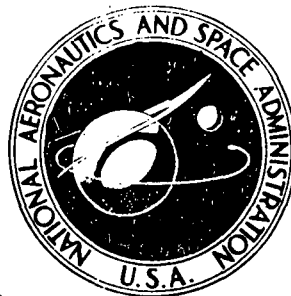


NASA CONTRACTOR REPORT



NASA CR-132432

**DATA AND RESULTS FROM A STUDY
OF
INTERNAL CONVECTIVE COOLING SYSTEMS
FOR
HYPERSONIC AIRCRAFT**

by **F. M. Anthony, W.H. Dukes, and R. G. Helenbrook**

| | | |
|-------------------|-------------------------------|------------|
| FACILITY FORM 602 | <u>1174-30422</u> | _____ |
| | (ACCESSION NUMBER) | (THRU) |
| | <u>365</u> | <u>G3</u> |
| | (PAGES) | (CODE) |
| | <u>CR 132432</u> | <u>02</u> |
| | (NASA CR OR TMX OR AD NUMBER) | (CATEGORY) |
| | | HC \$8.00 |

Prepared under Contract No. NAS 1-11357 by

textron Bell Aerospace
DIVISION

POST OFFICE BOX ONE
BUFFALO, NEW YORK 14240

for Langley Research Center

NATIONAL AERONAUTICS AND SPACE ADMINISTRATION - WASHINGTON, D. C. - JUNE, 1974

ERRATA FOR CR 132432

- Pg. 23 & 24, Table VIIA. Stations in column headings are incorrect. They should be equivalent to the stations in Table VIIB which are expressed in inches.
- Pg. 25, Table VIIB. Total gross weight is 43,875 lbs.
- Pgs. 130, 132, 134, 142, 144 and 146, (a) parts of figures 39, 40, 41, 45, 46 and 47. Delete $\times 10^2$ from the ordinate scale.
- Pg. 268, Table XXXIXB. In the 1st and 4th column headings, footnote (6) should be (7). In the 2nd, 3rd, and 5th column headings, footnote (7) should be (8).
- Pg. 267, Table XXXIXA, should carry the same footnote numbers in the column headings as Table XXXIXB, corrected.
- Pg. 273, Table XLIA, "Tankage and Insulation" column; footnote (6) should be (7) on entries 6, 7, and 8. Footnote (7) should be (8) on entries 9, 10 and 11.
- Pg. 274, Table XLIB. Footnotes on entries in "Tankage and Insulation" column and "Payload" column should be as in Table XLIA (corrected).
- Pg. 293-294, Tables XLIIIA and B. Delete footnote (3) from top line heading of table. Third entry in first column of Table B, 480 should be 80.
- Pg. 295, fifth line from bottom. 0.5 mm (20 mil) should be 0.25 (10 mil).
- Pg. 296-297, Tables XLIVA and B. Table lines and heading placement should indicate that the last column, "Baseline", is a separate concept and not a "Sphere-Core" subtype. Delete footnote (3) from the Nonredundant, Panel Residual item.
- Pg. 315, second paragraph last line. 0.62 cm (0.25 in) should be 62 cm (25 in).
- Pg. 320, Table XLVII A and B. The last three concepts, Plate fins, should all carry footnote (2).
- Pg. 326-327, figures 112a and b. The labels of the line keys should be interchanged.
- Pg. 269, Table XLA. In the column labeled "Other," 50, 394 should be 4990 in two places. Footnote 7 following 1271 should be Footnote 8 in three places.
- Pg. 270, Table XLB. In column labeled "Other," 111,000 should be 11,000 in two places.
- Pg. 74, 76, 78, Fig. 17b, 18b, 19b unit weight curves abscissa should be lb/ft^2 .

**DATA AND RESULTS FROM A STUDY OF INTERNAL CONVECTIVE
COOLING SYSTEMS FOR HYPERSONIC AIRCRAFT**

By F.M. Anthony, W.H. Dukes, and R.G. Helenbrook

**Prepared under Contract No. NAS 1-11357 by
Textron Bell Aerospace Division
Buffalo, New York**

for

**LANGLEY RESEARCH CENTER
NATIONAL AERONAUTICS AND SPACE ADMINISTRATION**

Page Intentionally Left Blank

FOREWORD

This document summarizes results of design, analysis, and experimental studies relating to internal convective cooling systems for hypersonic aircraft. The work was performed under contract NAS 1-11-357 for the National Aeronautics and Space Administration, Langley Research Center, Hampton, Virginia by Bell Aerospace Company, Buffalo, New York. At Bell, W. H. Dukes was the Project Manager and F. M. Anthony was the Technical Director. In addition to the authors other personnel who made significant contributions to this program were G. G. Chormann, A. Krivetsky, W. N. Meholick and A. L. Mistretta (loads, structural design and analysis), D. A. Brzezinski, J. A. Giafaglione, and J. D. Witsil, Jr. (cooling system and thermal analysis), E. O. Allen, K. M. Cooper, J. J. Early, C. Rossini, and W. Yurkowski (failure, hazard, and reliability analyses), and Dr. J. A. Davis, S. A. Long and Dr. A. A. Staklis (corrosion and compatibility studies).

CONTENTS

| | Page |
|--|------|
| INTRODUCTION | 1 |
| VEHICLE DATA | 2 |
| Hypersonic Transport | 2 |
| Hypersonic Research Airplane | 18 |
| MATERIAL SELECTION | 42 |
| Coolants | 42 |
| Construction Alloys | 47 |
| PANEL DESIGN STUDIES | 55 |
| Concepts | 55 |
| Thermal Analyses | 66 |
| Structural Analysis | 113 |
| Structural Assembly | 118 |
| Thermal Stresses | 121 |
| COOLING SYSTEM DESIGN STUDIES | 123 |
| Concepts | 123 |
| Distributing Line Sizing | 128 |
| Heat Exchanger Design | 154 |
| Pump Sizing | 181 |
| Failure Mode and Effect Analysis | 181 |
| Fault Hazard Analysis | 184 |
| Reliability | 198 |
| Fault Detection and Isolation Concepts | 202 |
| CONCEPTS FOR SELECTED REGIONS | 215 |
| Leading Edge Concepts | 215 |
| Heat Shielding | 224 |
| Concepts for Cooled Integral Tanks | 226 |
| Connection Concepts | 238 |
| Control Surface Concepts | 243 |
| Doors | 251 |
| SYSTEM SUMMARIES | 254 |
| Hypersonic Transport | 254 |
| Hypersonic Research Airplane | 281 |
| CONCLUSIONS AND RECOMMENDATIONS | 329 |
| APPENDIX A EXPERIMENTAL EVALUATIONS | 335 |
| Corrosion Potential Measurements | 335 |

CONTENTS (CONT)

| | Page |
|----------------------------------|------|
| Weight Change Measurements | 340 |
| Stress Corrosion Exposures | 340 |
| REFERENCES | 349 |

ILLUSTRATIONS

| Figure | | Page |
|--------|--|------|
| 1 | Delta Wing Configuration | 3 |
| 2 | Vehicle Load Histories for Various Wall Temperatures | 12 |
| 3 | Hypersonic Research Aircraft Configuration | 22 |
| 4 | Effect of Maneuvers on HRA Heat Load History, Mach 8 Trajectory, Unshielded Vehicle | 30 |
| 5 | Effect of Maneuvers on HRA Heat Load History, Mach 10 Trajectory, Unshielded Vehicle | 32 |
| 6 | Fuselage Bending Moment Diagram, Hypersonic Research Airplane | 38 |
| 7 | Fuselage Limit Loading Envelope | 40 |
| 8 | Nonredundant and Redundant Skin Panel Concepts | 56 |
| 9 | Manifold Arrangements for Parallel Flow in Nonredundant and Redundant Skin Panel Concepts | 59 |
| 10 | Insulated Panel Concepts | 61 |
| 11 | Qualitative Weights Trade for Insulated and Cooled Structure | 63 |
| 12 | Candidate Constructions | 64 |
| 13 | Crack Stopping Techniques | 65 |
| 14 | Parametric Coolant Passage Spacing Data, Water Glycol, Maximum Skin Temperature 450°K, $\Delta P/L = 11.3 \text{ k N/m}^2/\text{m}$, Semicircular Passage, Coolant Temperature Rise = 366°K, Coolant Inlet Temperature = 254°K | 67 |
| 15 | Parametric Coolant Passage Spacing Data, Water Glycol, Maximum Skin Temperature 450°K, $\Delta P/L = 45.2 \text{ k N/m}^2/\text{m}$, Semicircular Passage, Coolant Temperature Rise = 366°K, Coolant Inlet Temperature = 254° | 68 |
| 16 | Parametric Coolant Passage Spacing Data, Water Glycol, Maximum Skin Temperature 450°K, $\Delta P/L = 113 \text{ k N/m}^2/\text{m}$, Semicircular Passage, Coolant Temperature Rise = 366°K, Coolant Inlet Temperature = 254°K | 70 |
| 17 | Coolant Passage Spacing Data, Water Glycol, Plain Semicircular Passage, Coolant Temperature Rise = 111°K, Coolant Inlet Temperature = 253°K | 73 |
| 18 | Coolant Passage Spacing Data, Coolanol 20, Plain Semicircular Passage, Coolant Temperature Rise = 111°K, Coolant Inlet Temperature = 253°K | 75 |
| 19 | Coolant Unit Weight and Passage Spacing Data, Maximum Skin Temperature = 506°K, Plain Semicircular Passage, Coolant Temperature Rise = 111°K, Coolant Inlet Temperature = 256°K | 77 |
| 20 | Minimum Unit Weight for Plate Fin Panels, Ethylene Glycol/Water, Coolant in at 283°K/out at 367°K | 81 |
| 21 | Pressure Drop Through Optimum Plate Fin Panel, Ethylene Glycol/Water, Coolant in at 283°K/out at 367°K | 83 |
| 22 | Maximum Panel Temperature for Optimum Plate Fin Panel During Single Mode Operation, Ethylene Glycol/Water, Coolant in at 283°K/ out at 366°K | 85 |

ILLUSTRATIONS (CONT)

| Figure | | Page |
|--------|---|------|
| 23 | Minimum Unit Weight for 6.1 Meter Long Plate - Fin Panels with 6 Fins/cm, Coolant Inlet Temperature = 283°K | 88 |
| 24 | Optimized Unit Weights for Sphere-Core Panel Concept, Ethylene Glycol, Inlet Temperature = 283°K, Outlet Temperature = 367°K | 91 |
| 25 | Pressure Drop for Optimized 6m Long Sphere - Core Panels, Water Glycol Coolant, Coolant Temperature Rise from 283°K to 367°K | 93 |
| 26 | Maximum Stringer Spacing for Cooled Stringer Concept, Maximum Temperature = 422°K, Aluminum Structure | 95 |
| 27 | Maximum Stringer Spacing for Cooled Stringer Concept, Maximum Temperature = 533°K, Titanium Structure | 97 |
| 28 | Stringer Spacing as a Function of Interface Thermal Resistance, Heat Flux = W/cm^2 | 99 |
| 29 | Optimization of Unit Weight for Reusable Surface Insulation on an Actively Cooled Substructure at 366°K | 102 |
| 30 | Heat Flux, Temperature, Thermal Emittance Relationship | 104 |
| 31 | Heat Shield Temperature as a Function of Heat Flux and Effective Internal Emittance, External Emittance = 0.8, $T_r = 3810^\circ K$ | 107 |
| 32 | Cooling System Heat Load for Radiation Shielded Structure, $T_r = 3810^\circ K$... | 109 |
| 33 | Unit Weight of Radiation Shielded Cooling System, Effective Emittance = 0.67, Includes Heat Shield Weight $T_r = 3810^\circ K$ | 111 |
| 34 | Typical Thermal/Structural Integration Techniques for Sandwich Construction | 119 |
| 35 | Structural Details for Assembly of Cooled Airframe, Discrete Tubular Skin Panels | 120 |
| 36 | Redundant Cooling System Schematic | 125 |
| 37 | Multiple Systems, Mixed Materials | 127 |
| 38 | HST Distribution System | 129 |
| 39 | Minimum Weight of Coolant Distribution Lines and APS Fuel as a Function of Heat Load and Inlet Temperature, Outlet Temperature = 366°K, Ethylene Glycol/Water | 130 |
| 40 | Minimum Weight of Coolant Distribution Lines and APS Fuel as a Function of Heat Load and Inlet Temperature, Outlet Temperature = 366°K, FC-43 | 132 |
| 41 | Minimum Weight of Coolant Distribution Lines and APS Fuel as a Function of Heat Load and Inlet Temperature, Outlet Temperature = 366°K, Coolanol 45 | 134 |
| 42 | Pressure Drop for Minimum Weight Coolant Distribution Lines as a Function of Heat Load and Inlet Temperature, Outlet Temperature = 366°K, Ethylene Glycol/Water | 136 |

ILLUSTRATIONS (CONT)

| Figure | | Page |
|--------|---|------|
| 43 | Pressure Drop for Minimum Weight Coolant Distribution Lines as a Function of Heat Load and Inlet Temperature, Outlet Temperature = 366°K, FC-43 | 138 |
| 44 | Pressure Drop for Minimum Weight Coolant Distribution Lines as a Function of Heat Load and Inlet Temperature, Outlet Temperature = 366°K, Coolanol 45 | 140 |
| 45 | Minimum Weight of Coolant Distribution Lines and APS Fuel as a Function of Heat Load and Inlet Temperature, Outlet Temperature = 450°K, Coolanol 45 | 142 |
| 46 | Minimum Weight of Coolant Distribution Lines and APS Fuel as a Function of Heat Load and Inlet Temperature, Outlet Temperature = 450°K, Dow Corning XF-1-3755 | 144 |
| 47 | Minimum Weight of Coolant Distribution Lines and APS Fuel as a Function of Heat Load and Inlet Temperature, Outlet Temperature = 450°K, Freon E5 | 146 |
| 48 | Pressure Drop for Minimum Weight Coolant Distribution Lines as a Function of Heat Load and Inlet Temperature, Outlet Temperature = 450°K, Coolanol 45 | 148 |
| 49 | Pressure Drop for Minimum Weight Coolant Distribution Lines as a Function of Heat Load and Inlet Temperature, Outlet Temperature = 450°K, Dow Corning XF-1-3755 | 150 |
| 50 | Pressure Drop for Minimum Weight Coolant Distribution Lines as a Function of Heat Load and Inlet Temperature, Outlet Temperature = 450°K, Freon E5 | 152 |
| 51 | Separate Distribution System for Fuselage and Wing of HRA | 155 |
| 52 | Minimum Weight of Coolant Distribution Lines and APS Fuel as a Function of Heat Load and Inlet Temperature, Outlet Temperature = 366°K, Ethylene Glycol/Water | 156 |
| 53 | Minimum Weight of Coolant Distribution Lines and APS Fuel as a Function of Heat Load and Inlet Temperature, Outlet Temperature = 367°K, Methanol/Water | 158 |
| 54 | Minimum Weight of Coolant Distribution Lines and APS Fuel as a Function of Heat Load and Inlet Temperature, Outlet Temperature = 367°K, Coolanol 20 | 160 |
| 55 | Minimum Weight of Coolant Distribution Lines and APS Fuel as a Function of Heat Load and Inlet Temperature, Outlet Temperature = 367°K, Coolanol 40 | 162 |
| 56 | Pressure Drop for Minimum Weight Coolant Distribution Lines as a Function of Heat Load and Inlet Temperature, Outlet Temperature = 367°K, Ethylene Glycol/Water | 164 |
| 57 | Pressure Drop for Minimum Weight Coolant Distribution Lines as a Function of Heat Load and Inlet Temperature, Outlet Temperature = 367°K, Methanol/Water | 166 |

ILLUSTRATIONS (CONT)

| Figure | | Page |
|--------|---|------|
| 58 | Pressure Drop for Minimum Weight Coolant Distribution Lines as a Function of Heat Load and Inlet Temperature, Outlet Temperature = 367°K, Coolanol 20 | 168 |
| 59 | Pressure Drop for Minimum Weight Coolant Distribution Lines as a Function of Heat Load and Inlet Temperature, Outlet Temperature = 367°K, Coolanol 40 | 170 |
| 60 | Minimum Weight of Coolant Distribution Lines and APS Fuel as a Function of Heat Load and Inlet Temperature, Outlet Temperature = 506°K, Coolanol 40 | 172 |
| 61 | Pressure Drop for Minimum Weight Coolant Distribution Lines as a Function of Heat Load and Inlet Temperature, Outlet Temperature = 506°K, Coolanol 40 | 174 |
| 62 | Plate and Fin Heat Exchanger Weight as a Function of Heat Load, Low Temperature Coolants, Inlet Temperature = 367°K, Outlet Temperature = 283°K, H ₂ T _{in} /T _{out} = 33°K/339°K | 176 |
| 63 | Plate and Fin Heat Exchanger Weight as a Function of Heat Load, High Temperature Coolants, Inlet Temperature = 450°K, Outlet Temperature = 283°K, H ₂ T _{in} /T _{out} = 33°K/422°K | 178 |
| 64 | Impeller Diameter as a Function of Flow Rate and Head Requirements, N _s = 2000, η = 85% | 182 |
| 65 | Pump Weight as a Function of Flow Rate and Head Requirements, N _s = 2000, η = 85% | 182 |
| 66 | Nonredundant Cooling System Reliability Schematic | 200 |
| 67 | Instrumentation Schematic for Fault Isolation | 211 |
| 68 | Limited Instrumentation of Distribution System | 212 |
| 69 | Completely Instrumented Panel | 213 |
| 70 | Accumulator Schematic | 214 |
| 71 | Cooled Leading Edge Concepts | 216 |
| 72 | Fail-Safe Concepts for Cooled Leading Edges | 218 |
| 73 | Heat Capacity Envelope for Candidate Heat Sink Materials | 221 |
| 74 | External Heat Shielding Concepts | 225 |
| 75 | Unit Weights for Heat Shield and Supports | 227 |
| 76 | Typical Construction for Integral Tank | 229 |
| 77 | Coolant Passages Machined Into Exterior Tank Wall | 231 |
| 78 | External Tunnel Structure | 233 |
| 79 | Coolant Passages Integrated on Inside of Tank Wall | 234 |
| 80 | Wrap Around Cooled Skin | 236 |
| 81 | Actively Cooled Heat Shields | 237 |
| 82 | Actively Cooled Sandwich Tank | 239 |
| 83 | Concepts for Connecting Distribution Lines to Skin Panels | 242 |
| 84 | Fitting Concepts | 244 |
| 85 | Mechanically Attached Connectors | 245 |
| 86 | Metallurgically Attached Connectors | 246 |
| 87 | Control Surface Concepts, "Conventional" | 248 |

ILLUSTRATIONS (CONT)

| Figure | | Page |
|--------|--|------|
| 88 | Control Surface Concepts, Metallic Seals | 249 |
| 89 | Heat Load Attenuated Control Surface Concept | 250 |
| 90 | Extended Control Surface Concept | 252 |
| 91 | Typical Door Concepts | 253 |
| 92 | Hydrogen Availability as a Function of Flight Load Factor for Structural Wall Temperatures at Critical Times During Cruise and Descent, Shielded Airframe, 920 m ² (10,000 ft ²) of Shielding | 262 |
| 93 | Hydrogen Availability as a Function of Flight Load Factor for Structural Wall Temperatures at Critical Times During Cruise and Descent, Unshielded Airframe | 264 |
| 94 | Shielding Hypersonic Transport Concept, 1000 F Shields | 272 |
| 95 | Fatigue Characteristics of 2024-T3 Structure, HST Spectrum | 276 |
| 96 | Interaction of Life, Ultimate Design Allowable Stress and Initial Crack Size, Infinite 2024-T3 Sheet, HST Spectrum | 279 |
| 97 | Skin Stringer Dimensions for Hypersonic Research Aircraft | 283 |
| 98 | Fuselage Running Weight, Shell and Frames | 286 |
| 99 | Hydrogen Cooling Requirements and Fuel Flow Requirements for HRA, Coolant Temperatures In/Out = 283/366°K, Maximum Structural Temperature = 394°K | 289 |
| 100 | Distribution System Layout, Hypersonic Research Aircraft | 292 |
| 101 | Coolant Passage Size and Spacing | 299 |
| 102 | Temperature Distribution Between Passages, Fuselage Station 420, Passage Spacing = 1.78 cm, Mach 8, 71.8 kN/m ² Dynamic Pressure | 300 |
| 103 | Temperature Distribution Between Passages, Fuselage Station 900, Mach 8, 71.8 kN/m ² Dynamic Pressure Including Effect of Engine Exhaust | 302 |
| 104 | Temperature History for Nominal Flight and Boundaries for Maneuvers, HRA Station 420 | 304 |
| 105 | Temperature History for Nominal Flight and Boundaries for Maneuvers, HRA Station 900 | 306 |
| 106 | Temperature Distribution Between Passages, Fuselage Station 420, Passage Spacing = 1.78 cm, Mach 8, 71.8 kN/m ² Dynamic Pressure | 309 |
| 107 | Temperature Distribution Between Passages, Fuselage Station 900, Mach 8; 71.8 kN/m ² Dynamic Pressure | 311 |
| 108 | Temperature Distribution Along Panel Inbetween Passages for Single-Mode Operation at 50% of Total Design Coolant Flow, Station 420 | 313 |
| 109 | Dependence of Critical Passage Design Parameters on Panel Length, Baseline Length = 1.5 m (5.0 ft) | 318 |
| 110 | Pump Arrangements | 323 |
| 111 | Fatigue Characteristics of 2024-T3 Structure, Severe Research Airplane Spectrum | 324 |
| 112 | Interaction of Life, Ultimate Design Allowable Stress, and Initial Crack Size for a Surface Crack and Through-Crack in an Infinite 2024-T3 Sheet, Hypersonic Research Airplane Spectrum | 326 |

ILLUSTRATIONS (CONT)

| Figure | | Page |
|--------|---|------|
| 113 | Block Diagram of Automatic Polarization Apparatus | 336 |
| 114 | Polarization Diagram for 7075-T6 Aluminum Alloy Exposed to Apollo Grade 2 Ethylene Glycol at 200°F | 337 |
| 115 | Beryllium Bend Coupon Specimen Configuration | 347 |

TABLES

| Number | | Page |
|--------|---|------|
| I | Dead Weight Distribution - Estimated Hydrogen Fueled Air Breathing Cruise Aircraft | 5 |
| II | Trajectory and Fuel Flow Data | 9 |
| III | Maneuver Heat Loads, 366°K Wall Unshielded Vehicle | 14 |
| IV | Maneuver Heat Loads, 366°K Wall Shielded Vehicle | 16 |
| V | HST Structural Loading Intensities | 19 |
| VI | Suggested Loading Spectrum, Hypersonic Transport Cumulative Occurrences per 10,000 Flight Hours | 19 |
| VII | Initially Estimated Deadweight Distribution, Hypersonic Research Airplane .. | 23 |
| VIII | HRA Mission Profile and Weight History, Mach 8 Trajectory | 26 |
| IX | HRA Mission Profile and Weight History, Mach 10 Trajectory | 28 |
| X | Local Heat Fluxes, Hypersonic Research Airplane | 35 |
| XI | Suggested Loading Spectrum, Hypersonic Research Airplane Cumulative Occurrences per 1000 Flight Hours | 37 |
| XII | Candidate Coolants in Order of Decreasing Performance Potential | 43 |
| XIII | Comparison of Candidate Coolants, 366°K Shielded Nonredundant System, 340°K Temperature Rise 394°K Structural Temperature Limit, 54.5 x 10 ⁶ Watts | 46 |
| XIV | Comparison of Candidate Coolants, 450°K Shielded Nonredundant System 422°K Temperature Rise, 533°K Structural Temperature Limit, 33.4 x 10 ⁶ Watts | 46 |
| XV | Candidate Construction Materials Selected From Initial Review of Properties | 48 |
| XVI | Structural Efficiency of Construction Materials | 49 |
| XVII | Comparison of Candidate Materials and Panel Concepts for Hypersonic Trans- port Fuselage at 311°K, No Minimum Gage Constraint | 114 |
| XVIII | Comparison of Materials and Concepts for Wing Covers, Hypersonic Transport | 117 |
| XIX | Optimized Offset Fin Configuration for Heat Exchangers for Various Coolants | 180 |
| XX | Initial Failure Mode and Effect Analysis, Cooled Skin Panel | 185 |
| XXI | Initial Failure Mode and Effect Analysis, Panel Coolant Fittings and Lines | 187 |
| XXII | Initial Failure Mode and Effect Analysis, Panel Coolant Pump | 188 |
| XXIII | Initial Failure Mode and Effect Analysis, Panel Coolant Line Valves | 189 |
| XXIV | Initial Failure Mode and Effect Analysis, Expansion Tank | 190 |
| XXV | Initial Failure Mode and Effect Analysis, Heat Exchanger | 191 |
| XXVI | Initial Failure Mode and Effect Analysis, Hydrogen Control Valves | 195 |
| XXVII | Summary of Nonredundant Cooling System Failure Rates for a Hypersonic Transport | 201 |
| XXVIII | Summary of Non-Redundant Cooling System Failure Rates for a Hypersonic Research Airplane | 203 |
| XXIX | Summary of Fault Detection and Isolation Concepts | 205 |
| XXX | Candidate Heat Sink Materials | 219 |

TABLES (CONT)

| Number | | Page |
|---------|---|------|
| XXXI | Minimum Skin Gages for Candidate Materials | 255 |
| XXXII | Minimum Equivalent Thickness | 255 |
| XXXIII | Weight of Sandwich Construction Fuselage, 311°K | 256 |
| XXXIV | Weight of Zee Stiffened Fuselage, 311°K | 256 |
| XXXV | Weight of Zee Stiffened Wings*, 311°K | 258 |
| XXXVI | Weight of Symmetrical Double Beaded Wings, 311°K | 258 |
| XXXVII | Weight of Sandwich Construction Wings, 311°K | 259 |
| XXXVIII | Total Airframe Structural Weight | 261 |
| XXXIX | Cooling System Concept Comparison, Hypersonic Transport | 267 |
| XL | Cooled Airframe Weight Summary, Hypersonic Transport | 269 |
| XLI | Impact of Airframe Cooling On Payload, Hypersonic Transport | 273 |
| XLII | HRA Airframe Structure Weight Summary | 288 |
| XLIII | Cooling System Concept Comparison, Hypersonic Research Airplane Baseline Panel | 293 |
| XLIV | Cooling System Concept Comparison, Hypersonic Research Airplane, Plate-Fin and Sphere-Core Panels, Unshielded Aluminum Structure | 296 |
| XLV | Single Mode Operation, Station 420, 283°K Coolant Inlet Temperature | 316 |
| XLVI | Single Mode Operation, Station 900, 283°K Coolant Inlet Temperature | 316 |
| XLVII | Cooled Airframe Weight Summary, Hypersonic Research Airplane, Aluminum Alloy Construction | 320 |
| XLVIII | Cooling System Weight/Reliability As Related to Panel Size, Hypersonic Research Airplane | 321 |
| XLIX | Corrosion Rates in Aqueous Solutions | 338 |
| L | Corrosion Rates for 1300 Hours Exposure at 366°K In Coolanols | 341 |
| LI | Weight Change Results in Dielectric Coolants, 762 Hours of Exposure at 366°K | 341 |
| LII | Results of Stress Corrosion Tests in Apollo Grade 2 Ethylene Glycol/Water at 366°K, 90% of YTS | 342 |
| LIII | Results of Stress Corrosion Tests in Prestone*Water at 366°K, 90% of YTS .. | 342 |
| LIV | Results of Stress Corrosion Tests in Prestone II /Water at 366°K, 90% YTS .. | 343 |
| LV | Results of Stress Corrosion Tests in FC-43 , at 366°K, 90% YTS | 343 |
| LVI | Results of Stress Corrosion Tests in Coolanol 45 at 366°K, 90% YTS | 344 |
| LVII | Results of Stress Corrosion Tests in Coolanol 45 450°K, 90% YTS | 344 |
| LVIII | Results of Stress Corrosion Tests in XF-1-3755 at 450°K, 90% YTS | 345 |
| LIX | Results of Stress Corrosion Tests in E-5 at 450°K, 90% YTS | 345 |
| LX | Results of Stress Corrosion Tests in Coolanol 45 at 535°K, 90% YTS | 346 |
| LXI | Results of Stress Corrosion Tests in Dowtherm G at 535°K, 90% YTS | 346 |

INTERNAL CONVECTIVE COOLING SYSTEMS FOR HYPERSONIC AIRCRAFT

BY:

F. M. Anthony, W. H. Dukes, and R. G. Helenbrook

SUMMARY

Parametric studies were conducted to investigate the relative merits of construction materials, coolants and panel concepts for internal convective cooling systems applied to airframe structures of hypersonic aircraft. These parametric studies were then used as a means of comparing various cooled structural arrangements for hypersonic transport and a hypersonic research airplane. The cooled airplane studies emphasized weight aspects as related to the choice of materials, structural arrangements, and structural temperatures. Consideration was given to reliability and to fatigue and fracture aspects, as well.

Numerous candidate coolants were screened and coolant distribution systems sizing studies were conducted for the more promising coolants. Aqueous solutions, particularly ethylene glycol/water, were attractive for operation at temperatures below 394°K (250F). Operation at higher temperatures necessitated the use of non aqueous coolants whose lower specific heats required higher flow rates, but in some cases the pumping power penalty usually associated with a higher flow rate was compensated by a larger operating temperature range and the lower viscosity resulting from a higher maximum coolant temperature. Presently available coolants appear to be suitable for operation to 450°K (350F).

Because of the modest temperatures associated with actively cooled airframe structure the selection of construction materials closely parallels that for conventional aircraft structure except that consideration should be given to thermal conductivity as well as ratios of strength and stiffness to density. Beryllium and metal matrix composites are most attractive for minimizing weight in future applications while aluminum alloys are the most attractive of the materials commonly in use today for airframe structure.

Both tubular and plate-fin sandwich panels were attractive based on thermal design considerations. The former is attractive because of the relative ease of integration with the substructure; the latter is particularly well suited for regions of high heat flux. Both panel designs are adaptable to the incorporation of redundant coolant circuits. The choice of structural panel design was strongly influenced by the relatively low loading intensities associated with the types of hypersonic aircraft studied with highly swept delta wings and large fuselages required to house hydrogen fuel. Conventional stringer stiffened skin panels and honeycomb sandwich panels were attractive for fuselage and wing applications, respectively. Beaded skin designs showed lowest weight but the integration of coolant passages with such a structural configuration would pose significant problems.

Comparisons of non-redundant and redundant cooling systems indicated that the major weight increase associated with redundancy came from duplicating such items as the heat exchanger, the pump, and the coolant reservoir/accumulator; there was little weight penalty with respect to distribution

lines because of the design approach used. Minimization of the coolant distribution line weight for the redundant configuration was achieved by permitting half of the required flow through each of the redundant loops under normal operating conditions. With such a design it is necessary to increase coolant flow in the remaining loop in the event of a malfunction in one loop, or to accept higher operating temperatures after a malfunction.

For the Mach 6 hypersonic transport and the trajectory studied a surface temperature of about 544°K (575F) was required in order to have sufficient heat capacity in the fuel flow to absorb the heat loads for an unshielded airframe under all flight conditions including maneuvers. Operation at lower surface temperatures is possible if the heat load to the airframe is attenuated (by heat shielding or insulation) or if extra hydrogen is carried for cooling during specific flight conditions such as maneuvers. Combinations of these techniques were found to be attractive. Load factors near zero g are particularly adverse because the reduced drag reduces power requirements and fuel flow while heat loads are reduced to a lesser degree. For the configuration and trajectory studied, a structure operating at a maximum temperature of 394°K (250F) would require heat shielding and hydrogen flow in excess of fuel needs for maneuver involving load factors of between ± 0.8 g.

Even when auxiliary thermal protection system items, such as heat shielding, insulation, and excess hydrogen for cooling, are considered the more attractive actively cooled airframe concepts indicated potential payload increases of from 40% to over 100% as compared to the results of previous studies of the same vehicle configuration with an uncooled airframe. For the actively cooled hypersonic transport the use of a redundant cooling system reduced the indicated failure rate by two orders of magnitude, and added about 23% to the cooling system weight, (less than 0.7% of the aircraft gross weight).

Because of the nearer term aspects of a hypersonic research airplane as compared to the hypersonic transport, the active cooling studies for this application focused on aluminum alloy construction and aqueous coolants. Ethylene glycol/water was selected over methanol/water primarily on the basis of operational considerations of volatility, flammability, and toxicity. For the various cooled concepts examined weights of the airframe structure and total thermal protection system ranged from 30 to 40% of the launch weight. The smaller size of the research airplane necessitated fewer cooled panels and connectors than for the transport; this resulted in relatively higher reliability. Redundancy reduced the indicated failure rate by two orders of magnitude and added about 26% to the weight of the cooling system (about 2% of the aircraft gross weight).

INTRODUCTION

Preliminary studies in Ref 1-3 of a cooled structure for a hydrogen fueled Mach 6 transport indicated potential advantages of reduced thermal distortion and stresses, use of state-of-the-art materials and subsystems, and significant payload improvements when compared to hot structures. The cooling system found to be most attractive was an internal convective system which used a cooling fluid circulated through integral surface cooling passages to transfer the structural heat load to a centrally located hydrogen-fuel-cooled heat exchanger. A preliminary design for such a system was developed in Ref 3; however that study was limited in scope to two materials and coolants and a single cooled panel concept. Therefore, the purpose of this contract was to investigate a wide range of materials, coolants and panel concepts, such that optimum design concepts for cooled hypersonic structures could be more accurately defined.

An extensive survey of current and future airframe construction materials and coolants was conducted, so that the most promising candidates for cooled-panel, cooling-system and airframe concepts could be examined. Consideration was given to a wide range of structural materials, coolants, and structural panel concepts, several thermal panel concepts, and 3 cooled airframe design approaches, including unshielded, shielded, and dual temperature types. As an adjunct to the studies of materials and coolants, tests of corrosion potential and stress corrosion were carried out to investigate the compatibility of several promising structural materials and coolant fluids. The concept identification and parametric comparison phase of the study examined all major elements of the convectively cooled airframe, including the differing requirements at various locations on the aircraft.

The parametric results were used for the investigation of two separate vehicles, a hypersonic transport with a length of 96m (314 ft) and a weight of 240,000 kg (528,600 lb) and a hypersonic research airplane, with a length of 25m (80 ft) and a weight of 20,300 kg (44,700 lb). On the basis of NASA supplied trajectories, the heat loads and structural loads for both of these aircraft were predicted and used as baseline values for the comparative studies of different coolants and different cooling system concepts. In addition, consideration was given to cooling system concepts for selected regions of the vehicle, such as leading edges, integral tankage, and control surfaces. Fault hazard and reliability analyses were made to define critical cooling system components and to study the effects of redundancy on system weight and reliability.

Since the primary objective of this project was to compare materials and thermal/structural design approaches for cooled aircraft, emphasis was placed on cooling systems and primary load carrying airframe structure. Simplifying assumptions were used where it was felt that they would not influence comparisons seriously. Heat load calculations neglected control surface deflections and temperature variations over the vehicle surface. Approximations were used to account for secondary structural items such as leading edges, and control surfaces. With respect to the primary airframe structure, the analytical efforts were focused on the stiffened skin panels; allowances were made for frames, hard points, and non-optimum configurational features such as doors, based on prior experience, with an attempt to be conservative.

This report presents details of the work performed during this contract. A summary of the study is presented in NASA CR 2480, Internal Convective Cooling of Hypersonic Aircraft.

All computations were performed in the English system of units and then converted to SI units.

VEHICLE DATA

This section of the report provides a description of the hypersonic transport and the hypersonic research airplane that were studied during the project. Each description includes details of the configuration, flight trajectories, and fuel flow. Results of heating and structural load analyses are presented along with the flight load spectra used for analyses of fatigue and fracture mechanics characteristics.

Hypersonic Transport

The hypersonic transport investigated during this project was studied previously with respect to active cooling as reported in References 1, 2 and 3. The vehicle was originally defined during the studies of Reference 4. While the basic configuration of this Mach 6 transport remained the same as for the earlier studies, the trajectory and fuel flow data was updated by NASA, based on the recommendations of Reference 3, to minimize the peak heating near the end of the ascent phase and to increase the fuel flow during the descent phase. By reducing the peak heat load the size and weight of the cooling system and its components were decreased. Increasing the fuel flow during descent increased the heat sink capacity for structural cooling during this phase of flight with only a modest increase in weight, about 1360 kg (3,000 lb). Structural loading for the wing was updated from the modest levels specified in Reference 1 for cruise conditions to the more severe load factors defined in Reference 2 for flight at speeds below Mach 3.

Configuration. - The delta wing configuration of the hypersonic transport is shown in Figure 1 which also identifies the location of the fuel tankage, passenger and cargo compartments, and primary flight control surfaces. The 65° swept wing has a span of 32.9 meters (108 ft) and an area of approximately 650 m² (7,000 ft²). The horizontal tail has a span of about 15.25 meters (50 ft), a leading edge sweep of 55°, a trailing edge sweep of 30° and an area of approximately 100 m² (1,100 ft²). The vertical tail has a leading edge sweep of 65°, a trailing edge of 45°, and an area of approximately 85 m² (900 ft²). The fuselage is 95 meters (314 ft) long and has a wetted surface area of 1,700 m² (18,400 ft²). The wetted area of the hypersonic area is 3,200 m² (34,000 ft²).

Weights for the baseline configuration of Reference 4 were developed in Reference 3 as shown in Table I. The maximum design weight for the vehicle was assumed to be 236,000 kg (520,652 lb), which corresponds to a vehicle with a full load of fuel. The design cruise weight was 219,000 kg (484,500 lb), conservatively assuming only 20% of the fuel to be used during ascent, while the design landing weight was 761,000 kg (356,000 lb) with 10% of the fuel load retained. The weight distributions for each of these conditions was used in conjunction with the appropriate flight load factors to determine the structural loads presented in the Vehicle Data Section, Hypersonic Transport Airplane Subsection, Structural Loads.

Trajectory. - The nominal flight trajectory for the hypersonic transport is presented in Table II along with angle of attack, fuel flow, and vehicle weight data. The Mach 6 flight speed is reached at approximately 30,400 meters (100,000 ft) about 1,400 seconds after takeoff. By this time approximately 36,200 kg (80,000 lb) of fuel have been used. Although cruise is flown at a constant Mach number the altitude increases slightly as fuel is used. The descent begins at

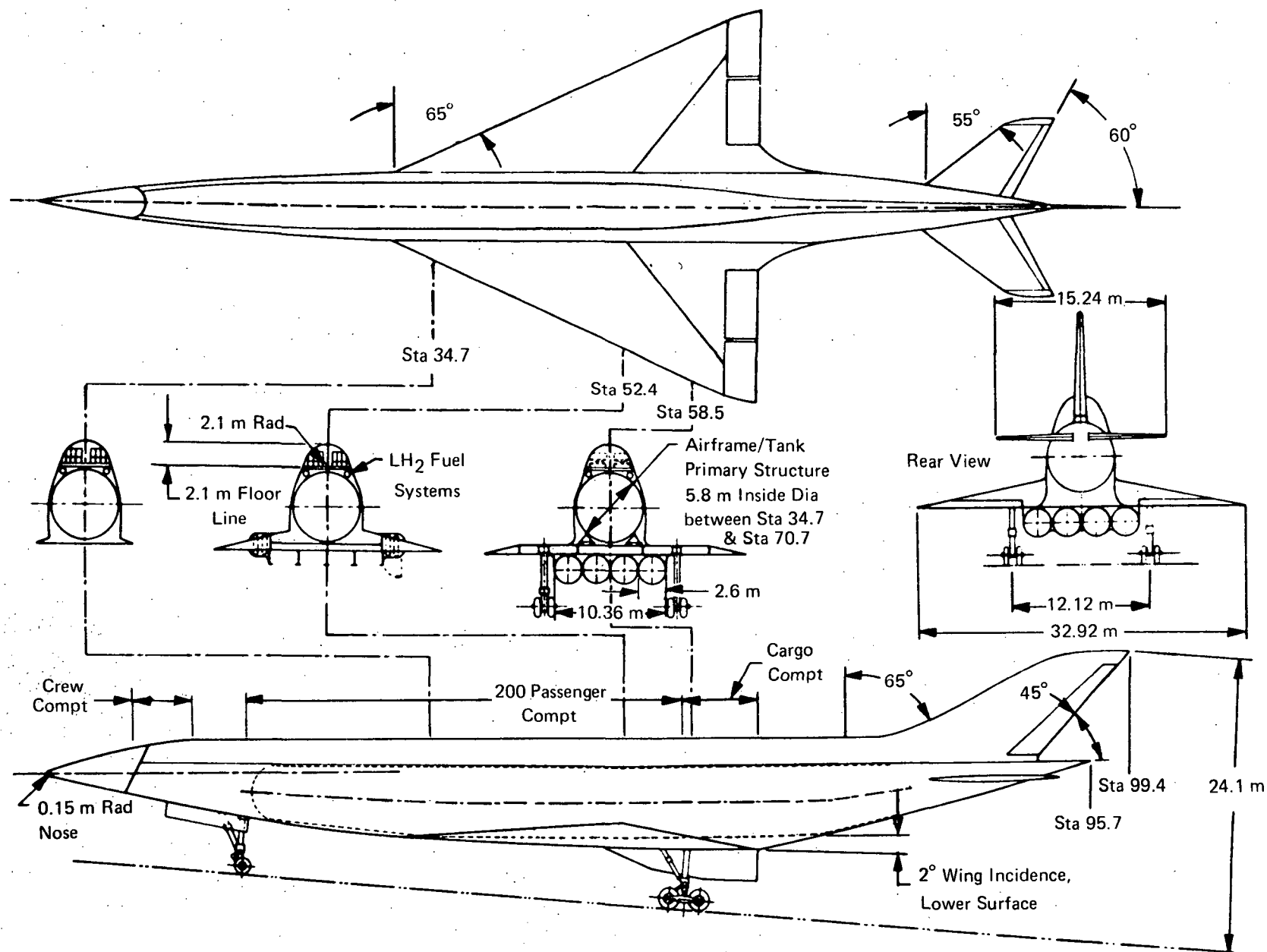


Figure 1a. Delta Wing Configuration (from Reference 5)

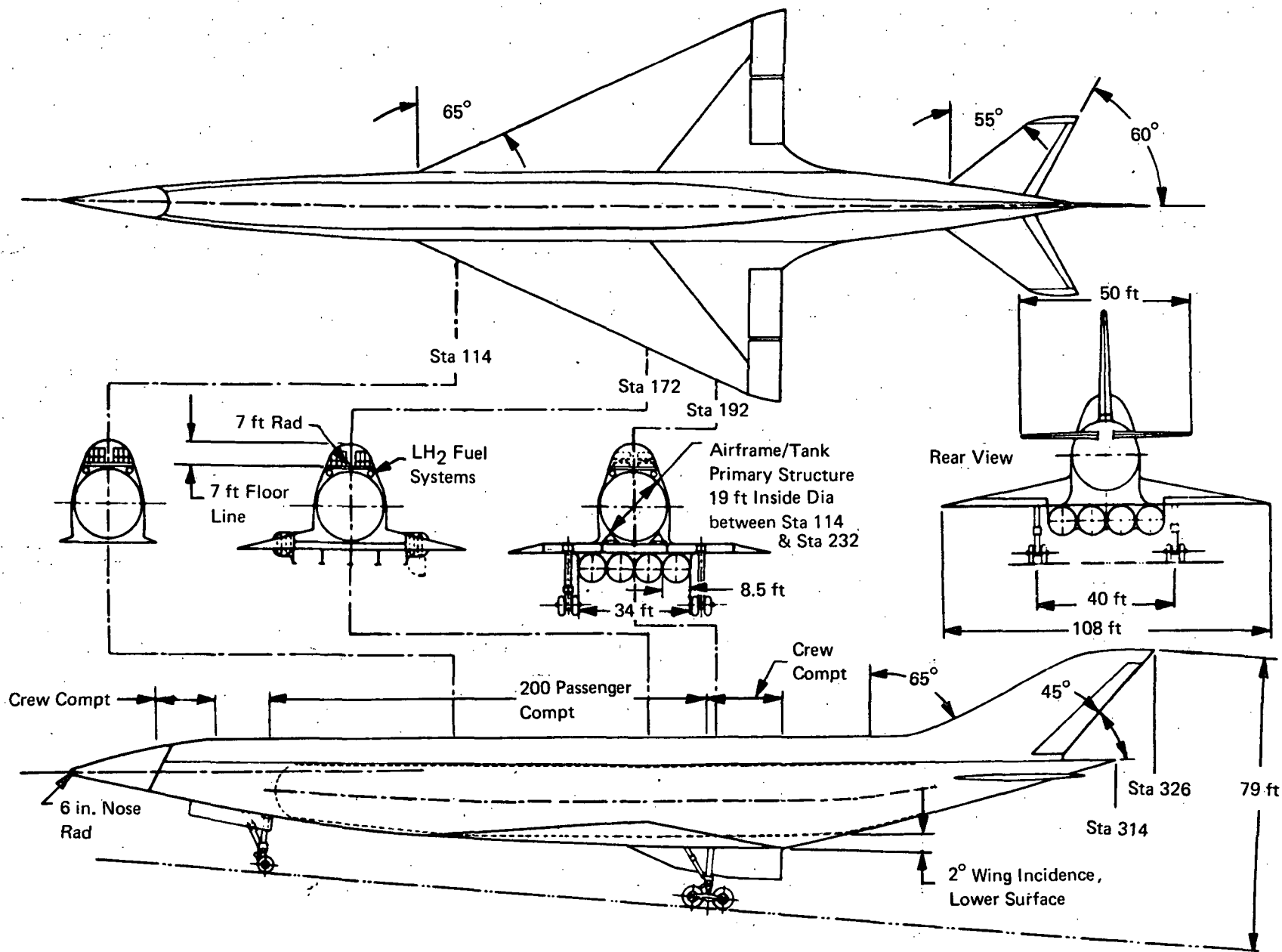


Figure 1b. Delta Wing Configuration (from Reference 5)

TABLE IA
DEAD WEIGHT DISTRIBUTION - ESTIMATED HYDROGEN FUELED AIR BREATHING CRUISE AIRCRAFT --- Kg

| Meters | Station Location | | | | | | | | | | | | | | | | |
|-----------------------------------|------------------|----------|-----------|-----------|-----------|-----------|-----------|-----------|-----------|-----------|-----------|-----------|-----------|-----------|-----------|-----------|----------|
| | 0-6.1 | 6.1-12.2 | 12.2-18.3 | 18.3-24.4 | 24.4-30.5 | 30.5-36.6 | 36.6-42.7 | 42.7-48.8 | 48.8-54.9 | 54.9-61.0 | 61.0-67.1 | 67.1-73.2 | 73.2-79.2 | 79.2-85.3 | 85.3-91.4 | 91.4-95.7 | |
| Body | | | | | | | | | | | | | | | | | |
| Basic Enclosing Structure | 525.6 | 1,478.0 | 2,138.3 | 2,660.7 | 3,047.1 | 3,247.1 | 2,543.7 | 2,490.6 | 2,450.7 | 2,584.0 | 2,715.1 | 2,511.5 | 1,950.5 | 1,471.2 | 851.2 | 189.0 | 32,854.3 |
| Pressurized Compartments | | 143.3 | 234.0 | 234.0 | 243.0 | 243.0 | 243.0 | 243.0 | 243.0 | 229.5 | 128.8 | | | | | | 2,139.6 |
| Main Propulsion | | | | | | | | | | | | | | | | | |
| Engine and Accessories | | | | | | | | | | 5,661.9 | 10,556.6 | | | | | | 16,218.5 |
| Air Induction | | | | | | | | | 2,560.9 | 4,088.3 | | | | | | | 6,649.2 |
| Nacelles, Pods, Pylons, Sup. | | | | | | | | | | 514.3 | 938.3 | | | | | | 1,452.6 |
| Fuel Containers and Supts. | | | | 1,138.7 | 1,264.8 | 1,264.8 | 1,264.8 | 1,264.8 | 1,264.8 | 1,228.3 | 1,264.8 | 1,264.8 | 1,289.3 | | | | 12,510.3 |
| Propellant Insulation | | | | 329.2 | 366.0 | 366.0 | 366.0 | 366.0 | 366.0 | 370.5 | 366.0 | 366.0 | 370.5 | | | | 3,632.1 |
| Fuel System | | | | | | 36.7 | 36.3 | 36.3 | 93.0 | 278.9 | 104.3 | 36.7 | | | | | 622.2 |
| Pressurization System | | | 578.7 | 34.5 | 34.5 | 34.5 | 34.5 | 34.5 | 34.5 | 596.8 | 317.5 | | | | | | 1,699.7 |
| Lubricating System | | | | | | | | | | | 72.6 | | | | | | 72.6 |
| Aerodynamic Controls (Body) | | | 31.7 | 335.1 | 27.2 | 27.2 | 27.2 | 27.2 | 27.2 | 27.2 | 27.2 | 27.2 | 13.6 | 13.6 | 13.6 | | 598.2 |
| Prime Power Sources | | | | | | | | | | | | | | | | | |
| Engine or Gas Generator Units | | | | 880.7 | | | | | | | | | | | | | 880.7 |
| Power Source Tanks and Systems | | | | 529.2 | | | | | | | | | | | | | 529.2 |
| Power Conversion and Distribution | | | | | | | | | | | | | | | | | |
| Electrical | | 399.1 | 399.1 | 36.3 | 36.3 | 36.3 | 36.3 | 36.3 | 36.3 | 299.3 | 263.0 | 14.1 | 27.2 | 27.2 | | | 1,646.7 |
| Hydraulic/Pneumatic | | | 90.7 | 9.1 | 9.1 | 9.1 | 9.1 | 9.1 | 9.1 | 374.6 | | | | | | | 519.7 |
| Guidance and Navigation | | | 317.6 | | | | | | | | | | | | | | 317.5 |
| Instrumentation | | 206.3 | | | | | | | | | | | | | | | 206.3 |
| Communication | | 204.1 | 736.9 | | | | | | | | | | | | | | 941.0 |
| Environmental Controls | | | | | | | | | | | | | | | | | |
| Equipment | | 79.8 | | | | | | | | | | | | | | | 79.8 |
| Personnel | | | 195.0 | 195.0 | | 97.5 | 97.5 | | 366.0 | | | | | | | | 951.0 |
| Compt. Insulation | | 239.9 | 239.0 | 239.0 | 239.0 | 239.0 | 239.0 | 239.0 | 239.0 | 240.4 | 239.9 | | | | | | 2,393.1 |
| Landing Gear | | | 1,814.0 | | | | | | | 5,439.3 | | | | | | | 7,253.3 |
| Aerodynamic Surfaces | | | | | | | | | | | | | | | | | |
| Wing and Wing Mounted | | | | | | | | | | | | | | | | | |
| Control Surfaces | | | | | | | | | | | | | | | | | |
| Vertical Surfaces | | | | | | | | | | | | | | | | | |
| Horizontal Surfaces | | | | | | | | | | | | | | | | | |
| Personnel Provisions | | | | | | | | | | | | | | | | | |
| Accommodations for Personnel | | | 83.9 | 299.3 | 299.3 | 383.2 | 383.2 | 199.3 | 299.3 | 93.0 | | | | | | | 2,140.5 |
| Fixed Life Support | | | 69.8 | | | | | | | 69.8 | | | | | | | 139.7 |
| Furnishings and Cargo Handling | | 907.0 | 362.8 | 204.1 | 204.1 | 204.1 | 204.1 | 204.1 | 566.9 | 432.2 | 411.8 | | | | | | 3,701.0 |
| Emergency Equipment | | 11.3 | 11.3 | | 6.8 | | 6.8 | | 6.8 | 54.4 | 11.3 | | | | | | 108.8 |

TABLE IB
DEAD WEIGHT DISTRIBUTION -ESTIMATED HYDROGEN FUELED
AIRBREATHING CRUISE AIRCRAFT, POUNDS

| | Station Location | | | | | | | | | | | | | | | | Total |
|--|------------------------|---------|----------|----------|----------|-----------|-----------|-----------|-----------|-----------|-----------|-----------|-----------|-----------|-----------|-----------|-----------|
| | 0-20' | 20'-40' | 40'-60' | 60'-80' | 80'-100' | 100'-120' | 120'-140' | 140'-160' | 160'-180' | 180'-200' | 200'-220' | 220'-240' | 240'-260' | 260'-280' | 280'-300' | 300'-314' | |
| Body | | | | | | | | | | | | | | | | | |
| Basic Enclosing Structure | 1,159 | 3,259 | 4,715 | 5,867 | 6,719 | 7,160 | 5,609 | 5,492 | 5,404 | 5,698 | 5,987 | 5,538 | 4,301 | 3,244 | 1,877 | 417 | 72,446 |
| Pressurized Compartments | | 316 | 516 | 516 | 516 | 516 | 516 | 516 | 516 | 506 | 284 | | | | | | 4,718 |
| Main Propulsion | | | | | | | | | | | | | | | | | |
| Engine and Accessories | | | | | | | | | | 12,485 | 23,278 | | | | | | 35,763 |
| Air Induction | | | | | | | | | 5,647 | 9,015 | | | | | | | 14,662 |
| Nacelles, Pods, Pylons, Sup. | | | | | | | | | | 1,134 | 2,069 | | | | | | 3,203 |
| Fuel Containers and Supts | | | | 2,511 | 2,789 | 2,789 | 2,789 | 2,789 | 2,789 | 2,709 | 2,789 | 2,789 | 2,843 | | | | 27,586 |
| Propellant Insulation | | | | 726 | 807 | 807 | 807 | 807 | 807 | 817 | 807 | 807 | 817 | | | | 8,009 |
| Fuel System | | | | | 81 | 80 | 80 | 80 | 205 | 615 | 230 | 81 | | | | | 1,372 |
| Pressurization System | | | 1,276 | 76 | 76 | 76 | 76 | 76 | 76 | 1,316 | 700 | | | | | | 3,748 |
| Lubricating System | | | | | | | | | | | 160 | | | | | | 160 |
| Aerodynamic Controls (Body) | | | 70 | 739 | 60 | 60 | 60 | 60 | 60 | 60 | 30 | 30 | 30 | 30 | 30 | | 1,369 |
| Prime Power Sources | | | | | | | | | | | | | | | | | |
| Engine or Gas Gen. Units | | | | 1,942 | | | | | | | | | | | | | 1,942 |
| Power Source Tanks and Systems | | | | 1,161 | | | | | | | | | | | | | 1,167 |
| Power Conversion and Distribution | | | | | | | | | | | | | | | | | |
| Electrical | | 880 | 880 | 80 | 80 | 80 | 80 | 80 | 80 | 660 | 580 | 31 | 60 | 60 | | | 3,631 |
| Hydraulic/Pneumatic | | | 200 | 20 | 20 | 20 | 20 | 20 | 20 | 826 | | | | | | | 1,146 |
| Guidance and Navigation | | | 700 | | | | | | | | | | | | | | 700 |
| Instrumentation | | 455 | | | | | | | | | | | | | | | 455 |
| Communication | | 450 | 1,625 | | | | | | | | | | | | | | 2,075 |
| Environmental Controls | | | | | | | | | | | | | | | | | |
| Equipment | | 176 | | | | | | | | | | | | | | | 176 |
| Personnel | | | 430 | 430 | | 215 | 215 | | 807 | | | | | | | | 2,097 |
| Compt Insulation | | 529 | 527 | 527 | 527 | 527 | 527 | 527 | 527 | 530 | 529 | | | | | | 5,277 |
| Landing Gear | | | 4,000 | | | | | | | 11,994 | | | | | | | 15,994 |
| Aerodynamic Surfaces | See Last Item of Table | | | | | | | | | | | | | | | | |
| Wing and Wing Mounted | | | | | | | | | | | | | | | | | |
| Control Surfaces | | | | | | | | | | | | | | | | | |
| Vertical Surfaces | | | | | | | | | | | | | | | | | |
| Horizontal Surfaces | | | | | | | | | | | | | | | | | |
| Personnel Provisions | | | | | | | | | | | | | | | | | |
| Accommodations for Personnel | | | 185 | 660 | 660 | 845 | 845 | 660 | 660 | 205 | | | | | | | 4,720 |
| Fixed Life Support | | | 154 | | | | | | | 154 | | | | | | | 308 |
| Furnishings and Cargo Hdlg. | | 2,000 | 800 | 450 | 450 | 450 | 450 | 450 | 1,250 | 953 | 908 | | | | | | 8,161 |
| Emergency Equipment | | 25 | 25 | | 15 | | 15 | | 15 | 120 | 25 | | | | | | 240 |
| Crew Station | | | | | | | | | | | | | | | | | |
| Controls and Panels | | 200 | 100 | | | | | | | | | | | | | | 300 |
| Dry Structure - Not Incl: Aero Surfaces and Aero Cont | (1,159) | (8,290) | (16,203) | (15,711) | (12,719) | (13,626) | (12,089) | (11,557) | (18,863) | (49,797) | (38,376) | (9,276) | (8,051) | (3,334) | (1,907) | (417) | (221,375) |
| Personnel | | | | | | | | | | | | | | | | | |
| Crew, Gear and Accessories | | 750 | 500 | | | | | | | | | | | | | | 1,250 |
| Crew, Life Support | | 25 | | | | | | | | | | | | | | | 25 |
| Payload | | | | | | | | | | | | | | | | | |
| Cargo | | | | 5,950 | 5,950 | 5,950 | 5,950 | 5,950 | 5,250 | 6,500 | 6,500 | | | | | | 13,000 |
| Passenger and Support | | | | | | | | | | | | | | | | | 35,000 |

[illegible]

TABLE IIA
TRAJECTORY AND FUEL FLOW DATA

| Time Sec. | Altitude Km | Mach | Alpha Deg. | Velocity m/sec. | Fuel Flow Kg/sec. | Gross Weight (Kg) |
|----------------|----------------|------|---------------|--------------------|----------------------|-------------------------|
| <u>ASCENT</u> | | | | | | |
| 0 | 0 | 0 | 0 | 0 | 41.08 | 236,274 |
| 379.4 | 10.66 | 1.01 | 0.60 | 299.7 | 19.90 | 226,990 |
| 643.4 | 10.66 | 1.51 | -0.20 | 449.3 | 32.41 | 220,591 |
| 719.3 | 12.81 | 2.00 | 0.81 | 590.8 | 36.04 | 217,830 |
| 779.3 | 15.68 | 2.51 | 1.13 | 739.9 | 34.04 | 215,739 |
| 837.3 | 18.03 | 3.02 | 1.51 | 889.8 | 34.61 | 213,757 |
| 887.2 | 19.94 | 3.50 | 1.97 | 1,033.9 | 35.03 | 211,961 |
| 954.2 | 21.91 | 4.08 | 1.92 | 1,210.1 | 30.99 | 209,766 |
| 1,012.2 | 23.21 | 4.51 | 2.20 | 1,341.7 | 29.30 | 208,011 |
| 1,084.2 | 24.54 | 5.00 | 2.44 | 1,491.0 | 27.73 | 205,957 |
| 1,165.2 | 25.81 | 5.51 | 2.52 | 1,646.7 | 26.17 | 203,776 |
| 1,165.2 | 25.81 | 5.51 | 3.72 | 1,646.7 | 28.72 | 203,776 |
| 1,374.9 | 30.70 | 6.01 | 5.24 | 1,815.7 | 17.35 | 199,939 |
| <u>CRUISE</u> | | | | | | |
| 1,375.0 | | 6.01 | 5.14 | 1,815.7 | 13.05 | 199,939 |
| 4,544 | 32.08 | 6.00 | 5.14 | 1,815.7 | 10.80 | 162,385 |
| <u>DESCENT</u> | | | | | | |
| 4,544.5 | 32.08 | 5.99 | 5.14 | 1,815.7 | 8.86 | 162,385 |
| 4,892.4 | 31.48 | 5.49 | 5.23 | 1,660.4 | 6.70 | 159,632 |
| 5,100.4 | 30.62 | 4.99 | 5.32 | 1,506.2 | 5.49 | 158,385 |
| 5,276.4 | 29.83 | 4.50 | 5.37 | 1,355.7 | 4.74 | 157,487 |
| 5,440.4 | 28.84 | 4.00 | 5.42 | 1,203.8 | 4.03 | 156,770 |
| 5,584.4 | 28.05 | 3.50 | 5.47 | 1,051.9 | 3.04 | 156,267 |
| 5,698.4 | 26.91 | 3.01 | 5.52 | 901.0 | 1.20 | 156,013 |
| 5,778.4 | 25.81 | 2.50 | 5.50 | 748.0 | 0.0 | 155,986 |
| 5,866.4 | 24.04 | 1.98 | 5.49 | 591.0 | 0.0 | 343,960 |
| 5,946.4 | 22.14 | 1.49 | 5.71 | 442.5 | 0.0 | 343,960 |
| 6,056.4 | 17.60 | 0.99 | 5.05 | 291.2 | 0.0 | 343,960 |

TABLE IIB
TRAJECTORY AND FUEL FLOW DATA

| Time Sec. | Altitude Ft. | Mach | Alpha Deg. | Velocity FPS | Fuel Flow Lb/Sec. | Gross Weight Lb |
|----------------|-----------------|-------|---------------|-----------------|----------------------|-----------------------|
| <u>ASCENT</u> | | | | | | |
| 0 | 0 | 0 | 0 | 0 | 90.574 | 521,000 |
| 379.4 | 34,965 | -1.01 | 0.60 | 983.3 | 43.873 | 500,530 |
| 643.4 | 34,965 | 1.51 | 0.20 | 1,474.1 | 71.456 | 486,420 |
| 719.3 | 42,035 | 2.00 | 0.81 | 1,938.3 | 79.466 | 480,330 |
| 779.3 | 51,444 | 2.51 | 1.13 | 2,427.5 | 75.058 | 475,720 |
| 837.3 | 59,163 | 3.02 | 1.51 | 2,919.4 | 76.313 | 471,350 |
| 887.2 | 65,446 | 3.50 | 1.97 | 3,392.0 | 77.233 | 467,390 |
| 954.2 | 71,901 | 4.08 | 1.92 | 3,970.0 | 68.345 | 462,550 |
| 1,012.2 | 76,153 | 4.51 | 2.20 | 4,401.8 | 64.611 | 458,680 |
| 1,084.2 | 80,534 | 5.00 | 2.44 | 4,891.7 | 61.151 | 454,150 |
| 1,165.2 | 84,686 | 5.51 | 2.52 | 5,402.5 | 57.702 | 449,340 |
| 1,165.2 | 84,686 | 5.51 | 3.72 | 5,402.5 | 63.336 | 449,340 |
| 1,374.9 | 100,750 | 6.01 | 5.24 | 5,957.0 | 38.252 | 440,880 |
| <u>CRUISE</u> | | | | | | |
| 1,375.0 | 100,800 | 6.01 | 5.14 | 5,957.0 | 28.604 | 440,880 |
| 4,544.0 | 105,260 | 6.00 | 5.14 | 5,957.0 | 23.550 | 358,070 |
| <u>DESCENT</u> | | | | | | |
| 4,544.5 | 105,260 | 5.99 | 5.14 | 5,957.0 | 19.527 | 358,070 |
| 4,892.4 | 103,310 | 5.49 | 5.23 | 5,447.5 | 14.765 | 352,000 |
| 5,100.4 | 100,470 | 4.99 | 5.32 | 4,941.7 | 12.104 | 349,250 |
| 5,276.4 | 97,879 | 4.50 | 5.37 | 4,447.9 | 10.454 | 347,270 |
| 5,440.4 | 94,649 | 4.00 | 5.42 | 3,949.5 | 8.876 | 345,690 |
| 5,584.4 | 92,050 | 3.50 | 5.47 | 3,451.2 | 6.710 | 344,580 |
| 5,698.4 | 88,311 | 3.01 | 5.52 | 2,956.1 | 2.640 | 344,020 |
| 5,778.4 | 84,703 | 2.50 | 5.50 | 2,454.0 | 0.0 | 343,960 |
| 5,866.4 | 78,888 | 1.98 | 5.49 | 1,939.0 | 0.0 | 343,960 |
| 5,946.4 | 72,634 | 1.49 | 5.71 | 1,451.8 | 0.0 | 343,960 |
| 6,056.4 | 57,744 | 0.99 | 5.05 | 955.3 | 0.0 | 343,960 |

31,920 meters (105,000 ft) about 4,500 seconds after takeoff. Fuel flow is stopped when aerodynamic heating is no longer significant and subsonic flight is achieved at 6,000 seconds; at the time of engine shutdown 80,500 kg (177,000 lb) of hydrogen fuel has been consumed. Note that the weights assumed for the calculation of structural loadings are conservatively higher than actual values based on fuel usage.

Heating Conditions. - Heat loads were computed for nominal and maneuver flight conditions for three assumed average structural temperatures 366° K (200F), 477° K (400F), and 589° K (600F). Consideration of a range of structural temperatures was consistent with the purpose of the investigations to consider a variety of construction materials. In addition, prior studies had indicated difficulty in matching structural cooling requirements and available hydrogen heat capacity for average structural temperatures below 477° K (400F). Therefore, heat loads were also computed for a partially shielded airframe with an average structural temperature of 366° K (200F). The shielding consisted of external superalloy semi-structural panels, without intermediate insulation, over those portions of the aircraft where radiation equilibrium temperatures would have exceeded 811° K (1,000F), except that the first 0.61 meters (2 feet) of the fuselage, the first 1.52 meters (5 ft) of the wing leading edge, as measured perpendicular to the leading edge, and the first 0.609 m (2 ft) of the tail surfaces were not shielded. The lack of shielding in the stagnation regions was dictated by a desire for very sharp leading edges. The relatively large unshielded portion of the wing, as compared to the tail, was based on a conservative assumption that a leading edge slat would be employed and that it might not be desirable to utilize partially shielded construction for this component.

Heat loads for the nominal flight trajectory and various wall temperatures of the unshielded and shielded configurations are presented in Figure 2. Maneuver heat loads for the 366° K (200F) wall temperature unshielded and shielded vehicle are presented in Tables III and IV. Similar data was computed for the 477° K (400F) and 588° (600F) unshielded configurations. For the nominal flight trajectory adequate heat capacity is available in the fuel flow for all situations considered except the unshielded 366° K (200F) configuration. For all configurations positive load factors resulted in increased fuel flow requirements that more than offset increased heating inputs. This was true even for the unshielded 366° K (200F) configuration when the positive load factor exceeded 1.2 g. Cooling requirements become more critical as the load factor approaches 0 g because drag is reduced and the decreased thrust requirements mean reduced hydrogen fuel flow. Even though the heat loads decrease the fuel flow decreases to a greater extent so that it is not possible to cool the structure adequately at maneuver conditions for flight speeds above approximately Mach 3.0 for the unshielded 366° K (200F) configuration or Mach 4.0 for the 477° K (400F) unshielded configuration. Adequate cooling was available when the average structural temperature was 588° K (600F). Shielding of 33% of the external surface area for a structural temperature of 366° K (200), or 15% for an average structural temperature of 477° K (400F), resulted in adequate heat capacity in the fuel flow to deal with the heat loads resulting from any flight conditions within the flight envelope of the hypersonic transport at an average temperature of 561° K (550F) the fuel flow just matched the cooling requirements for an unshielded aircraft under all flight conditions.

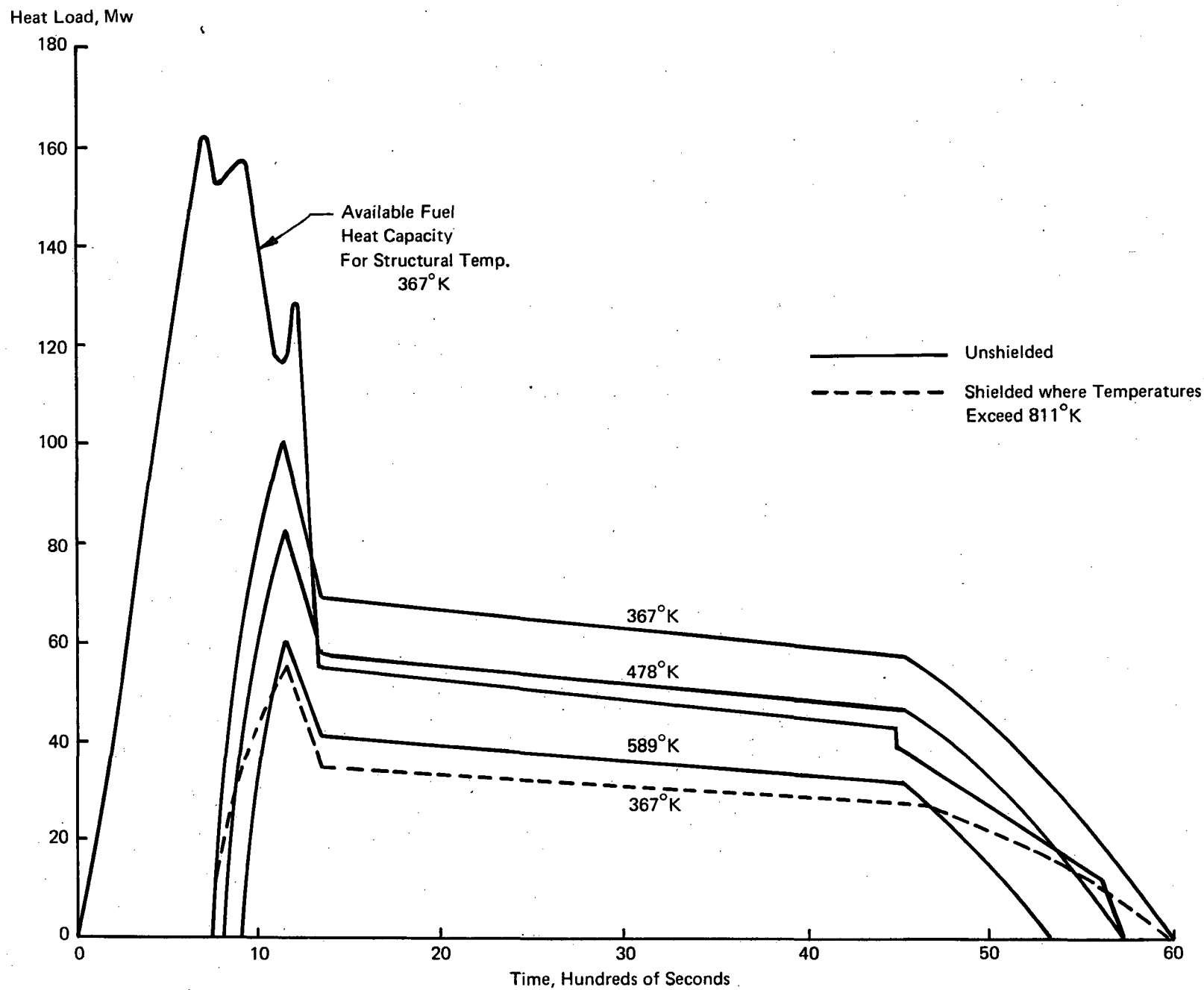


Figure 2a. Vehicle Load Histories for Various Wall Temperatures

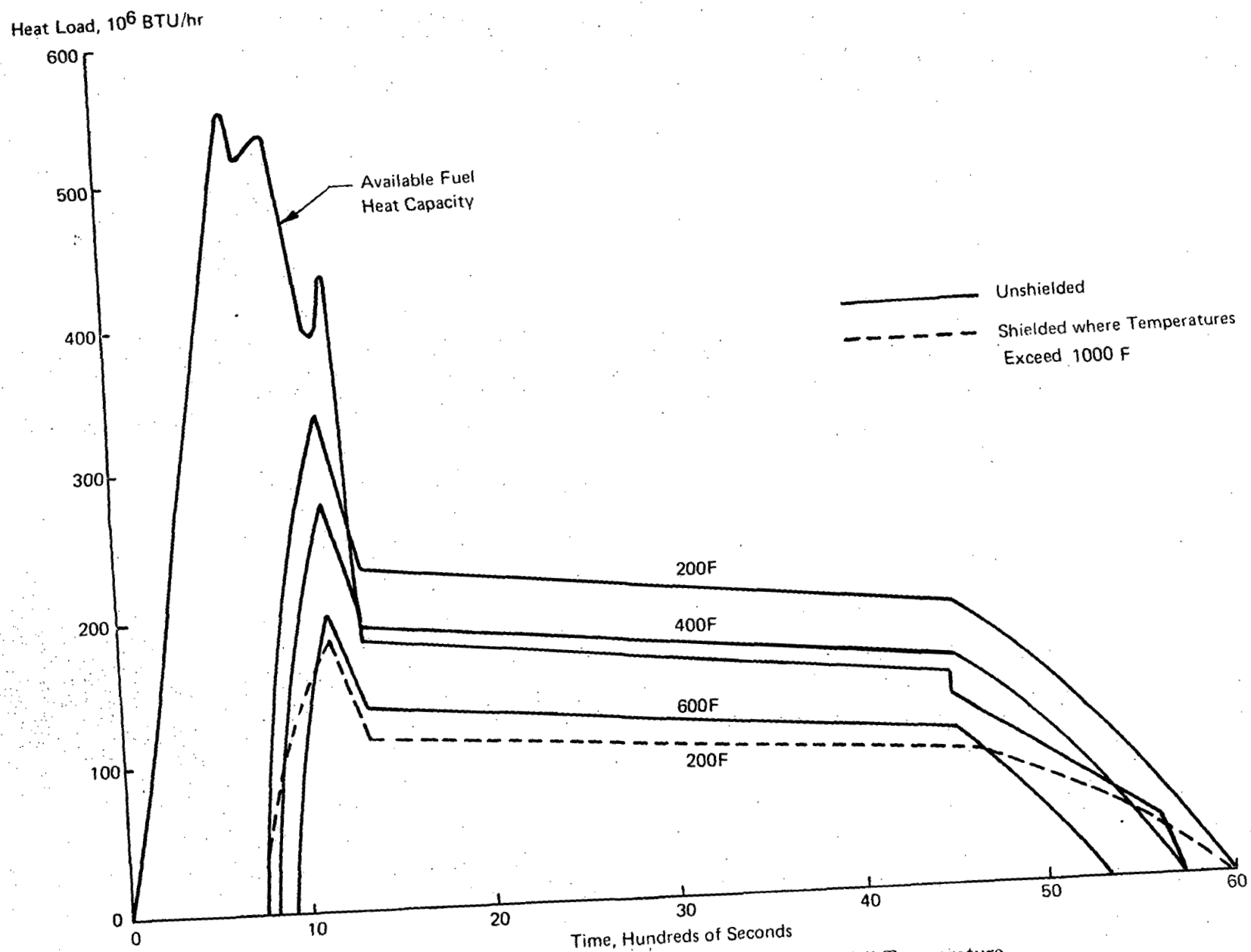


Figure 2b. Vehicle Heat Load Histories for Various Wall Temperature

TABLE IIIA
MANEUVER HEAT LOADS, 366°K WALL UNSHIELDED VEHICLE

| Flight Condition | Mach Number | Altitude km | Angle of Attack deg | Heat Load meg watt | | | | Hydrogen Flowrate kg/sec | |
|--------------------|-------------|-------------|---------------------|--------------------|----------|-------|--------|--------------------------|----------|
| | | | | Wing | Fuselage | Tail | Total | Available | Required |
| Nominal Trajectory | 3.01 | 18.0 | 1.51 | 12.05 | 22.93 | 6.40 | 41.38 | 34.6 | 9.24 |
| | 5.50 | 25.8 | 3.72 | 31.08 | 54.09 | 15.33 | 100.50 | 30.1 | 22.45 |
| | 6.01 | 30.7 | 5.24 | 21.96 | 36.66 | 10.44 | 69.06 | 17.4 | 15.65 |
| | 6.0 | 32.1 | 5.14 | 18.21 | 30.35 | 8.77 | 57.33 | 8.9 | 12.81 |
| | 4.0 | 28.8 | 5.42 | 8.80 | 14.54 | 4.15 | 27.25 | 4.0 | 6.09 |
| Banked Turn, 2 G | 3.01 | 18.0 | 3.81 | 12.34 | 22.51 | 6.40 | 41.24 | 18.9 | 9.21 |
| | 5.50 | 25.8 | 6.11 | 33.77 | 55.61 | 15.33 | 104.71 | 26.9 | 23.39 |
| | (1) 6.01 | 30.7 | 7.798 | 25.49 | 38.80 | 10.44 | 65.94 | 24.0 | 14.73 |
| | (2) 6.00 | 32.1 | 7.82 | 21.34 | 32.29 | 8.77 | 62.40 | 20.1 | 13.94 |
| | (3) 4.00 | 28.8 | 8.48 | 9.82 | 14.95 | 4.15 | 28.92 | 21.3 | 6.46 |
| Pushover 0 G | 3.01 | 18.0 | -0.987 | 11.49 | 22.73 | 6.40 | 40.62 | 10.8 | 9.07 |
| | 5.50 | 25.8 | -1.166 | 26.19 | 52.99 | 15.33 | 94.51 | 9.8 | 21.11 |
| | 6.01 | 30.7 | -1.194 | 17.43 | 35.03 | 10.44 | 62.90 | 5.8 | 14.05 |
| | 6.00 | 32.1 | -1.193 | 14.60 | 29.14 | 8.77 | 52.51 | 4.8 | 11.73 |
| | 4.00 | 28.8 | -1.07 | 15.95 | 14.46 | 4.15 | 35.57 | 3.7 | 7.72 |
| Pushover -0.5 G | 3.01 | 18.0 | -2.34 | 11.35 | 22.67 | 6.40 | 40.42 | 11.5 | 9.03 |
| | 5.50 | 25.8 | -3.29 | 26.21 | 52.66 | 15.33 | 94.19 | 11.0 | 21.04 |
| | 6.01 | 30.7 | -5.05 | 18.13 | 35.08 | 10.44 | 63.66 | 8.3 | 14.22 |
| | 6.00 | 32.1 | -5.06 | 15.18 | 29.18 | 8.77 | 53.14 | 0.8 | 11.87 |
| | 4.00 | 28.8 | -4.79 | 7.53 | 14.34 | 4.15 | 26.02 | 5.1 | 5.81 |
| Pushover -1.0 G | 3.01 | 18.0 | -3.59 | 11.32 | 22.56 | 6.40 | 40.28 | 13.0 | 9.00 |
| | 5.50 | 25.8 | -5.33 | 27.14 | 52.91 | 15.33 | 95.38 | 15.0 | 21.31 |
| | (4) 6.01 | 30.7 | -5.80 | 18.65 | 35.34 | 10.44 | 64.42 | 9.9 | 14.39 |
| | (5) 6.00 | 32.1 | -5.81 | 15.51 | 29.40 | 8.77 | 53.68 | 8.3 | 11.99 |
| | (6) 4.00 | 28.8 | -6.94 | 7.73 | 14.44 | 4.15 | 26.33 | 7.9 | 5.88 |

- (1) 1.4 G due to insufficient thrust
- (2) 1.4 G due to insufficient thrust
- (3) 1.5 G due to insufficient thrust
- (4) -0.6 G due to insufficient thrust
- (5) -0.6 G due to insufficient thrust
- (6) -0.8 G due to insufficient thrust

TABLE IIIB
MANEUVER HEAT LOADS, 200F WALL UNSHIELDED VEHICLE

| Flight Condition | Mach Number | Altitude (ft) | Angle of Attack deg | Heat Load (Million BTU/hr) | | | | Hydrogen Flowrate (lb/hr) | |
|--------------------|-------------|---------------|---------------------|----------------------------|----------|-------|--------|---------------------------|----------|
| | | | | Wing | Fuselage | Tail | Total | Available | Required |
| Nominal Trajectory | 3.01 | 59,163 | 1.51 | 41.14 | 78.26 | 21.83 | 141.23 | 274,716 | 73,366 |
| | 5.50 | 84,692 | 3.72 | 106.06 | 184.62 | 52.31 | 342.99 | 238,788 | 178,176 |
| | 6.01 | 100,700 | 5.24 | 74.95 | 125.11 | 35.64 | 235.70 | 137,700 | 124,240 |
| | 6.0 | 105,260 | 5.14 | 62.16 | 103.58 | 29.94 | 195.68 | 70,272 | 101,650 |
| | 4.0 | 94,650 | 5.42 | 30.02 | 49.61 | 14.17 | 93.01 | 31,953 | 48,316 |
| Banked Turn, 2 G | 3.01 | 59,163 | 3.81 | 42.10 | 76.83 | 21.83 | 140.76 | 150,160 | 73,125 |
| | 5.50 | 84,692 | 6.11 | 115.27 | 189.78 | 52.31 | 357.36 | 212,990 | 185,641 |
| | (1) 6.01 | 100,700 | 7.798 | 86.98 | 132.44 | 35.64 | 225.06 | 190,250 | 116,918 |
| | (2) 6.00 | 105,260 | 7.82 | 72.82 | 110.20 | 29.94 | 212.96 | 159,340 | 110,631 |
| | (3) 4.00 | 94,650 | 8.48 | 33.51 | 51.02 | 14.17 | 98.71 | 168,990 | 51,280 |
| Pushover 0 G | 3.01 | 59,163 | -0.987 | 39.22 | 77.57 | 21.83 | 138.62 | 85,985 | 72,012 |
| | 5.50 | 84,692 | -1.166 | 89.37 | 180.85 | 52.31 | 322.53 | 77,479 | 167,551 |
| | 6.01 | 100,700 | -1.194 | 59.48 | 119.57 | 35.64 | 214.69 | 46,393 | 111,528 |
| | 6.00 | 105,260 | -1.193 | 49.82 | 99.44 | 29.94 | 179.20 | 38,245 | 93,093 |
| | 4.00 | 94,650 | -1.07 | 54.44 | 49.35 | 14.17 | 117.97 | 28,978 | 61,284 |
| Pushover - 0.5 G | 3.01 | 59,163 | -2.34 | 38.74 | 77.37 | 21.83 | 137.95 | 90,929 | 71,665 |
| | 5.50 | 84,692 | -3.29 | 89.44 | 179.71 | 52.31 | 321.46 | 87,374 | 166,996 |
| | 6.01 | 100,700 | -5.05 | 61.89 | 119.74 | 35.64 | 217.27 | 65,908 | 112,868 |
| | 6.00 | 105,260 | -5.06 | 51.81 | 99.60 | 29.94 | 181.36 | 54,285 | 94,216 |
| | 4.00 | 94,650 | -4.79 | 25.70 | 48.95 | 14.17 | 88.82 | 40,267 | 46,144 |
| Pushover - 1.0 G | 3.01 | 59,163 | -3.59 | 38.64 | 76.99 | 21.83 | 137.46 | 103,050 | 71,411 |
| | 5.50 | 84,692 | -5.33 | 92.64 | 180.58 | 52.31 | 325.53 | 119,070 | 169,109 |
| | (4) 6.01 | 100,700 | -5.80 | 63.64 | 120.60 | 35.64 | 219.88 | 78,455 | 114,223 |
| | (5) 6.00 | 105,260 | -5.81 | 52.94 | 100.33 | 29.94 | 183.21 | 66,002 | 95,174 |
| | (6) 4.00 | 94,650 | -6.94 | 26.39 | 49.28 | 14.17 | 89.85 | 62,777 | 46,675 |

- (1) 1.4 G due to insufficient thrust
(2) 1.4 G due to insufficient thrust
(3) 1.5 G due to insufficient thrust
(4) -0.6 G due to insufficient thrust
(5) -0.6 G due to insufficient thrust
(6) -0.8 G due to insufficient thrust

TABLE IVA
MANEUVER HEAT LOADS, 366°K WALL SHIELDED VEHICLE *

| Flight Condition | Mach Number | Altitude km | Angle of Attack deg | Heat Load (Million megawatts) | | | | Hydrogen Flowrate kg/sec | |
|--------------------|-------------|-------------|---------------------|----------------------------------|----------|------|-------|-----------------------------|----------|
| | | | | Wing | Fuselage | Tail | Total | Available | Required |
| Nominal Trajectory | 3.01 | 18.0 | 1.51 | 6.57 | 16.31 | 2.74 | 25.62 | 34.6 | 5.7 |
| | 5.50 | 25.8 | 3.72 | 14.41 | 33.03 | 7.16 | 54.60 | 30.1 | 12.2 |
| | 6.0 | 30.7 | 5.24 | 9.36 | 20.57 | 5.03 | 34.95 | 17.4 | 7.8 |
| | 6.0 | 32.1 | 5.14 | 7.86 | 17.08 | 4.24 | 27.38 | 8.9 | 6.1 |
| | 4.0 | 28.8 | 5.42 | 4.06 | 9.21 | 1.68 | 14.95 | 4.0 | 3.3 |
| Banked Turn, 2G | 3.01 | 18.0 | 3.810 | 6.29 | 15.55 | 2.74 | 24.58 | 18.9 | 5.5 |
| | 5.50 | 25.8 | 6.110 | 14.20 | 31.47 | 7.16 | 52.82 | 26.9 | 11.8 |
| | (1) 6.01 | 30.7 | 7.798 | 9.91 | 19.83 | 5.03 | 34.77 | 24.0 | 7.8 |
| | (2) 6.00 | 32.1 | 7.820 | 8.35 | 16.46 | 4.24 | 29.06 | 20.1 | 6.5 |
| | (3) 4.00 | 28.8 | 8.480 | 4.12 | 8.82 | 1.68 | 14.63 | 21.3 | 3.3 |
| Pushover 0.0 G | 3.01 | 18.0 | -0.987 | 7.03 | 16.54 | 2.74 | 26.32 | 10.8 | 5.9 |
| | 5.50 | 25.8 | -1.166 | 16.97 | 36.48 | 7.16 | 60.61 | 9.8 | 13.5 |
| | 6.01 | 30.7 | -1.194 | 11.52 | 23.77 | 5.03 | 40.31 | 5.8 | 9.0 |
| | 6.00 | 32.1 | -1.193 | 9.68 | 19.76 | 4.24 | 33.68 | 4.8 | 7.5 |
| | 4.00 | 28.8 | -1.070 | 4.83 | 10.29 | 1.68 | 16.80 | 3.7 | 3.8 |
| Pushover -0.5 G | 3.01 | 18.0 | -2.34 | 7.30 | 16.65 | 2.74 | 26.70 | 11.5 | 6.0 |
| | 5.50 | 25.8 | -3.29 | 18.95 | 37.60 | 7.16 | 63.72 | 11.0 | 14.2 |
| | 6.01 | 30.7 | -5.05 | 14.57 | 25.75 | 5.03 | 45.34 | 8.3 | 10.1 |
| | 6.00 | 32.1 | -5.06 | 12.23 | 21.42 | 4.24 | 37.88 | 6.8 | 8.5 |
| | 4.00 | 28.8 | -4.79 | 5.60 | 10.70 | 1.68 | 17.98 | 5.1 | 4.0 |
| Pushover -1.0 G | 3.01 | 18.0 | -3.59 | 7.60 | 16.79 | 2.74 | 27.12 | 13.0 | 6.1 |
| | 5.50 | 25.8 | -5.33 | 21.54 | 39.26 | 7.16 | 67.96 | 15.0 | 15.2 |
| | (4) 6.01 | 30.7 | -5.80 | 15.32 | 26.29 | 5.03 | 46.63 | 9.9 | 10.4 |
| | (5) 6.00 | 32.1 | -5.81 | 12.85 | 21.87 | 4.24 | 38.96 | 8.3 | 8.7 |
| | (6) 4.00 | 28.8 | -6.94 | 6.17 | 11.05 | 1.68 | 18.91 | 7.9 | 4.2 |

*920 m² of shielding

- (1) 1.4 G due to insufficient thrust
- (2) 1.4 G due to insufficient thrust
- (3) 1.5 G due to insufficient thrust
- (4) -0.6 G due to insufficient thrust
- (5) -0.6 G due to insufficient thrust
- (6) -0.8 G due to insufficient thrust

TABLE IVB
MANEUVER HEAT LOADS, 200F WALL SHIELDED VEHICLE *

| Flight Condition | Mach Number | Altitude (ft) | Angle of Attack deg | Heat Load (Million BTU/hr) | | | | Hydrogen Flowrate (lb/hr) | |
|--------------------|-------------|---------------|---------------------|----------------------------|----------|-------|--------|---------------------------|----------|
| | | | | Wing | Fuselage | Tail | Total | Available | Required |
| Nominal Trajectory | 3.01 | 59,163 | 1.51 | 22.44 | 55.66 | 9.34 | 87.44 | 274,716 | 45,423 |
| | 5.50 | 84,692 | 3.72 | 49.19 | 112.74 | 24.43 | 186.36 | 238,788 | 96,810 |
| | 6.0 | 100,700 | 5.24 | 31.93 | 70.19 | 17.15 | 119.27 | 137,700 | 61,960 |
| | 6.0 | 105,260 | 5.14 | 26.83 | 58.29 | 14.48 | 93.45 | 70,272 | 48,540 |
| | 4.0 | 94,650 | 5.42 | 13.85 | 31.44 | 5.74 | 51.03 | 31,953 | 26,510 |
| Banked Turn | 3.01 | 59,163 | 3.810 | 21.48 | 53.08 | 9.34 | 83.90 | 150,160 | 43,588 |
| | 5.50 | 84,692 | 6.110 | 48.46 | 107.39 | 24.43 | 180.28 | 212,990 | 93,655 |
| | 6.01 | 100,700 | 7.798 | 33.83 | 67.69 | 17.15 | 118.67 | 190,250 | 61,649 |
| | 6.00 | 105,260 | 7.820 | 28.51 | 56.19 | 14.48 | 99.19 | 159,340 | 51,528 |
| | 4.00 | 94,650 | 8.480 | 14.07 | 30.10 | 5.74 | 49.92 | 168,990 | 25,935 |
| Pushover 0.0 G | 3.01 | 59,163 | -0.987 | 24.01 | 56.46 | 9.34 | 89.82 | 85,985 | 46,661 |
| | 5.50 | 84,692 | -1.166 | 57.92 | 124.51 | 24.43 | 206.86 | 77,479 | 107,462 |
| | 6.01 | 100,700 | -1.194 | 39.31 | 81.13 | 17.15 | 137.59 | 46,393 | 71,479 |
| | 6.00 | 105,260 | -1.193 | 33.03 | 67.44 | 14.48 | 114.96 | 38,245 | 59,719 |
| | 4.00 | 94,650 | -1.070 | 16.50 | 35.11 | 5.74 | 57.35 | 28,978 | 29,796 |
| Pushover -0.5 G | 3.01 | 59,163 | -2.34 | 24.93 | 56.84 | 9.34 | 91.11 | 90,929 | 47,334 |
| | 5.50 | 84,692 | -3.29 | 64.69 | 128.34 | 24.43 | 217.46 | 87,374 | 112,970 |
| | 6.01 | 100,700 | -5.05 | 49.72 | 87.87 | 17.15 | 154.74 | 65,908 | 80,385 |
| | 6.00 | 105,260 | -5.06 | 41.73 | 73.09 | 14.48 | 129.30 | 54,285 | 67,169 |
| | 4.00 | 94,650 | -4.79 | 19.12 | 36.51 | 5.74 | 61.38 | 40,267 | 31,889 |
| Pushover -1.0 G | 3.01 | 59,163 | -3.59 | 25.93 | 57.29 | 9.34 | 92.56 | 103,050 | 48,086 |
| | 5.50 | 84,692 | -5.33 | 73.52 | 133.98 | 24.43 | 231.93 | 119,070 | 120,484 |
| | 6.01 | 100,700 | -5.80 | 52.27 | 89.73 | 17.15 | 159.16 | 78,455 | 82,680 |
| | 6.00 | 105,260 | -5.81 | 43.85 | 74.64 | 14.48 | 132.98 | 66,002 | 69,084 |
| | 4.00 | 94,650 | -6.94 | 21.05 | 37.73 | 5.74 | 64.53 | 62,777 | 33,525 |

*10,000 ft² of shielding

- (1) 1.4 G due to insufficient thrust
- (2) 1.4 G due to insufficient thrust
- (3) 1.5 G due to insufficient thrust
- (4) -0.6 G due to insufficient thrust
- (5) -0.6 G due to insufficient thrust
- (6) -0.8 G due to insufficient thrust

Structural Loads - The loads used for sizing the structure of the hypersonic transport were computed for maneuver, landing, and taxi conditions as described in Reference 2. Maneuver load factors were assumed to be 2.5 g for speeds less than Mach 3 and 2.0 g for speeds greater than Mach 3. Positive and negative gust conditions were considered for hypersonic and subsonic speeds. Since structural loads due to negative load factors were not computed, the loads resulting from the design conditions considered were conservatively assumed to be applied in both directions; that is, at a particular station the shear and bending moment values were assumed to be of equal magnitude in the positive and negative directions. This assumption is in line with the preliminary design nature of the analysis. The resulting loading intensities for the wing and fuselage are presented in Table V for a structure of constant equivalent thickness at any vehicle station.

Load Spectrum - The load spectrum used for assessing fatigue and fracture mechanics characteristics of the structure is presented in Table VI. This was derived from References 5, 6 and 7. The mission flight time from takeoff to landing was assumed to be two hours so that during a 3.6×10^7 -second block of operating time there would be 5,000 ground-air-ground cycles where, for purposes of analysis, the loads on the ground were assumed to be equivalent to a 0 g condition.

TABLE VI
SUGGESTED LOADING SPECTRUM, HYPERSONIC TRANSPORT
CUMULATIVE OCCURRENCES PER 10,000 FLIGHT HOURS

| <u>Load Factor, g</u> | <u>Occurrences</u> |
|-----------------------|--------------------|
| 0 | 5,000 |
| 0.2 | 1 |
| 0.4 | 18 |
| 0.6 | 2,475 |
| 0.7 | 13,750 |
| 0.8 | 59,200 |
| 0.9 | 160,000 |
| 1.0 | |
| 1.2 | 363,000 |
| 1.4 | 20,700 |
| 1.6 | 2,210 |
| 1.8 | 445 |
| 2.0 | 125 |
| 2.7 | 11 |
| 2.4 | 4 |
| 2.6 | 1 |

Hypersonic Research Airplane

The configuration used for this aircraft was one of several identified during in-house studies at NASA and features integral hydrogen tankage. Configuration, weight, and trajectory data were provided by NASA. Heating conditions and structural loads were computed as part of the project.

TABLE V A
HST STRUCTURAL LOADING INTENSITIES

| Wing Station m | Axial Loading, Nx (Limit), k N/m | | |
|----------------------|----------------------------------|-----------|----------|
| | Original | Room Temp | Use Temp |
| 0 | 297.7 | 372.1 | 276.7 |
| 3.12 | 297.7 | 372.1 | 276.7 |
| 5.08 | 218.9 | 273.5 | 203.5 |
| 7.62 | 122.6 | 153.2 | 113.8 |
| 12.70 | 42.0 | 52.5 | 39.2 |
| 15.22 | 8.8 | 11.0 | 8.2 |
| Wing Station m | Shear Flow, Q (Limit), k N/m | | |
| | Original | Room Temp | Use Temp |
| 0 | 0 | 0 | 0 |
| 3.12 | 367.7 | 458.0 | 341.5 |
| 5.08 | 269.7 | 338.0 | 252.2 |
| 7.62 | 150.6 | 189.1 | 141.0 |
| 10.16 | 51.8 | 64.8 | 48.3 |
| 12.70 | 10.9 | 13.7 | 10.2 |
| 15.22 | 0 | 0 | 0 |

| Station, m | 12.7 | 25.4 | 38.1 | 50.8 | 54.8 | 63.5 | 76.2 |
|------------------|--------|--------|--------|--------|---------|--------|--------|
| Nx (Limit) k N/m | 175.12 | 367.75 | 700.47 | 945.64 | 1050.71 | 612.91 | 280.19 |
| Q (Limit) k N/m | 175.12 | 122.58 | 105.07 | 166.36 | 201.39 | 140.09 | 78.80 |

*Loadings are similar for flight above and below
M = 3.0, therefore maximum values will be used
at room and use temperatures.

TABLE VB
HST STRUCTURAL LOADING INTENSITIES

| Wing Station, In. | Axial Loading, Nx (Limit) lb/in. | | |
|----------------------|----------------------------------|-----------|----------|
| | Original | Room Temp | Use Temp |
| 0 | 1700 | 2125 | 1580 |
| 123 | 1700 | 2125 | 1580 |
| 200 | 1250 | 1562 | 1162 |
| 300 | 700 | 875 | 650 |
| 400 | 240 | 300 | 224 |
| 500 | 50 | 63 | 47 |
| 600 | 0 | 0 | 0 |

| Wing Station, In. | Shear Flow, Q (Limit) lb/in. | | |
|----------------------|------------------------------|-----------|----------|
| | Original | Room Temp | Use Temp |
| 0 | 0 | 0 | 0 |
| 123 | 2100 | 2620 | 1950 |
| 200 | 1540 | 1930 | 1440 |
| 300 | 860 | 1080 | 805 |
| 400 | 296 | 370 | 276 |
| 500 | 62 | 78 | 58 |
| 600 | 0 | 0 | 0 |

FUSELAGE*

| Station, In. | 500 | 1000 | 1500 | 2000 | 2150 | 2500 | 3000 |
|--------------------|------|------|------|------|------|------|------|
| Nx (Limit), lb/in. | 1000 | 2100 | 4000 | 5400 | 6000 | 3500 | 1600 |
| Q (Limit) lb/in. | 1000 | 700 | 600 | 950 | 1150 | 800 | 450 |

*Loadings are similar for flight above and below
M = 3.0, therefore maximum values will be used
at room and use temperatures.

Configuration. - The hypersonic research airplane configuration is shown in Figure 3. The highly swept wing is mounted near the fuselage mid-plane. The tip-mounted fins are towed-in slightly. The fuselage is somewhat oval in shape with the upper surface more rounded than the lower. Aft of the engine the lower fuselage is flat to serve as an expansion nozzle surface for the air-breathing engines. The upper portion of the rear fuselage is boat-tailed slightly around the upper engine. The wing has a span of 9.91 m (32.5 ft) and a planform area of 38.1 m² (410 ft²). The wetted fin and rudder area is 16.7 m² (180 ft²) per side. The fuselage length is 26.4 m (80 ft) and has a wetted surface area of 196 m² (2110 ft²). The total wetted area of the hypersonic research airplane is 305 m² (3290 ft²).

A detailed weight statement for the aircraft is presented in Table VII. The gross weight of 19,800 kg, (43,875 lb) was representative of a version which employed rocket acceleration to Mach 3.0 after drop from a carrier aircraft and scram jet operation for the remainder of the flight. The gross weight was used for taxi, captive flight on the carrier aircraft, and free-flight conditions. The landing gross weight was 12,900 kg (28,500 lb). The weight distribution appropriate for each of these conditions was used in conjunction with the design flight load factor to determine the structural loads presented in the Structural Loads portion of the Hypersonic Research Airplane Section on Vehicle Data.

Trajectory. - Two normal flight trajectories were examined for the hypersonic research aircraft and are presented in Tables VIII and IX along with angle of attack, fuel flow, and vehicle weight data. For the Mach 8 cruise trajectory the maximum Mach number is reached at an altitude of 28,040 m (92,000 ft) at which point a sudden angle of attack change is assumed to obtain an equilibrium cruise condition beginning at an altitude of 36,000 m (118,000 ft). By the end of the 71,800 newtons/m² (1500 psf) dynamic pressure ascent phase, which takes 320 seconds, 6,450 kg (14,200 lb) of fuel are used. Since the cruise is flown at a constant Mach number and angle of attack the altitude increases slightly during cruise. A constant angle of attack descent was assumed with the vehicle in a banked condition so as to execute a 180° turn during descent; approximately 2.0 g is experienced during the turn. The duration of cruise is approximately 340 seconds.

The Mach 10 trajectory is quite similar to the Mach 8 although the ascent and descent phases are longer and the cruise portion of flight is shorter. The Mach 10 cruise speed is obtained about 540 seconds after vehicle release, at an altitude of 35,420 m (116,200 ft). The cruise condition is initiated at 37,620 m (123,400 ft) and the cruise duration is 130 seconds. A banked constant angle of attack descent trajectory is assumed such that a 180° turn is accomplished.

Heating Conditions. - Heat loads were computed for nominal and maneuver flight conditions for three assumed average structural temperatures, 366° K (200F), 477° K (400F), and 588° K (600F). Consideration of this temperature range was consistent with the initial purpose of the investigation to consider a variety of construction material. Heat loads corresponding to nominal and maneuver flight conditions are shown in Figures 4 and 5 for the two flight trajectories. Positive load factors of up to 3.0 g and negative load factors as low as -1.0 g were considered. The heat load lines representative of the maneuver conditions are really envelopes of the maximum value of heat load that

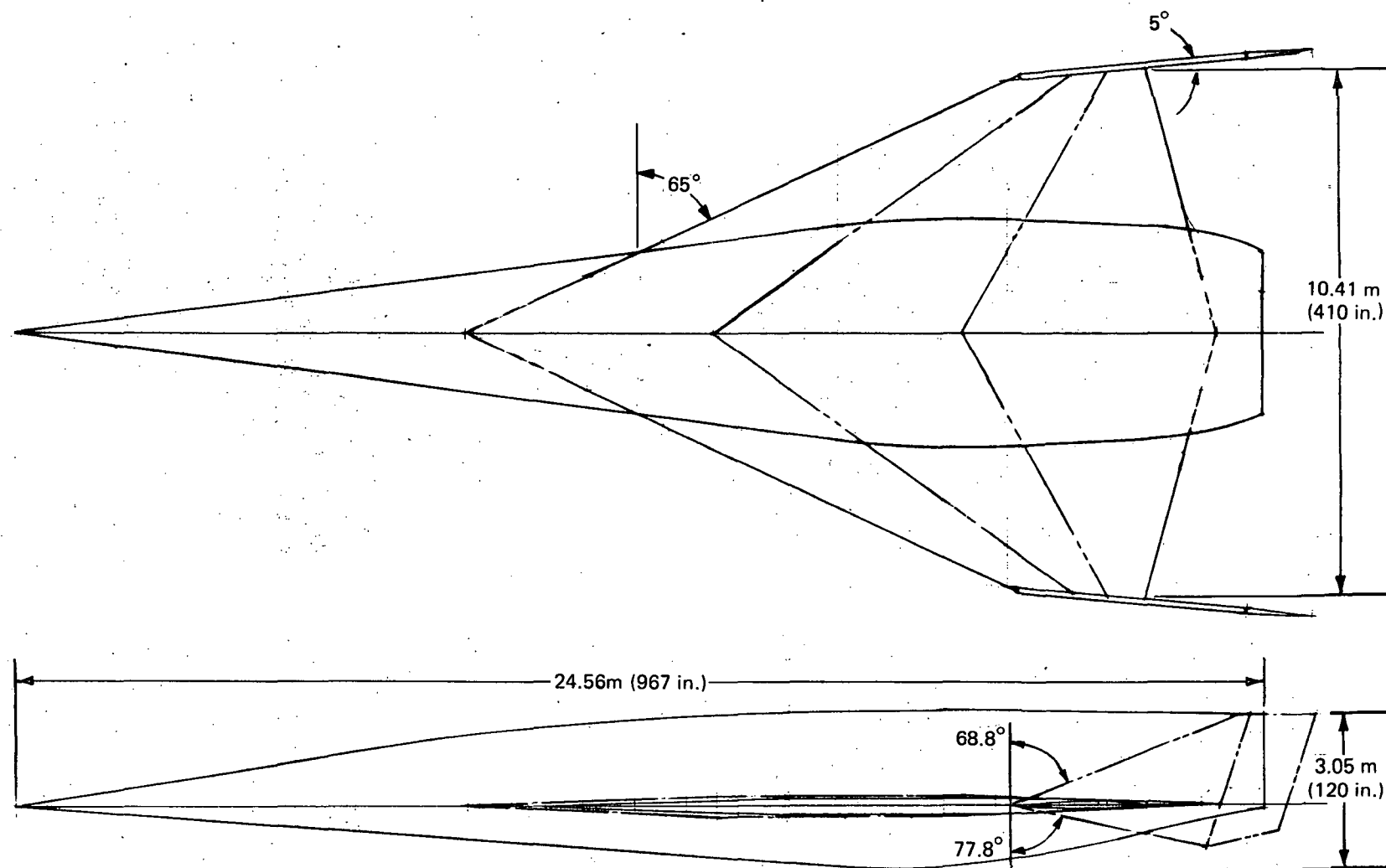


Figure 3. Hypersonic Research Aircraft Configuration

TABLE VIIA
INITIALLY ESTIMATED DEADWEIGHT DISTRIBUTION, HPERSONIC RESEARCH AIRPLANE

| | Weight Between Stations ---- Kg (Station in Inches) | | | | | | | | | | | | | | | | | |
|------------------------|---|--------------|---------------|---------------|---------------|---------------|---------------|---------------|---------------|---------------|----------------|-----------------|-----------------|-----------------|-----------------|-----------------|-----------------|-----------------|
| | 0- 9.1 | 9.1- 18.3 | 18.3- 27.4 | 27.4- 36.6 | 36.6- 45.7 | 45.7- 54.9 | 54.9- 64.0 | 64.0- 73.2 | 73.2- 82.3 | 82.2- 91.4 | 91.4- 100.6 | 100.6- 109.7 | 109.7- 118.9 | 118.9- 128.0 | 128.0- 137.2 | 137.2- 146.3 | 146.3- 154.4 | 154.4- 164.6 |
| Wing | | | | | | | | | | | | | | | | | | |
| Body | 5.89 | 16.31 | 27.18 | 37.60 | 48.47 | 58.43 | 68.86 | 78.82 | 89.24 | 99.20 | 109.17 | 118.69 | 128.65 | 139.98 | 148.58 | 157.64 | 166.25 | 175.31 |
| Tail | | | | | | | | | | | | | | | | | | |
| Fwd Landing Gear | | | | | | 52.10 | 43.04 | 43.04 | 43.04 | | | | | | | | | |
| Main Landing Gear | | | | | | | | | | | | | | | | | | |
| Surface Controls | | | | | | | 22.65 | 4.53 | 4.53 | 4.53 | 4.53 | 4.53 | 4.53 | 4.53 | 4.53 | 4.53 | 4.53 | 4.53 |
| Rockets | | | | | | | | | | | | | | | | | | |
| Scramjet | | | | | | | | | | | | | | | | | | |
| Fuel System | | | | | | | | | | | | | | 9.06 | 18.12 | 13.59 | 13.59 | 18.12 |
| Miscellaneous | | | | | | | | | | | | | | | | | | |
| APU | | | | | | | | | | | 140.43 | | | | | | | |
| Motor Controls | | | | | | | | 27.18 | | | | | | | | | | |
| Instruments | | | | | | | 79.28 | | | | | | | | | | | |
| Hydraulics | | | | | | | | | 9.06 | 9.06 | 6.80 | 2.27 | 2.27 | 2.27 | 2.27 | 2.27 | 2.27 | 2.27 |
| Electrical | | | | | | | 13.59 | 4.53 | 4.53 | 4.53 | 4.53 | 2.27 | 2.27 | 2.27 | 2.27 | 2.27 | 2.27 | 2.27 |
| Electronics | | | | | | | | 6.80 | 190.26 | 126.8 | | | | | | | | |
| Furnishings | | | | | | | 45.30 | 135.9 | | | | | | | | | | |
| ECS | | | 22.85 | 31.71 | 36.24 | 22.65 | | | | | | | | | | | | |
| Contingency | 1.36 | 1.81 | 2.27 | 2.72 | 4.53 | 4.53 | 6.80 | 6.80 | 6.80 | 6.80 | 6.80 | 6.80 | 6.80 | 6.80 | 6.80 | 4.53 | 4.53 | 4.53 |
| Weight Empty | 7.25 | 17.67 | 52.10 | | | 137.71 | 279.50 | 308.27 | 347.45 | 250.96 | 272.25 | 134.54 | 144.51 | 164.89 | 182.56 | 184.82 | 193.43 | 207.02 |
| Crew and Equipment | | | | | | | 18.12 | 90.60 | | | | | | | | | | |
| Payload | | | | | | | | | | | | 588.90 | 90.60 | | | | | |
| Ullage | | | | | | | | | | | | | | 3.62 | 3.62 | 3.62 | 3.62 | 4.08 |
| Pressurant | | | | | | | | | | | | | 40.77 | | | | | |
| APU Fuel | | | | | | | | | | 8.15 | 45.30 | | | | | | | |
| LOX | | | | | | | | | | | | | 27.63 | 1676.1 | 1676.1 | 27.63 | | |
| LH ₂ Rkt | | | | | | | | | | | | | | | | | | |
| LH ₂ SJ ACC | | | | | | | | | | | | | | | | 67.95 | 196.15 | 196.15 |
| LH ₂ SJ CR | | | | | | | | | | | | | | | | | | |
| Coolant | | | | | | 2.27 | 2.27 | 2.27 | 2.27 | 2.27 | 2.27 | 2.27 | 2.27 | 2.27 | 2.27 | 2.27 | 2.27 | 2.27 |
| Gross Weight | 7.25 | 17.67 | 52.10 | 72.03 | 89.24 | 139.98 | 299.89 | 400.45 | 349.72 | 261.38 | 319.82 | 725.71 | 305.78 | 1846.9 | 1864.5 | 286.29 | 395.47 | 409.51 |

TABLE VIIA (CONTD)

| | Weight Between Stations - - - - Kg | | | | | | | | | | | | | | | | | Total |
|------------------------|------------------------------------|------------------|------------------|------------------|------------------|------------------|------------------|------------------|------------------|------------------|------------------|------------------|------------------|------------------|------------------|------------------|------------------|----------|
| | 164.6 - 173.7 | 173.7 - 182.9 | 182.9 - 192.0 | 192.0 - 201.3 | 201.3 - 210.3 | 210.3 - 219.5 | 219.5 - 228.6 | 228.6 - 237.7 | 237.7 - 246.9 | 246.9 - 256.0 | 256.0 - 265.2 | 265.2 - 274.3 | 274.3 - 283.5 | 283.5 - 292.6 | 292.6 - 301.8 | 301.8 - 310.9 | 310.9 - 320.0 | |
| Wing | | 15.86 | 30.80 | 46.66 | 62.51 | 78.37 | 94.22 | 110.08 | 126.84 | 154.02 | 158.55 | 158.55 | 158.55 | 158.55 | | | | 1,352.7 |
| Body | 183.47 | 190.71 | 198.41 | 204.76 | 210.65 | 217.44 | 219.71 | 219.71 | 219.71 | 216.99 | 212.46 | 207.02 | 200.68 | 192.98 | | | | 4,568.5 |
| Tail | | | | | | | | | | 6.34 | 42.13 | 84.26 | 125.93 | 166.25 | 194.79 | 184.39 | 60.25 | 864.3 |
| Fwd Landing Gear | | | | | | | | | | | | | | | | | | 181.2 |
| Main Landing Gear | | | | | | 45.30 | 90.60 | 90.60 | 226.50 | 67.95 | | | | | | | | 543.6 |
| Surface Controls | 4.53 | 4.53 | 4.53 | 4.53 | 4.53 | 4.53 | 4.53 | 4.53 | 4.53 | 4.53 | 4.53 | 13.59 | 4.53 | 4.53 | 13.59 | | | 158.6 |
| Rockets | | | | | | | | | | | | | | 195.22 | 387.72 | | | 582.9 |
| Scramjet | | | 226.50 | 1,261.2 | 1,261.2 | 226.50 | | | | | | | | | | | | 2,975.3 |
| Fuel System | 18.12 | 18.12 | 8.12 | 18.12 | 18.12 | 18.12 | 18.12 | 18.12 | 90.60 | 18.12 | 18.12 | 18.12 | 67.45 | | | | | 430.4 |
| Miscellaneous | | | | | | | | | | | | | | | | | | |
| APU | | | | | | | | | | | | | | | | | | 140.4 |
| Motor Controls | | | | | | | | | | | | | | | | | | 27.2 |
| Instruments | | | | | | | | | | | | | | | | | | 79.3 |
| Hydraulics | 2.27 | 2.27 | 2.27 | 2.27 | 2.27 | 2.27 | 2.27 | 2.27 | 2.27 | 2.27 | 2.27 | 6.80 | 11.78 | 2.27 | 11.78 | | | 98.3 |
| Electrical | 2.27 | 2.27 | 2.27 | 2.27 | 2.27 | 2.27 | 2.27 | 2.27 | 2.27 | 2.27 | 2.27 | 18.12 | 9.06 | 18.12 | 18.12 | | | 135.9 |
| Electronics | | | | | | | | | | | | | | | | | | 323.9 |
| Furnishings | | | | | | | | | | | | | | | | | | 181.2 |
| ECS | | | | | | | | | | | | | | | | | | 113.3 |
| Contingency | 4.53 | 5.89 | 9.06 | 11.33 | 11.33 | 11.33 | 13.59 | 13.59 | 14.50 | 13.14 | 9.97 | 9.97 | 11.33 | 11.33 | 4.98 | 1.36 | | 249.2 |
| Weight Empty | 215.18 | 238.73 | 491.96 | 1551.1 | 1572.8 | 606.11 | 467.95 | 461.15 | 687.20 | 485.62 | 450.28 | 516.42 | 589.81 | 748.81 | 630.12 | 185.73 | 60.25 | 13,005.0 |
| Crew and Equipment | | | | | | | | | | | | | | | | | | 108.7 |
| Payload | | | | | | | | | | | | | | | | | | 679.5 |
| Ullage | 4.08 | 4.08 | 4.08 | 4.08 | 3.62 | 3.62 | 3.62 | 3.62 | 3.62 | | | | | | | | | 53.0 |
| Pressurant | | | | | | | | | | | | | | | | | | 40.8 |
| APU Fuel | | | | | | | | | | | | | | | | | | 53.5 |
| LOX | | | | | | | | | | | | | | | | | | 3,407.5 |
| LH ₂ Rkt | | | | | | | | | | | | | | | | | | 570.8 |
| LH ₂ SJ ACC | 196.15 | 196.15 | 196.15 | 196.15 | 196.15 | 196.15 | 196.15 | 196.15 | 45.3 | 90.60 | 90.60 | | | | | | | 1,277.5 |
| LH ₂ SJ CR | | | | | | | | | | | | | | | | | | 407.7 |
| Coolant | 2.27 | 2.27 | 12.23 | 12.23 | 12.23 | 14.50 | 14.50 | 14.50 | 14.50 | 12.23 | 57.53 | 57.53 | 5.89 | 6.34 | 3.62 | | | 271.8 |
| Gross Weight | 417.67 | 441.22 | 704.42 | 1763.50 | 1784.8 | 820.38 | 682.22 | 675.42 | 750.62 | 588.45 | 598.41 | 573.95 | 595.70 | 755.15 | 633.75 | 185.73 | 60.25 | 19,875.4 |

TABLE VIIB
INITIALLY ESTIMATED DEADWEIGHT DISTRIBUTION, HYPERSONIC RESEARCH AIRPLANE

| | Weight Between Stations Indicated, Pounds | | | | | | | | | | | | | | | | | | | | | | | | | | | | | | Total | | | | | | | |
|------------------------|---|-------|-------|--------|---------|---------|---------|---------|---------|---------|---------|---------|---------|---------|---------|---------|---------|---------|---------|---------|---------|---------|---------|---------|---------|---------|---------|---------|---------|---------|-------|---------|---------|---------|----------|-----------|--------|-------|
| | 0-30 | 30-60 | 60-90 | 90-120 | 120-150 | 150-180 | 180-210 | 210-240 | 240-270 | 270-300 | 300-330 | 330-360 | 360-390 | 390-420 | 420-450 | 450-480 | 480-510 | 510-540 | 540-570 | 570-600 | 600-630 | 630-660 | 660-690 | 690-720 | 720-750 | 750-780 | 780-810 | 810-840 | 840-870 | 870-900 | | 900-930 | 930-960 | 960-990 | 990-1020 | 1020-1050 | | |
| Wing | | | | | | | | | | | | | | | | | | | 35 | 68 | 103 | 138 | 173 | 208 | 243 | 280 | 340 | 350 | 350 | 350 | | | | | | 2,986 | | |
| Body | 13 | 35 | 60 | 83 | 107 | 129 | 152 | 174 | 197 | 219 | 241 | 262 | 284 | 309 | 328 | 348 | 367 | 387 | 405 | 421 | 438 | 452 | 465 | 480 | 485 | 485 | 479 | 469 | 457 | 443 | 426 | | | | | | 10,085 | |
| Tail | | | | | | | | | | | | | | | | | | | | | | | | | | | 14 | 93 | 186 | 278 | 367 | 430 | 407 | 133 | | | 1,908 | |
| Fwd Landing Gear | | | | | | 115 | 95 | 95 | 95 | | | | | | | | | | | | | | | | | | | | | | | | | | | | 400 | |
| Main Landing Gear | | | | | | | | | | | | | | | | | | | | | | | 100 | 250 | 200 | 500 | 150 | | | | | | | | | | 1,200 | |
| Surface Controls | | | | | | | 50 | 10 | 10 | 10 | 10 | 10 | 10 | 10 | 10 | 10 | 10 | 10 | 10 | 10 | 10 | 10 | 10 | 10 | 10 | 10 | 10 | 10 | 10 | 30 | 10 | 10 | 30 | | | | 350 | |
| Rockets | | | | | | | | | | | | | | | | | | | | | | | | | | | | | | | | | 430 | 854 | | | | 1,284 |
| Scramjet | | | | | | | | | | | | | | | | | | | | | 500 | 2784 | 2784 | 500 | | | | | | | | | | | | | | 6,568 |
| Fuel System | | | | | | | | | | | | | | 20 | 40 | 30 | 30 | 40 | 40 | 40 | 40 | 40 | 40 | 40 | 40 | 40 | 200 | 40 | 40 | 40 | 150 | | | | | | 950 | |
| Miscellaneous | | | | | | | | | | | | | | | | | | | | | | | | | | | | | | | | | | | | | | |
| APU | | | | | | | | | | | | 310 | | | | | | | | | | | | | | | | | | | | | | | | | | 310 |
| Motor Controls | | | | | | | | 60 | | | | | | | | | | | | | | | | | | | | | | | | | | | | | | 60 |
| Instruments | | | | | | | 175 | | | | | | | | | | | | | | | | | | | | | | | | | | | | | | | 175 |
| Hydraulics | | | | | | | | | 20 | 20 | 15 | 5 | 5 | 5 | 5 | 5 | 5 | 5 | 5 | 5 | 5 | 5 | 5 | 5 | 5 | 5 | 5 | 5 | 5 | 15 | 26 | 5 | 26 | | | | 217 | |
| Electrical | | | | | | | 30 | 10 | 10 | 10 | 10 | 5 | 5 | 5 | 5 | 5 | 5 | 5 | 5 | 5 | 5 | 5 | 5 | 5 | 5 | 5 | 5 | 5 | 5 | 5 | 40 | 20 | 40 | 40 | | | | 300 |
| Electronics | | | | | | | | 15 | 420 | 280 | | | | | | | | | | | | | | | | | | | | | | | | | | | | 715 |
| Furnishings | | | | | | | 100 | 300 | | | | | | | | | | | | | | | | | | | | | | | | | | | | | | 400 |
| ECS | | | 50 | 70 | 80 | 50 | | | | | | | | | | | | | | | | | | | | | | | | | | | | | | | | 250 |
| Contingency | 3 | 4 | 5 | 6 | 10 | 10 | 15 | 15 | 15 | 15 | 15 | 15 | 15 | 15 | 15 | 10 | 10 | 10 | 10 | 13 | 20 | 25 | 25 | 25 | 30 | 30 | 32 | 29 | 22 | 22 | 25 | 25 | 11 | 3 | | | 550 | |
| Weight Empty | 16 | 39 | 115 | 159 | 197 | 304 | 617 | 679 | 767 | 554 | 601 | 297 | 319 | 364 | 403 | 408 | 427 | 457 | 475 | 527 | 1086 | 3424 | 3472 | 1338 | 1033 | 1018 | 1517 | 1072 | 994 | 1140 | 1302 | 1653 | 1391 | 410 | 133 | | 28,708 | |
| Crew and Equipment | | | | | | | 40 | 200 | | | | | | | | | | | | | | | | | | | | | | | | | | | | | | 240 |
| Payload | | | | | | | | | | | | 1300 | 200 | | | | | | | | | | | | | | | | | | | | | | | | | 1,500 |
| Ullage | | | | | | | | | | | | | | 8 | 8 | 8 | 8 | 9 | 9 | 9 | 9 | 9 | 8 | 8 | 8 | 8 | | | | | | | | | | | 117 | |
| Pressurant | | | | | | | | | | | | | 90 | | | | | | | | | | | | | | | | | | | | | | | | | 90 |
| APU Fuel | | | | | | | | | | 18 | 100 | | | | | | | | | | | | | | | | | | | | | | | | | | | 118 |
| LOX | | | | | | | | | | | | | 61 | 3700 | 3700 | 61 | | | | | | | | | | | | | | | | | | | | | | 7,522 |
| LH ₂ RKT | | | | | | | | | | | | | | | | | | | | | | | | | | | | | | | | | | | | | | 1,260 |
| LH ₂ SJ AAC | | | | | | | | | | | | | | | | 150 | 433 | 433 | 433 | 433 | 433 | 433 | 433 | 433 | 433 | 433 | 100 | 200 | 200 | | | | | | | | 2,820 | |
| LH ₂ SJ CR | | | | | | | | | | | | | | | | | | | | | | | | | | | | | | | | | | | | | | 900 |
| Coolant | | | | | | 5 | 5 | 5 | 5 | 5 | 5 | 5 | 5 | 5 | 5 | 5 | 5 | 5 | 5 | 5 | 27 | 27 | 27 | 32 | 32 | 32 | 32 | 27 | 127 | 127 | 13 | 14 | 8 | | | | 600 | |
| Gross Weight | 16 | 39 | 115 | 159 | 197 | 309 | 662 | 884 | 772 | 577 | 706 | 1602 | 675 | 4077 | 4116 | 632 | 873 | 904 | 922 | 974 | 1555 | 3893 | 3940 | 1811 | 1506 | 1491 | 1657 | 1299 | 1321 | 1267 | 1315 | 1667 | 1399 | 410 | 133 | | | |

TABLE VIIIA
HRA MISSION PROFILE AND WEIGHT HISTORY, MACH 8 TRAJECTORY

| Time (Sec) | Mach Number | Altitude Km | Angle of Attack (deg) | Fuel Flowrate (kg/sec) | Weight (kg) |
|-----------------------|------------------------|------------------------|--------------------------------------|---------------------------------------|------------------------|
| 0 | 0.82 | 10.64 | 0 | 0 | 19,800 |
| 68 | 3.5 | 17.34 | 2.32 | 3.55 | 14,903 |
| 116 | 4.0 | 19.05 | 2.40 | 4.38 | 14,273 |
| 145 | 4.5 | 20.57 | 2.51 | 5.37 | 14,587 |
| 169 | 5.0 | 21.92 | 2.52 | 6.04 | 14,451 |
| 191 | 5.5 | 23.13 | 2.54 | 6.36 | 14,314 |
| 213 | 6.0 | 24.26 | 2.60 | 6.69 | 14,179 |
| 236 | 6.5 | 25.33 | 2.63 | 6.51 | 13,997 |
| 261 | 7.0 | 26.30 | 2.66 | 6.39 | 13,862 |
| 289 | 7.5 | 27.19 | 2.71 | 6.31 | 13,681 |
| 303 | 7.7 | 27.61 | 2.72 | 6.30 | 13,590 |
| 318 | 8.0 | 35.36 | 8.00 | 1.45 | 13,499 |
| 660 | 8.0 | 36.24 | 14.0 | 0 | 12,820 |
| 707 | 7.0 | 36.69 | 14.0 | 0 | 12,820 |
| 758 | 6.0 | 33.13 | 14.0 | 0 | 12,820 |
| 801 | 5.0 | 31.18 | 14.0 | 0 | 12,820 |
| 847 | 4.0 | 30.05 | 14.0 | 0 | 12,820 |
| 900 | 3.0 | 27.46 | 14.0 | 0 | 12,820 |
| 968 | 2.0 | 21.34 | 14.0 | 0 | 12,820 |
| 1127 | 1.0 | 15.64 | 14.0 | 0 | 12,820 |

TABLE VIIIB
HRA MISSION PROFILE AND WEIGHT HISTORY,
MACH 8 TRAJECTORY

| Time | Mach | Altitude | Angle of | Fuel | Weight |
|-------|--------|----------|----------|---------|--------|
| (sec) | Number | (ft) | (deg) | (lb/hr) | (lb) |
| 0 | 0.82 | 35,000 | 0 | 0 | 43,875 |
| 68 | 3.5 | 56,900 | 2.32 | 28,200 | 32,900 |
| 116 | 4.0 | 62,500 | 2.40 | 34,800 | 32,500 |
| 145 | 4.5 | 67,500 | 2.51 | 42,600 | 32,200 |
| 169 | 5.0 | 71,900 | 2.52 | 47,900 | 31,900 |
| 191 | 5.5 | 75,900 | 2.54 | 50,500 | 31,600 |
| 213 | 6.0 | 79,600 | 2.60 | 53,100 | 31,300 |
| 236 | 6.5 | 83,100 | 2.63 | 51,700 | 30,900 |
| 261 | 7.0 | 86,300 | 2.66 | 50,700 | 30,600 |
| 289 | 7.5 | 89,200 | 2.71 | 50,100 | 30,200 |
| 303 | 7.7 | 90,600 | 2.72 | 50,000 | 30,000 |
| 318 | 8.0 | 116,000 | 8.00 | 11,500 | 29,800 |
| 660 | 8.0 | 118,900 | 14.00 | 0 | 28,300 |
| 707 | 7.0 | 117,100 | 14.00 | 0 | 28,300 |
| 758 | 6.0 | 108,700 | 14.00 | 0 | 28,300 |
| 801 | 5.0 | 102,300 | 14.00 | 0 | 28,300 |
| 847 | 4.0 | 98,600 | 14.00 | 0 | 28,300 |
| 900 | 3.0 | 90,100 | 14.00 | 0 | 28,300 |
| 968 | 2.0 | 70,000 | 14.00 | 0 | 28,300 |
| 1127 | 1.0 | 51,300 | 14.00 | 0 | 28,300 |

TABLE IXA
HRA MISSION PROFILE AND WEIGHT HISTORY MACH 10 TRAJECTORY

| Time (Sec) | Mach Number | Altitude 1 (Km) | Angle of Attack (deg) | Fuel Flowrate (kg/sec) | Weight (kg) |
|-----------------------|------------------------|----------------------------|--------------------------------------|---------------------------------------|------------------------|
| 0 | 0.8 | 10.64 | 0 | 0 | 19,900 |
| 123 | 4.0 | 19.050 | 2.57 | 4.36 | 16,353 |
| 183 | 5.0 | 21.915 | 2.70 | 6.06 | 16,036 |
| 232 | 6.0 | 24.262 | 2.82 | 6.75 | 15,719 |
| 285 | 7.0 | 26.304 | 2.88 | 6.46 | 15,402 |
| 349 | 8.0 | 28.042 | 3.04 | 6.43 | 14,949 |
| 426 | 9.0 | 29.627 | 3.00 | 6.22 | 14,496 |
| 473 | 9.5 | 30.358 | 3.02 | 6.19 | 14,043 |
| 498 | 9.7 | 30.693 | 2.94 | 6.12 | 13,910 |
| 612 | 10.0 | 37.612 | 6.69 | 3.18 | 13,499 |
| 740 | 10.0 | 37.948 | 12.00 | 0 | 12,820 |
| 791 | 9.0 | 37.247 | 12.00 | 0 | 12,820 |
| 844 | 8.0 | 35.022 | 12.00 | 0 | 12,820 |
| 889 | 7.0 | 33.315 | 12.00 | 0 | 12,820 |
| 936 | 6.0 | 32.339 | 12.00 | 0 | 12,820 |
| 986 | 5.0 | 30.541 | 12.00 | 0 | 12,820 |
| 1038 | 4.0 | 28.346 | 12.00 | 0 | 12,820 |
| 1093 | 3.0 | 26.274 | 12.00 | 0 | 12,820 |
| 1196 | 2.0 | 23.073 | 12.00 | 0 | 12,820 |
| 1346 | 1.0 | 15.545 | 12.00 | 0 | 12,820 |

TABLE IXB
HRA MISSION PROFILE AND WEIGHT HISTORY, MACH 10 TRAJECTORY

| Time | Mach | Altitude | Angle of | Fuel | Weight |
|-------|--------|----------|----------|---------|--------|
| (sec) | Number | (ft) | (deg) | (lb/hr) | (lb) |
| 0 | 0.8 | 35,000 | 0 | 0 | 43,875 |
| 123 | 4.0 | 62,500 | 2.57 | 34,600 | 36,100 |
| 183 | 5.0 | 71,900 | 2.70 | 48,100 | 35,400 |
| 232 | 6.0 | 79,600 | 2.82 | 53,600 | 34,700 |
| 285 | 7.0 | 86,300 | 2.88 | 51,300 | 34,000 |
| 349 | 8.0 | 92,000 | 3.04 | 51,000 | 33,000 |
| 426 | 9.0 | 97,200 | 3.00 | 49,400 | 32,000 |
| 473 | 9.5 | 99,600 | 3.02 | 49,100 | 31,000 |
| 498 | 9.7 | 100,700 | 2.94 | 48,600 | 30,600 |
| 612 | 10.0 | 123,400 | 6.69 | 25,200 | 29,800 |
| 740 | 10.0 | 124,500 | 12.00 | 0 | 28,300 |
| 791 | 9.0 | 122,200 | 12.00 | 0 | 28,300 |
| 844 | 8.0 | 114,900 | 12.00 | 0 | 28,300 |
| 889 | 7.0 | 109,300 | 12.00 | 0 | 28,300 |
| 936 | 6.0 | 106,100 | 12.00 | 0 | 28,300 |
| 986 | 5.0 | 100,200 | 12.00 | 0 | 28,300 |
| 1038 | 4.0 | 93,000 | 12.00 | 0 | 28,300 |
| 1093 | 3.0 | 86,200 | 12.00 | 0 | 28,300 |
| 1196 | 2.0 | 75,700 | 12.00 | 0 | 28,300 |
| 1346 | 1.0 | 51,000 | 12.00 | 0 | 28,300 |

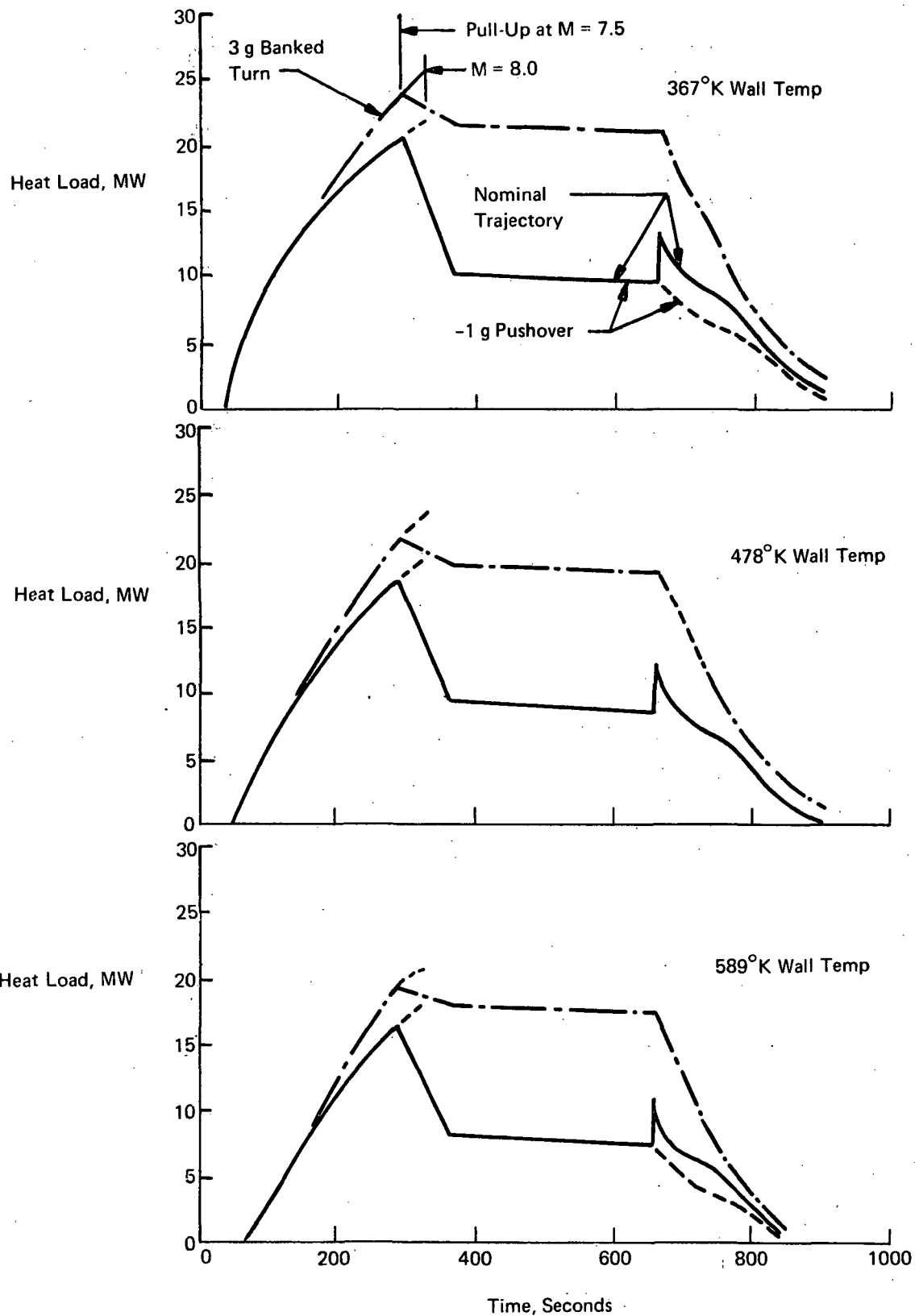


Figure 4a. Effect of Maneuvers on HRA Heat Load History, Mach 8 Trajectory, Unshielded Vehicle

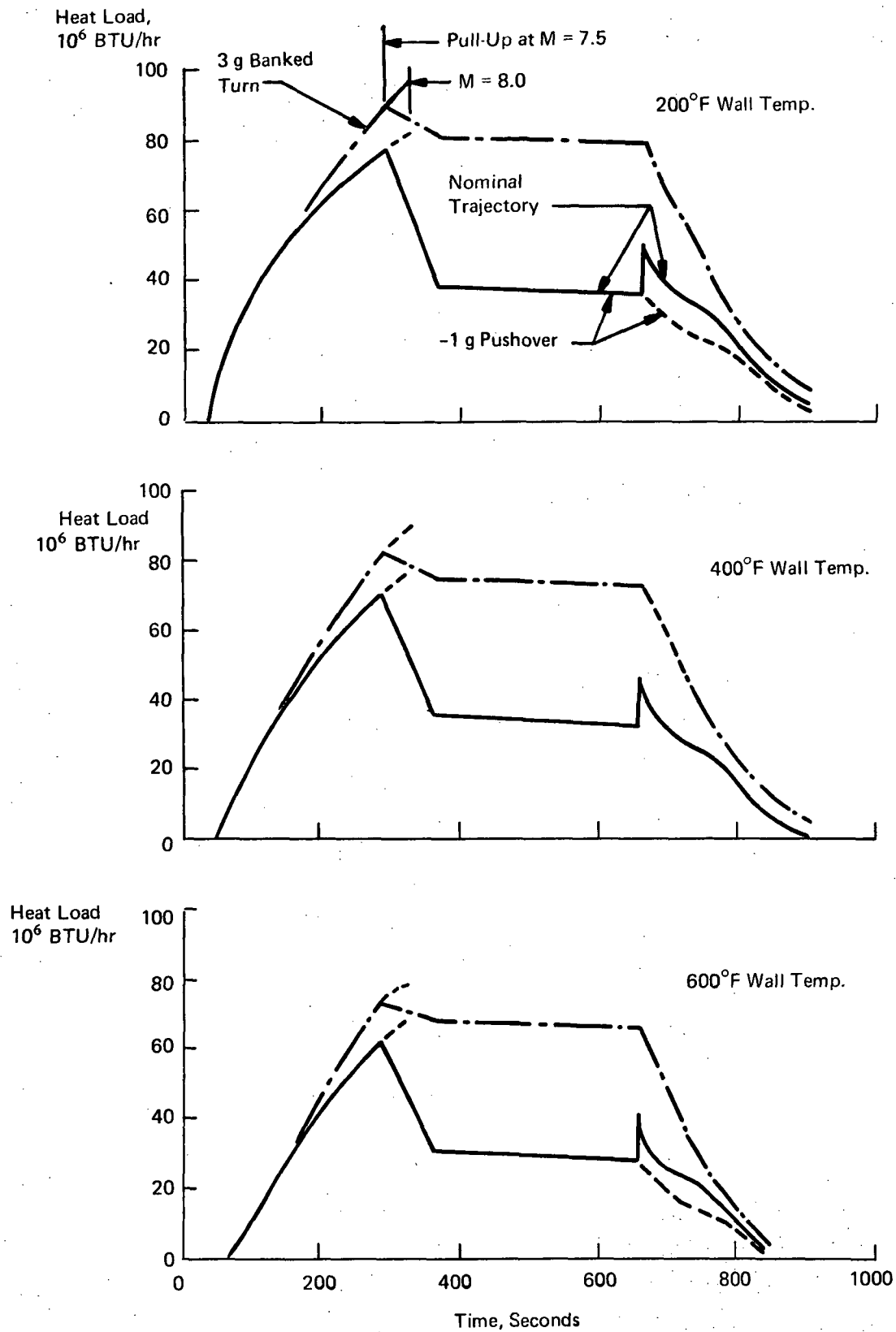


Figure 4b. Effect of Maneuvers on HRA Heat Load History, Mach 8 Trajectory, Unshielded Vehicle

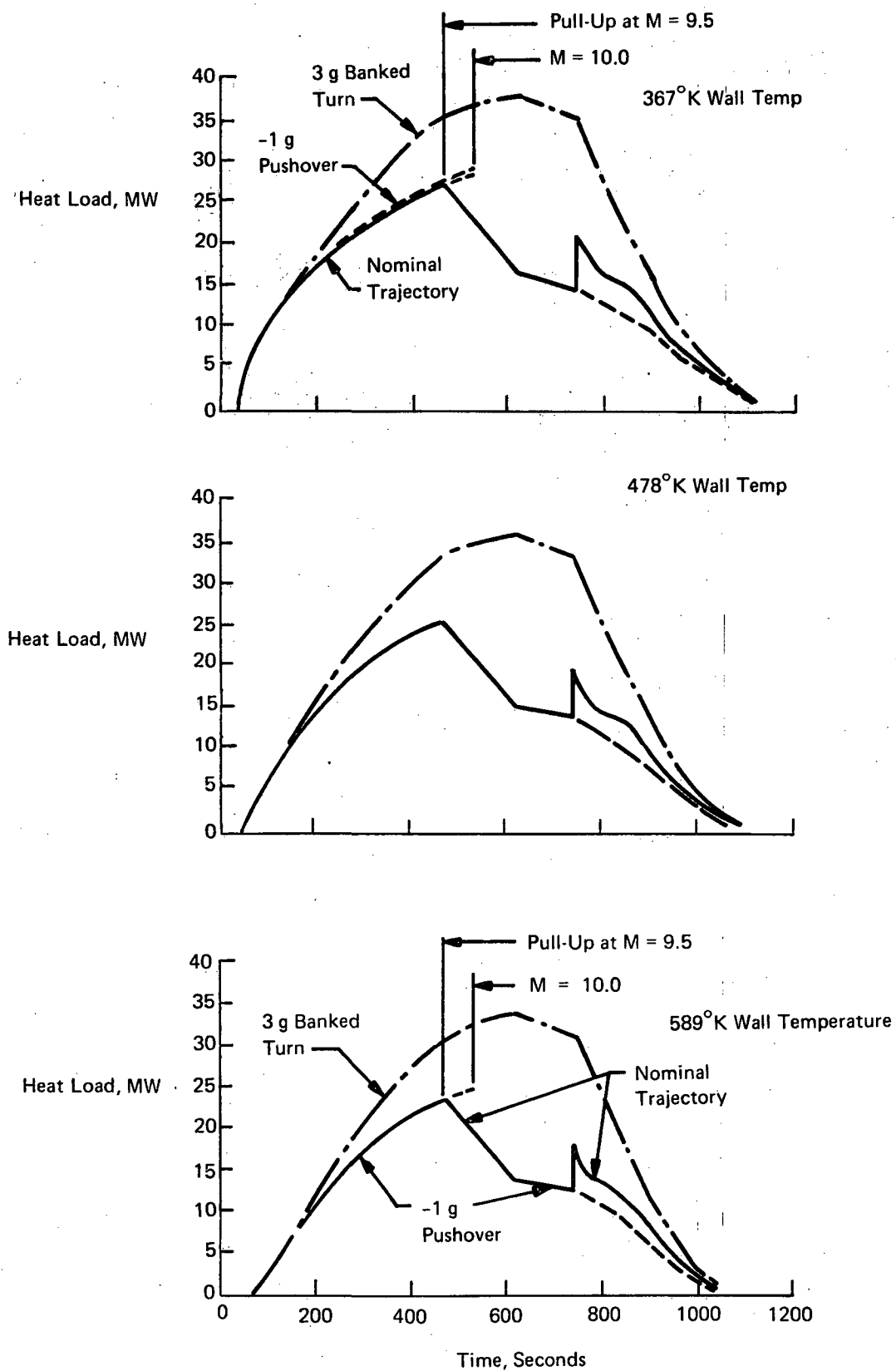


Figure 5a. Effect of Maneuvers on HRA Heat Load History, Mach 10 Trajectory, Unshielded Vehicle

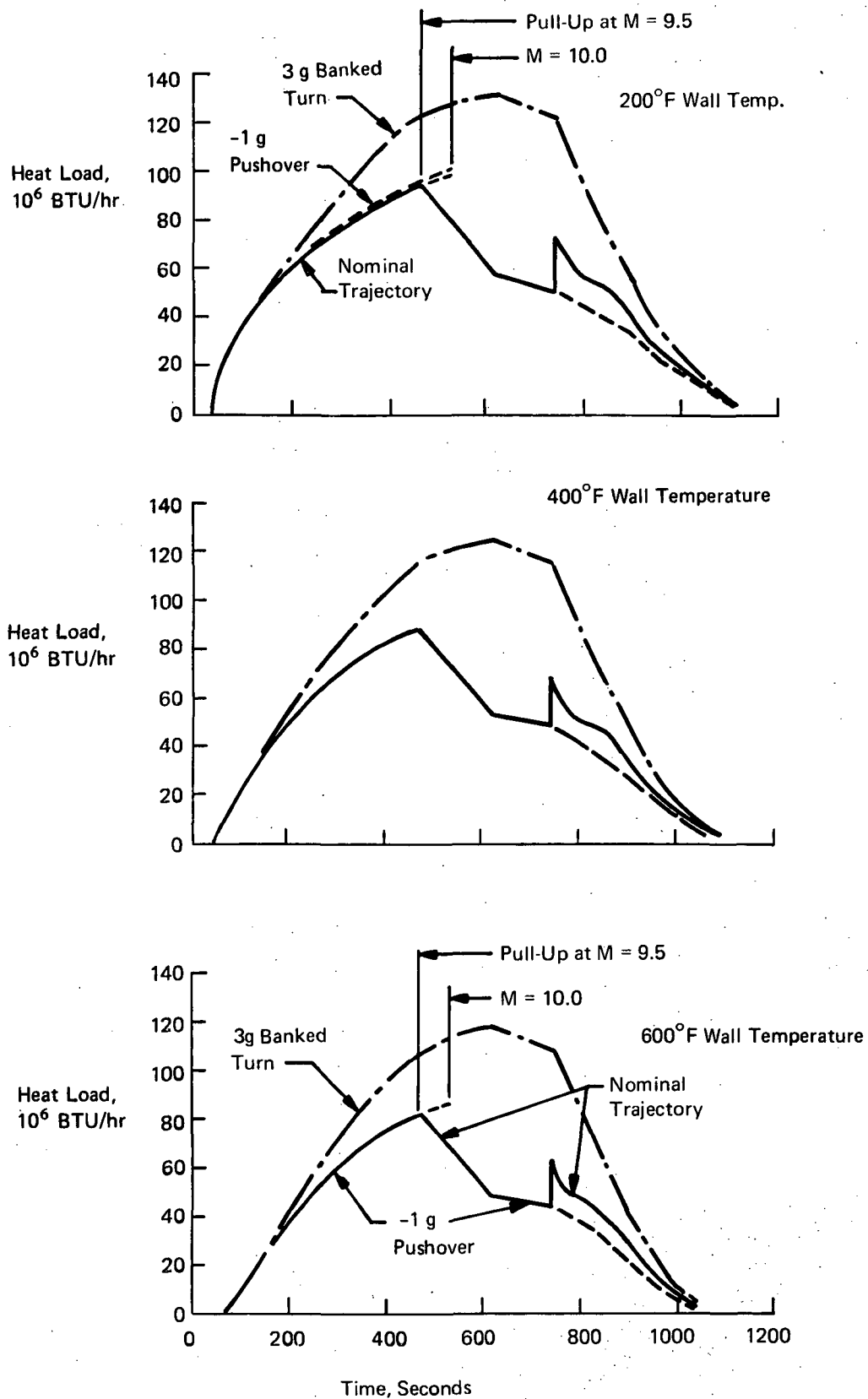


Figure 5b. Effect of Maneuvers on HRA Heat Load History, Mach 10 Trajectory, Unshielded Vehicle

would result if a maneuver was initiated at any point along the nominal trajectory such that the maximum positive or negative load factor was reached instantaneously.

To obtain an accurate prediction of the heat loads, heating rates were determined at 234 zones on the wings, 156 zones on the vertical fins and 280 zones on the fuselage. The wing consisted of 39 streamwise zones at 3 span locations on the wing; i.e., root chord, mid span, and tip chord. These 3 span locations were required to account for the variations in streamwise distance to the point of maximum thickness as well as the change in wedge angles with span location. The vertical fins, even though they are of constant cross-section, require two zones for analysis, i.e., one above the wing and one below the wing. These must be analyzed separately because of the different sweep angles. The fuselage data, on the other hand, was computed along 14 streamlines of the fuselage in order to account for local effective wedge angles. Ten axial stations were considered. A total of over 900,000 data points were computed.

For the Mach 8 trajectory the maximum maneuver conditions during ascent require a hydrogen flow of 6.30 kg/sec (50,000 lb/hr) which is slightly less than engine fuel flow requirements at that time. An increase in wall temperature from 366°K (200F) to 588°K (600F) reduces that heat load by about 16%. At the cruise condition, the required hydrogen flow for the 366°K (200F) vehicle is about 2.52 kg/sec (20,000 lb/hr) which is more than the available fuel flow. Because the vehicle configuration is nearly symmetrical, heating conditions for the nominal and 1-g conditions are very similar. The peak heat load for the 3.0 g maneuver condition is 31,000 kW (106 million BTU/hr), assuming that the load factor is 3.0 g at Mach 8 with a dynamic pressure of 71,900 newtons/m² (1,500 psf). Although the area of the HRA is only about 10% of that of that for the HST, the design heat load for the Mach 8 trajectory is about 25% of the HST design value. For the Mach 10 trajectory the peak heat load is about 38% higher than for the Mach 8 flight path while the trends are nearly identical.

In order to size the coolant passages and to determine required passage spacing to maintain skin temperatures at desired levels the maximum aerodynamic heat flux is needed at specific locations on the vehicle. In addition, the variations of the heat fluxes and heat loads must be known as a function of time if cooling system performance is to be evaluated. Such data was computed. Maximum heat fluxes are presented in Table X at various vehicle locations for the two design trajectories. Results for both the nominal flight conditions and for maximum maneuver load factors are presented. In analyzing these results, the balancing effect of vehicle symmetry on heat loads was observed. As positive load factors were experienced, heating on the upper surface decreased while heating on the lower surface increased; the opposite was true for negative load factors. This observation lead to studies of coolant flow routing around the vehicle perimeter which tended to minimize the difference in heat load in a particular coolant circuit network as vehicle attitude was changed. These studies are described in the Plate Fin portion of the Thermal Analyses section on Panel Design Studies.

Structural Loads. - The loads used for sizing the structure of the HRA were computed for taxi, captive flight, maneuver, and landing conditions that are described as follows:

TABLE XA
LOCAL HEAT FLUXES, HYPERSONIC RESEARCH AIRPLANE

| Location | Heat Flux, W/cm ² | | | | | |
|----------------------------|------------------------------|-------|-------|-------|-------|-------|
| | 3.0g | | 1.0g | | -1.0g | |
| | M=8 | M=10 | M=8 | M=10 | M=8 | M=10 |
| Nose, 5.08 cm Dia | 198.6 | 352.0 | 198.6 | 351.9 | 198.6 | 352.0 |
| Sta. 2.5, Lower ζ | 36.3 | 62.4 | 18.7 | 23.3 | 10.7 | 2.6 |
| Sta. 5.0, Lower ζ | 33.1 | 56.2 | 16.8 | 21.0 | 9.6 | 2.4 |
| Sta. 25, Lower ζ | 28.9 | 46.0 | 13.6 | 17.0 | 7.6 | 1.9 |
| Sta. 50, Lower ζ | 24.4 | 42.0 | 12.3 | 15.3 | 6.9 | 1.7 |
| Sta. 2.5, Upper ζ | 9.6 | 0.11 | 15.9 | 19.9 | 28.4 | 39.2 |
| Sta. 5.0, Upper ζ | 8.7 | 0.11 | 14.2 | 18.2 | 25.1 | 35.2 |
| Sta. 25, Upper ζ | 7.2 | 0.11 | 12.0 | 15.5 | 21.8 | 30.1 |
| Sta. 50, Upper ζ | 1.2 | 0.0 | 2.8 | 2.8 | 6.2 | 7.0 |
| Leading Edge, 0.635 cm dia | 175.9 | 295.1 | 175.9 | 295.1 | 172.5 | 295.1 |
| Sta. 2, Lower Wing Surf. | 29.2 | 44.9 | 15.5 | 18.4 | 6.3 | 1.4 |
| Sta. 8, Lower Wing Surf. | 18.2 | 30.1 | 8.2 | 9.1 | 3.7 | 0.57 |
| Sta. 2, Upper Wing Surf. | 2.75 | 1.5 | 6.8 | 6.8 | 13.1 | 14.2 |
| Sta. 8, Upper Wing Surf. | 1.23 | 0.91 | 4.0 | 2.8 | 6.8 | 7.4 |

TABLE XB
LOCAL HEAT FLUXES, HYPERSONIC RESEARCH AIRPLANE

| Location | Heat Flux, BTU/Ft ² Sec | | | | | |
|-----------------------------|------------------------------------|--------|-------|--------|-------|--------|
| | 3.0g | | 1.0g | | -1.0g | |
| | M = 8 | M = 10 | M = 8 | M = 10 | M = 8 | M = 10 |
| Nose, 2.0 In. Dia. | 175.0 | 310.0 | 175.0 | 310.0 | 175.0 | 310.0 |
| Sta. 2.5, Lower ζ | 32.0 | 55.0 | 16.5 | 20.5 | 9.4 | 2.3 |
| Sta. 5.0, Lower ζ | 29.2 | 49.5 | 14.8 | 18.5 | 8.5 | 2.1 |
| Sta. 25, Lower ζ | 25.5 | 40.5 | 12.0 | 15.0 | 6.7 | 1.7 |
| Sta. 50, Lower ζ | 21.5 | 37.0 | 10.8 | 13.5 | 6.1 | 1.5 |
| Sta. 2.5, Upper ζ | 8.5 | 0.1 | 14.0 | 17.5 | 25.0 | 34.5 |
| Sta. 5.0, Upper ζ | 7.7 | 0.1 | 12.5 | 16.0 | 22.1 | 31.0 |
| Sta. 25, Upper ζ | 6.3 | 0.1 | 10.6 | 13.7 | 19.2 | 26.5 |
| Sta. 50, Upper ζ | 1.1 | 0.0 | 2.5 | 2.5 | 5.5 | 6.2 |
| Leading Edge, 0.25 In. Dia. | 155.0 | 260.0 | 155.0 | 260.0 | 152.0 | 260.0 |
| Sta. 2, Lower Wing Surf. | 25.7 | 39.6 | 13.7 | 16.2 | 5.54 | 1.2 |
| Sta. 8, Lower Wing Surf. | 16.0 | 26.5 | 7.2 | 8.0 | 3.22 | 0.5 |
| Sta. 2, Upper Wing Surf. | 2.42 | 1.3 | 6.0 | 6.0 | 11.5 | 12.5 |
| Sta. 8, Upper Wing Surf. | 1.08 | 0.8 | 3.5 | 2.5 | 6.0 | 6.5 |

- (1) 2.0 g taxi, 3-point attitude, 20,000 kg (44,000 lb) gross weight, 0 lift; considered to account for possible horizontal takeoff, nose gear at Station 265, main gear at Station 721.
- (2) Same as Condition (1) but with main gear at Station 641 so that 90% of the aircraft weight is on the main gear.
- (3) Carrier captive flight with 2.0 g load factor, 20,000 kg (44,000 lb) gross weight, forward hook at Station 457 and rear hook at Station 721.
- (4) Same as Condition (3) but with forward hook at Station 521 and rear hook at Station 641.
- (5) Symmetrical 3-point landing at 2.0 g, gross weight of 12,900 kg (28,500 lb), main gear at Station 721.
- (6) Same as Condition (5) but with the main landing gear at Station 641.
- (7) Tail down landing with spring back, ground reaction of 2.0 g and a spring back load equal to 50% of the vertical reaction, 12,900 kg (28,500 lb) gross weight, main landing gear at Station 721.
- (8) Same as Condition (7) but with the main landing gear at Station 641.
- (9) Tail-down landing with spin-up, ground reaction of 2.0 g with a spin-up load equal to 50% of the vertical reaction, 12,900 kg (28,500 lb) gross weight, main landing gear at Station 721.
- (10) Same as Condition (9) but with the main landing gear at Station 641.
- (11) 3.0 g banked turn, 71,800 newtons/m² (1,500 psf) dynamic pressure, M = 4.0, Alpha = 6.18°, 20,000 kg (44,000 lb) gross weight.
- (12) -1.0 g push-over, 71,800 newtons/m² (1,500 lb) dynamic pressure, M = 4.0, Alpha = 0.83°, 20,000 kg (44,000 lb) gross weight.
- (13) 3.0 g pull-up, 71,800 newtons/m² (1,500 psf) dynamic pressure, M = 0.8, Alpha = 24.5°, 20,000 kg (44,000 lb) gross weight.
- (14) -1.0 g push-over, 71,800 newtons/m² (1,500 psf) dynamic pressure, M = 0.8, Alpha = -5.85°, 20,000 kg (44,000 lb) gross weight.

Because of some uncertainty in the location of the main landing gear and the carrier aircraft attachment hooks, two locations were investigated for each.

The weight distribution employed for the airplane load computations is presented in Table VII. For this loading distribution a longitudinal cg location was computed to be at Station 603.2. For the loading conditions that involve lift, surface pressure distributions were integrated to establish point loads at numerous locations on the airframe. These were integrated for the purposes of obtaining the shears and bending moments. There were 41 fuselage stations used with 28 node points around the circumference of each for a total of over 1,000 node points. A total of 192 node points were used for the wings and 40 for the vertical tails.

When loads were defined for all ground and flight conditions, envelopes were established for the shear and bending moment loadings. Since only a limited number of flight conditions had been examined the loading curves were rotated about the horizontal axis which was equivalent to assuming maximum loads to be either positive or negative. This assumption is believed to be conservative. The bending moment and axial loading envelopes are shown as Figures 6 and 7.

Load Spectrum. - The load spectrum used for assessing fatigue and fracture mechanics characteristics of the structure is presented in Table XI. It was derived from References 5 and 6. The more severe maneuver conditions associated with fighter, fighter bomber, and trainer aircraft were normalized with respect to the design limit load factor for the particular aircraft type. The normalized curves were then used with the design limit load factors for the HRA to obtain the spectrum presented in Table XI. A design life of 250 missions of one hour each was assumed along with a life scatter factor of 4.0, hence the 3.60×10^6 sec (1,000 hr) increment of time as the basis for the total number of cycles at the various load factors.

TABLE XI
SUGGESTED LOADING SPECTRUM, HYPERSONIC RESEARCH AIRPLANE
CUMULATIVE OCCURRENCES PER 1000 FLIGHT HOURS

| Load Factor, g | Occurrences |
|----------------------|-------------|
| -1.0 | — |
| -0.8 | 1 |
| -0.6 | 5 |
| -0.4 | 20 |
| -0.2 | 100 |
| 0 | 350 |
| 0.2 | 1,300 |
| 0.4 | 3,000 |
| 0.6 | 42,000 |
| 0.8 | — |
| 1.0 | — |
| 1.2 | — |
| 1.4 | 350,000 |
| 1.6 | 150,000 |
| 1.8 | 70,000 |
| 2.0 | 35,000 |
| 2.2 | 10,000 |
| 2.4 | 4,000 |
| 2.6 | 2,400 |
| 2.8 | 1,300 |
| 3.0 (Positive Limit) | 650 |
| 3.2 | 300 |
| 3.4 | 150 |
| 3.6 | — |
| 3.66 | 35 |

Limit Bending, Moment, km-N

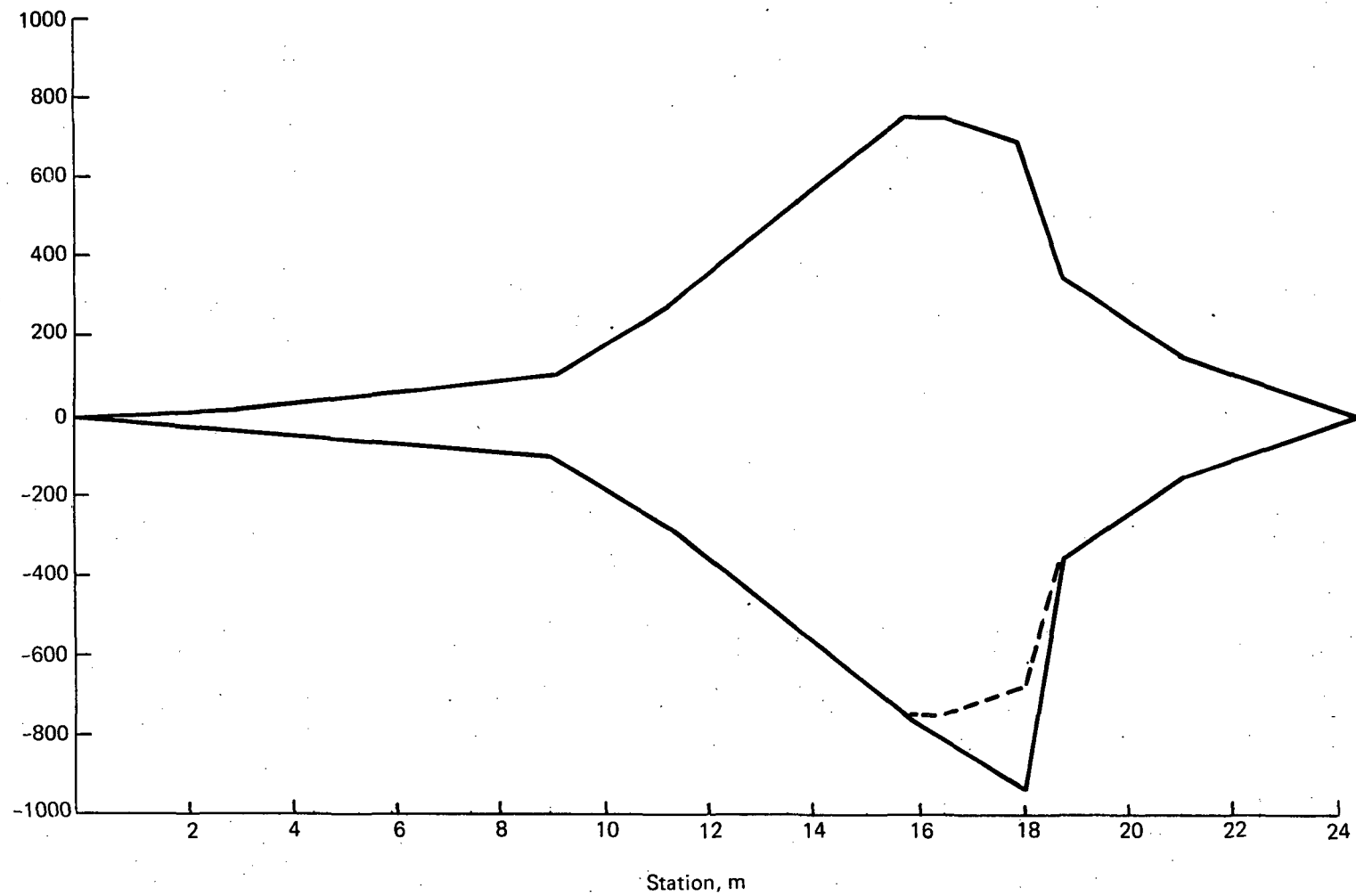


Figure 6a. Fuselage Bending Moment Diagram, Hypersonic Research Airplane

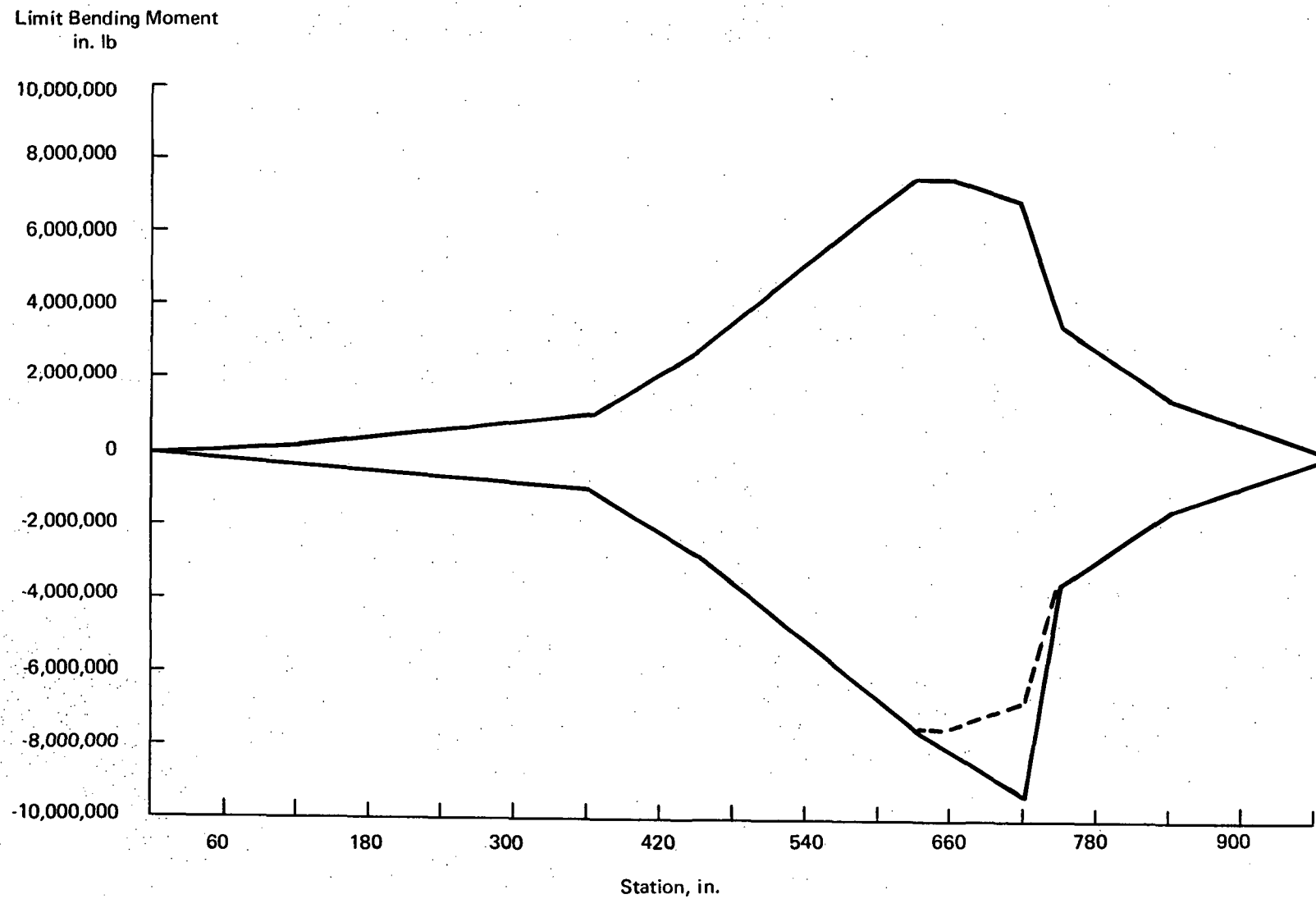


Figure 6b. Fuselage Bending Moment Diagram, Hypersonic Research Airplane

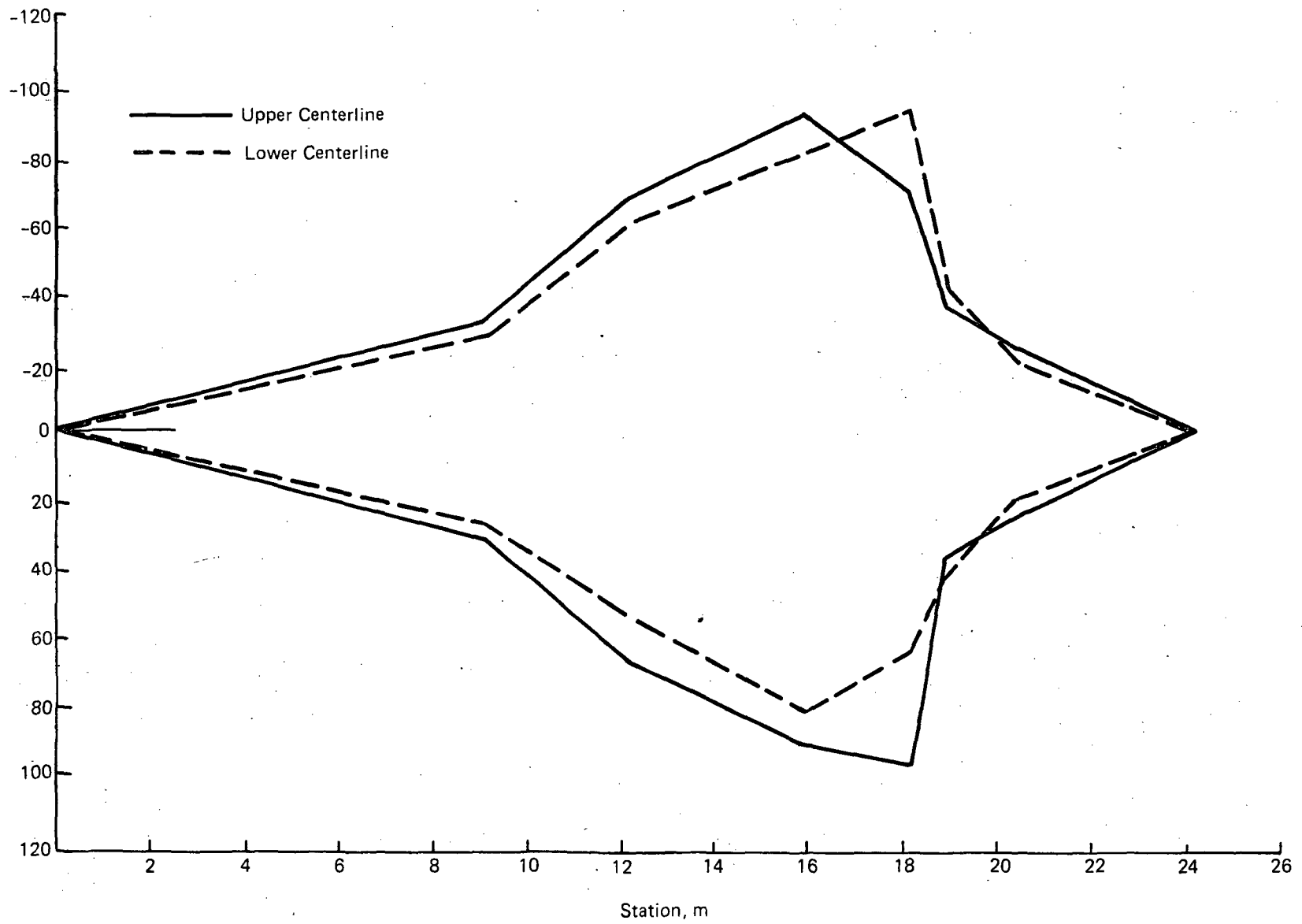
Limit Axial Loading Intensity, N_x , kN/m

Figure 7a. Fuselage Limit Loading Envelope

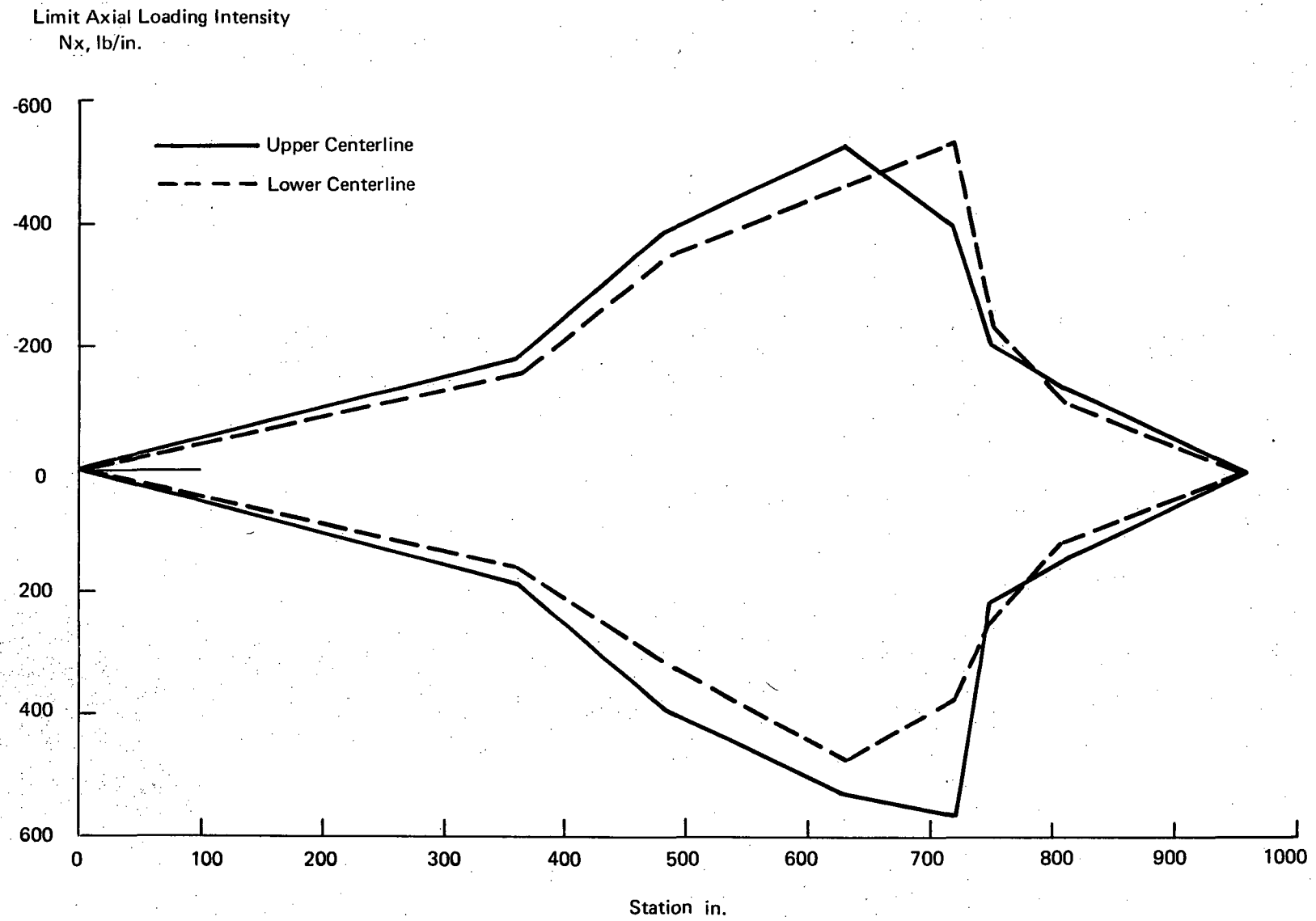


Figure 7b. Fuselage Limit Loading Envelope

MATERIAL SELECTION

The operational time for the hypersonic transport studied is estimated to begin around the year 2000. Such timing will permit advances in materials technology to be factored into its design and construction. Prior studies had indicated some advantages of operating at temperatures up to 589°K (600F). On the other hand, the hypersonic research airplane was envisioned for the 1980 time period so that presently available materials were the most likely candidates for its construction. Because of these considerations the types of construction materials considered ranged from aluminum alloys through metal matrix composites. Since there appears to be far less development effort on advanced coolants as compared to the efforts on construction materials, only rather conventional and available coolants were considered. Some of the high temperature coolants are quite expensive but these were not excluded since a significant demand might reduce coolant costs.

No projections were made as to future material developments. All studies and comparisons were based on available material property data. This approach was adopted as a means of obtaining a conservative estimate of the benefits of cooled airframe structure. Further advances in materials technology would have to provide a meaningful improvement in vehicle performance before they would be considered. Hence, the results presented in this report are likely to be improved by future developments.

Coolants

Screening. — Liquid convective cooling was the only approach considered. Aerodynamic heat input to the structure was transferred to a heat exchanger where it was rejected to the hydrogen fuel. For this heat transport function the coolant characteristics of primary importance are the thermal and physical properties that define coolant flow rate, heat transfer, and pumping power penalties as well as safety considerations and chemical compatibility with candidate construction materials. Properties of primary interest include minimum and maximum temperature limits, specific heat, density, thermal conductivity, and viscosity. Based on these considerations the 26 candidate coolants listed in order of decreasing performance in Table XII were chosen from more than 50 preliminary candidates, References 8 through 20. The coolant performance factor is a ratio of pumping power to heat transfer conductance for turbulent flow. The two temperature levels used for the assessment were based on the use of aluminum alloy and higher temperature construction materials. The number of coolants that can be used above 450°K (350F) is quite limited so that comparisons at higher temperatures were not required during the screening phase.

Detailed considerations of safety, toxicity, and thermal stability were not included during the screening, and in most cases chemical compatibility data was sparse. At temperatures below 394°K (250F), thermal degradation is not likely and oxidation is slow except for the glycols. At higher temperatures oxidation is faster and most coolants tend to form residues, with the prefluorinated fluorocarbons being most resistant.

TABLE XII A
CANDIDATE COOLANTS IN ORDER OF DECREASING PERFORMANCE POTENTIAL

| Coolant | Chemical Formula or Chemical Name | Operating Range | | | | Coolant Performance Factor* at | | Corrosion Resistance of Materials to Coolant | | | | |
|------------------------------------|--|---------------------------|---------------|-------------|---------------------------------|---|--------|--|-----------|-----------|-----------|-----------|
| | | Pour or Freezing °K | Boiling °K | Flash °K | Pressure at 366° K psi | 366° K | 450° K | Aluminum | Titanium | Stainless | Magnesium | Beryllium |
| | | | | | | | | | | | | |
| Methanol - Water (80-20) | CH ₃ OH | 170 | 343 | | 283 | 0.0013 | | Fair | No Data | Fair | Resistant | No Data |
| Propylene Glycol - Water (60-40) | CH ₃ CH ₂ OH·CH ₂ ·OH | 212 | 381 | 381 | | 0.0026 | | Fair | No Data | Resistant | Resistant | No Data |
| Triethylene Glycol - Water (60-40) | CH ₂ O·CH ₂ CH ₂ ·OH·CH ₂ ·O·CH ₂ CH ₂ ·OH | 233 | 378 | | | 0.0037 | | Fair | No Data | Fair | Resistant | No Data |
| Ethylene Glycol - Water (60-40) | CH ₂ OH·CH ₂ OH | 223 | 383 | 389 | | 0.0038 | | Fair | No Data | Resistant | Resistant | No Data |
| Dow Therm E | O-Dichlorobenzene | 255 | 450 | 342 | | 0.015 | | Unsatisfactory | No Data | Resistant | No Data | No Data |
| FC-43 | Fluorinated Compound | 288 | 450 | | — | 0.017 | 0.0064 | Resistant | No Data | Resistant | Resistant | Resistant |
| Dow Therm A | Diphenyl and Diphenyl Oxide | 289 | 533 | 394 | | 0.018 | — | Fair | No Data | Resistant | No Data | No Data |
| Freon 21 | CHCl ₂ F | 373 | 282 | | 344 | 0.020 | — | Resistant | Resistant | Resistant | Resistant | No Data |
| Coolanol 15 | Silicate Ester Compound | 333 | 383 | 350 | — | 0.021 | — | Fair | No Data | Fair | Fair | No Data |
| Freon E1 | F (CF ₃ ·CF ₂ ·O) ₄ CH FCH ₃ | 392 | 314 | | 296 | 0.021 | — | Resistant | No Data | Resistant | Resistant | No Data |
| FC-75 | Fluorinated Compound | 181 | 376 | — | — | 0.025 | — | Resistant | No Data | Resistant | Resistant | Resistant |
| Coolanol 25 | Silicate Ester Compound | 189 | 578 | 436 | — | 0.025 | 0.012 | Fair | No Data | Fair | Fair | No Data |
| FC-78 | Fluorinated Compound | 200 | 323 | — | 272 | 0.025 | — | Resistant | No Data | Resistant | Resistant | Resistant |
| Freon E2 | F (CF ₃ ·CF ₂ ·O) ₂ ·CHFCF ₃ | 150 | 378 | — | — | 0.028 | — | Resistant | No Data | Resistant | Resistant | No Data |
| Coolanol 45 | Silicate Ester Compound | 208 | 611 | 461 | — | 0.029 | 0.0054 | Fair | No Data | Fair | Fair | No Data |
| OS 59 | — | 208 | — | 461 | — | 0.029 | 0.014 | No Data | No Data | No Data | No Data | No Data |
| Freon E3 | F (CF ₃ ·CF ₂ ·O) ₃ ·CHFCF ₃ | 167 | 426 | — | — | 0.029 | 0.015 | Resistant | No Data | Resistant | Resistant | No Data |
| Freon 113 | CCl ₂ F·CClF ₂ | 238 | 321 | | 283 | 0.033 | — | Resistant | Resistant | Resistant | Resistant | Resistant |
| Stauffer 3664 | Polyol Ester Compound | 236 | — | 533 | — | 0.036 | 0.0070 | Resistant | No Data | Resistant | Resistant | Resistant |
| Dow Therm G | Mixture of Di and Tri-ary | 246 | 589 | 469 | — | 0.039 | 0.016 | Resistant | No Data | Resistant | No Data | No Data |
| Freon E4 | F (CF ₃ ·CF ₂ ·O) ₄ ·CHFCF ₃ | 179 | 467 | — | — | 0.039 | 0.022 | Resistant | No Data | Resistant | Resistant | No Data |
| Freon E5 | F (CF ₃ ·CF ₂ ·O) ₅ ·CHFCF ₃ | 189 | 497 | — | — | 0.048 | 0.024 | Resistant | No Data | Resistant | Resistant | No Data |
| Dow Corning 200 | Silicone Compound | 208 | 438 | 473 | — | 0.067 | 0.045 | Resistant | No Data | Resistant | Resistant | No Data |
| AF-1-3755 | Silicone Compound | 201 | 473 | 488 | — | 0.069 | 0.047 | Resistant | No Data | Resistant | Resistant | No Data |
| Oronite 8200 | Hydrocarbon | 292 | — | 472 | — | 0.130 | 0.058 | No Data | No Data | No Data | No Data | No Data |
| Dow Corning 710 | Silicone Compound | 253 | 523 | 573 | — | 0.560 | 0.170 | Resistant | No Data | Resistant | Resistant | No Data |

* Pumping Power (Turbulent Flow) = $\frac{\mu^{0.72}}{\rho^2 c_p 2.28 k^{0.67}}$
Heat Transfer Conductance

TABLE XII B
CANDIDATE COOLANTS IN ORDER OF DECREASING PERFORMANCE POTENTIAL

| Coolant | Chemical Formula or Chemical Name | Operating Range | | | | Coolant Performance Factor* at | | Corrosion Resistance of Materials to Coolant | | | | |
|------------------------------------|--|---------------------------|---------------|-------------|---------------------------------|---|--------|--|-----------|-----------|-----------|-----------|
| | | Pour or Freezing °F | Boiling °F | Flash °F | Pressure at 200° F psi | 200° F | 350° F | Aluminum | Titanium | Stainless | Magnesium | Beryllium |
| | | | | | | | | | | | | |
| Methanol - Water (80-20) | CH ₃ OH | -154 | 158 | | 50 | 0.0013 | | Fair | No Data | Fair | Resistant | No Data |
| Propylene Glycol - Water (60-40) | CH ₃ CH·OH·CH ₂ ·OH | - 78 | 225 | 225 | | 0.0026 | | Fair | No Data | Resistant | Resistant | No Data |
| Triethylene Glycol - Water (60-40) | CH ₂ O·CH ₂ CH ₂ ·OH·CH ₂ ·O·CH ₂ CH ₂ ·OH | - 40 | 220 | 330 | | 0.0037 | | Fair | No Data | Fair | Resistant | No Data |
| Ethylene Glycol - Water (60-40) | CH ₂ OH·CH ₂ OH | - 58 | 230 | 240 | | 0.0038 | | Fair | No Data | Resistant | Resistant | No Date |
| Dow Therm E | O-Dichlorobenzene | 0 | 350 | 155 | | 0.015 | | Unsatisfactory | No Data | Resistant | No Data | No Data |
| FC-43 | Fluorinated Compound | - 58 | 350 | | — | 0.017 | 0.0064 | Resistant | No Data | Resistant | Resistant | Resistant |
| Dow Therm A | Diphenyl and Diphenyl Oxide | 60 | 500 | 250 | | 0.018 | — | Fair | No Data | Resistant | No Data | No Data |
| Freon 21 | CHCl ₂ F | -211 | 48 | | 160 | 0.020 | — | Resistant | Resistant | Resistant | Resistant | No Data |
| Coolanol 15 | Silicate Ester Compound | -140 | 230 | 170 | — | 0.021 | — | Fair | No Data | Fair | Fair | No Data |
| Freon E1 | F (CF ₃ ·CF ₂ ·O) ₄ ·CHFCF ₃ | -246 | 105 | | 73 | 0.021 | — | Resistant | No Data | Resistant | Resistant | No Data |
| FC-75 | Fluorinated Compound | -135 | 216 | — | — | 0.025 | — | Resistant | No Data | Resistant | Resistant | Resistant |
| Coolanol 25 | Silicate Ester Compound | -120 | 580 | 325 | — | 0.025 | 0.012 | Fair | No Data | Fair | Fair | No Data |
| FC-78 | Fluorinated Compound | -100 | 122 | — | 30 | 0.025 | — | Resistant | No Data | Resistant | Resistant | Resistant |
| Freon E2 | F (CF ₃ ·CF ₂ ·O) ₂ ·CHFCF ₃ | -190 | 220 | — | — | 0.028 | — | Resistant | No Data | Resistant | Resistant | No Data |
| Coolanol 45 | Silicate Ester Compound | - 85 | 640 | 370 | — | 0.029 | 0.0054 | Fair | No Data | Fair | Fair | No Data |
| OS 59 | — | - 85 | — | 370 | — | 0.029 | 0.014 | No Data | No Data | No Data | No Data | No Data |
| Freon E3 | F (CF ₃ ·CF ₂ ·O) ₃ ·CHFCF ₃ | -160 | 306 | — | — | 0.029 | 0.015 | Resistant | No Data | Resistant | Resistant | No Data |
| Freon 113 | CCl ₂ F·CClF ₂ | - 32 | 117 | — | 50 | 0.033 | — | Resistant | Resistant | Resistant | Resistant | No Data |
| Stauffer 3664 | Polyol Ester Compound | - 35 | — | 500 | — | 0.036 | 0.0070 | Resistant | No Data | Resistant | Resistant | Resistant |
| Dow Therm G | Mixture of Di and Tri-aryl | - 18 | 600 | 385 | — | 0.039 | 0.016 | Resistant | No Data | Resistant | No Data | No Data |
| Freon E4 | F (CF ₃ ·CF ₂ ·O) ₄ ·CHFCF ₃ | -138 | 380 | — | — | 0.039 | 0.022 | Resistant | No Data | Resistant | Resistant | No Data |
| Freon E5 | F (CF ₃ ·CF ₂ ·O) ₅ ·CHFCF ₃ | -119 | 435 | — | — | 0.048 | 0.024 | Resistant | No Data | Resistant | Resistant | No Data |
| Dow Corning 200 | Silicone Compound | - 85 | 329 | 392 | — | 0.067 | 0.045 | Resistant | No Data | Resistant | Resistant | No Data |
| AF-1-3755 | Silicone Compound | - 99 | 392 | 419 | — | 0.069 | 0.047 | Resistant | No Data | Resistant | Resistant | No Data |
| Oronite 8200 | Hydrocarbon | - 65 | — | 390 | — | 0.130 | 0.058 | No Data | No Data | No Data | No Data | No Data |
| Dow Corning 710 | Silicone Compound | - 4 | 482 | 572 | — | 0.560 | 0.170 | Resistant | No Data | Resistant | Resistant | No Data |

*Pumping Power (Turbulent Flow) = $\frac{\mu \cdot 0.72}{\rho^2 \cdot c_p^{2.28} \cdot k^{0.67}}$

Heat Transfer Conductance

Based on performance ratings and the desire to retain candidates from generically different classes, the 26 more promising candidates were reviewed. Nine of the coolants screened were eliminated because of either high freezing points, similarity to other coolants, and/or high pumping power penalties over the temperature range of interest.

Parametric Comparisons and Selections. — The 17 remaining coolants were divided into two categories, those for use to a maximum temperature of 366°K (200F) and those which could be used at higher temperatures. Computer analyses were then conducted using the cooling system configuration selected and described in Reference 3 and the peak heat load corresponding to the new trajectory assuming partially shielded vehicles (shielding in those areas which would exceed 811°K (1,000F) if uncooled). The analysis employed an optimization technique to size the distribution lines and to trade off line size and pumping power. Results are summarized in Tables XIII and XIV for the 366° (200F) and 450°K (350F) maximum coolant temperatures. For the 366° (200F) coolant temperature, aluminum alloy construction was assumed along with a maximum structural operating temperature of 394°K (250F), while for the higher temperature, titanium alloy construction was assumed along with a maximum operating temperature of 533°K (500F). The results presented in Tables XIII and XIV include the system pressure drop and the weight of the distribution lines and APS fuel required to circulate the coolant for an equivalent steady state time of 2,700 seconds under the peak heat load of 54,500 kw (186×10^6 BTU/hr) for the 366°K (200F) system and 33,400 kw (114×10^6 BTU/hr) for the 450°K (350F) system. However, the tabulated weights do not include the allowances for residual coolant in the skin panels, heat exchanger, pumps, or other system items not specifically mentioned above.

In reviewing Table XIII pressure drops from 0.76×10^6 newton/m² (110 psi) up to 1.19×10^6 newton/m² (174 psi) are noted. The weight of the distribution lines and APS fuel ranges from approximately 2270 kg (5,000 lb) up to 5900 kg (13,000 lb). It can be noted that high pressure drop is not synonymous with the high system weight. The silicate ester coolants (Coolanols) tended to have relatively lower pressure drops while those for the heavier fluoroinated coolants tended to be relatively higher. Of the coolants considered, the use of the glycols resulted in substantially lighter system weights, about 2270 kg (5,000 lb), than other candidates. The next most attractive candidates, Coolanol 15 and Coolanol 25 yielded comparable system weights of about 3630 kg (8000 lb). The next most promising candidates, Stauffer 3664 and Coolanol 45, also have comparable system weights of about 4080 kg (9,000 lb). The distribution system and APS weights for all other candidates are more than twice as high as for the water-glycol coolants.

In selecting coolants for further study, water-glycol is obviously the most promising candidate. However, because of the unknown chemical compatibility with candidate construction materials it is desirable to include some alternate coolants as well. In reviewing the nonaqueous coolants, consideration was given to the likelihood of their use in airframes which use more than one construction material. This approach is desirable since it would reduce the amount of shielding which would be required for an all aluminum airframe, see Sections titled Cooling System Design Studies, Concepts and System Summaries. Consideration was given to system weight, boiling and freezing points and to the desirability of including coolants of basically different formulations. Coolanol 45 was selected as a conservative silicate ester candidate which could be used to the highest

TABLE XIII A
COMPARISON OF CANDIDATE COOLANTS, 366°K
SHIELDED NON-REDUNDANT SYSTEM,
340°K TEMPERATURE RISE, 394°K
STRUCTURAL TEMPERATURE LIMIT, 54.5×10^6 WATTS

| Coolant | Total System | | Rating |
|------------------|---------------------------------|-------------------------------|--------|
| | MN/m ² ΔP | Line + APS Fuel Weight, kg | |
| Ethylene Glycol | 0.9079 | 2304.0 | 2 |
| Propylene Glycol | 0.9145 | 2279.2 | 1 |
| FC-43 | 1.1970 | 5487.2 | 9 |
| Freon 21 | 0.8893 | 5066.6 | 7 |
| Coolanol 15 | 0.7569 | 3564.0 | 3 |
| Freon E1 | 0.9474 | 5264.5 | 8 |
| FC-75 | 1.1196 | 5504.7 | 10 |
| Coolanol 25 | 0.7697 | 3676.0 | 4 |
| Freon E2 | 1.0534 | 5525.7 | 11 |
| Coolanol 45 | 0.8503 | 4086.6 | 6 |
| Freon E3 | 1.1052 | 5790.2 | 12 |
| Freon 113 | 0.9723 | 5950.9 | 13 |
| Stauffer 3664 | 0.9329 | 4078.5 | 5 |

TABLE XIII B
COMPARISON OF CANDIDATE COOLANTS, 200F
SHIELDED NON-REDUNDANT SYSTEM,
150F TEMPERATURE RISE, 250F
STRUCTURAL TEMPERATURE LIMIT, 186×10^6 BTU/hr.

| Coolant | Total System | | Rating |
|------------------|------------------|-------------------------------|--------|
| | ΔP , psi | Line + APS Fuel Weight, lb | |
| Ethylene Glycol | 131.67 | 5086.2 | 2 |
| Propylene Glycol | 132.63 | 5031.4 | 1 |
| FC-43 | 173.61 | 12113.11 | 9 |
| Freon 21 | 127.98 | 11184.6 | 7 |
| Coolanol 15 | 109.77 | 7867.6 | 3 |
| Freon E1 | 137.40 | 11621.5 | 8 |
| FC-75 | 162.38 | 12151.6 | 10 |
| Coolanol 25 | 111.63 | 8114.8 | 4 |
| Freon E2 | 152.78 | 12198.1 | 11 |
| Coolanol 45 | 123.32 | 9021.2 | 6 |
| Freon E3 | 160.29 | 12782.0 | 12 |
| Freon 113 | 141.02 | 13136.7 | 13 |
| Stauffer 3664 | 135.30 | 9003.3 | 5 |

TABLE XIVA
COMPARISON OF CANDIDATE COOLANTS,
450°K SHIELDED NON-REDUNDANT
SYSTEM, 422°K TEMPERATURE RISE,
533°K STRUCTURAL TEMPERATURE LIMIT, 33.4×10^6 WATTS

| Coolant | Total System | | Rating |
|--------------------------|---------------------------------|-------------------------------|--------|
| | MN/m ² ΔP | Line + APS Fuel Weight, kg | |
| FC-43 | 1.2703 | 2035.8 | 6 |
| Coolanol 25 | 0.8440 | 1436.0 | 1 |
| Coolanol 45 | 0.9148 | 1570.6 | 2 |
| Stauffer 3664 | 0.9947 | 1619.9 | 3 |
| Dow Therm G | 1.0351 | 1774.4 | 5 |
| Freon E4 | 1.1972 | 2255.5 | 7 |
| Freon E5 | 1.2384 | 2360.6 | 8 |
| Dow Corning XF-1-3755 | 0.8741 | 1672.5 | 4 |

TABLE XIV B
COMPARISON OF CANDIDATE COOLANTS, 350F
SHIELDED NON-REDUNDANT SYSTEM,
300F TEMPERATURE RISE,
500F STRUCTURAL TEMPERATURE LIMIT, 114×10^6 BTU/hr.

| Coolant | Total System | | Rating |
|--------------------------|------------------|-------------------------------|--------|
| | ΔP , psi | Line + APS Fuel Weight, lb | |
| FC-43 | 184.23 | 4494 | 6 |
| Coolanol 25 | 122.41 | 3170 | 1 |
| Coolanol 45 | 132.68 | 3467 | 2 |
| Stauffer 3664 | 144.26 | 3576 | 3 |
| Dow Therm G | 150.13 | 3917 | 5 |
| Freon E4 | 173.64 | 4979 | 7 |
| Freon E5 | 179.61 | 5211 | 8 |
| Dow Corning XF-1-3755 | 126.78 | 3692 | 4 |

operating temperature and appeared to be least corrosive based on manufacturer's data. FC-43 was selected as the representative fluorinated coolant because of its high boiling point.

For the high temperature coolants listed in Table XIV pressure drops range from approximately 0.827×10^6 newtons/m² (120 psi) to 1.27×10^6 newtons/m² (185 psi) while weights ranged from approximately 1450 kg (3,200 lb) to about 2360 kg (5,200 lb). There is a definite trend of system weight increasing with pressure drop. For the high temperature systems the primary selection criteria included weight, maximum use temperature, freezing point, and basically different chemical nature. These considerations led to the choice of Cooanol 45, Freon E-5, and Dow Corning XF-1-3755. While Dow Therm G was used during the experimental evaluations its relatively high freezing point makes it unattractive for actual use and its retention in the experimental program was based on the fact that it is the most attractive hydrocarbon.

Construction Alloys

Screening. - In considering a hypersonic transport for the 2,000 + time period the relative merits of current work horse materials and developmental types must be assessed. Requirements include high strength and stiffness to density ratios, high fatigue strength, relative insensitivity to notches, and acceptable corrosion resistance at operating temperatures. At elevated temperature high thermal conductivity minimizes gradients, and low expansion coefficients minimize thermal stresses. The material must be chemically compatible with the coolant, available in the sizes of interest, and capable of being manufactured into required shapes at reasonable cost. In recognition of these needs over 100 specific structural materials from eleven different categories were reviewed, References 21 through 35, and the 40 most applicable are listed in Table XV. Extensive property data are available for most of these candidates but are not repeated here. It should be noted that different heat treatments are included for some alloys since they influence mechanical properties, corrosion resistance, and fabricability. Depending upon the coolant selected, tradeoffs among these parameters may be important. In addition, materials likely to be developed by 1990 may be considered. For example, laminated beryllium/titanium offers potential advantages in tailoring properties and provides a slight compressive prestress in the beryllium at all operating temperatures. However, analyses were based on data for presently available materials. New developments will only be used if they are superior to existing materials, hence by using available data rather than projections conservative results are obtained.

As a further step in reducing the number of candidates, Table XVI was prepared, primarily from the data of Reference 21 and supplements of Reference 22, and presents structural efficiency parameters at room and use temperatures. Bare aluminum alloy properties are presented in Table XVI and the reader must bear in mind that the structural efficiencies parameters would be reduced by about 5% if cladding is used. In addition to consideration of structural efficiency, comparisons were made among fracture toughness, notch sensitivity and fatigue strength for each particular class of alloy.

On this basis, the four aluminum alloys selected were 2021, 2024, 2219, and 7475. The first shows highest performance potential, the second is a work horse alloy, the third has one of the lowest efficiencies, and the fourth is intermediate. Among the magnesium alloys AZ31B and HK31A appeared to be the more promising for inclusion in the panel efficiency studies. For the titanium

TABLE XV
CANDIDATE CONSTRUCTION MATERIALS SELECTED FROM
INITIAL REVIEW OF PROPERTIES

ALUMINUM ALLOYS

2021-T62, -T87
 2024-T3, -T4, -T6, -T81, -T861
 2048-T851
 2219-T62, -T851, -T87
 7050
 7075-T6, -T73
 7178-T6, -T76
 7475-T61, -T761

MAGNESIUM ALLOYS

AZ31B-H24
 HM21A-T8
 HM31A-T5
 HK31A-H24

TITANIUM ALLOYS

4Al-3Mo-IV STA
 6Al-4V A AND STA
 6Al-6V-2Sn STA
 6Al-2Cb-1Ta-0.8 Mo
 8Al-1Mo-1V A
 13V-11Cr-3Al STA
 16V-2.5 Al STA
 2Cr-2Fe-2Mo

STAINLESS STEELS

AM350 SCT850, SCT1000, CRT
 AM355 SCT850, SCT1000, SCCRT
 17-7 PH CH900, RH950, TH1050
 PH 14-8Mo CH950, CH1050, SRH950, SRH1050
 PH 15-7Mo CH900, RH950, TH1050
 MARAGING, 250 GRADE

SUPERALLOYS

INCONEL 625 A
 INCONEL 718 STA, STA-CW
 INCONEL 901 STA
 RENE 41
 HAYNES 188 ST
 TD NICKEL A
 TD NICKEL CHROME

BERYLLIUM

BERYLLIUM, CRS
 LOCKALLOY

METAL MATRIX COMPOSITIES

BORON/ALUMINUM
 BORON/TITANIUM
 BERYLLIUM/ALUMINUM
 BERYLLIUM/TITANIUM
 GRAPHITE/ALUMINUM

TABLE XVIA
STRUCTURAL EFFICIENCY OF CONSTRUCTION MATERIALS

| Material | Room Temperature Struct. Efficiency Parameters, cm. | | | Use Temperature (1) | | | | | |
|-------------------------|---|------|------|-------------------------------|----------|------|--|-----------------------------------|------------------------------|
| | | | | Correction Factors (2) (3) | | | Structural Efficiency Parameters, cm. | | |
| | | | | F_{tu} | F_{cy} | E | $F_{tu} \times 10^{-3}$ ρ | $F_{cy} \times 10^{-3}$ ρ | $E \times 10^{-6}$ ρ |
| Aluminum Alloys | | | | | | | | | |
| 2021-T62 | 1791 | 1537 | 262 | 2.36 | 2.41 | 2.36 | 1664 | 1461 | 244 |
| 2021-T81 | 1791 | 1511 | 262 | 2.36 | 2.41 | 2.36 | 1664 | 1435 | 244 |
| 2024-T4 | 1575 | 1016 | 272 | 2.34 | 2.44 | 2.49 | 1448 | 965 | 262 |
| 2024-T62 | 1626 | | 272 | 2.46 | 2.39 | 2.49 | 1575 | | 262 |
| 2024-T81 | 1702 | 1473 | 272 | 2.44 | 2.39 | 2.49 | 1625 | 1384 | 262 |
| 2024-T86 | 1778 | 1600 | 272 | 2.39 | 2.39 | 2.49 | 1676 | 1511 | 267 |
| 2219-T62 | 1346 | 947 | 264 | 2.34 | 2.41 | 2.46 | 1232 | 902 | 257 |
| 2219-T81 | 1549 | 1194 | 264 | 2.34 | 2.41 | 2.46 | 1422 | 1130 | 257 |
| 2219-T87 | 1575 | 1295 | 264 | 2.29 | 2.39 | 2.46 | 1422 | 1219 | 257 |
| 7075-T6 | 1905 | 1715 | 259 | 2.13 | 1.91 | 2.41 | 1600 | 1283 | 246 |
| 7075-T73 | 1689 | 1410 | 259 | 2.08 | 1.91 | 2.41 | 1384 | 1054 | 246 |
| 7173-T6 | 2070 | 1816 | 256 | 1.98 | 1.91 | 2.41 | 1613 | 1359 | 244 |
| 7173-T76 | 1842 | 1626 | 256 | 1.93 | 1.91 | 2.41 | 1397 | 1219 | 244 |
| 7475-T61 | 1867 | 1638 | 259 | 2.13 | 1.91 | 2.41 | 1575 | 1232 | 246 |
| 7475-T761 | 1740 | 1537 | 259 | 2.08 | 1.91 | 2.41 | 1435 | 1156 | 246 |
| Magnesium Alloys | | | | | | | | | |
| AZ31B-H24 | 1575 | 808 | 262 | 1.91 | 2.13 | 2.44 | 1181 | 686 | 251 |
| HK31A-H24 | 1181 | 787 | 254 | 1.78 | 2.41 | 2.44 | 826 | 749 | 244 |
| HM21A-T8 | 1308 | 597 | 257 | 1.68 | 2.29 | 2.39 | 864 | 533 | 241 |
| HM31A-T5 | 1638 | 737 | 254 | 1.98 | 2.46 | 2.44 | 1283 | 584 | 244 |
| Titanium Alloys | | | | | | | | | |
| 6Al-4V STA | 2375 | 2286 | 262 | 1.98 | 1.60 | 2.24 | 1854 | 1549 | 231 |
| 4Al-3Mo-1V STA | 2565 | 2261 | 241 | 1.98 | 1.78 | 2.24 | 2007 | 1575 | 213 |
| 8Al-1Mo-1V A | 2121 | 1956 | 284 | 2.03 | 1.83 | 2.24 | 1689 | 1410 | 251 |
| 6Al-6V-2Sn STA | 2400 | 2235 | 262 | 2.16 | 2.03 | 2.24 | 1793 | 1791 | 231 |
| 6Al-2Cb-1Ti-.8Mo | 1842 | 2032 | 274 | 1.85 | 1.65 | 2.24 | 1715 | 1321 | 241 |
| 13V-11Cr-3Al | 2464 | 2337 | 210 | 2.34 | 2.08 | 2.36 | 2261 | 1905 | 196 |
| 16V-2.5 Al | 2769 | 2616 | 231 | 2.29 | 2.03 | 2.29 | 2489 | 2083 | 206 |
| Alloy Steels | | | | | | | | | |
| AM350-SCT | 1664 | 1422 | 262 | 2.24 | 1.93 | 2.08 | 1461 | 1080 | 216 |
| AM355-SCT | 1702 | 1486 | 262 | 2.18 | 1.98 | 2.29 | 1461 | 1156 | 234 |
| 17-7 pH, CH900 | 2197 | 2108 | 269 | 2.03 | 2.03 | 2.31 | 1765 | 1689 | 244 |
| 17-7 pH, RH950 | 1956 | 1829 | 267 | 2.16 | 2.03 | 2.31 | 1664 | 1473 | 241 |
| 17-7 pH, TH1050 | 1626 | 1372 | 264 | 2.16 | 2.03 | 2.29 | 1384 | 1105 | 236 |
| PH 14-8Mo, CH950 | 2324 | 2235 | 264 | 2.16 | 2.16 | 2.29 | 1981 | 1905 | 236 |
| PH 14-8Mo, CH1050 | 2235 | 2134 | 264 | 2.16 | 2.16 | 2.29 | 1905 | 1816 | 236 |
| PH 14-8Mo, SRH950 | 1956 | 1740 | 264 | 2.21 | 2.16 | 2.29 | 1702 | 1486 | 236 |
| PH 14-8Mo, SRH1050 | 1765 | 1639 | 264 | 2.13 | 2.16 | 2.29 | 1486 | 1397 | 236 |
| PH 15-7Mo, CH950 | 2248 | 2146 | 267 | 1.96 | 2.13 | 2.29 | 1702 | 1791 | 239 |
| PH 15-7Mo, RH950 | 2019 | 1880 | 267 | 2.18 | 2.21 | 2.29 | 1740 | 1626 | 239 |
| PH 15-7Mo, TH1050 | 1740 | 1549 | 267 | 2.18 | 2.18 | 2.29 | 1499 | 1334 | 239 |
| 250 Maraging | 2235 | 2146 | 254 | 2.24 | 2.26 | 2.29 | 1956 | 1880 | 229 |
| Superalloys | | | | | | | | | |
| Haynes 188 | 1003 | 500 | 254 | 2.24 | 1.47 | 2.31 | 876 | 264 | 231 |
| Inconel 625 | 1207 | 498 | 241 | 1.93 | 1.85 | 2.41 | 914 | 363 | 229 |
| Inconel 718 STA | 1537 | 1283 | 254 | 2.29 | 2.39 | 2.34 | 1384 | 1207 | 234 |
| Inconel 901 STA | 1283 | 851 | 257 | 2.16 | 2.34 | 2.34 | 1092 | 775 | 236 |
| Rene 41, STA 1400 | 1448 | 1143 | 269 | 2.31 | 2.44 | 2.34 | 1321 | 1092 | 250 |
| Rene 41, STA 1650 | 1702 | 1283 | 269 | 2.39 | 2.44 | 2.34 | 1600 | 1232 | 250 |
| TD Nickel | 450 | 330 | 157 | 1.98 | 2.08 | 2.29 | 348 | 267 | 142 |
| Beryllium CR/SR | 2464 | 1588 | 1613 | 1.98 | 1.98 | 2.44 | 1918 | 1245 | 1549 |
| Lockalloy (32-68) | 1877 | 1433 | 973 | 1.35 | 1.47 | 2.74 | 991 | 836 | 1057 |
| Composite | | | | | | | | | |
| Boron/Aluminum L | 4534 | 4534 | 907 | 2.31 | 2.31 | 2.31 | 4145 | 4145 | 828 |
| Boron/Aluminum T | 648 | 777 | 490 | 1.52 | 1.70 | 2.13 | 389 | 518 | 414 |

(1) The following mean use temperatures were assumed:

Aluminum and magnesium alloys 366°K
Titanium and beryllium alloys 533°K
Stainless steels and superalloys 588°K

(2) Numbers in () are estimates where data was not available in MIL-HDBK-5 or in AFML Aerospace Structural Metals Handbook

(3) Includes the effects of 10,000 hour exposure at use temperature except for magnesium and beryllium alloys. Short time data for titanium alloys, stainless steels and superalloys was assumed to be equivalent to 10,000 hour data at the use temperatures chosen.

TABLE XVIB
STRUCTURAL EFFICIENCY OF CONSTRUCTION MATERIALS

| Material | Room Temperature Struct. Efficiency Parameters, Inch | | | Use Temperature (1) | | | | | |
|-------------------------|--|--------------------------------------|---------------------------------|-------------------------------|----------|--------|---|--------------------------------------|---------------------------------|
| | | | | Correction Factors (2) (3) | | | Structural Efficiency Parameters, Inch | | |
| | $\frac{F_{tu} \times 10^{-3}}{\rho}$ | $\frac{F_{cy} \times 10^{-3}}{\rho}$ | $\frac{E \times 10^{-6}}{\rho}$ | F_{tu} | F_{cy} | E | $\frac{F_{tu} \times 10^{-3}}{\rho}$ | $\frac{F_{cy} \times 10^{-3}}{\rho}$ | $\frac{E \times 10^{-6}}{\rho}$ |
| Aluminum Alloys | | | | | | | | | |
| 2021-T62 | 705 | 605 | 103 | (0.93) | (0.95) | (0.93) | 655 | 575 | 96 |
| 2021-T81 | 705 | 595 | 103 | 0.93 | (0.95) | 0.93 | 655 | 565 | 96 |
| 2024-T4 | 620 | 400 | 107 | 0.92 | 0.96 | 0.98 | 570 | 380 | 105 |
| 2024-T62 | 640 | | 107 | 0.97 | 0.94 | 0.98 | 620 | | 105 |
| 2024-T81 | 670 | 580 | 107 | 0.96 | 0.94 | 0.98 | 640 | 545 | 105 |
| 2024-T86 | 700 | 630 | 107 | 0.94 | 0.94 | 0.98 | 660 | 595 | 105 |
| 2219-T62 | 530 | 373 | 104 | 0.92 | (0.95) | 0.97 | 485 | 355 | 101 |
| 2219-T81 | 610 | 470 | 104 | 0.92 | (0.95) | 0.97 | 560 | 445 | 101 |
| 2219-T87 | 620 | 510 | 104 | 0.90 | (0.94) | 0.97 | 560 | 480 | 101 |
| 7075-T6 | 750 | 675 | 102 | 0.84 | 0.75 | 0.95 | 630 | 505 | 97 |
| 7075-T73 | 665 | 555 | 102 | 0.82 | (0.75) | (0.95) | 545 | 415 | 97 |
| 7173-T6 | 815 | 715 | 101 | 0.78 | (0.75) | (0.95) | 635 | 535 | 96 |
| 7173-T76 | 725 | 640 | 101 | (0.76) | (0.75) | (0.95) | 550 | 480 | 96 |
| 7475-T61 | 735 | 645 | 102 | (0.84) | (0.75) | (0.95) | 620 | 485 | 97 |
| 7475-T761 | 685 | 605 | 102 | (0.82) | (0.75) | (0.95) | 565 | 455 | 97 |
| Magnesium Alloys | | | | | | | | | |
| AZ31B-H24 | 620 | 318 | 103 | 0.75 | 0.84 | 0.96 | 465 | 270 | 99 |
| HK31A-H24 | 465 | 310 | 100 | 0.70 | 0.95 | 0.96 | 325 | 295 | 96 |
| HM21A-T8 | 515 | 235 | 101 | 0.66 | 0.90 | 0.94 | 340 | 210 | 95 |
| HM31A-T5 | 645 | 290 | 100 | 0.78 | 0.97 | 0.96 | 505 | 280 | 96 |
| Titanium Alloys | | | | | | | | | |
| 6Al-4V STA | 935 | 900 | 103 | 0.78 | 0.63 | 0.88 | 730 | 610 | 91 |
| 4Al-3Mo-1V STA | 1010 | 890 | 95 | 0.78 | 0.70 | 0.88 | 790 | 620 | 84 |
| 8Al-1Mo-1V A | 835 | 770 | 112 | 0.80 | 0.72 | 0.88 | 665 | 555 | 99 |
| 6Al-6V-2Sn STA | 945 | 880 | 103 | 0.85 | 0.80 | (0.88) | 805 | 705 | 91 |
| 6Al-2Cb-1To-8Mo | 935 | 800 | 108 | 0.73 | 0.65 | (0.88) | 675 | 520 | 95 |
| 13V-11Cr-3Al | 970 | 920 | 82.5 | 0.92 | 0.82 | 0.93 | 890 | 750 | 77 |
| 16V-2.5 Al | 1090 | 1030 | 91 | (0.90) | (0.80) | (0.90) | 980 | 820 | 81 |
| Alloy Steels | | | | | | | | | |
| AM350-SCT | 655 | 560 | 103 | 0.88 | 0.76 | 0.82 | 575 | 425 | 85 |
| AM355-SCT | 670 | 585 | 103 | 0.86 | 0.78 | 0.90 | 575 | 455 | 92 |
| 17-7 pH, CH900 | 865 | 830 | 106 | 0.80 | (0.80) | (0.91) | 695 | 665 | 96 |
| 17-7 pH, RH950 | 770 | 720 | 105 | 0.85 | 0.80 | 0.91 | 655 | 580 | 95 |
| 17-7 pH, TH1050 | 640 | 540 | 104 | 0.85 | 0.80 | 0.90 | 545 | 435 | 93 |
| PH 14-8Mo, CH950 | 915 | 880 | 104 | (0.85) | (0.85) | (0.90) | 780 | 750 | 93 |
| PH 14-8Mo, CH1050 | 880 | 840 | 104 | (0.85) | (0.85) | (0.90) | 750 | 715 | 93 |
| PH 14-8Mo, SRH950 | 770 | 685 | 104 | 0.87 | (0.85) | 0.90 | 670 | 585 | 93 |
| PH 14-8Mo, SRH1050 | 695 | 645 | 104 | 0.84 | (0.85) | 0.90 | 585 | 550 | 93 |
| PH 15-7Mo, CH950 | 865 | 845 | 105 | 0.77 | 0.84 | (0.90) | 670 | 705 | 94 |
| PH 15-7Mo, RH950 | 795 | 740 | 105 | 0.86 | 0.87 | (0.90) | 685 | 640 | 94 |
| PH 15-7Mo, TH1050 | 685 | 610 | 105 | 0.86 | 0.86 | 0.90 | 590 | 525 | 94 |
| 250 Maraging | 880 | 845 | 100 | 0.88 | 0.89 | 0.90 | 770 | 740 | 90 |
| Superalloys | | | | | | | | | |
| Haynes 188 | 395 | 197 | 100 | 0.88 | 0.58 | 0.91 | 345 | 104 | 91 |
| Inconel 625 | 475 | 196 | 95 | 0.76 | 0.73 | 0.95 | 360 | 143 | 90 |
| Inconel 718 STA | 605 | 505 | 100 | 0.90 | (0.94) | 0.92 | 545 | 475 | 92 |
| Inconel 901 STA | 505 | 335 | 101 | 0.85 | (0.92) | 0.92 | 430 | 305 | 93 |
| Rene 41, STA 1400 | 570 | 450 | 106 | 0.91 | 0.96 | 0.92 | 520 | 430 | 98 |
| Rene 41, STA 1650 | 670 | 505 | 106 | 0.94 | (0.96) | (0.92) | 630 | 485 | 98 |
| TD Nickel | 177 | 130 | 62 | 0.78 | 0.82 | 0.90 | 137 | 105 | 56 |
| Beryllium CR/SR | 970 | 625 | 635 | 0.78 | (0.78) | 0.96 | 755 | 490 | 610 |
| Lockalloy (32-68) | 739 | 564 | 383 | 0.53 | 0.58 | | 390 | 329 | 416 |
| Composite | | | | | | | | | |
| Boron/Aluminum L | 1785 | 1785 | 357 | 0.91 | (0.91) | 0.91 | 1632 | 1632 | 326 |
| Boron/Aluminum T | 255 | 306 | 193 | 0.60 | 0.67 | 0.84 | 153 | 204 | 163 |

(1) The following mean use temperatures were assumed:

Aluminum and magnesium alloys 200F
Titanium and beryllium alloys 500F
Stainless steels and superalloys 600F

(3) Includes the effects of 10,000 hour exposure at use temperature except for magnesium and beryllium alloys. Short time data for titanium alloys, stainless steels and superalloys was assumed to be equivalent to 10,000 hour data at the use temperatures chosen.

(2) Numbers in () are estimates where data was not available in MIL-HDBK-5 or in AFML Aerospace Structural Metals Handbook

alloys the choices include 6 Al-4V STA, 6 Al-2Cb-1Ta-0.8Mo, and 16V-2.5Al. The first alloy was selected because of the extensive data available with respect to properties and fabricability. The second alloy has demonstrated outstanding resistance to stress corrosion. The third alloy has the highest structural efficiency within the titanium alloy class. Among the alloy steels, 17-7 pH and the 250 grade maraging steel are generally representative of this class and were compared in greater detail. None of the superalloy materials are particularly promising with respect to structural efficiency. Inconel 718 STA was chosen as the single candidate from this class because of its representative properties, excellent fabricability, extensive property data, and high fracture toughness. TD Nickel is considered as a possible candidate for leading edge application where its high thermal conductivity is expected to be of significant value. Cross-roll beryllium sheet, lockalloy, and boron/aluminum composite were considered to be representative of more advanced materials.

Parametric Comparisons and Selections. - Having narrowed the field from over 100 candidate materials to 15 from seven classes, it was appropriate to introduce considerations of structural approach as well as material properties. Since the fuselage structure is essentially a shell subjected to bending three types of shell structures were compared:

- (1) Sandwich
- (2) Stringer and ring stiffened
- (3) Symmetrical double beaded
- (4) Unsymmetrical double beaded

The methods of References 36 and 37 were used. Minimum gage thickness considerations did not constrain these comparisons but were introduced later when structural weights were computed. Parametric comparisons were made for wing and tail structure also, using Reference 38 to compare the following types of wide columns:

- (1) Symmetrical double beaded (turbular)
- (2) Unsymmetrical double beaded (convex beaded)
- (3) Honeycomb sandwich
- (4) Z stiffened

The structural efficiency curves for the first two configurations were developed in Reference 38; this reference is a convenient source for the efficiency curves for the other two configurations but they were obtained from other references.

For the sandwich construction a core to face sheet density of 0.03 was assumed. When allowances are made for bonding or brazing material, the corresponding core densities in kg/m^3 (lb/ft^3) are approximately 48 (3.0) for aluminum, 32 (2.0) for magnesium, 96.1 (6.0) for titanium, 192 (12.0) for stainless steel and superalloys and 32 (2.0) for beryllium. To account for the fact that joints between sandwich skins and other members such as rings are significantly heavier for sandwich construction than for conventional ring-shell or stringer-ring configurations, the weights of the sandwich panels were increased by 20%. For these comparative analyses, only overall sandwich buckling was considered; neither wrinkling nor core buckling were included.

In comparing the various materials for sandwich construction, beryllium is outstanding with respect to structural efficiency at all temperature and loading levels considered. However, these comparisons were only approximate at loadings which result in stresses in excess of the compressive yield strength for a particular material since plasticity effects were not included in these analyses. Prior analyses, including plasticity effects, have shown beryllium to be superior to all other construction materials of the types considered here, although the comparisons did not include the exact materials analyzed during the present series of analyses. For use to maximum temperatures in the 394°K (250°F) range magnesium alloys have structural efficiencies about 25% higher than aluminum alloys; but because of their higher yield strengths, the aluminum alloys can be used to loading intensities which are approximately twice as high as those for magnesium alloys. Therefore, if optimum advantage is to be taken of magnesium alloys, they would be used in lightly loaded regions such as the forward section of the fuselage and the outer wing panels. In the lower temperature range, the aluminum and magnesium alloys are substantially more efficient than the titanium alloys, alloy steels or superalloys. For operation in the 533°K (500°F) to 588°K (600°F) range, the titanium alloys are superior to the alloy steels and superalloys, having an advantage of about 25%.

The trends for the ring-stiffened shells were generally similar to those found for the sandwich shells, although the sandwich construction is much more efficient at any particular loading index. The stringer and ring stiffened shells were the most efficient type of construction and permitted high loading intensities to be reached for the various candidate materials. Efficiency trends among material classes were the same as for the other types of shells.

With respect to narrowing the choice of materials within an alloy class, the parametric analyses indicated relatively small differences. This made the choices difficult, but it suggested that the particular choice within an alloy class was not particularly critical for the preliminary design studies of this project. Depending upon the type of construction, the 7475 aluminum alloy is from 2% to 7% more efficient than the others. The relative merits of the two magnesium alloys and the three titanium alloys are very close within each class. In the alloy steel and superalloy classes 17-7 PH is up to 5% more efficient than the other candidates. Beryllium is about 30% more efficient than lockalloy. While it was difficult to make clear choices of a single candidate from each of the classes of construction material the following choices were made for further analytical studies:

1. 2021-T81 Aluminum Alloy
2. 7475-T76 Aluminum Alloy
3. AZ31B-H24 Magnesium Alloy
4. 6Al-4V Titanium Alloy

5. 250 M Maraging Steel
6. Beryllium
7. Boron/Aluminum

It should be noted that the choices were made on the basis of being representative, and having desirable characteristics in addition to structural efficiency, and NOT on maximum structural efficiency alone. Future studies are likely to yield slightly superior structural performance than indicated by these studies.

Two aluminum alloys were selected, 2021-T81 because of representative properties and weldability and 7475-T76 because of its good structural efficiency and high fracture toughness. The AZ31-H24 magnesium alloy was chosen over HK31A-H24 because of its slightly higher efficiency when used in stringer and ring stiffened construction and because its somewhat higher compressive yield permits it to be used at higher loading intensities. The 6Al-4V alloy of titanium was selected as being typical of the class and because of the extensive data and experience with this alloy. The maraging steel was chosen to represent this higher density class of materials because of its weldability, good fracture toughness characteristics, similarity to the 10 Ni types being developed, and its representative structural efficiency, being somewhat lower than 17-7 PH and slightly higher than Inconel 718. Beryllium was chosen over Lockalloy despite its somewhat lower yield strength because of its substantially higher structural efficiency. The boron/aluminum composite was not compared parametrically to other composite materials; it was chosen on the basis of its developmental status which might make it a viable candidate for the 2,000 time frame for aircraft design and development. Other metal matrix composites are emerging but their availability is projected to be about 10 years later than boron/aluminum when considering the sheet sizes and quantities needed for a hypersonic transport fleet; however, this might change, depending on developmental emphasis, so that the graphite/aluminum might be a better choice because of its higher thermal conductivity.

While structural considerations are of primary concern when construction materials are compared, the use of active cooling implies temperature gradients, thermal stresses and coolant passage spacing. A comparison of passage spacing is provided below for sheets of equal weight and thermal stresses equal to 15% of the compressive yield strength. Aluminum alloys are the obvious choice with the stainless steels least attractive. Metal matrix composites were not compared because of property dependence on fiber orientation content, but such materials would be between beryllium and titanium with the graphite reinforced near the former and the boron reinforced near the latter.

| Material | Thickness (mm) | Spacing at Heat Flux* Indicated, cm | | | |
|-----------------|-------------------|-------------------------------------|------|------|------|
| | | 1.1 | 3.3 | 11.0 | 33.6 |
| Aluminum | 1.3 | 8.26 | 5.07 | 2.52 | 1.57 |
| Beryllium | 2.0 | 5.60 | 3.56 | 1.78 | 1.09 |
| Magnesium | 2.0 | 6.90 | 4.35 | 2.19 | 1.37 |
| Titanium | 0.8 | 2.92 | 1.83 | 0.92 | 0.51 |
| Stainless Steel | 0.5 | 1.83 | 1.09 | 0.59 | 0.38 |

*W/cm²

| Material | Thickness (in.) | Spacing at Heat Flux* Indicated, in. | | | |
|-----------------|--------------------|--------------------------------------|------|------|------|
| | | 1.0 | 3.0 | 10.0 | 30.0 |
| Aluminum | 0.05 | 3.30 | 2.00 | 1.00 | 0.62 |
| Beryllium | 0.08 | 2.20 | 1.40 | 0.70 | 0.43 |
| Magnesium | 0.08 | 2.72 | 1.72 | 0.86 | 0.54 |
| Titanium | 0.03 | 1.15 | 0.72 | 0.36 | 0.23 |
| Stainless Steel | 0.018 | 0.72 | 0.43 | 0.23 | 0.15 |

*BTU/ft² sec

For the analysis leading to the above results the coolant inlet and outlet temperatures were 283 and 366° K (50 and 200° F) respectively. Maximum skin temperatures were varied from 394 to 556° K (250 to 450° F) depending upon the material being analyzed.

PANEL DESIGN STUDIES

In an actively cooled airframe the skin panels must satisfy two sets of requirements, high structural efficiency and an integral capability for heat removal. Panel design characteristics defined by one set of requirements can adversely influence the second set. Because of the necessity for meeting both sets of requirements in an efficient manner, studies were conducted of thermal and structural concepts, as discussed in this section.

Concepts

Thermal. - Four basic skin panel thermal design concepts were considered for use on actively cooled airframe assemblies:

- | | |
|------------------------|--------------------------------|
| (1) Tubular | (3) Sphere-core sandwich |
| (2) Plate-fin sandwich | (4) Plain/cooled substructure. |

As shown in Figure 8, there are a number of variations for each concept. The tubular approach, using either a dual sheet skin, a tube on a sheet, or a combination of both, Figure 8.A-1, was considered to be the baseline. It can be modified to include a redundant set of coolant circuits if three sheets or two sheets and tubing are employed rather than just two sheets. The passages may be alternately spaced as in Figure 8.A-2 or can be nested as illustrated in Figure 8.A-3. The former involves somewhat simpler forming but the latter minimizes the change in passage spacing when only one circuit is operating. In the dual operating mode concept, Figure 8.A-2 has a passage spacing equal to approximately 1/2 the spacing for single mode operation. Thus, the temperature gradient in the skin for dual mode operation is only about 1/4 of that for single mode operation. The redundancy is difficult to obtain with the tube-on-sheet design unless a serpentine design is used to avoid cross-overs. However, a serpentine configuration results in higher pressure drop and more coolant hold-up than parallel flow passages. The use of concept A-3 (Figure 8) results in a passage spacing increase equal to the width of the quarter round coolant passage when operation is shifted from dual to single mode; estimates indicated that the skin temperature gradient would increase by less than 50% even for high heat flux regions where spacings are small and passage widths are large.

The specific tubular arrangement used will depend upon the particular material of construction and the types of joining processes that are most appropriate for the construction material. The formed skin approach is relatively simple, but high peel stresses can exist at the joint between the sheets, and it is necessary that the construction be highly efficient and compatible with the coolant. Installation of tubing onto the structural skin separates the structural efficiency and chemical compatibility considerations but necessitates metallurgical joining which might limit or restrict material choices. By sandwiching the coolant passage tubing between two formed skins, the advantages of both concepts can be achieved while the high stresses in the joints near the coolant passage are reduced significantly. For adhesively bonded aluminum alloy tubular panels, in-house experimental evaluations demonstrated an increase in pressurization capability of nearly an order of magnitude when the sandwiched tube design was used. This concept also appears to be well suited to incorporation of crack arrestors in the form of wires or filaments adjacent to the tubes which should enhance the damage - tolerance of the cooled panel.

Variations of the plate-fin concept can also provide nonredundant or redundant skin panels. The somewhat greater thickness of this type of skin permits a reduction in the amount of substructure necessary to stabilize against buckling under design loads. However, this panel thickness cannot be particularly great because the weight of residual coolant contained within the skin assembly is

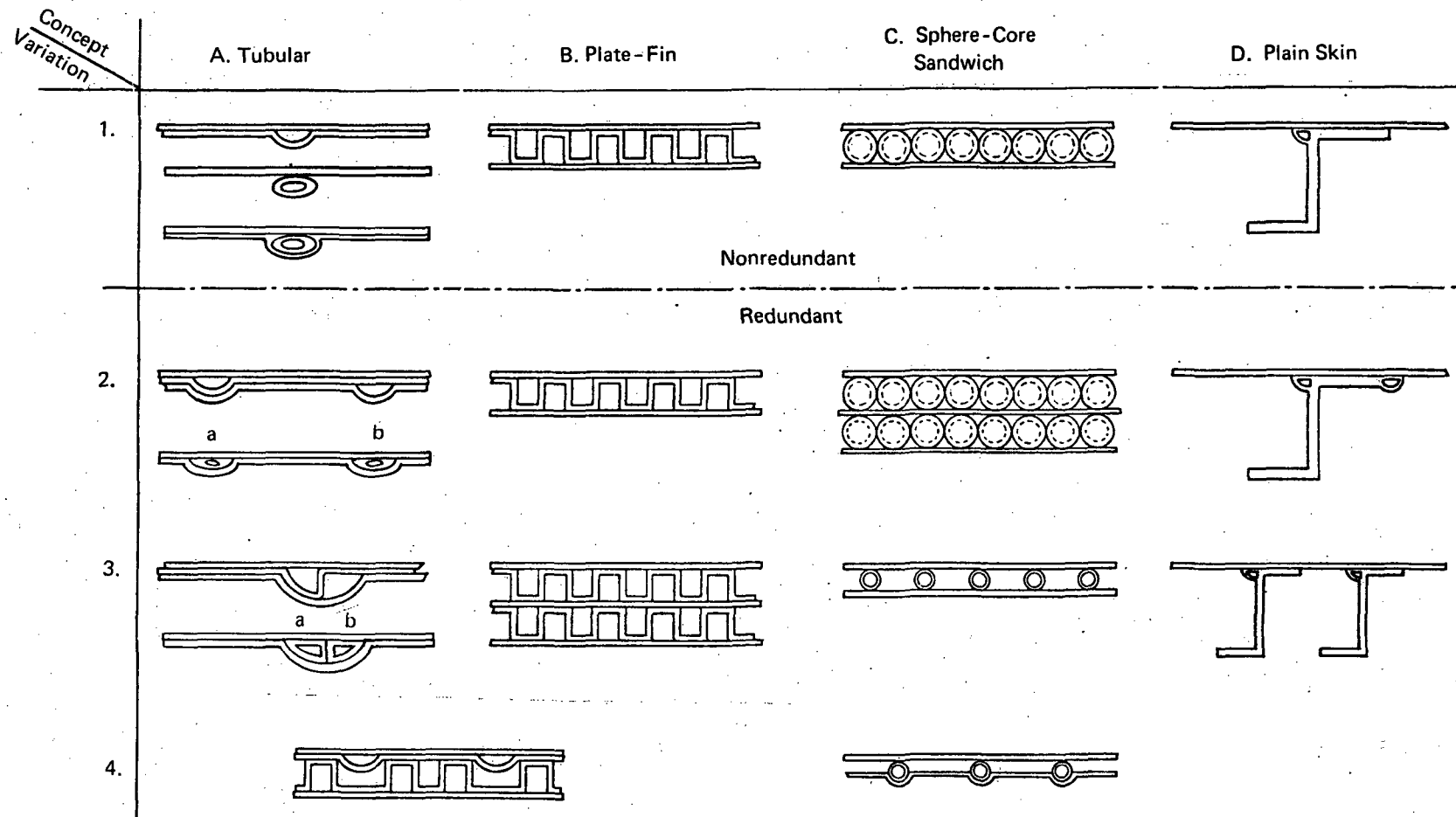


Figure 8. Nonredundant and Redundant Skin Panel Concepts

directly proportional to the sandwich thickness. Estimates suggested that thicknesses must be less than 2.54 mm (0.1 inch) if reasonable residual coolant weights, less than 2.4 kg/m^2 (0.5 psf), are to be obtained. Concept B-1 (Figure 8) utilizes parallel once-through flow since other studies have shown it to be the most effective in minimizing thermal stresses. Although concept B-2 (Figure 8) is similar schematically to B-1 (Figure 8), the flow is assumed to be contained in two independent networks of alternate passages established by proper manifolding at the ends of the panels. This variation results in very small passage spacings and small in-plane temperature gradients during single mode operation and no in-plane skin gradients of any consequence for dual mode operation. This characteristic of the plate-fin design permits a larger rise of transport coolant temperature than is possible with the discrete tubular passage concepts. The larger coolant temperature rise reduces the coolant flow rate which, in turn, reduces the weight of the cooling system distribution lines and pumps.

Another approach to redundancy is provided by Figure 8, concept B-3. Here, two plate-fin arrangements are stacked to provide continuous cooling across each level. However, if residual coolant weight is to be minimized, the total thickness of this approach must be about the same as for other plate-fin arrangements so that flexural rigidity to resist buckling tendencies will be similar. The weight will be greater in as much as the developed fin length for two sets of fins is greater than for one having twice the depth and also because an extra skin is required which is not particularly effective in increasing flexural rigidity.

It is also possible to combine the tubular and plate-fin approach as shown in concept AB-4 (Figure 8). An advantage of this approach is the simplified manifolding as compared to the strictly plate-fin concept while retaining the desirable large allowable temperature rise in the coolant during dual mode operation and during single mode operation with the plate-fin portion of the skin panel. If this larger coolant temperature rise is to be utilized during single mode operation with the tubular portion of the skin panel a higher than normal skin temperature must be tolerated because of the skin temperature gradient that will develop.

A disadvantage of the plate-fin concept is the difficulty of accommodating mechanical fastening and cutouts such as doors. However, it is expected that solutions to such problems can be found. For example, manifolding could be arranged to exclude flow from selected passages so that fasteners could be installed without regard to leakage. Other potential disadvantages of the various plate-fin concepts include sensitivity to crack growth which will cause leakage, and the relatively long heat flow path associated with the stacked configuration in the event of a malfunction of the outer coolant loop.

Although not as structurally efficient as honeycomb or truss core sandwich (to which the plate-fin is a close cousin) the sphere-core sandwich, Reference 39, appeared to be a potentially attractive approach for cooled structural skin. Since hollow spheres are used, the amount of residual coolant within the sandwich is less than 40% of the volume contained between the skins. For a similar weight of residual coolant the sphere-core sandwich can be about 2.5 times the thickness of the plate-fin panel, thereby increasing flexural rigidity and the spacing between substructural members. This should be helpful in reducing weight for the lightly loaded structure of the HST and HRA. Since structural loadings are relatively low the face skins will not be loaded to compressive yield and the difference in structural efficiency between the sphere-core, plate-fin, and honeycomb sandwiches should be minimized.

Primary disadvantages of the sphere-core sandwich include its sensitivity to skin cracks, the large number and potential cost of the spheres, and the complexity associated with accommodating mechanical fasteners and doors. With respect to mechanical fastening this concept is somewhat more flexible than plate-fin since all channels are interconnected. This same situation could be obtained for the nonredundant plate-fin or the stacked configuration if off-set fins were used rather than plain fins.

For the sphere-core sandwich, redundancy can only be achieved by stacking, concept C-2 (Figure 8), manifolding is expected to be at least as complex as that associated with stacked plate-fin configuration; somewhat greater complexity might be experienced because of the interconnected nature of the coolant flow.

Degenerate forms of the sphere-core sandwich are shown as concepts C-3 and C-4 (Figure 8) where the spheres have been replaced with cylindrical tubes so as to form separate coolant passages within the tubes and between the tubes. This reduces sensitivity to skin cracks. Somewhat simplified manifolding is anticipated with these concepts as compared to concept C-2 (Figure 8). The primary difference between concepts C-3 and C-4 (Figure 8) is the effective thickness. For a constant residual coolant volume it is expected that the flexural rigidity parallel to the tube will be greater for concept C-4 than for concept C-3 (Figure 8). However, neither of these variations are expected to be as efficient in resisting buckling than the basic sphere-core sandwich.

The plain skin concept, D-1 (Figure 8), is least sensitive to skin cracks but has disadvantages with respect to gradients within the skin. Analyses indicated that this approach was most suitable for low heat fluxes and that it was quite sensitive to contact resistance. Redundancy may be achieved by dual passages in a single stiffener, D-2, or by closely spaced stringers, D-3 (Figure 8). This latter approach may not be applicable except at the very lowest heating intensities. A relatively large number of connections may be required with this design approach. There may be design situations where it is desirable for the coolant passages and the stringers to have non-parallel orientations.

Coolant inlet and outlet connections are required for each panel as well as a means of distributing coolant flow uniformly through the coolant passages. A number of concepts and variations thereof are shown in Figure 9. These manifolding arrangements correspond to the panel concepts marked with identical alpha numeric codes in Figure 8. As shown in concept A-1 (Figure 9), the manifold and coolant passages are formed into one sheet which is joined to the smooth external airframe skin so that each skin panel of a nonredundant system requires only one inlet and one outlet despite the fact that there may be dozens of individual coolant passages in a skin panel. Redundant coolant passage designs, A-2 and A-3 (Figure 9), can be achieved by using two formed inner skins such that dual manifold and dual coolant passage networks are provided. For such redundant skin panels, two sets of inlets and outlets are required.

The plate-fin concept, B-1 (Figure 9), can be treated similarly in that an external manifold can be used at each end of the panel, with holes cut through the inner skin of the plate-fin sandwich to permit coolant to flow from the manifold to each individual passage. When the redundant coolant flow network concept involves connecting alternate coolant passages to different manifolds, the concept shown in B-2 can be used. If the stacked plate-fin sandwich concept is employed, manifolding the coolant becomes more complex. If the manifold design requires flat surfaces, a triangular truss core can be used to stiffen the flat sides and make them act as a sandwich, see Figure 9, B-3.

The manifold design approaches for the nonredundant and for the stacked redundant sphere-core sandwich are identical to those for the similar plate-fin sandwich design, as shown in C-1 and C-2 (Figure 9). When tubes are used as spacers for the inner and outer panel skins, it is possible to join all ends of the tubes to a tubular manifold while forming the manifold for the other passages integral with the inner skin, C-3 (Figure 9). Indentations in the tubular header allows coolant flow from the outboard manifold through the nontubular passages.

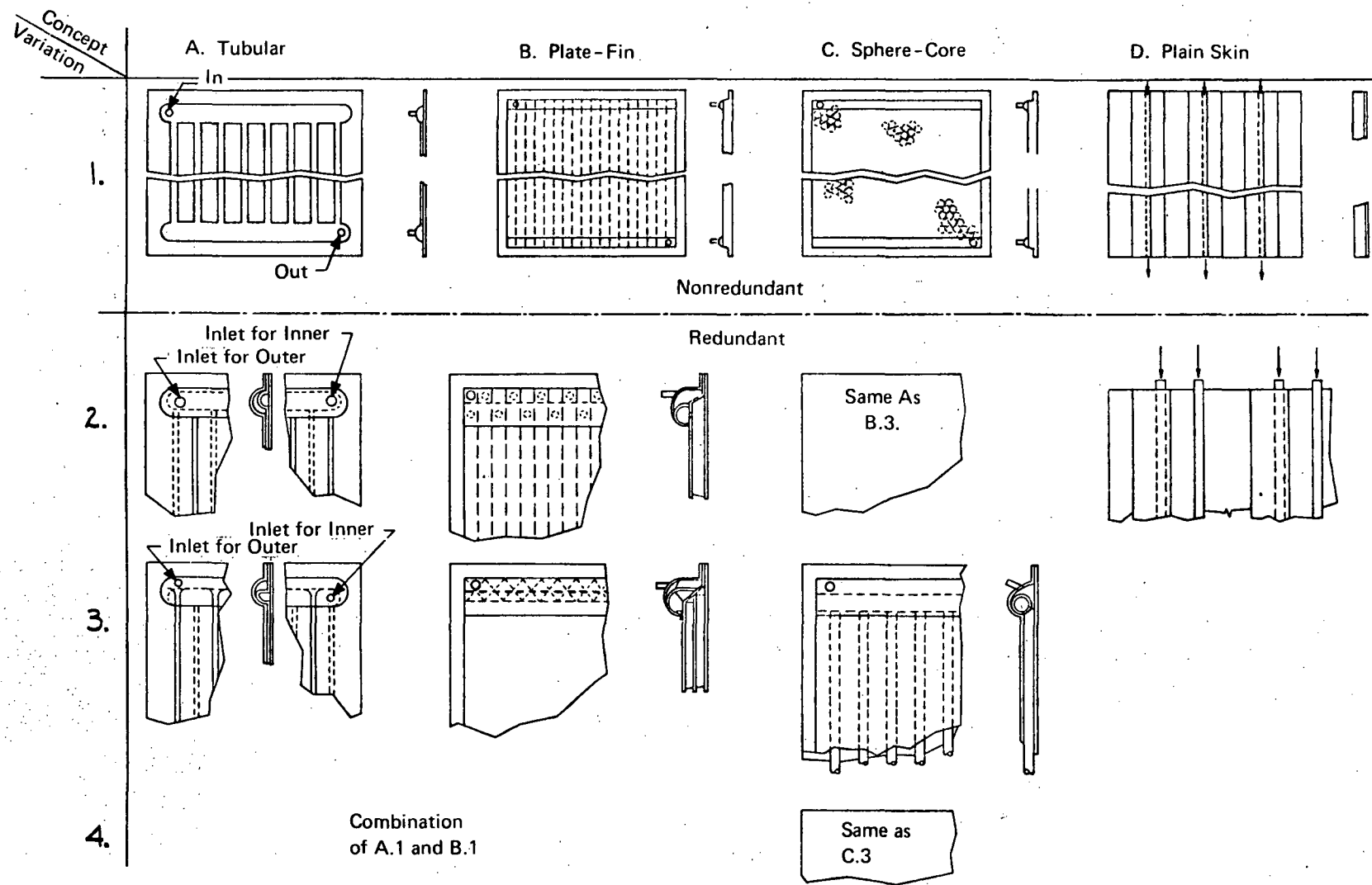


Figure 9. Manifold Arrangements for Parallel Flow in Nonredundant and Redundant Skin Panel Concepts

Connection of the coolant passages that are integrated with stringers is somewhat more difficult than manifolding coolant passages that are integrated with the skin. A relatively large number of individual joints will be required; a situation that is avoided with the other design concepts. The number of connections can be minimized by using long continuous stringers, but this tends to increase the weight of the residual coolant and/or the pumping power penalty due to the higher pressure drop associated with longer runs. The use of long continuous stringers may tend to dictate the location of the inlets and outlets to extreme locations on the structure of a relatively small airframe. This may have adverse influences on the weight of coolant distribution lines and/or the location of the heat exchanger and pump. As the aircraft size increases it will become impractical to employ full-length stringers, so that adverse influences associated with locations of inlets and outlets will be reduced. However, the number of connectors would increase. In the case of the HST, if stringer lengths of 30.5m (100 feet) are assumed, an estimated 1800 stringer connectors would be required for a non-redundant system, compared with about 300 panel connectors for the tubular skin baseline design discussed in Reference 3.

As indicated by the heat load and fuel flow comparisons of the section on Vehicle Data, the airframe cooling requirements exceed fuel flow heat capacity during some flight conditions for structural temperatures below about 560°K (550 F) for the hypersonic transport. While extra hydrogen could be carried to meet cooling requirements, such an approach is usually heavy. An alternate approach is that of reducing the heat load to the cooled structure by the introduction of insulation between the boundary layer and the cooled structure. Three such approaches are illustrated in Figure 10, an insulating coating, reusable surface insulation, and metallic heat shielding that radiates both to space and to the cooled structure. The heat load to the structure is reduced by 50% or more, depending upon radiant interchange characteristics.

The coating concept offers simplicity. Even a relatively thin layer of insulating material will reduce the heat load to the cooled structure. The reusable surface insulation concept would exploit the advances made as a result of the space shuttle efforts on lightweight ceramic insulating surface materials. Basic requirements include favorable thermal properties, mechanical strength, and strain compatibility with the load carrying airframe structure as well as moisture and erosion resistance. For a research airplane, the level of serviceability can be minimal, but becomes increasingly important as the need for high vehicle utilization increases, as for a commercial transport.

A more rugged external insulation is provided by metallic heat shields that prevent the hot boundary layer from contacting the cooled structure. The heat flux to the cooled structure is defined by radiant heat transmission from the heat shield and conduction through the heat shield supports. With this concept no intermediate insulation is used. The radiant heat transfer depends upon the relative temperatures of the heat shield and the structure as well as the absorptance and emittance characteristics of the two materials used.

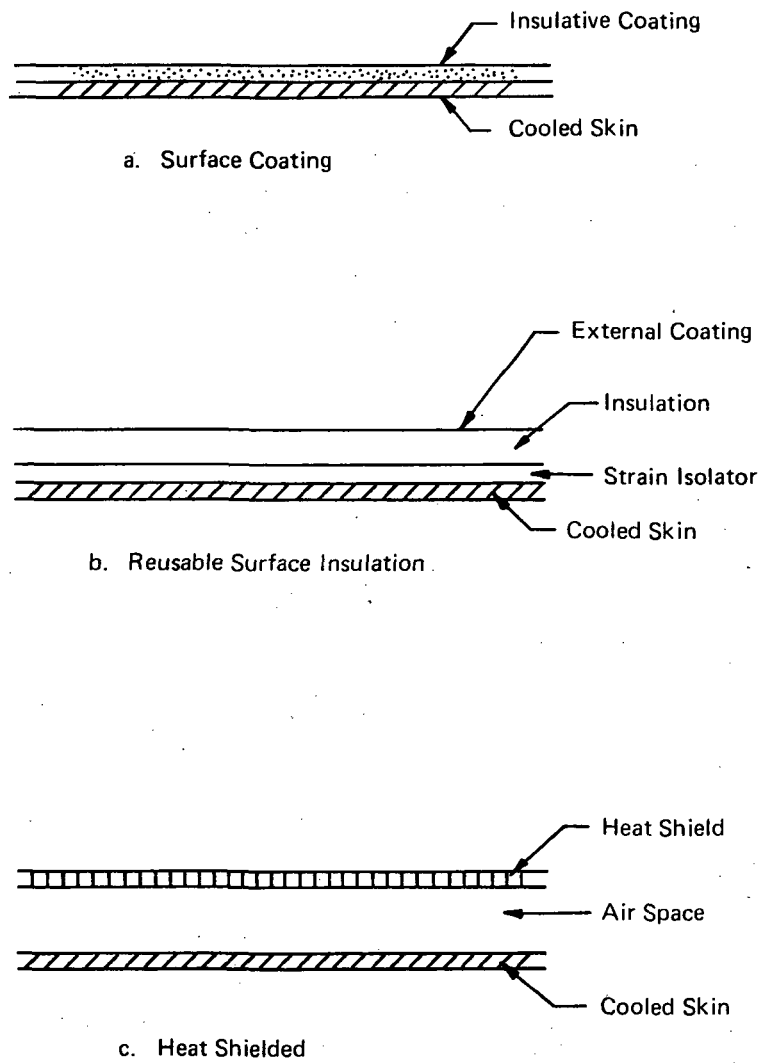


Figure 10. Insulated Panel Concepts

If either the reusable surface insulation or the radiative heat shield approach is used the weight of these auxiliary thermal protection elements should be considered as part of a thermal protection system weight. They would be used to reduce the absorbed heat load so that it would match the vehicle fuel flow under all flight conditions and thus to reduce the weight of the cooling system that would be required for an unshielded vehicle that required excess fuel just for cooling purposes. Figure 11 indicates the qualitative weight trends for a unit area (not for the total airframe). Increasing the insulation thickness decreases the heat load to the cooling system and reduces the weight of the cooling system. As the insulation thickness increases the total weight begins to rise. The same general trend is noted when heat shields are used in addition to insulation.

Structural. - The work of References 1 and 2 utilized very conventional airframe structure. Fuselage construction featured Z-stringer stiffened skin supported by frames, while for the wing the Z-stringer stiffened skin was supported by ribs and spars, in keeping with its purpose of examining a variety of coolant/cooling concept combinations. The promising potential of the cooled airframe warranted a more detailed examination of structural concepts to define a more nearly optimum structure, including possible variations in construction that might be dictated by differences in the loading intensity and the geometry of the major airframe components. Twenty-four skin stiffening concepts were considered on the basis of structural efficiency and relative complexity. The six shown in Figure 12 were selected as candidates for fuselage construction:

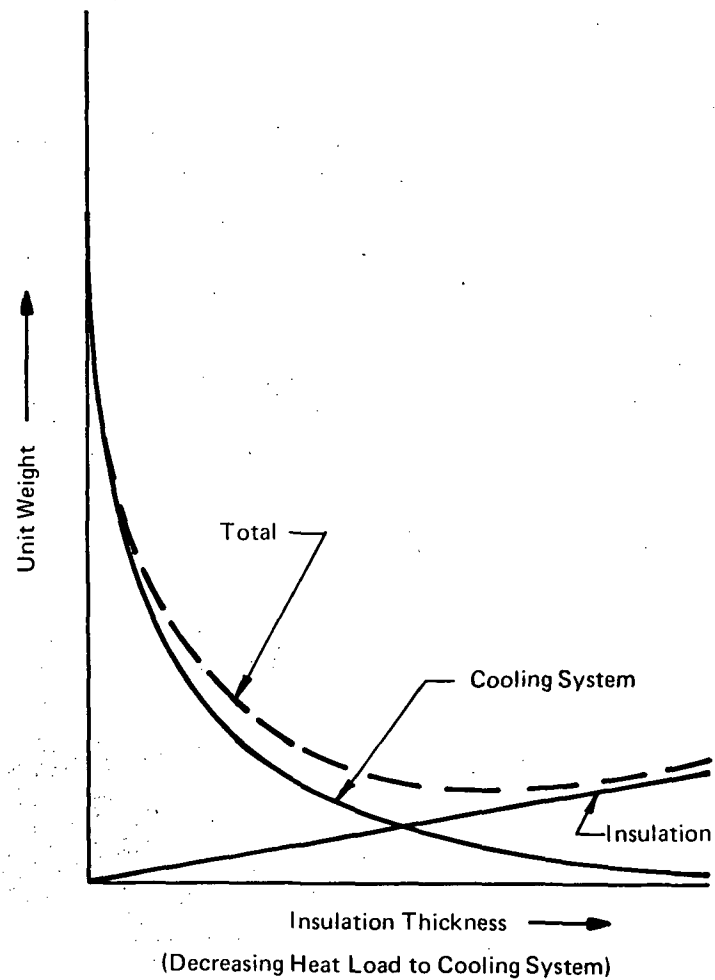
- (1) Ring-stiffened monocoque shell
- (2) Sandwich monocoque shell
- (3) Ring and Z-stringer stiffened shell
- (4) Ring and corrugated skin
- (5) Ring and symmetrical double-beaded skin
- (6) Ring and unsymmetrical double-beaded skin.

For the wing covers the following types of construction were compared in a preliminary manner as wide columns:

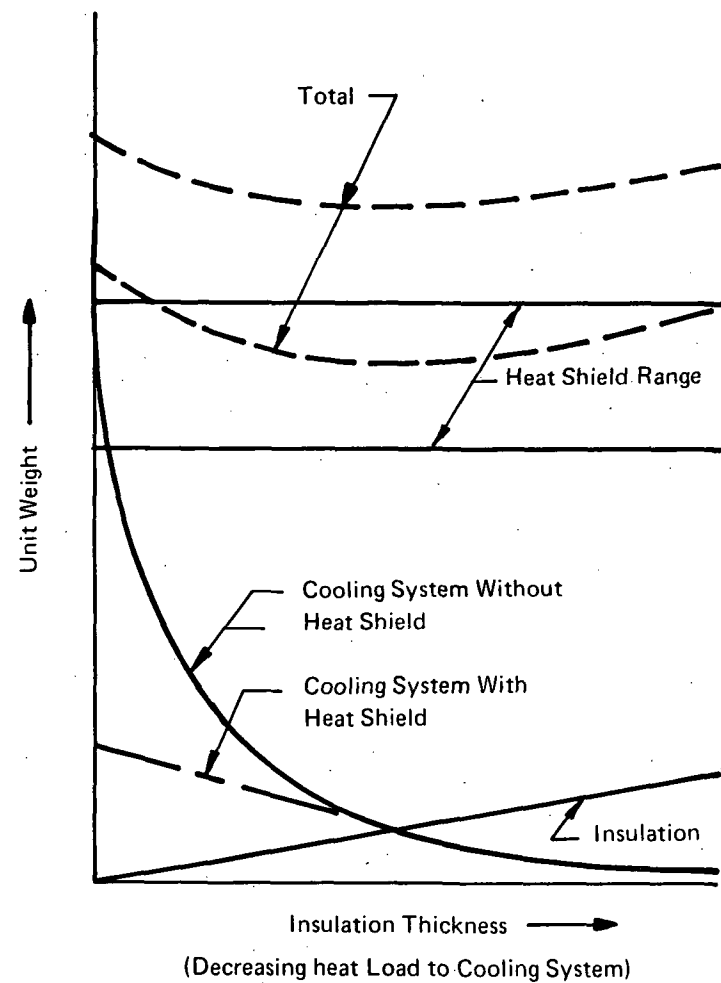
- (1) Honeycomb sandwich
- (2) Z-stringer stiffened
- (3) Symmetrical double-beaded skin
- (4) Unsymmetrical double-beaded skin.

Weights for the fuselage and wing structure are discussed in the section on Panel Design Studies subsection, Structural Analysis for a number of candidate construction materials.

The structural concepts described thus far do not reflect their use for a cooled airframe. Emphasis was on stiffening the skin to achieve minimum airframe weight. However, this is not the only important structural design consideration. Experience indicates a tendency for skin cracks to initiate from structural discontinuities such as fasteners and changes in cross section or panel stiffness. Obviously the growth of such cracks could be catastrophic for an actively cooled aircraft flying at hypersonic speed if the cooling system was drained of fluid. One means of minimizing such adverse effects is to introduce redundant coolant passages within the cooled skin panels as discussed in the Panel Design Studies section, under Concepts, Thermal. A structural approach for minimizing skin crack damage to the cooling system is to introduce crack arrestors near the coolant passages. Figure 13 illustrates a number of variations of this concept. The overlay material could be the same as or different from the skin construction. Adhesive bonding is probably preferable to mechanical fastening.



a. Cooling System and Insulation



b. Cooling System, Insulation and Heat Shield

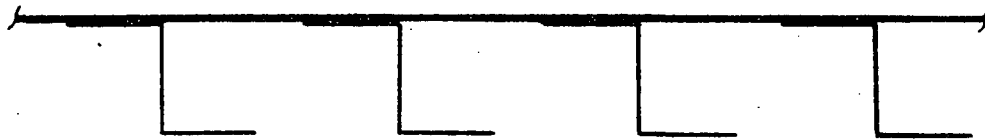
Figure 11. Qualitative Weight Trade for Insulated and Cooled Structure



A. Monocoque



B. Sandwich



C. Z Stringer



D. Corrugation



E. Symmetrical Double Bead



F. Unsymmetrical Double Bead

Figure 12. Candidate Constructions



a. Overlay



b. Metallic Strips



c. Composite Strips

Figure 13. Crack Stopping Techniques

Metallic strips could be bonded near the edge of the coolant passage, or composite strips could be installed. In all cases the objective is to decrease the stress at the tip of the crack before the crack causes leakage, thereby delaying crack growth sufficiently so that the crack can be found during air-frame inspection. The first two concepts are similar with the first involving fewer pieces of material while the second maximizes the amount of useful material at the locations of most benefit. The composite reinforcement has an additional potential advantage over the others in that the number of cycles required to propagate a crack through a multiplicity of elements may be greater than the number required for a single element of the same weight.

Thermal Analyses

As a means of assessing the relative merits of the many thermal concepts, a series of analyses was conducted. The analyses were parametric in nature and included the four cooled panel concepts (tubular, plate-fin, sphere-core, and plain skin/cooled stringer) as well as various insulative approaches (coatings, reusable surface insulation, and heat shielding). Except for the plain skin/cooled stringer and the coating approaches, the various concepts appeared to have potential merits for certain applications.

Baseline. - A series of parametric analyses was initiated to define the characteristics of cooled skin panels which incorporate discrete coolant passages, Concept A of Figure 8. The parameters of significance in the cooled panel design include:

- | | |
|--------------------------------|------------------------------|
| (1) Heat flux | (9) Coolant (properties) |
| (2) Panel area | (10) Passage spacing |
| (3) Panel aspect ratio | (11) Passage shape |
| (4) Skin thickness | (12) Passage width |
| (5) Skin material (properties) | (13) Passage height |
| (6) Maximum skin temperature | (14) Pressure drop |
| (7) Coolant outlet temperature | (15) Residual coolant weight |
| (8) Coolant inlet temperature | (16) Pumping power weight |

Ranges of variables were selected to encompass requirements of both the HST and the HRA. The heat flux, skin material, and skin thickness were combined as a heat input/conductance parameter, q/kt , so that results are applicable for a range of materials and thicknesses.

Typical results, for glycol/water, are presented in Figures 14, 15, and 16 as passage spacing minus passage width as a function of the coolant bulk temperature and the heat input/conductance parameter q/kt . For these three curves, the maximum skin temperature is 450°K (350°F), the coolant inlet temperature is 254°K (0°F), the outlet temperature is 366°K (200°F), and a plain semicircular passage is assumed. Thus, the coolant bulk temperature increases in the flow direction. Figures 14, 15, and 16 all indicate that for large values of q/kt the minimum passage spacing may be at the inlet end of the panel rather than at the outlet. This will be discussed later. Each curve is for a different unit pressure drop, so that the results are insensitive to panel length to a first approximation. Examination of curves show striking and subtle trends. The space between passage edges decreases quite rapidly as heat flux is increased or as thermal conductivity and/or skin thickness is decreased. For low values of q/kt , the space decreases as the bulk temperature increases; that is, as the skin temperature

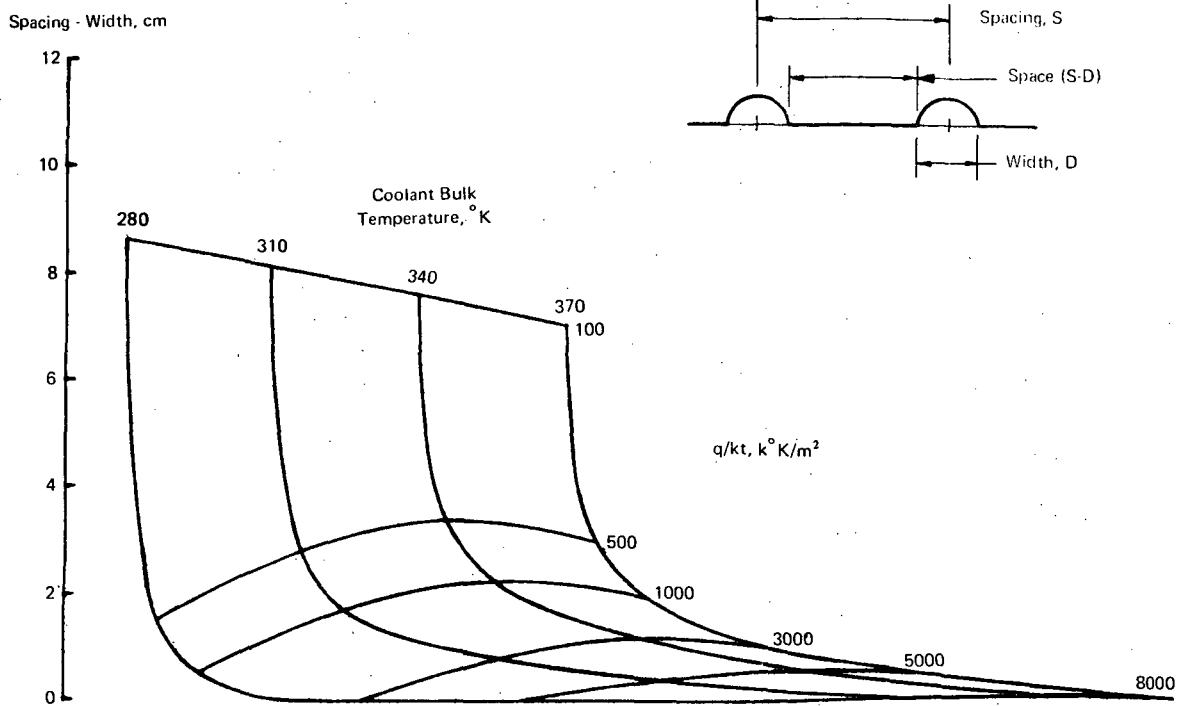


Figure 14a. Parametric Coolant Passage Spacing Data, Water Glycol, Maximum Skin Temperature $450^{\circ}K$, $\Delta P/L = 11.3 \text{ kN/m}^2/\text{m}$, Semicircular Passage, Coolant Temperature Rise = $366^{\circ}K$, Coolant Inlet Temperature = $254^{\circ}K$

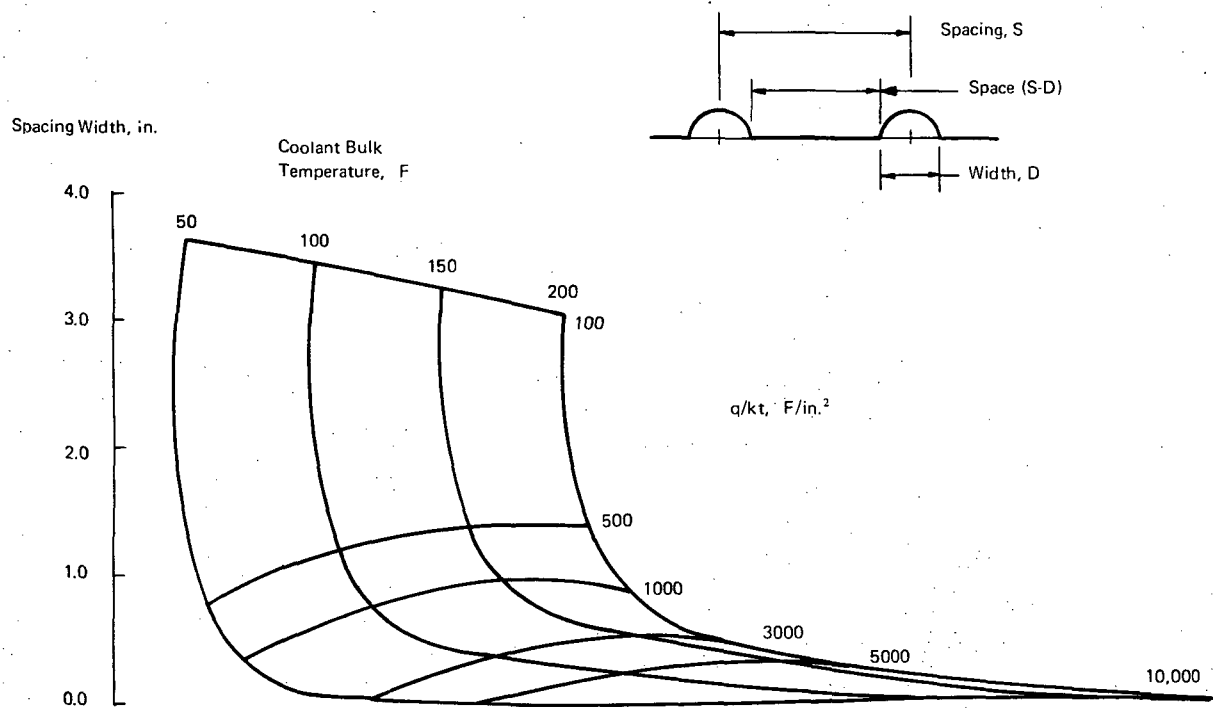


Figure 14b. Parametric Coolant Passage Spacing Data, Water Glycol, Maximum Skin Temperature $350^{\circ}F$, $\Delta P/L = 0.5 \text{ psi/ft}$, Semicircular Passage, Coolant Temperature Rise = $200^{\circ}F$, Coolant Inlet Temperature = $0^{\circ}F$

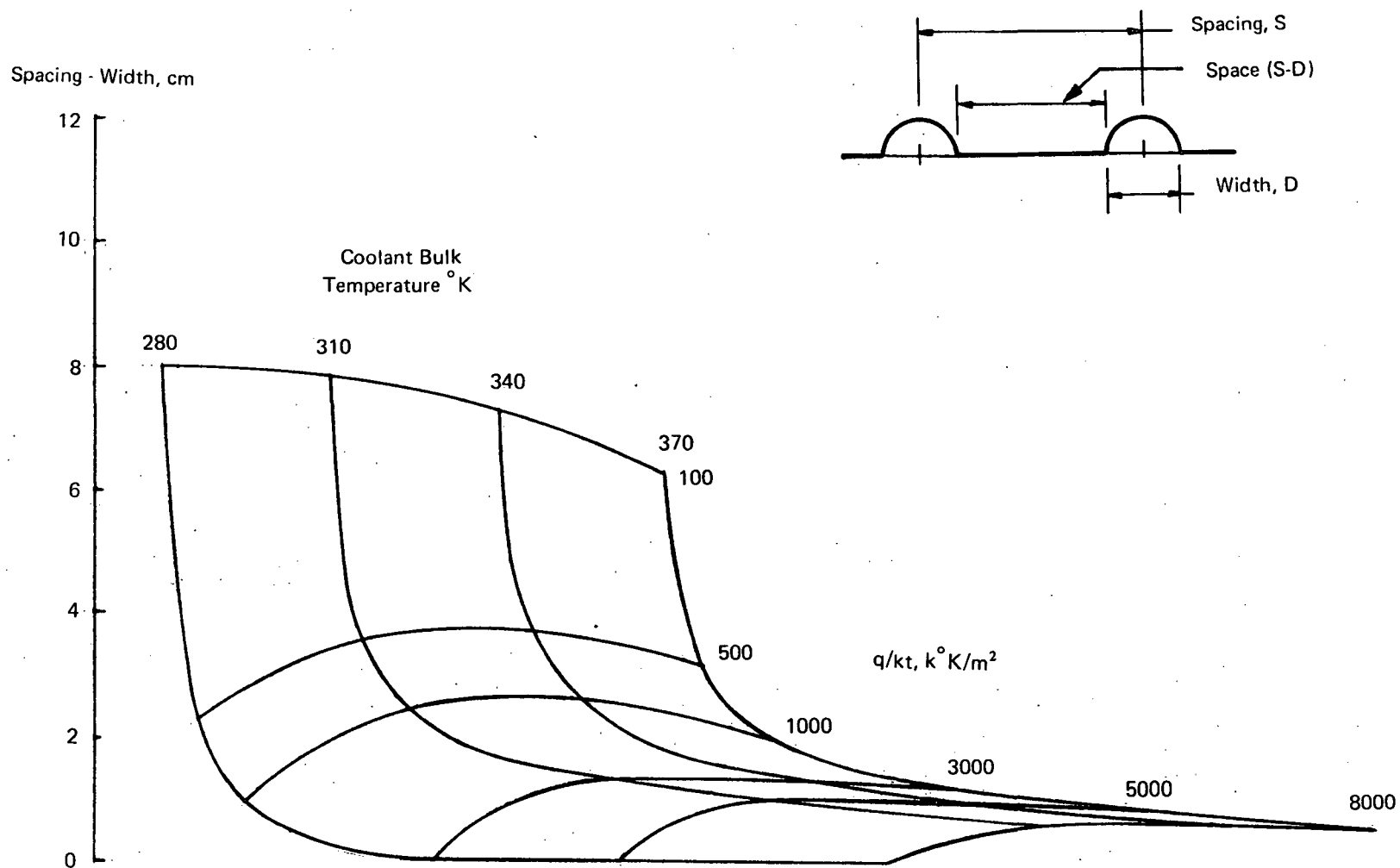


Figure 15a. Parametric Coolant Passage Spacing Data, Water Glycol, Maximum Skin Temperature $450^{\circ}K$, $\Delta P/L = 45.2 \text{ kN/m}^2/\text{m}$, Semicircular Passage, Coolant Temperature Rise = $366^{\circ}K$, Coolant Inlet Temperature = $254^{\circ}K$

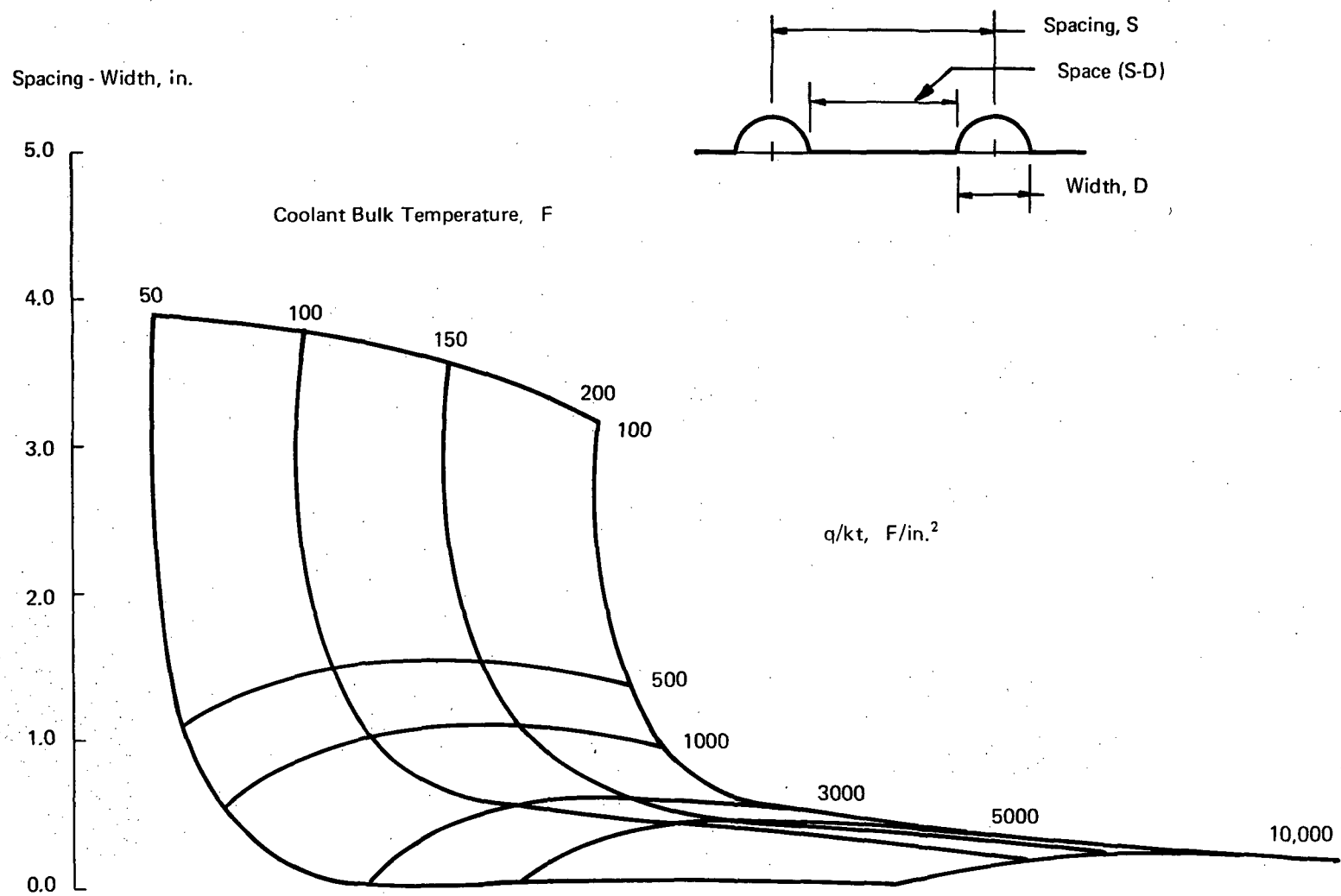


Figure 15b. Parametric Coolant Passage Spacing Data, Water Glycol, Maximum Skin Temperature 350°F, $\Delta P/L = 2.0$ psi/ft, Semicircular Passage Coolant Temperature Rise = 200°F, Coolant Inlet Temperature = 0°F

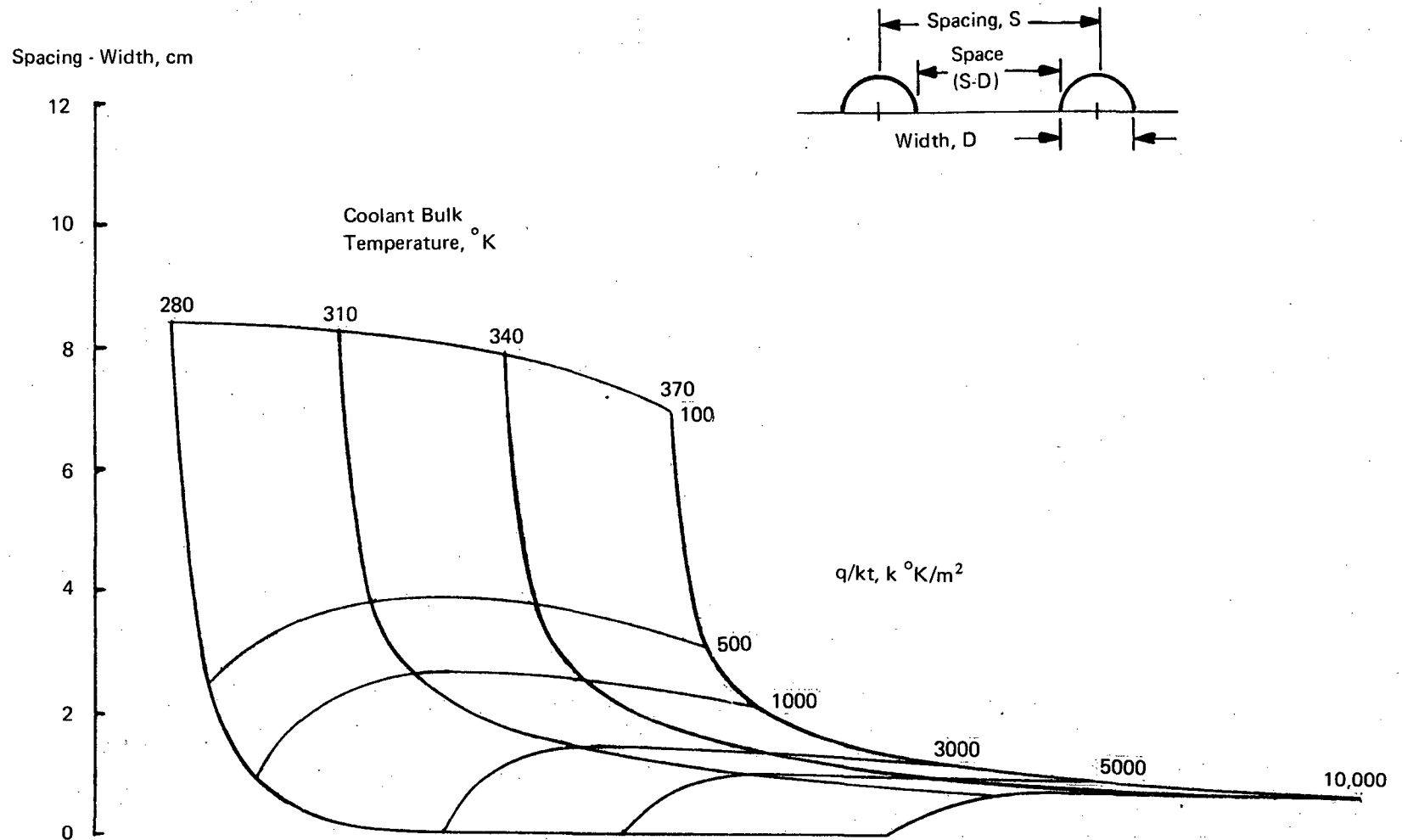


Figure 16a. Parametric Coolant Passage Spacing Data, Water Glycol, Maximum Skin Temperature 450°K , $\Delta P/L = 113 \text{ kN/m}^2/\text{m}$, Semicircular Passage, Coolant Temperature Rise = 366°K , Coolant Inlet Temperature = 254°K

Spacing - Width, in.

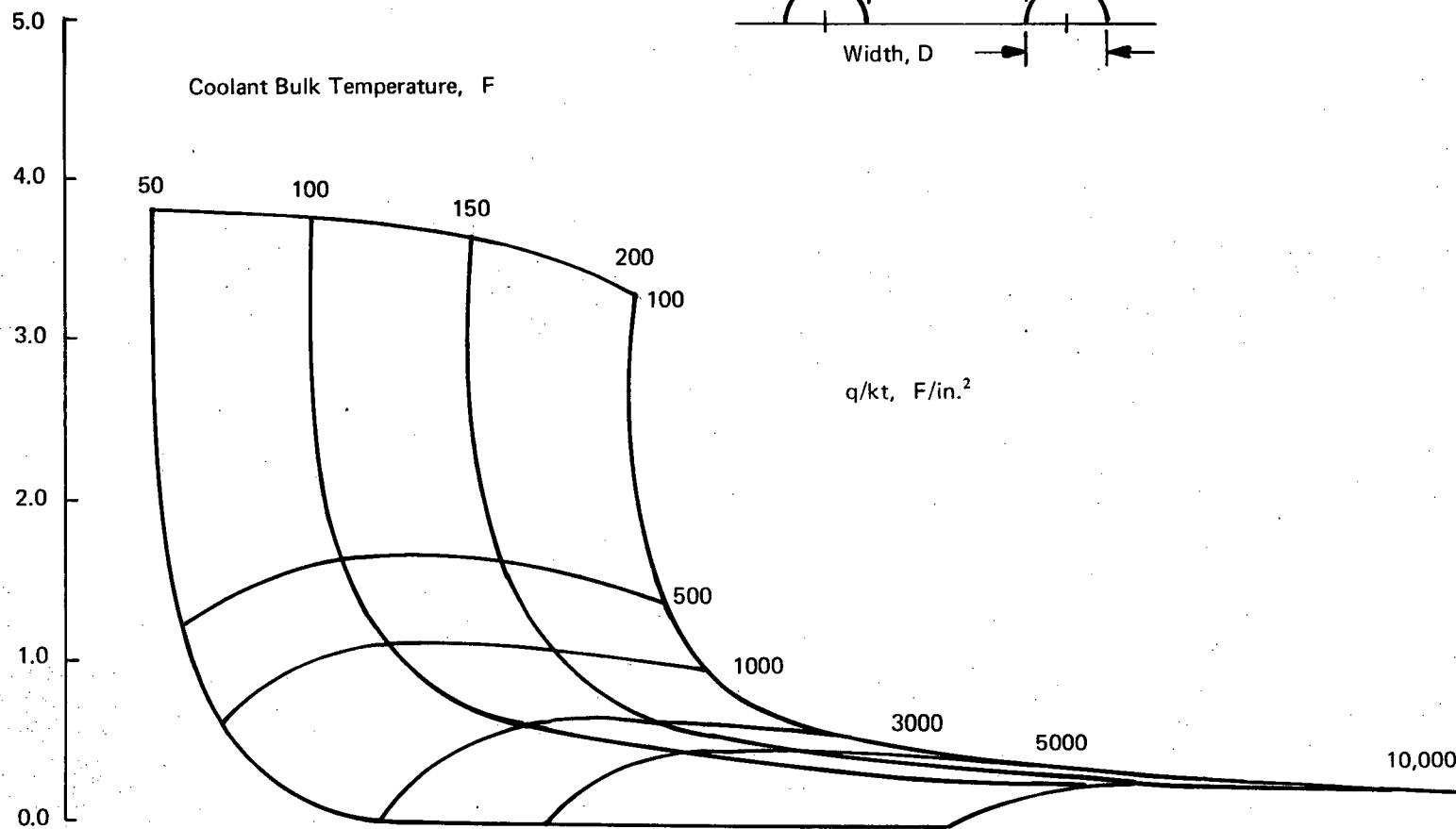


Figure 16b. Parametric Coolant Passage Spacing Data, Water Glycol, Maximum Skin Temperature 350°F, $\Delta P/L = 5.0$ psi/ft, Semicircular Passage, Coolant Temperature Rise = 200°F, Coolant Inlet Temperature = 0°F

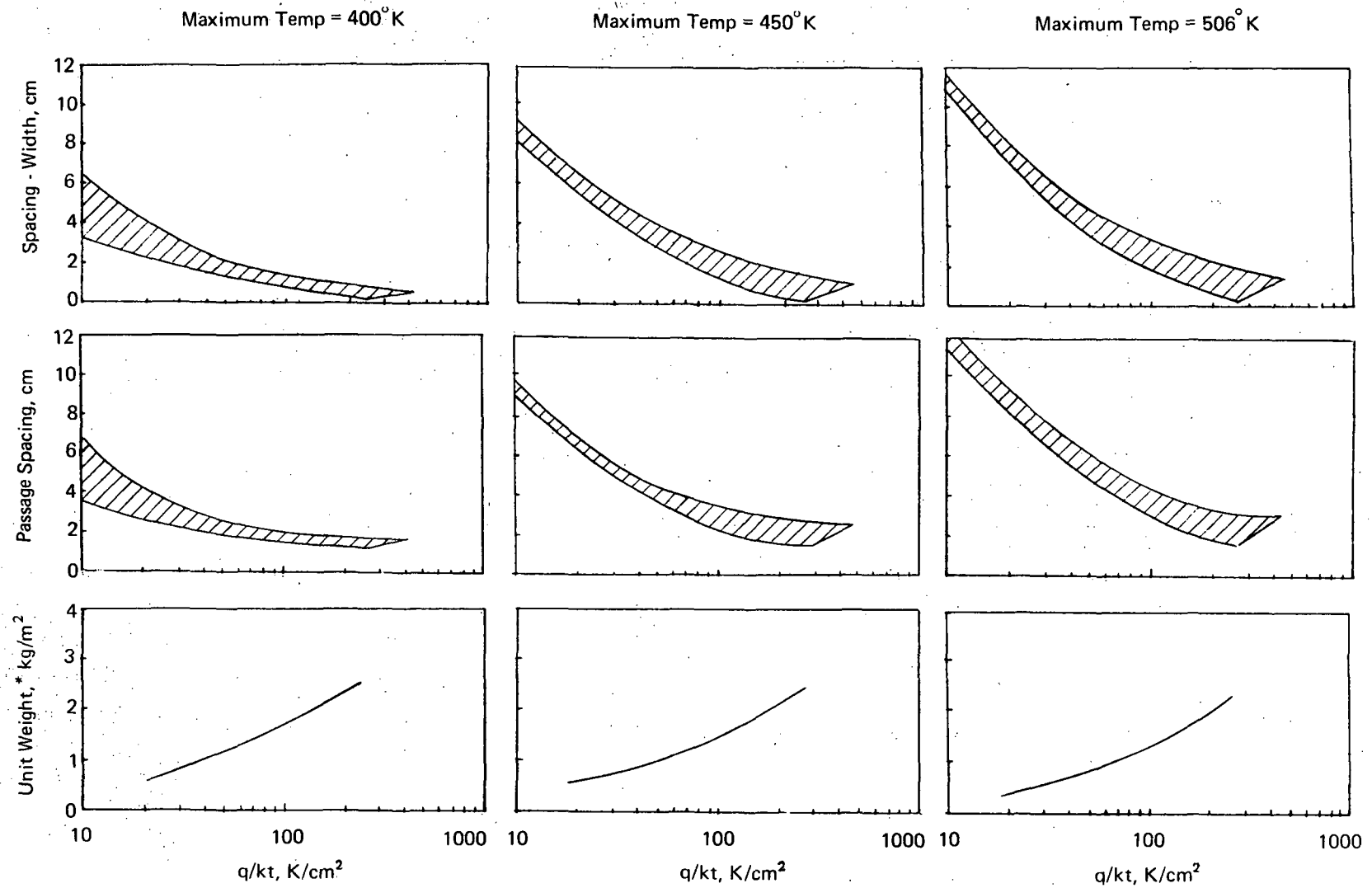
gradient is reduced. For high q/kt values the opposite tends to be true and a maximum appears to exist. This rather strange shape (for constant values of q/kt) is related to the flow conditions which range from laminar through transition to turbulent.

It can also be noted that for pressure drops per foot above about $45.2 \text{ kN/m}^2/\text{m}$ (2.0 psi/ft) the space between passages is no longer a function of pressure drop for values of q/kt above $0.43 \text{ M}^\circ\text{K/m}^2$ (500°F/in^2) and is only a weak function of pressure drop per foot at low values of q/kt . However, the pressure drop influences the pumping power penalty and the quantity of residual coolant within the passages. The passage width is reduced by about 60% as the pressure drop increases from $11.3 \text{ kN/m}^2/\text{m}$ (0.5 psi/ft) to $450 \text{ kN/m}^2/\text{m}$ (20 psi/ft). Residual coolant weight decreases even more rapidly as the pressure drop is increased with reductions of about 50% and 80% from $11.3 \text{ kN/m}^2/\text{m}$ (0.5 psi/ft) to $45 \text{ kN/m}^2/\text{m}$ (2.0 psi/ft) and $450 \text{ kN/m}^2/\text{m}$ (20 psi/ft), respectively. The weight tradeoff between residual coolant and pumping power penalty (fuel) appears to optimize at about $113 \text{ kN/m}^2/\text{m}$ (5 psi/ft) in a rather flat manner.

As noted in Figures 14 through 16, at low heat fluxes the (s-d) value decreases with an increase in bulk temperature whereas at high heat fluxes a maximum is reached as bulk temperature is increased. At low heat fluxes the internal heat transfer coefficient is not critical, hence the effect of a variation in viscosity due to a change in coolant bulk temperature has only a slight effect and the difference between the coolant bulk temperature and maximum surface temperature is controlling. At high heat fluxes, the viscosity has a significant effect and causes the (s-d) value to be quite small at the inlet. As the temperature increases the internal heat transfer coefficient increases and the spacing can increase until the temperature difference between the coolant bulk temperature and the maximum skin temperature begins to control at which time the spacing must decrease again. This trend for close passage spacing at the inlet end of a panel can be countered by: (1) a higher inlet temperature so that viscosity effects are minimized, (2) location of the inlet in a region of low heat flux to reduce the q/kt parameter, (3) increasing the thermal conductivity or thickness of the panel, or (4) providing extended surface area within the coolant passage. The second of these approaches usually involves the least impact on the total system since few long panels are subjected to a uniform heat flux. An alternative to any of the above design approaches is to vary the spacing of the coolant passage by using a technique similar to that shown in Reference 3 for a typical fuselage panel.

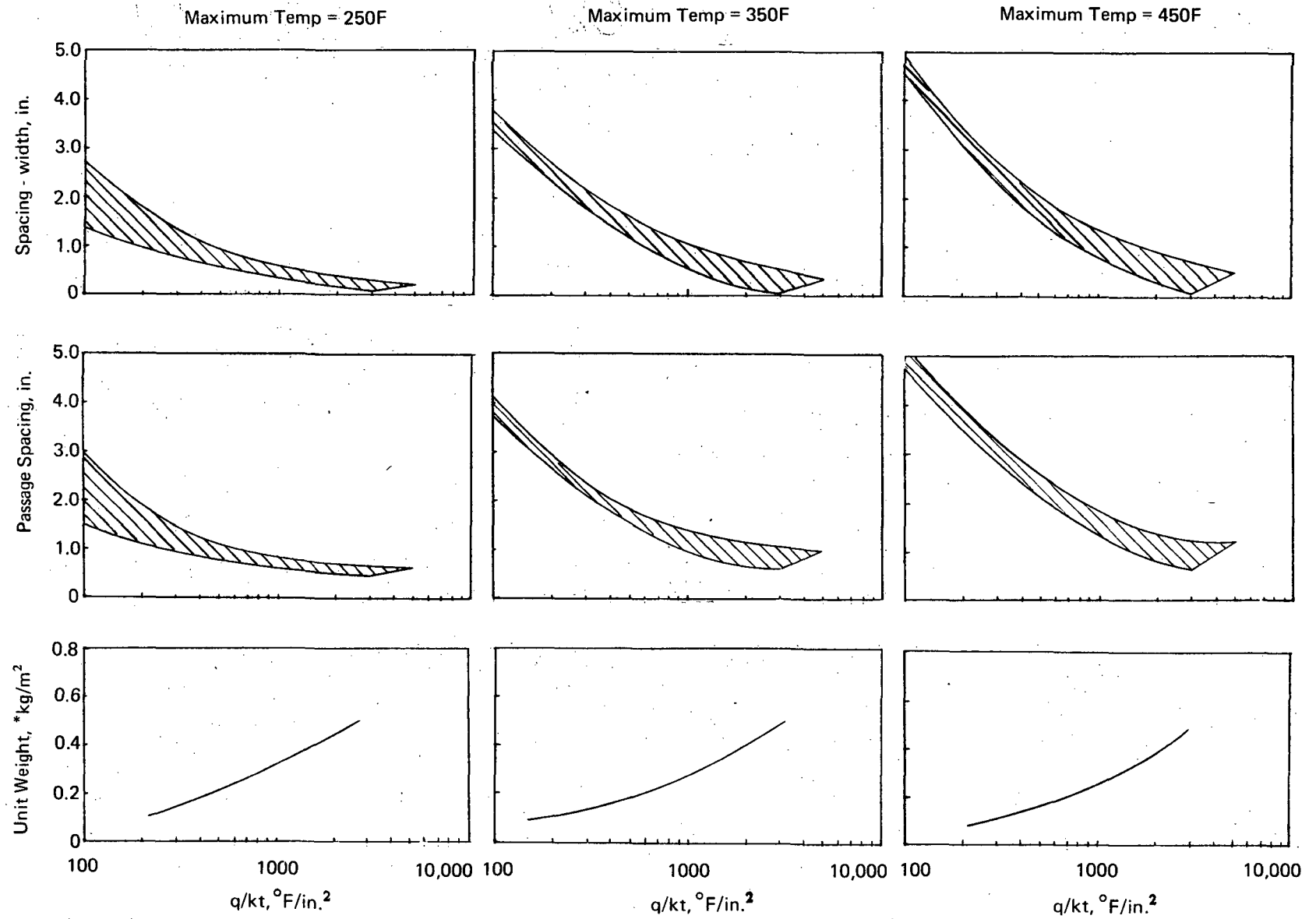
Passage spacing results are presented in Figures 17, 18, and 19 for selected coolants. The coolant temperature rise is 111°K , (200°F) and the outlet temperature is 366°K (200°F) for all of these plots. Figures 17 and 18 show the effect of wall temperature on both the passage spacing and (s-d) value for various heat flux levels with glycol/water and Coolanol 20 coolants. The band width accounts for variations in coolant bulk temperature and unit pressure drops along the panel. As the maximum surface temperature increases the difference between the bulk temperature and skin temperature increases, hence the effect of the internal heat transfer is smaller. This results in a much narrower band width as long as one particular type of flow is maintained. However, for the glycol/water, the high viscosity at the low temperature inlet end of the panel causes laminar flow with a resultant low heat transfer coefficient. This requires a closer spacing at the inlet end than at the outlet end particularly as higher maximum skin temperatures are used for higher heating intensities, hence the widening of the band of passage spacing for such combinations of parameters.

Comparing the results for each coolant at a constant maximum temperature, it is surprising to note that the absolute values of spacing and (S-d) are similar for high values of q/kt because for such conditions heat transfer coefficients tend to be high. At the lower values of q/kt the passage spacings are different for the various coolants because the differences in properties become greater in a relative sense. With respect to the various coolants it should be noted that coolanol 45 and Dow XF-1-3755 cannot be used at values of q/kt above about 90°K/cm^2 (1000 F/in^2) because there is no distance



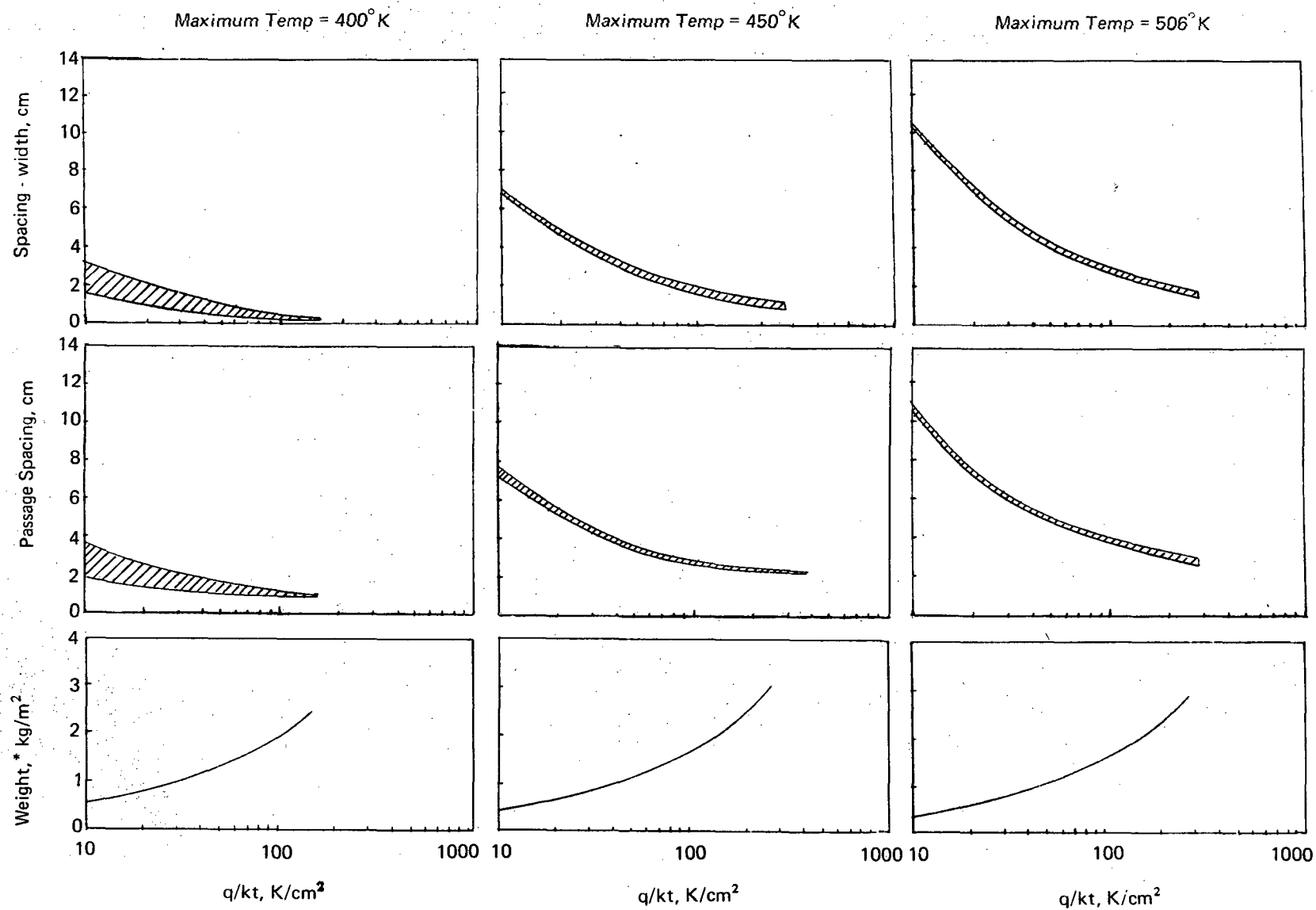
* Coolant in Panel Passages and Manifolds plus Pumping Power Penalty

Figure 17a. Coolant Passage Spacing Data, Water Glycol, Plain Semicircular Passage, Coolant Temperature Rise = 111°K, Coolant Inlet Temperature = 253°K



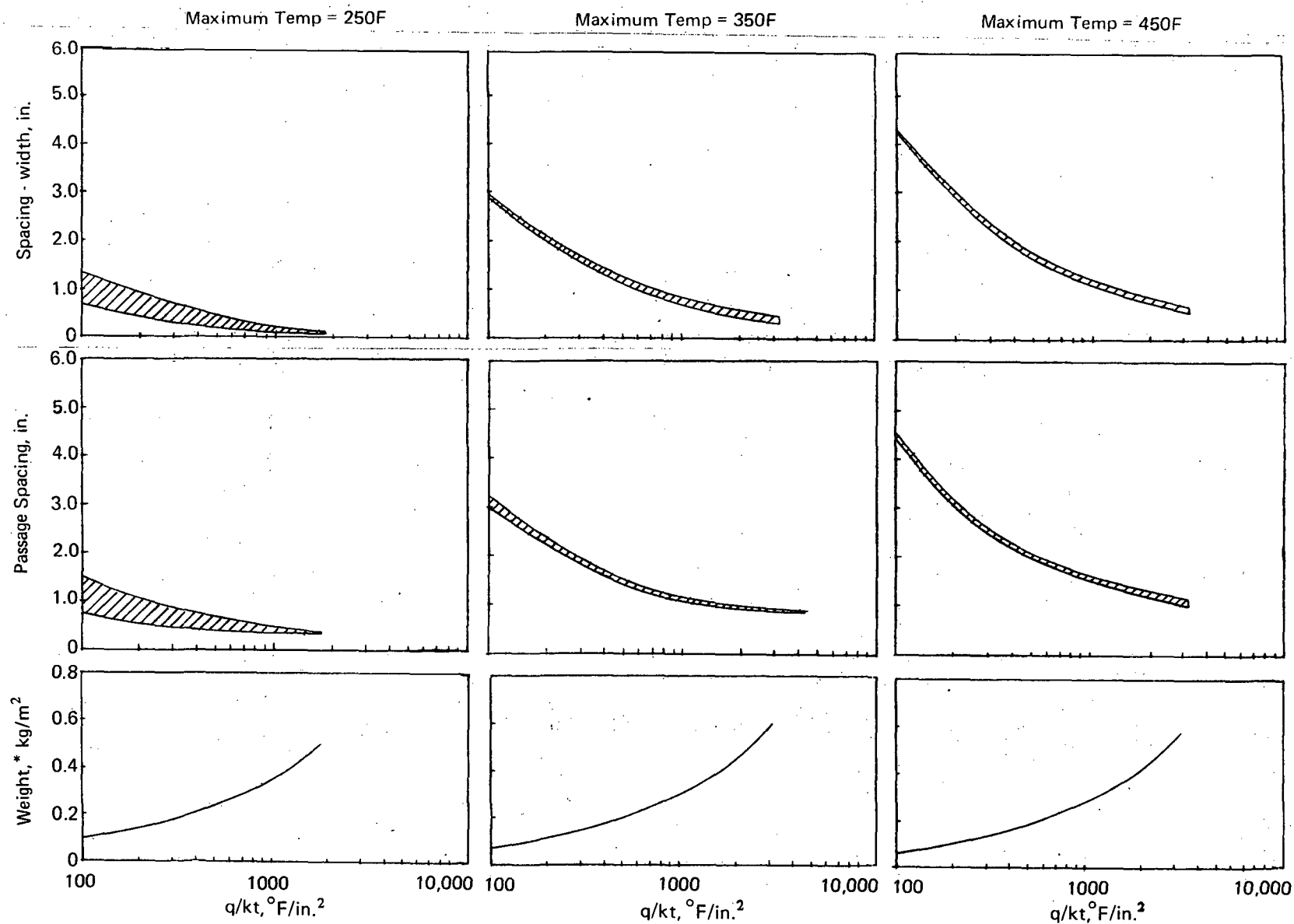
*Coolant in Panel Passages and Manifolding plus Pumping Power Penalty

Figure 1.7b. Coolant Passage Spacing Data, Water Glycol, Plain Semicircular Passage,
Coolant Temperature Rise = 200°F, Coolant Inlet Temperature = 0°F



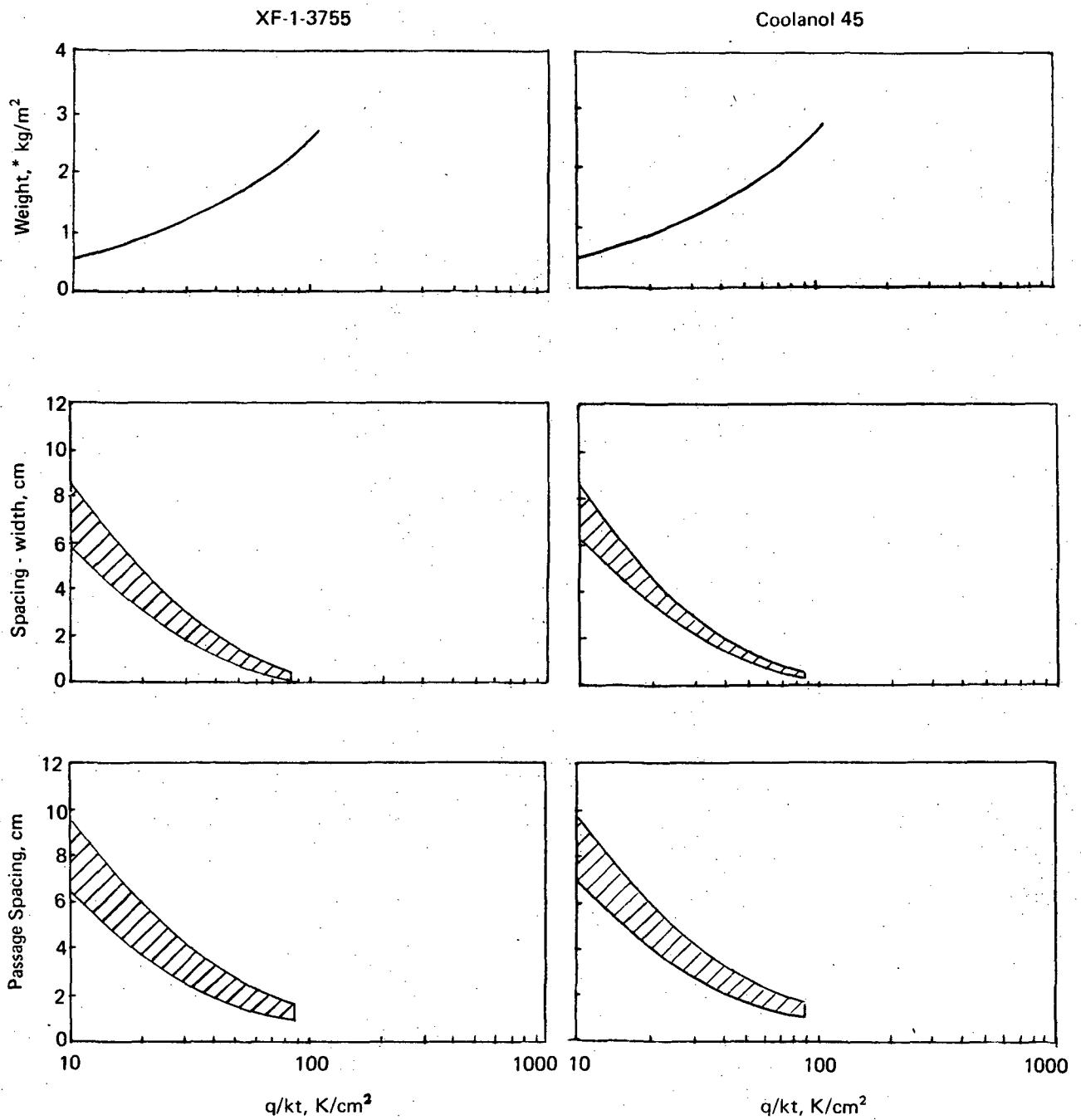
*Coolant in Panel Passages and Manifolds plus Pumping Power Penalty

Figure 18a: Coolant Passage Spacing Data, Coolanol 20, Plain Semicircular Passage, Coolant Temperature Rise = 111° K, Coolant Inlet Temperature = 253° K



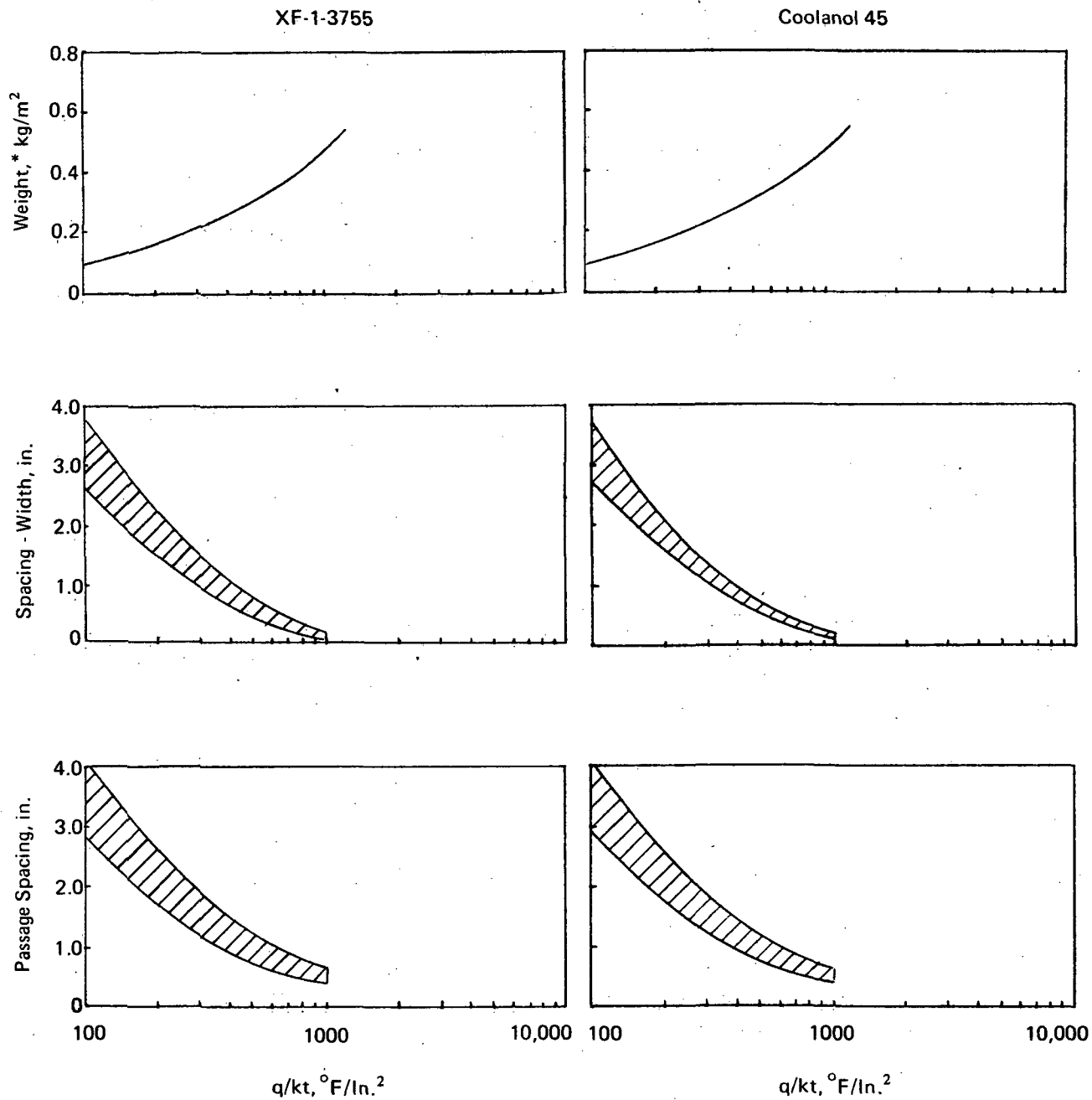
*Coolant in Panel Passages and Manifolds plus Pumping Power Penalty

Figure 18b. Coolant Passage Spacing Data, Coolanol 20, Plain Semicircular Passage, Coolant Temperature Rise = 200°F , Coolant Inlet Temperature = 0°F



*Coolant in Panel Passages and Manifolds plus Pumping Power Penalty

Figure 19a. Coolant Unit Weight and Passage Spacing Data, Maximum Skin Temperature = 506°K,
Plain Semicircular Passage, Coolant Temperature Rise = 111°K,
Coolant Inlet Temperature = 256°K



*Coolant in Panel Passages and Manifolds plus Pumping Power Penalty

Figure 19b. Coolant Unit Weight and Passage Spacing Data, Maximum Skin Temperature = 450F,
Plain Semicircular Passage, Coolant Temperature Rise = 200F,
Coolant Inlet Temperature = 0F

between the edges of adjacent passages. For Coolanol 20 and glycol/water such a limiting geometric condition will occur at values of q/kt ranging from about 200 to $1000^{\circ}\text{K}/\text{cm}^2$ (2000 to 10,000 F/in^2) depending upon maximum skin temperature and other design parameters.

The results presented in Figures 17, 18, and 19 can be used to obtain preliminary estimates of the weight of coolant contained in skin panels. For a design value of q/kt it is possible to read the corresponding values of the passage spacing and the spacing minus width. The passage spacing defines the number of passages per unit of panel width. The area of the coolant passage can be determined from the passage width, knowing that the passages are assumed to be hemispherical. The unit weight of the contained coolant can be estimated by summing the cooling passage cross-sectional area per unit of panel width, and then multiplying by a unit length and coolant density. Unit weights can be determined at a number of locations on the aircraft and integrated to obtain an estimate of the total weight of coolant contained in the skin panels. This preliminary estimate can be refined as the cooled airframe design is developed in greater detail.

Plate-Fin. - As the heat flux to the vehicle increases the passage spacing must decrease in order to maintain reasonable structural temperatures. In the limit no significant spacing remains between them and the plate-fin concept evolves. For an aluminum alloy skin of 1.0 mm (40 mils) the crossover from discrete passages to plate-fin appears to be about 34.3 W/cm^2 ($30 \text{ BTU/ft}^2/\text{sec}$). This transition heat flux can be altered by various design parameters such as skin thickness, allowable structural temperature, and maximum coolant temperature. While the plate-fin concept can be used to very high heat fluxes it is more difficult to integrate with substructure since mechanical fastening is more complicated, and it is sensitive to even very small skin cracks which result in leakage and loss of coolant.

The weight of plate-fin construction is minimized, from a thermal point of view, by defining the depth that minimizes the residual coolant and the pumping power penalty. If redundancy is desired, it is more appropriate for half of the coolant to flow through each of the plate-fins stacks (B3 of Figure 8), rather than to size each stack for total flow without pressure drop penalties at times of emergency. Further considerations of redundancy are discussed in "Cooling System Design Studies." Since the weight of the sheet material is not considered the weights of nonredundant and 50/50 flow - redundant panels are the same.

The weights and pressure drops for the optimum panels of various lengths are shown in Figures 20 and 21. The weight is only that of the thermal elements (fins, coolant contained in passages and manifolds, and APS fuel) and does not include the skins which were considered to be part of the structure. The pressure drop penalty associated with employing a greater number of fins per unit width is clearly evident especially at larger panel lengths. If large panels are to be used it may be desirable to employ larger than optimum fin heights so that the pressure drops can be reduced. The weight and pressure drop results suggest the use of relatively short panels in regions subjected to high heating intensities.

Figure 22 presents the maximum temperatures of aluminum alloy panels, optimized for 1.52 m (5 ft), 3.04 m (10 ft), and 6.08 m (20 ft) lengths, during single mode operation. For the five-foot length, the 15 FPI panel exceeds the design value of 450°K (350°F) at a heat flux of 31.6 W/cm^2 ($28 \text{ BTU/ft}^2/\text{sec}$) whereas the 35 FPI panel does not exceed the design value until a heat flux in excess of 56.6 W/cm^2 ($50 \text{ BTU/ft}^2/\text{sec}$) is achieved. This suggests the use of off-optimum panel designs with smaller passage heights, higher fin counts, and subsequently higher pressure drops. Reference to Figure 21 indicates that the pressure drop increases substantially from 0.41 MN/m^2 (60 psi) to 0.55 MN/m^2 (80 psi) as the fin count is increased from 15 to 35 per inch, but the weight increase is only 0.24 kg/m^2 (0.05 psf). For the 6.08 m (20 ft) panel maximum heat fluxes of

Unit Weight of Residual Coolant and APS Fuel, kg/m^2

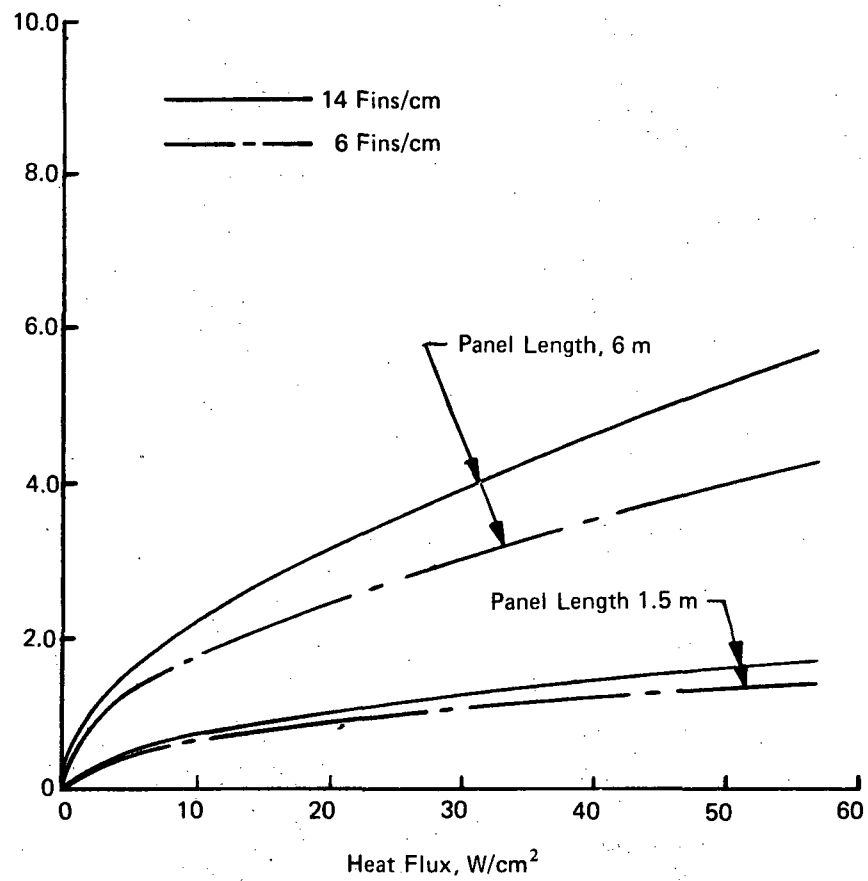


Figure 20a. Minimum Unit Weight for Plate Fin Panels, Ethylene Glycol/Water, Coolant in at 283°K /Out at 367°K

Unit Weight of Residual Coolant, Fins, and APS Fuel, psf

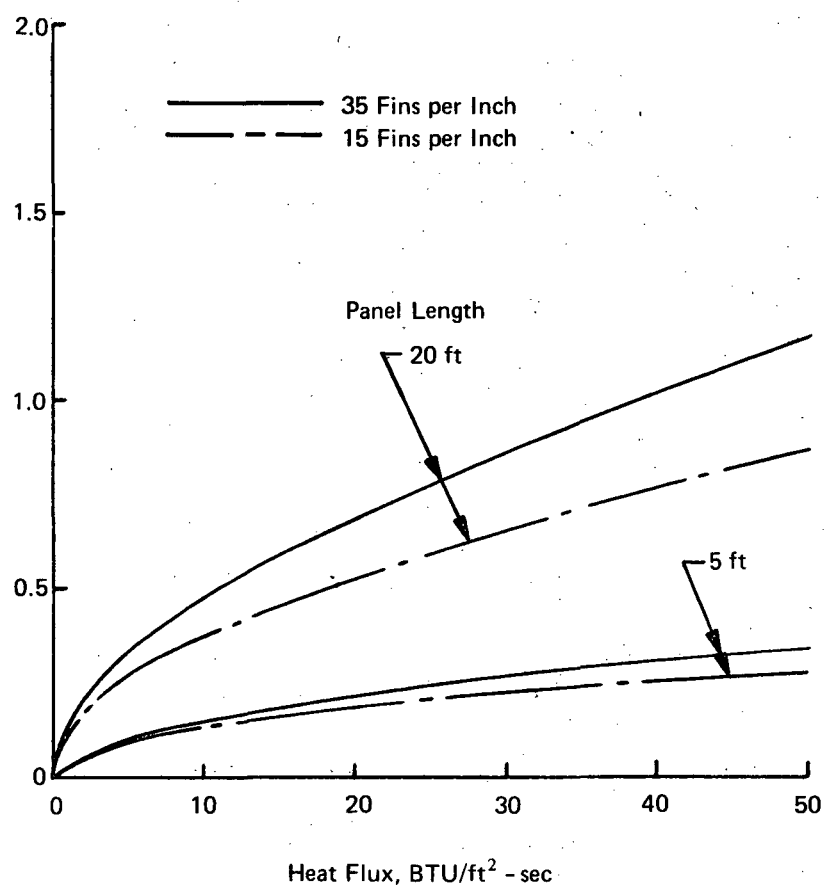


Figure 20b. Minimum Unit Weight for Plate Fin Panels, Ethylene Glycol/Water, Coolant in at 50F/Out at 200F

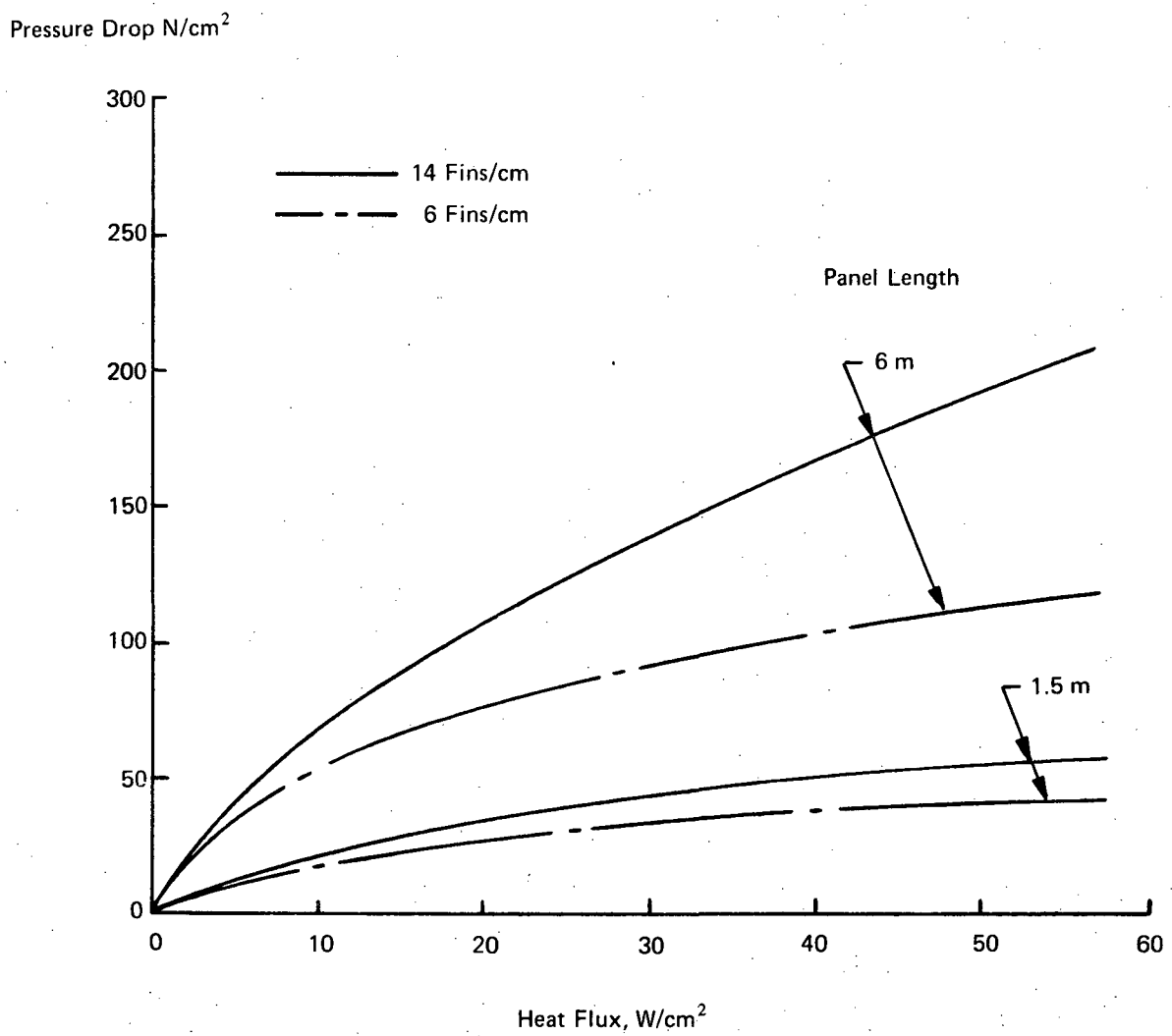


Figure 21a. Pressure Drop Through Optimum Plate Fin Panel, Ethylene Glycol/Water, Coolant in at 283°K /Out at 367°K

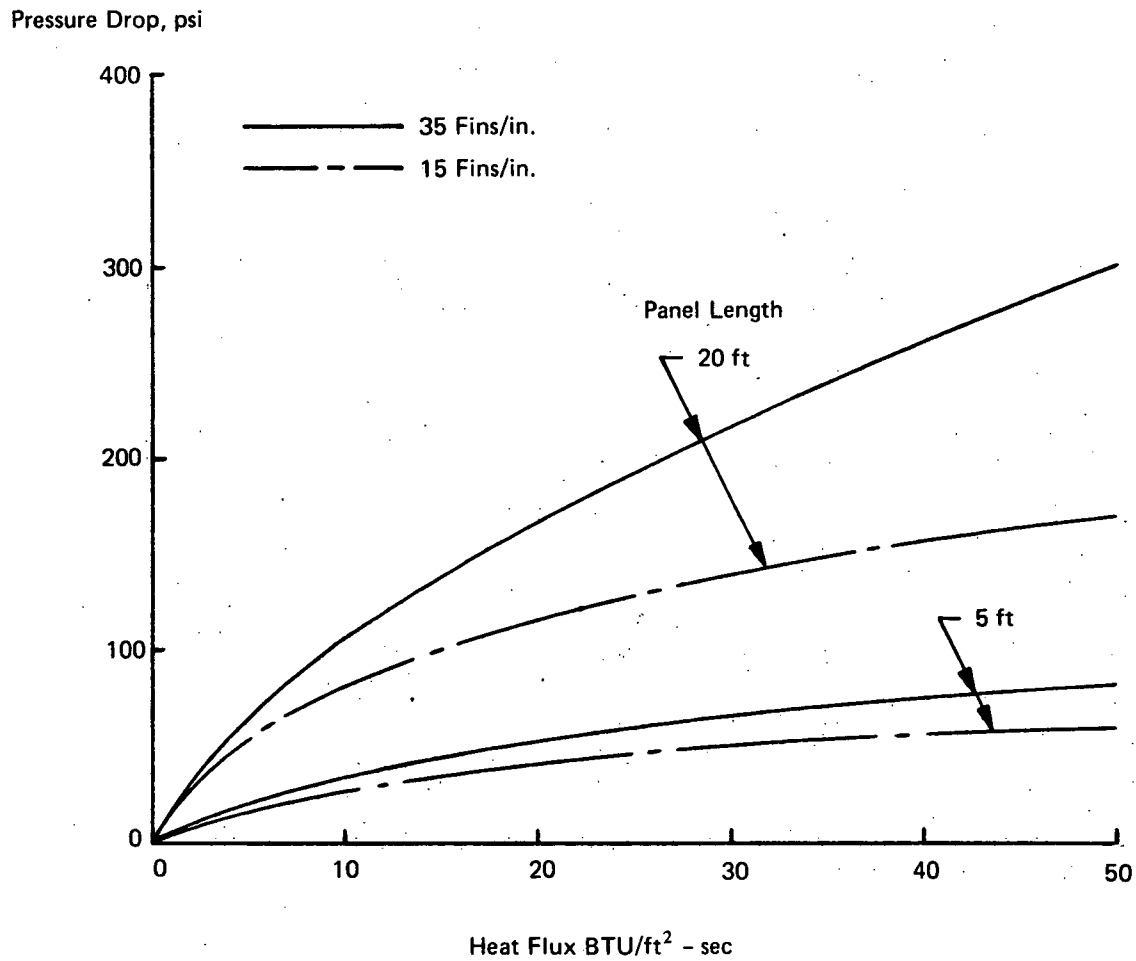


Figure 21b. Pressure Drop Through Optimum Plate Fin Panel, Ethylene Glycol/Water, Coolant in at 50F/Out at 200F

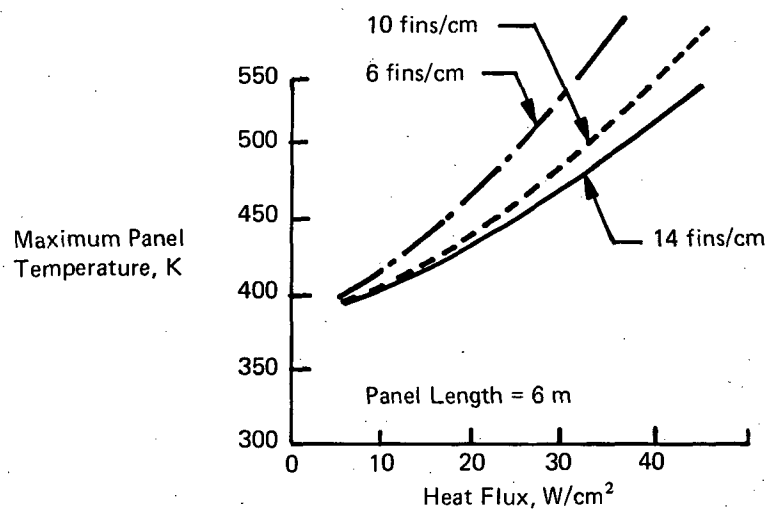
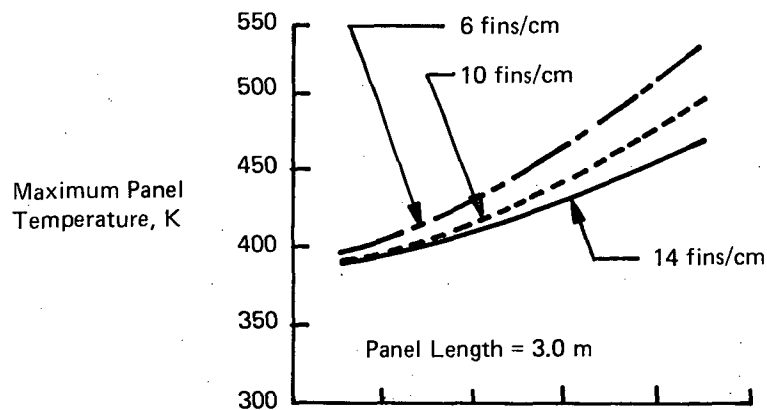
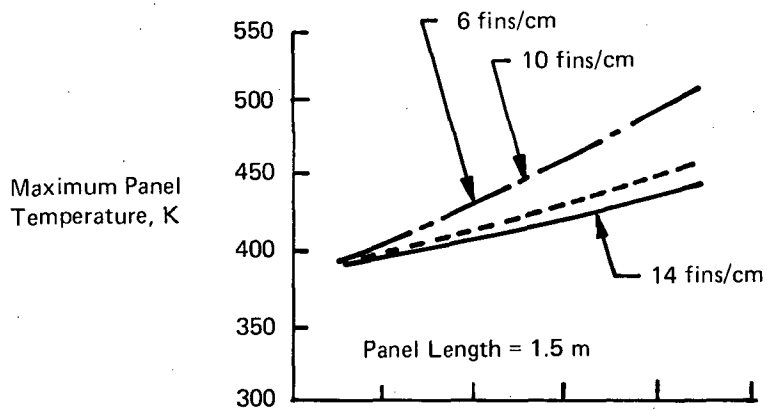


Figure 22a. Maximum Panel Temperature for Optimum Plate Fin Panel During Single Mode Operation, Ethylene Glycol/Water, Coolant in at 283K/Out at 366K

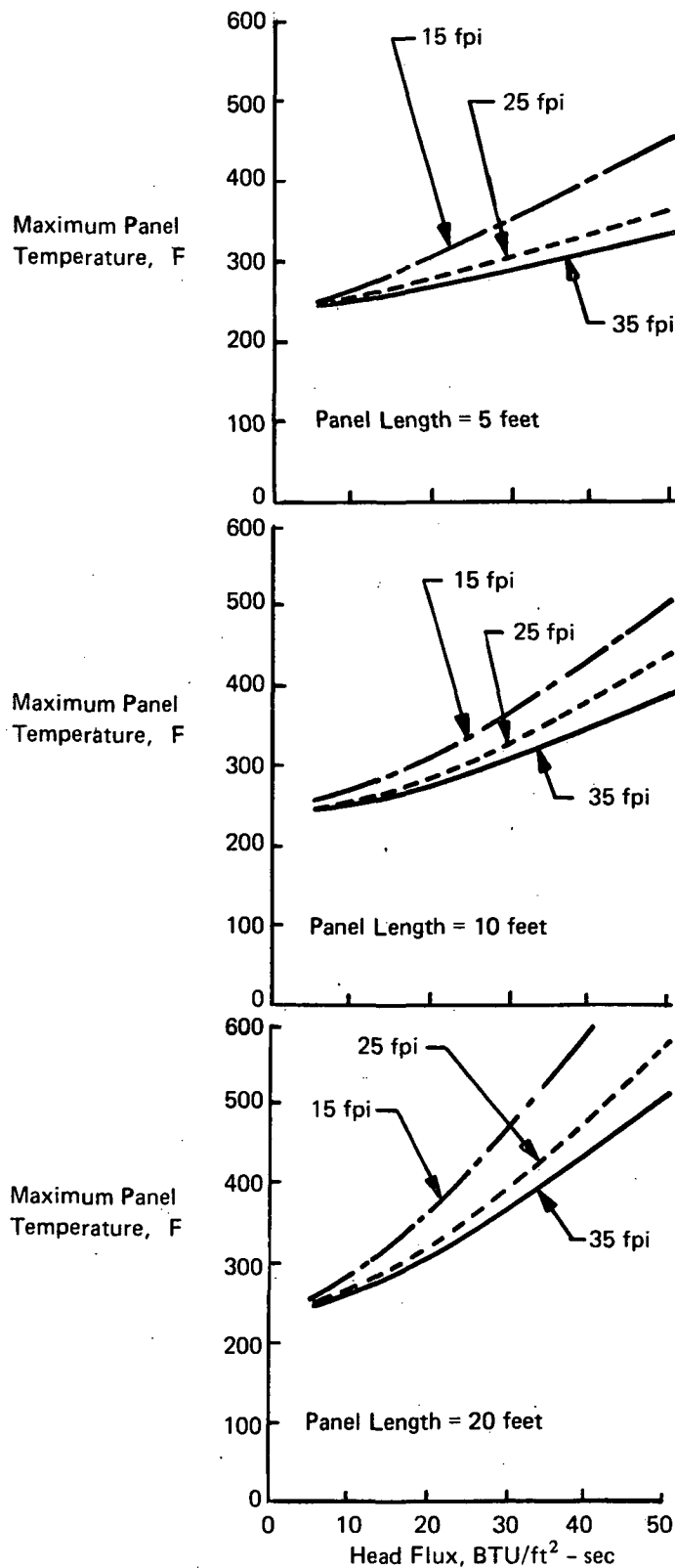


Figure 22b. Maximum Panel Temperature for Optimum Plate Fin Panel During Single Mode Operation, Ethylene Glycol/Water, Coolant in at 50 F/Out at 200 F

20.4 and 30.5 w/cm² (18 and 27 BTU/ft²/sec) can be sustained within the 450°K (350F) limit for 15 and 35 FPI, respectively. This change in fin count increases panel pressure drop from 1.17 MN/m² (135 psi) to 2.05 MN/m² (200 psi) at the higher heat flux while the weight increases from 2.93 kg/m² (0.6 psf) to 3.91 kg/m² (0.8 psf).

As a guide to the trends for other coolants and construction materials analyses were conducted for Coolanol 20/aluminum, Coolanol 45/titanium, and Coolanol 45/beryllium. For the last two, a maximum coolant temperature of 450°K (350F) was assumed rather than the 366°K (200F) assumed for the aluminum panels. Results are summarized in Figure 23 for 6.1 m (20 ft) long panels with 15 fins per inch. The poorer thermal properties of Coolanol 20, particularly the low specific heat as compared to aqueous solutions, resulted in a 50% weight increase. A further weight increase would be expected for Coolanols of higher molecular weight. Similarly, the weights for other dielectric coolants would be higher than for water-based coolants. When the maximum coolant temperature is increased to 450°K (350F) the coolant temperature rise is doubled, the flowrate is halved, and the weight decreases. The higher operating temperature increases the heat transfer effectiveness as well. The choice of panel material has no significant influence on the unit weight of the thermal elements of the panel but can influence the weight of the splitter plate between the two layers of fins. In the case of titanium 0.20 mm (8 mil) sheet was assumed while for beryllium 0.50 mm (20 mil) sheet was assumed. The combinations of thickness and density resulted in equal weights. A significant difference in skin temperature was noted, however, between the titanium and beryllium with the temperature of panels made from the former being from 283°K (50F) to 340°K (150F) higher than for the latter, depending upon the heat flux.

Sphere-Core. - This concept is similar to the plate-fin approach except that the fin stock is replaced by hollow spheres thereby reducing the quantity of coolant within a sandwich of a given thickness. From a thermal point of view the merit of this concept is dependent upon the savings in coolant weight overshadowing any weight increases due to pumping power penalties. For initial studies the heat transfer and friction factor data for packed beds of spherical particles was used, Reference 40. Although the free flow area for a packed bed is less than for a layer of spheres between two plates, more appropriate correlations could not be found. After the initial analyses were completed it was apparent that a high price had been paid in pumping power penalty due to the conservative assumption made with respect to friction factors. Therefore, as part of an in-house project pressure drop measurements were made for spheres between parallel plates. When a tight packing was used the measured friction factors were about 15% lower than those based on a packed bed of spheres. When a square pattern array was used the friction factor was less than half that predicted by Reference 40. Thus, the results presented for this concept are conservative.

The sphere-core panel sizing studies were conducted similarly to those for the plate-fin concept. Various sandwich heights were assumed and weights were computed for residual coolant and for the pumping power penalty at each of several heat fluxes and panel lengths. Thus, the sandwich thickness that resulted in the lightest panel weight for each combination of variables could be identified. The analyses were conducted at heat fluxes from 1.13 to 56.5 W/cm² (1 to 50 BTU/ft²/sec) for panel lengths of 1.5 and 6.1 m (5 and 20 ft). For the range of heat fluxes considered, the sandwich thickness varied from 0.12 to 1.1 cm (0.05 to 0.44 in.) for the 1.5 m (5 ft) panels and from

Weight of Residual Coolant and APS Fuel, Kg/m^2

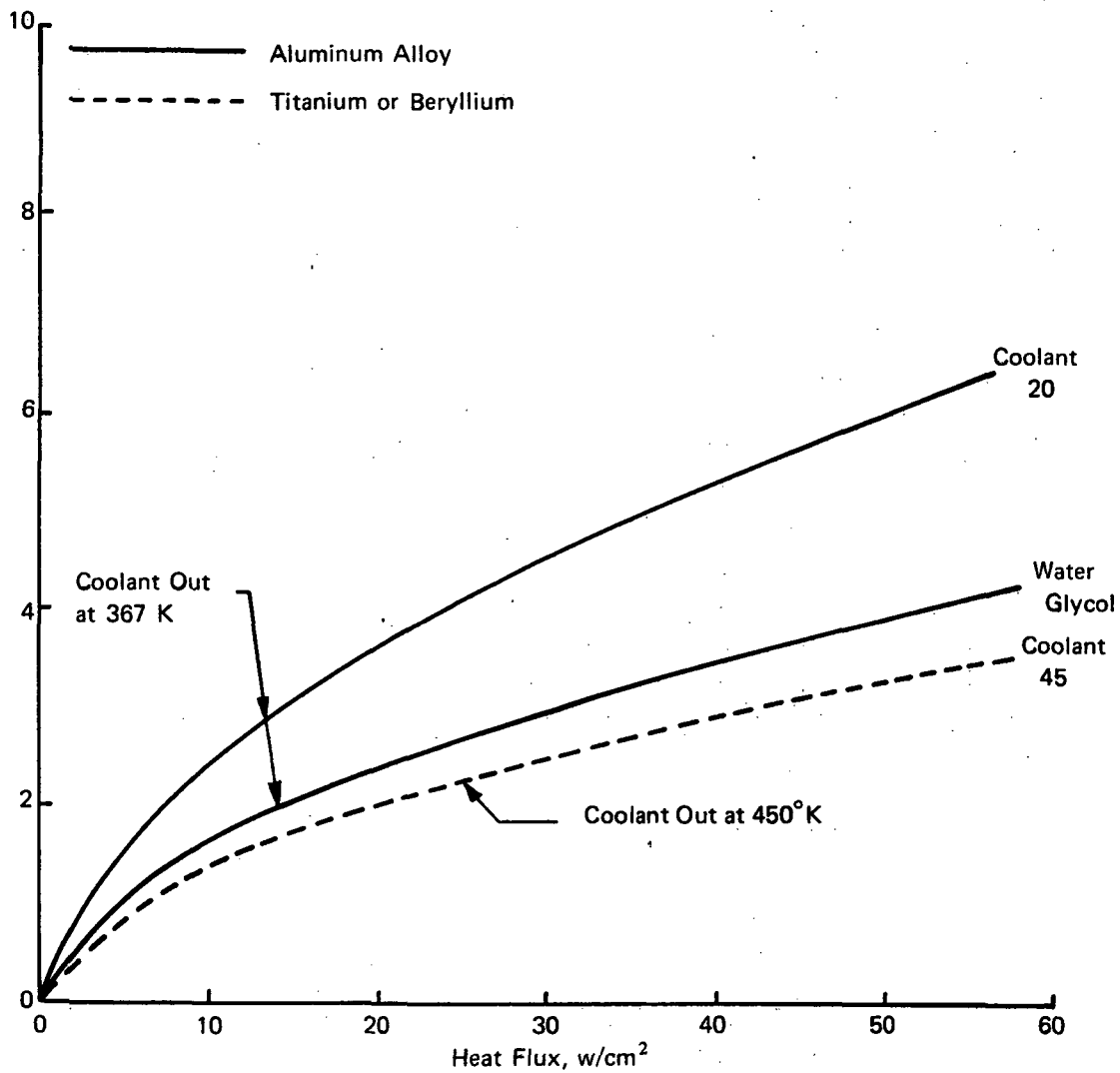


Figure 23a. Minimum Unit Weight for 6.1 Meter Long Plate - Fin Panels with 6 Fins/cm, Coolant Inlet Temperature = 283°K

Weight of Residual Coolant,
Fins, and APS Fuel, psf

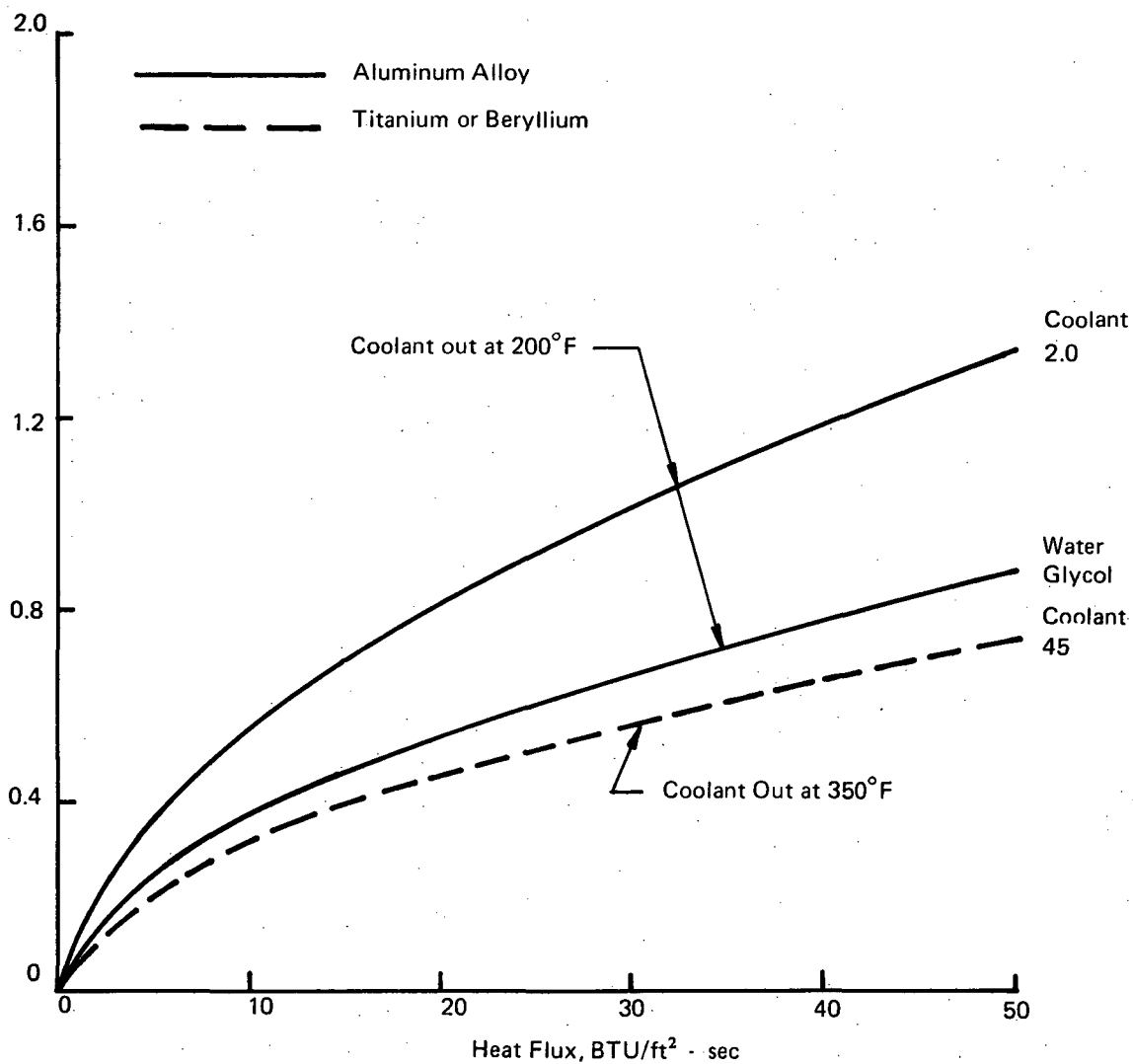


Figure 23b. Minimum Unit Weight for 20 Foot Lower-Plate-Fin Panels
with 15 Fins for Inch, Coolant Inlet Temperature = 50°F

0.44 to 3.2 cm (0.175 to 1.25 in.) for the 6.1 m (20 ft) panels. The weight results are shown in Figure 24. The difference in pressure drop characteristics for the two panel lengths are shown in Figure 25 as a function of heat flux. As in the case of the plate-fin concept, shorter panel lengths led to significantly lighter panels with lower pressure drops.

As compared to the plate-fin concept the initial predictions of sphere-core panels indicated weights to be about three times as high and pressure drops to be about 50% higher. When the in-house experimental friction factor data was used the sphere-core concept results were approximately twice as high as for plate-fin designs which utilize a fin count of between 15 and 25 per inch.

Plain Skin/Cooled Stringer. - Of the panel concepts considered, this approach is probably the most tolerant to skin cracks that might occur in service. As illustrated as Concept D of Figure 8, the coolant passage is integral with the stringer. Such a design requires good thermal contact between the skin and the stringer. Therefore, the applicability of this concept was assessed by thermal analysis to define the relationships among operating temperature, heat flux, and geometric proportions of the concept. The skin and stringer thicknesses were assumed to be 1 mm (40 mils). Initial studies assumed infinite conductance between the stringer and the skin. Stringer spacings were computed such that the maximum temperature between passages was 420°K (300F) aluminum construction and 530°K (500F) for titanium. The coolant passage was sized to yield minimum weight between residual coolant and pumping power penalty.

For the aluminum alloy construction, spacings were determined for three coolants, ethylene glycol/water, FC-43, and Coolanol 45. In all cases the coolant outlet temperature was assumed to be 366°K (200F) while the inlet temperature was 293°K (50F). Results of these analyses are shown in Figure 26. For the Coolanol 45 heat fluxes had to be less than 1.13 w/cm² (1 BTU/ft² sec) before attractive designs could be achieved, hence results are not indicated. The dashed line indicates limiting heat flux/size characteristics; to the right of the dashed line skin temperatures between stringers cannot be maintained at maximum values unless more than one coolant passage is formed in each cooled stringer. For the titanium structure the maximum temperature between coolant passages was assumed to be 530°K (500F) while the coolant outlet temperature was 450°K (350F) and its inlet temperature was 293°K (50F). Results of the analysis are summarized in Figure 27. Note that the higher temperature levels appear to compensate for the lower thermal conductivity of the titanium.

Additional analyses were conducted to assess the influence of joint resistance on the results. Only one geometry/heat flux combination was considered, a stringer flange width of 1.9 cm (0.75 in.) at 1.13 w/cm² (1 BTU/ft² sec). Results are presented in Figure 28. The interface resistances for representative joining techniques are also included on the figure. Unless metallurgical joining by brazing or diffusion bonding can be achieved a significant decrease in stringer spacing results. The stringer spacings are significantly less than those determined during the work of References 1 and 2 for the hypersonic transport, further indicating the general unattractiveness of this concept. The relatively low heat flux levels indicated for this design suggests that it is not a good candidate for use at even moderate heating intensities. However, it may be attractive as a backup concept.

Coated/Cooled. - The application of an external coating to the cooled panels will reduce the heat load to the cooling system and the cooling system weight. Whether the weight savings would

Unit Weight, Residual Coolant, Spheres, and APS Fuel, kg/m^2

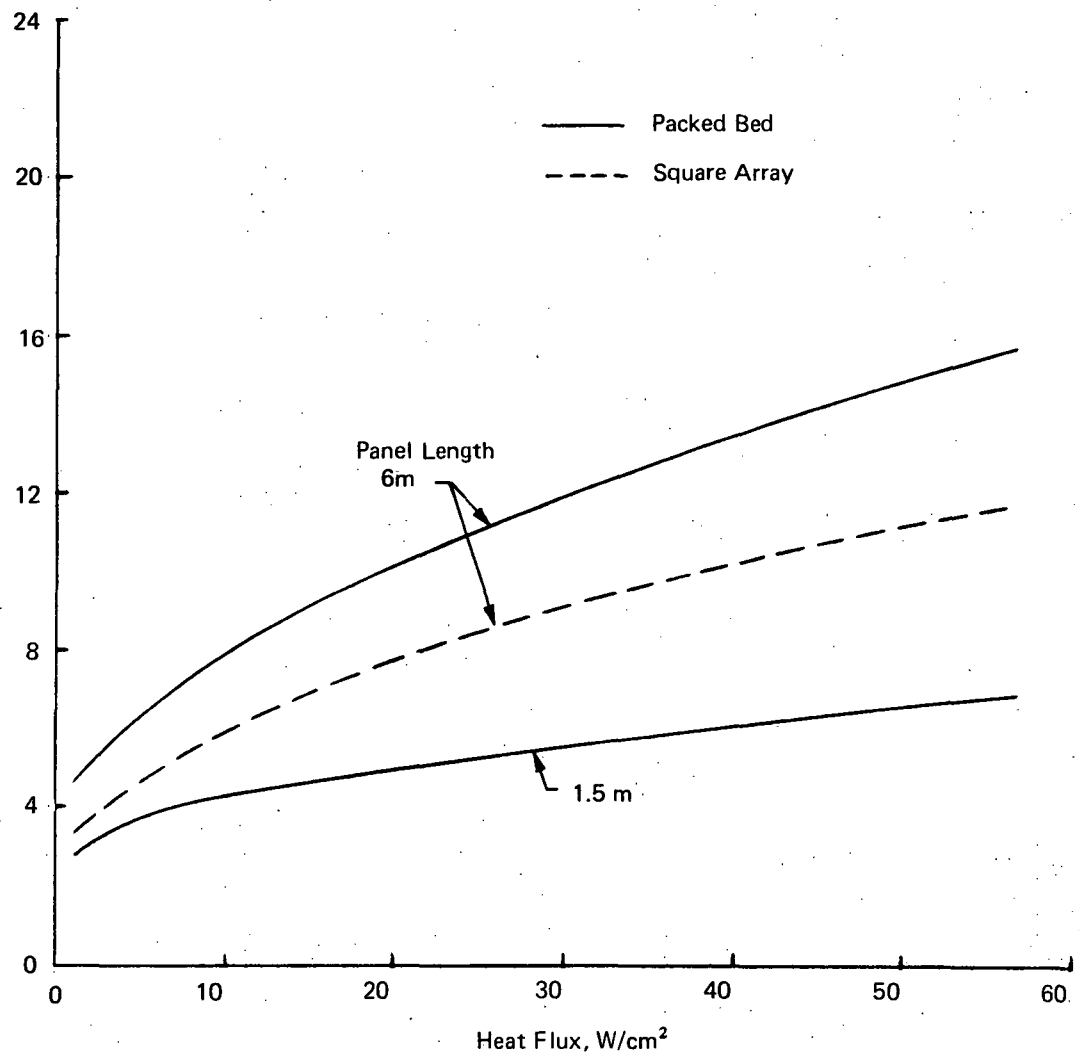


Figure 24a. Optimized Unit Weights for Sphere-Core Panel Concept, Ethylene Glycol, Inlet Temperature = 283°K , Outlet Temperature = 367°K

Unit Weight, Residual Coolant, Spheres, and APS Fuel, psf

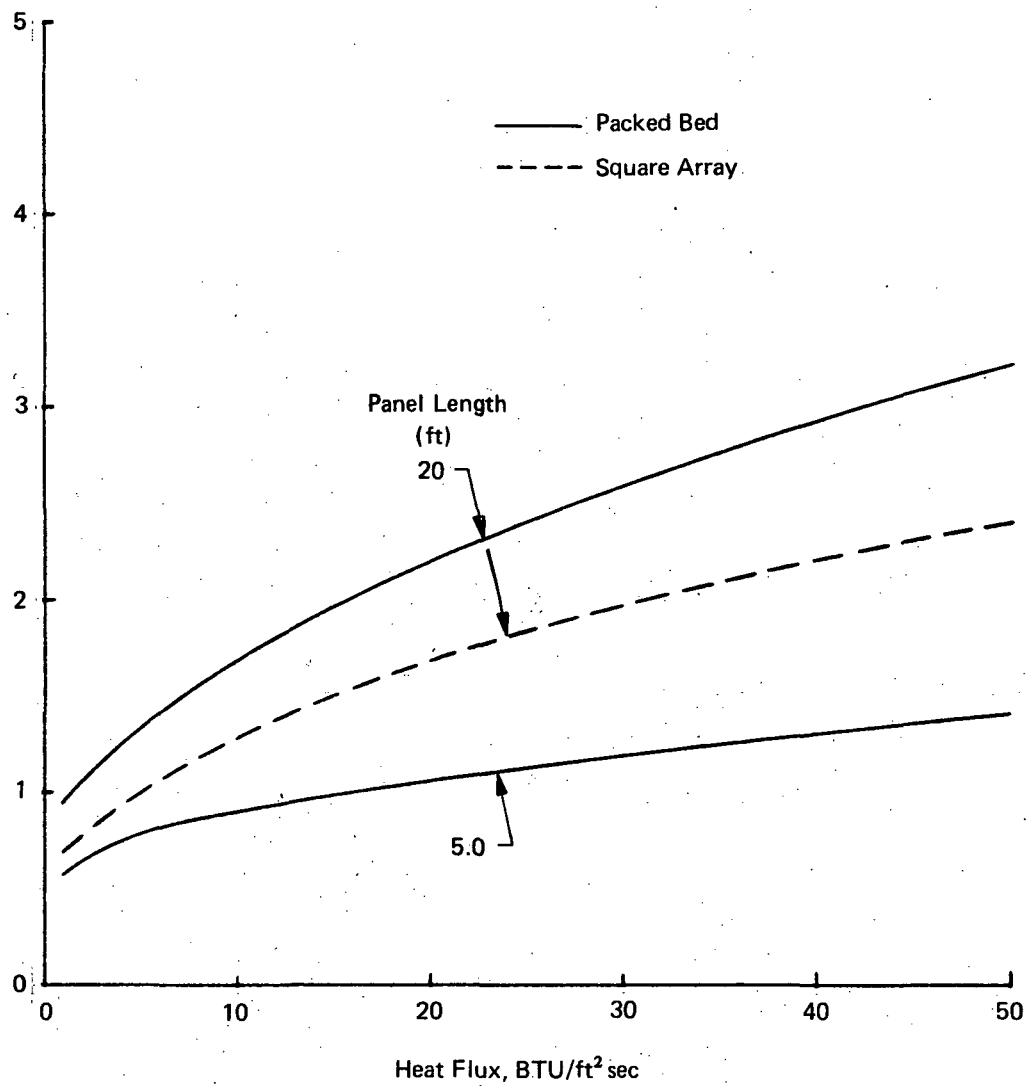


Figure 24b. Optimized Unit Weights for Sphere-Core Panel Concept, Ethylene Glycol, Inlet Temperature = 50F, Outlet Temperature = 200F

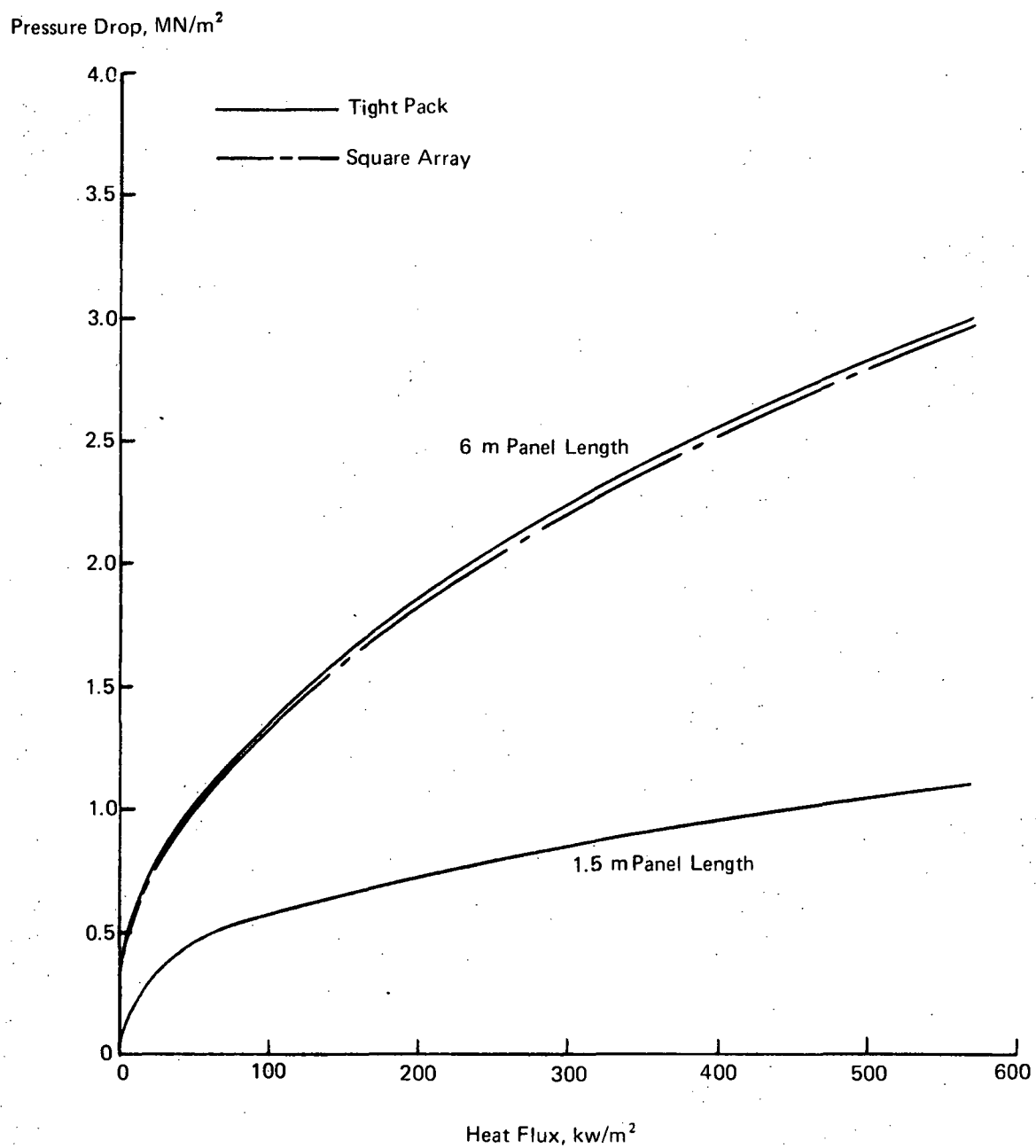


Figure 25a. Pressure Drop for Optimized 6m Long Sphere-Core Panels, Water Glycol Coolant, Coolant Temperature Rise from 283°K to 367°K

Pressure Drop, psi

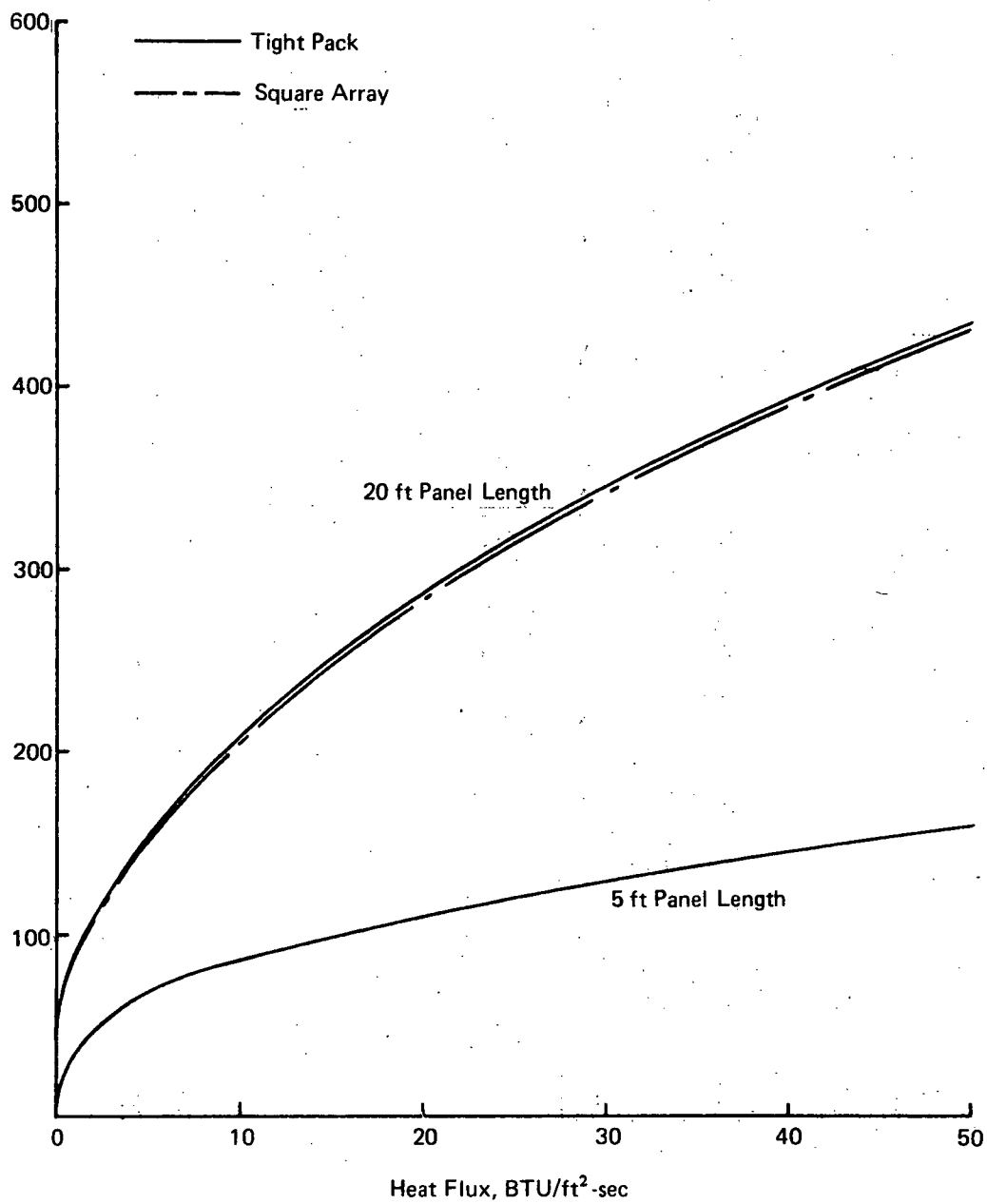


Figure 25b. Pressure Drop for Optimized 20 ft Long Sphere-Core Panels,
Water Glycol Coolant, Coolant Temperature Rise from 50F to 200F

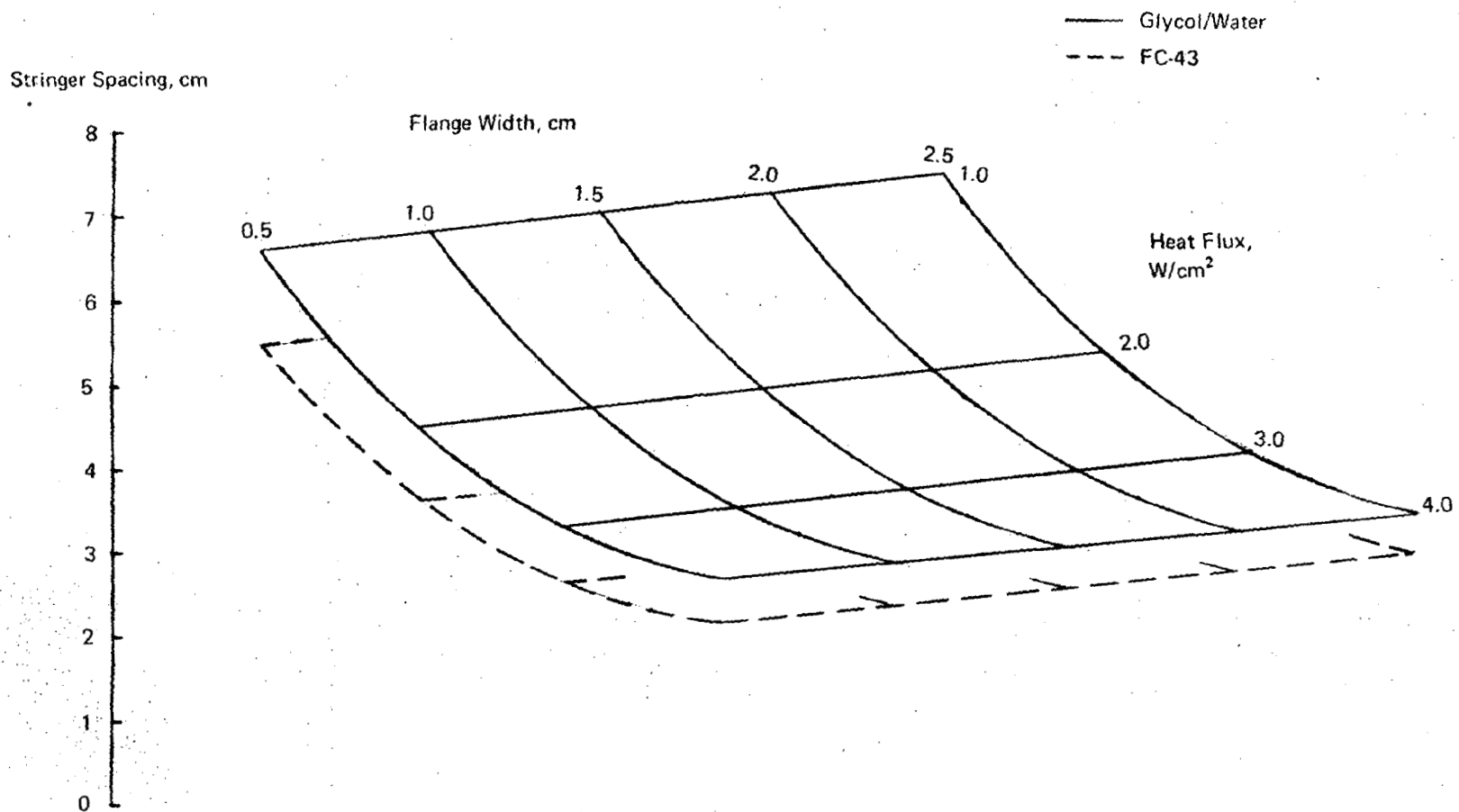


Figure 26a. Maximum Stringer Spacing for Cooled Stringer Concept, Maximum Temperature = 422° K
Aluminum Structure

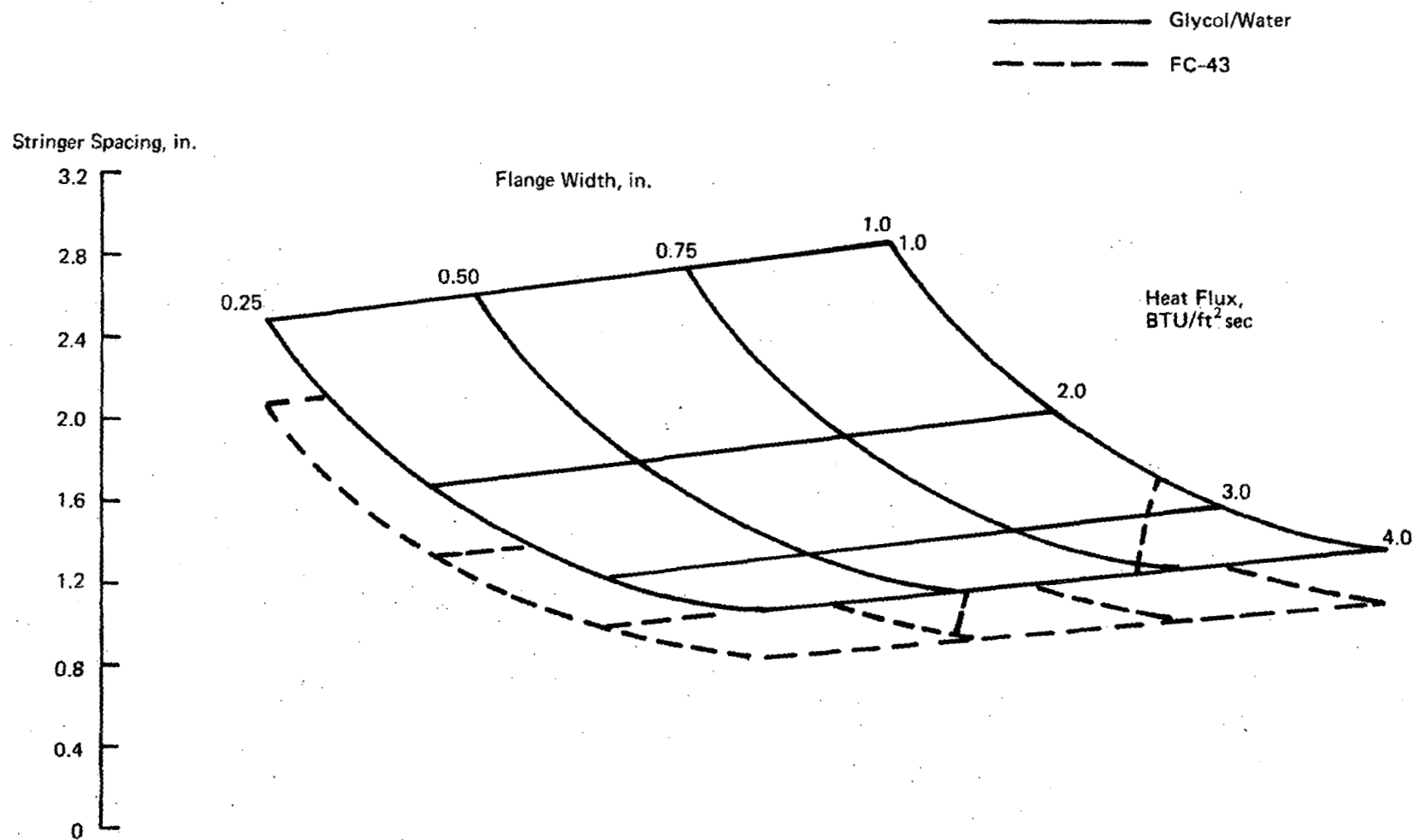


Figure 26b. Maximum Stringer Spacing for Cooled Stringer Concept, Maximum Temperature = 300 F
Aluminum Structure

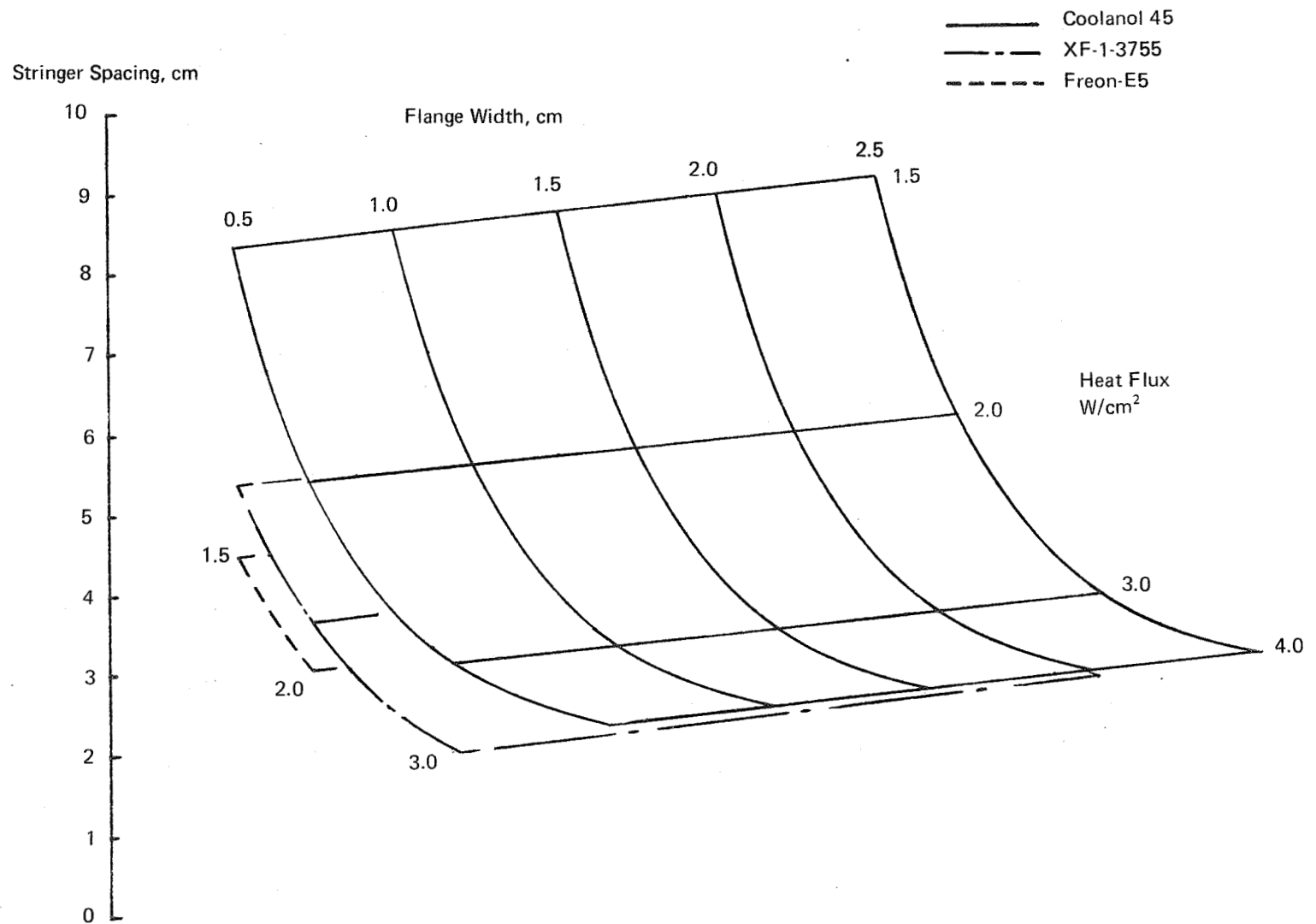


Figure 27a. Maximum Stringer Spacing for Cooled Stringer Concept, Maximum Temperature = 533°K
Titanium Structure

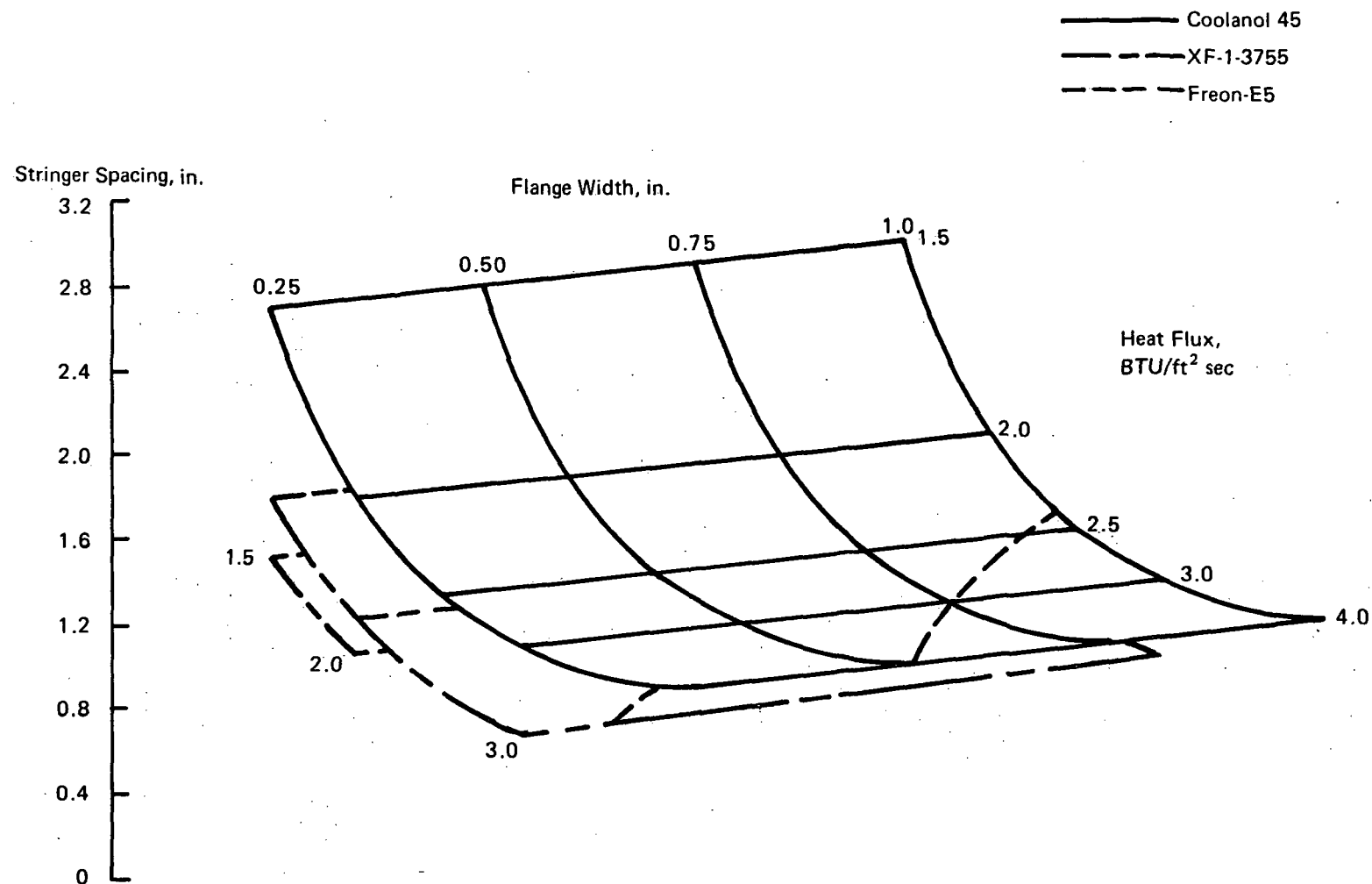


Figure 27b. Maximum Stringer Spacing for Cooled Stringer Concept, Maximum Temperature = 500F
Titanium Structure

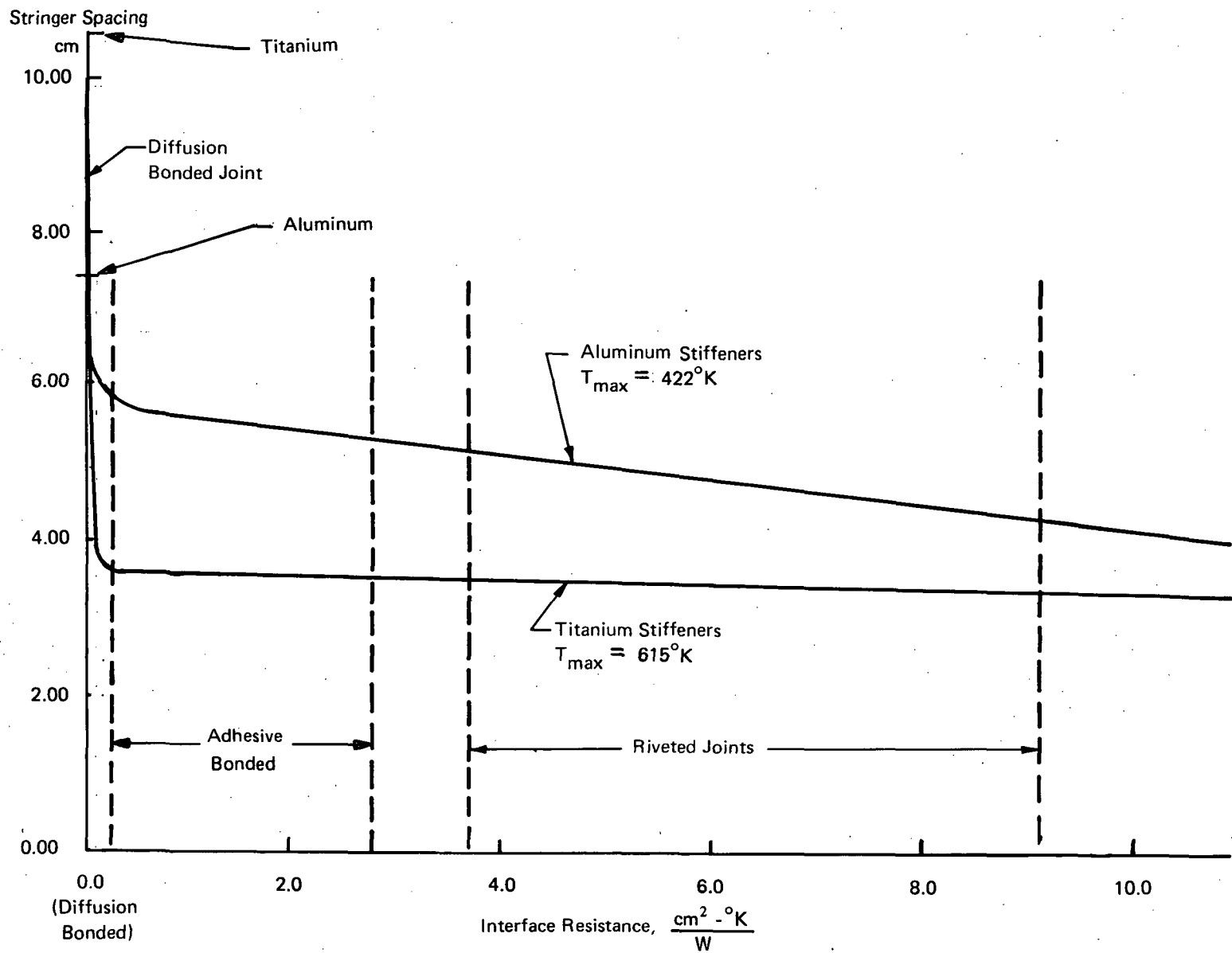


Figure 28a. Stringer Spacing as a Function of Interface Thermal Resistance, Heat Flux = W/cm^2

Stringer Spacing, in.

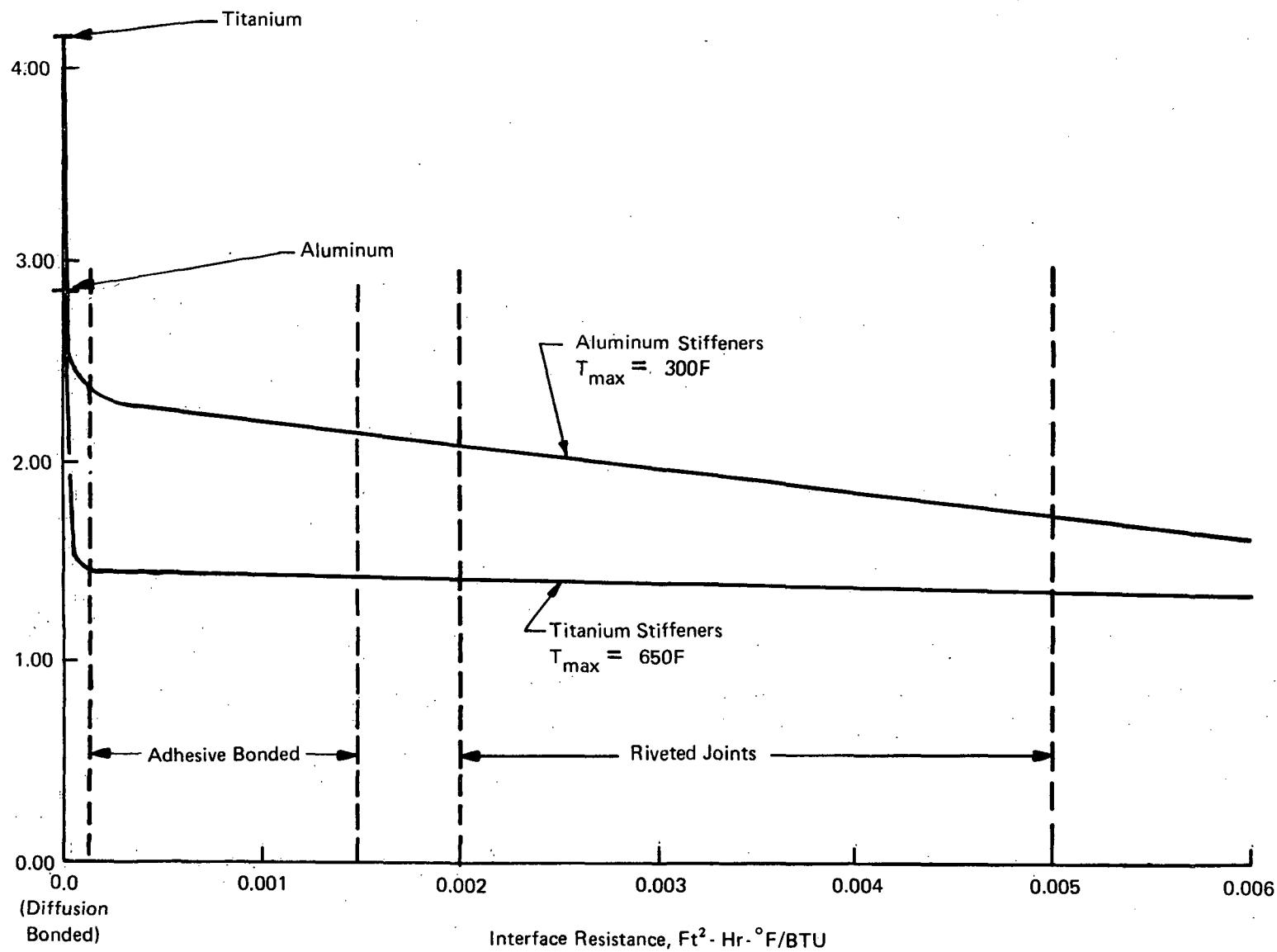


Figure 28b. Stringer Spacing as a Function of Interface Thermal Resistance,
Heat Flux = $1.0 \text{ BTU}/\text{Ft}^2 \cdot \text{Sec}$

offset the weight of the coating depends on the coating characteristics. While organic, metallic, or ceramic coatings can be considered only the latter were examined. Analyses were conducted for flame sprayed aluminum oxide having densities of 65% and 80% of theoretical. Thicknesses were varied from 0.025 to 1.5 mm (1 to 60 mils) but in all cases the reduction in cooling system weight was less than the weight increase due to the external surface coating.

Reusable Surface Insulation/Cooled. - Although the dense ceramic coatings were not attractive prior studies, Reference 41 suggested that ceramics of lower density, like the RSI concept being investigated for the Space Shuttle thermal protection, could be quite attractive. However, when cooling is used the insulation thickness is significantly less than that required for an uncooled structure. This means that a nearly linear temperature gradient is established quite early during the heating history between the equilibrium temperature due to aerodynamic heating of the outer surface and the panel temperature as controlled by the cooling system. This temperature gradient and the conductivity determines the heat flow to the cooling system, generally between 1 and 10% of the aerodynamic heat input, so that the influence on radiation equilibrium temperature is slight.

In considering the RSI concept in conjunction with cooling the presence of the strain isolator must be taken into account because of its maximum temperature limitation in the order of 590°K (600F). Since the heat flow from the outer surface to the cooling system is representative of a quasi steady-state situation it is necessary that the conductance and temperature gradient of the strain isolator bear a particular relationship to that of the surface insulation. Such a constraint was used during the analysis in the form of a correction to the thermal conductivity of the RSI material. In addition, the weight of the strain isolator and the waterproof/emittance control external coating were assumed to be 2.3 kg/m² (0.50 psf). This is somewhat lower than values that had been documented at the time the analyses were performed in order to reflect expected improvements in the material system.

The parametric study of the RSI/cooled panel concept utilized the thermal characteristics of Lockheed LI-1500 as presented in Reference 42. Account was taken for high-altitude operation and local surface pressure by using properties measured at 10 Torr. Since the forcing function for internal heat flow is the difference between the external surface temperature and that of the cooled structure, the parametric results of Figure 29 are presented as a function of external temperature rather than heat flux. In addition to providing weights as a function of insulation thickness and external temperature, Figure 29 yields two interesting observations. Except for the highest operating temperature levels, the weight of the strain isolator and protective coating exceeds that of the insulation and cooling system combined. Also, the optimum amount of insulation is very thin. These observations suggest that the reusable surface insulation system being developed for the space shuttle may not be ideal for hypersonic cruise aircraft.

The relationship between external temperature and heat flux is provided in Figure 30 for various thermal emittance that might be of interest. A value of about 0.8 is representative of a good external coating.

Heat Shielded/Cooled. - As shown in Reference 1 the introduction of external heat shielding, with or without intermediate insulation, can reduce heating of cooled panels to between 2 and 40% of the heating when the panel is exposed directly to the boundary layer. Large reductions in panel heating intensity permit widest passage spacings and greatest reductions in cooling system weight.

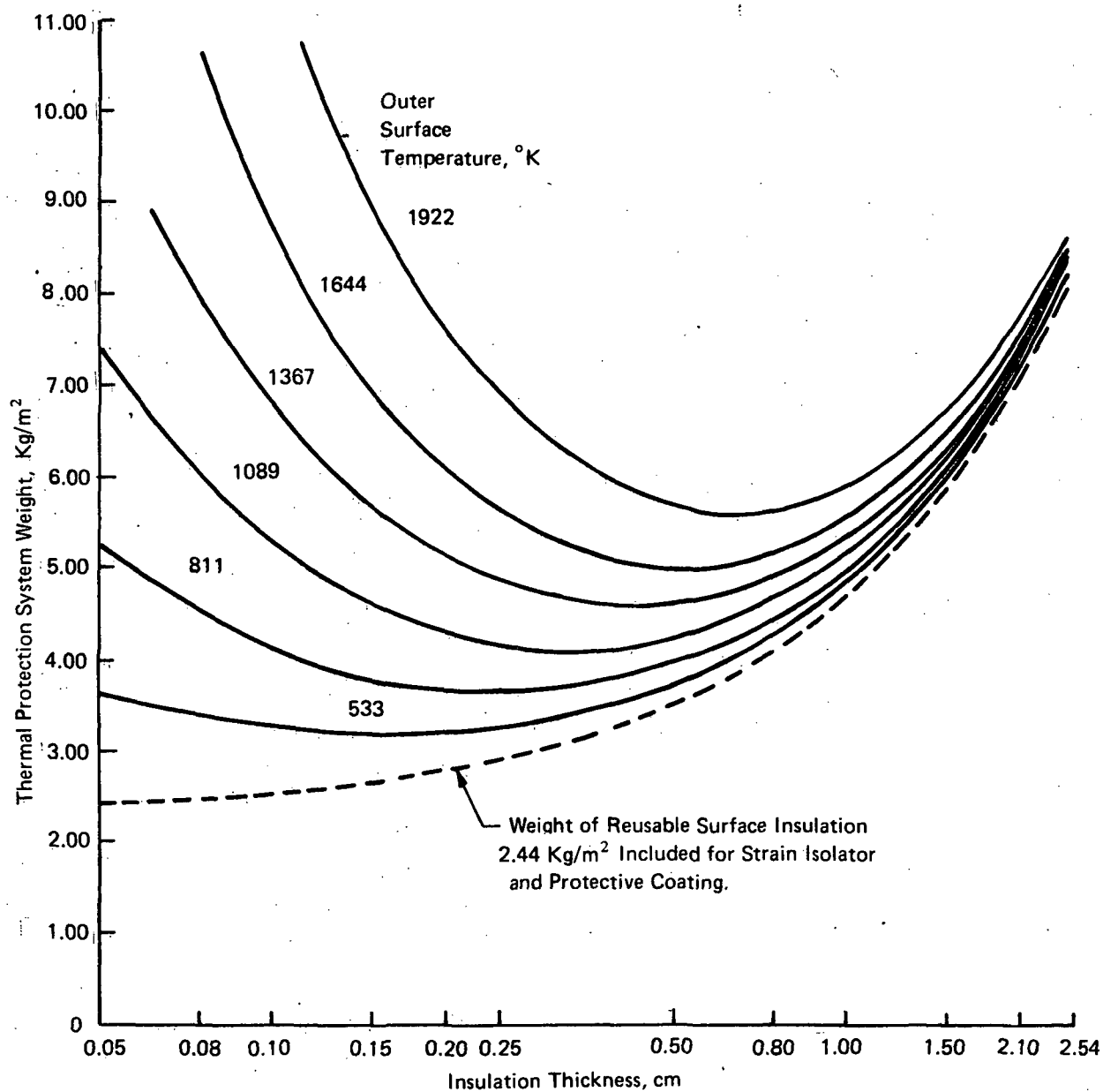


Figure 29a. Optimization of Unit Weight for Reusable Surface Insulation on an Actively Cooled Substructure at 366° K

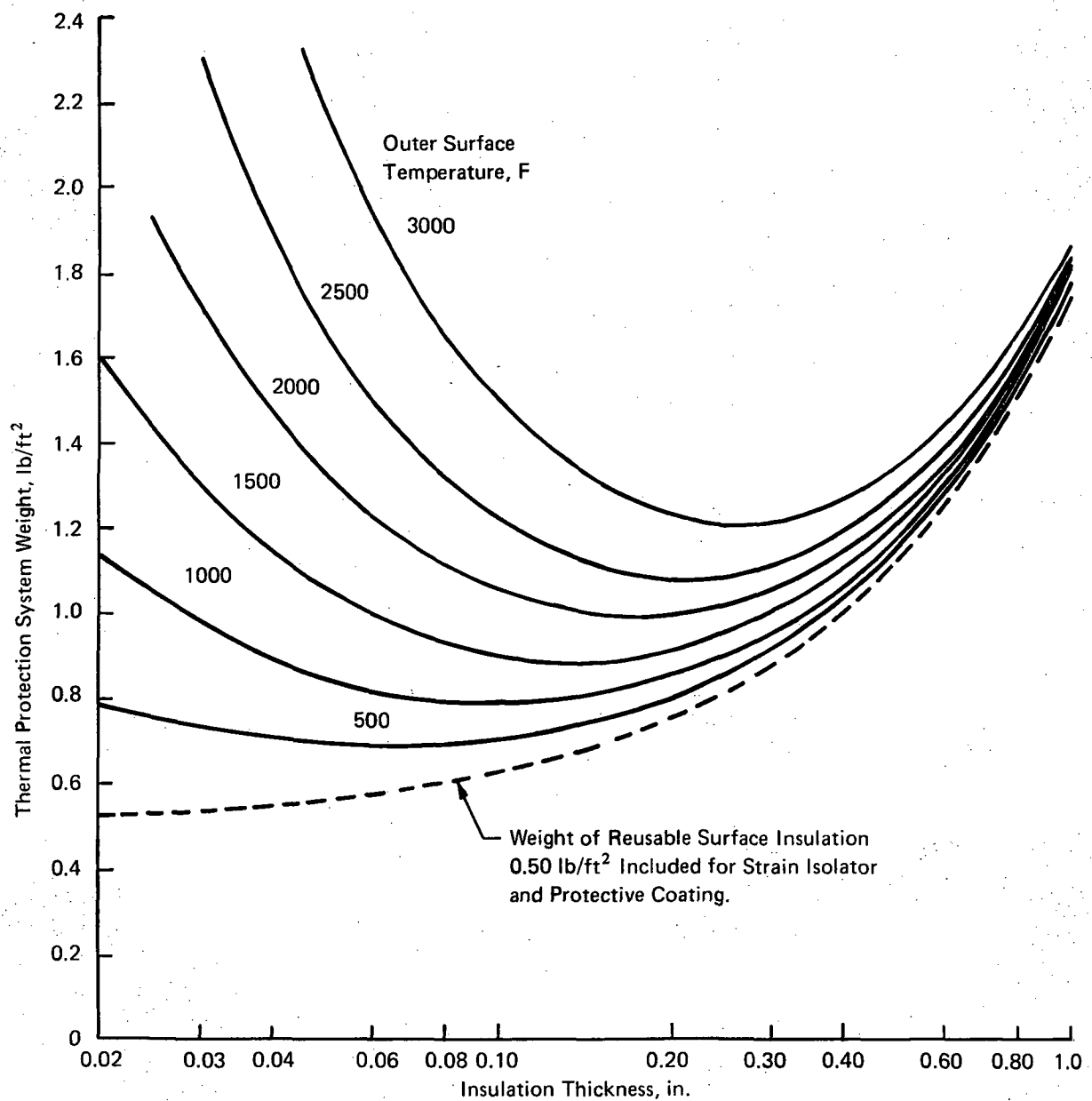


Figure 29b. Optimization of Unit Weight for Reusable Surface Insulation on an Actively Cooled Substructure at 200F

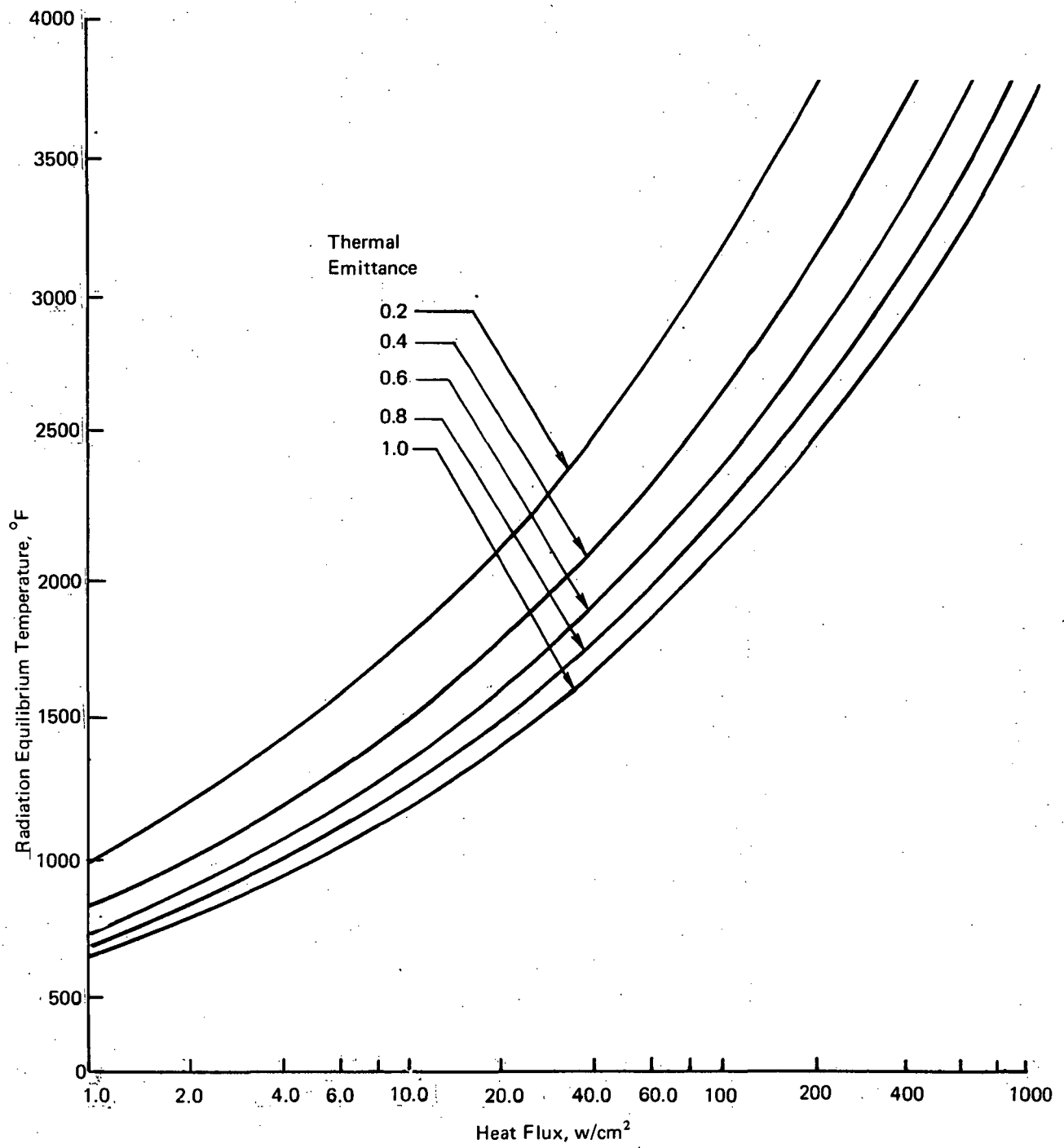


Figure 30a. Heat Flux, Temperature, Thermal Emittance Relationship

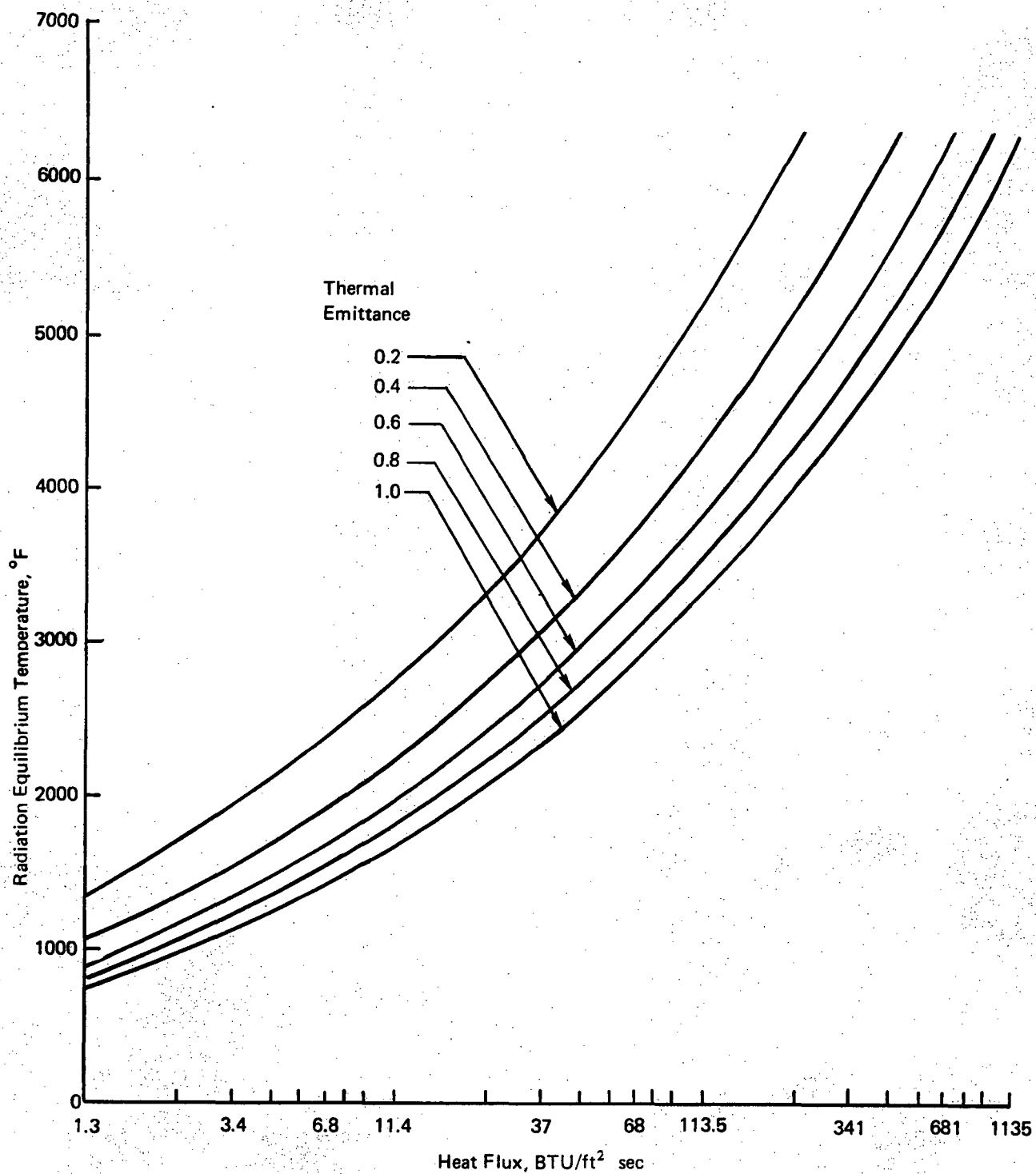


Figure 30b. Heat Flux, Temperature, Thermal Emittance Relationship

In order to be of benefit the weight reductions must be greater than the weight added due to the heat shields. In some instances it may be desirable to radiate a relatively large amount of heat to the cooled internal panels in order to control heat shield temperature so that a change of heat shield material can be avoided if such a change would lead to a significant weight penalty. A variety of heat shield concepts have been studied by a number of investigators; a later section discusses selected concepts and weights.

For analyses of this concept, heat shield weights were taken along the lower boundary of the weight envelope in Figure 75, corresponding to honeycomb sandwich construction with minimum gauge constraints of 0.25 mm (10 mils) for superalloys and 0.37 mm (15 mils) for refractory metals. A review of the heat shield weights indicates significant penalties when temperatures exceed 1360°K (2000F); coated refractory metals are assumed to be necessary. Therefore, it is advantageous to maintain the heat shield operating temperature to values less than 1360°K (2000F). In the high heat flux regions of the vehicle, the radiation equilibrium temperatures exceed 1360°K (2000F), hence contrary to usual heat shielded TPS designs it is advantageous to permit a considerable percentage of the aerodynamics heat input to flow from the heat shield to the cooled panel. As the heat flow to the cooled panel increases, less heat must be radiated to space and the heat shield operating temperature is reduced.

Figure 31 is a typical plot of heat shield operating temperature as a function of effective thermal emittance of the two inner surfaces, (in this case for the HRA Mach 10 cruise condition where $T_{AW} = 6400^{\circ}\text{F}$). The effective emittance is related to the actual surface emittances by the following equation:

$$\epsilon_{\text{EFF}} = \frac{1}{\frac{1}{\epsilon_o} + \frac{1}{\epsilon_s} - 1}$$

where ϵ_o is the emittance of the inner surface of the heat shield and ϵ_s is the emittance of the skin panel. An emittance of 0.8 was assumed for both of the surfaces and resulted in an effective emittance of 0.67. A study of Figure 31 shows that with such an arrangement the heat shield temperatures will be less than 1360°K (2000F) for cold wall heat fluxes below 45 W/cm² (40 BTU/ft²/sec) for these flight conditions.

Before the cooling system weights can be computed, the heat load to the cooling system must be known. Figure 32 presents the heat flow to the cooled panel as a function of effective emittance and aerodynamic heat flux for the flight condition noted above. For an emittance of 0.67 the heat flow to the cooling system is about 30 percent of cold wall heating rate. Figure 33 presents the unit weights of the TPS system with a heat shield arrangement having an emittance of 0.8 on both surfaces of the heat shield and on the skin panel. Note that a relatively high percentage of the total weight is due to the heat shielding until high heat fluxes are reached.

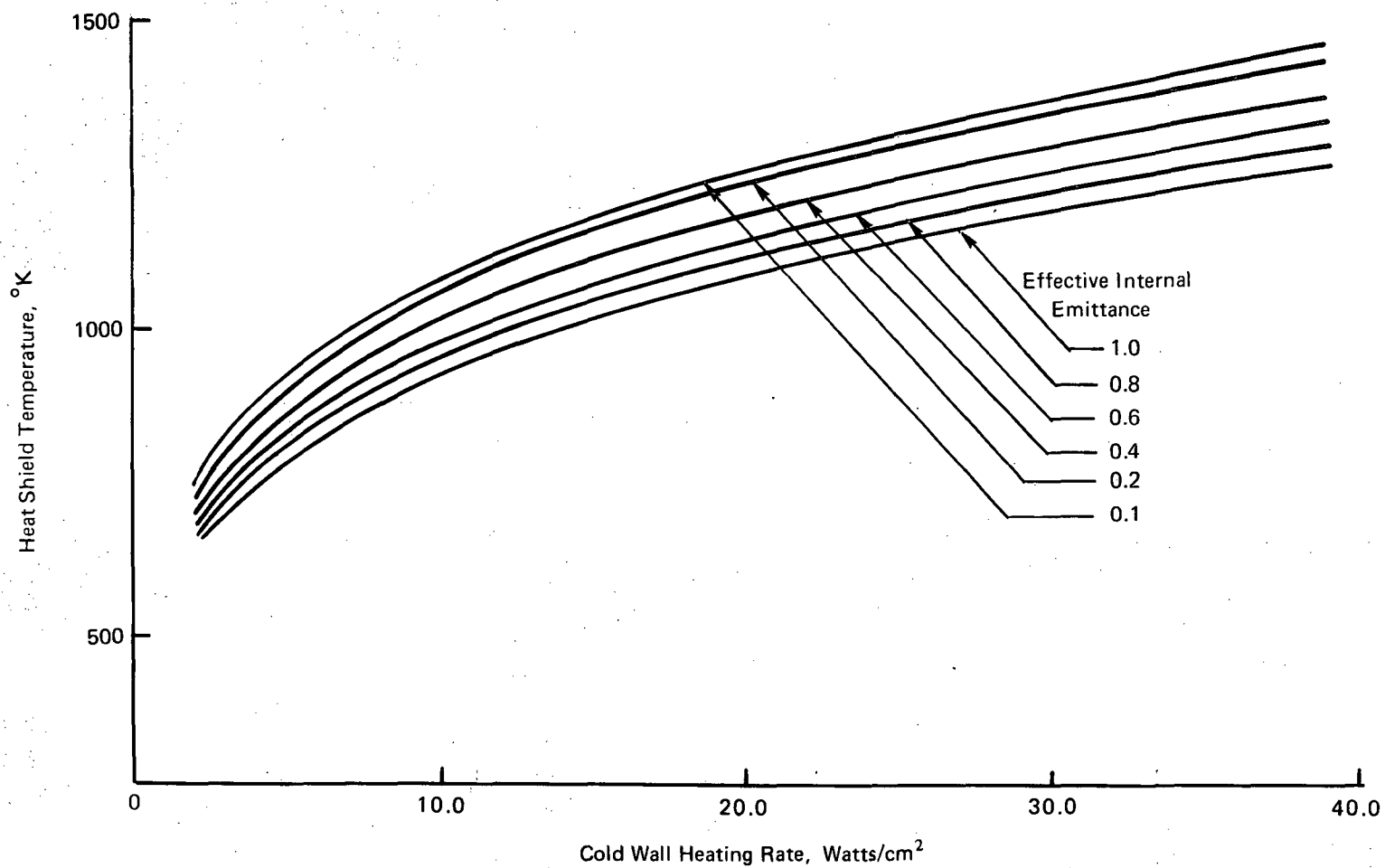


Figure 31a. Heat Shield Temperature as a Function of Heat Flux and Effective Internal Emittance, External Emittance = 0.8, $T_r = 3810^\circ\text{K}$

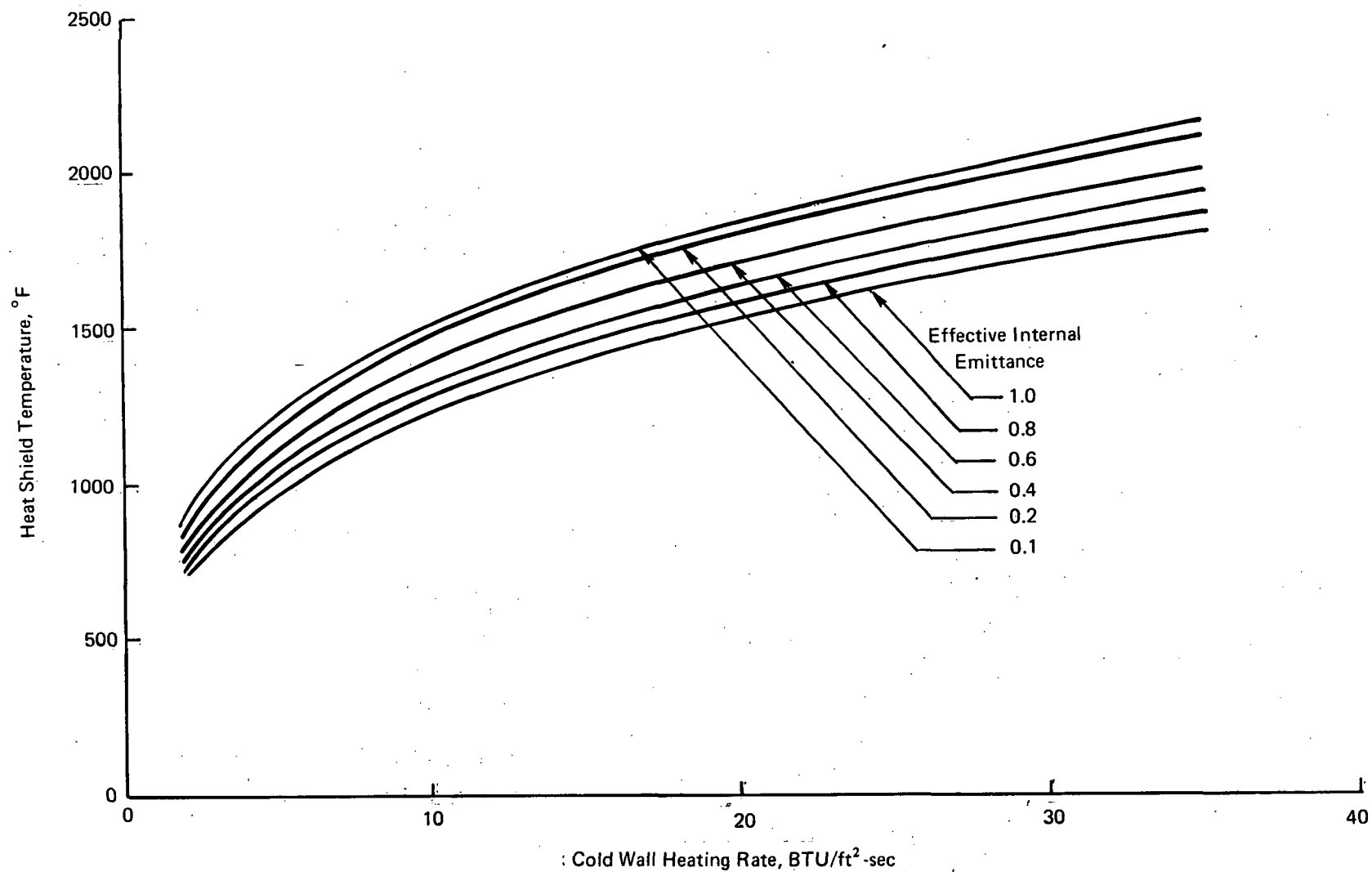


Figure 31b. Heat Shield Temperature as a Function of Heat Flux and Effective Internal Emittance, External Emittance = 0.8, $T_r = 6400F$

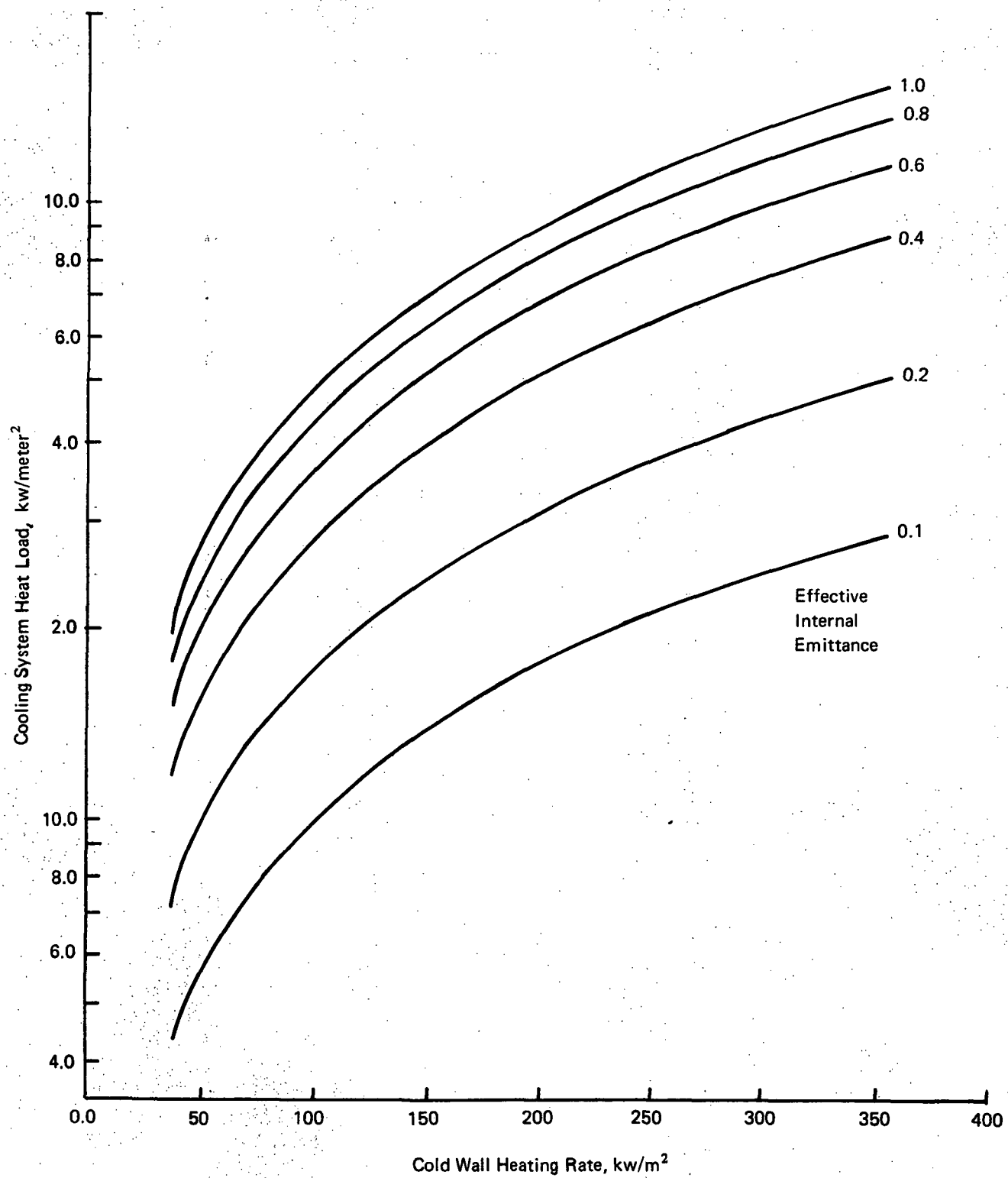


Figure 32a. Cooling System Heat Load for Radiation Shielded Structure, $T_r = 3810^\circ\text{K}$

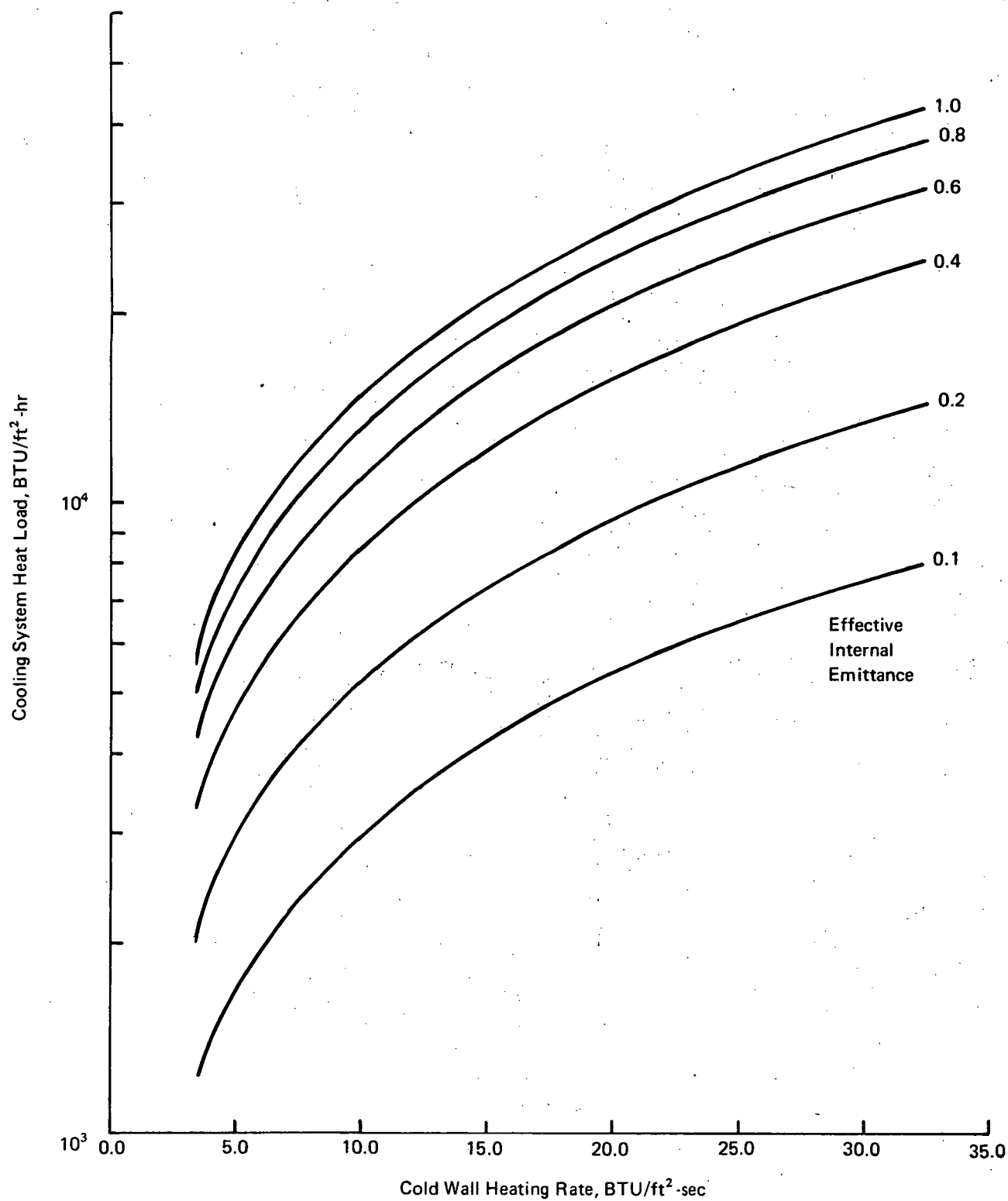


Figure 32b. Cooling System Heat Load for Radiation Shielded Structure, $T_r = 6400F$

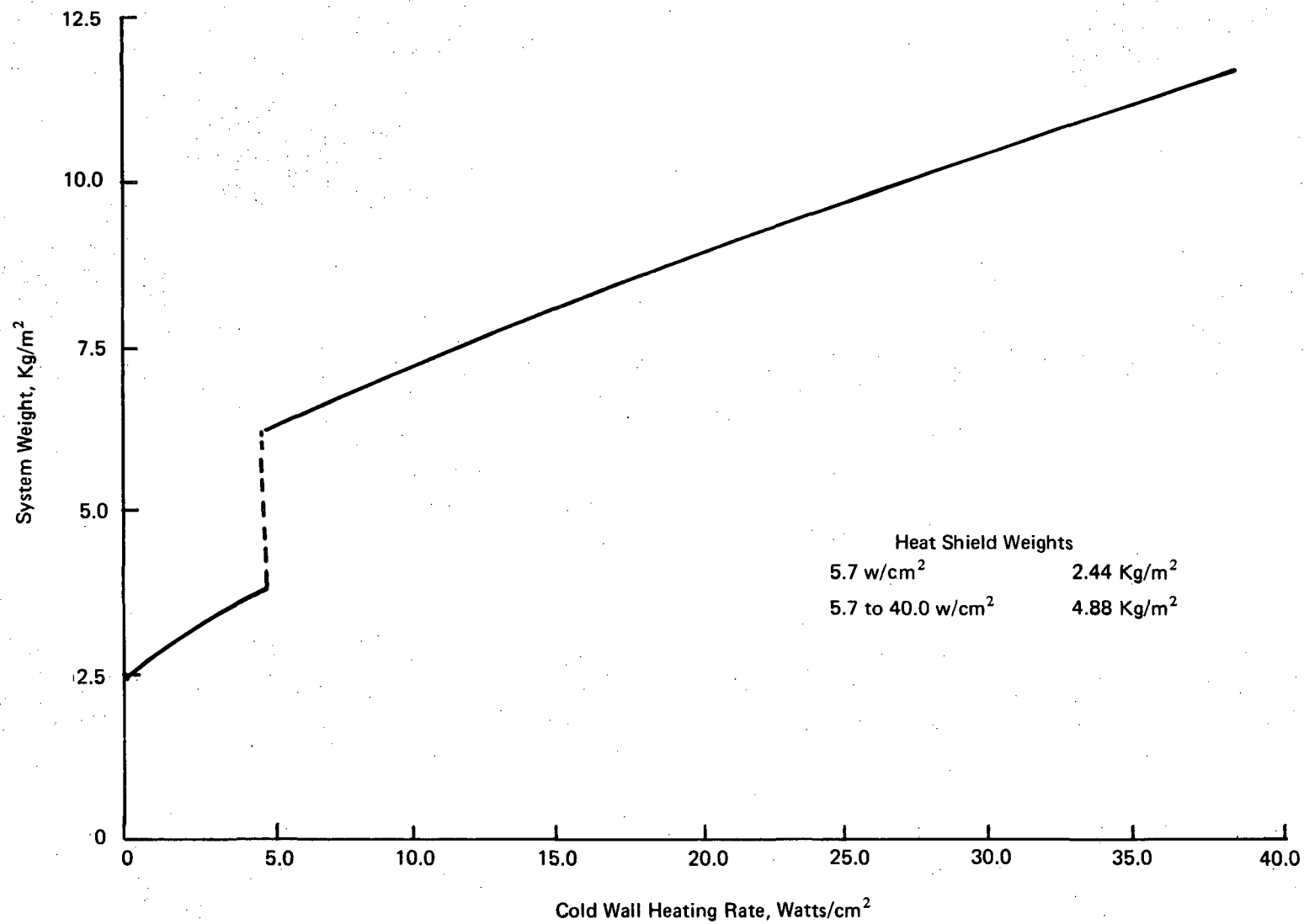


Figure 33a. Unit Weight of Radiation Shielded Cooling System, Effective Emittance
 = 0.67, Includes Heat Shield
 Weight, $T_r = 3810^\circ\text{K}$

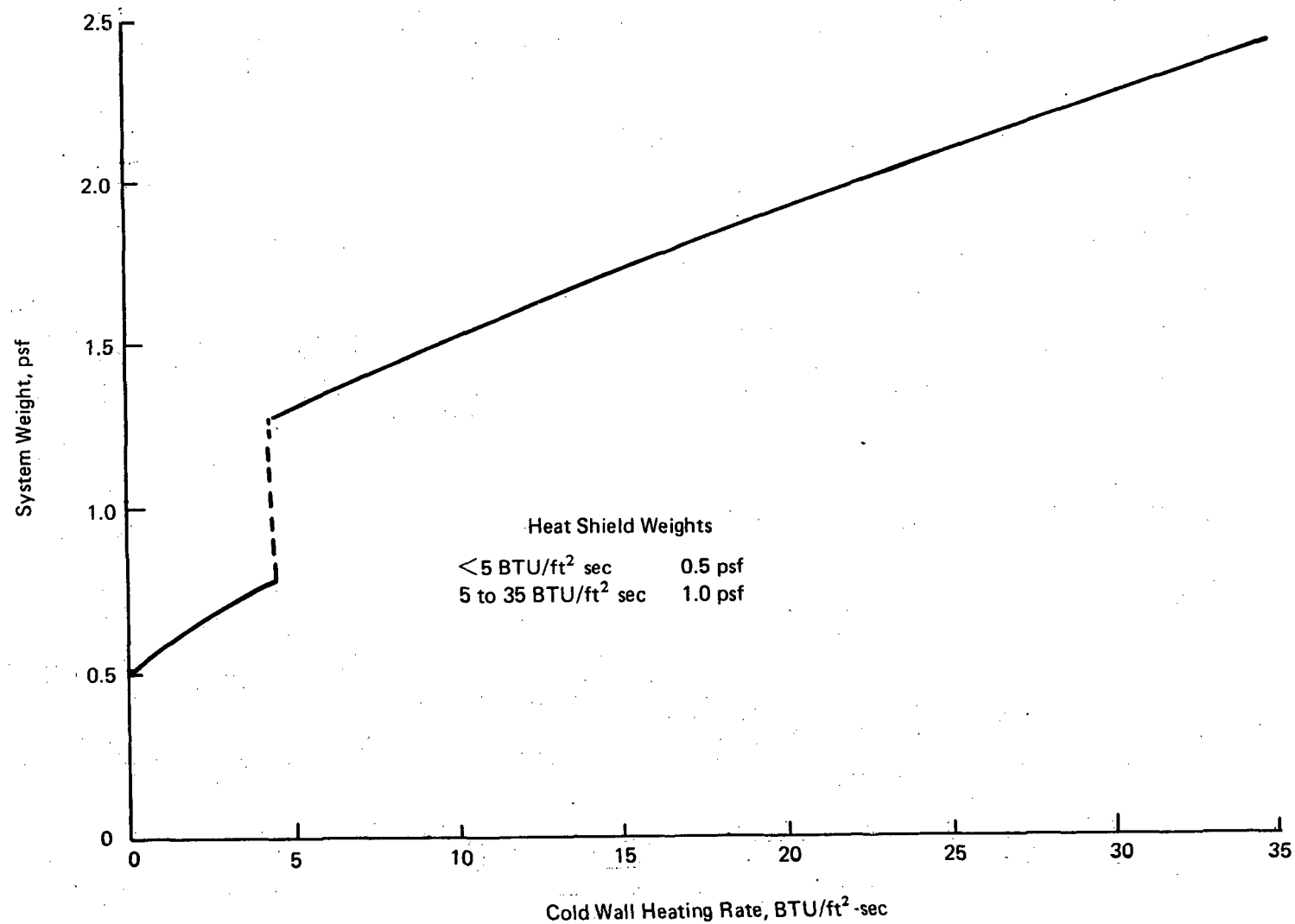


Figure 33b. Unit Weight of Radiation Shielded Cooling System, Effective Emittance = 0.67, Includes Heat Shield Weight, $T_r = 6400\text{F}$

Structural Analyses

The structural design studies of panel concepts included all of the types shown in Figure 12 and the more promising material from the selection studies of construction alloys. Initially the method of Reference 36 was used to examine cylindrical shells in bending and included the influence of temperature on material properties but was limited to monocoque, honeycomb sandwich, and skin/stringer/frame constructions. These results were used to reduce the number of candidate construction materials; the more promising construction materials were then compared for fuselage and wing structures of the types shown in Figure 12.

Fuselage Panels. Initial studies of fuselage panels compared aluminum alloys (2021-T81, 2219-T8, and 7475-T76), magnesium alloys (AZ31B-H24 and HK31A-H24) titanium alloys (6Al-4V, 6Al-2Cb-1Ta-0.8Mo, 16V-2.5Al), stainless/super alloys types 17-7 PH, 250 maraging steel, and Inconel 718), beryllium, and Lockalloy. Data was available from Reference 36 on the 2024-T3 and 7075-T6 aluminum alloy, HM21A-T8 and FSI-H24 magnesium alloy, and Inconel X nickel alloy. For the aluminum and magnesium alloys, temperatures of up to 300F were examined while for the other materials maximum temperatures were assumed to reach 600F.

The results of these comparisons indicated that:

- (1) Over the range of temperature of interest for each alloy the temperature dependence of properties had a modest influence on weight, less than 25%,
- (2) The differences among alloys of a given class were small compared to differences among classes,
- (3) Monocoque construction would be of interest only under very light loading conditions.

The fact that temperature dependence of properties had a minor influence on the weight of structural panels for hypersonic aircraft results from the active cooling of the airframe to temperature levels where structural efficiencies are highest. If the structure is to be cooled actively the temperature should be low enough to maximize structural efficiencies and to minimize thermal degradation effects including those on fatigue and due to creep and thermal stresses.

As a result of the initial studies the number of candidate materials of interest was decreased and the number of construction types was increased. The materials included 2021-T81 and 7475-T76 aluminum alloys, AZ31B-H24 magnesium alloy, 6Al-4V titanium alloy, 250 maraging steel, beryllium, and boron/aluminum composite. The types of construction included honeycomb sandwich, skin/stringer/frame, ring and corrugation stiffened skin, ring and symmetrical double beaded skin, and ring and unsymmetrical double beaded skin. These comparisons were all done at an assumed temperature of 100F since the prior studies showed relatively little influence of temperature over the range of interest for each alloy. With the exception of the honeycomb sandwich analyses the method of Reference 37 was used. Equivalent thicknesses and weights were determined at eight stations for the fuselage of the hypersonic transport. The results were plotted and integrated to obtain the skin panel weights presented in Table XVII for the materials and construction of interest. For purposes of this comparison no consideration was given to minimum gauge limitations. This practical consideration was introduced later when aircraft weights were determined, see "SYSTEM SUMMARIES." In referring to Table XVII, it appears that the most advanced materials, beryllium and boron/aluminum, result in

TABLE XVIII
COMPARISON OF CANDIDATE MATERIALS AND PANEL CONCEPTS FOR
HYPERSONIC TRANSPORT FUSELAGE AT 311°K, NO MINIMUM GAGE CONSTRAINT

| Concept/Alloy | Running Weight at Indicated Station, kg/m | | | | | | | | Total Weight, kg |
|-------------------------|---|-------|-------|-------|-------|-------|-------|-------|------------------|
| | 45 | 60 | 111 | 150 | 177 | 190 | 211 | 257 | |
| Ring/Stringer | | | | | | | | | |
| Aluminum | 42.9 | 64.3 | 164.8 | 206.1 | 212.6 | 224.4 | 181.8 | 69.7 | 10,580 |
| Magnesium | 45.1 | 60.6 | 184.8 | 274.9 | 332.0 | 323.0 | 197.9 | 68.1 | 12,770 |
| Titanium | 52.3 | 78.4 | 201.4 | 236.0 | 260.6 | 273.0 | 220.0 | 82.0 | 12,850 |
| Steel | 68.5 | 100.7 | 261.8 | 315.0 | 336.0 | 342.2 | 279.5 | 108.2 | 16,600 |
| Beryllium | 22.6 | 32.0 | 90.3 | 131.4 | 155.6 | 159.9 | 93.3 | 33.4 | 6,220 |
| Boron/Aluminum* | 21.2 | 29.7 | 83.4 | 122.9 | 146.6 | 149.5 | 86.3 | 31.0 | 5,820 |
| Ring/Symmetrical Bead | | | | | | | | | |
| Aluminum | 32.6 | 47.7 | 124.1 | 162.4 | 193.4 | 196.7 | 135.3 | 52.2 | 8,450 |
| Magnesium | 45.1 | 62.3 | 184.8 | 268.5 | 319.6 | 316.5 | 197.9 | 68.1 | 12,570 |
| Titanium | 37.8 | 57.8 | 150.5 | 187.7 | 201.2 | 208.9 | 160.9 | 61.8 | 9,580 |
| Steel | 49.0 | 70.8 | 169.4 | 232.9 | 251.8 | 257.0 | 201.6 | 76.0 | 11,610 |
| Beryllium | 22.6 | 32.0 | 95.1 | 133.7 | 155.6 | 159.9 | 96.0 | 34.3 | 6,300 |
| Boron/Aluminum* | 21.0 | 29.8 | 74.5 | 123.7 | 146.6 | 149.4 | 88.7 | 31.6 | 5,900 |
| Ring/Unsymmetrical Bead | | | | | | | | | |
| Aluminum | 44.0 | 65.6 | 170.2 | 207.7 | 227.2 | 231.4 | 183.7 | 71.1 | 10,530 |
| Magnesium | 48.0 | 65.6 | 189.2 | 262.2 | 307.4 | 316.5 | 201.6 | 69.0 | 12,740 |
| Titanium | 52.3 | 78.4 | 204.1 | 241.4 | 265.6 | 278.6 | 219.8 | 82.0 | 12,900 |
| Steel | 68.5 | 96.9 | 256.3 | 320.4 | 340.5 | 352.5 | 279.5 | 108.2 | 16,500 |
| Beryllium | 24.9 | 34.6 | 101.0 | 145.0 | 171.8 | 169.1 | 106.2 | 35.8 | 6,880 |
| Boron/Aluminum* | - | - | - | - | - | - | - | - | - |
| Ring/Corrugation | | | | | | | | | |
| Aluminum | 53.0 | 78.7 | 203.8 | 247.9 | 270.7 | 269.7 | 201.2 | 84.9 | 12,680 |
| Magnesium | 51.0 | 75.4 | 207.1 | 288.8 | 332.0 | 343.0 | 222.5 | 83.1 | 14,200 |
| Titanium | 63.2 | 92.8 | 249.7 | 287.1 | 324.8 | 331.5 | 269.2 | 101.8 | 15,920 |
| Steel | 84.6 | 130.7 | 317.8 | 382.9 | 424.4 | 438.4 | 346.7 | 129.9 | 20,620 |
| Beryllium | 26.5 | 35.5 | 103.4 | 145.0 | 175.1 | 176.1 | 111.5 | 38.4 | 7,000 |
| Boron/Aluminum* | 24.6 | 32.8 | 96.4 | 141.0 | 148.1 | 156.5 | 103.4 | 35.8 | 6,440 |
| Sandwich | | | | | | | | | |
| Aluminum | 40.5 | 71.1 | 191.5 | 233.2 | 276.4 | 229.5 | 197.1 | 92.2 | 12,390 |
| Magnesium | 31.9 | 54.1 | 212.3 | 370.7 | 436.4 | 329.3 | 184.5 | 121.1 | 15,300 |
| Titanium | 43.4 | 76.7 | 194.0 | 272.7 | 291.9 | 274.2 | 219.0 | 107.7 | 13,490 |
| Steel | 66.6 | 116.5 | 320.4 | 395.9 | 403.0 | 393.1 | 329.1 | 155.0 | 20,320 |
| Beryllium | 13.6 | 34.3 | 135.4 | 238.4 | 280.1 | 211.6 | 118.2 | 78.5 | 9,680 |
| Boron/Aluminum* | 12.7 | 32.0 | 125.2 | 221.3 | 260.0 | 196.7 | 110.6 | 72.6 | 9,005 |

*50% 0° + 50% ±30° Laminate

TABLE XVIIB
COMPARISON OF CANDIDATE MATERIALS AND PANEL CONCEPTS FOR
HYPERSONIC TRANSPORT FUSELAGE AT 100F, NO MINIMUM GAGE CONSTRAINT

| Concept/Alloy | Running Weight at Indicated Station, lb/ft | | | | | | | | Total Weight, lb |
|-------------------------|--|------|-------|-------|-------|-------|-------|-------|------------------|
| | 45 | 60 | 111 | 150 | 177 | 190 | 211 | 257 | |
| Ring/Stringer | | | | | | | | | |
| Aluminum | 28.8 | 43.2 | 110.6 | 138.3 | 142.7 | 150.6 | 122.0 | 46.8 | 23,300 |
| Magnesium | 30.3 | 40.7 | 124.0 | 184.5 | 222.8 | 216.8 | 132.8 | 45.7 | 28,160 |
| Titanium | 35.1 | 52.6 | 135.2 | 158.4 | 174.9 | 183.2 | 147.5 | 55.0 | 28,300 |
| Steel | 46.0 | 67.6 | 175.7 | 211.4 | 225.5 | 229.7 | 187.6 | 72.6 | 36,550 |
| Beryllium | 15.2 | 21.5 | 60.6 | 88.2 | 104.4 | 107.3 | 62.6 | 22.4 | 13,730 |
| Boron/Aluminum* | 14.2 | 19.9 | 56.0 | 82.5 | 98.4 | 100.3 | 57.9 | 20.8 | 12,850 |
| Ring/Symmetrical Bead | | | | | | | | | |
| Aluminum | 21.9 | 32.0 | 83.3 | 109.0 | 129.8 | 132.0 | 90.8 | 35.0 | 18,640 |
| Magnesium | 30.3 | 41.8 | 124.0 | 180.2 | 214.5 | 212.4 | 132.8 | 45.7 | 27,630 |
| Titanium | 25.4 | 38.8 | 101.0 | 126.0 | 135.0 | 140.2 | 108.0 | 41.5 | 21,170 |
| Steel | 32.9 | 47.5 | 113.7 | 156.3 | 169.0 | 172.5 | 135.3 | 51.0 | 25,630 |
| Beryllium | 15.2 | 21.5 | 63.8 | 89.7 | 104.4 | 107.3 | 64.4 | 23.0 | 13,900 |
| Boron/Aluminum* | 14.1 | 20.0 | 59.0 | 83.0 | 98.4 | 100.3 | 59.5 | 21.2 | 13,010 |
| Ring/Unsymmetrical Bead | | | | | | | | | |
| Aluminum | 29.5 | 44.0 | 114.2 | 139.4 | 152.5 | 155.3 | 123.3 | 47.7 | 23,260 |
| Magnesium | 32.2 | 44.0 | 127.0 | 176.0 | 206.3 | 212.4 | 135.3 | 46.3 | 28,140 |
| Titanium | 35.1 | 52.6 | 137.0 | 162.0 | 178.3 | 187.0 | 147.5 | 55.0 | 28,530 |
| Steel | 46.0 | 65.0 | 172.0 | 215.0 | 228.5 | 236.6 | 187.6 | 72.6 | 36,400 |
| Beryllium | 16.7 | 23.2 | 67.8 | 97.3 | 115.3 | 113.5 | 71.3 | 24.0 | 15,180 |
| Boron/Aluminum* | | | | | | | | | |
| Ring/Corrugation | | | | | | | | | |
| Aluminum | 35.6 | 52.8 | 136.8 | 166.4 | 181.7 | 181.0 | 135.0 | 57.0 | 27,940 |
| Magnesium | 34.2 | 50.6 | 139.0 | 193.8 | 222.8 | 230.2 | 149.3 | 55.8 | 31,330 |
| Titanium | 42.4 | 62.3 | 167.6 | 192.7 | 218.0 | 222.5 | 180.7 | 68.3 | 35,040 |
| Steel | 56.8 | 87.7 | 213.3 | 257.0 | 284.8 | 294.2 | 232.7 | 87.2 | 45,500 |
| Beryllium | 17.8 | 23.8 | 69.4 | 97.3 | 117.5 | 118.2 | 74.8 | 25.8 | 15,440 |
| Boron/Aluminum* | 16.5 | 22.0 | 64.7 | 94.6 | 99.4 | 105.0 | 69.4 | 24.0 | 14,200 |
| Sandwich | | | | | | | | | |
| Aluminum | 27.2 | 47.7 | 128.5 | 156.5 | 185.5 | 154.0 | 132.3 | 61.9 | 27,300 |
| Magnesium | 21.4 | 36.3 | 142.5 | 248.8 | 292.9 | 221.0 | 123.8 | 81.3 | 33,650 |
| Titanium | 29.1 | 51.5 | 130.2 | 183.0 | 195.3 | 184.0 | 147.0 | 72.3 | 29,760 |
| Steel | 44.7 | 78.2 | 215.0 | 265.7 | 270.5 | 263.8 | 220.9 | 104.0 | 44,785 |
| Beryllium | 9.1 | 23.0 | 90.9 | 160.0 | 188.0 | 142.0 | 79.3 | 52.7 | 21,390 |
| Boron/Aluminum* | 8.5 | 21.5 | 84.0 | 148.5 | 174.5 | 132.0 | 74.2 | 48.7 | 19,850 |

*50% 0° + 50% ±30° Laminate

lightest weight regardless of the type of construction. In general, the aluminum alloys are next most attractive, the magnesium and titanium alloys are comparable in weight, and the maraging steel results in highest weight. On a total fuselage basis the symmetrical double beaded skin is the lightest construction, particularly for alloys of high density such as titanium and steel, while the honeycomb sandwich is the heaviest. Weights for the ring and Z stringer stiffened construction were comparable to those for the unsymmetrical double beaded skin for any particular material. For the unsymmetrical double beaded and the stringer stiffened skin constructions there is little difference in weight between the aluminum and magnesium material in the lightly loaded forward and rear portions of the fuselage. For the other types of construction magnesium is somewhat lighter. It is apparent from the comparative weights of fuselage skins that regardless of the type of construction used, the materials in order of increasing structural weight, are:

- (1) beryllium or boron/aluminum
- (2) aluminum alloys
- (3) alloys of magnesium or titanium
- (4) steel alloys

In addition, there appeared to be little weight saving potential that could be realized by utilizing different materials at various locations of the fuselage in attempting to tailor material choices for variations in loading intensity.

It should be noted that the weights summarized in Table XVII represent the skin and stiffening elements with only sufficient frame to provide stability. Not included in these weights are the passenger compartment, the floor, and the effect of internal pressurization requirements on frame weights, as well as minimum gage considerations. Thus, the weight of the fuselage fabricated from any candidate material will be heavier than the values listed in Table XVII.

When considering aerodynamic smoothness, the incorporation of integral coolant passages and minimum gage constraints, the use of corrugated types of skins is highly questionable. On the fuselage, the stiffening should be oriented axially while the coolant passages should be circumferentially oriented. Thus, the stiffened skin and the honeycomb sandwich concepts appear to be most attractive. The apparent weight penalty associated with eliminating the symmetrical double beaded design as a candidate is reduced to zero when minimum gage constraints are introduced.

Wing Panels. - The fuselage panel studies preceded similar analyses of wing panels so that design trends permitted a narrowing of the materials and the types of construction considered. Materials included alloys of aluminum, magnesium, titanium, maraging steel, beryllium, and boron aluminum composite. Structural arrangements included Z-stiffened skins, symmetrical and unsymmetrical beaded skins, and honeycomb sandwich. The method of Reference 38 was used to obtain basic weights for axial loadings. These weights were doubled to correct, in an approximate manner, for torsional and shear loadings based on the work of Reference 1. Minimum gage constraints were introduced; results are summarized in Table XVIII. In order of increasing weight the material ranking is beryllium, boron/aluminum, aluminum, titanium, and maraging steel. A weight factor of approximately 3.0 exists between the steel and beryllium materials. Sandwich construction was found to be lightest regardless of the type of material used, with the symmetrical double beaded second followed by Z stiffened sheet and the unsymmetrical double beaded skin.

TABLE XVIII
COMPARISON OF MATERIALS AND CONCEPTS FOR
WING COVERS, HYPERSONIC TRANSPORT

| Material | Z - Stiffened | Symmetrical Double Bead | Unsymmetrical Double Bead | Honeycomb Sandwich |
|-----------------|---------------|----------------------------|------------------------------|-----------------------|
| Aluminum | 8,300 | 6,700 | 8,600 | 6,300 |
| Magnesium | 9,800 | — | 10,400 | — |
| Titanium | 11,900 | 7,600 | 12,300 | 6,400 |
| Maraging Steel | 16,300 | — | — | — |
| Beryllium | 5,600 | 5,700 | 5,800 | 5,400 |
| Boron/Aluminum* | 6,300 | 6,300 | 6,500 | 5,700 |

*Laminate Consisting of 50% 0° and 50% ±30° plies

TABLE XVIII B
COMPARISON OF MATERIALS AND CONCEPTS FOR
WING COVERS, HYPERSONIC TRANSPORT

| Material | Weight of Cover Panels for Concept Indicated, Pounds | | | |
|-----------------|--|----------------------------|------------------------------|-----------------------|
| | Z - Stiffened | Symmetrical Double Bead | Unsymmetrical Double Bead | Honeycomb Sandwich |
| Aluminum | 18,200 | 14,600 | 18,900 | 13,900 |
| Magnesium | 21,800 | — | 22,800 | — |
| Titanium | 26,000 | 16,600 | 27,100 | 14,000 |
| Maraging Steel | 35,600 | — | — | — |
| Beryllium | 12,200 | 12,500 | 12,700 | 11,800 |
| Boron/Aluminum* | 13,600 | 13,800 | 14,150 | 12,600 |

*Laminate Consisting of 50% 0° and 50% ±30° plies

For purposes of comparing wing panel designs the stiffened skins were assumed to be wide columns and panel lengths were varied from 0.5 to 1.0 m (20 to 40 inches) for loading intensities of up to 14,000 N/cm (8,000 pounds/inch). With no consideration given to minimum gage limitations, substructural weights, or nonoptimum factors the lightest type of construction was the symmetrical double beaded skin, with sandwich construction about 15% heavier, unsymmetrical double beaded skin about 33% heavier, and Z stringer stiffened skin about twice as heavy. When minimum gauge requirements are introduced the honeycomb sandwich becomes the lightest followed by the symmetrical double beaded skin, the Z-stiffened skin, and the unsymmetrical double beaded skin. However, it is difficult to incorporate coolant passages with optimum beaded skins when minimum gauge constraints are considered. Therefore, only the honeycomb sandwich and the Z-stiffened skin concepts are considered to be promising.

Structural Assembly

The smooth aerodynamic surface desired for the cooled unprotected airframe structure necessitates the inward protrusion of coolant passages in the skin panels. Unless a sandwich type of construction is used, assembly of the skin with substructural elements such as stiffeners, rings, etc., requires careful consideration of design details. Structural assembly concepts for cooled sandwich panels are shown in Figure 34 while discrete tubular passage panel concepts are shown in Figure 35. Both shielded and unprotected honeycomb skin panels are illustrated, and in addition, plate-fin sandwich panels are shown in Figure 34. With the shielded approach titanium or superalloy honeycomb could be adhesively bonded to the cooled inner structure. The high thermal stresses that might result could be minimized by not joining the outer sheet and core assembly to the cooled structure, but rather to hold it in place with strips as shown. Since the spacing of stiffening elements are expected to range from about 5.0 to 15 cm (2 to 6 inches) the unsupported width of the open face honeycomb sandwich should not be excessive. If strips are not provided for joining the cooled skin to the substructure, it would be necessary to install mechanical fasteners through the sandwich thickness as shown. Inserts would probably be needed and would increase the heat flow from the outer skin to the cooled inner skin. However, this should not be a problem in view of the similarity of this technique to the shielded panel concept discussed previously. When the cooled surface is external to the sandwich assembly, adhesive bonding can be used, the number of internal stiffening elements can be reduced, and final assembly to substructural elements can be accommodated with relative ease by eliminating the honeycomb core in the joint region as shown.

The assembly techniques envisioned for plate-fin construction are different from those currently used in airframe construction. Inserts are essential if mechanical fastenings are to be used, except perhaps at edges where the core can be eliminated. For low temperature alloys, substructural elements can be adhesive bonded to the cooled skin panels while for the high temperature alloys brazing can be used. With this type of an approach, it should be possible to utilize an integrally machined inner skin, so that it can be attached to substructural elements using the conventional mechanically fastened techniques. However, the complexity of matching the integrally machined skins with previously installed substructural elements is a major challenge. This suggests that the stiffening could be integral with or integrated with the cooled plate-fin panel before the panels are assembled with the major substructural elements such as stringers, frames, spars, and ribs. With such an arrangement it would be necessary to attach the panel stiffening element to the major substructural elements by means of clips.

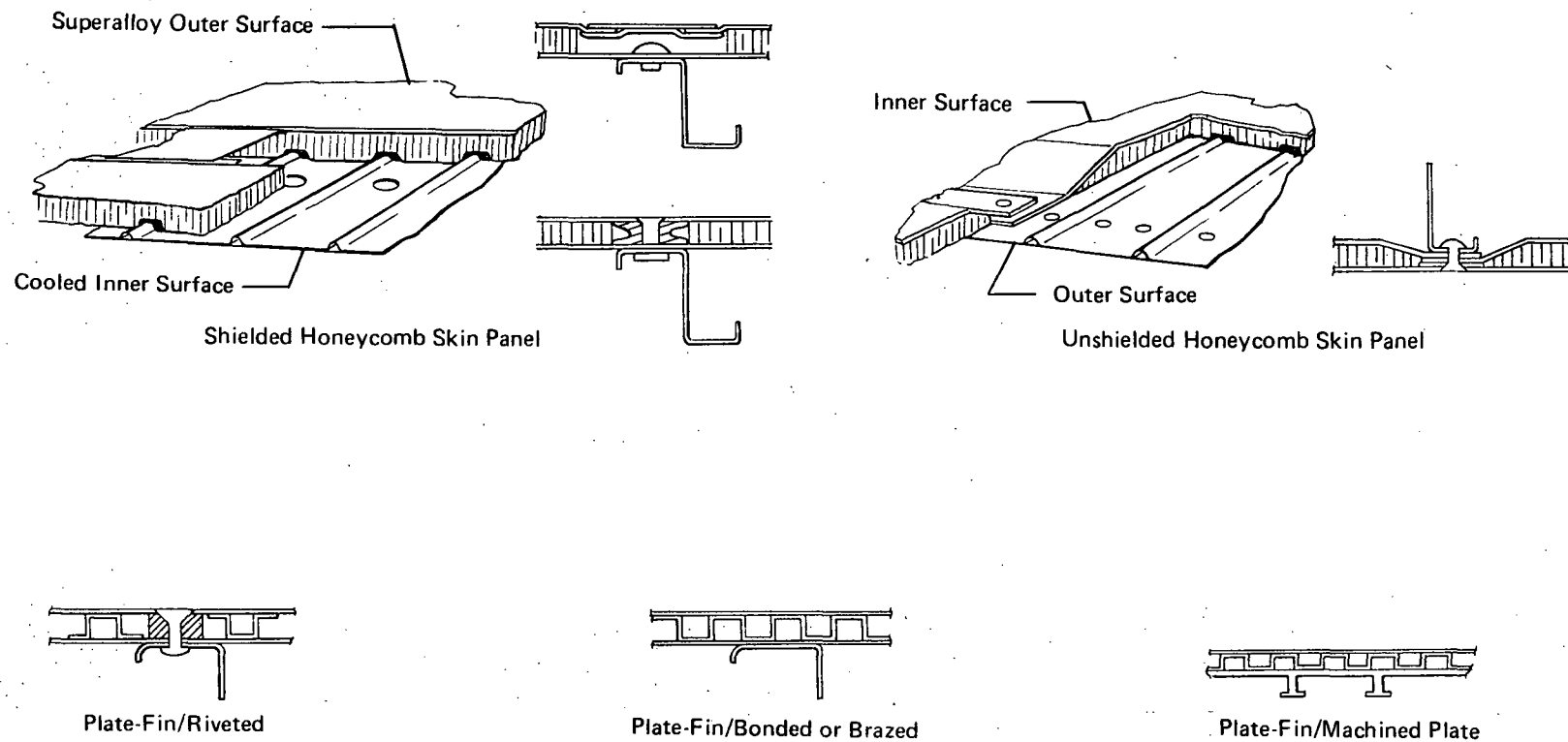
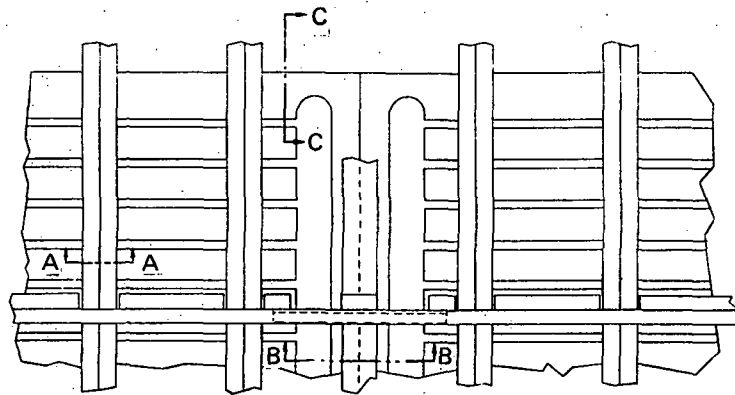
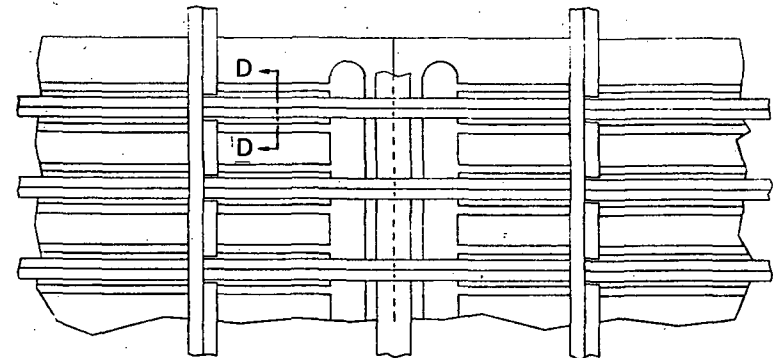


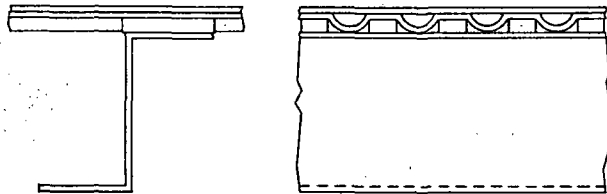
Figure 34. Typical Thermal/Structural Integration Techniques for Sandwich Construction



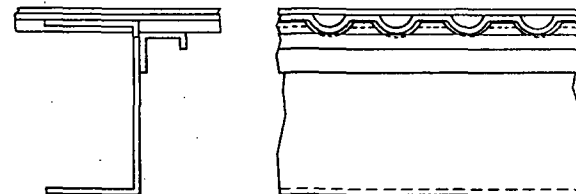
Stringers Perpendicular to Coolant Passages



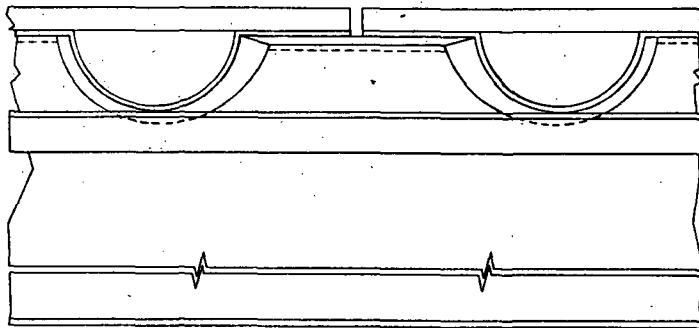
Stringers Parallel to Coolant Passages



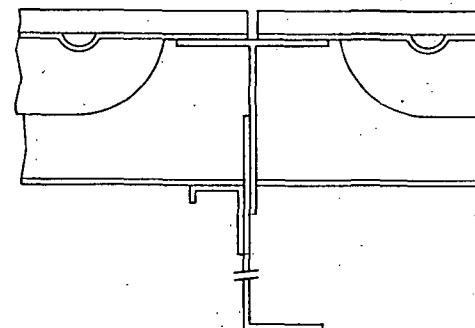
A-A



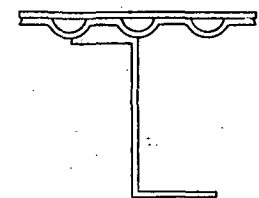
Alternate A-A



B-B



C-C



D-D

Figure 35. Structural Details for Assembly of Cooled Airframe, Discrete Tubular Skin Panels

In Figure 35, consideration was given to stringer orientations perpendicular and parallel to coolant passages. Assembly problems become most difficult when very close passage spacing is required, as shown on the detailed sections. It is left to the reader to envision the simplification possible as passage spacing is increased. Attachment of the stringers perpendicular to the coolant passages, Sections A-A and alternate A-A, require a spacer to clear the passage height. The first detail utilizes a filler strip between the skin and the stringer. Such fillers could be adhesively bonded to the skin to minimize local stresses due to mechanical fasteners. It should be possible to obtain a thin gage stringer extrusion with one thick flange which is subsequently machined to provide local bearing pads between the coolant passages. The alternate involves notching the stringer to achieve integral shear clips for joining to the skin plus the addition of an angle to replace the continuity lost by notching. The notches can be of large radius to minimize stress concentration. The reinforced stringer can be assembled by riveting or adhesive bonding. It is also possible to procure special thin gage extrusions which would provide an integral angle just below the level of the notch bottom. The choice of approach depends upon the space between edges of the coolant tubes, the height of the coolant passages, and the loads involved.

When the stringers are perpendicular to the coolant passages, the frames or rib caps will be paralleled to the passages and perpendicular to the inlet and outlet manifolds. The manifolds must have significant height so that a means of maintaining structural continuity past a manifold is required. Section B-B shows one approach. The frame is notched to clear the header and the notch is reinforced with an angle. The width of the flat header side will be sufficiently large that an internal double plate is likely to be needed. An internal splice plate can be used between skin panels; the use of an external plate would introduce a thermal resistance between the external plate and the cooled skin panel which might cause excessive temperature.

Splicing of the panel edges parallel to the coolant passages is illustrated in Section C-C. For this particular illustration a curved fuselage frame is envisioned to be assembled from two formed angles and a tee. Skin edge doublers are shown to minimize stress concentration if mechanical fasteners are used; these doublers also enhance in-plane conduction of heat. The frame could be assembled by riveting or adhesive bonding. The stringers are continuous through the frame with flange attachment to the short angle of the frame. Alternatively, shear clips could be used between the webs of the stringers and notched frames. In the case of a rib cap where the degree of curvature is small a single piece extrusion might be used with a significant weight saving achieved by eliminating overlap areas.

When the stringers are oriented parallel to the coolant passages a most promising approach is that previously illustrated in A-A and shown in D-D with an appropriate variation to account for the change in orientation between the stringer and the coolant passages. Here, a stringer with a thick flange is shown as an extruded member. This minimizes costs and provides local reinforcement for the stiffer flange. However, it is generally more desirable to reinforce the skin since the growth of skin cracks could endanger operation of the cooling system by inducing leakage.

Thermal Stresses

Despite the fact that active cooling is employed some temperature gradients exist. For the baseline panel configuration heat is removed along discrete lines while heat input is more or less uniformly applied. Temperatures are a maximum between coolant passages and are at minimum levels

at the passages. The temperature distribution is defined by hyperbolic functions but can be approximated rather closely by simple algebraic functions. In the case of the plate-fin and spherical core sandwiches the temperature of the outer face is higher than that of the inner face although the temperature along any line perpendicular to the direction of coolant flow is practically constant on each face.

The shape of the thermal stress distribution is practically identical to that of the temperature distribution, deviating only as a result of temperature dependence of material properties. The magnitude of the total thermal stress, as an absolute value, is determined by multiplying the temperature gradient by the product of the expansion coefficient and the modulus of elasticity. The apportionment of this overall stress magnitude into tension and/or compression increments depends upon the restraint on the component subjected to the temperature gradient. In the case of a completely restrained component all thermally induced stresses will be compressive and their magnitudes will be directly proportional to the difference between the final temperature distribution and the initial temperature distribution. If the component is prevented from bending under the thermally induced loads the relative proportions of the tension and compression stresses can be estimated by integrating the thermal stresses into forces and balancing the tension and compression loads.

A number of texts and other reports can be consulted to obtain more accurate predictions of thermal stresses resulting from temperatures gradients. However, one of the major objectives of a cooled airframe is to minimize thermal degradation influences on airframe designs. Therefore, the magnitude of the thermal stresses is likely to range between 10 and 20% of the yield strength of the construction material. Hence, small errors in thermal stress estimation are not of extreme criticality. Some coolant passage spacings for different materials based on thermal stress equal to 15% f_{cy} are shown in the section on Materials Selection.

COOLING SYSTEM DESIGN STUDIES

Within the scope of this study the cooling system is of the liquid convective type that absorbs heat from actively cooled panels and transports it to a heat exchanger where it is rejected to the hydrogen fuel used to power the aircraft. The primary objectives in designing such a system include minimization of weight and maximization of reliability. In addition, there may be situations where the operating temperature levels of the coolant limit the percentage of the fuel heat capacity that can be used for airframe cooling. For example, if aluminum alloy is used to minimize costs its maximum operating temperature will be in the order of 423°K (300°F) such that the coolant temperature cannot exceed about 395°K (250°F) and the hydrogen cannot be heated to more than about 366°K (200°F). This permits the hydrogen fuel to absorb about 4.9 J/g (2100 BTU/lb). If the airframe heat load requires greater cooling capacity a number of alternatives can be considered such as providing external thermal protection, flowing hydrogen in excess of fuel flow requirements, or changing structural material so that operating temperatures can be increased thereby increasing the heat capacity of the hydrogen fuel that can be used for airframe cooling requirements. This last approach, however, does not change the total heat capacity of the fuel, rather, the portion that can be utilized for airframe cooling is increased while that portion that can be used for engine cooling is decreased.

Concepts

Since continuous cooling is essential to the safe operation of an actively cooled airframe a single nonredundant system, as discussed in Reference 3, may not be an optimum solution. It may be desirable to consider varying degrees of redundancy so that the most reliable and economical concept can be determined from among:

1. A single nonredundant system,
2. A single system with some duplicate components such as pumps, controls, and heat exchangers,
3. Redundant cooling loops for critical regions such as leading edges with a nonredundant or partially redundant system for less critical areas,
4. A single full capacity system and a second system of lesser capacity such that the flight operation would be restricted should the primary system fail,
5. Two completely duplicate systems.

In order to obtain an assessment of the relative merits of the various design approaches weight and reliability analyses were conducted for the two extreme situations, nonredundancy and complete redundancy. From these basic analyses estimates of the weights and reliabilities of other variations can be made.

Figure 36 depicts the completely redundant cooling system. Each loop of the distribution system contains a network of lines that connect the airframe skin panels to a hydrogen cooled heat exchanger with a pump to provide circulation, an expansion tank, and appropriate temperature sensors, pressure transducers, flow meter, and valves. Coolant can be ducted to various vehicle subsystems as desired. In addition to accommodating volumetric changes of the coolant, the expansion tank provides a pressure head for the pump intake and serves as a coolant reservoir to replenish minor leakage. A portion of the hydrogen flow to the engines is ducted through each heat exchanger as required, with the excess being bypassed. The hydrogen exhausted from each heat exchanger is supplied to the engine as heated fuel.

By measuring the coolant flow rate and the coolant inlet and outlet temperatures at the heat exchanger it is possible to compute the heat load absorbed by the skin panels. A knowledge of the heat exchanger performance characteristics, the skin panel coolant flow rate and temperatures, and the hydrogen inlet temperature will allow control of the proportioning valves so that proper hydrogen flow is achieved through the heat exchanger. In Figure 36, no flow meter is shown for the hydrogen nor is a temperature transducer shown in the hydrogen inlet line. It is assumed that these transducers would be part of the fuel system instrumentation and that appropriate signals could be provided to the cooling system controls. In addition to the system components shown in Figure 36 there is likely to be a need for shutoff valves at various locations to facilitate installation and removal of equipment, fill and drain connections, bleed valves, and other items which might be desired to facilitate inspection, fault detection, and fault isolation. Such aspects are discussed in the "Fault Isolation" section of this chapter.

In reviewing Figure 36 it is apparent that each of the redundant distribution systems is quite independent. If desired, separate bypass lines could be provided for each heat exchanger rather than the common line shown schematically. The separate identity of each loop can be preserved during detailed design of an aircraft by physical separation of components and by slight differences in detailed design features for each loop. However, the close proximity of coolant passages within the skin panels raises the question as to whether the cooling systems are truly redundant. In a sense, the skin panels contain separate independent coolant passage networks, a redundant feature. But these passages are quite close together so that an incident likely to damage one system may damage the other. The likelihood of one incident damaging both coolant circuits within a panel depends upon the incident as well as on the panel design. The use of a crack arrestor, Figure 13, in the vicinity of the coolant passages might make the panel redundant with respect to crack growth but the panel may not be redundant with respect to a foreign object that damages two adjacent coolant passages simultaneously. Experimental evaluations are required to define the true degree of redundancy provided by a particular design.

Within the concept of complete redundancy at least two variations are possible: (1) the flowrate in each system is sufficiently large to absorb the total heat load, and (2) each loop is sized for a flowrate somewhat less than that required to absorb the total heat load. The first approach results in significant over cooling under all but the most severe maneuver conditions when only one loop is functioning, single mode operation. As will be shown later this constitutes a substantial weight penalty, about 15% of the distribution system weight. The weight penalty can be reduced by reducing the flow rate in each loop so that in the case of emergency it is necessary to increase the flow rate in the remaining operational cooling loop or to suffer a rise of structural temperature.

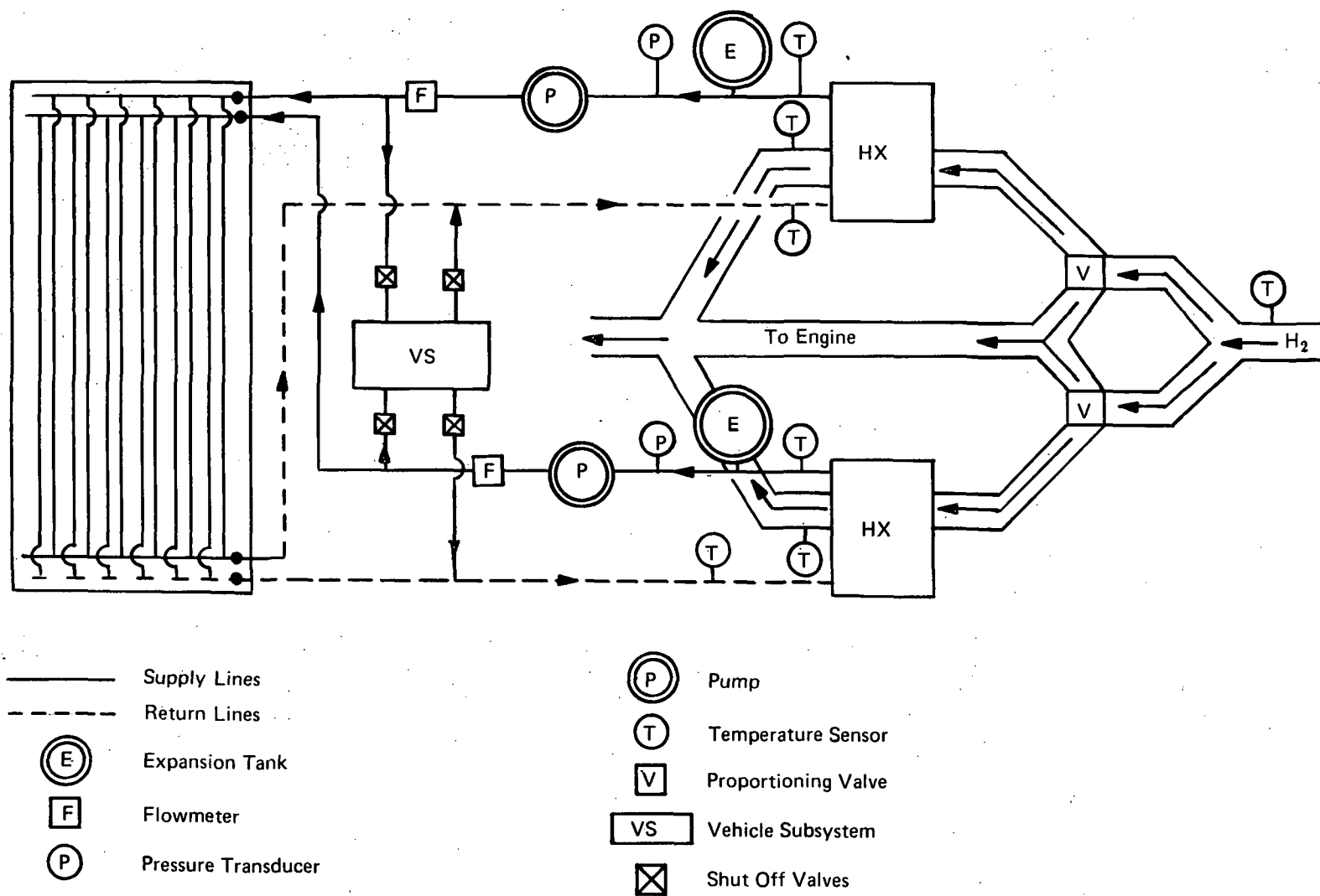


Figure 36. Redundant Cooling System Schematic

However, studies indicated the desirability of sizing each loop for approximately half of the required coolant flow rate and of increasing the flow rate when one loop became inoperative. As will be discussed later for the hypersonic research airplane, the inability to increase coolant flow rate when single mode operation is initiated will not result in catastrophic conditions although it may be desirable to restrict the flight envelope. If the coolant flow rate is increased to the full flow rate required to absorb the aerodynamic heat input associated with the mission, without increasing structural temperatures significantly, it would be possible to complete the mission without an abort. If a second failure precludes increasing the coolant flow rate it would be desirable to reduce air speed so that the aerodynamic heat input would tend to match the heat capacity at reduced coolant flow rate.

Referring back to the five liquid convective cooling system concepts described earlier in this section it is apparent that a single full capacity system combined with a second system of lesser capacity would be schematically similar to the completely redundant concept of Figure 36. System weight would be less than for the completely redundant approach. The reduction in capacity for the second system could be based on the fact that the number of maximum load factor maneuvers to be encountered during the life of an aircraft is quite small and that the likelihood of such a condition occurring during a time of emergency is very unlikely. Thus, a rationale might be established for designing the secondary system for a heat load corresponding to a load factor between 1.5 g and 2.0 g, so that a degree of maneuverability is retained. Furthermore, the maximum structural temperature might be allowed to increase by a relatively small amount, perhaps 14 to 28° K (25 to 50F), because the time accumulated at the higher temperature level would be very small; the cooling system would be repaired before another flight. Once the heat load and coolant operating temperature levels are defined for the secondary system its weight can be estimated using the data contained in other sections of this chapter.

If only critical regions have redundant cooling loops, weight estimates can be made by introducing appropriate corrections to either reduce the weight of a redundant system or to increase the weight of the nonredundant system. This is equally true for a single system that contains duplicate components. Obviously, the system of lightest weight and least complexity is the nonredundant one. However, the reliability of such a system is lower than for alternative concepts, but may be satisfactory for some applications.

In earlier cooled airframe structure studies, References 1, 2, and 3, a single construction material and a single cooling system were used. This simplifies fabrication and development efforts, but does not necessarily lead to an optimum aircraft. When low cost aluminum alloy construction is used, heat shields or other heat load reducing techniques may be required, but if the maximum coolant temperature is increased to increase the airframe heat input that can be absorbed by the hydrogen fuel such attenuating devices may be eliminated. However, fabrication costs increase when higher temperature materials are used. Therefore, it is possible that an optimum aircraft may use more than one structural material and two or more coolant loops, possibly with different fluids, such that the hydrogen fuel temperature is raised to a level above that associated with the primary construction material and coolant before entering the engine structure. Figure 37 shows an example which uses aluminum alloy for the major portion of the airframe with beryllium and superalloys in selected regions to permit coolant flow requirements to match the fuel flow schedule. Heat shields are eliminated, smooth external surfaces are provided, the higher cost materials are limited in usage, and in the case of beryllium, the areas are lightly loaded. Thermal stress checks of the beryllium and

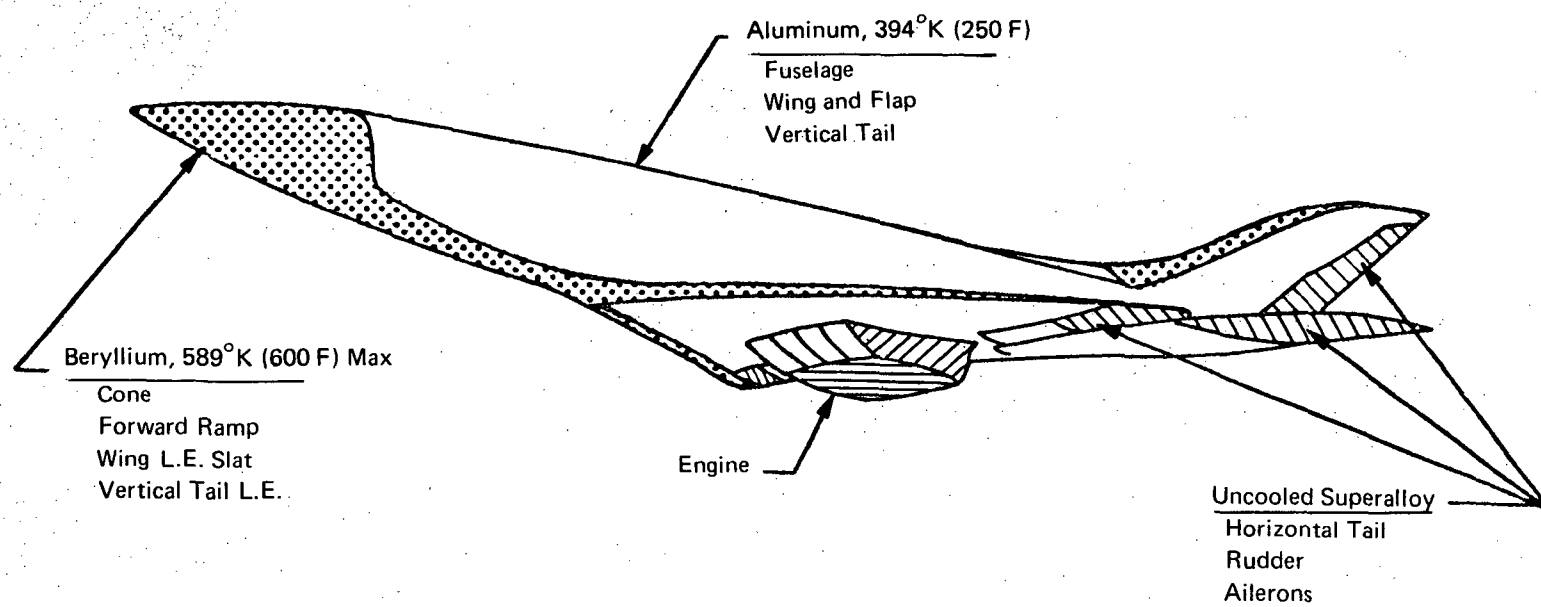


Figure 37. Multiple Systems, Mixed Materials

aluminum interface indicate modest levels, less than 103 MN/m^2 (15,000 psi). It is obvious that the beryllium and/or aluminum structures can be replaced by titanium or stainless steel alloys and the relative areas of the material combinations can be altered to suit particular design requirements. Systems of this type were examined for the hypersonic transport and for the hypersonic research airplane; results are summarized in "System Summaries".

Distribution Line Sizing

Hypersonic Transport. - Nonredundant and redundant distribution system line characteristics were defined for selected coolants. For a maximum coolant outlet temperature of 366°K (200F), compatible with aluminum alloy structure, ethylene glycol/water, FC-43, and Coolanol 45 were compared. Coolants were also examined for an outlet temperature of 450°K (350F), suitable for use with titanium, beryllium, superalloy, or boron/aluminum construction materials. The coolants included were Coolanol 45, Dow Corning XF-1-3755, and Freon E-5. These comparisons were based on the cooling system configuration developed in Ref 3 and shown in Figure 38. For this geometric arrangement heat loads were varied from 11.7 MW to 117 MW (40 million to 400 million BTU/hr) and coolant inlet temperatures were varied from 228°K (-50F) to 310°K (100F). The weight penalty for fuel to drive the coolant pump was computed as in Ref 3. Coolant flow was programmed during the mission in the 3-step mode described in Ref 3. Distribution line weights, including the pumping power penalty, are presented in Figures 39, 40 and 41 for the lower temperature coolants while the corresponding pressure drops are shown in Figures 42, 43 and 44. The nonredundant and two redundant concepts are compared. As discussed previously the 100% flow/loop redundancy approach results in significant overcooling while the 50% flow/loop design requires an increase in flowrate or yields an increase in structural temperature if one loop malfunctions. The pressure drop curves include a 0.35 MN/m^2 (50 psi) allowance for the heat exchanger and the skin panel farthest from the pump. The glycol/water coolant yields lightest weights and lowest pressure drops. The FC-43 coolant results in the highest line weights.

Weight results for the higher temperature coolants are presented in Figures 45, 46 and 47 while pressure drop data is presented in Figures 48, 49 and 50. The increase in maximum coolant temperature reduces coolant flow rate, pressure drop, and line size as compared to the values for the same coolant used with a lower maximum temperature. The trend is illustrated by comparison of the Coolanol 45 data at the two maximum temperature levels. In fact, the benefits of the higher coolant temperature rise is sufficiently large so that the system weights for the Coolanol 45 system with a maximum temperature of 450°K (350F) are lower than for glycol/water at 366°K (200F) and the pressure drops are very slightly higher than for glycol/water.

In reviewing the data it can be noted that the distribution line weight increases by a factor of about 6 when the heat load increases by a factor of 10. In general, weight decreases as inlet temperature decreases. However, in the case of Coolanol 45 and Freon E-5 with outlet temperatures of 450°K (350F), and for high heat loads, a minimum weight is indicated at an inlet temperature of about 265°K (0F). In comparing the redundant, 100% flow, and nonredundant cooling system weights the former is found to be heavier by about 50% to 70% depending upon the particular coolant, the heat load, and the inlet temperature.

Hypersonic Research Airplane. - Parametric studies of the distribution lines and pumping power penalty for this aircraft were conducted in a manner similar to those for the hypersonic transport. Initially four arrangements of distribution lines were compared for a single heat load and the glycol/water coolant with an inlet temperature of 283°K (50F) and an outlet temperature of 366°K

S - Supply Line
R - Return Line

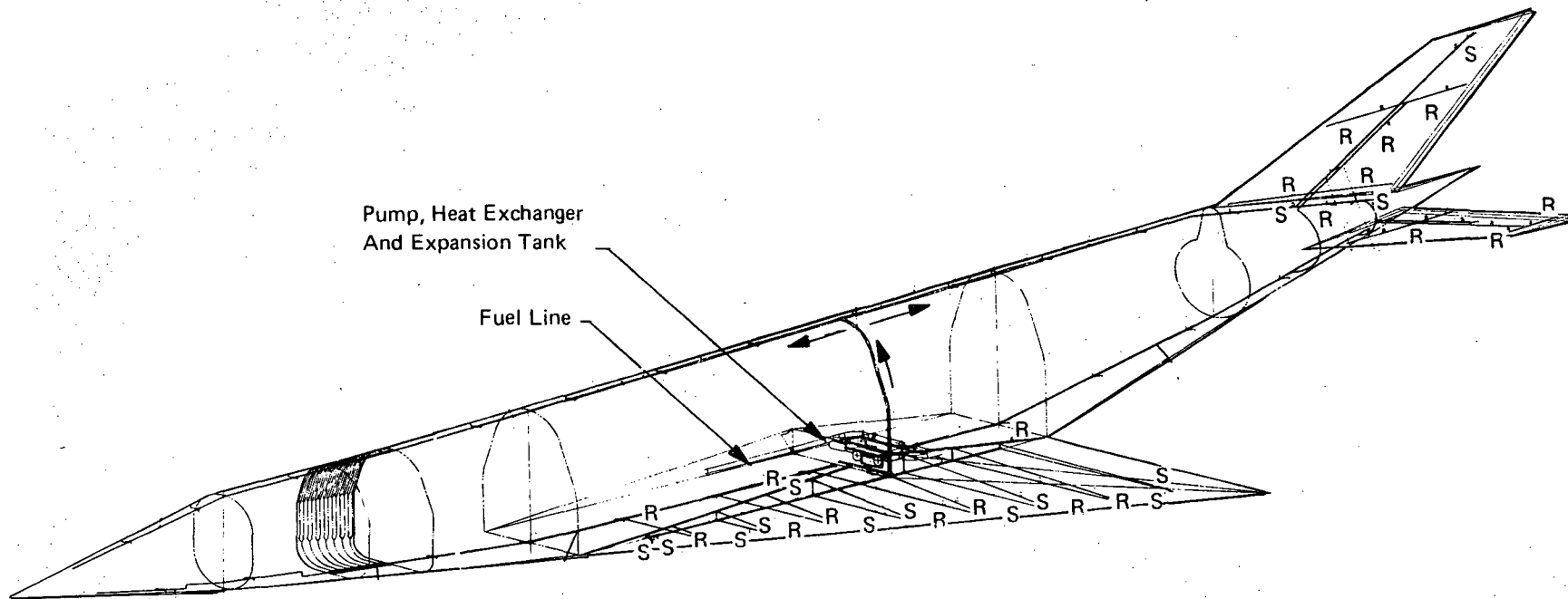


Figure 38. HST Distribution System

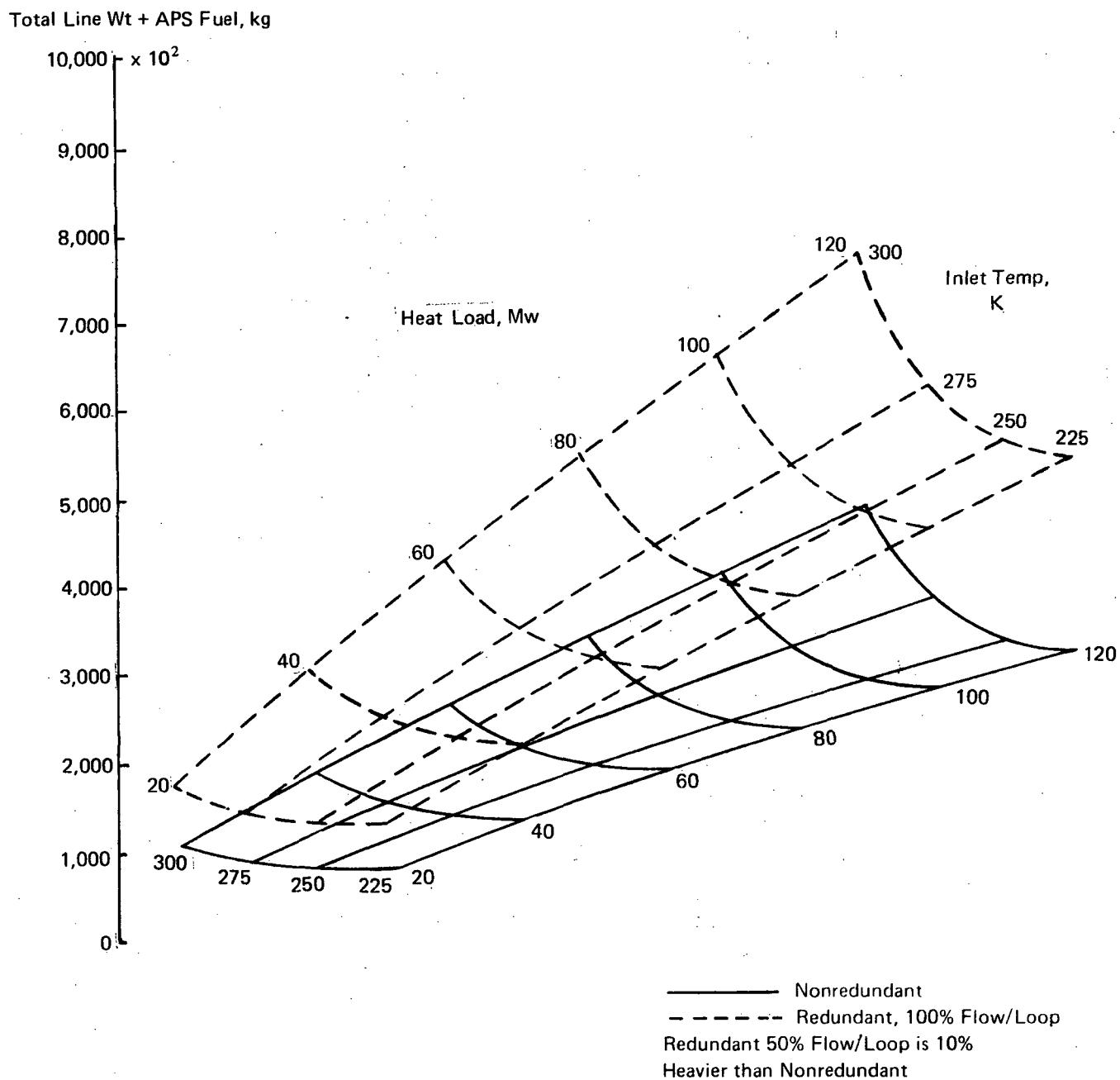


Figure 39a. Minimum Weight of Coolant Distribution Lines and APS Fuel as a Function of Heat Load and Inlet Temperature, Outlet Temperature = 366°K, Ethylene Glycol/Water

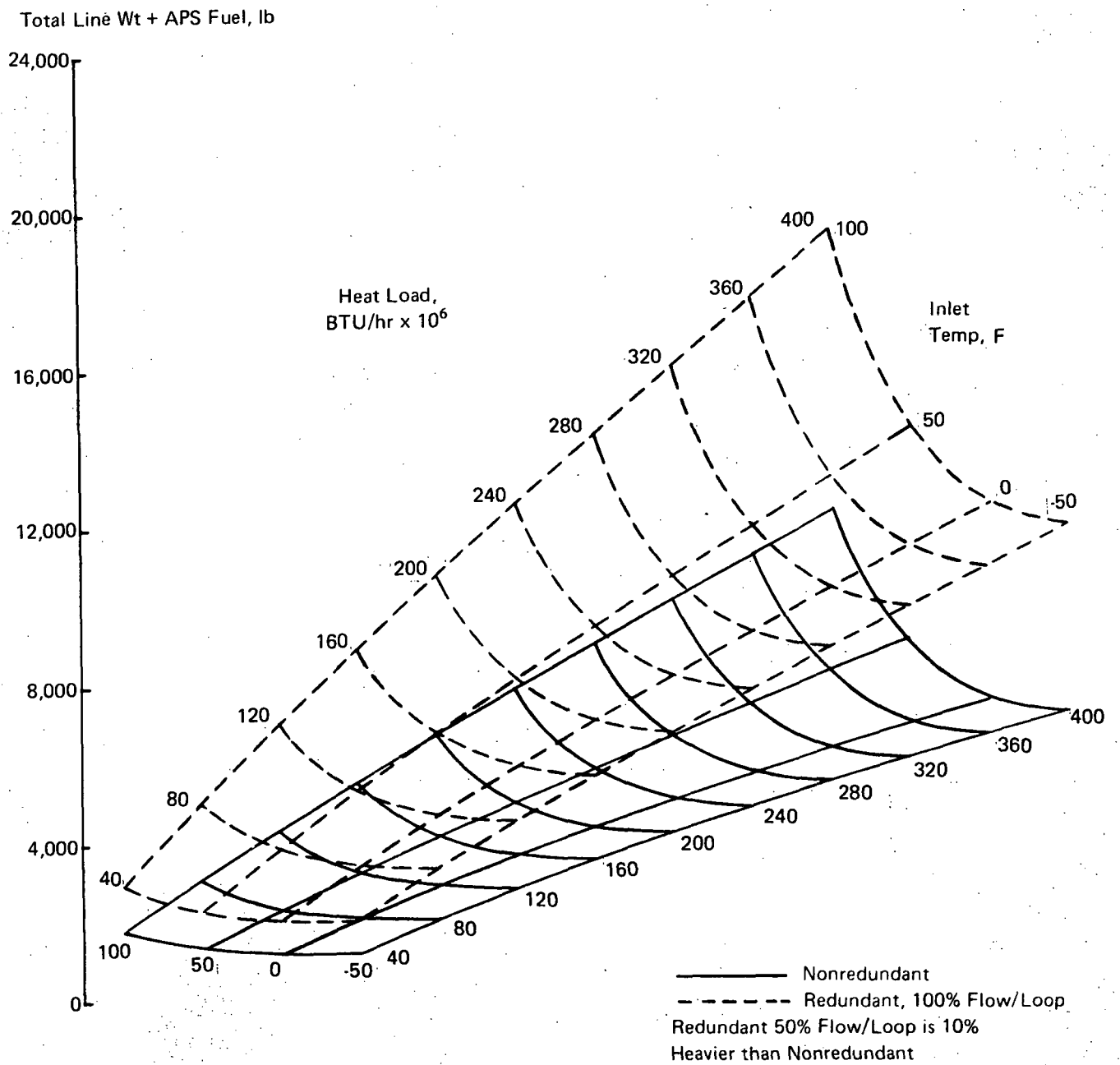


Figure 39b. Minimum Weight of Coolant Distribution Lines and APS Fuel as a Function of Heat Load and Inlet Temperature, Outlet Temperature = 200F, Ethylene Glycol/Water

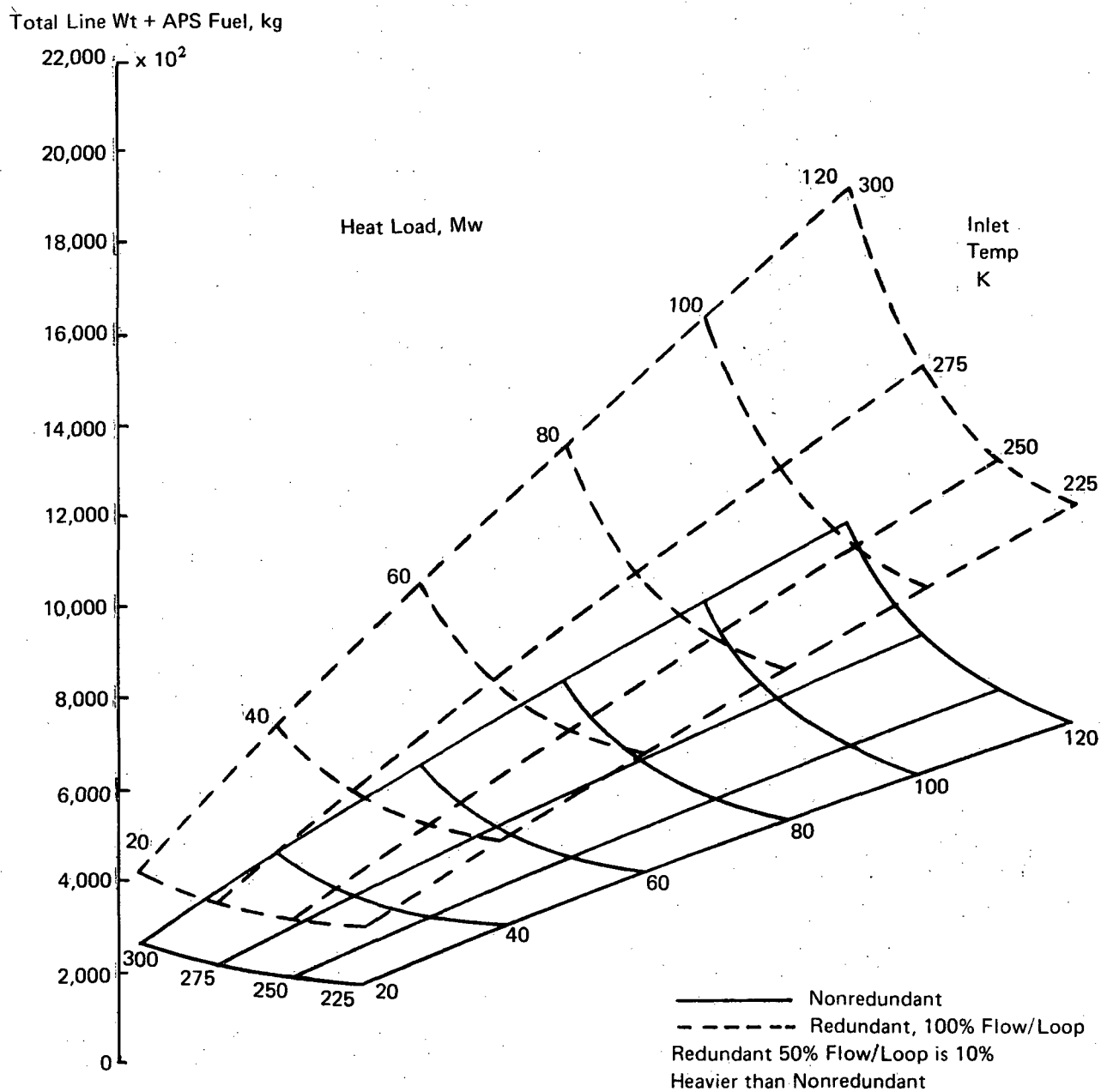


Figure 40a. Minimum Weight of Coolant Distribution Lines and APS Fuel as a Function of Heat Load and Inlet Temperature, Outlet Temperature = 366°K, FC-43

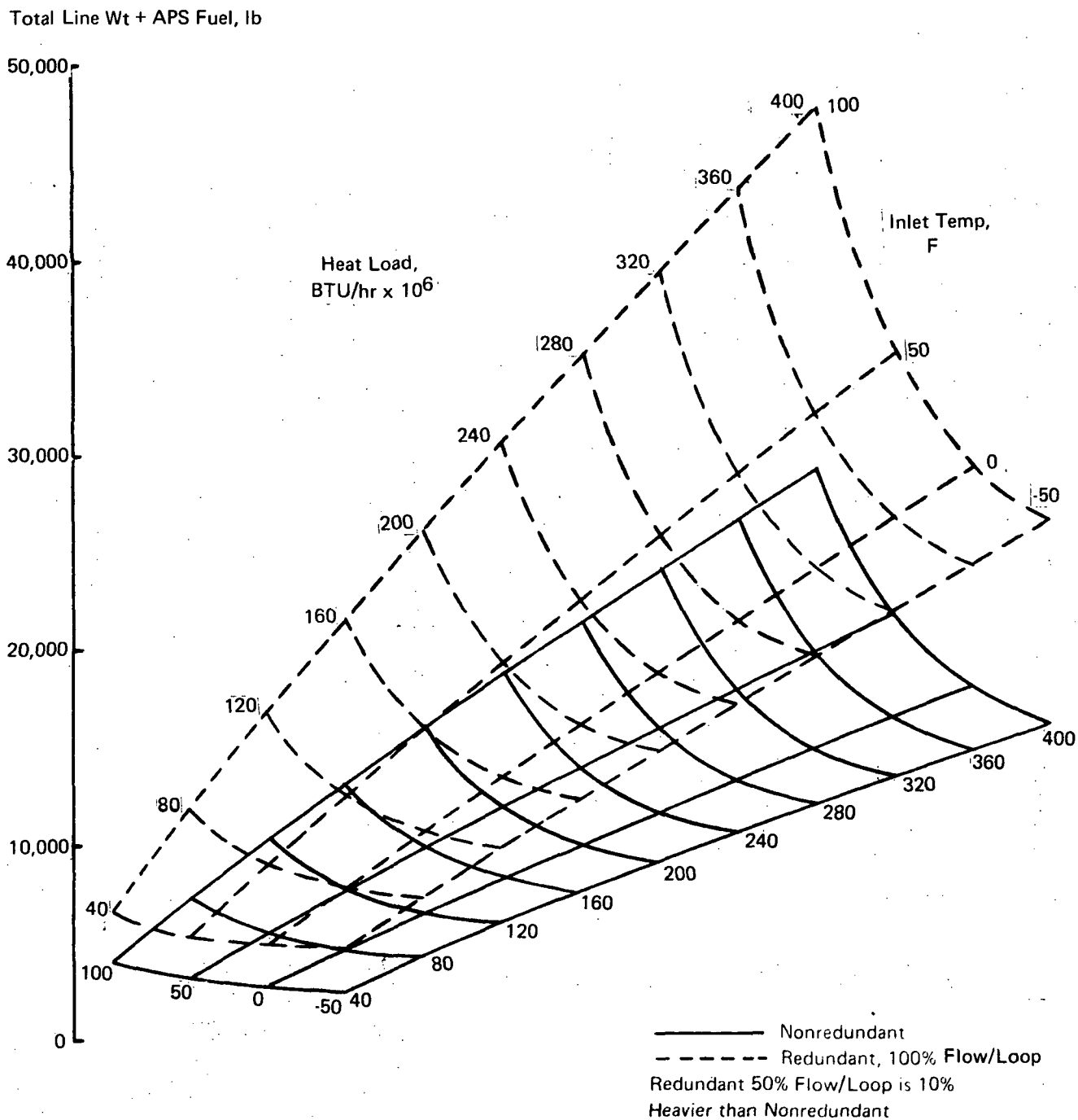


Figure 40b. Minimum Weight of Coolant Distribution Lines and APS Fuel as a Function of Heat Load and Inlet Temperature, Outlet Temperature = 200F, FC-43

Total Line Wt + APS Fuel, kg

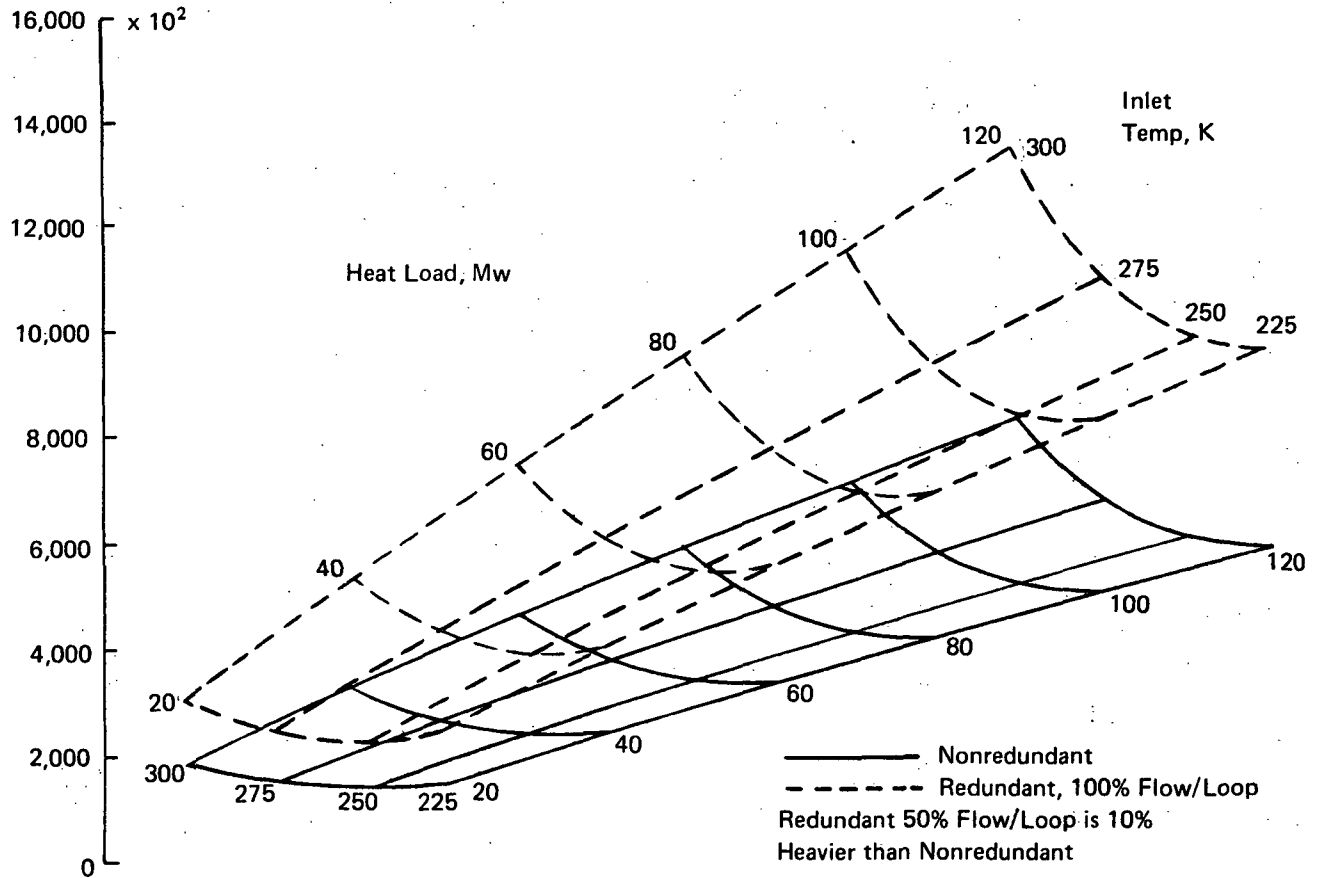


Figure 41a. Minimum Weight of Coolant Distribution Lines and APS Fuel as a Function of Heat Load and Inlet Temperature, Outlet Temperature = 366°K, Coolanol 45

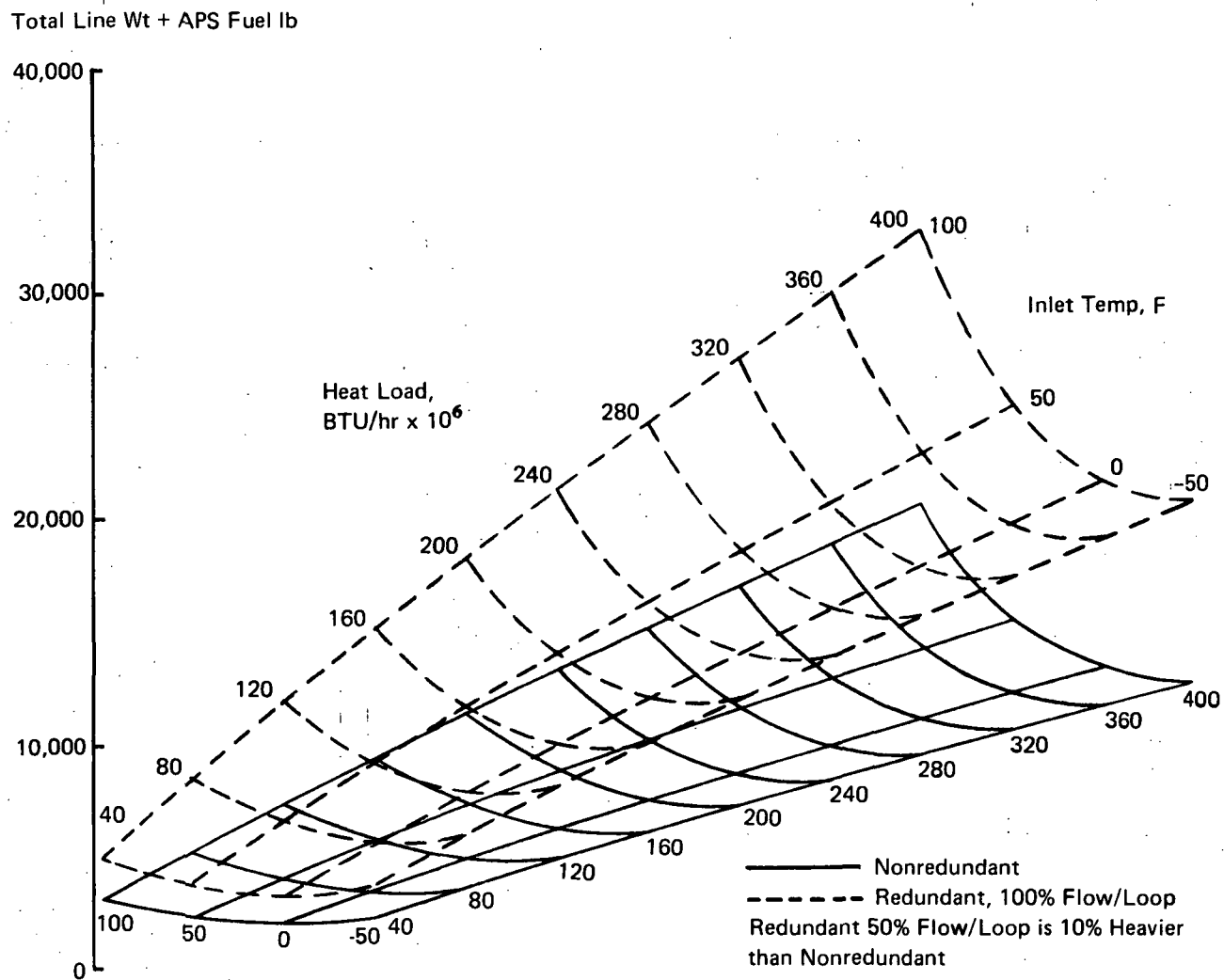


Figure 41b. Minimum Weight of Coolant Distribution Lines and APS Fuel as a Function of Heat Load and Inlet Temperature, Outlet Temperature = 200F, Coolanol 45

Total System ΔP , MN/m²

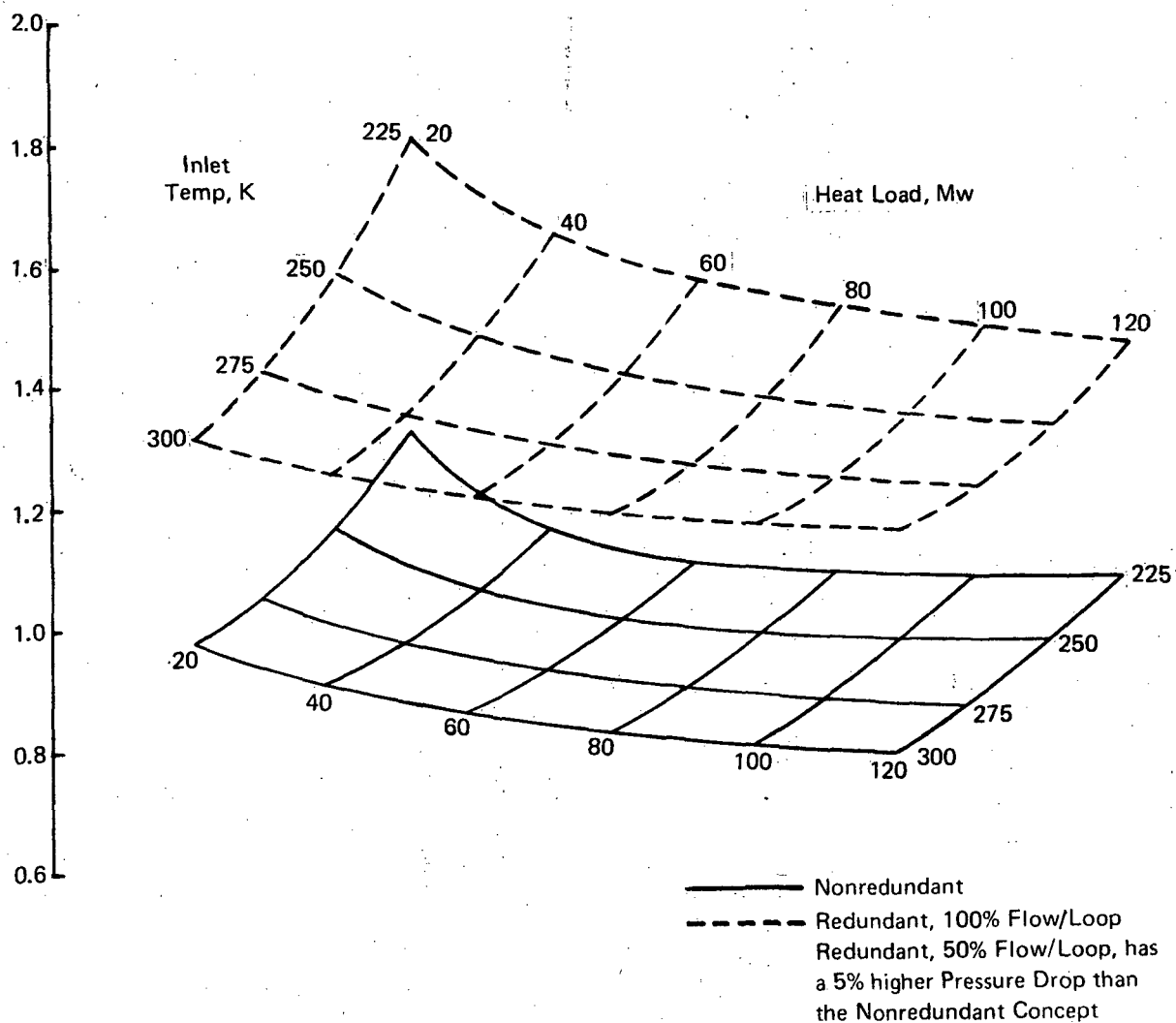


Figure 42a. Pressure Drop for Minimum Weight Coolant Distribution Lines as a Function of Heat Load and Inlet Temperature, Outlet Temperature = 366°K, Ethylene Glycol/Water

Total System ΔP , psi

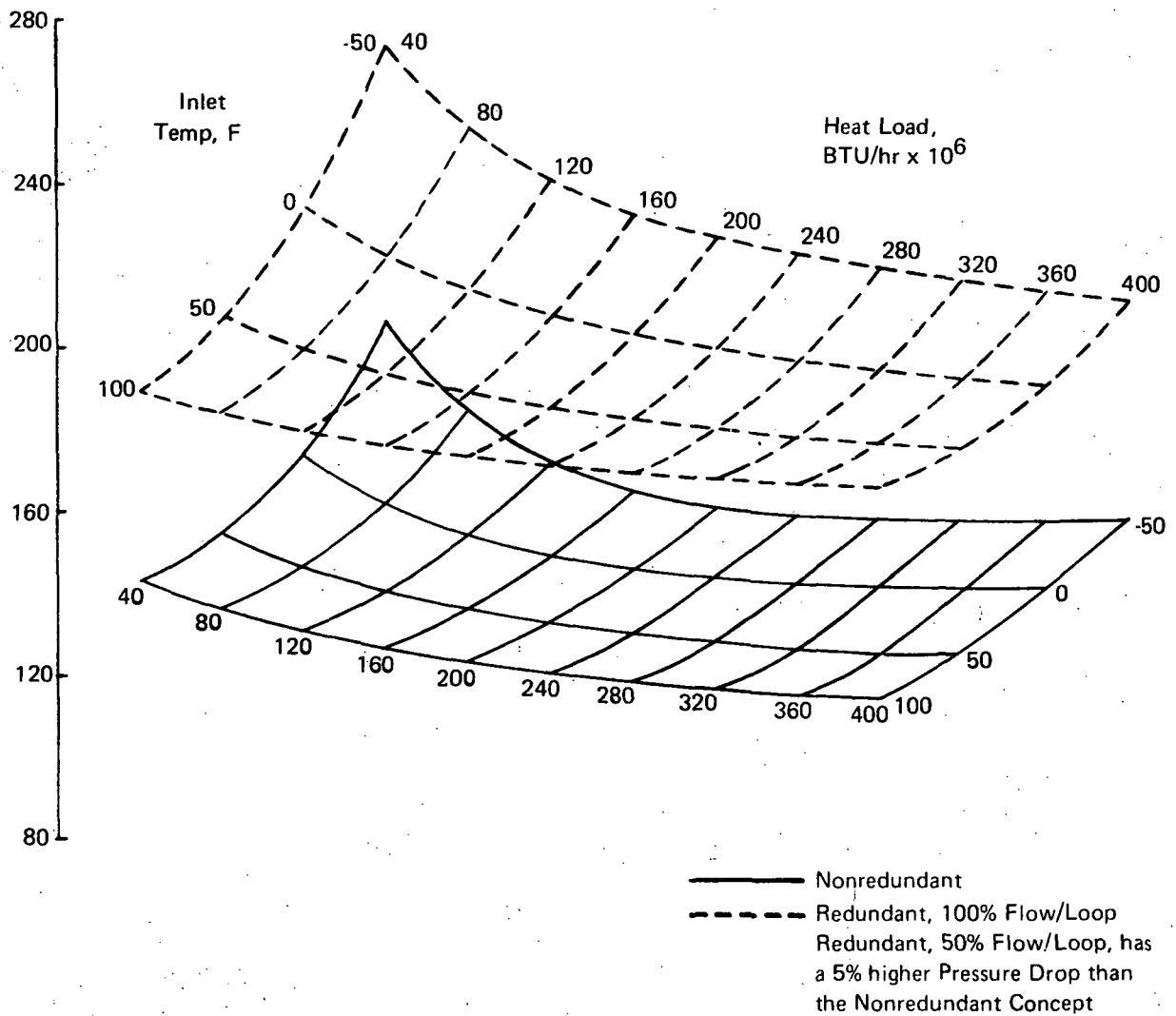


Figure 42b. Pressure Drop for Minimum Weight Coolant Distribution Lines as a Function of Heat Load and Inlet Temperature, Outlet Temperature = 200F, Ethylene Glycol/Water

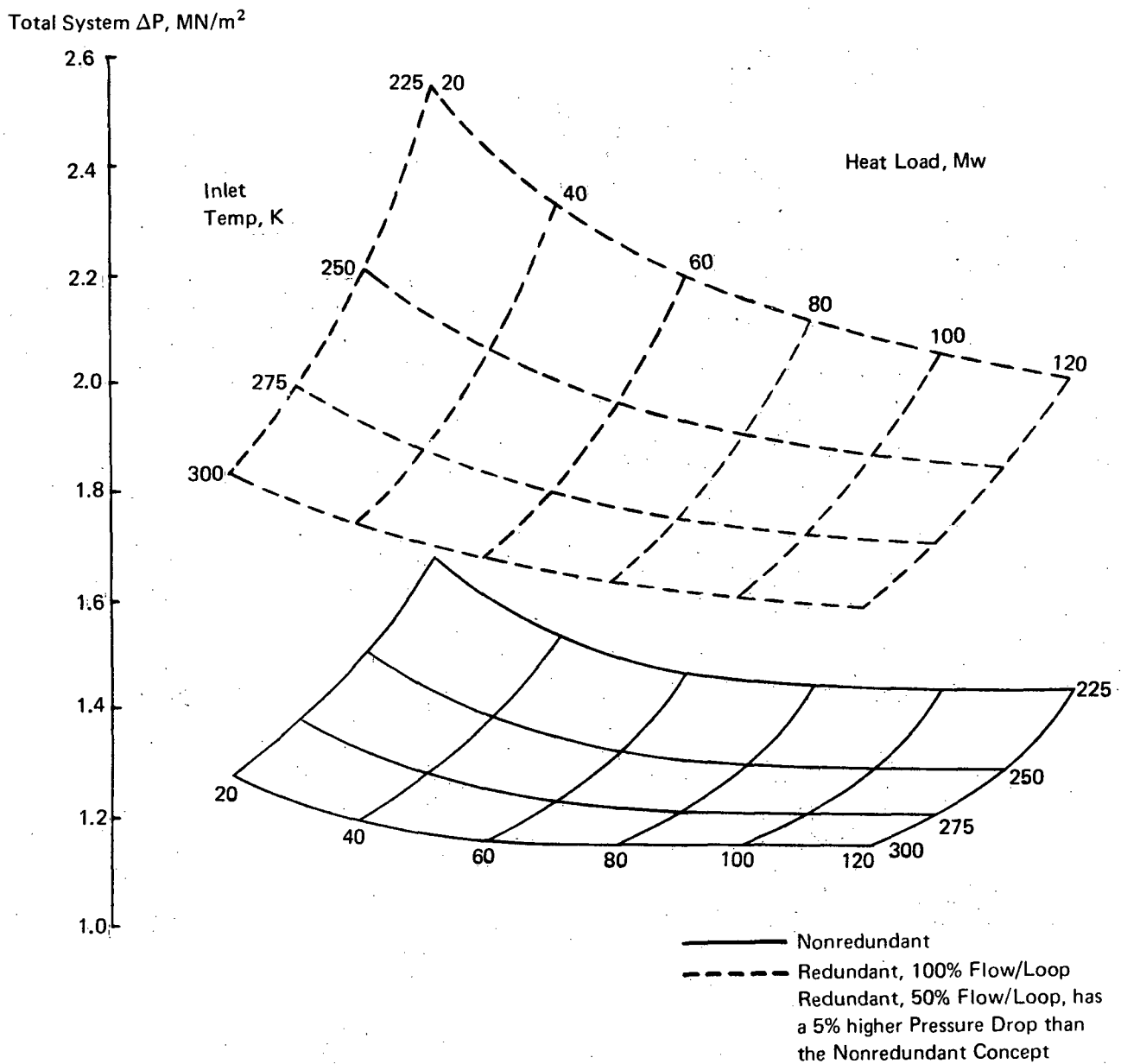


Figure 43a. Pressure Drop for Minimum Weight Coolant Distribution Lines as a Function of Heat Load and Inlet Temperature, Outlet Temperature = 366°K, FC-43

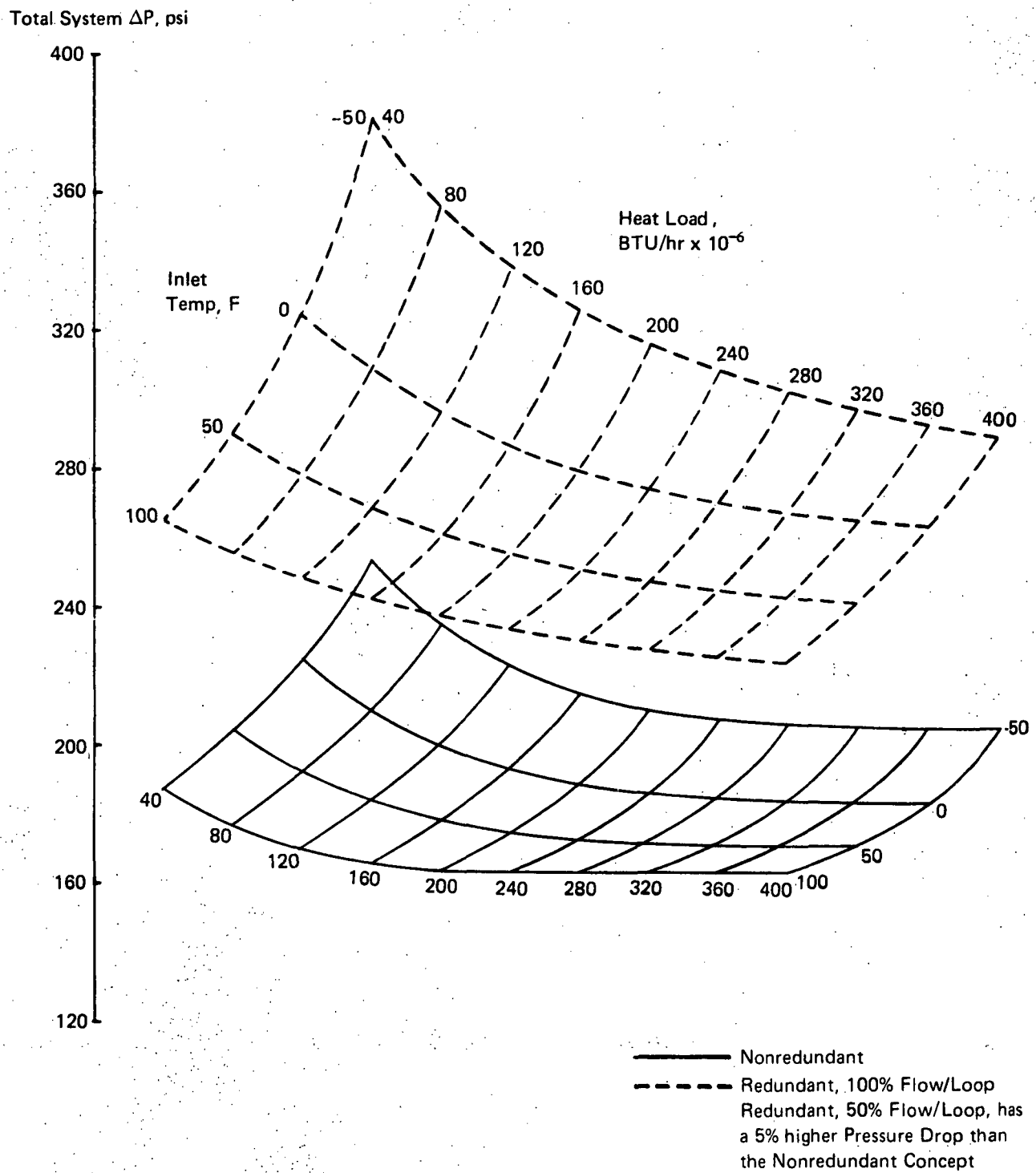


Figure 43b. Pressure Drop for Minimum Weight Coolant Distribution Lines as a Function of Heat Load and Inlet Temperature, Outlet Temperature = 200F, FC-43

Total System ΔP , MN/m²

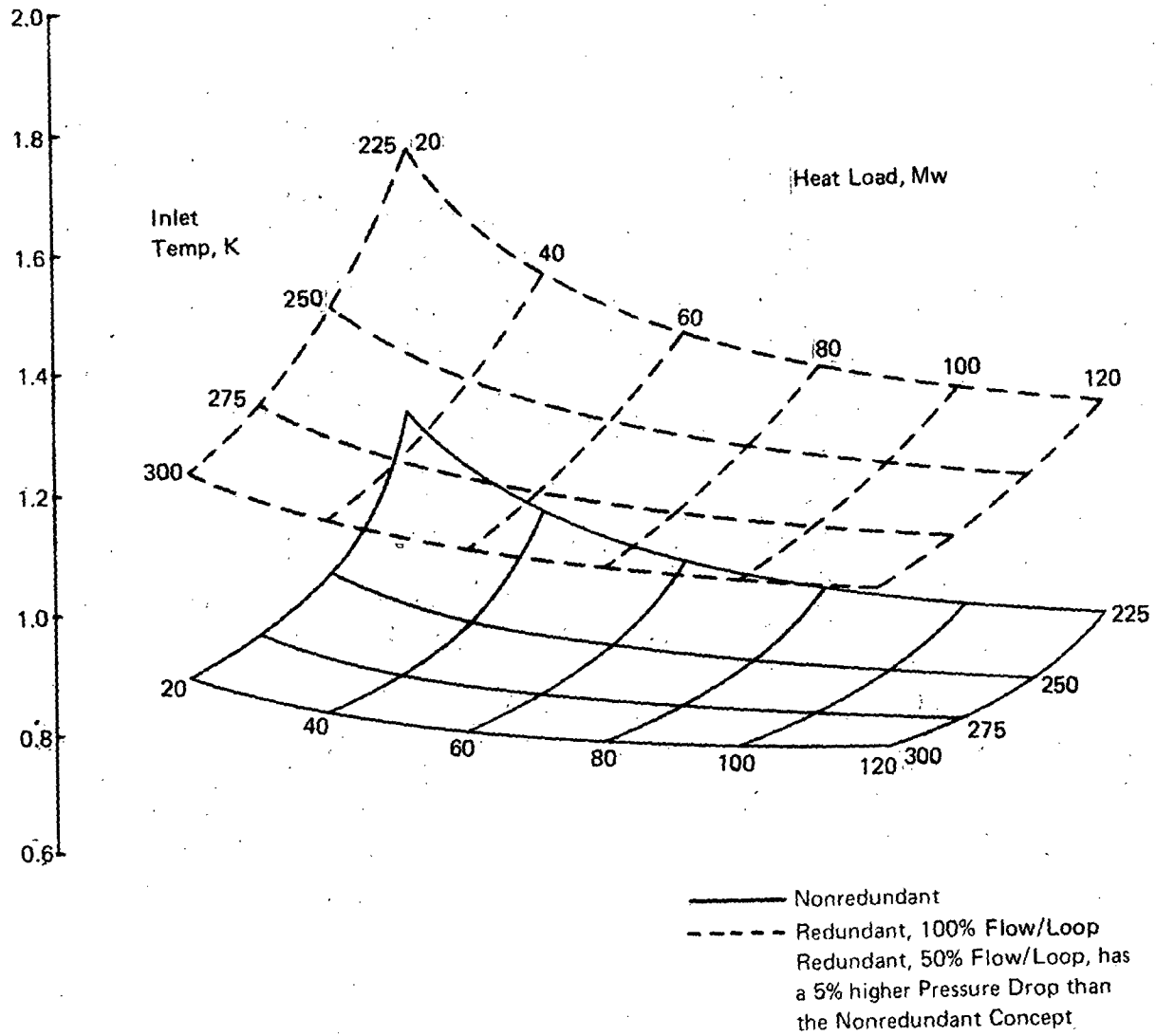


Figure 44a. Pressure Drop for Minimum Weight Coolant Distribution Lines as a Function of Heat Load and Inlet Temperature, Outlet Temperature = 366° K, Coolant 45

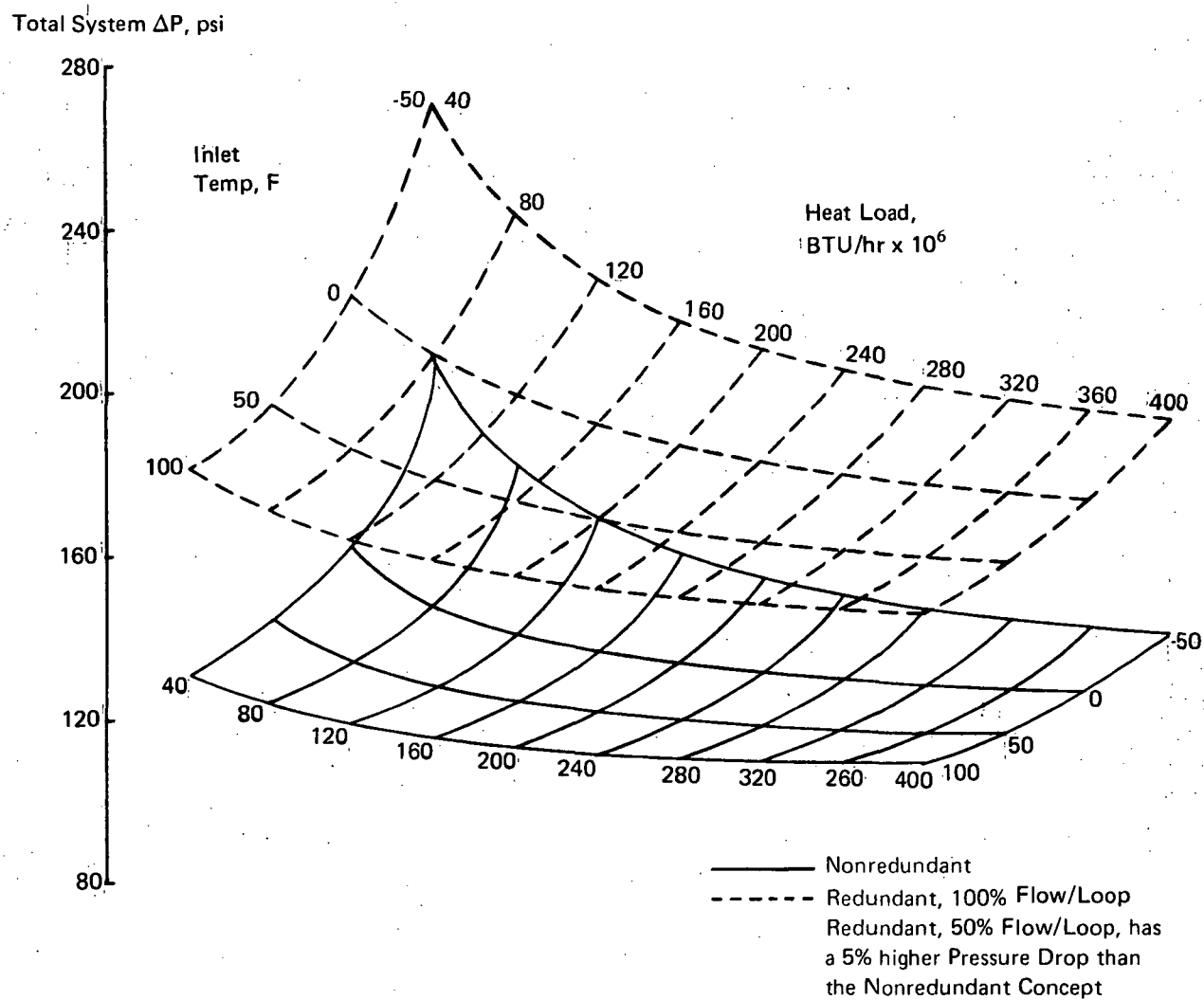


Figure 44b. Pressure Drop for Minimum Weight Coolant Distribution Lines as a Function of Heat Load and Inlet Temperature, Outlet Temperature = 200F, Coolant = 45

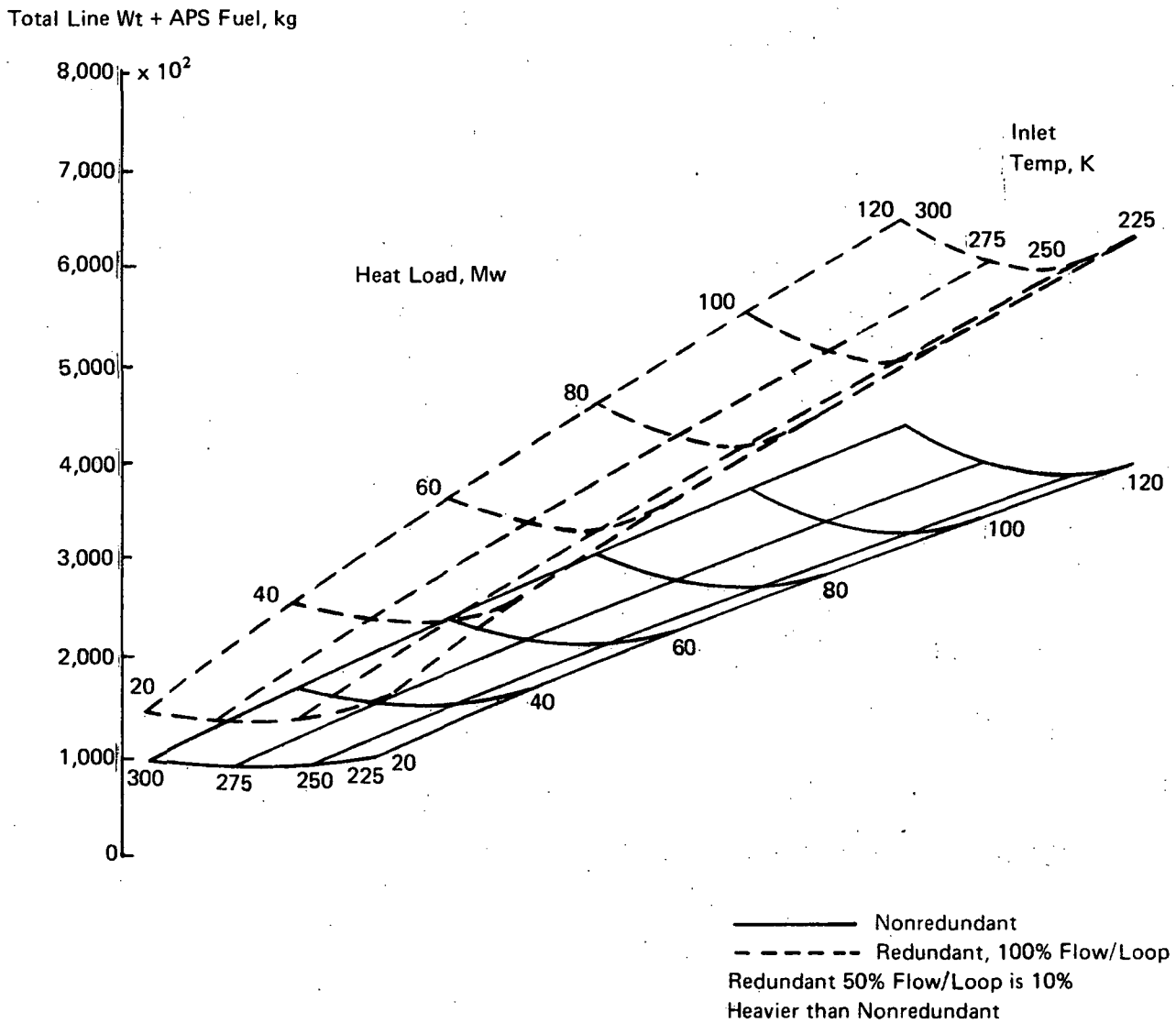


Figure 45a. Minimum Weight of Coolant Distribution Lines and APS Fuel as a Function of Heat Load and Inlet Temperature, Outlet Temperature = 450°K, Coolant 45

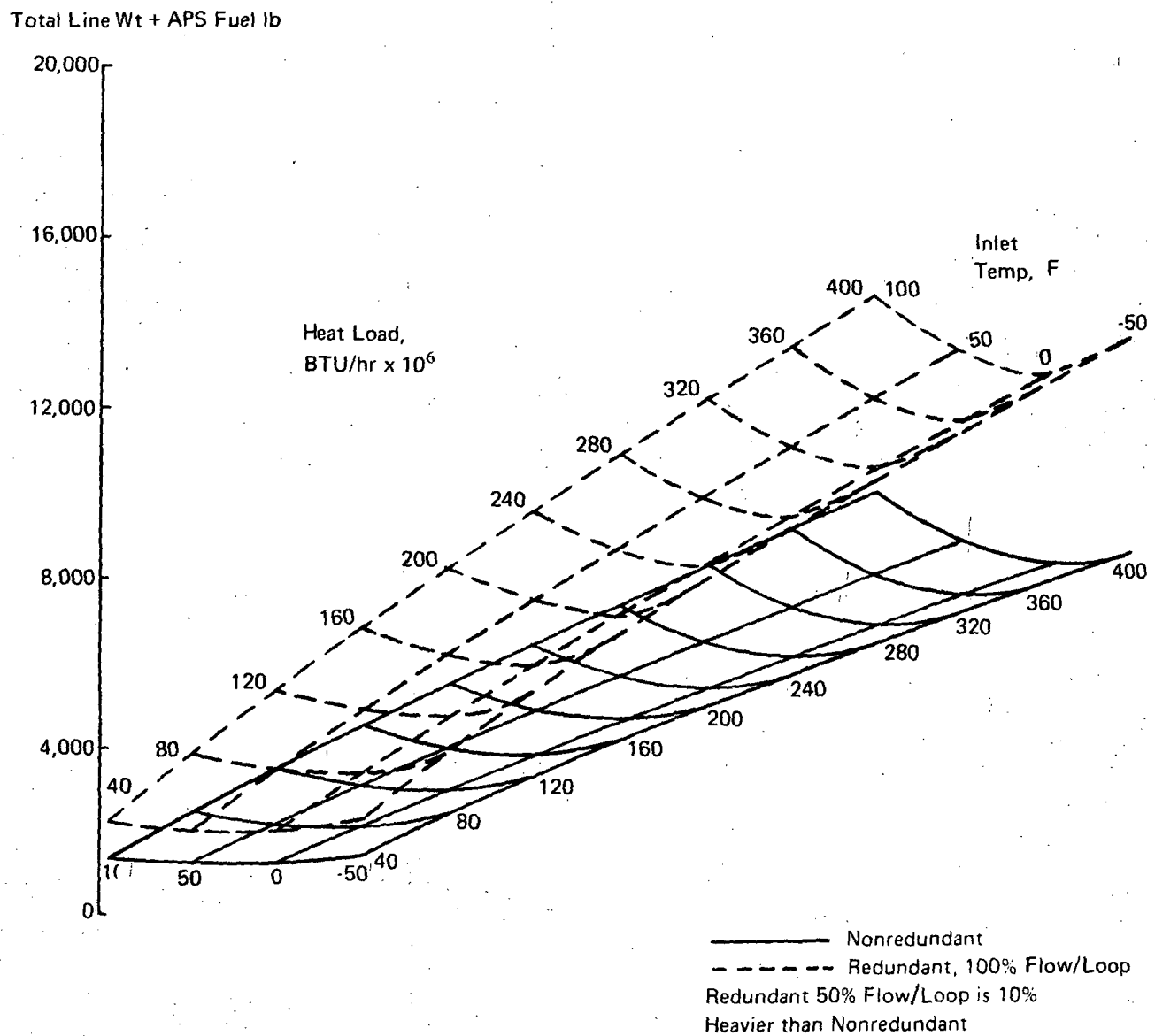


Figure 45b. Minimum Weight of Coolant Distribution Lines and APS Fuel as a Function of Heat Load and Inlet Temperature, Outlet Temperature = 350F, Coolanol 45

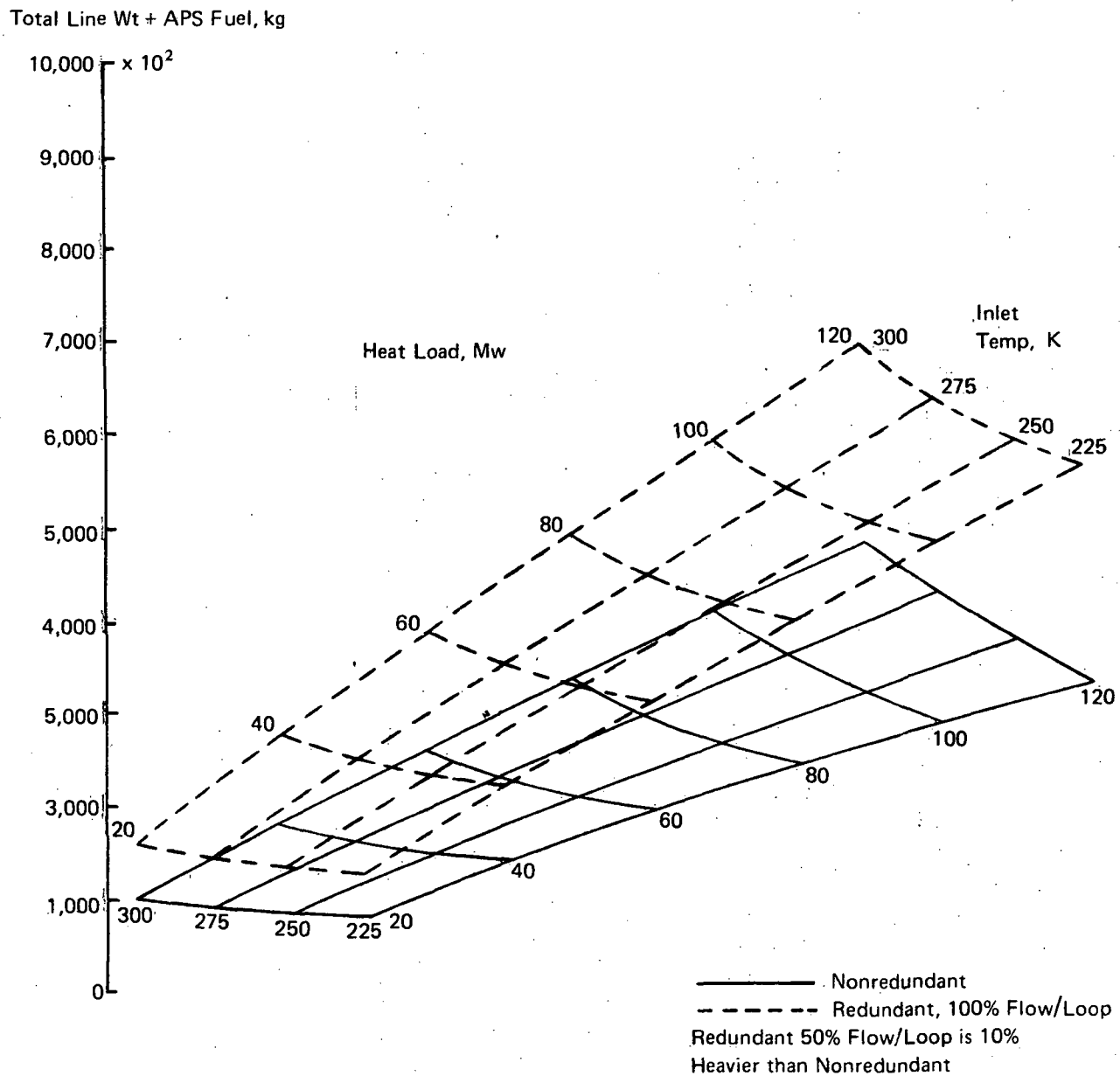


Figure 46a. Minimum Weight of Coolant Distribution Lines and APS Fuel as a Function of Heat Load and Inlet Temperature, Outlet Temperature = 450°K , Dow Corning XF-1-3755

Total Line Wt + APS Fuel, lb

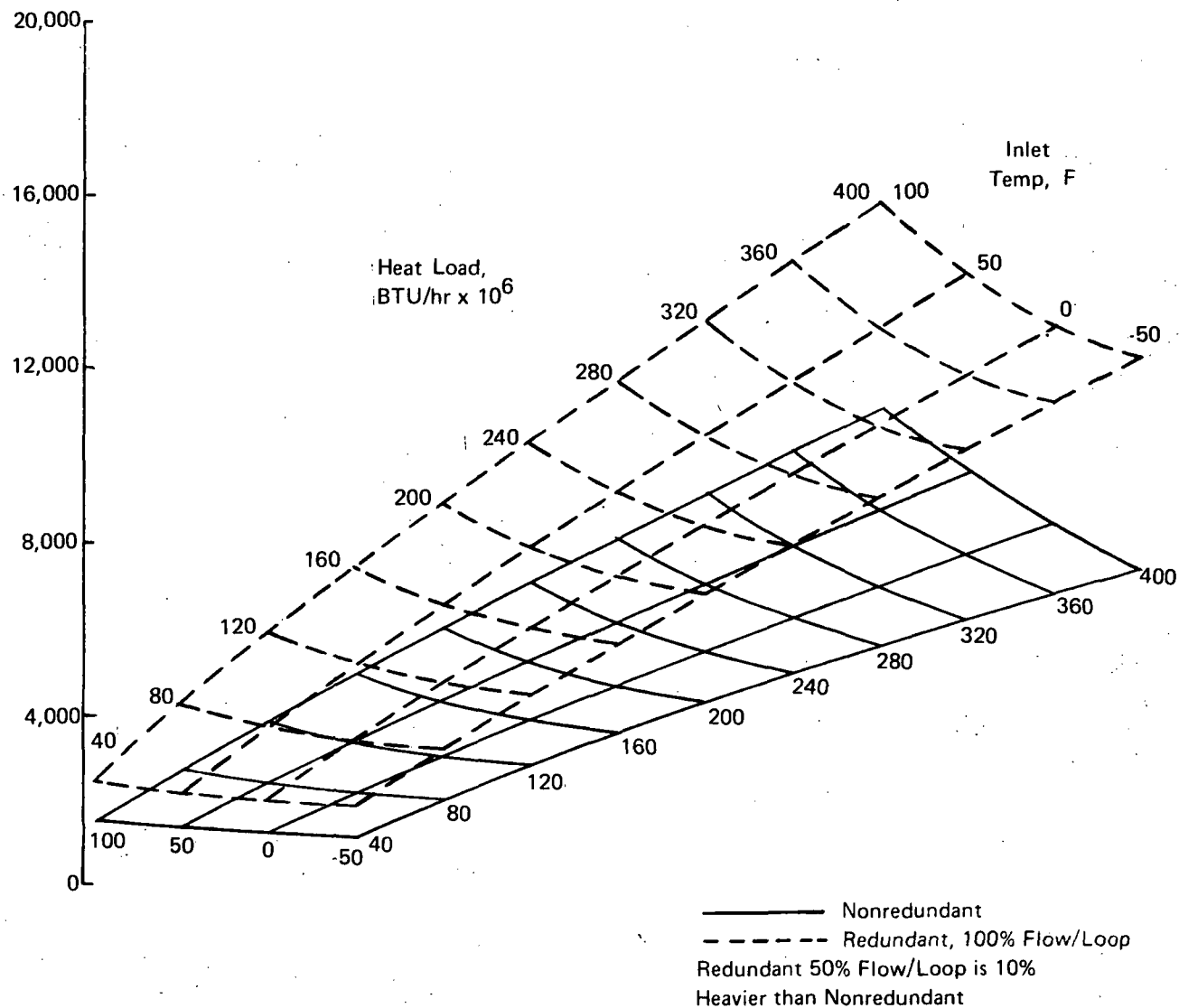


Figure 46b. Minimum Weight of Coolant Distribution Lines and APS Fuel as a Function of Heat Load and Inlet Temperature, Outlet Temperature = 350F, Dow Corning XF-1-3755 Fluid

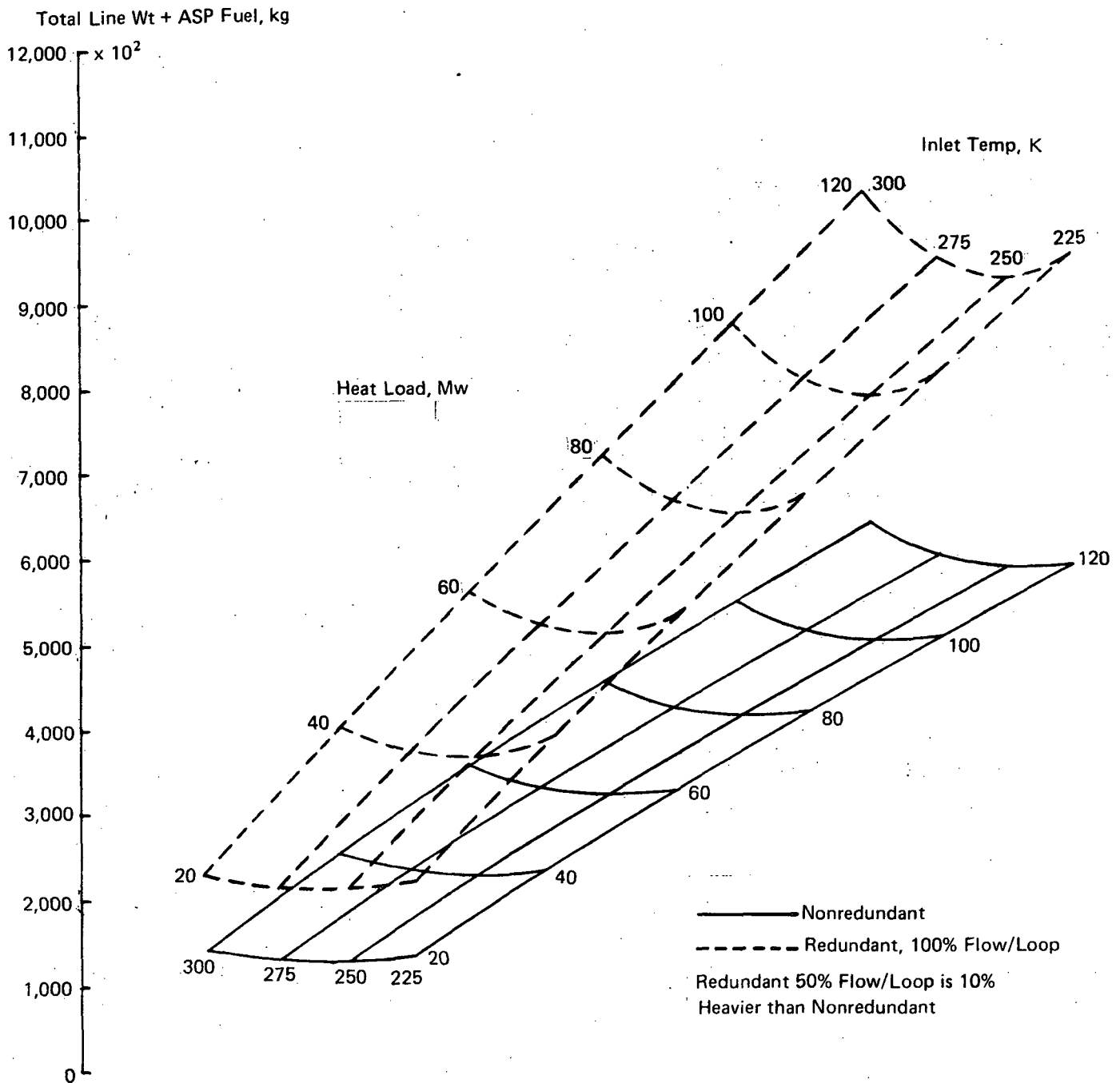


Figure 47a. Minimum Weight of Coolant Distribution Lines and APS Fuel as a Function of Heat Load and Inlet Temperature, Outlet Temperature = 450°K, Freon E5

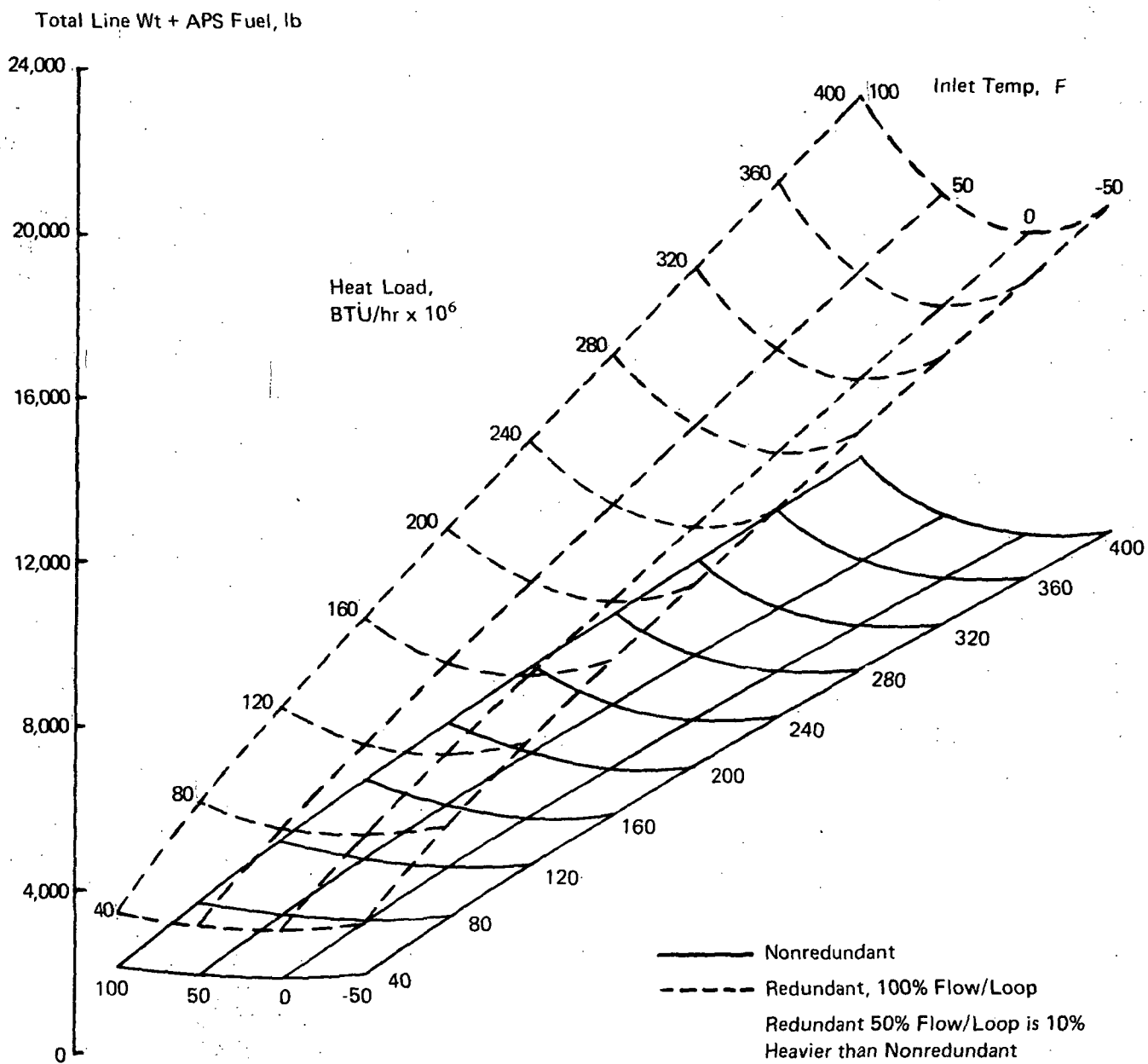


Figure 47b. Minimum Weight of Coolant Distribution Lines and APS Fuel as a Function of Heat Load and Inlet Temperature, Outlet Temperature = 350F, Freon E5

Total System ΔP , MN/m²

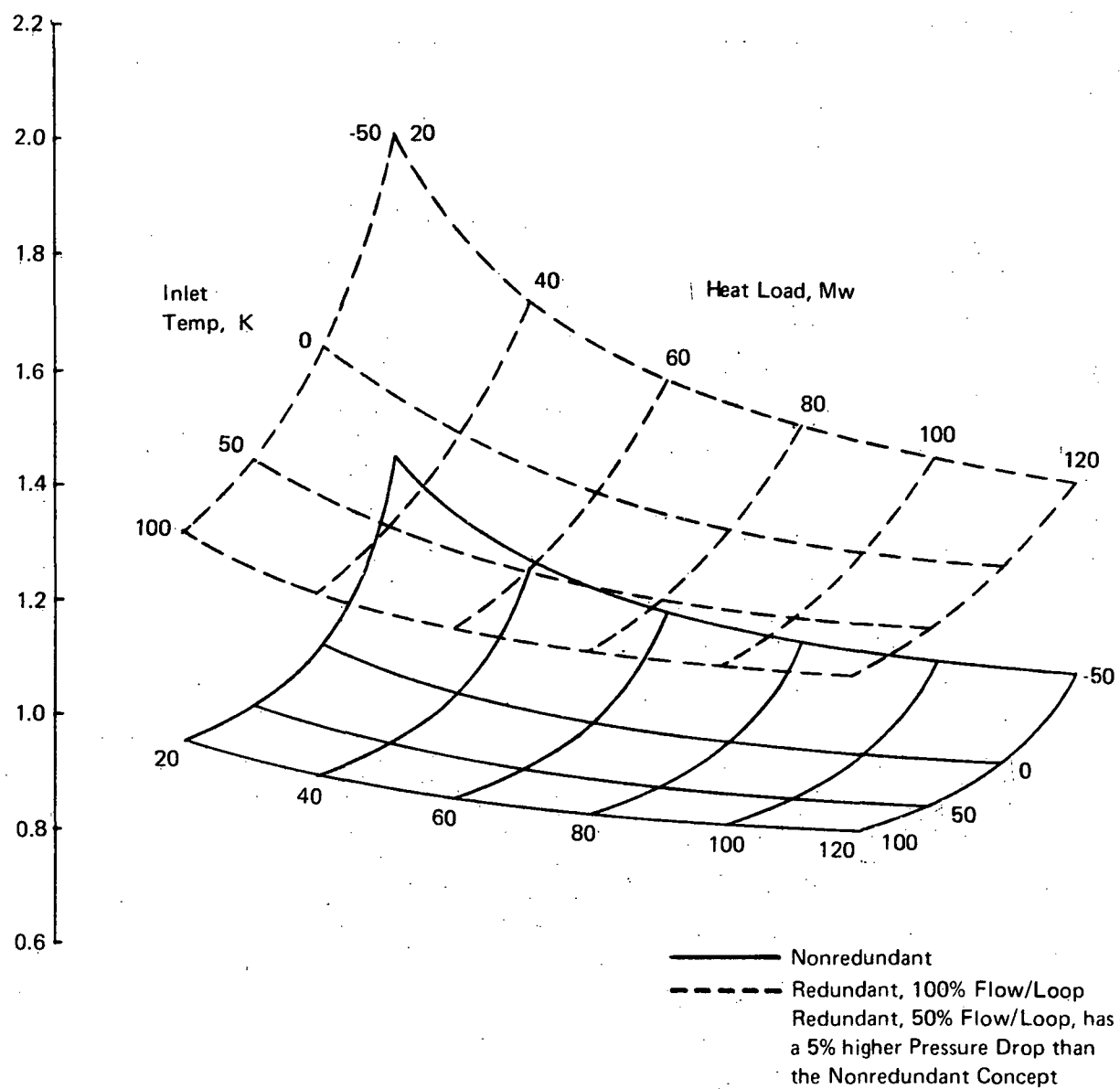


Figure 48a. Pressure Drop for Minimum Weight Coolant Distribution Lines as a Function of Heat Load and Inlet Temperature, Outlet Temperature = 450°K, Coolant = 45

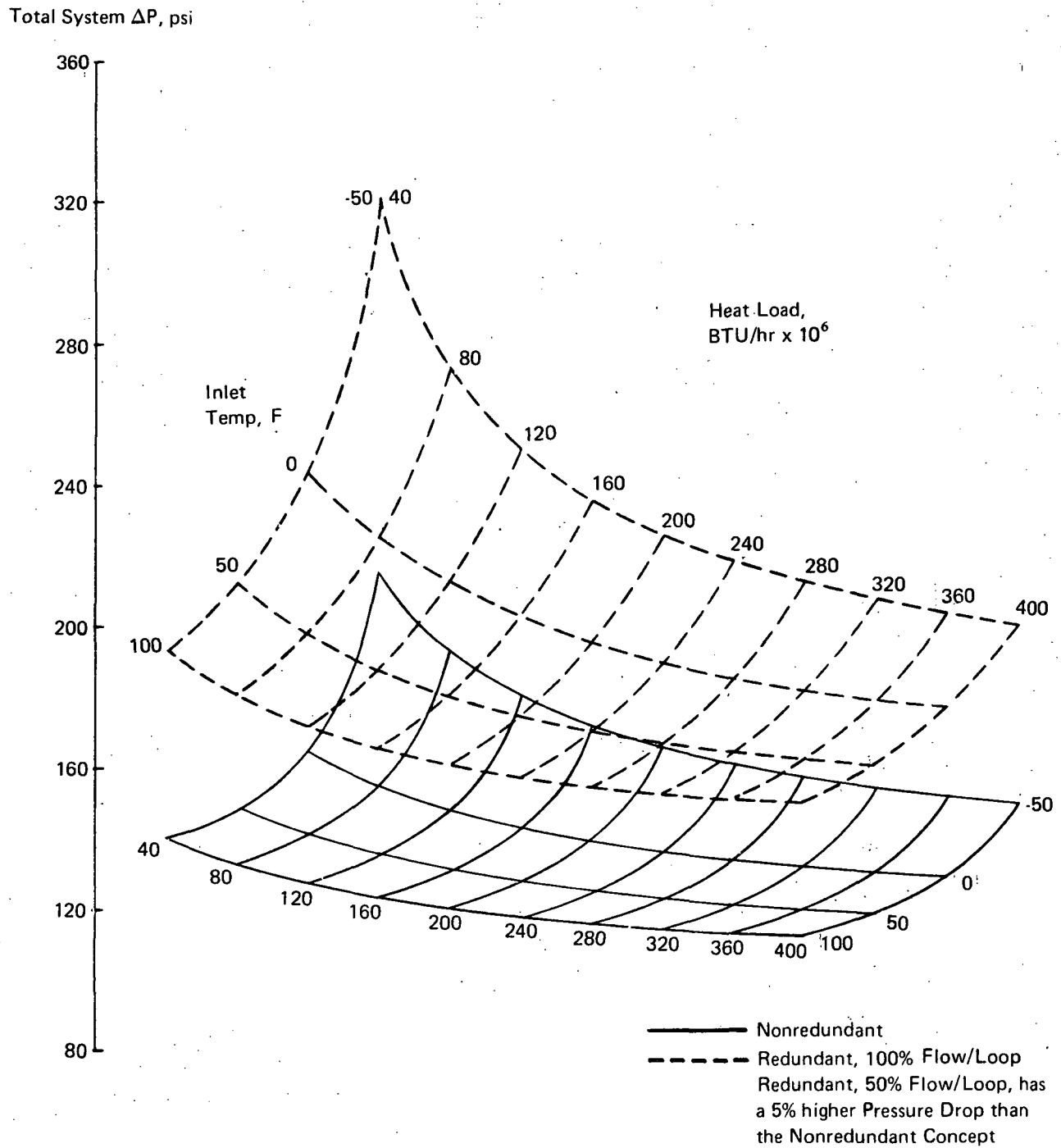


Figure 48b. Pressure Drop for Minimum Weight Coolant Distribution Lines as a Function of Heat Load and Inlet Temperature, Outlet Temperature = 350F, Coolanol 45

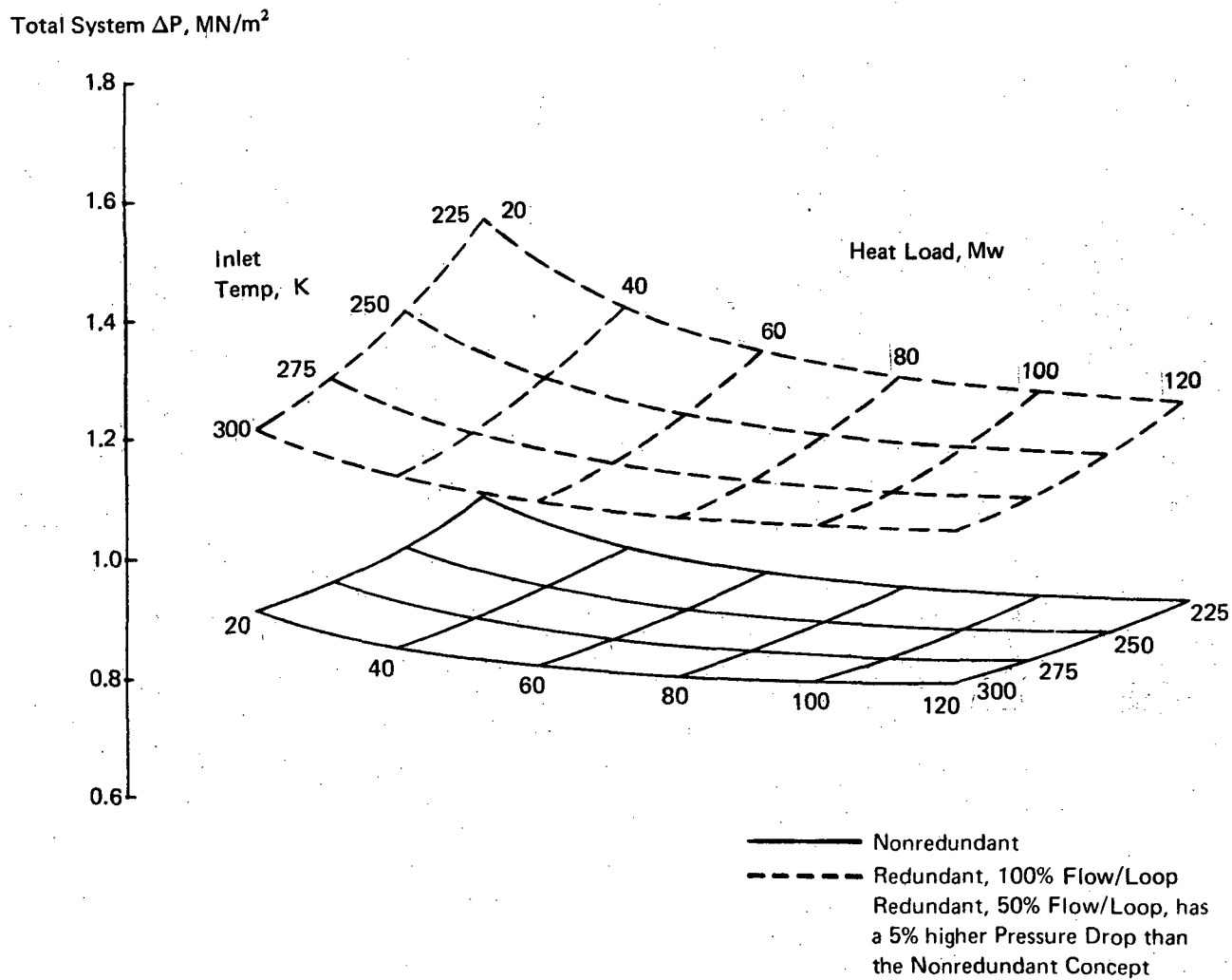


Figure 49a. Pressure Drop for Minimum Weight Coolant Distribution Lines as a Function of Heat Load and Inlet Temperature, Outlet Temperature = 450°K, Dow Corning XF-1-3755

Total System ΔP , psi

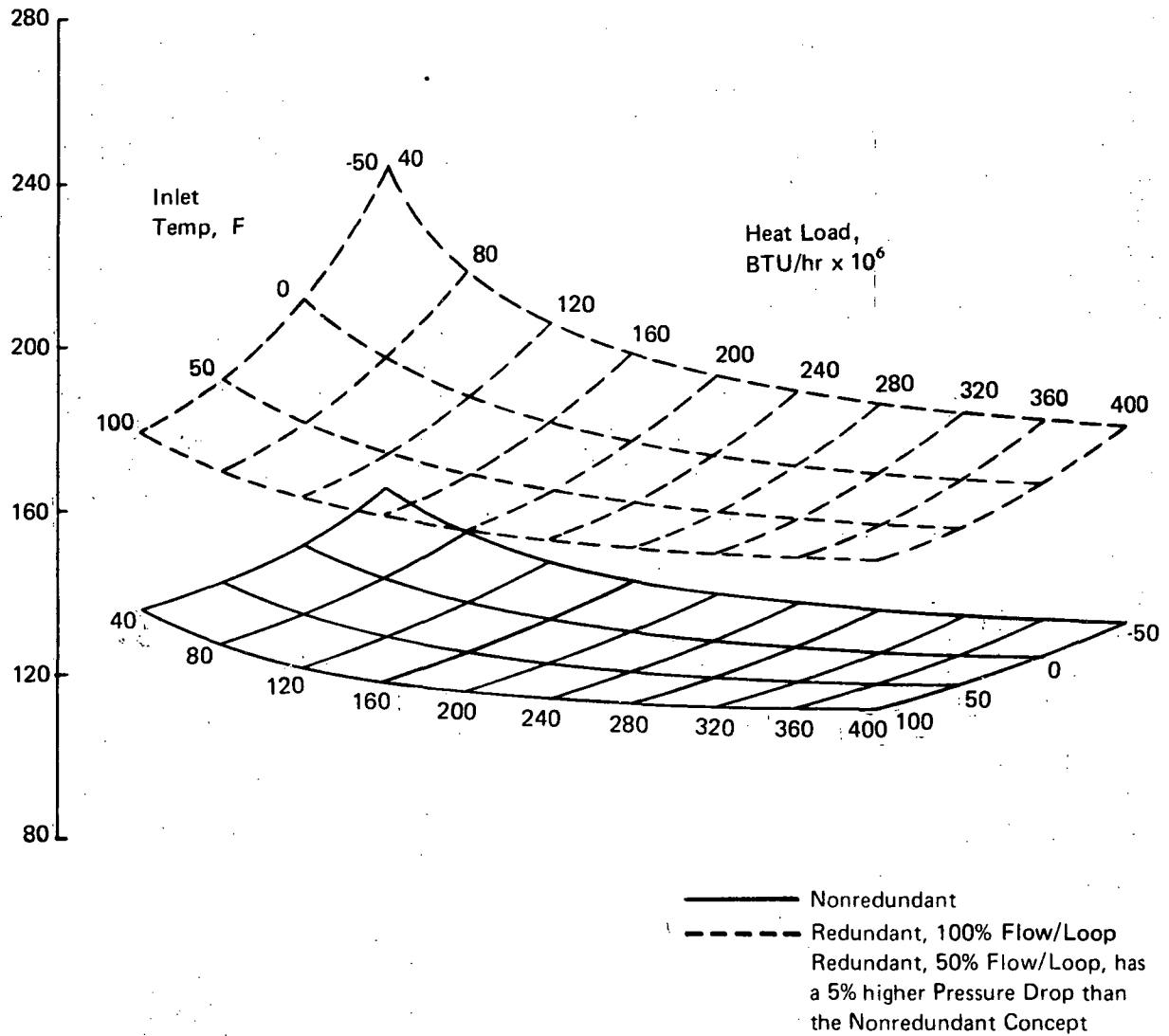


Figure 49b. Pressure Drop for Minimum Weight Coolant Distribution Lines as a Function of Heat Load and Inlet Temperature, Outlet Temperature = 350F, Dow Corning XF-1-3755

Total System ΔP , MN/m²

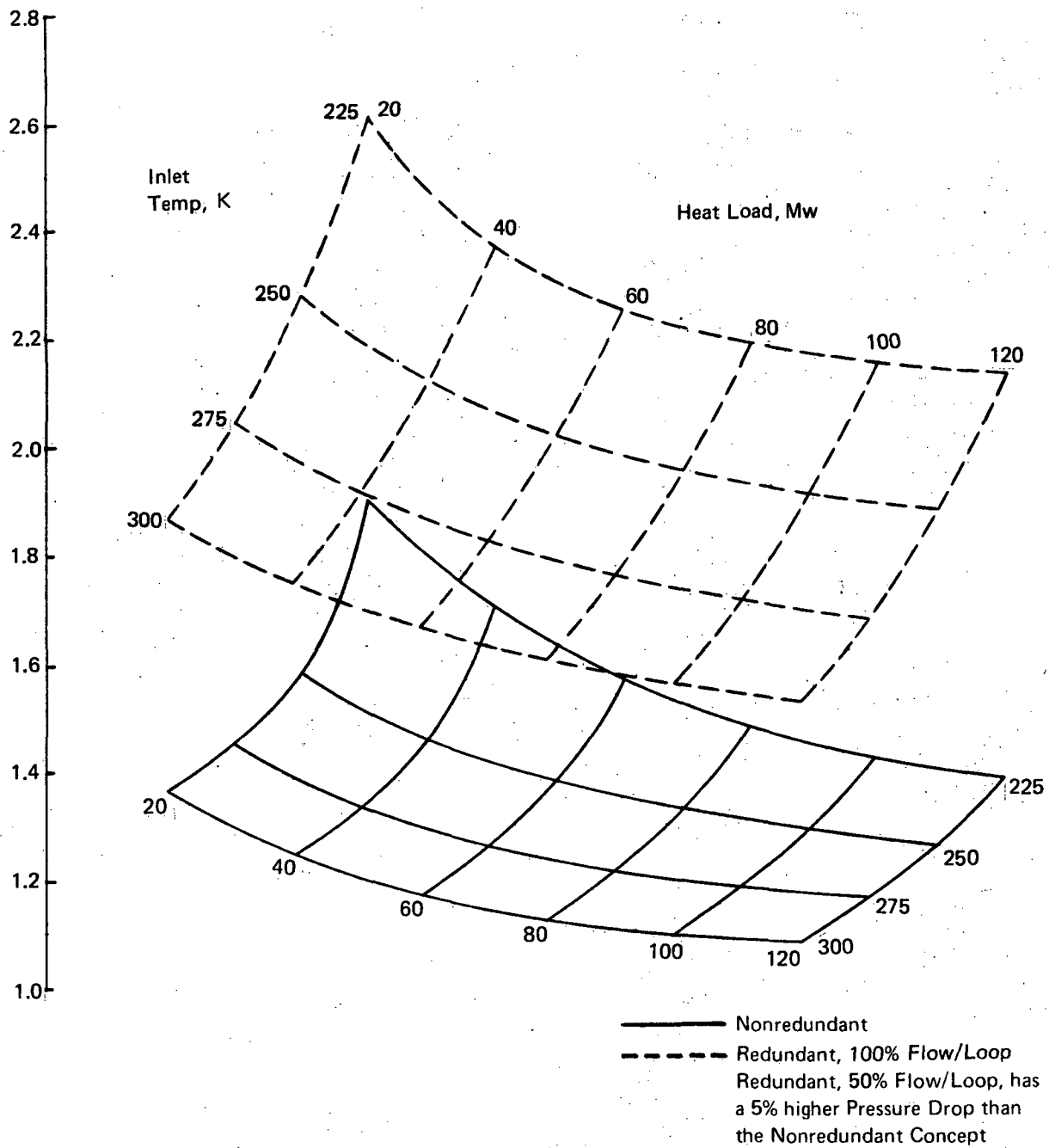


Figure 50a. Pressure Drop for Minimum Weight Coolant Distribution Lines as a Function of Heat Load and Inlet Temperature, Outlet Temperature = 450°K, Freon E5

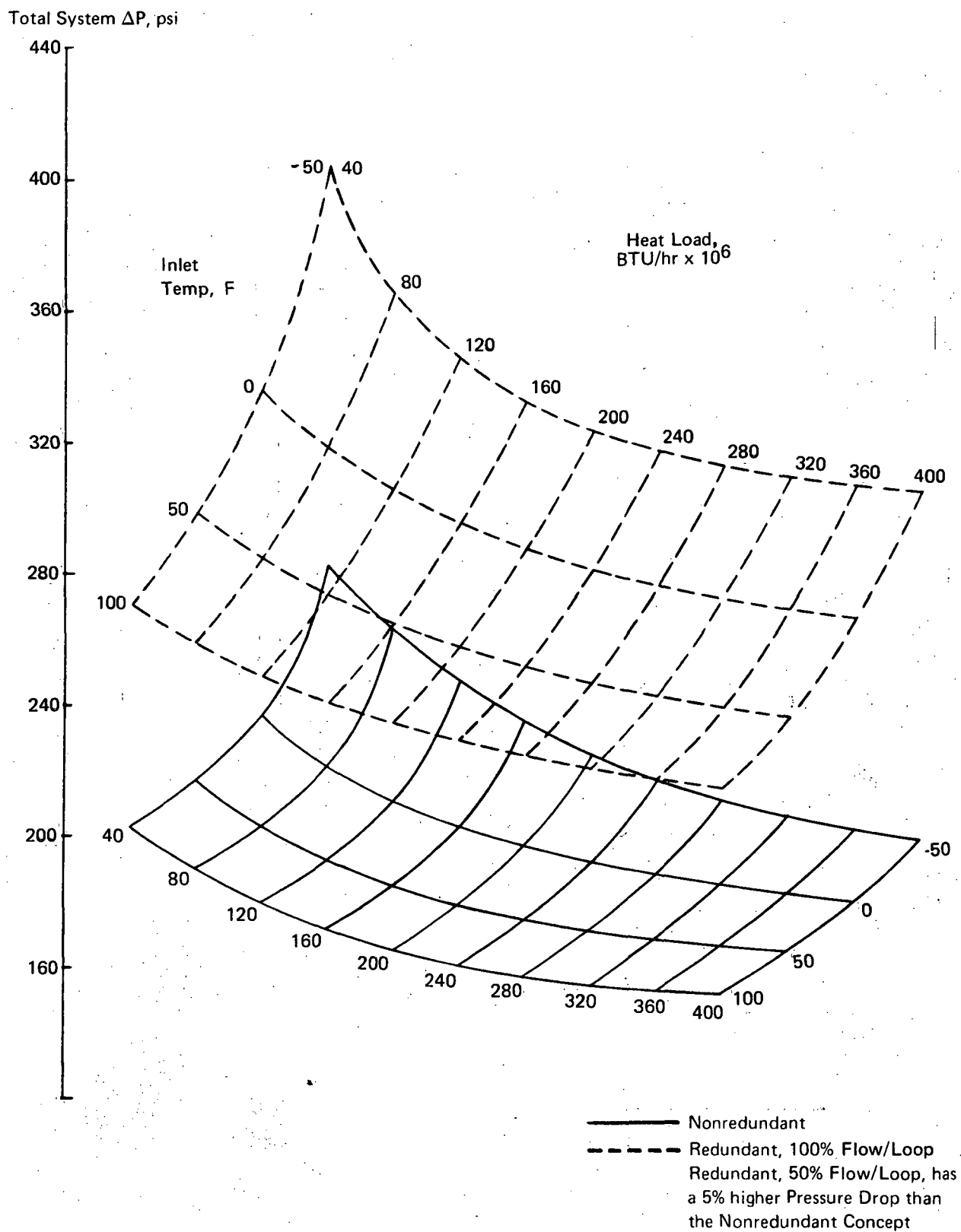


Figure 50b. Pressure Drop for Minimum Weight Coolant Distribution Lines as a Function of Heat Load and Inlet Temperature, Outlet Temperature = 350F, Freon E5

(200F). Although the weights of the various distribution systems, including pumping penalties varied by as much as 30% the percentage difference in total cooling system weight was less than 7% when the weight of coolant within the skin panels was included. The similarity of weights, despite the diversity of distribution line arrangements, indicated that the weights obtained for a typical system would provide realistic estimates for most likely system arrangements. Therefore, the parametric weights were generated for the distribution line arrangement shown in Figure 51. Because of its nearer term aspect aluminum alloy construction was emphasized for the HRA, thus focusing attention on coolants with operating temperature levels in the 394°K (250F) range. Results of parametric analysis for ethylene glycol/water, methanol/water, Coolanol 20 and Coolanol 40 are presented in Figures 52 through 55, while associated pressure drop data are presented in Figures 56 through 59. In all cases the nonredundant and the redundant, 50% flow/loop, concepts were compared; the redundant, 100% flow/loop, was analyzed only for two of the coolants. Pressure drop data is shown only for the nonredundant and the redundant, 100% flow/loop, concepts. For the redundant, 50% flow/loop concept the pressure drops were between 2 and 8% higher than for the nonredundant systems with the largest difference occurring at lowest heat loads for the lowest inlet temperature and the smallest difference for the highest heat load and highest inlet temperature. The pressure drop data includes an allowance of 0.38 MN/m² (55 psi) to account for the heat exchanger and the skin panel farthest from the pump. The 10% increase above the value used for the hypersonic transport was to account for the higher heat flux to which the HRA is subjected which was expected to require a somewhat larger pressure drop through the remote panels.

In order to provide an indication of the influence of using a cooled structure with higher temperature capability, weight and pressure drop characteristics were computed for Coolanol 40 assuming an outlet temperature of 506°K (450F). The results are presented in Figures 60 and 61. These data are also useful in assessing the merits of dual temperature mixed material airframe concepts discussed previously.

Heat Exchanger Design

While many heat exchanger designs are available for aircraft use, past experience suggests that the brazed aluminum plate and fin type is most appropriate for hypersonic aircraft cooling systems. Since the desired temperature levels are incompatible with either parallel flow or cross flow designs only a counterflow arrangement was considered. With these constraints the heat exchanger design problem is one of determining the optimum fin configuration. A heat exchanger sizing computer program, which determines system weight as a function of Reynolds number in the passage, was used to select the optimum system for the (UA) requirement specified. Sixty fin configurations were considered. For each fin configuration, the dimensions, thermal characteristics and pressure drop characteristics are input to the program. In addition the parting sheet thickness, APS fuel weight penalty of 2.27 mg/J (5.0 lb/hp-hr), (see Ref 3), and the fluid properties of both hydrogen and the panel coolant are required.

The wet weight of the heat exchanger plus APS fuel are presented in Figures 62 and 63 for the five candidate coolants in addition to water-glycol. Because the thermal and pumping characteristics of each coolant are different, the fin types utilized for each were different. Table XIX lists the fin configurations for each coolant as determined by the heat exchanger optimization program. In all cases an offset fin 1.9 mm (0.075 inch) high with 24 FPI was selected as the fin type on the hydrogen side.

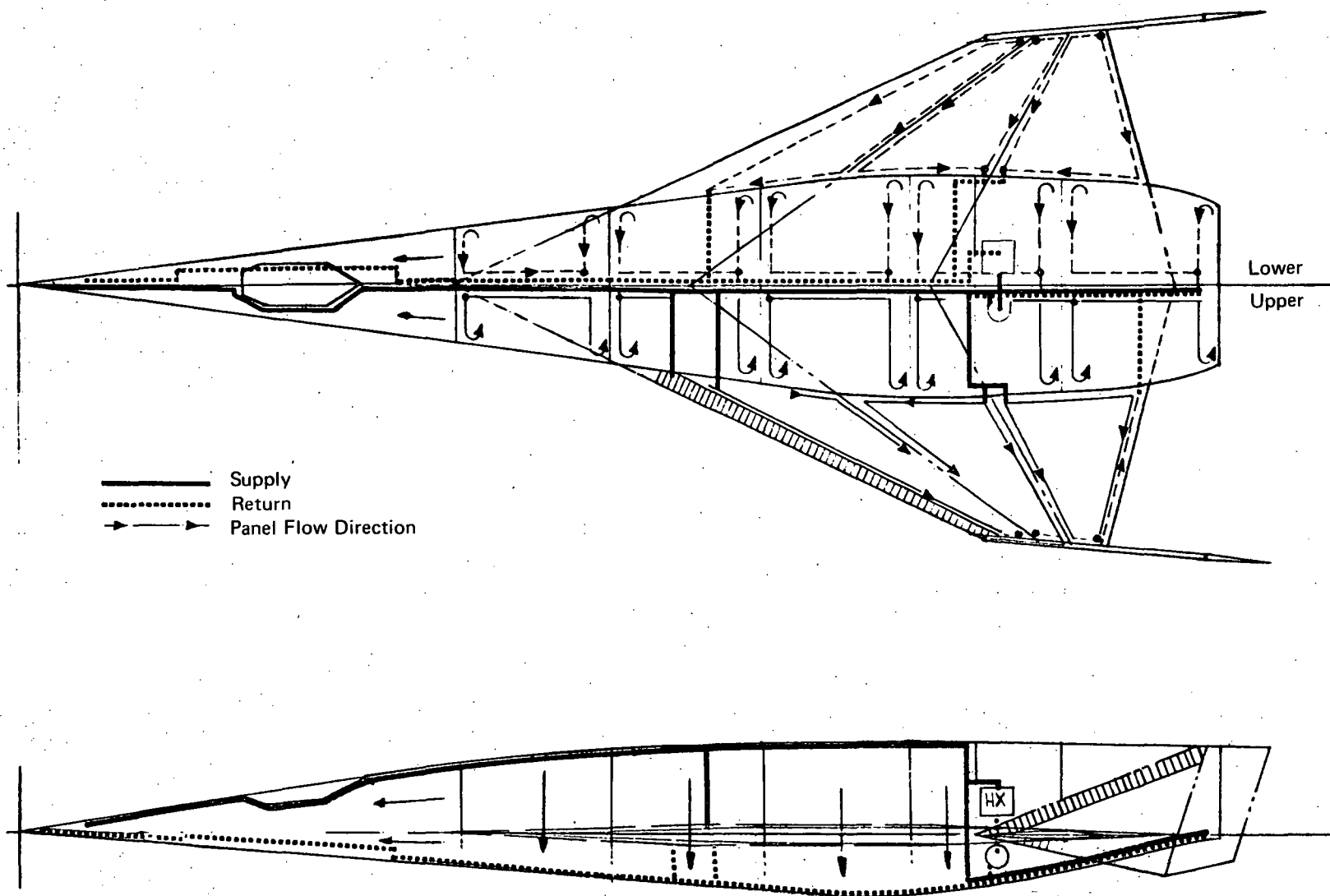


Figure 51. Separate Distribution System for Fuselage and Wing of HRA

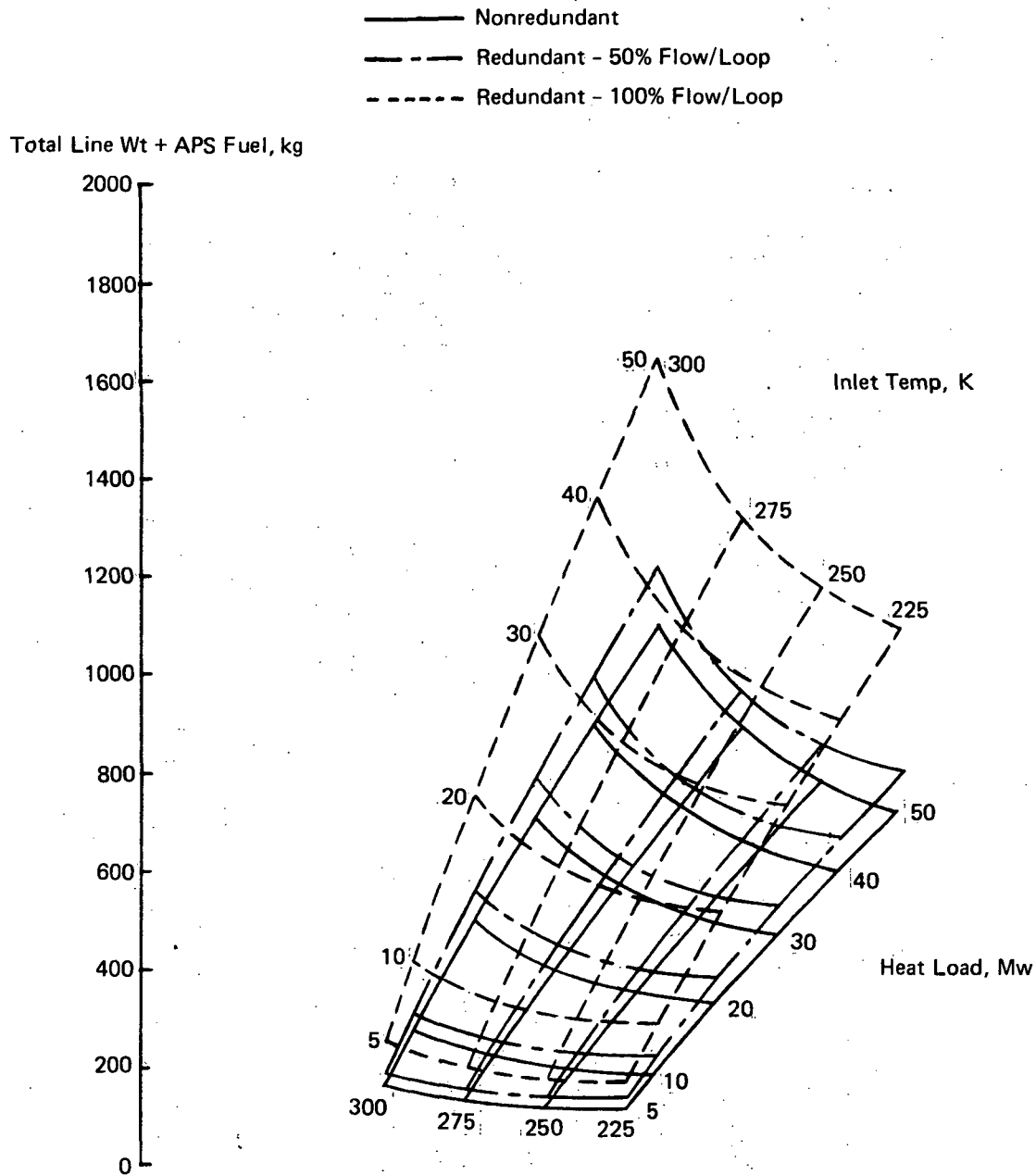


Figure 52a. Minimum Weight of Coolant Distribution Lines and APS Fuel as a Function of Heat Load and Inlet Temperature, Outlet Temperature = 366°K, Ethylene Glycol/Water

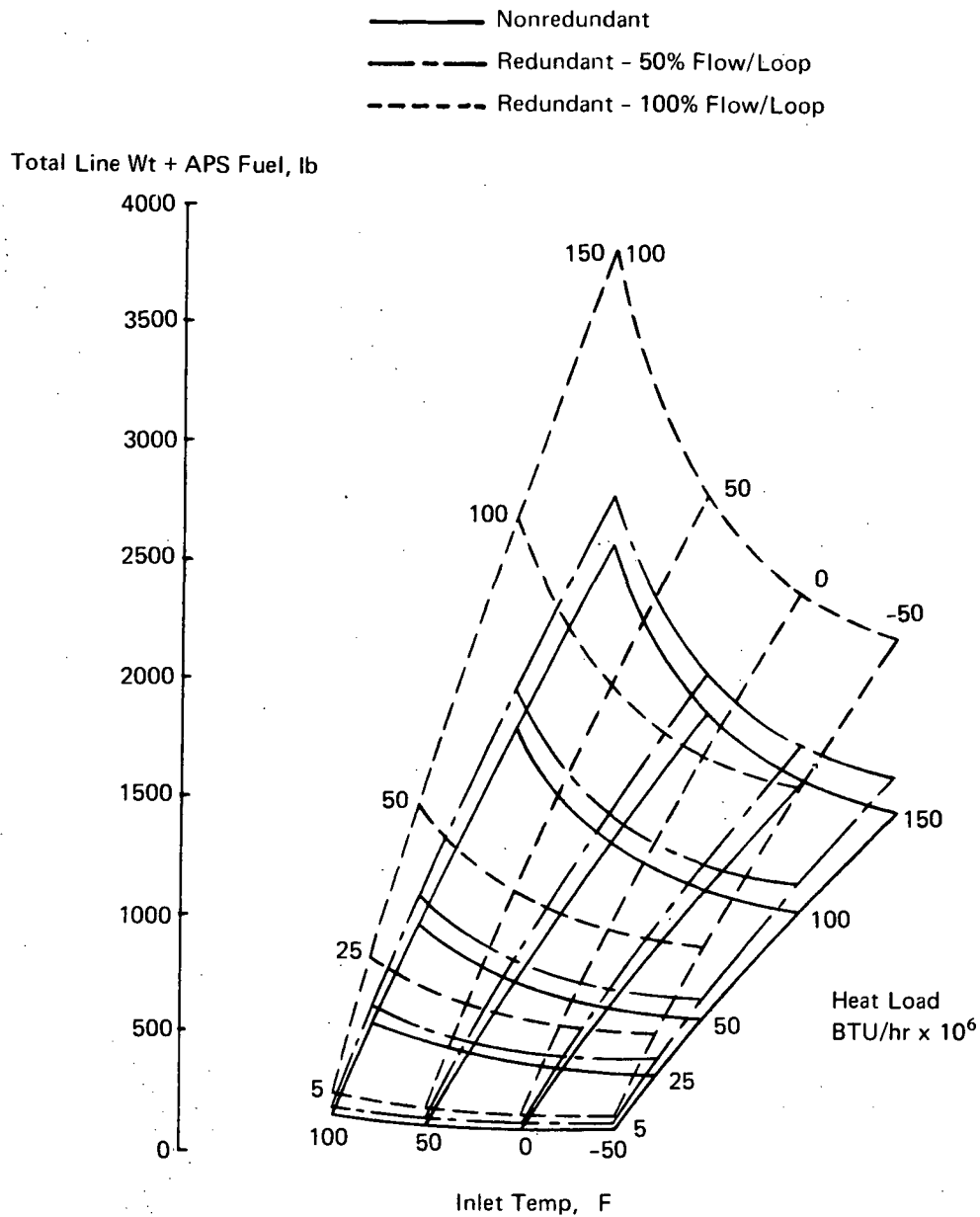


Figure 52b. Minimum Weight of Coolant Distribution Lines and APS Fuel as a Function of Heat Load and Inlet Temperature, Outlet Temperature = 200F, Ethylene Glycol/Water

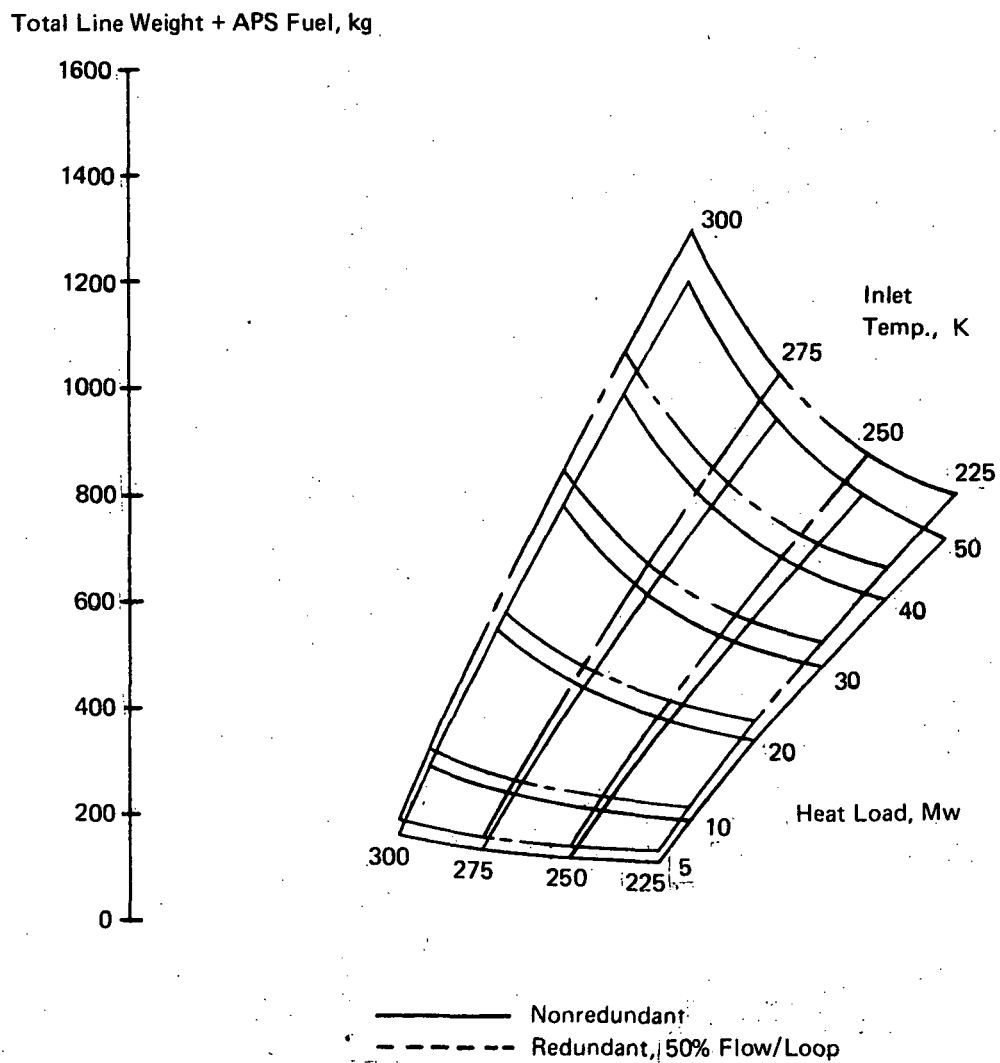


Figure 53a. Minimum Weight of Coolant Distribution Lines and APS Fuel as a Function of Heat Load and Inlet Temperature Outlet Temperature = 367°K, Methanol/Water

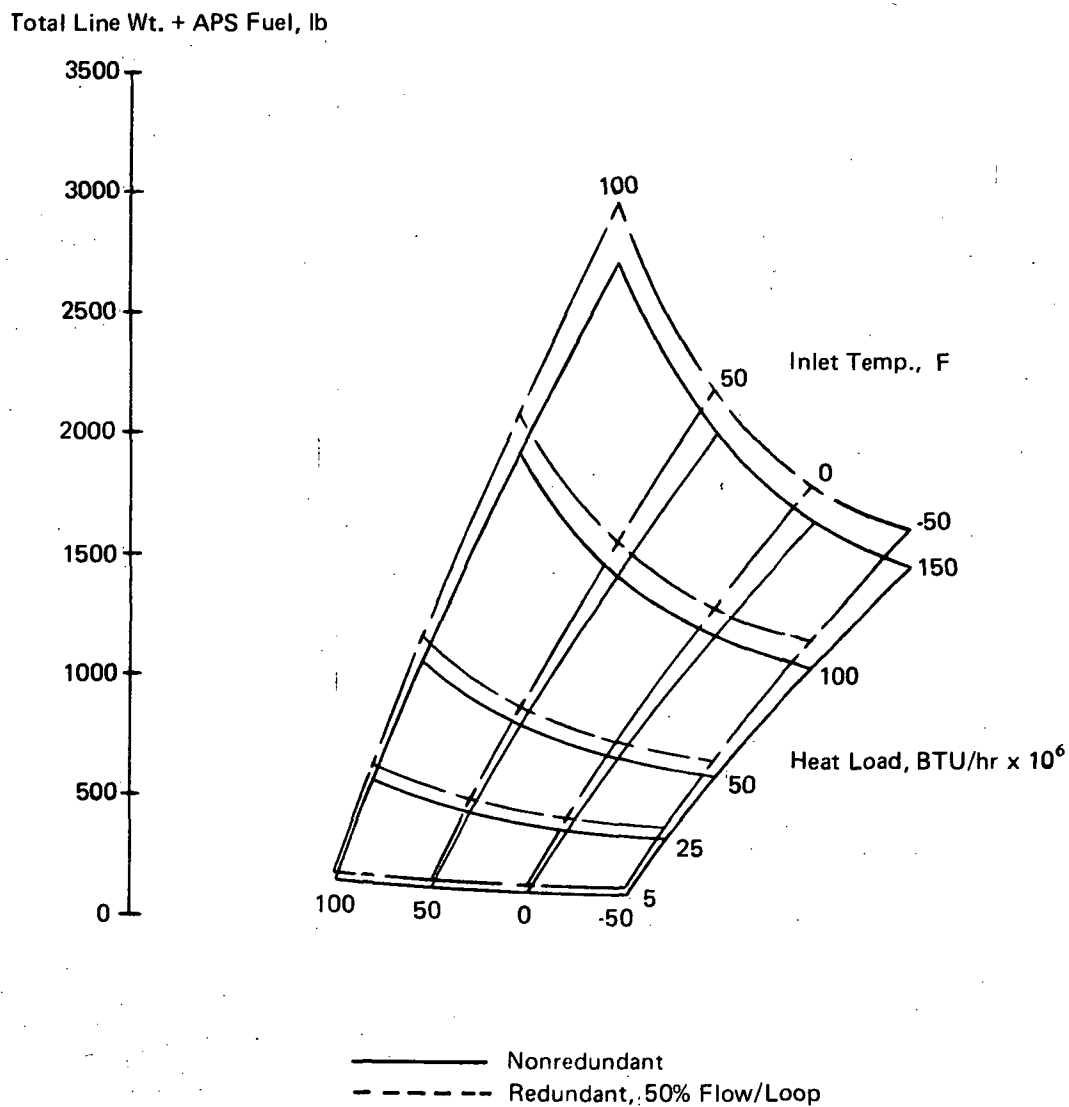


Figure 53b. Minimum Weight of Coolant Distribution Lines and APS Fuel as a Function of Heat Load and Inlet Temperature Outlet Temperature = 200F, Methanol/Water

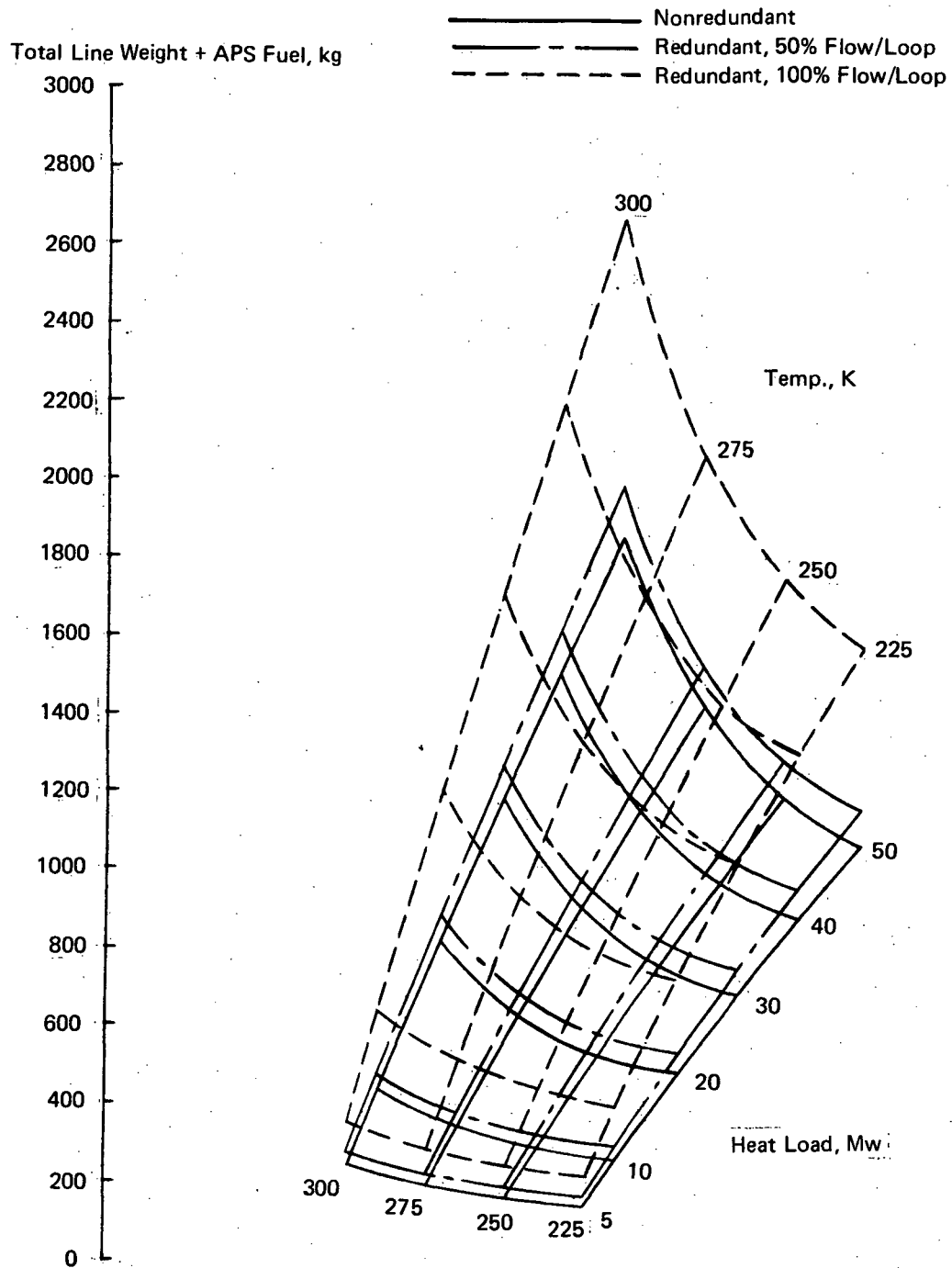


Figure 54a. Minimum Weight of Coolant Distribution Lines and APS Fuel as a Function of Heat Load and Inlet Temperature, Outlet Temperature = 367°K, Coolant 20

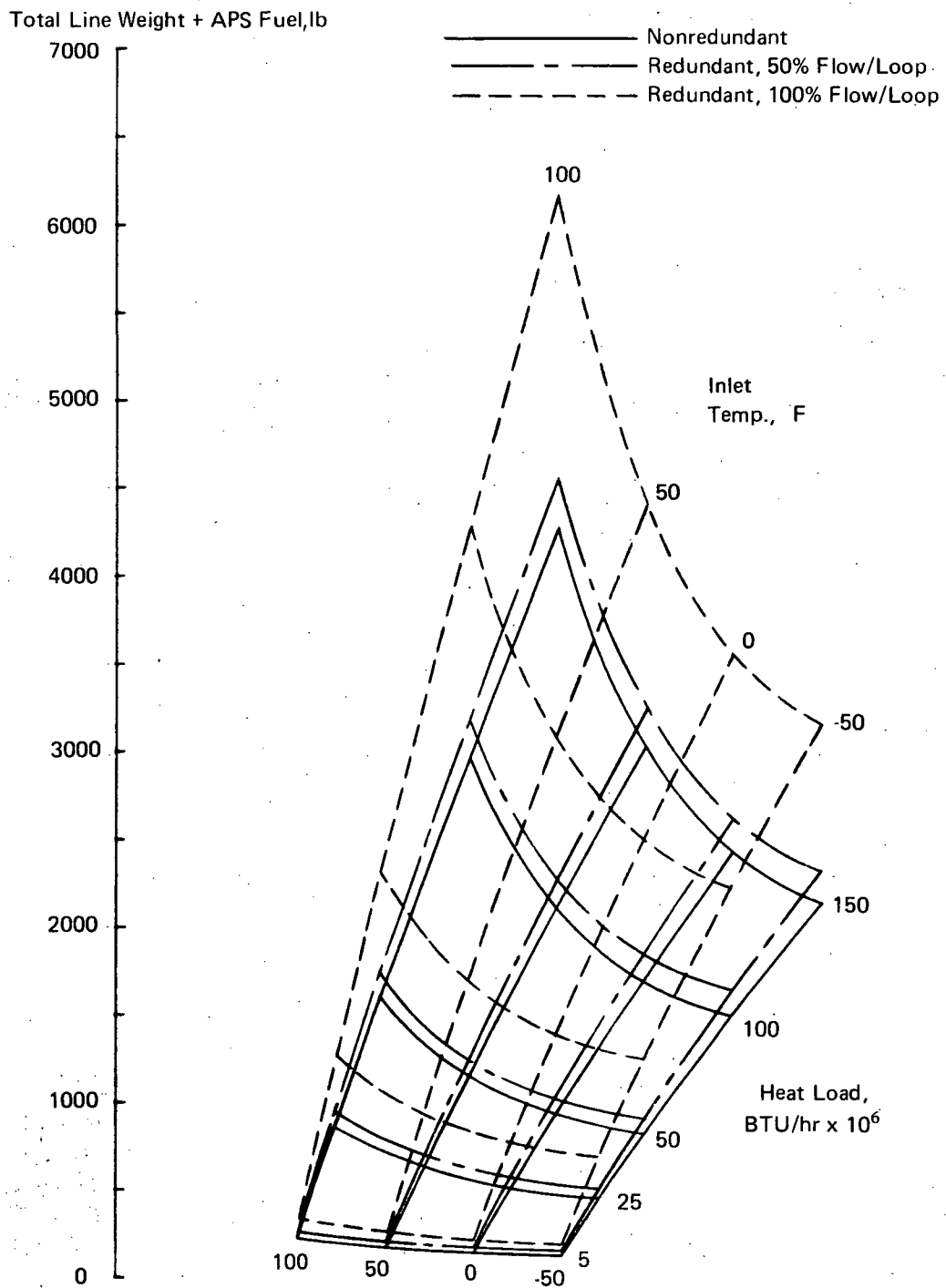


Figure 54b. Minimum Weight of Coolant Distribution Lines and APS Fuel as a Function of Heat Load and Inlet Temperature, Outlet Temperature = 200F, Coolanol 20

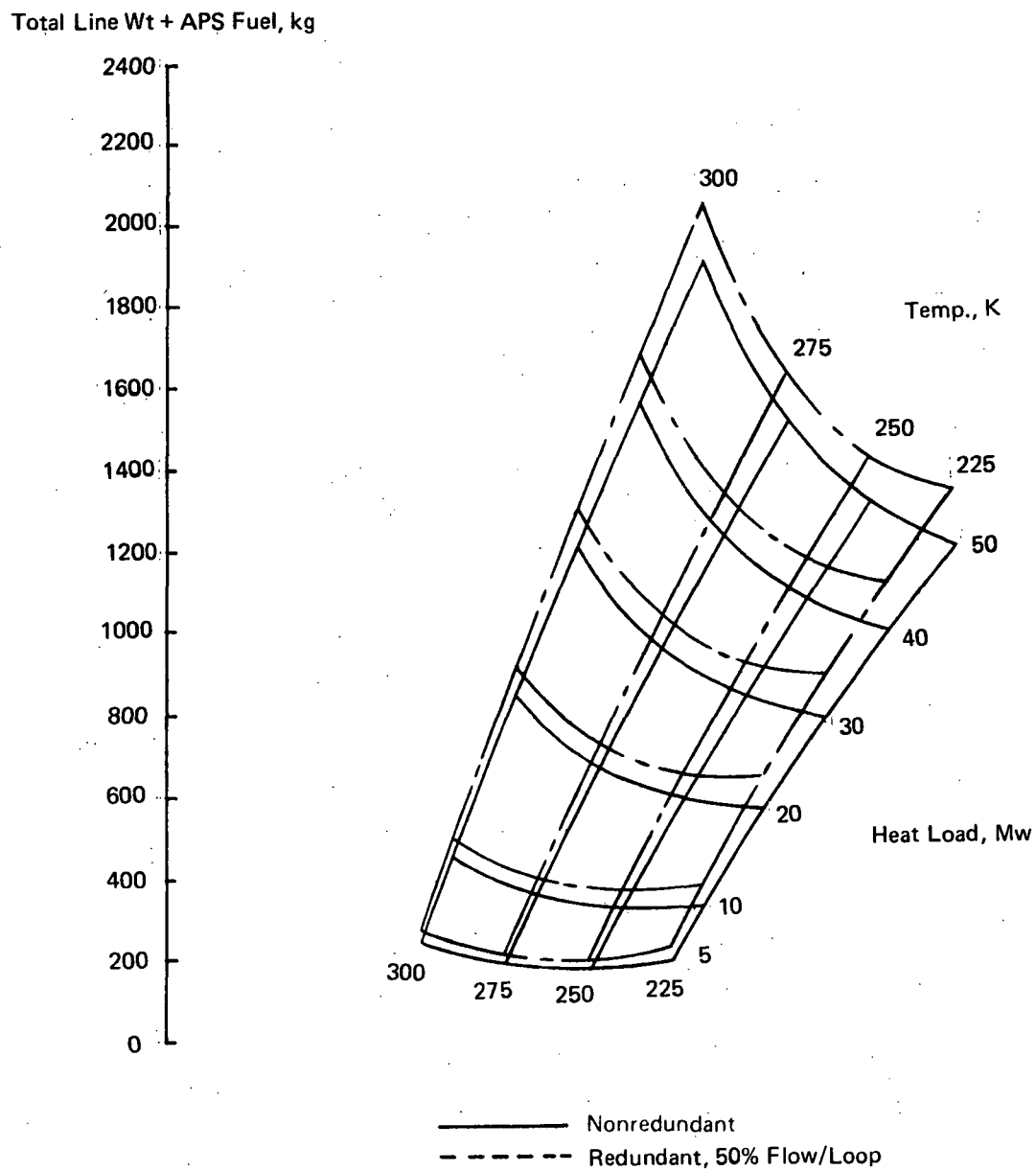


Figure 55a. Minimum Weight of Coolant Distribution Lines and APS Fuel as a Function of Heat Load and Inlet Temperature, Outlet Temperature = 367°K, Coolant 40

Total Line Wt + APS Fuel, lb

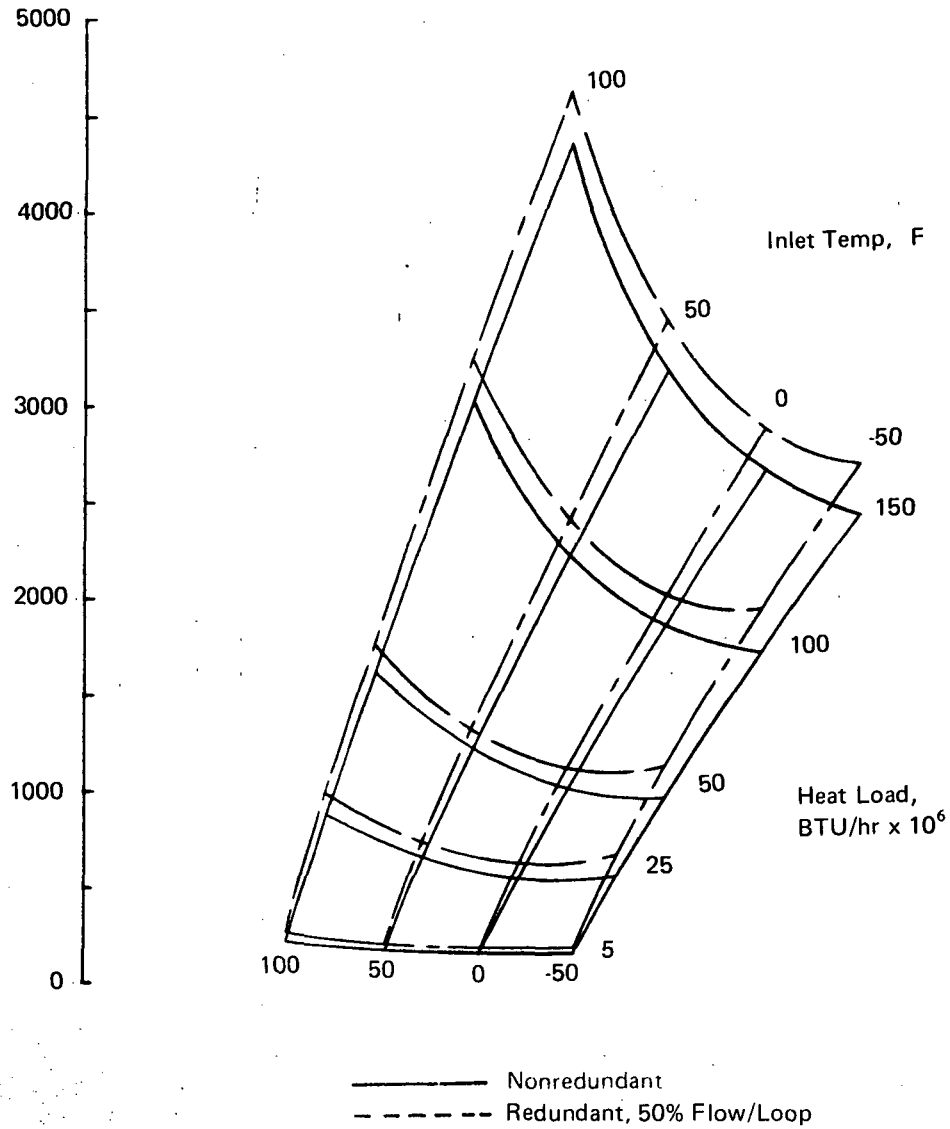


Figure 55b. Minimum Weight of Coolant Distribution Lines and APS Fuel as a Function of Heat Load and Inlet Temperature, Outlet Temperature = 200F, Coolant 40

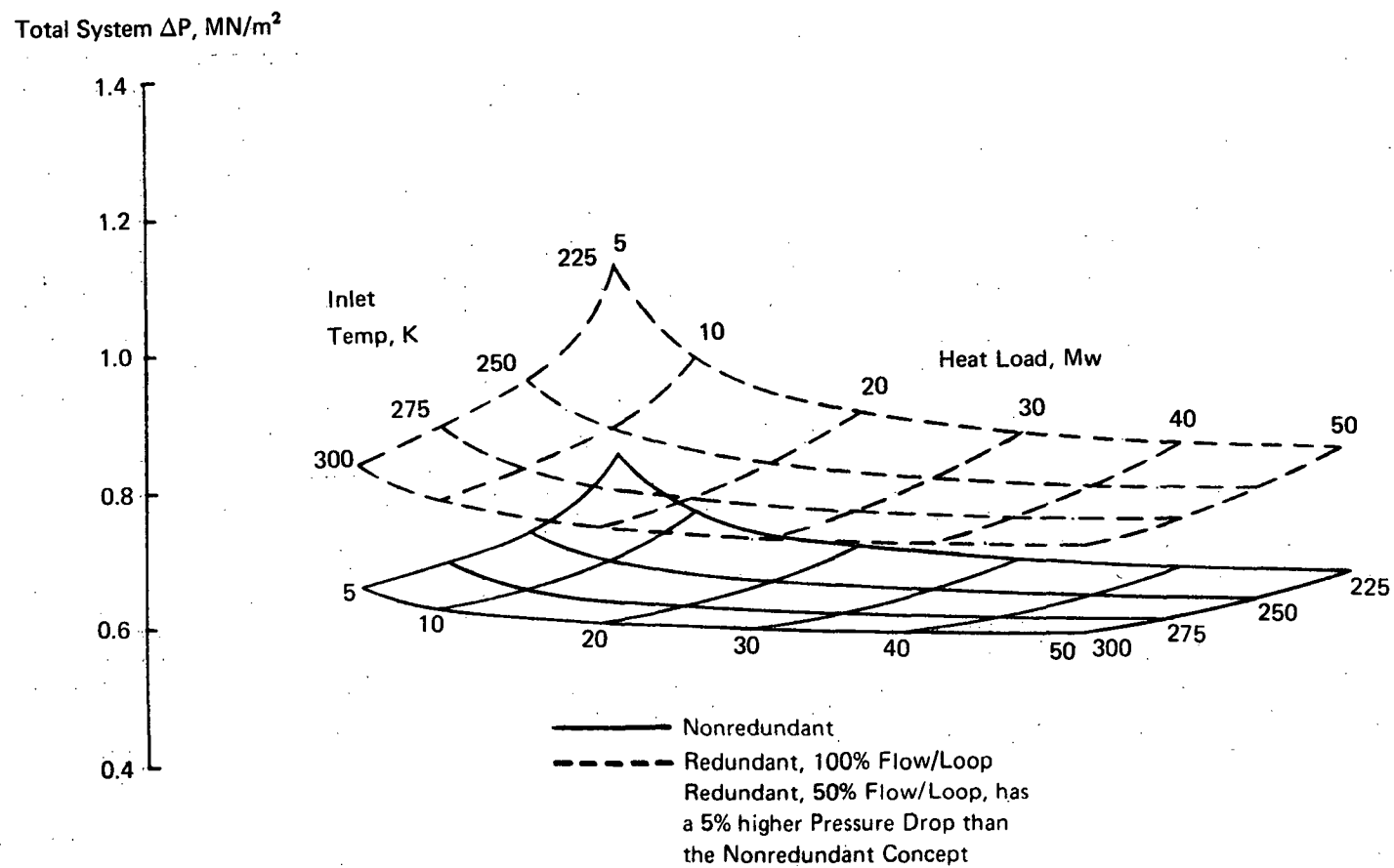


Figure 56a. Pressure Drop for Minimum Weight Coolant Distribution Lines as a Function of Heat Load and Inlet Temperature, Outlet Temperature = 367° K, Ethylene Glycol/Water

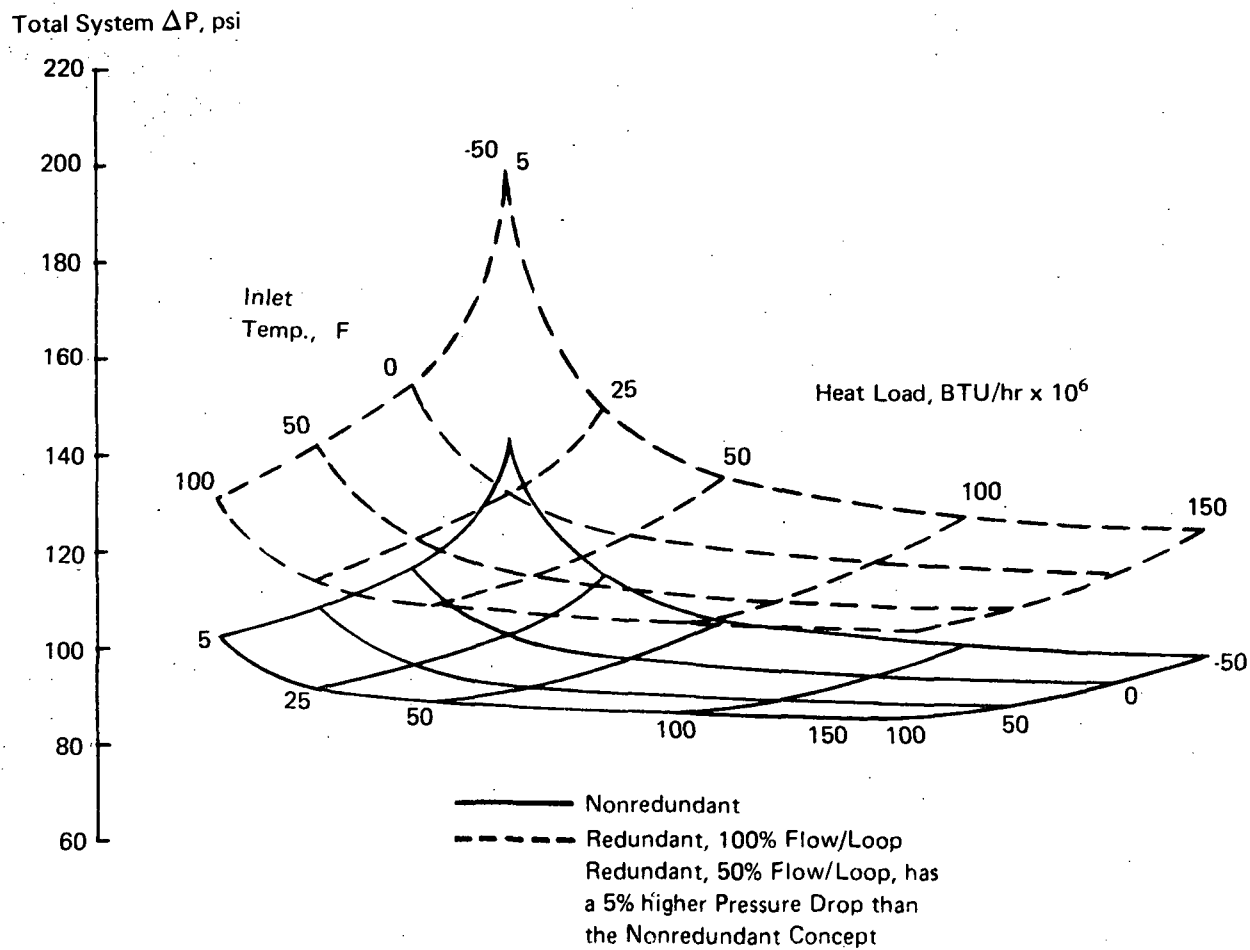


Figure 56b. Pressure Drop for Minimum Weight Coolant Distribution Lines as a Function of Heat Load and Inlet Temperature, Outlet Temperature = 200F, Ethylene Glycol/Water

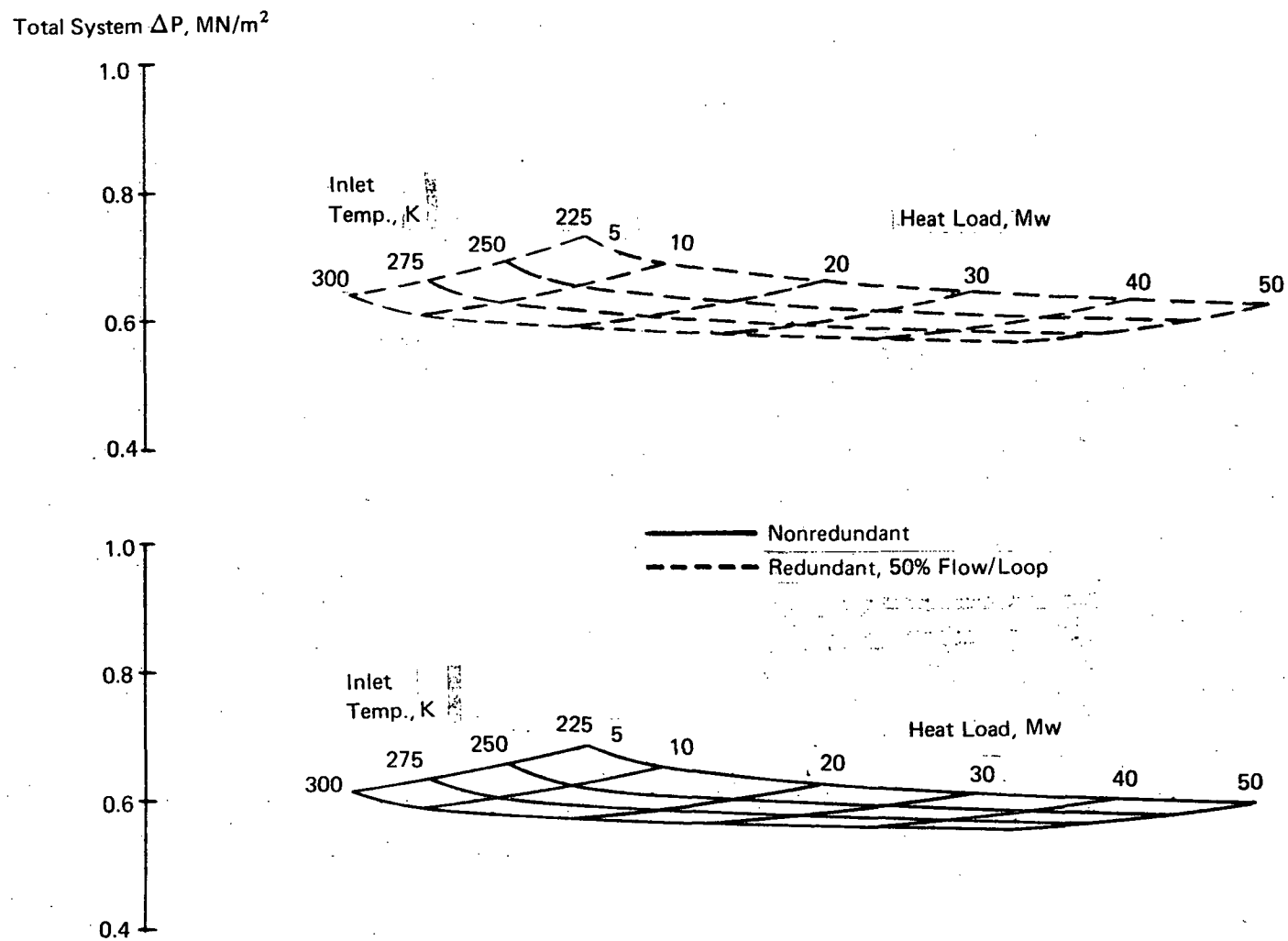


Figure 57a. Pressure Drop for Minimum Weight Coolant Distribution Lines as a Function of Heat Load and Inlet Temperature Outlet Temperature = 367°K, Methanol/Water

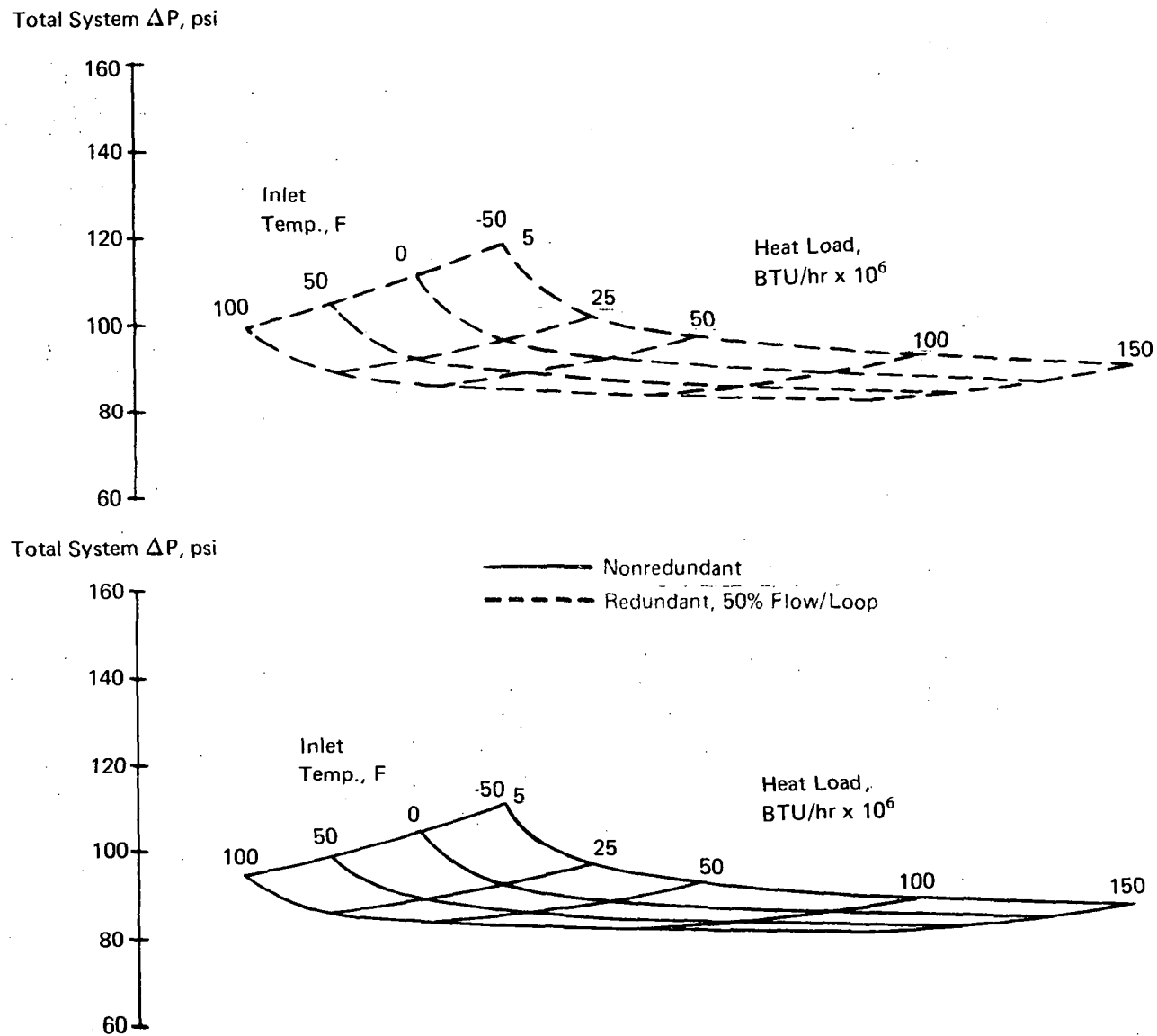


Figure 57b. Pressure Drop for Minimum Weight Coolant Distribution Lines as a Function of Heat Load and Inlet Temperature, Outlet Temperature = 200F, Methanol/Water

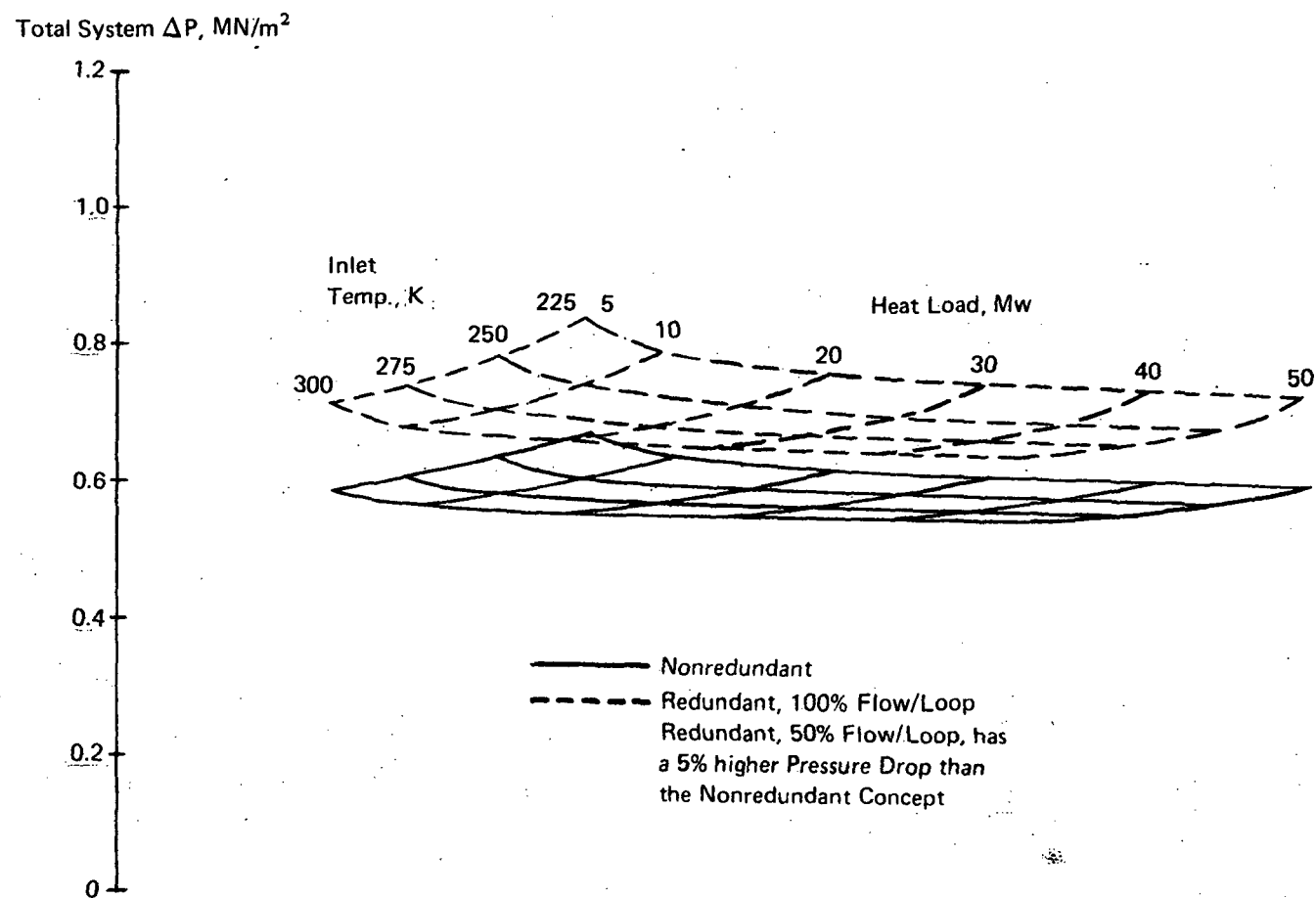


Figure 58a. Pressure Drop for Minimum Weight Coolant Distribution Lines as a Function of Heat Load and Inlet Temperature, Outlet Temperature = 367°K, Coolanol 20

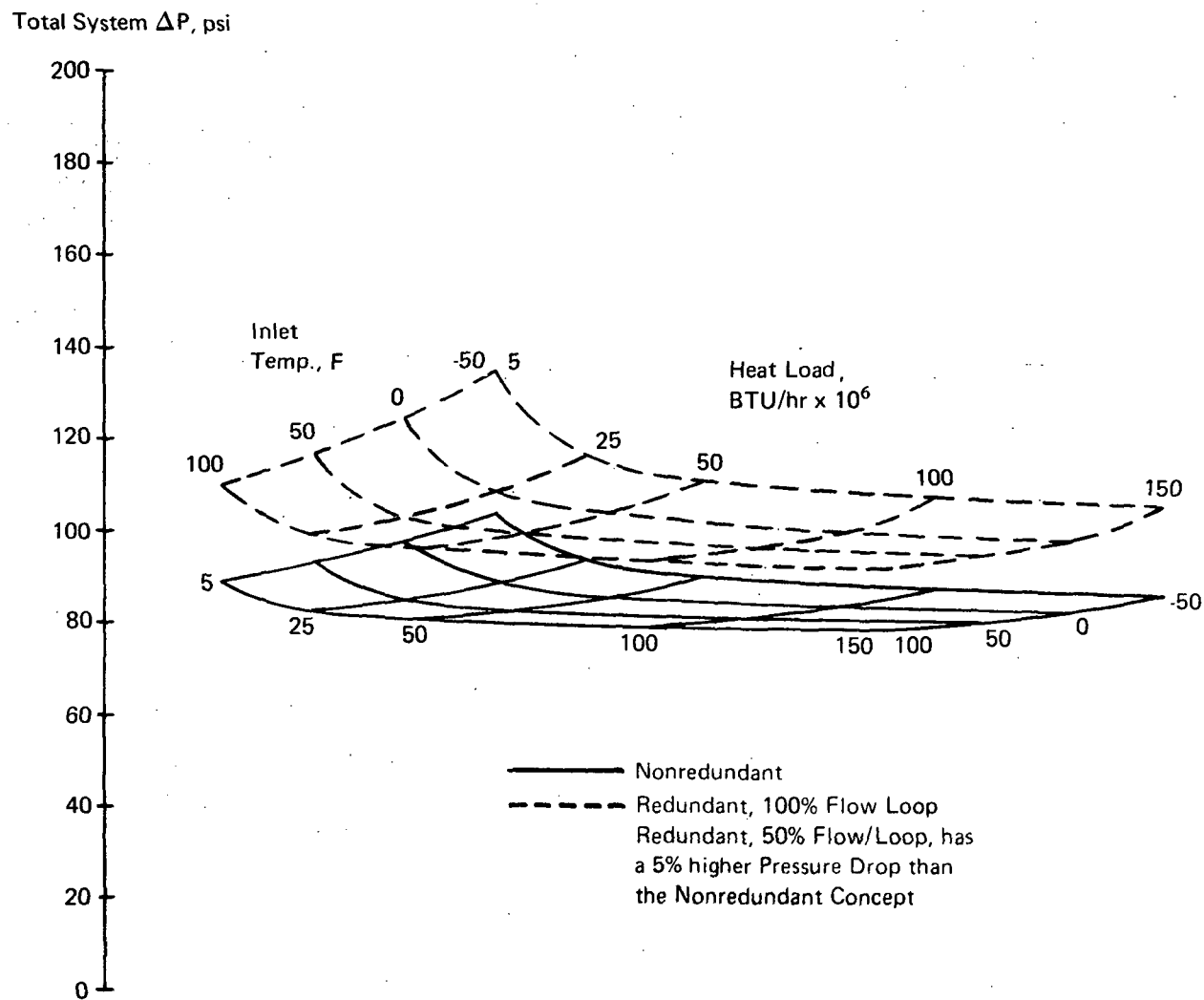


Figure 58b. Pressure Drop for Minimum Weight Coolant Distribution Lines as a Function of Heat Load and Inlet Temperature, Outlet Temperature = 200F, Coolant 20

Total System ΔP , MN/m²

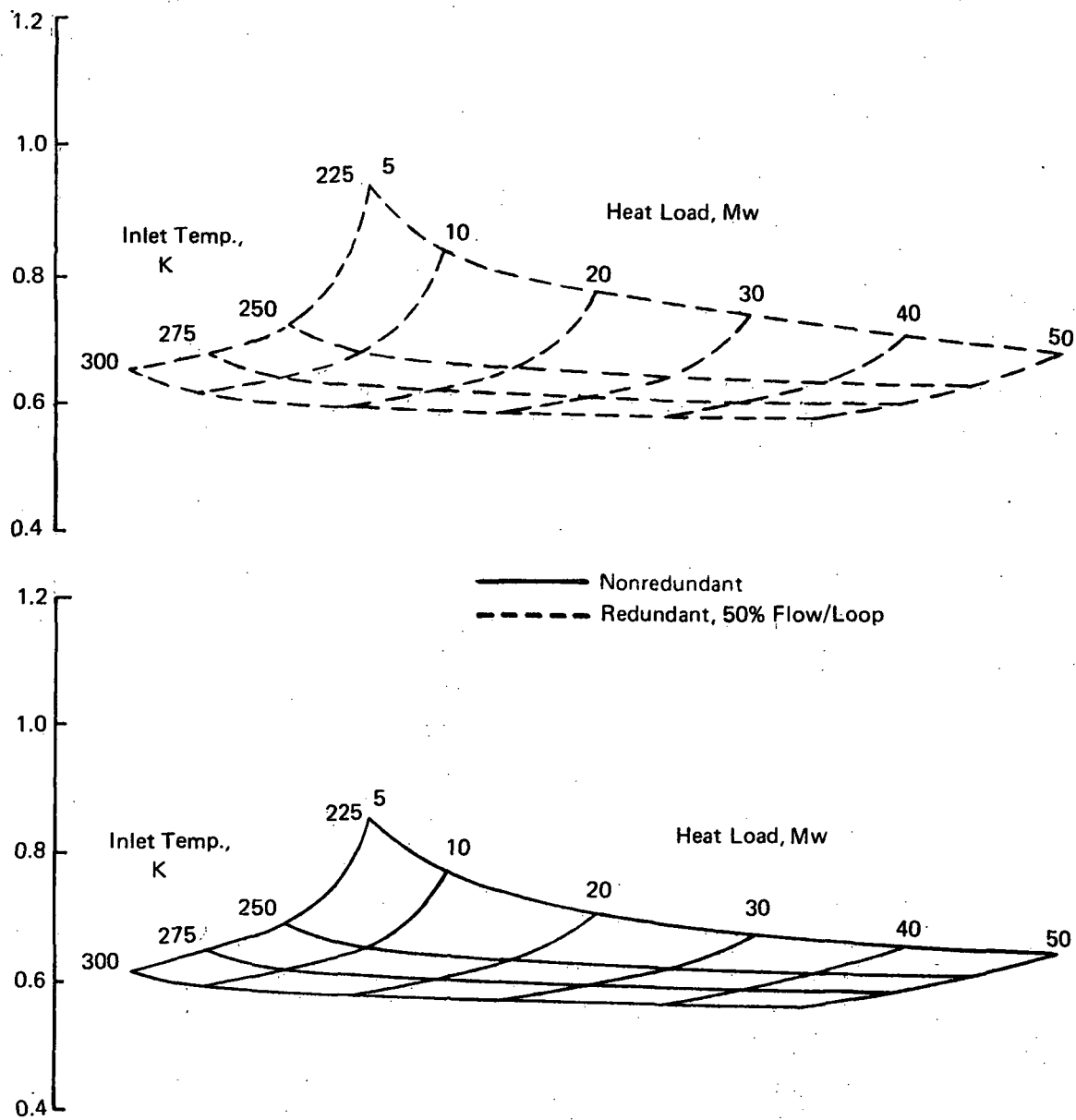


Figure 59a. Pressure Drop for Minimum Weight Coolant Distribution Lines as a Function of Heat Load and Inlet Temperature, Outlet Temperature = 367°K, Coolant 40

Total System ΔP , psi

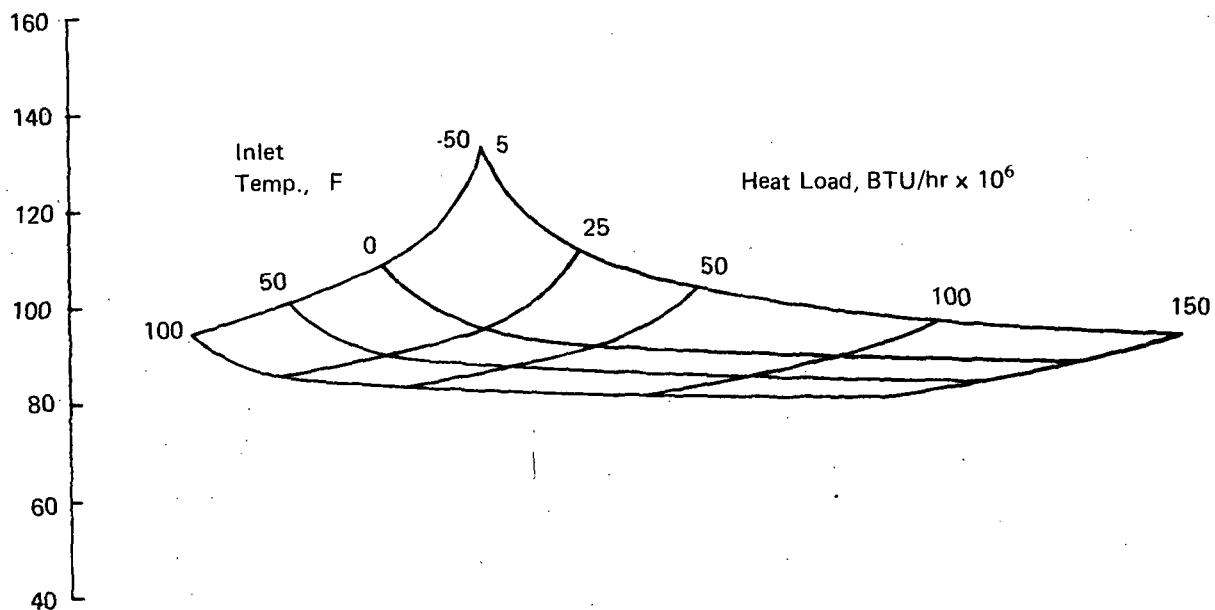
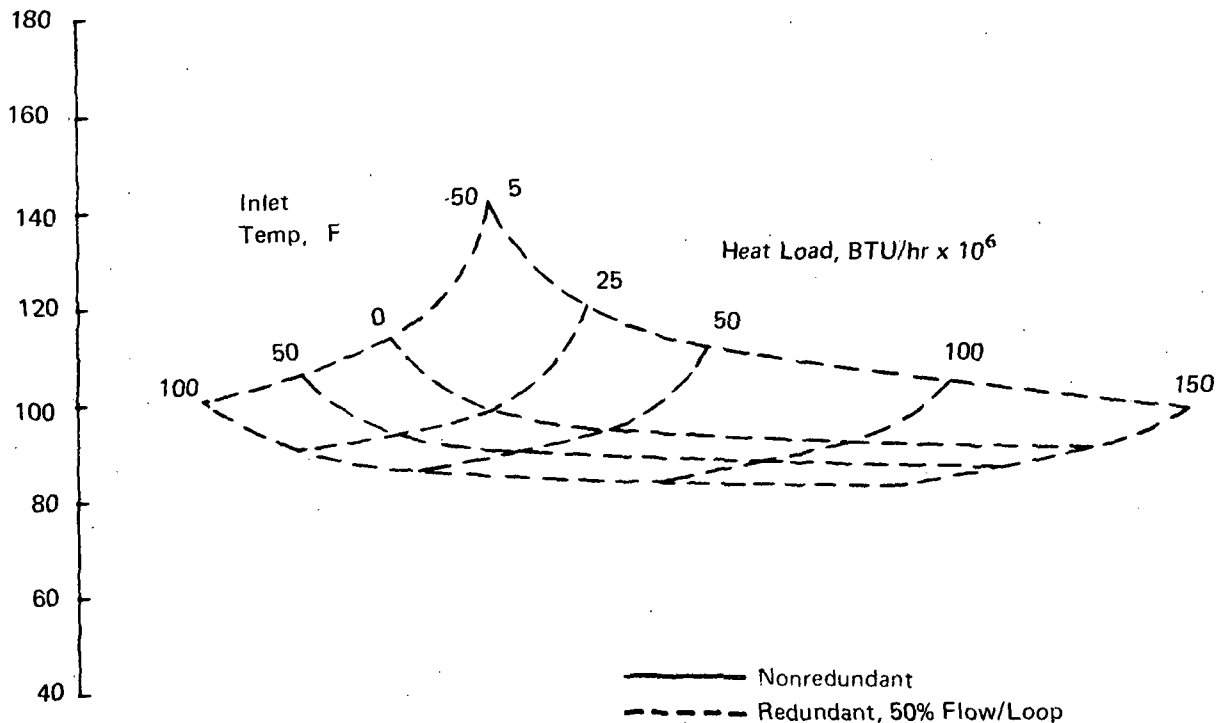


Figure 59b. Pressure Drop for Minimum Weight Coolant Distribution Lines as a Function of Heat Load and Inlet Temperature, Outlet Temperature = 200F, Coolanol 40

Total Line Wt + APS Fuel, kg

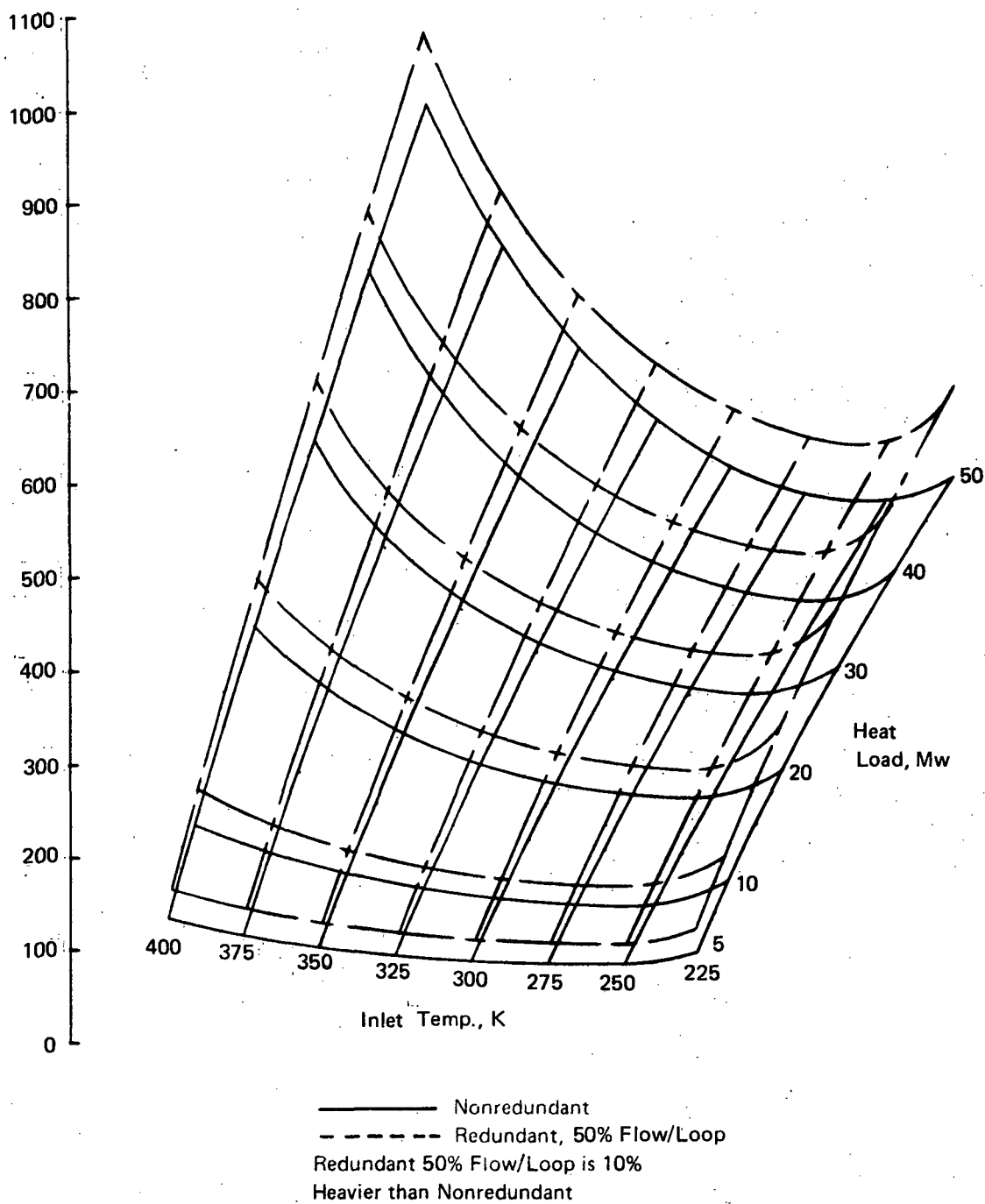


Figure 60a. Minimum Weight of Coolant Distribution Lines and APS Fuel as a Function of Heat Load and Inlet Temperature, Outlet Temperature = 506°K, Coolant 40

Total Line Wt + APS Fuel, lb

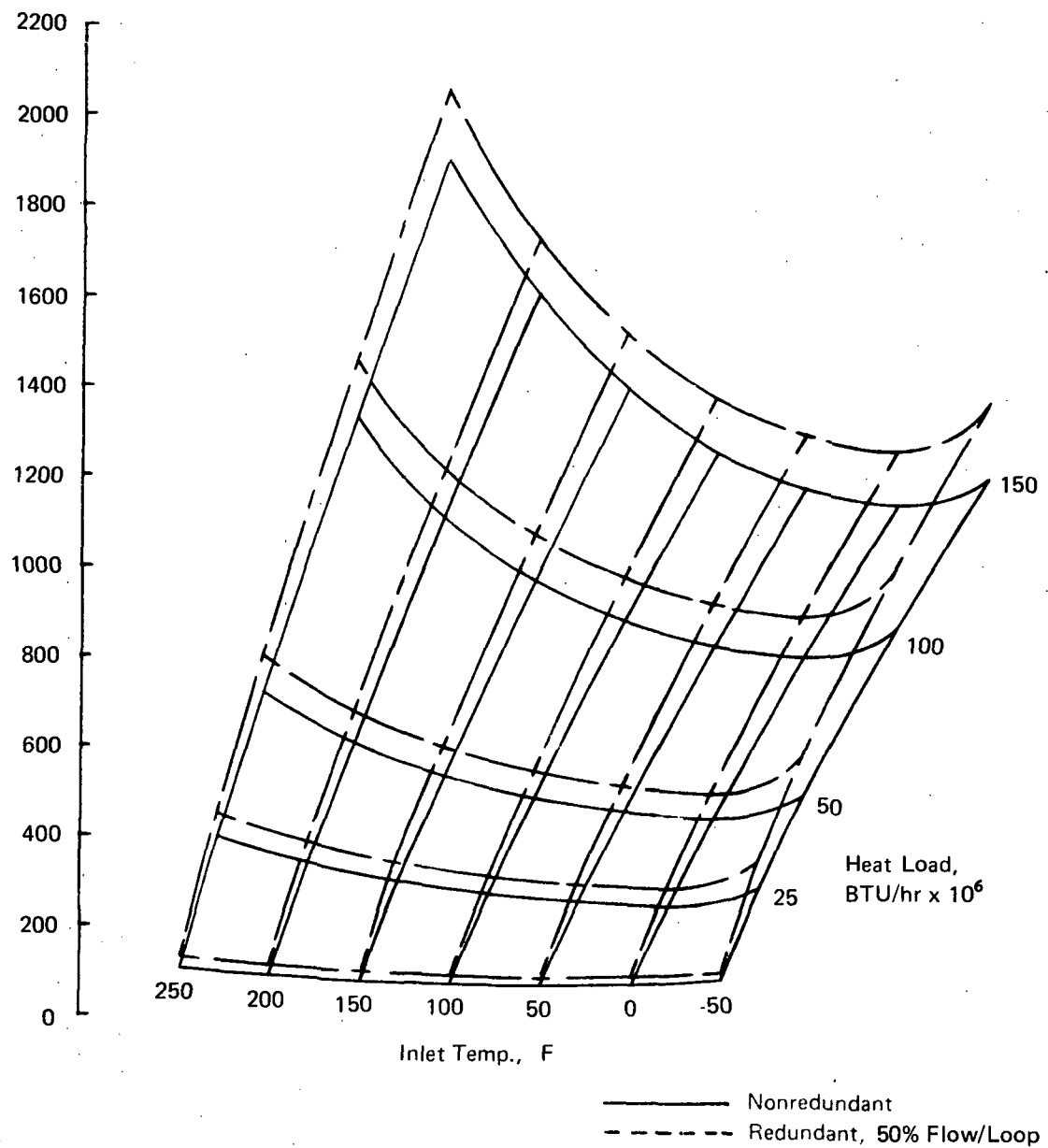


Figure 60b. Minimum Weight of Coolant Distribution Lines and APS Fuel as a Function of Heat Load and Inlet Temperature, Outlet Temperature = 450F, Coolanol 40

Total System ΔP , MN/m²

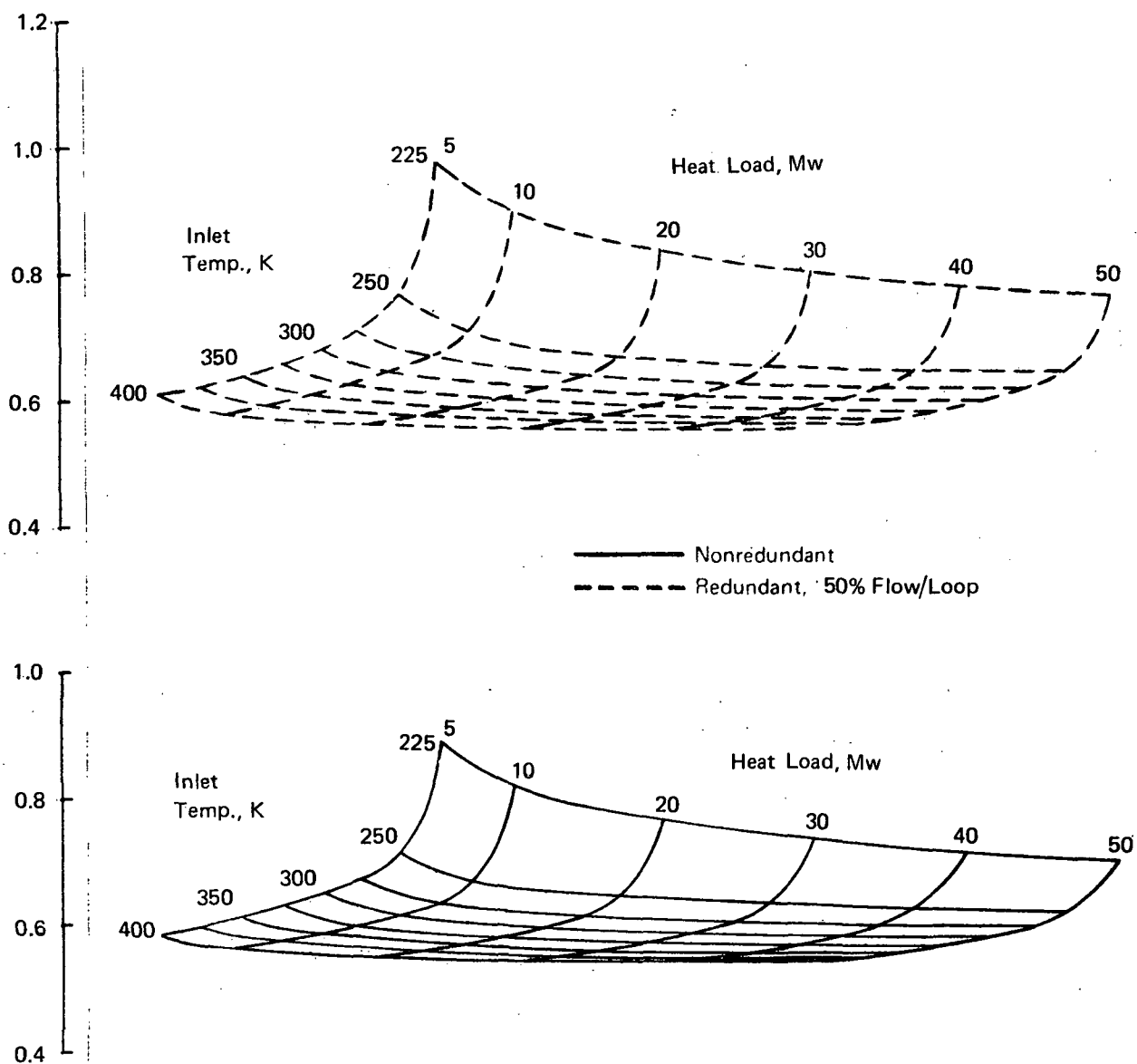


Figure 61a. Pressure Drop for Minimum Weight Coolant Distribution Lines as a Function of Heat Load and Inlet Temperature, Outlet Temperature = 506°K, Coolant 40

Total System ΔP , psi

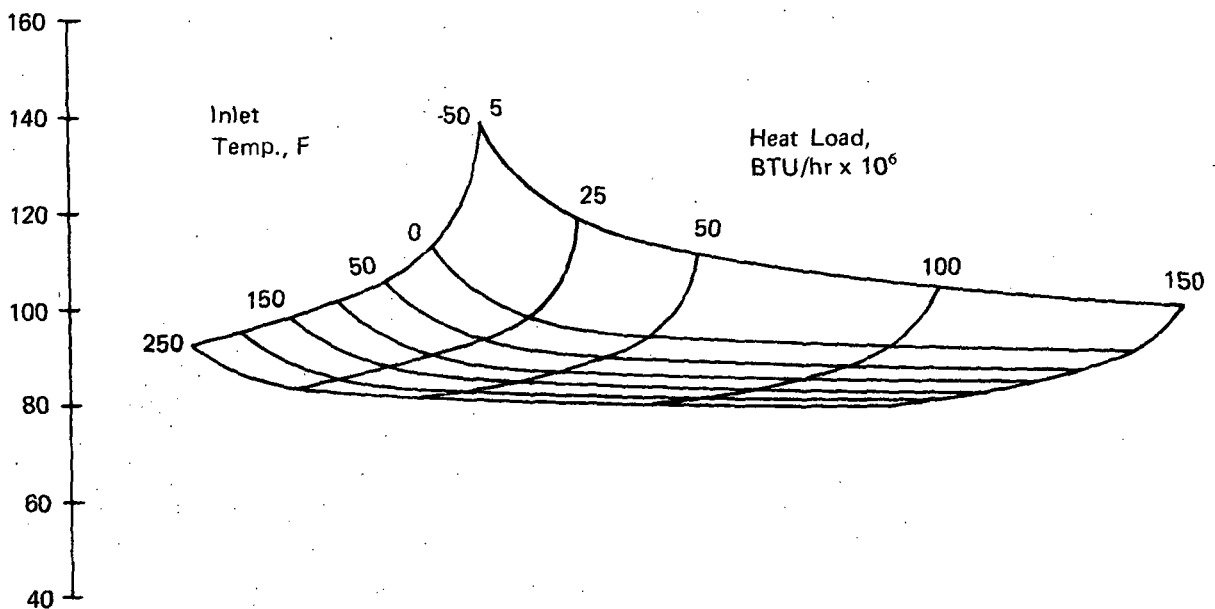
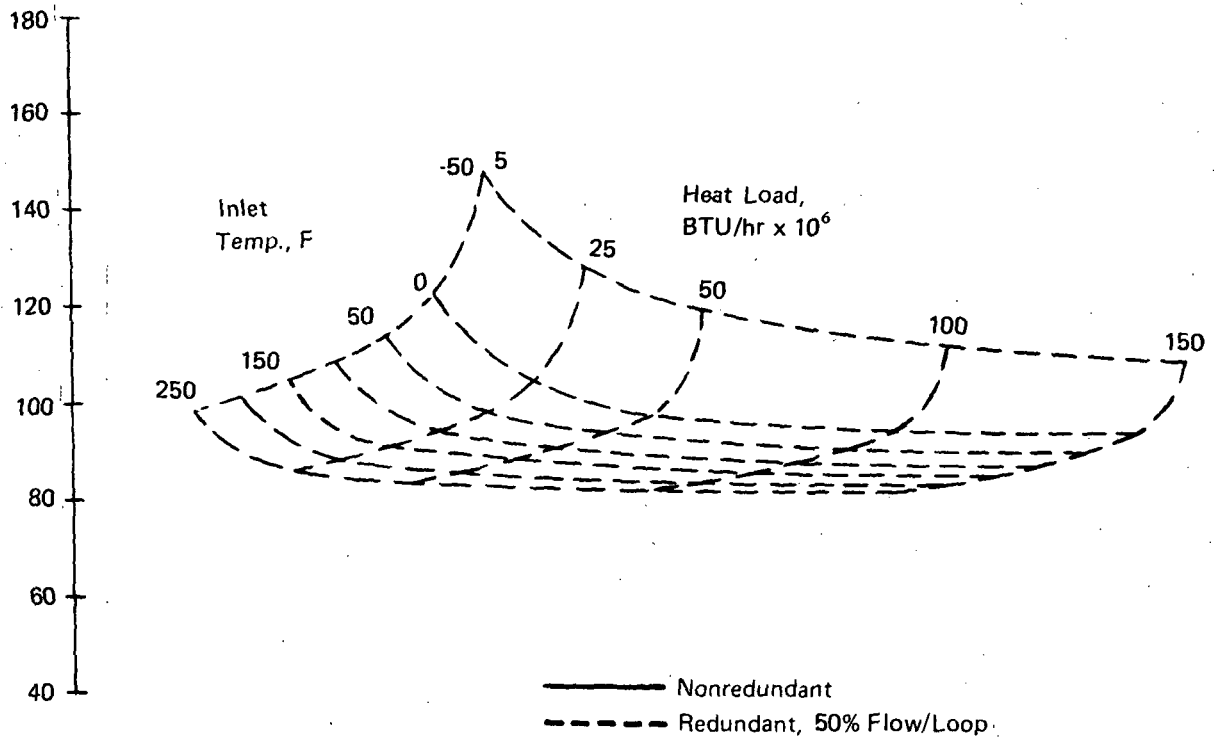


Figure 61b. Pressure Drop for Minimum Weight Coolant Distribution Lines as a Function of Heat Load and Inlet Temperature, Outlet Temperature = 450F, Coolanol 40

Fuel + Heat Exchanger Weight, kg

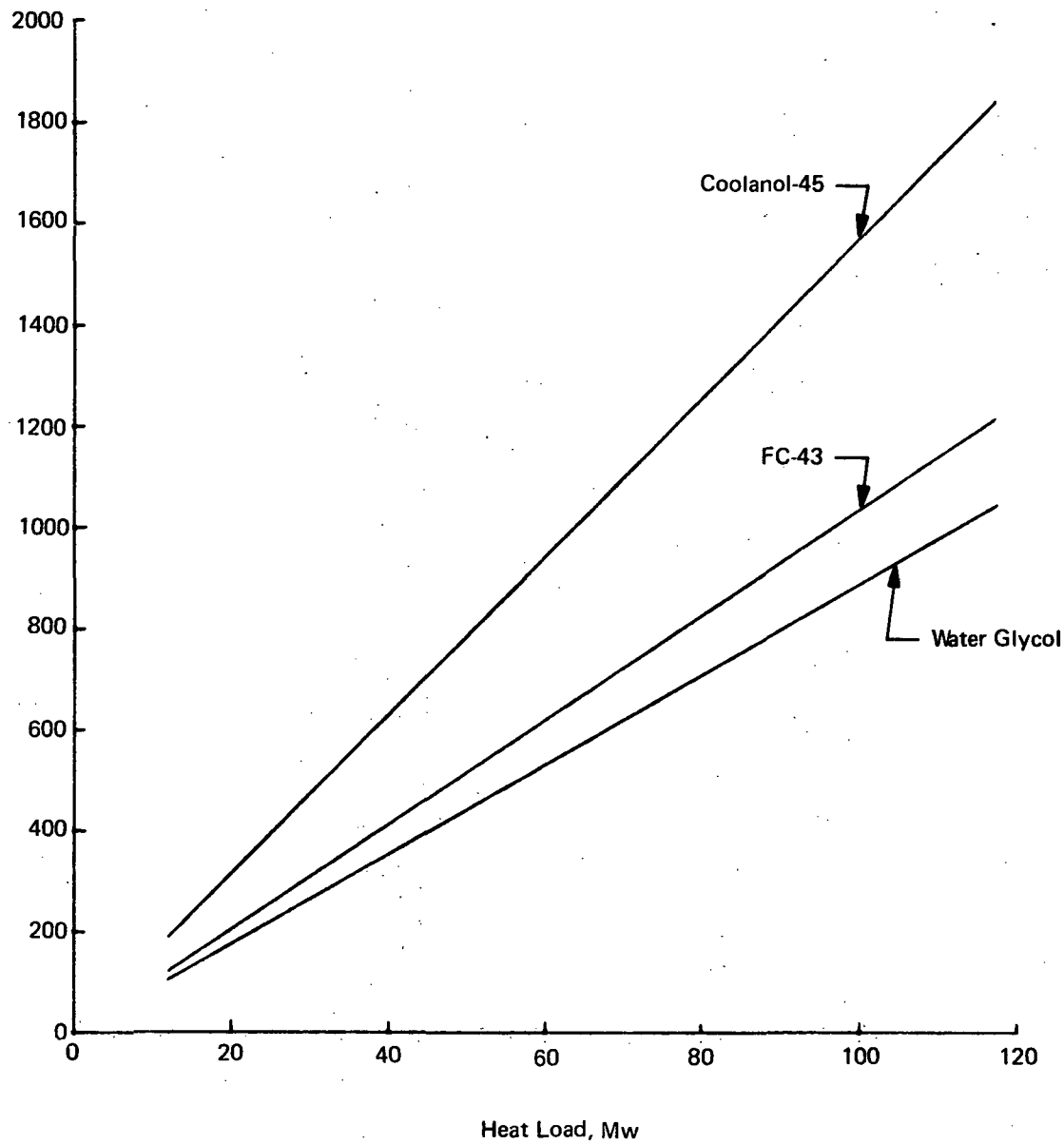


Figure 62a. Plate and Fin Heat Exchanger Weight as a Function of Heat Load, Low Temperature Coolants, Inlet Temperature = 367°K, Outlet Temperature = 283°K, H_2 $T_{in}/T_{out} = 33^\circ K/339^\circ K$

Fuel + Heat Exchanger Weight, lb

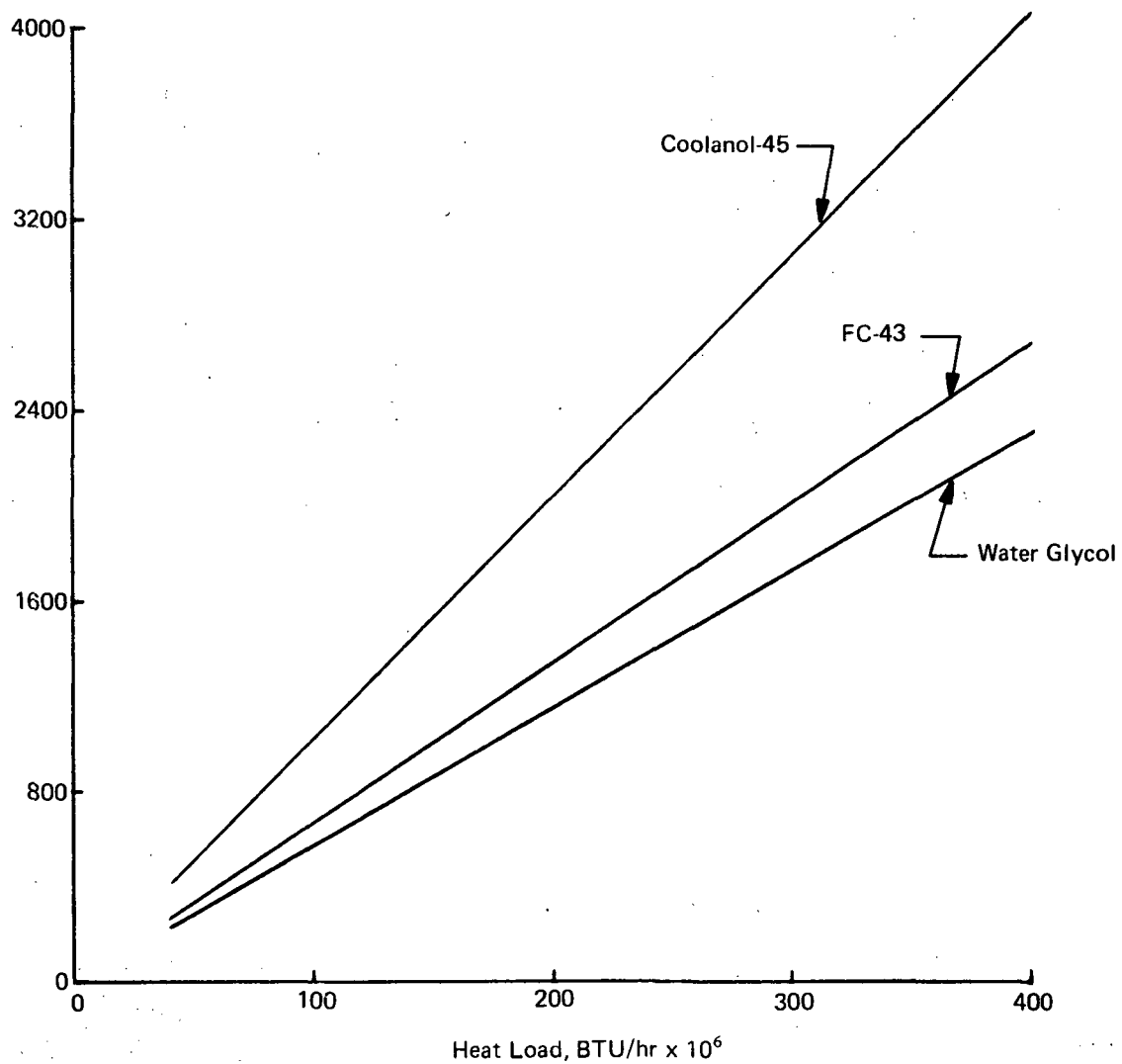


Figure 62b. Plate and Fin Heat Exchanger Weight as a Function of Heat Load, Low Temperature Coolants, Inlet Temperature = 200F, Outlet Temperature = 50F, H₂ T_{in}/T_{out} = -400F/150F

Fuel + Heat Exchange Weight, kg

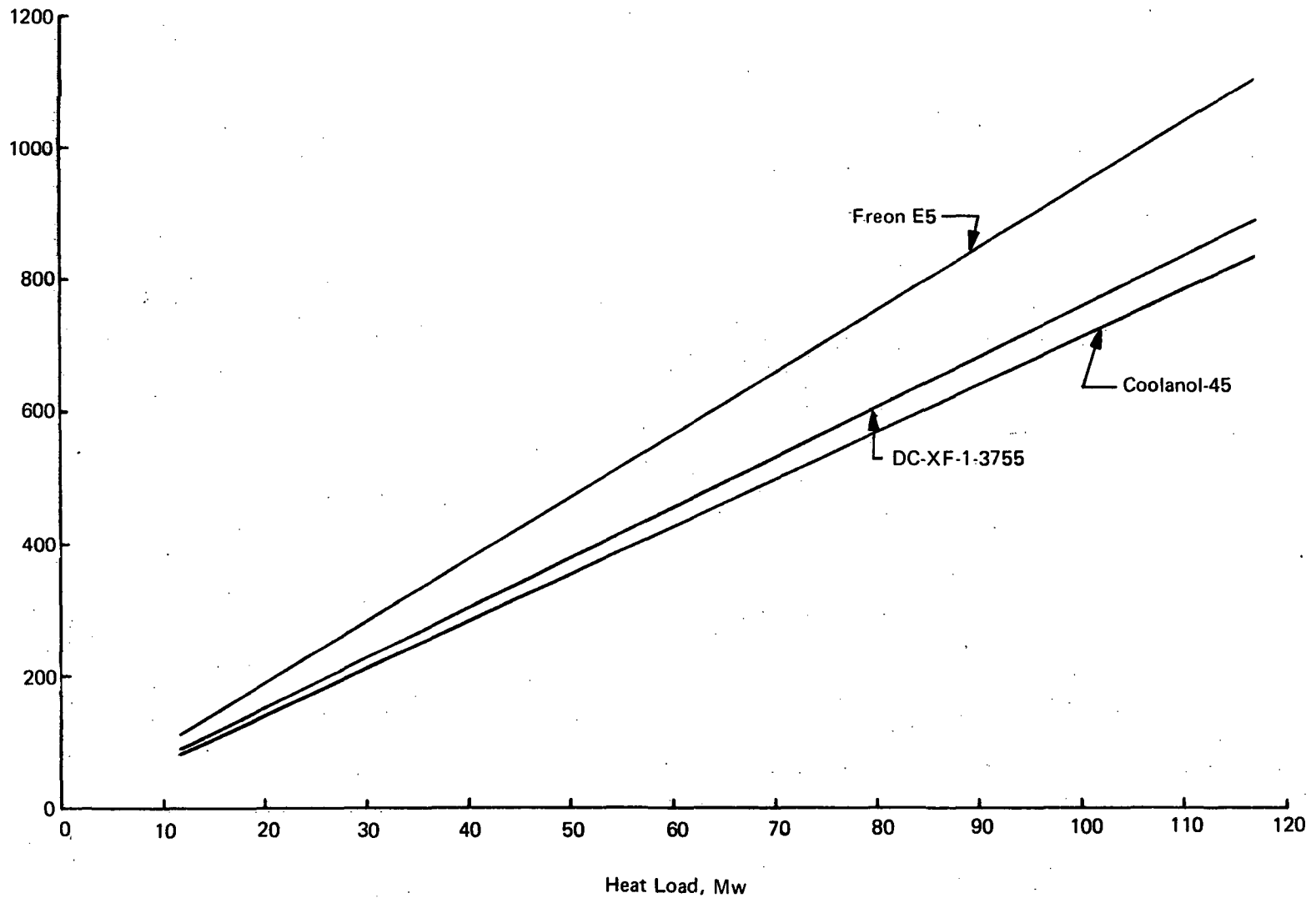


Figure 63a. Plate and Fin Heat Exchanger Weight as a Function of Heat Load, High Temperature Coolants, Inlet Temperature = 450°K, Outlet Temperature = 283°K, H_2 $T_{in}/T_{out} = 33^\circ\text{K}/422^\circ\text{K}$

C-3

Fuel and Heat Exchanger Weight, lb

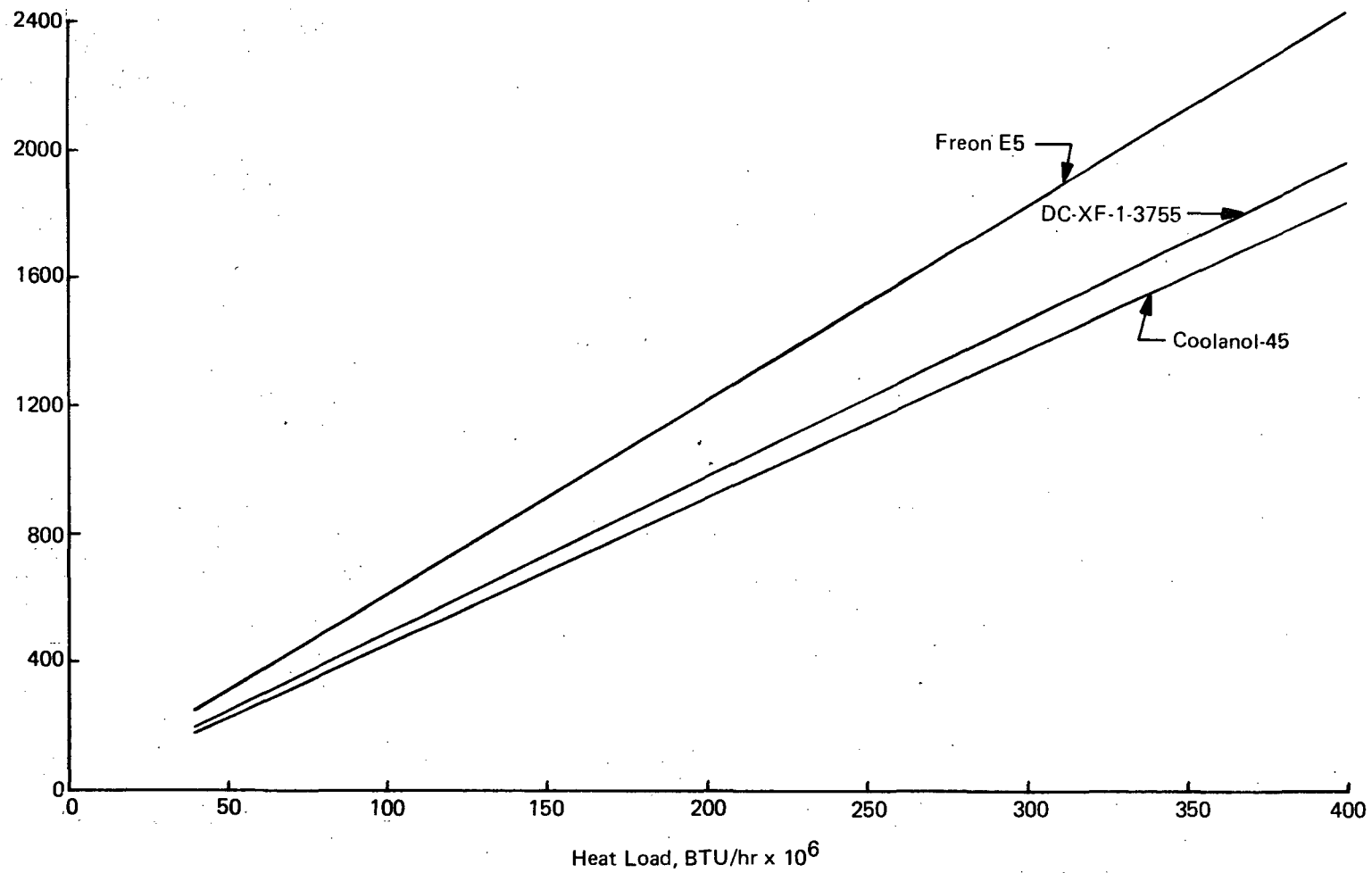


Figure 63b. Plate and Fin Heat Exchanger Weight as a Function of Heat Load, High Temperature Coolants, Inlet Temperature = 350°F, Outlet Temperature = 50°F, H₂ T_{in}/T_{out} = -400F/300F

TABLE XIX
OPTIMIZED OFFSET FIN CONFIGURATION FOR
HEAT EXCHANGERS FOR VARIOUS COOLANTS

| Coolant | Fin Configuration | | | | | |
|--------------------------|-------------------|-------|--------|----------|---------------|-------|
| | Fin Height | | Fins | | Fin Thickness | |
| | mm | inch | per cm | per inch | mm | inch |
| Water Glycol | 1.9 | 0.075 | 9.5 | 24 | 0.1 | 0.004 |
| FC-43 | 1.9 | 0.075 | 9.5 | 24 | 0.1 | 0.004 |
| Coolanol 45 (Low Temp.) | 3.2 | 0.126 | 6.3 | 16 | 0.15 | 0.006 |
| Coolanol 45 (High Temp.) | 2.5 | 0.100 | 7.9 | 20 | 0.1 | 0.004 |
| DC XF-1-3755 | 3.2 | 0.100 | 7.9 | 20 | 0.1 | 0.004 |
| Freon E5 | 1.9 | 0.075 | 9.5 | 24 | 0.1 | 0.004 |

Figure 62 presents the weights for three low temperature coolants as a function of transferred heat load. For each coolant, the inlet temperature to the heat exchanger was considered to be 366°K (200F) and the outlet was 283°K (50F) whereas the hydrogen inlet temperature was 33°K (-400F) and its outlet was 340°K (150F). Because the water glycol exhibits the lowest pumping power to heat transfer parameter, it results in the lowest heat exchanger weight. For similar reasons, FC-43 ranks better than Coolanol 45.

The weights for the high temperature coolants are shown in Figure 63. The spread between these curves is much less than for the low temperature coolants, however, the ranking is again directly related to their pumping power/heat transfer parameter. These weights were generated on the basis of a coolant inlet temperature of 450°K (350F), a coolant outlet temperature of 283°K (50F), a hydrogen inlet temperature of 33°K (-400F) and a hydrogen outlet temperature of 422°K (300F).

Pump Sizing

The size, weight, and power requirements for the pump needed to circulate coolant through the airframe depend upon the flow rate and system pressure drop. Reference 3 describes the method of sizing pumps and presents the appropriate equations along with representative pump sizing charts. Figures 64 and 65 were extracted from that reference. Although they are applicable strictly to glycol/water the similarity of densities for coolants of interest permit the use of the impeller diameter and weight charts to obtain first approximations of pump characteristics. The error introduced will be relatively small unless the densities vary substantially from that of glycol/water. Furthermore, since the weight of the pump is very small compared to the cooling system weight, efforts to refine pump sizing characteristics for various candidate coolants were not warranted.

Failure Mode and Effect Analysis

In the design of operational hardware, careful attention must be given to reliability. One tool required by NASA Document NHB 5300.4, "Reliability Program Provisions for Aeronautical and Space System Contractors," is a failure mode and effect analysis normally prepared for design reviews with an updating provided at about the time when qualification testing is completed. Although there was no requirement for the implementation of this approach, the lack of experience with the cooled airframe concept suggested that significant benefits might be derived from the application of this methodology at an early point in the development cycle. Therefore, a failure mode and effect analysis was prepared on the basis of the representative cooling system design presented in Figure 38.

The FMEA was used as a design tool to identify possible failure modes, failure causes, effects upon hardware and mission capability, and controls which can be exercised to preclude these failure modes. While many of the potential problems can be avoided through the routine application of good design, manufacturing, and quality control practices, it is considered desirable to adopt a more formal procedure for a new type of structural system. The formal nature of the FMEA enhances the visibility of potential problems and the need for their early consideration.

The analysis must be considered as a first step and a guide in assuring implementation of the design and development actions necessary to produce hardware of maximum reliability. Emphasis was placed on the system and major component level since the components were not designed as yet. This is in contrast to the normally conducted FMEA analyses which are performed on finalized sys-

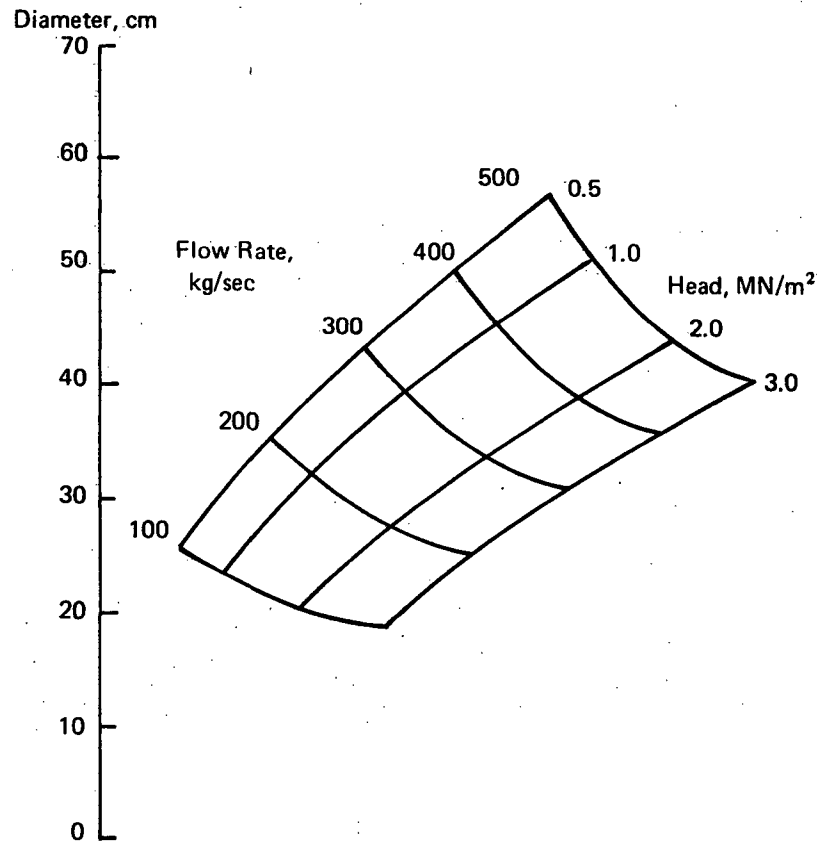


Figure 64a. Impeller Diameter as a Function
of Flow Rate and Head Requirements,
 $N_s = 2000$, $\eta = 85\%$

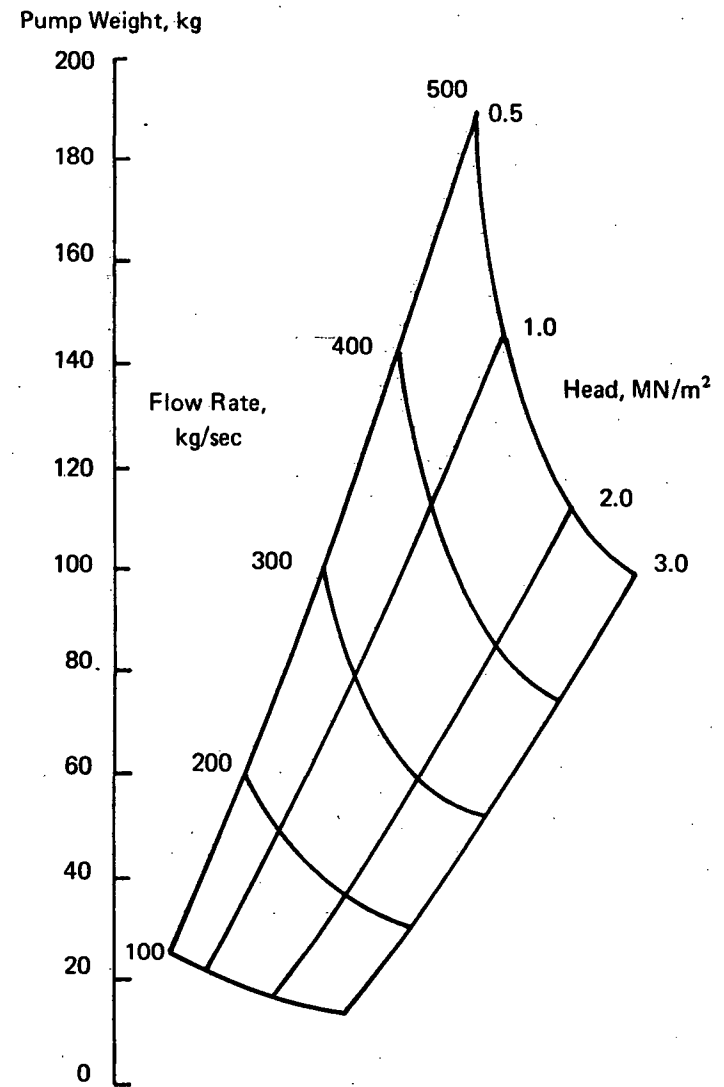


Figure 65a. Pump Weight as a Function
of Flow Rate and Head Requirements
 $N_s = 2000$, $\eta = 85\%$

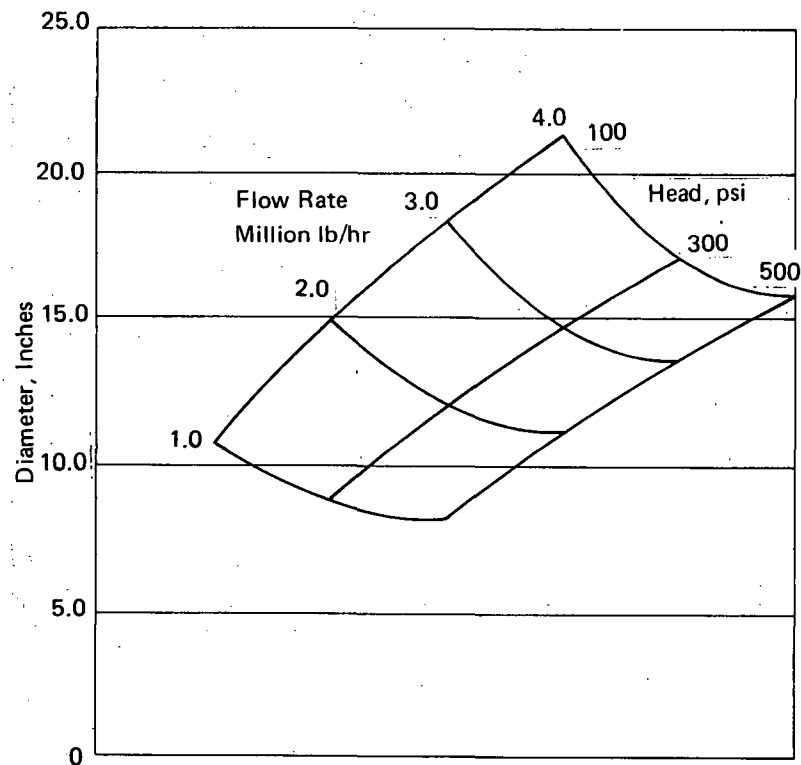


Figure 64b. Impeller Diameter as a Function of Flow Rate and Head Requirements,
 $N_s = 2000$, $\eta = 85\%$

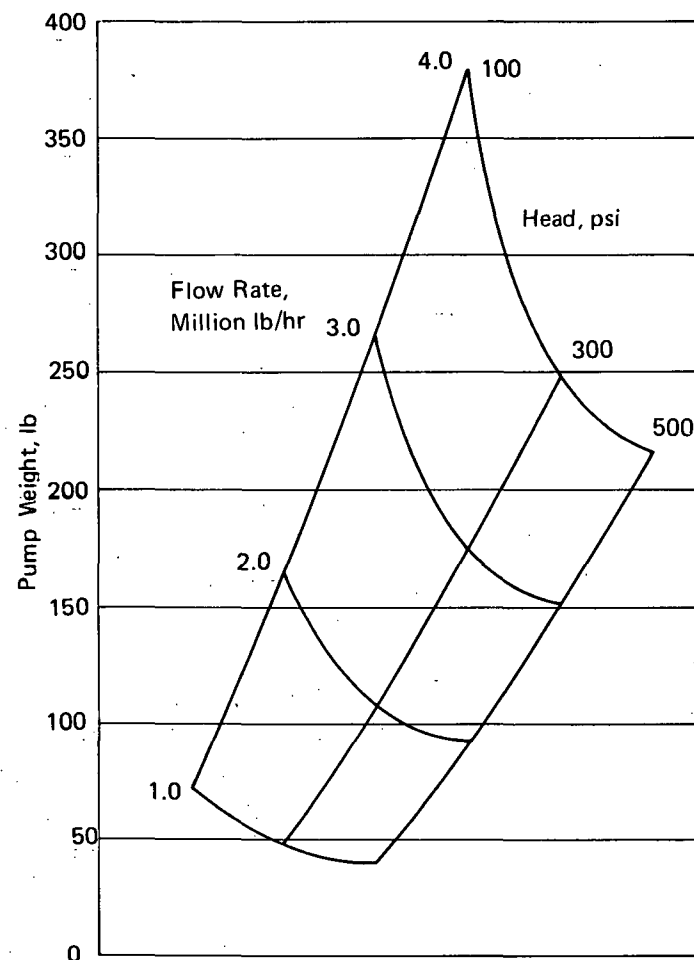


Figure 65b. Pump Weight as a Function of Flow Rate and Head Requirements
 $N_s = 2000$, $\eta = 85\%$

tem and component designs. The results of the initial analysis are presently in Tables XX through XXVI. Some important design considerations are clearly identified.

In reviewing the failure causes, it will be noted that no attempt has been made to differentiate between the various environmental conditions which act upon individual components, such as vibration levels, thermal cycling, repeated loads, pressure levels, and pressure cycling, as well as chemical compatibility considerations. Failures due to the operationally induced loadings cannot be covered in detail until specific designs and sizes of design details are defined. As detailed designs become available for components, failure mode and effect analyses can consider each design feature and detail so that adequate failure control can be exercised. The applicability of the recommended controls is generally demonstrated during experimental demonstrations of the integrity of the components and the system of interest both during developmental and qualification phases.

Fault Hazard Analysis

A qualitative fault hazard analysis was conducted for the major components of the convective cooling system. Although it closely parallels the failure mode and effect analysis, its purpose was to identify potentially hazardous system failure modes in order to provide design insight to minimize undesirable conditions resulting from cooling system component malfunctions. In many instances the degree of hazard varied depending upon the magnitude of failure. For example, a small unchecked leak may be of little consequence as long as there is coolant in the expansion reservoir whereas a large leak could result in the loss of the aircraft.

The two most hazardous categories were hydrogen leakage and coolant flow interruption. The problems in the first category must be resolved for any hydrogen fueled vehicle; the use of a cooled structure simply introduces a few additional components whose characteristics must be considered. Within the second category flow leakage and flow obstructions are important. The former is minimized by careful design, quality control, and maintenance. The second category can be resolved by attention in material selection to minimize corrosion and degradation products, careful design, coolant filtration, and maintenance. System redundancy in the form of a backup cooling system, or another alternative that temporarily controls structural temperature, provides a means of enhancing system safety with respect to coolant flow disruptions.

TABLE XX
INITIAL FAILURE MODE AND EFFECT ANALYSIS, COOLED SKIN PANEL

| FAILURE MODE | FAILURE CAUSE | FAILURE EFFECT | CONTROL |
|----------------------------|--|--|---|
| 1. Leak, External | 1. A leak in the fluid passages of the cooled skin panel could be induced by: a. Corrosion b. Cyclic stresses c. Defective material d. Incorrect drilling of fastener holes. | 1. Depletion of reserve coolant endangering the overall effectiveness of the cooling system. A hot spot may develop downstream of the leak in the vicinity of the affected tube. With a leak as a nucleation site, a panel crack may propagate to cause further degradation. | 1. a. Proper materials can be selected for both coolant and panel to minimize corrosion. Coolant may contain a corrosion inhibitor. Design can include provision for coating the inside of passages and/or cathodic protection. b. Panel design can include features which reduce the likelihood of stress risers, such as bonded stiffeners, and doublers at edges where fasteners are required, and crack stoppers to limit damage. c. Panels can be thoroughly inspected and proof pressure tested prior to acceptance. d. Templates can be used for drilling operations. Hole and passage locations can be printed on outside of panels. |
| 2. Crimped coolant passage | 2. Accidental damage or operationally stress induced | 2. Reduced or stopped flow will allow overheating on either side of the affected tube. Crimp could act as stress riser for crack initiation in the panel. | 2. Care must be taken during fabrication to preclude crimped passage in the final product. Panel stiffeners can be provided to guard against flight stressed induced crimping. Skin gages could be restricted to thicknesses greater than minimum allowed by present specification to minimize damage effect. |
| 3. Cracked panel | 3. Operationally stress induced | 3. a. For cracks parallel to fluid passages, panel manifolds will be endangered. A manifold crack may allow coolant depletion causing degraded system performance. If enough coolant is lost, the system may become non-functional b. For cracks normal to fluid passages, the coolant passages may be endangered. The panel may develop a hot area downstream of the cracked tube. If enough coolant is lost, the system will become non-functional. | 3. a. Panel design can employ laminated skins and can specify crack arresters at critical locations. The panels can be designed to withstand the worst anticipated stress level and be tested to demonstrate this capability. Redundant flow passages can be provided. b. Similar to 3.a. |
| 4. Peeling, internal leaks | 4. Stress riser at passage junctions where upper and lower panel skins are joined, coupled with coolant pressure level | 4. Panel may develop a structural bubble. Coolant mass velocity may decrease locally causing a reduction in heat transfer coefficient. Aerodynamic heating will increase at the protruding panel deformation into the air stream. These conditions may cause a local hot | 4. Tube form design within the panels can emphasize the minimization of stress risers. Joining techniques of high strength can be used. Proof pressure testing will verify structural integrity. |

TABLE XX (CONT)

| FAILURE MODE | FAILURE CAUSE | FAILURE EFFECT | CONTROL |
|------------------------------|---|--|---|
| 4. Continued | | spot in the affected area of the panel. A severe structural bubble may burst causing coolant loss with further effects associated with leaks. Or, the peeling action may reach an exposed edge thereby permitting coolant leakage. | |
| 5. Buckling | 5. Operational stress induced | 5. Design margin degradation which could cause coolant panel cracking, coolant passage crimping or leak initiation and the failure effects associated with these conditions. | 5. Panel stiffeners can be provided to guard against stress induced buckling. The panels can be tested to demonstrate structural integrity under the worst anticipated loads. |
| 6. Clogging | 6. Contamination accumulation | 6. Panel may develop hot region on either side of the affected coolant passage. This localized overheating may contribute to secondary effects deleterious to the mission. | 6. Care can be exercised to avoid the possibility of contaminant generation due to coolant panel material interaction. Filters can be specified upstream of the coolant panels. Coolant passages could be located somewhat closer than necessary to minimize the chance of destructive secondary effects. |
| 7. Unequal flow distribution | 7. Unequal passage and/or header sizes, poor dimensional control. | 7. Adverse temperature gradients and temperature levels may be established. Temperature capability of material may be exceeded with corresponding excessive deformation. | 7. Strict quality control procedures can be followed. The detailed design and close tolerance tools can assure a constant hydraulic impedance throughout the flow field. System coolant flow can be increased above the minimum required so that all passages receive sufficient or excessive coolant. Provision can be made for adjusting, or fine tuning, coolant flow in each passage of the skin panel. |
| 8. Burn through | 8. Encountered high aerodynamic heating due to bulging into air-flow stream | 8. Opening generated causing loss of coolant and attendant system degradation. | 8. Quality control must be rigid for purchased materials and fabricated parts. |

TABLE XXI
INITIAL FAILURE MODE AND EFFECT ANALYSIS, PANEL COOLANT FITTINGS AND LINES

| FAILURE MODE | FAILURE CAUSE | FAILURE EFFECT | CONTROL |
|---|--|--|--|
| 1. Leakage of fittings or connectors | 1. Defective material, cracks, misalignment and inadequate mating surface finishes, operational stresses. | 1. Depletion of coolant fluid reserve. If enough coolant is lost, the system may become nonfunctional. | 1. Fitting designs can emphasize leak tight objective and redundancy. Quality control can be rigidly enforced. Mechanical and welded joints can be leak tested at system installation. Preference can be given to the use of metallurgical joints. Special emphasis can be given to panel connectors where hose and tubing inertial loads may cause local bending. |
| 2. Leaks of flexible hoses, tubing, supply and return lines | 2. Defective material chemical degradation, abrasion, vibration induced torque relaxation. | 2. Same as 1 above. | 2. Quality control can be rigidly enforced. Coolant compatibility with hoses and tubing can be demonstrated. Leak and proof pressure tests can be specified. Hoses with braided covering can be specified as well as lock wiring of connectors. |
| 3. Rupture of flexible hoses, tubing, supply and return lines | 3. Inability of hose, tubing or line to withstand pressure or excessive unsupported length culminating in fatigue failure. | 3. Same as 1 above. | 3. Design margin can be specified in requirement for tubing wall thickness. Hoses with braided covering can be specified. Cooling lines should be adequately supported to minimize induced bending stresses, to avoid resonant vibrations, and to allow for thermal expansion and contraction. Proof pressure tests can be specified. |

TABLE XXII
INITIAL FAILURE MODE AND EFFECT ANALYSIS, PANEL COOLANT PUMP

| FAILURE MODE | FAILURE CAUSE | FAILURE EFFECT | CONTROL |
|--|---|--|---|
| 1. Instability | 1. Loss of an excessive amount of coolant through leakage or loss of expansion tank pressurant. | 1. Loss of net positive suction pressure may be experienced. Cavitation within the pump may be experienced which may cause pump performance to be erratic. Pump may attain speeds inconsistent with safe operation. The cooling system will become inoperative when flow ceases. | 1. System leak suppression must be a prime design objective. Adequate net positive suction pressure can be provided and/or pump can be designed for low net positive suction head with flat characteristics of wide range of net positive suction head. |
| 2. External seal leak | 2. Ineffective seal/shaft design. | 2. Loss of coolant. If severe, this failure mode could effect system performance with regard to conditions associated with loss of coolant reservoir content. | 2. The effectiveness of the seal/shaft design can be demonstrated under the worst anticipated flight conditions. Redundant seals can be specified. |
| 3. Overheating of coolant side of pump | 3. Thermal short circuits from the turbine drive side of the pump to coolant chambers. | 3. An increase of vapor pressure may result, thus losing some margin in net positive suction pressure. Cavitation may result both upstream and downstream of the impeller with a resultant loss of pump performance and system effectiveness. | 3. The pump can be designed with adequate thermal resistance between the turbine drive and the coolant chambers. A test demonstration can be required to insure pump performance under worst anticipated thermal load conditions. |
| 4. Overheating of pump | 4. Loss of lubricant, imperfect bearings. | 4. Excessive thermal expansion may cause seizing of bearings with subsequent loss of pump performance. | 4. Pump can be designed to assure lubricant will be available at all times. Quality control must rigidly maintain. |
| 5. Internal leakage | 5. Seal leak from gas turbine chamber to coolant chamber. | 5. Loss of system effectiveness when gas is ingested into the coolant loop. May eventually lose pump capability if a large gas pocket enters pump inlet. | 5. Redundant seals with a vent between seals can be specified. |
| 6. Casing leak, coolant side | 6. Porous material, stress or wear induced defects. | 6. Loss of coolant with resultant degradation of cooling capability. If enough coolant is lost, the system may become nonfunctional. | 6. Chamber walls can be leak tested and the total pump can be life tested under severe operating conditions to demonstrate survivability. A defective pump can be isolated from the coolant system through valving if another pump is provided to sustain coolant flow. |
| 7. Leaking flanges | 7. Defective flange faces and seal surfaces, improper seals. | 7. Degraded system performance caused by coolant loss. If enough coolant is lost, system may become nonfunctional. | 7. For flange and sealing surfaces, quality control can be assured through a thorough inspection. Redundant seals can be specified to assure minimal leakage overboard. A defective pump can be isolated from the coolant system through valving if another is available. |

TABLE XXIII
INITIAL FAILURE MODE AND EFFECT ANALYSIS, PANEL COOLANT LINE VALVES

| FAILURE MODE | FAILURE CAUSE | FAILURE EFFECT | CONTROL |
|--------------------------------|--|--|---|
| 1. Failure to open | 1. Inoperative solenoid, seized mechanical linkage, or plugged sensing passages. | 1. Total coolant system nonfunctional. | 1. The pump associated with the failed valve can be bypassed and a redundant pump can be utilized. The redundant pump can be serviced by its own valving. Dual solenoids can be utilized. Adequate surface finish and part tolerance can be specified and inspected. Special coatings for internal surfaces and slightly tapered internal fittings can be specified in design. The system can contain filters to preclude the possibility of clogging pressure sensor passages. |
| 2. Failure to open fully | 2. Seized mechanical linkage | 2. Degraded system performance during peak load periods. | 2. Adequate surface finish and part tolerances can be specified and inspected. Life testing can be performed to demonstrate capability. Special coatings for internal fittings can be specified in design. |
| 3. Failure to close | 3. Inoperative solenoid, seized mechanical linkage, or plugged pressure sensing passages. | 3. Inability to isolate nonfunctional pump. For failure mode of external leakage from pump, loss of coolant with subsequent deterioration of coolant system. | 3. A high margin of activation load to internal frictional resistance can be specified and demonstrated to preclude this failure mode. Dual solenoids can be utilized. Adequate surface finish and part tolerance can be specified and inspected. Special coatings for internal surfaces and slightly tapered internal fittings can be specified in design. The system can contain filters to preclude the possibility of clogging pressure sensor passages. |
| 4. Failure to close completely | 4. Inability of spring force to completely overcome frictional resistance of moving parts. | 4. Similar but less serious than Failure Effect 3. | 4. A high margin of actuation load to internal frictional resistance can be specified and demonstrated to preclude this failure mode. Special coatings for internal surfaces and slightly tapered internal fittings can be specified in design. |

TABLE XXIV
INITIAL FAILURE MODE AND EFFECT ANALYSIS, EXPANSION TANK

| FAILURE MODE | FAILURE CAUSE | FAILURE EFFECT | CONTROL |
|---|---|--|--|
| 1. Outer shell leak | 1. Defective material and/or inadequate joints. Stresses induced by vibration, repeated cycling and/or system pressurization. | 1. Loss of pressure head up-stream of pump. Decreased net positive suction pressure creating a condition which may cause cavitation within the pump. | 1. Metallurgical joints can be eliminated or can be carefully inspected to detect voids and/or cracks. Acceptance tests can include leak checks and proof pressure tests. Pressure can be monitored in flight for alert below a prescribed minimum value. |
| 2. Bladder leak, internal | 2. Excessive abrasion between bladder and outer shell or defective material. | 2. Gas may be ingested into the panel coolant loop thus affecting overall system thermal performance. Ingested gas may also create pump cavitation problems as a long term effect. | 2. Adequate clearance can be provided between the bladder and outer shell. Also a non-abrasive coating can be applied to the inside surface of the outer shell. The tank can be spatially oriented to minimize the forces potentially destructive to the bladder. Acceptance tests can include leak checks and proof pressure tests. |
| 3. Bladder movement restricted or impossible. | 3. Interference between bladder and outer shell. | 3. Possible loss of pressure head or cavitation of pump. | 3. Adequate clearance can be provided between bladder and outer shell. Also low friction coating can be applied to the inside surface of the outer shell. |
| 4. Seal leak | 4. Improper seal or improper torque | 4. Loss of gas and/or panel coolant resulting in possible loss of pressure head or cavitation of pump. | 4. Application of strict Quality Control to monitor assembly and installation instructions. Adequate torquing procedures. |

TABLE XXV
INITIAL FAILURE MODE AND EFFECT ANALYSIS, HEAT EXCHANGER

| FAILURE MODE | FAILURE CAUSE | FAILURE EFFECT | CONTROL |
|---------------------------------------|--|--|---|
| 1. Loss of heat exchanger performance | <p>1. a. Freezing of panel coolant fluid at exit region of heat exchanger.</p> <p>b. Clogging of fluid passages as a result of installed and/or generated particulate impurities.</p> <p>c. Non-homogeneous fin density</p> <p>d. Reverse installation</p> | <p>1. a. Inability of the cooling system to accommodate the heat load; excessive pressure drop and maldistribution of fluid flow resulting in unpredictable temperatures and thermal stresses; also potentially destructive stresses will be experienced as constrained panel coolant fluid expands during phase change. Total loss of heat exchanger performance would dictate a mission abort condition since the cooling system would be rendered useless.</p> <p>b. Ineffective heat exchanger performance due to variant hydraulic impedance in region of affected passages. Undesirable thermal stress in areas of restricted flow. Stagnant panel coolant fluid could freeze, further effecting cooling system performance.</p> <p>c. Maldistribution of heat transfer fluids aggravates nonuniform temperature distribution transverse to flow direction. This condition creates unpredictable heat exchanger performance.</p> <p>d. Hydrogen and/or panel coolant fluid might be introduced in opposition to design flow direction which will affect exchanger performance.</p> | <p>1. a. Heat transfer resistance can be designed into the parting sheets at the panel coolant fluid exit region of the heat exchanger. Temperature sensors can be included at both the entrance and exit of the coolant fluid side of the heat exchanger. The entrance sensor can indicate the heat load being experienced, while the exit sensor can warn against incipient freezing. This information can allow hydrogen flow modulation to preclude freezing while maintaining system effectiveness. A check valve at the hydrogen exit side of the heat exchange can be used to isolate the heat exchanger from the hydrogen system during periods of non-usage.</p> <p>b. Care can be taken during component manufacture and installation to preclude the inclusion of contaminants into the system. A corrosion inhibitor can be used in the coolant fluid which will retard generation of corrosion products. Care can be taken in the selection of an inhibitor to assure system and material compatibility. A filter and/or a cold trap can be considered as part of system analysis to maintain system cleanliness. Additionally, the coolant can be sampled periodically and checked for contamination levels, chemical composition and acidity. On-board monitoring can also be used.</p> <p>c. Design, fabrication, inspection and test can deliver, within the operating range, constant hydraulic impedance per passage. This most likely can be accomplished through the installation of manifold diffusers and in-process production controls.</p> <p>d. Manifold flanges can be designed to preclude the possibility of reverse installation; by using a different size for each connection point.</p> |

TABLE XXV (CONT)

| FAILURE MODE | FAILURE CAUSE | FAILURE EFFECT | CONTROL |
|--------------------------------|--|--|---|
| 2. Parting sheet internal leak | 2. Defective material and/or improperly tested | <p>2. a. During normal operation a higher pressure will exist on the hydrogen side than on the panel coolant fluid side of the heat exchanger. Hydrogen leaking into the coolant loop may cause ice formation and increase coolant system pressure and/or volume. This condition will tend to degrade cooling system performance.</p> <p>b. During periods when hydrogen is bypassed around the heat exchanger the pressure on the coolant fluid side may be higher than the hydrogen side. Coolant fluid which leaks into the hydrogen side will freeze when hydrogen enters. Freezing may cause structural damage to the heat exchanger and particulate ice will contaminate the hydrogen system.</p> <p>c. During initial fluid charging and maintenance performance the parting sheet may be subjected to high pressure on the panel coolant side. Same effect as 2.b.</p> | 2. Heat exchanger can be vacuum dried before leak testing with dry helium or nitrogen. Proof pressure testing on both sides of the heat exchanger can assure safe operation at the specified operating pressures. During proof pressure testing, the heat exchanger can be monitored with acoustic recording equipment to detect any internal fractures or loss of bond between fins and plates. The heat exchanger can be subjected to maximum anticipated thermal stress before leak checking. Incorporate bypass valve control sensor to detect the condition so operational status of engine can be maintained in the event of heat exchanger freeze-out. |
| 3. Parting sheet bulge | 3. Defective bond at fin-to-plate joints | 3. See Failure Effects 1.b. and 1.c. Also sheet material flow will cause localized sheet thinning which will reduce design margin. Unaffected fin to plate joints at the periphery of the bulge will be acted upon by peel stresses which may further increase the size of the deformation. Rupture may result - see Failure Effect 2.a. | 3. During fabrication, manufacturing processes and inspection techniques can be employed that can provide effective material joining prior to heat exchanger assembly. During proof pressure testing, the heat exchanger can be monitored with acoustic recording equipment to detect any loss of bond between fin and plate. The heat exchanger can also be subjected to maximum anticipated thermal stress before pressure testing. |

TABLE XXV (CONT)

| FAILURE MODE | FAILURE CAUSE | FAILURE EFFECT | CONTROL |
|---|--|--|--|
| 4. Hydrogen manifold leak - external | 4. Defective manifold joints. | 4. External leakage of hydrogen will create a fire and/or explosion safety hazard. Also, loss of fuel will impact aircraft propulsion capability. Impinging cryogen from a high pressure leak could cause damage to adjacent components. | 4. Manifolds can be designed as pressure vessels with care taken to avoid stress risers. Material of high fracture toughness and slow crack growth rate can be used providing they meet other requirements. Design can also consider careful nondestructive inspection of all joints during fabrication and in-process inspection to insure compliance with manufacturing process instructions. Proof pressure tests can demonstrate structural integrity and leak testing can assure a leak tight assembly. Additionally the heat exchanger could be subjected to maximum anticipated thermal stresses before pressure testing. Continuous on-board purging and monitoring of hydrogen areas can assure minimum risk due to formation of gas pockets. |
| 5. Panel coolant fluid manifold leak-external | 5. Defective manifold joints. | 5. Degraded system cooling capacity. If enough coolant is lost, the accumulator reservoir will be depleted making it impossible to cool the aircraft effectively. | 5. See Control 4 |
| 6. Leaks at manifold flanges | 6. Improper alignment, cracked flange or defective seals. Inadequate or non-existent expansion/contraction features at heat exchanger to-system installation, different coefficients of expansion of mating flanges. | 6. See Failure Effects 4 and 5. | 6. Heat exchanger installation procedure can document proper alignment and bolt torquing procedure. Seals and flange faces can be inspected for any irregularities prior to installation. System design can consider compensation for differential expansion as well as assure the compatibility of mating parts from the stand point of coefficient of expansion. Post installation leak check can be required. |
| 7. External hydrogen leak | 7. Ineffective sheet to spacer joint. | 7. See Failure Effect 4. | 7. Heat exchanger can be leak and proof pressure tested. The subject joints are visually accessible and easily leak checked. Heat exchanger can be subjected to maximum anticipated thermal stress before pressure testing. |
| 8. External panel coolant fluid leak | 8. Ineffective sheet to spacer joint | 8. See Failure Effect 5. | 8. See Control 7 |

TABLE XXV (CONT)

| FAILURE MODE | FAILURE CAUSE | FAILURE EFFECT | CONTROL |
|---|---------------------------------------|---|--|
| 9. Panel coolant fluid parting sheet to spacer leak in hydrogen manifold | 9. Ineffective sheet to spacer joint | 9. Particulate ice will contaminate the hydrogen loop with more massive pieces of ice jeopardizing the structural integrity of the heat exchanger. Ultimate effect would be to stall hydrogen flow, thus losing the function of the heat exchanger. | 9. Panel coolant fluid sheet to spacer joints can be leak checked before manifolds are installed. A proof pressure check can also be specified. Leak and proof pressure checks can also be required after heat exchanger is subjected to maximum anticipated thermal stress. |
| 10. Hydrogen parting sheet to spacer leak into panel coolant fluid manifold | 10. Ineffective sheet to spacer joint | 10. Hydrogen will enter violently into the panel coolant fluid tank with potential further structural damage to the ice formation will occur causing a decrease in heat exchanger efficiency. | 10. Hydrogen parting sheet to spacer joints can be leak checked before manifolds are installed. A proof pressure check can also be specified before installing manifolds. |

TABLE XXVI
INITIAL FAILURE MODE AND EFFECT ANALYSIS, HYDROGEN CONTROL VALVES

| FAILURE MODE | FAILURE CAUSE | FAILURE EFFECT | CONTROL |
|---|---|---|--|
| 1. Failure of heat exchanger supply valve to open | 1. Binding of poppet, malfunction in operating mechanism, or failure of feed back control system. | 1. This valve will operate in conjunction with the hydrogen by-pass line valve. Dependent on cooling system demands for more or less heat sink, these valves will control hydrogen flow through the heat exchanger. During periods of high cooling system demands the hydrogen control valve for the heat exchanger circuit will tend to open to allow more hydrogen through the heat exchanger and the parallel hydrogen by-pass line valve will tend to close to divert more hydrogen as required through the heat exchanger. During flight the quantity of hydrogen that must flow through the heat exchanger varies from 0 to 100%. If the hydrogen heat exchanger valve fails to open, the by-pass valve would be instructed by the feed back control circuit to divert more hydrogen to the heat exchanger by tending to close. This could cut off all fuel to the aircraft propulsion system. This failure mode would be most likely to occur during the critical ascent phase of the flight and may create a hazardous condition. | 1. Design and qualification test criteria for this valve and associated control system can stress maximum reliability including consideration of redundant and/or overriding controls and circuits and in corporation of fail-safe devices. Additionally, quality inspection and test during fabrication and assembly and preflight checks can provide confidence in system flight operation. Additional design consideration can be given to a single three-way flow control valve in place of the two hydrogen control valves. The single valve design would provide a simple flow diversion feature which would be responsive to cooling system demands, with a positive shut-off to the heat exchanger. |
| 2. Failure of heat exchanger supply valve to open fully | 2. See Failure Cause 1 | 2. The effect of this failure mode will be dependent on the extent of valve opening and the sequence of flight. The failure effect could be quite hazardous or merely require a low performance flight abort mode of operation. During landing approaches or any other period of low cooling system demand if locked in a partially open position (will not close) hydrogen could continue to flow through the heat exchanger providing a larger heat sink than desired. Freezing in the panel coolant fluid side could result causing damage to the heat exchanger and rendering the cooling system inoperative. | 2. See Control 1. |

TABLE XXVI (CONT)

| FAILURE MODE | FAILURE CAUSE | FAILURE EFFECT | CONTROL |
|--|---|---|-------------------|
| 3. Failure of heat exchanger supply valve to close, locked full open | 3. See Failure Cause 1. | 3. This situation would not be hazardous except during landing approach or other flight mode requiring low speeds and low cooling system demands. A greater heat sink would be available than required and freezing of the panel coolant fluid could result. This in turn could cause structural damage to the heat exchanger, with the additional possibility of ruptures which could allow internal or external leakage of hydrogen. See FMEA for heat exchanger. | 3. See Control 1. |
| 4. Closing of heat exchanger supply valve during flight | 4. Broken actuation linkage or malfunction in feedback system | 4. Cooling system nonfunctional condition. | 4. See Control 1. |
| 5. Failure of by-pass valve to open | 5. See Failure Cause 1. | 5. Failure to open for the hydrogen by-pass control valve would normally only occur on the ground. The hydrogen heat exchanger control valve would also be closed and fuel would not be provided to the aircraft propulsion system. | 5. See Control 1. |
| 6. Failure of by-pass valve to open fully | 6. See Failure Cause 1. | 6. Failure of the hydrogen by-pass control valve to open fully could affect propulsion system performance during take-off and ascent (prior to opening of hydrogen heat exchanger control valve). Less than maximum available power during this flight mode could be critical. | 6. See Control 1. |
| 7. Failure of by-pass valve to partially close, full open | 7. See Failure Cause 1. | 7. Insufficient heat sink would be available for peak ascent or cruise flight mode. Aircraft would have to operate at speeds commensurate with available heat sink. | 7. See Control 1. |

TABLE XXVI (CONT)

| FAILURE MODE | FAILURE CAUSE | FAILURE EFFECT | CONTROL |
|---|--|---|--|
| 8. Closing of by-pass valve during flight | 8. See Failure Cause 4. | 8. Continued full performance propulsion system will be dependent on impedance of heat exchanger. If impedance is high performance will be low. During landing approach more heat sink than required will be available causing freezing of panel coolant fluid with results as described in Failure Effect 3. | 8. See Control 1. Additionally design considerations can be given to minimizing heat exchanger hydrogen impedance. |
| 9. Hydrogen Leaks | 9 Valve packing, flange connections, defective seals and valve materials. Cryogenic operation and cycling of valves may facilitate breakdown of materials. | 9. Hydrogen leakage could create pockets of highly combustible gas, additionally, impingement of the cryogen fluid could effect operation of other near-by components and controls. | 9. Design consideration can be given to choosing materials which will withstand worst case conditions of operation with cryogens. Qualification testing can be conducted under overstressed conditions to verify integrity of design. Inspections of materials, fabrication, assembly, and test will assure product quality. |

Reliability

In the broad sense system reliability is concerned with two aspects, safety and maintainability; the former is of paramount importance but the latter has a profound impact on profitability. A primary technique for enhancing reliability is to utilize increasing levels of redundancy until total redundancy is achieved. As a means of comparing the reliability to be achieved in this manner analyses were conducted for a representative aircraft systems as shown in Figure 38 for the hypersonic transport and in Figure 51 for the hypersonic research airplane. The reliability weight characteristics of non-redundant and completely redundant systems will be discussed as part of "SYSTEM SUMMARIES". In this present discussion the primary purposes are to define the reliabilities of the nonredundant and redundant approaches and to identify those components which have a major influence on vehicle reliability as influenced by vehicle size. The components in the analyses are as follows:

- (1) Cooled skin panels
- (2) Coolant to liquid hydrogen heat exchanger
- (3) Coolant expansion tank
- (4) Coolant control valves
- (5) Hydrogen control valves
- (6) Coolant centrifugal pumps
- (7) Marman clamps
- (8) Connectors to the cooled panel
- (9) Braided flexible hoses
- (10) Machined tee fitting
- (11) Mechanical connections
- (12) Coolant supply and return lines
- (13) Welded connections

It should be noted that the reliability analyses for the cooling systems were performed using failure rate data for components used in other types of fluid flow systems at pressures generally higher than that of the cooled airframe structure. While the failure rates obtained from References 44 to 47 represent actual experience, the lower operating pressure of a cooled airframe structure is likely to enhance reliability.

Hypersonic Transport. - The baseline system for the hypersonic transport was assumed to be made from aluminum alloy and to use ethylene glycol/water coolant. All of the joints in the coolant distribution lines were assumed to be welded or brazed except for two mechanical joints in the fuselage supply and return lines. Mechanical connections were assumed between the distribution lines and the connections to the cooled panel. The mission duration was taken as two hours and the design life has 15,000 flights. The system operating pressure was assumed to be 2.0 MN/m^2 (300 psi) at the pump outlet and 0.4 MN/m^2 (50 psi) at the pump inlet.

Reliability prediction was performed first for a nonredundant system containing only redundant pumps and then for a totally redundant system comprised of two nonredundant systems in parallel. Recognizing the questionable nature of reliability prediction in the early design phases of a non-state-of-the-art concept, a qualitative reliability assessment was also performed. The results of the qualitative phase of the reliability analysis are in the form of specific comments directed at the systems components. The comments relate desirable design features which, if utilized, could enhance ultimate system reliability.

The reliability model for the nonredundant cooling system is shown in Figure 66. All components are in series with a parallel pump arrangement. The failure of any one of the depicted components, with the exception of the loss of one pump, constitutes a system failure. It is recognized that this is a conservative assumption since many of the anticipated failure modes may result in only degraded performance rather than complete system failure. Nevertheless, it should be recognized that for the purpose of this analysis, any type of component failure mode, regardless of severity, was assumed equivalent to a system failure. With the redundant arrangement a failure that renders one loop useless does not incapacitate the entire system; the cooling function is assumed by the undamaged loop. A necessary assumption in redundancy analysis is that the environment causing failure of the primary system does not simultaneously cause failure of the standby system. System design must be directed at attaining a configuration capable of satisfying the assumption.

Reliability was predicted for the nonredundant system by subtracting the summation of failure rates for components in series. The failure rate of the redundant pump configuration was first computed by squaring the single failure rate of a pump before adding its contribution to the total component failure rate summation. This was necessary since the redundant pumps are in series with the other components. Failure rate summation is mathematically justified when component failure rates are low (1.0×10^{-4} events/unit time) and the failure density function is exponential. Table XXVII summarizes the information found most applicable. The predicted failure rate for the nonredundant system is $6,182.08 \times 10^{-6}$ failures per mission. This yields a predicted system reliability of 0.99382 per mission or approximately seven failures per 1000 flights. The reliability prediction for a totally redundant system is 0.99996 or approximately four failures per 100,000 flights.

As seen in Table XXVII, the greatest contributors to predicted mission failure rates are the skin panels and the flexible hoses. However, the source data for the panel failure rate specified "pressurized panels" and it is not certain if the data is truly applicable to the aircraft skin panels with integral coolant passages. This requires further examination. The high failure rate associated with the use of flexible hoses to connect skin panels to the return and supply lines might be reduced by substituting formed metal lines with loops to accommodate differential expansion. Furthermore, the high failure rates assigned to these two items include incidents which would not necessarily result in a catastrophic system failure. About two-thirds of the failures are due to leakage which can be detected as a change of liquid level in the expansion tank. By using an expansion tank of larger capacity than necessary, it is possible to provide make-up coolant to offset minor leakage. Suitable design of the expansion tank can enhance the detectability of small changes in coolant volume. This would permit a mission abort before a significant risk of aircraft loss could develop. Of the 45 detailed failure modes identified in the Failure Mode and Effects Analysis the risk can be reduced by careful attention to design in about 30 of the cases while specialized quality assurance procedures may reduce risk in about 25 instances; some failure modes are significantly influenced by both the design and the quality assurance efforts. The design of the system was reviewed in light of the reliability analysis results and lead to the following observation:

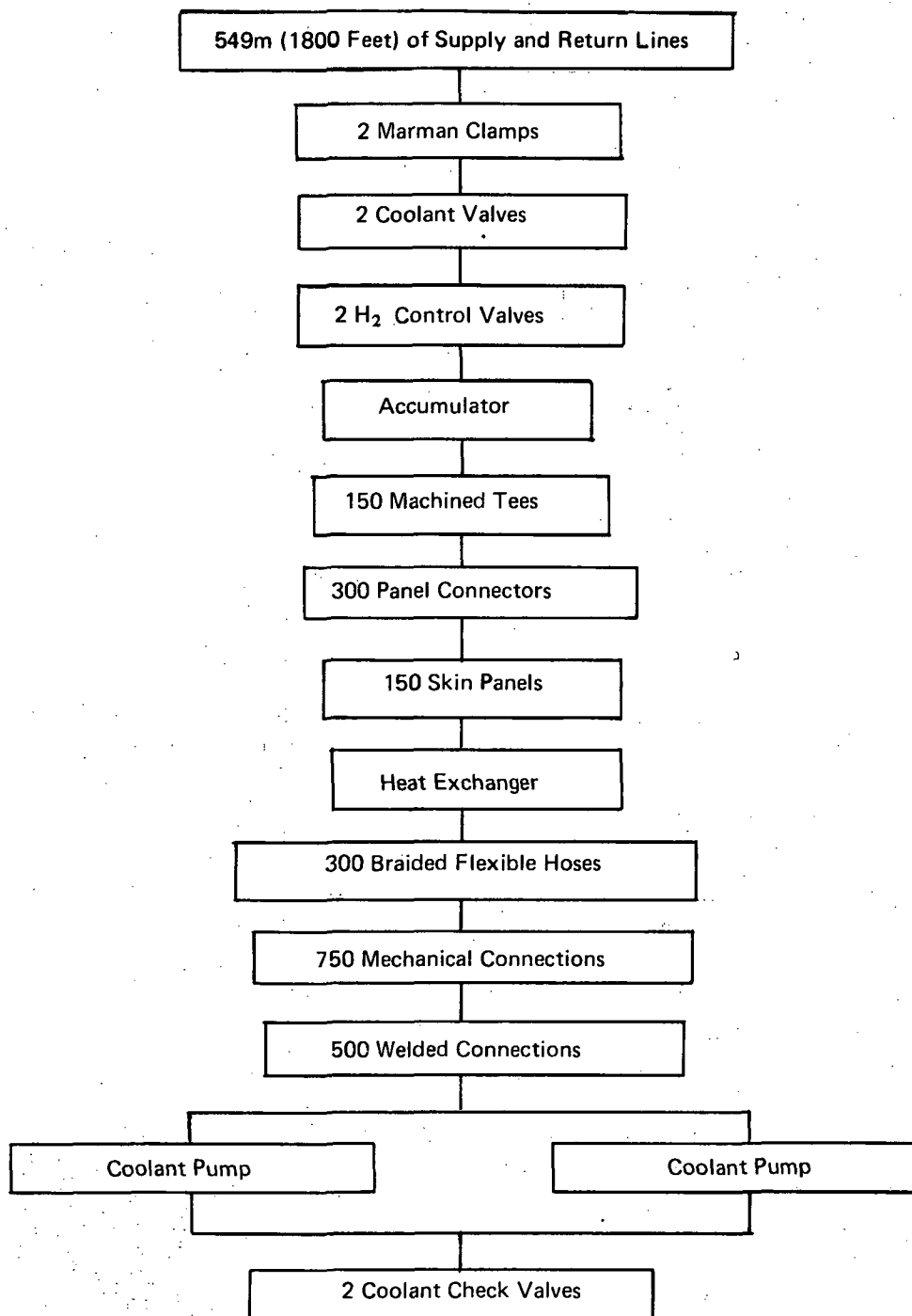


Figure 66. Nonredundant Cooling System Reliability Schematic

TABLE XXVII
SUMMARY OF NONREDUNDANT COOLING SYSTEM
FAILURE RATES FOR A HYPERSONIC TRANSPORT

| Component | Number in System | Failure Rate (Failures/hr) x 10 ⁻⁶ | Failure Rate for Total Number of Each Component (Failures/hr) x 10 ⁻⁶ | Failure Rate Per Mission x 10 ⁻⁶ (2 Hrs Per Mission) |
|---|------------------------|--|---|---|
| Supply and Return Lines (H ₂ O) | 549 m (1800 ft) | 0.224* | 403.2 | 806.4 |
| Marman Clamp | 2 | 2.02 | 4.04 | 8.08 |
| Gate Valve (H ₂ O) | 2 | 11.0 | 22.0 | 44.0 |
| Control Valve (H ₂) | 2 | 67.1 | 134.2 | 268.4 |
| Accumulator (H ₂ O) | 1 | 6.2 | 6.2 | 12.4 |
| Heat Exchanger (H ₂ O - H ₂) | 1 | 5.0 | 5.0 | 10.0 |
| Skin Panels (H ₂ O) | 150 | 8.3 | 1245.0 | 2490.0 |
| Panel Connectors (H ₂ O) | 300 | 0.056 | 16.8 | 33.6 |
| Machined Tees (H ₂ O) | 150 | 0.02 | 3.0 | 6.0 |
| Flexible Hoses (H ₂ O) | 300 | 3.93 | 1179.0 | 2358.0 |
| Mechanical Connections (H ₂ O) | 750 | 0.056 | 42.0 | 84.0 |
| Welded Connections (H ₂ O) | 500 | 0.052 | 26.0 | 52.0 |
| Check Valves (H ₂ O) | 2 | 2.3 | 4.6 | 9.2 |
| Centrifugal Pump (H ₂ O) | 2 | 8.7 | 0.00007569 (8.7 x 10 ⁻⁶) ² | 0.00015138 |
| Total System | | | | 6182.08 x 10 ⁻⁶ |

*(Failures/ft/hr) x 10⁻⁶

- (1) The integral construction and compactness of the plate-fin heat exchanger makes inspection difficult and places high reliance on quality control. Consideration might be given to the shell and tube design which provides a higher level of inspectability but a lower level of heat transfer effectiveness.
- (2) A temperature sensor at the outlet of the coolant flow from the heat exchanger may be warranted as a check on freezing of the glycol/water that might occur during a system malfunction.
- (3) An alternative to flexible hoses should be investigated. If hoses are used they must be adequately restrained to preclude loading due to aircraft maneuvers or fluid pressure pulses.
- (4) It may be desirable to orient coolant passages perpendicular to the panel stress field so as to minimize damage by skin cracks and therefore require protection and/or low stress levels only around the manifolding.
- (5) Care should be exercised in the design of a redundant system to ensure that redundancy is obtained in fact. Skin panels with integral redundant coolant passages warrant special attention in this regard.

Hypersonic Research Airplane. - The reliability analyses for the hypersonic research airplane paralleled those for the transport. The mission duration was assumed to be one hour and the design life was 1,000 flights. Aluminum alloy construction was assumed with a glycol/water coolant. All joints in the coolant distribution line were assumed to be welded or brazed except for two mechanical joints in the fuselage supply and return lines. Table XXVIII summarizes the failure rate data found to be most applicable for a vehicle with 1.5 m (5 ft) wide skin panels extending from the upper fuselage centerline to the lower fuselage centerline, and in a case of the wing from the root to the tip. The predicted failure rate for the nonredundant system is 773.1×10^{-6} failures per mission, a reliability of 0.99922 per mission or about 7 failures per 10,000 flights. This failure rate is about an order of magnitude lower than for the hypersonic transport that had a wetted area about one order of magnitude greater. By using a totally redundant system the reliability of the HRA is increased to 0.9999994 or approximately 1 failure per million flights. The greatest contributors to predicted mission failure rates are the flexible hoses, control valves, and skin panel. Note that the failure rate of the skins becomes less important for a smaller research vehicle than it was for the transport whose wetted area was about an order of magnitude greater. As discussed for the transport it is important to recognize that the failure rate data includes a great many failures that would not result in catastrophic consequences, as discussed previously for the hypersonic transport.

Fault Detection and Isolation Concepts

During the operation of actively cooled hypersonic aircraft, particularly transports, the basic maintenance philosophy of removal/replacement of line replaceable units appears to be most likely. Removed components can be returned to a depot and/or vendors for repair and disposition. Reliability analyses provide one means of identifying those system elements which should receive major attention, initially to enhance reliability, and secondarily to provide an indication of potential maintainance

TABLE XXVIII
SUMMARY OF NON-REDUNDANT COOLING SYSTEM FAILURE RATES
FOR A HYPERSONIC RESEARCH AIRPLANE

| Component | Number in System | Failure Rate (Failures/hr) $\times 10^{-6}$ | Failure Rate For Total Number of Each Component (Failures/Mission) $\times 10^{-6}$ |
|---|------------------|--|--|
| Supply and Return Lines (H ₂ O) | 91 m (300 ft) | 0.224* | 67.0 |
| Marmian Clamp | 2 | 2.02 | 4.04 |
| Gate Valve (H ₂ O) | 2 | 11.0 | 22.0 |
| Control Valve (H ₂) | 2 | 67.1 | 134.2 |
| Accumulator (H ₂ O) | 1 | 6.2 | 6.2 |
| Heat Exchanger (H ₂ O-H ₂) | 1 | 5.0 | 5.0 |
| Skin Panels (H ₂ O) | 51 | 2.08 | 106.0 |
| Panel Connectors (H ₂ O) | 102 | 0.056 | 5.7 |
| Machined Tees (H ₂ O) | 51 | 0.02 | 1.02 |
| Flexible Hoses (H ₂ O) | 102 | 3.93 | 400.8 |
| Mechanical Connection (H ₂ O) | 153 | 0.056 | 8.6 |
| Welded Connections (H ₂ O) | 153 | 0.052 | 7.9 |
| Check Valves (H ₂ O) | 2 | 2.3 | 4.6 |
| Centrifugal Pump (H ₂ O) | 2 | 8.7 | 0.00007569 (8.7 $\times 10^{-6}$) ² |
| Total System | | | 773.1 $\times 10^{-6}$ |

*(Failures/ft/hr) $\times 10^{-6}$

problems. As a further aid to the safety and maintainability activities, fault detection and isolation equipment is essential. In practice, a certain amount of built-in test equipment will probably be desirable. Since the number of access panels in a cooled airframe structure should be minimized, many of the major system elements are likely to be packaged in close proximity to each other. This might permit a grouping of the fault detection and isolation equipment as well.

Of primary importance to the safety and operation of an actively cooled airframe structure is the flow of coolant during high speed flight. Redundancy increases reliability at a relatively modest cost in aircraft weight, and reliability analyses indicate very low failure rates for redundant structural cooling systems even when using component failure rate data that is believed to be conservative. Furthermore, analyses that will be discussed later suggest that even if one loop of a redundant system becomes inoperative and the flow in the second loop is not increased it is likely to cause loss of the aircraft. Nevertheless, repairs must be made in a timely fashion, and preventive maintenance should be practiced to maximize safety. In addition, despite the fact that analyses indicate very high reliabilities for the structural cooling system, there is always a concern for "infant mortality" failures when mechanical components are involved. Therefore, it is desirable to include sensors on various types of components to indicate incipient failure tendencies, as well as at various system locations to indicate system performance data that may be useful for detecting and isolating malfunctions.

Table XXIX presents an analysis of techniques for detecting cooling system component failures. The failure modes identified in the prior failure mode and effects analysis were examined for each major system component. In the analysis, various alternatives are included, but this does not constitute a recommendation for their incorporation in any particular cooled aircraft structural system. Items most likely to be included in any cooled airframe structures are:

- (1) Liquid level indicator
- (2) Flowmeter in main line from the pump
- (3) Pressure sensors downstream of the pump and on the accumulator
- (4) Temperature sensors at the inlet and the outlet of heat exchanger
- (5) Acoustic sensors on pump

These items are all related to overall system conditions and may be adequate for safety, particularly when redundancy is incorporated. Other instruments aid in locating problem areas.

Various features of the fault detection and isolation approaches are illustrated schematically in Figures 67 through 70. Here too, it should be noted that various alternatives are being discussed without making specific recommendations. Figure 67 shows instrumentation associated with overall cooling system performance and is typical of what may be installed in a large vehicle such as the HST. Figure 68 suggests a method for isolating portions of a cooling system while retaining the major portion of the system. For a redundant system, this approach could provide added safety if the controls fail to increase pump speed for the fully operational loop after a malfunction is detected in one loop. Figure 69 depicts instrumentation for a single panel but such an approach is considered to be overly complex, particularly if applied throughout the airframe. Temperature sensors between coolant passages were considered also, but this could lead to excessive maintenance for data of very limited value. There are a number of alternate liquid level devices in addition to the magnet approach depicted in Figure 70. However, experience with positive expulsion propellant tankage indicates the magnetic system to be superior to, though somewhat more expensive than, potentiometric devices of either linear or wind-up types.

TABLE XXIX
SUMMARY OF FAULT DETECTION AND ISOLATION CONCEPTS (SHEET 1 OF 6)

| Item Identification | Failure Mode | Failure Detectable by | | Alternate Means of Operation | Remarks |
|---------------------|--------------------|--|--|---|---|
| | | in Flight | on Ground | | |
| 1. Cooled Panel | A. External Leak | <p>Decrease in indicated accumulator liquid level.</p> <p>Decrease in indicated coolant flowrate leaving pump.</p> <p>Nonuniform variation in pump speed.</p> <p>Glycol sniffers located throughout vehicle.</p> <p>Different mass flowrates at inlet and outlet of panel.</p> | <p>Cannot hold accumulator liquid level.</p> <p>Glycol sniffers located throughout vehicle.</p> <p>Discoloration of vehicle paint by coolant leak.</p> <p>Pump heated coolant through panels and use infrared sensor to determine leakage point.</p> <p>Visual examination of aircraft skin.</p> | <p>If leakage rate exceeds prespecified value.</p> <p>Shut down affected circuit and operate other circuit in the redundant mode.</p> <p>Shut down affected circuit and operate other circuit in redundant mode.</p> <p>Of little value for inflight decisions but helpful for ground servicing.</p> <p>Switch to other circuit or close off one circuit of affected panel.</p> | <p>Liquid level indicator requires a logic circuit to account for variations in coolant density. Must work under all 'g' level conditions.</p> <p>Automatic shut down of affected circuit should occur prior to these indications as a result of a low level sensor in the accumulator. Requires a switching network.</p> <p>Does not differentiate which circuit has leak, little advantage.</p> <p>Requires a special paint that changes color when contacted by coolant and reverts to original color when cleaned.</p> <p>Transient type of test makes detection of differences difficult. Structural details (differences in thermal mass) will influence temperature patterns.</p> <p>Requires extensive instrumentation and a logic circuit to correct for temperature level. Consider transmitter and receiver rather than wire bundles. Failure of valves may be of higher probability than an external leak.</p> <p>Cracks are readily visible on a highly polished surface, but difficult to detect on a painted or tarnished surface.</p> <p>Addition of coloring to the coolant would make crack detection easier.</p> <p>Utilization of a coolant with a leak preventive compound would cause small leaks to seal themselves.</p> |
| | B. Restricted Flow | <p>Reduction in total system flowrate.</p> <p>Increase as indicated pressure at pump outlet.</p> <p>Flowmeter at panel does not exhibit consistent performance when compared with design expectations.</p> | | <p>Operate unaffected system in redundant mode.</p> <p>Same as above.</p> <p>Same as above.</p> | |

TABLE XXIX (CONT'D) (SHEET 2 OF 6)

| Item Identification | Failure Mode | Failure Detectable by | | Alternate Means of Operation | Remarks |
|----------------------------|-----------------------------|---|--|---|---|
| | | In Flight | On Ground | | |
| 1. Cooled Panel (Cont'd) | B. Restricted Flow (Cont'd) | | Infrared scanner of coolant heated by ground cart shows restricted area as a cold section. Sample coolant and perform chemical composition test for contaminants or corrosion products. | | Transient test hence it requires many tests to be performed or quick inspection. Preventative test for accumulation of foreign particulate matter. |
| | | Increase in temperature between passages. | Visual examination of skin for changes in color of temperature sensitive paint. | | Requires extensive instrumentation. A special paint is required. |
| | C. Entrapped Gas | Variation in pump speed. | | No action required unless acoustic sensor indicates amplitudes in excess of a prespecified limit. | Utilization of a self bleeding valve should eliminate problem. |
| | | Acoustic sensor indicates abnormal sound levels. Same as 1.A | | | |
| 2. Fittings and Connectors | A. External Leakage | | Same as 1.A | Same as 1.A | Proof pressure test on ground or previous to hypersonic flight at 1.5 times operating pressure level and subsequent check of accumulator liquid level during this period will indicate if external leaks exist. If leak exists abort. Enclosure around each connector is required. |
| | | Tuning fork with absorbent pad operates at different frequency level. Complete electrical circuit. | | | |
| 3. Flexible Hoses | External Leakage | Same as 2.A | Same as 2.A | Same as 2.A | Extensive instrumentation with enclosures around each connector is required. Leak location is identified exactly. Same as 2.A |
| 4. Centrifugal Pump | A. External Leakage | Same as 2.A | Same as 2.A | Same as 2.A | Same as 2.A |
| | B. Internal Leakage | Variation in Pump Speed. Decrease of pump outlet pressure. | | Operate unaffected system in redundant mode. | Liquid is not lost from the system, hence operation at a lower flowrate can be tolerated without any change in flight plan. |

TABLE XXIX (CONT'D) (SHEET 3 OF 6)

| Item Identification | Failure Mode | Failure Detectable by | | Alternate Means of Operation | Remarks |
|---------------------------------|---|--|--|---|--|
| | | In Flight | On Ground | | |
| 4. Centrifugal Pump (Cont'd) | C. Failure to Deliver Rated Flowrate 1. Cavitation 2. Bearing Failure 3. Failure of Drive System 4. Contamination 5. Loss of Speed Control | Coolant inlet temperature to heat exchanger in unaffected loop would increase. Acoustic sensors would detect abnormal sound levels. | Acoustic sensors would detect abnormal sound levels. | Operate unaffected circuit in redundant mode. If sound levels do not exceed allowable limits continue operation. Otherwise operate other circuit in redundant mode. Attempt to pressurize accumulator, if unsuccessful operate other circuit in redundant mode. | If an increase in accumulator pressure does not solve the problem, the problem is a result of a foreign gas leaking into the coolant loop. |
| | | Reduction in indicated flowrate. | Pump is not capable of delivering its rated flowrate. | | |
| | | Reduction in pump outlet pressure with very erratic fluctuations. Pump speed fluctuates. | Pump speed fluctuates. | | |
| | | Acoustic sensors would detect abnormal sound levels. | Same as flight detection. | If sound levels do not exceed allowable limits continue operation, otherwise operate other circuit in redundant mode. | |
| | | Pump speed and pressure indicators will be erratic. Loss of pump speed. | | Shut down affected system and operate other system in redundant mode. | |
| 5. Coolant F Flow Control Valve | A. Failure to Open Command signal failed or valve stem interferes with valve body. | High pump outlet pressure. | High outlet pressure. Sample coolant chemical composition for foreign particles and corrosion products. | | Filter should be added to trap large particles such as corrosion products but not to remove small soft sludge like particles that are formed by some inhibitors and are necessary for proper inhibitor action. |
| | | Pump speed does not achieve desired value. | Speed does not vary. | | |
| | | 1. Flowmeter in affected circuit will indicate no flow. | Same as 5.A.1 and 5.A.2 Flight Condition | Activate redundant command circuit. If that does not eliminate problem, shut down pump, and operate on one circuit only. | |
| | | 2. Valve position indicator will indicate closed. | | | |
| | | 3. Coolant inlet temperature of other loop will exceed normal operating level. | | | Presently, this type of valve is not included in the system design. Valves will be open before hypersonic flight is initiated, hence this failure would only cause an abort from low speed. |

TABLE XXIX (CONT'D) (SHEET 4 OF 6)

| Item Identification | Failure Mode | Failure Detectable by | | Alternate Means of Operation | Remarks |
|--|--|--|---|---|---|
| | | In Flight | On Ground | | |
| 5. Coolant Flow Control Valve (Cont'd) | B. Failure to Open Fully | Flowmeter in affected circuit will show a reduced flow. Valve position indicator will not indicate fully opened. Coolant inlet temperature to HX of unaffected loop will read high. Pressure drop of loop will be low. | Same as for flight operation except the inlet temperature of other loop will not read high because there is no heating. | | |
| 6. Accumulator | A. External Leak | Liquid level sensor which would indicate loss of liquid. | Liquid level indicator would indicate loss of liquid. | If depletion rate exceeds a pre-specified value the pump would be stopped and the speed of the pump in the other loop would be increased. An automatic shutdown will occur when the liquid in the accumulator is less than a low level requirement. | |
| | B. Internal Leak | The flowmeter in the pressurization line would register an abnormal rate and would cause a light to appear on the control panel. A variation in pump speed may be detected because of the entrained gas. Reduction in gas supply pressure level. | Flowmeter in pressurization line would register an abnormal rate. Reduction in gas supply pressure level. | | System would remain operative with this type of failure. |
| | C. External Leak On Pressurization Side of Accumulator | Flowmeter in pressurization line will record a reading and cause a light to appear on control panel. However, liquid level will remain constant. Reduction in gas supply pressure level. | Flowmeter in pressurization line will record a reading. Reduction in gas supply pressure level. | No action required unless the pressurization gas flow exceeds the available gas supply at which time the system would be shut down and the other system would be operated in the redundant mode. | |
| 7. Heat Exchanger | A. Internal Leak | | | | |
| | 1. Hydrogen flows into coolant stream. | Increase in accumulator liquid level with no flow on accumulator gas supply. | Same as flight detection controls. | Shut down system and operate other system in redundant mode. | Preflight check at 1.5 times of the redundant operating pressure should insure that such a failure will not occur during hypersonic flight. |

TABLE XXIX (CONT'D) (SHEET 5 OF 6)

| Item Identification | Failure Mode | Failure Detectable by | | Alternate Means of Operation | Remarks |
|---|--|--|---|---|---|
| | | In Flight | On Ground | | |
| 7. Heat Exchanger (Cont'd) | A. Internal Leak | | | | |
| | 1. (Cont'd) | If the leak is significant, a reduction in coolant outlet temperature from the heat exchanger would be detected. | | | |
| | 2. Coolant flows into hydrogen stream. | Decrease in accumulator liquid level. | Decrease in accumulator liquid level. However, an increase in pressure on the hydrogen side will decrease this flow rate. | If leakage rate exceeds a pre-specified value shut down system and operate other system in redundant mode. | |
| | B. External Leak | | | | |
| | 1. Hydrogen | Hydrogen sensors located in the HX region will cause a light to appear on the control panel. | Same. | None required, if the concentrations are less than a prespecified amount since the purge gas will eliminate the explosion hazard. If leak is major, pilot must reduce speed to low supersonic range and then shut down both HX. | Same as above. This failure mode suggests separate compartments for each of the HX's so that the failed heat exchanger can be identified and the mission can be completed using the other system. Hydrogen sensor may be a tuning fork with absorbent pads. |
| | 2. Coolant | Loss of liquid level in accumulator. | Same as flight. | If leak is too severe the system would shut down automatically and the other system would operate in the redundant mode. | |
| 8. Heat Exchanger Hydrogen Control Valves | A. Failure to Open | | | | |
| | 1. No command signal | Valve position indicator will indicate closed. Coolant temperature at outlet will be greater than acceptance limit and coolant inlet temperature will increase. | Valve position indicator will indicate closed. | Use redundant command circuit. | |
| | 2. Contaminated Valve | Same as above. | Same as above. | Shut down affected system and operate other system in redundant mode. | Utilization of filters to remove foreign particles in hydrogen line may be necessary. |
| | B. Failure to Fully Open | | | | |
| | 1. Improper command signal. | Coolant temperature at heat exchanger inlet and outlet will increase. Valve position indicator will indicate not fully opened. | Same as flight. | Use redundant command circuit. | |

TABLE XXIX (CONT'D) (SHEET 6 OF 6)

| Item Identification | Failure Mode | Failure Detectable by | | Alternate Means of Operation | Remarks |
|---|---|--|---|--|--|
| | | In Flight | On Ground | | |
| 8. Heat Exchanger Hydrogen Control Valves. (Cont'd) | B. Failure to Fully Open (Cont'd) 2. Contaminated Valve | Same as above. | Same as above. | Shutdown affected system and operate other system in redundant mode. | Utilization of filters to remove foreign particles in hydrogen line may be necessary. |
| | C. Failure to Close 1. Improper Command Signal 2. Contamination | Coolant inlet and outlet temperature are below acceptable limits. Valve position indicator indicates valve is open. Same as above. | Valve position indicator indicates valve is open. Same as above. | Use redundant command circuit. Shut down affected system and operate other system in redundant mode. Close hydrogen supply valve to prevent freezing in the HX. | It may be necessary to vent water Glycol heat exchanger outlet overboard in order to prevent freezing within heat exchanger. |
| Filter | D. External Leak | Hydrogen gas sensor will detect an increase in hydrogen concentration and will light a light on the control panel. | | None required unless concentration becomes an explosion hazard at which time pilot must increase purge gas flow and abort the mission. | Suggests separate compartment for each valve so that the failed component can be identified. |
| | Clogged | Pressure drop across filter reads high. | | None required unless flow is restricted in which case the filter bypass line would be opened. | Cleaning of filter regularly would eliminate this failure since buildup would be slow. |

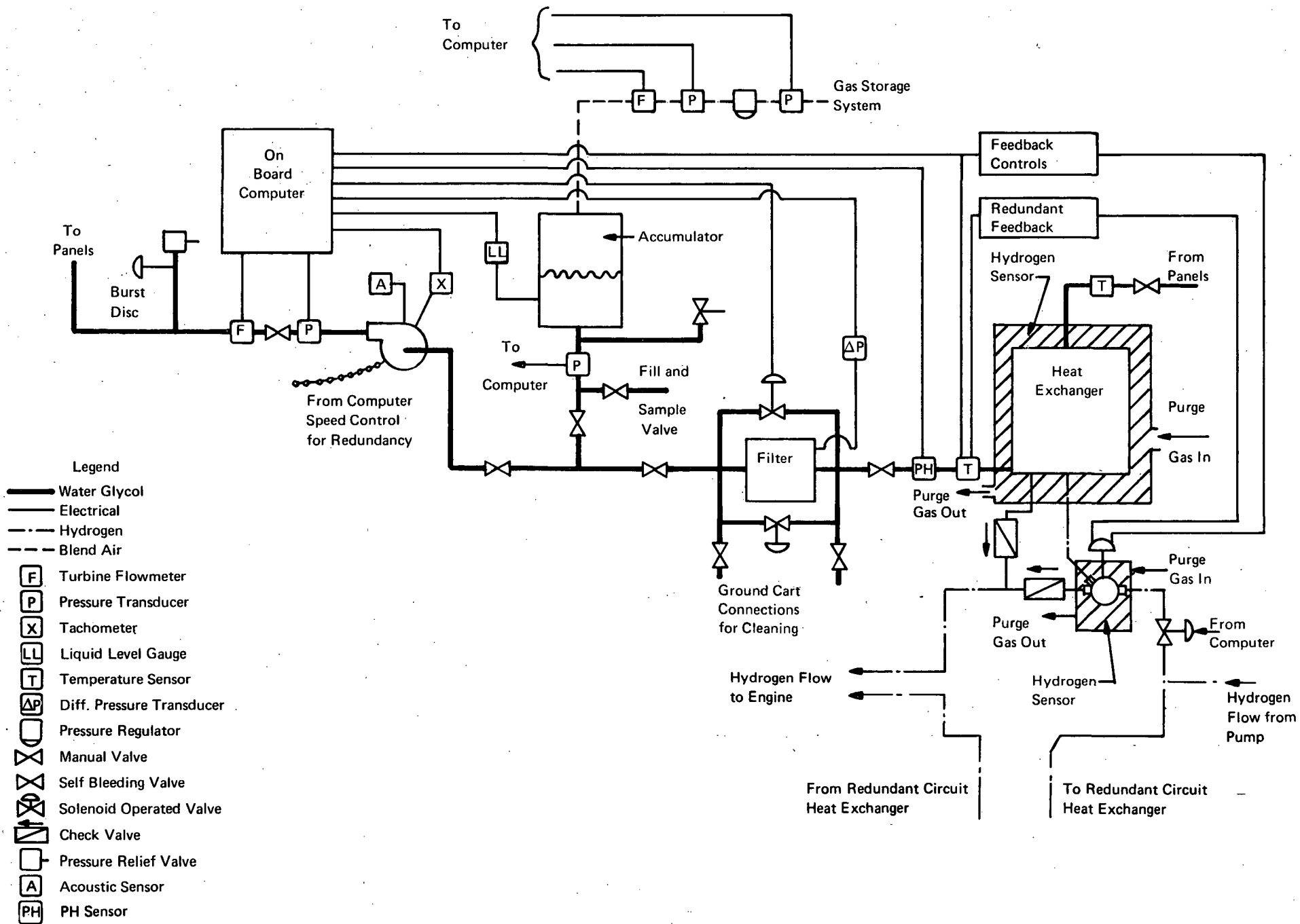


Figure 67. Instrumentation Schematic for Fault Isolation

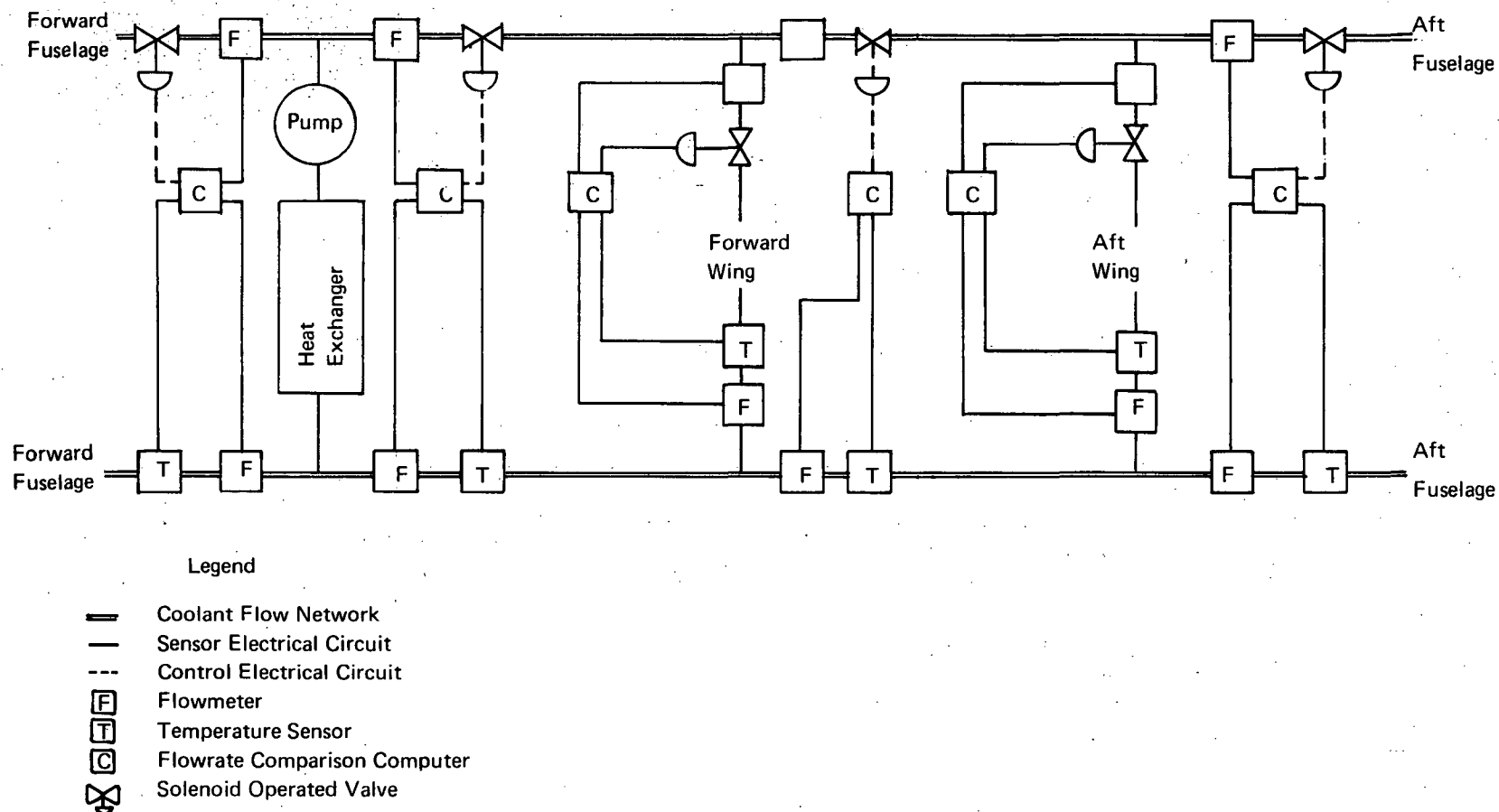


Figure 68. Limited Instrumentation of Distribution System

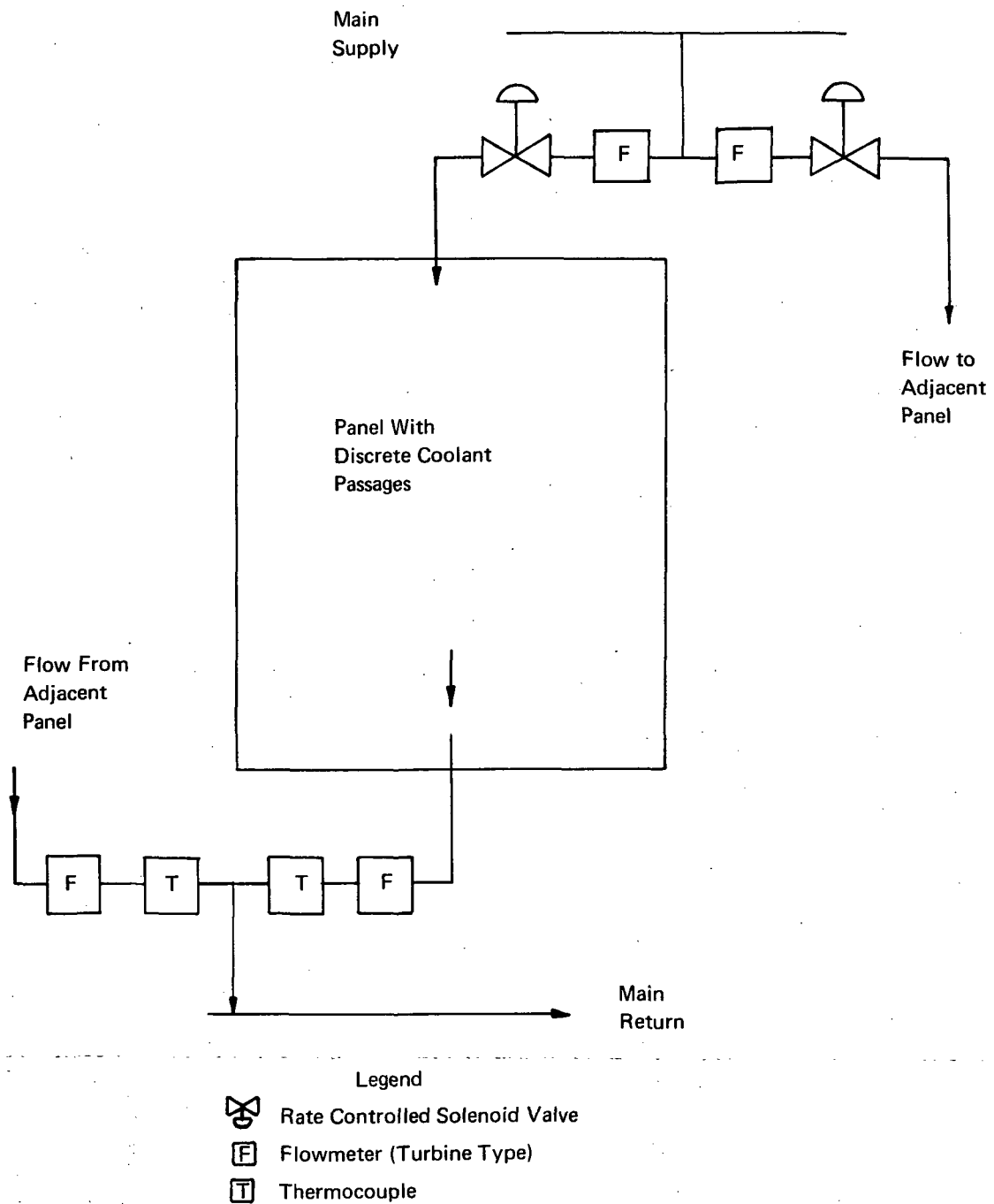


Figure 69. Completely Instrumented Panel

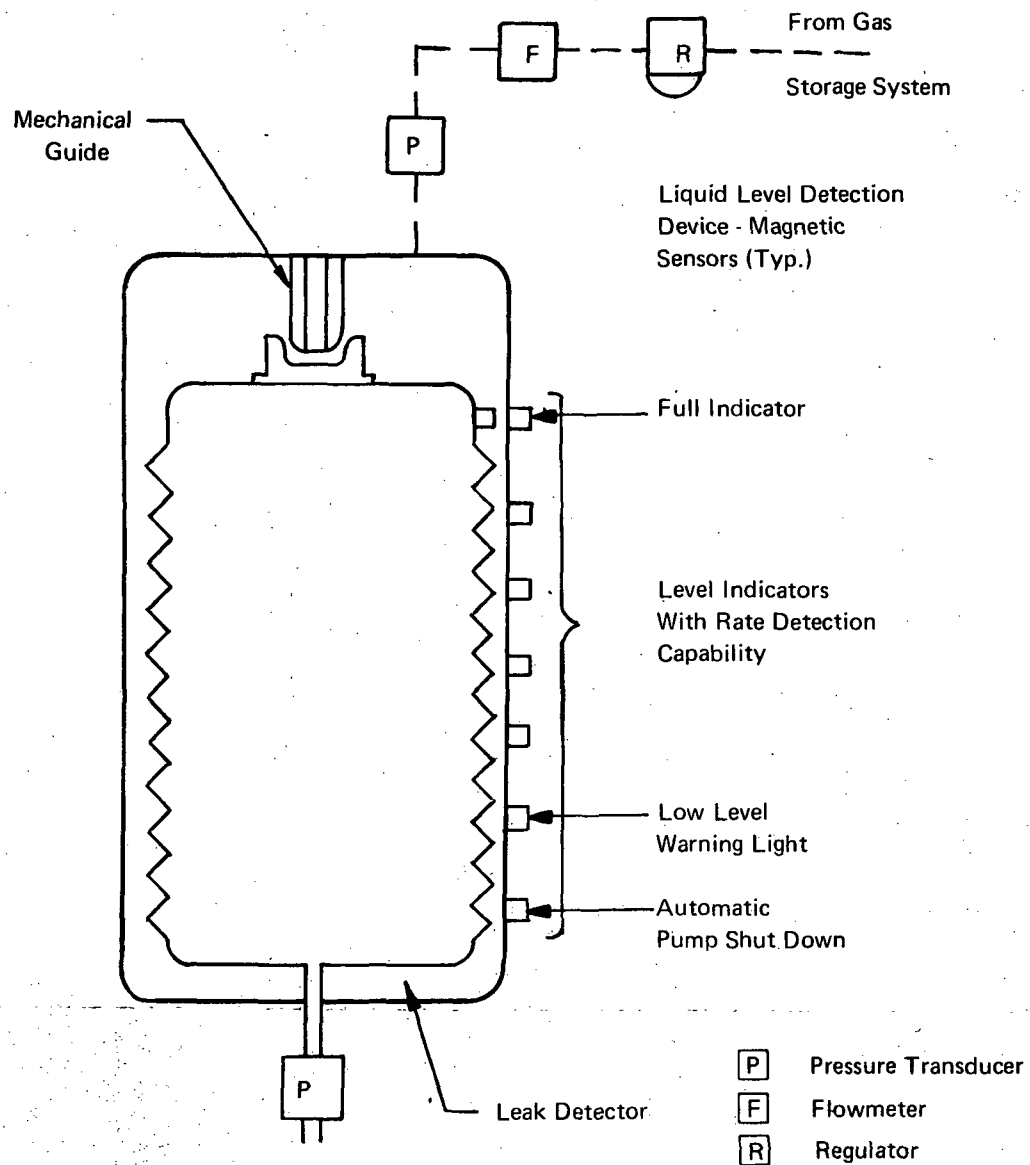


Figure 70. Accumulator Schematic

CONCEPTS FOR SELECTED REGIONS

The primary factors influencing the viability of the cooled airframe concept are related to the weight and size of components, ability to integrate the cooling system with the structure, and reliability/maintainability considerations. However, a number of questions arise pertaining to some areas where weight is not as important as indications of feasibility. A number of such areas were examined qualitatively to identify problems and possible solutions. Attention was directed to concepts for sharp leading edges (including redundancy and fail-safe approaches), heat shields, cooling of integral propellant tanks, connections of cooling system lines and control surface panels, and doors and access panels. The concepts discussed subsequently can provide the basis for future studies of a more detailed nature.

Leading Edge Concepts

The use of actively cooled leading edges of small diameter reduces drag and enhances aircraft performance. The minimum practical leading edge diameter will be established either by fabrication limitation, by the maximum heating intensity that can be absorbed or possibly by the depth of coolant passage needed to accommodate the coolant flow from inlet to outlet header. Although the heat flux increases as the diameter is decreased, the heat load decreases. Therefore, sharp leading edges decrease the vehicle heat load but would be subjected to temperatures in excess of coated refractory metals if coolant flow should cease. Therefore, it is important to consider leading edge designs with redundant coolant flow passages and also to examine techniques for achieving fail-safe features.

Figure 71 illustrates a number of nonredundant and redundant leading edge approaches. As part of an in-house effort, an aluminum alloy leading edge based on the upper design concept was successfully exposed to a radiant heat source that produced stagnation line heat fluxes of up to 110 w/cm^2 ($100 \text{ BTU/ft}^2 \text{ sec}$) without exceeding allowable temperatures for the aluminum alloy. Superalloy structure similar to Concept b was used successfully for the hydrogen research engine. The beaded construction of Concept c utilizes stretch forming operations for the forward and rear portions of the inner sheet to achieve a small radius and to eliminate one of the joints used to attach the manifolds. Concepts d and e are redundant versions of the first and third concepts. The redundant version of Concept b would be similar to the stacked plate-fin panel illustrated in Figure 8. For any of the redundant concepts good conduction from the external mold line to the inner cooling system passage network is essential if excessive temperatures are to be avoided. In general, brazing or diffusion bonding are the preferred joining techniques because of the large area of intimate contact achieved. If welding is used, the designs should utilize narrow vertical webs between inner and outer sheets, such as truss core, to avoid long conduction paths before absorbed aerodynamic heating can be transferred to the coolant.

The use of thin gage material and elevated temperature forming should permit the fabrication of leading edge diameters in the order of 2.5 mm (0.10 inch). Such small diameters would result in very small passage heights particularly with redundant concepts. To minimize the pressure drop through such coolant passages, it would be possible to increase passage depth behind the hemicylindrical portion where the heat flux is lower, so that the internal heat transfer coefficient can be reduced without exceeding structural temperature limits. This increase in passage depth tends to relieve tolerance requirements, thereby reducing the cost of fabrication, but is more difficult to incorporate with the plate-fin concept than with the machined core of formed sheet approaches. Satisfactory thermal performance of a redundant system with one loop inoperative (i.e., sufficient lateral conduction in the skin) may not be attainable with the smallest leading edge diameters that could be fabricated.

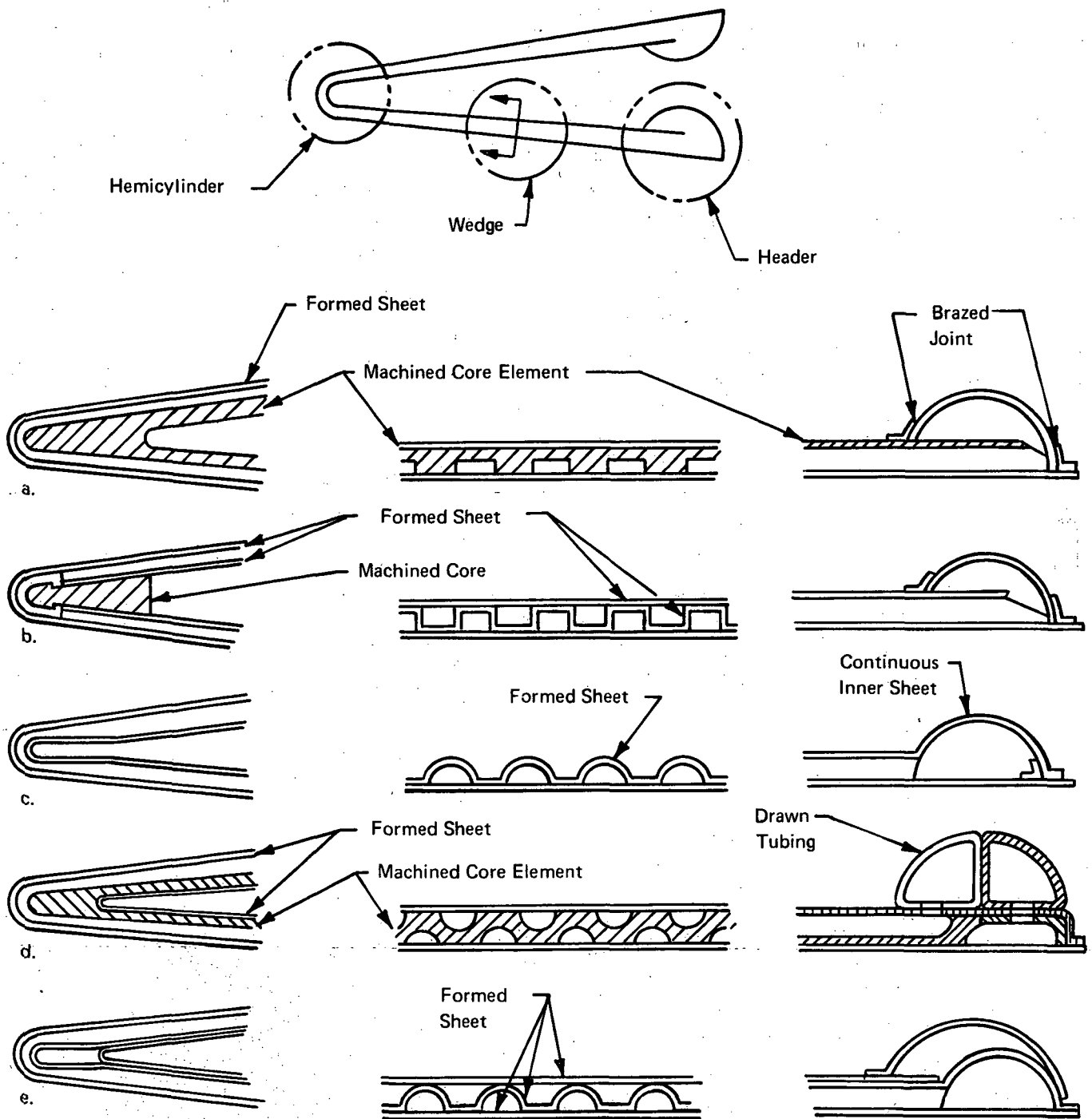


Figure 71. Cooled Leading Edge Concepts

For the nonredundant designs the leading edge diameter might be fabricated as small as 1.5 mm (0.06 inch). For these very small diameters consideration would have to be given to handling and erosion aspects. A small dent in the very shallow coolant passages around the hemicylinder might restrict flow to such a degree as to result in a burn through. Severe erosion could result in a similar malfunction.

A number of fail-safe concepts are suggested schematically in Figure 72. The first incorporates a heat sink material that does not absorb much of the heat load while the cooling system is operating properly at maximum temperatures between 366° K (200F) and 590° K (600F) depending upon the particular design. The choice of construction material will determine the maximum operating temperature that would activate the fail-safe features under emergency conditions. If superalloy construction is used the maximum emergency temperatures could be about 1140° K (1600F). This still requires heat sink materials of a high heat absorbing capacities since radiation equilibrium temperatures would be in the order of 1640° K (2500F) for the hypersonic transport and up to 3900° K (6600F) for the hypersonic research airplane.

Table XXX lists candidate heat sink materials, identifies melting and boiling points, and presents heat capacity. Approximately 150 elements and compounds were reviewed prior to the selection of these more promising candidates. The first three phase change materials have been considered for temperature control of insulated space shuttle structure, but are not particularly attractive for the leading edge application because of their modest heat capacities. Of the elemental materials, those with lowest atomic numbers and lowest melting points provide the highest heat capacity per pound; lithium is particularly outstanding with its heat capacity of over 23 MJ/kg (10,000 BTU/lb). However, for space limited applications the heat capacity per unit volume may be important; here, zinc is somewhat superior to lithium. Water is included for comparative purposes and is certainly the most attractive of the more easily handled materials.

A more explicit presentation of the heat capacity/temperature characteristics of available heat sinks is provided by Figure 73, which is an envelope of the tabulated data with consideration of likely vent pressures. For one minute of flight time the first 0.61 meters (2 feet) of leading edge, as measured perpendicular to the leading edge, would absorb 402 MJ (381,000 BTU) for the hypersonic transport and 116 MJ (110,000 BTU) for the HRA. If a water heat sink is evaporated the heat sink weights would be 172 kg (380 lb) and 50 kg (110 lb) respectively. While this would fit within the HST leading edge there is insufficient volume within the HRA leading edge. Another class of heat sinks that are attractive are the hydrides, particularly lithium hydride which has a heat capacity comparable to lithium.

There appears to be little advantage in operating the leading edge cavity between 422° K (300F) and 1080° K (1500F) since the maximum heat capacity of the candidates is nearly constant at about 2.3 MJ/kg (1000 BTU/lb) over this range. However, assuming the temperature difference between the outer skin and heat sink is independent of the type of heat sink used, the quantity of aerodynamic heat to be absorbed is decreased as the heat sink temperature increases. For flight conditions with low recovery temperatures there is an advantage in using high temperature heat sinks. Other design aspects of importance include:

- (1) Maintaining thermal contact between the heat sink and the leading edge shell

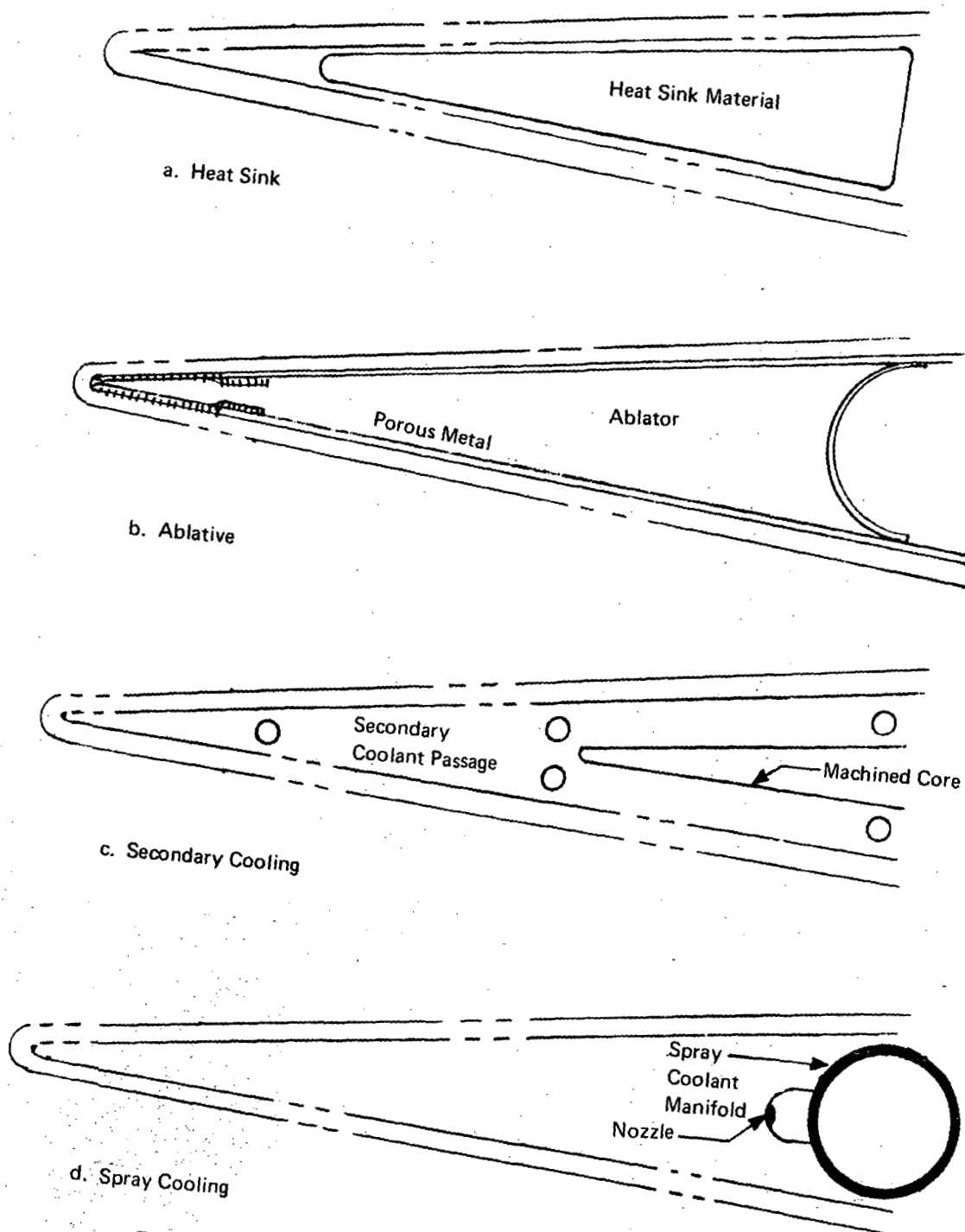


Figure 72. Fail-Safe Concepts for Cooled Leading Edges

TABLE XXXA
CANDIDATE HEAT SINK MATERIALS

| Material | Density Kg/m ³ | T _{Melt} °K | T _{Boil} °K | H _{fl} Kj/Kg | H _v Kj/Kg | Total Heat Capacity, Kj/Kg, From 294° To | | | | | | |
|---------------|------------------------------|-------------------------|-------------------------|--------------------------|-------------------------|--|-------|-------|--------|--------|--------|--------|
| | | | | | | 366°K | 533°K | 811°K | 1089°K | 1367°K | 1644°K | 1922°K |
| TH190A(1) | 1650.1 | 361 | (2) | 258 | - | 378 | - | - | - | - | - | - |
| Polyethylene | 961.2 | 410 (3) | - | 138 | - | 161 | 686 | - | - | - | - | - |
| Polypropylene | 913.4 | 449 (3) | - | 237 | - | 150 | 710 | - | - | - | - | - |
| Aluminum | 2723.7 | 933 | 2723 | 396 | 12,620 | 69 | 226 | 555 | 1200 | 1520 | 1,745 | 2120 |
| Beryllium | 1842.3 | 1558 | 3056 | 1,080 | - | 157 | 579 | 1268 | 1960 | 2660 | 4,410 | 5040 |
| Boron | 2531.1 | 2572 | 2856 | 2,025 | - | 150 | 485 | 1080 | 1690 | 2280 | 2,880 | 3480 |
| Carbon | 2114.6 | 3867 (4) | - | - | - | 76 | 328 | 750 | 1150 | 1540 | 1,960 | 2360 |
| Lithium | 560.7 | 458 | 1617 | 656 | 19,300 | 300 | 1640 | 2355 | 3070 | 3810 | 24,050 | (5) |
| Magnesium | 1602.0 | 924 | 1381 | 339 | 5,550 | 76 | 286 | 610 | 1290 | 1605 | 1,940 | 2260 |
| Potassium | 853.0 | 336 | 1047 | 60 | 2,060 | 92 | 224 | 445 | 3730 | (5) | (5) | (5) |
| Sodium | 1025.3 | 371 | 1166 | 113 | 4,180 | 99 | 444 | 830 | 1220 | 5820 | (5) | (5) |
| Zinc | 6888.6 | 693 | 1181 | 101 | 1,740 | 35 | 110 | 339 | 474 | 2330 | (5) | (5) |
| Water | 999.6 | 273 | 373 | 319 | 2,240 | 300 | 2885 | (5) | - | - | - | - |

Note:

- (1) Trademark of Royal Industries.
- (2) Decomposition may occur at temperatures above 394°K, neither temperature or the related heat absorption are well defined.
- (3) Transition temperature.
- (4) Sublimes.
- (5) Selection of vent location can permit vaporization over a range of temperatures, approximately 0.8T_B to 1.2T_B without significantly influencing total heat capacity.

TABLE XXXB
CANDIDATE HEAT SINK MATERIALS

| Material | Density pcf | T _{melt} °F | T _{boil} °F | H _{fl} BTU/lb | H _v BTU/lb | Total Heat Capacity, BTU/lb, From 70F To | | | | | | |
|---------------|----------------|-------------------------|-------------------------|---------------------------|--------------------------|--|------|-------|-------|-------|-------|-------|
| | | | | | | 200F | 500F | 1000F | 1500F | 2000F | 2500F | 3000F |
| TH190A(1) | 103 | 190 | (2) | 112 | - | 164 | - | - | - | - | - | - |
| Polyethylene | 60 | 278 (3) | - | 60 | - | 70 | 297 | - | - | - | - | - |
| Polypropylene | 57 | 349 (3) | - | 102 | - | 65 | 308 | - | - | - | - | - |
| Aluminum | 170 | 1220 | 4442 | 172 | 5480 | 30 | 98 | 240 | 520 | 660 | 778 | 920 |
| Beryllium | 115 | 2345 | 5040 | 470 | - | 68 | 255 | 550 | 850 | 1150 | 1910 | 2180 |
| Boron | 158 | 4170 | 4680 | 880 | - | 65 | 210 | 470 | 730 | 990 | 1250 | 1510 |
| Carbon | 132 | 6500 (4) | - | - | - | 33 | 142 | 325 | 500 | 670 | 850 | 1025 |
| Lithium | 35 | 365 | 2450 | 284 | 8410 | 130 | 710 | 1020 | 1330 | 1650 | 10410 | (5) |
| Magnesium | 100 | 1204 | 2025 | 147 | 2400 | 33 | 123 | 264 | 560 | 697 | 840 | 980 |
| Potassium | 52 | 144 | 1425 | 26 | 894 | 40 | 97 | 193 | 1185 | (5) | (5) | (5) |
| Sodium | 64 | 208 | 1638 | 49 | 1810 | 43 | 192 | 360 | 530 | 2520 | (5) | (5) |
| Zinc | 430 | 787 | 1665 | 44 | 755 | 15 | 48 | 147 | 205 | 1010 | (5) | (5) |
| Water | 62.4 | 32 | 212 | 138 | 970 | 130 | 1250 | (5) | - | - | - | - |

- (1) Trademark of Royal Industries.
- (2) Decomposition may occur at temperatures above 250F, neither temperature or the related heat absorbtion are well defined.
- (3) Transition temperature.
- (4) Sublimes.
- (5) Selection of vent location can permit vaporization over a range of temperatures, approximately $0.8T_B$ to $1.2T_B$ without significantly influencing total heat capacity.

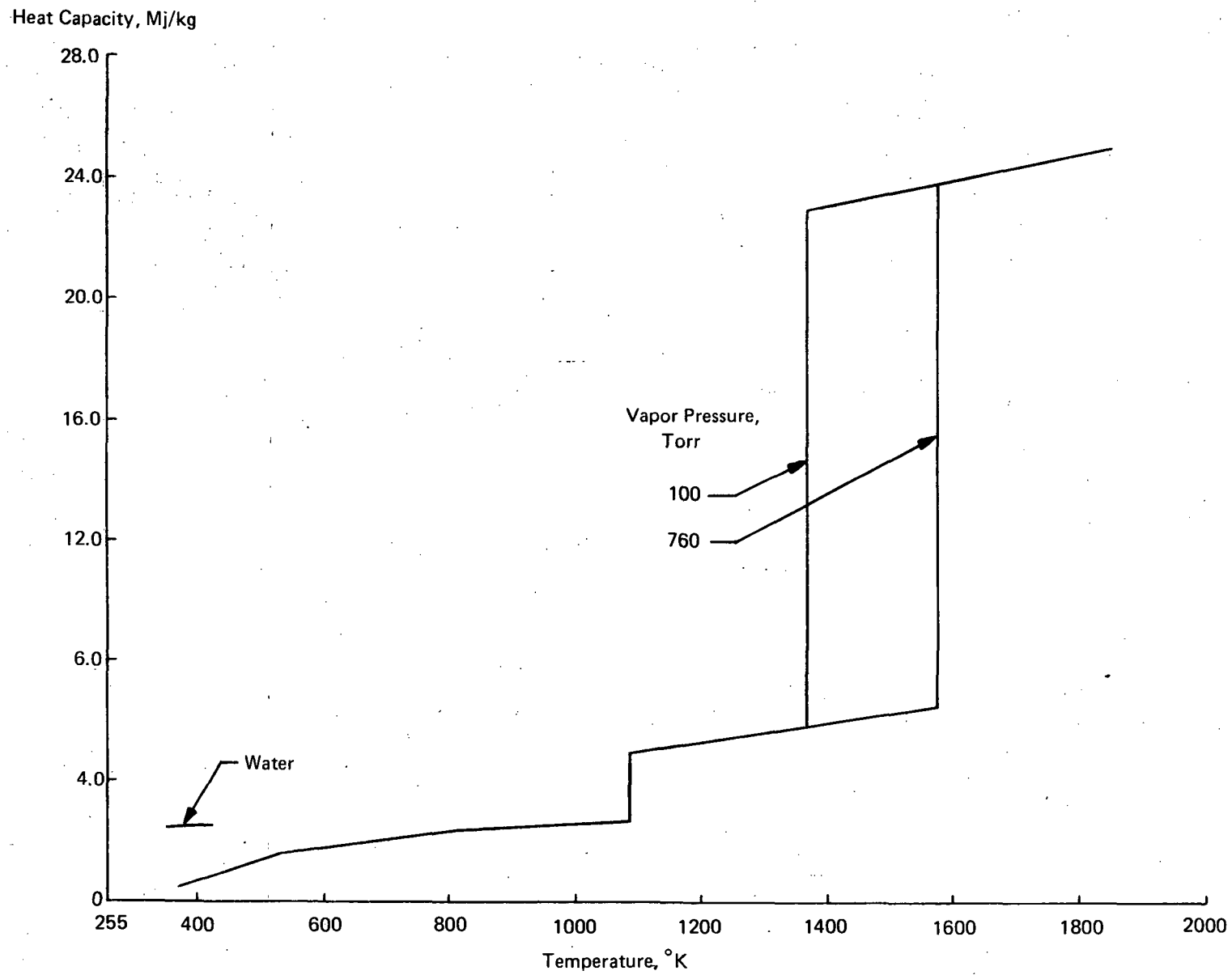


Figure 73a. Heat Capacity Envelope for Candidate Heat Sink Materials

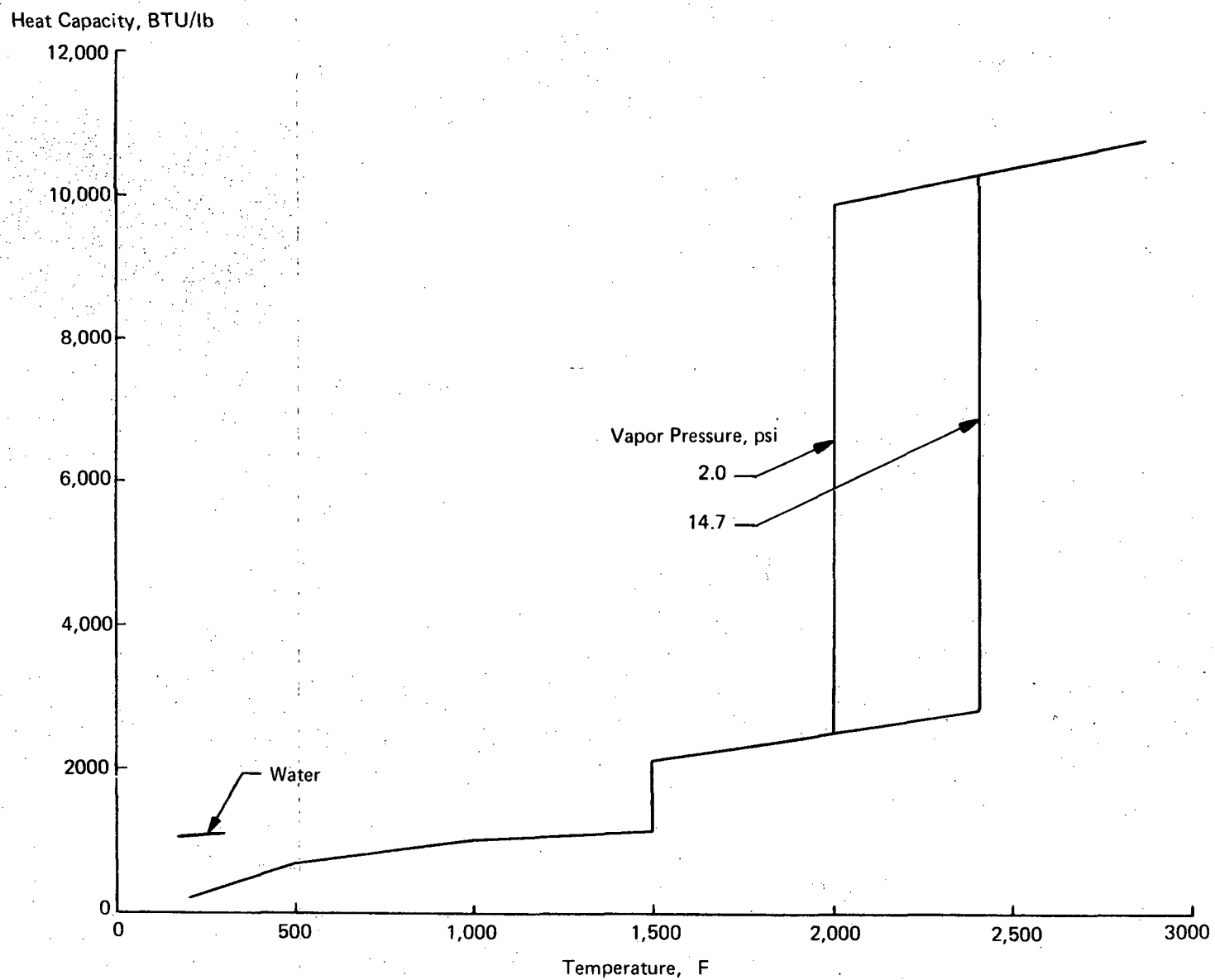


Figure 73b. Heat Capacity Envelope for Candidate Heat Sink Materials

- (2) Economic tradeoffs between concepts which require replacement of the leading edge in the event of an emergency and those which involve simple recharging of an expended heat sink
- (3) Compatibility of the heat sink with the leading edge construction material
- (4) Compatibility of expendable heat sink material with surfaces downstream of exhaust vents
- (5) Vent design to control vaporization temperature of expendable heat sinks

Detailed investigations of such design questions are well suited for future efforts.

Concept b of Figure 72 attempts to utilize an ablator as the heat sink material. It is obvious that the ablation process would generate high internal pressures and gradually would eliminate effective thermal contact between the leading edge shell and the ablator. Therefore, a porous material nose section is provided to vent the decomposition products through the most highly heated region. A low temperature ablator with a high thermal absorbance is desired so that heat from the structure can be transferred to the ablator by radiation. While effective heats of ablation of between 11.5 and 2.3 MJ/kg (5000 and 1000 BTU/lb) can be achieved under certain conditions, it is highly doubtful whether values of more than 4.6 MJ/kg (2000 BTU/lb) could be achieved with a concept that does not permit boundary layer modification or thermal radiation from a hot char layer. Note also that a minimum amount of ablative material is adjacent to the most highly heated section of the structure. The small portion of the inner wall that is made from porous material could be infiltrated with a low melting point material so that it is solid at operating temperatures for the cooled leading edge. It might be possible to utilize a similar design approach for the outer skin thereby achieving some blockage of aerodynamic heating. A further consideration for the ablative material is that it be noncharring, since the char layer would insulate the leading edge shell structure from the actively decomposing portion of the ablator and char fragments might plug the porous material.

Another technique for incorporating cooling system redundancy is shown in the third sketch of Figure 72. Here, a number of coolant passages are introduced parallel to the leading edge to absorb heat if the primary coolant loop malfunctions. Cooling effectiveness is greatly reduced so that the leading edge temperatures would rise substantially. It may be desirable to use a higher temperature coolant for this emergency system and to reject heat to a portion of other aircraft structure without the need of continuing the loop to the primary heat exchanger. A number of high temperature coolants are available for use in the 650°K (700F) to 700°K (800F) range that might be used for such an emergency system but could not be used for the primary system since they would not be liquid at 218°K (-65F).

Still another redundant approach is to provide a spray system quite independent of the leading edge structure as shown in Figure 72 d. A pressurized water reservoir would feed coolant to a number of spray nozzles mounted within each leading edge segment. If the primary cooling system malfunctions

the spray nozzles produce an essentially rectangular spray pattern of high aspect ratio so that the spray is concentrated toward the most forward section of the leading edge. Excess liquid would flow across the lower wedge thereby providing maximum cooling to the more highly heated wedge surface. At least two options are open with respect to emergency system activation. A sensor could open a valve to initiate coolant flow to the desired leading edge section, or the system could be fully charged and a controlled melting point alloy used to preclude flow through the nozzle until an over heated condition melts the alloy nozzle plug. A variation of this system might be achieved by closing the interior leading edge structure and providing a porous forward region as described for the ablative concept such that the steam generated would be exhausted through the leading edge coolant passages thereby providing improved cooling.

Heat Shielding

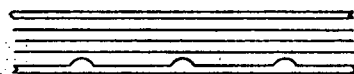
A number of concepts are shown in Figure 74 for external heat shielding, heat shields, and attachments. The first three shielding concepts have a common disadvantage of decreasing the available structural depth for a fixed moldline configuration. The fourth approach minimizes this penalty, but care must be exercised to adequately insulate the points of contact between the heat shield and the coolant passages or the manifolds. The concept that employs intermediate insulation has been studied by several investigators, References 41, 48 and 49. For most prior applications it was necessary to consider the weight of expendable coolant. Thus the minimum system weight was found by trading off the weight of insulation against the weight of the cooling system and expendable coolant. However, when the vehicle fuel provides the heat sink the insulation weight is traded against the weight of the cooling system only. This results in a shift of the optimum design to a point where very little insulation is needed. Obviously this system is substantially lighter than one that requires expendable coolant.

The very small amount of insulation required to optimize a shielded system when no expendable coolant is required suggests the possibility of controlling heat flow between the external shield and the cooled structure by the radiant heat transfer characteristics of the two construction materials. As shown in Reference 1 this approach is very attractive. This design approach decreases the heat load to the cooling system thereby reducing cooling system weight, and providing a match of airframe heat load to fuel flow cooling capacity. The heat shielding approach, even without insulation, is lighter than the weight of expendable coolant that would have to be carried to deal with the added heat load if there was no shielding. With regard to weight, however, it is heavier than direct surface cooling, when the fuel can absorb the heat load. Another disadvantage is the presence of the heat shielding which involves a significant expense both initially and for maintenance.

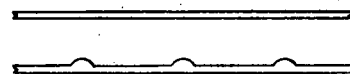
The various types of heat shields have been studied by many investigators over the years and require little discussion. The corrugation is the lightest and least expensive but is not smooth. The honeycomb is the lightest of the remaining heat shield types, is very smooth but is probably the most expensive. Its use with refractory metal construction is questionable because of the light weight core which becomes relatively brittle if coated or is highly susceptible to oxidation if uncoated and the panel seal is destroyed. The corrugation and integrally stiffened design are probably most attractive for coated refractory metals because of the elimination of faying surfaces and the accessibility for inspection.



Heat Shield Plus
Insulation



Heat Shield Plus
Radiation Barriers



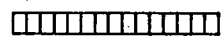
Heat Shield Only



Heat Shield On
Cooled Structure



Corrugation



Honeycomb



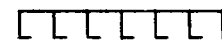
Channel



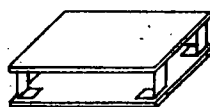
Truss Core



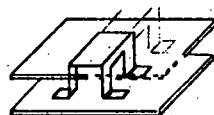
Single Face



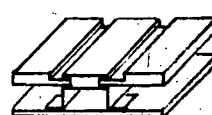
Integrally
Stiffened



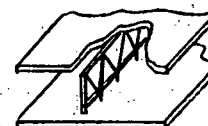
Multiple
Clip



Internal
Rail



Edge
Clamp



Truss

Figure 74. External Heat Shielding Concepts

The range of heat shield weights for various materials, operating temperatures, and surface pressure differentials from 67 to 120 kn/m^2 (1400 to 2500 psf) are presented in Figure 75. The data was accumulated from a number of space shuttle reports. The relationship between temperature and heat flux as shown in Figure 75 assumes no internal heat flow. This is essentially true when insulation or low radiation transfer characteristics are provided. However, for a particular temperature a higher heat flux can be sustained if significant radiative heat transfer is allowed between the heat shield and the cooled panel. Although much prior work has been done it has served to demonstrate feasibility and to identify problem areas which require further attention, such as thermal stress minimization, creep life under cyclic conditions, oxidation effects, damage tolerance, sealing against water and gas flow, improved fabrication and inspection procedures particularly for refractory metals, and cost aspects. While it should be possible to resolve present short comings the time and effort involved must be compared with the benefits to be derived.

The important aspects of heat shield attachment concepts include the number of attachment points and the thermal resistance of each. The number of attachment points may influence the type of cooled panel to be used. Note that except for the multiple clip type (that suffers from relatively large out of plane panel deformation) the various attachment approaches have a large number of contact points with the cooled structural panel. Hence the discrete tubular panel concept is favored. The use of plate-fin or sphere-core sandwich concepts would require local inserts at the heat shield attachment points in order to permit connections without leakage. Such inserts would add to cost and weight. With respect to thermal resistance, prior studies indicate that well designed attachment (without local insulation) increase the heat flow to the panel to about 140% of that through an optimized insulation system. When local insulation is installed at each attachment the total heat flow can be reduced to about 115% of that through the thermal insulation alone. Note that when only a heat shield is used the heat flow to the cooled panel is higher than when insulation or radiation barriers are used; thus, the influence of the attachment is relatively less, even though the actual heat flow through the attachments may be somewhat higher.

Concepts For Cooled Integral Tanks

As used in this discussion, an integral tank carries primary airframe bending, torsion and shear loads but its surface does not necessarily form the external mold line; heat shielding can be used. A number of concepts were identified for incorporating cooling with integral tanks; they fall into one of two categories:

- (1) Coolant passages integrated with the tank wall
- (2) Coolant passages separated from the tank wall

The first grouping is not applicable to LOX tankage because of coolant freezing, but can be used for cryogenics when internal insulation is employed so that coolant freezing is not a potential problem. The wall thickness dictated by structural requirements would probably permit wider passage spacing if designs are based on the first concept, particularly if the construction material has a high thermal conductivity such as aluminum.

Structural Arrangements for Basic Tank. - The propellant tank consists of seven major elements: the cylindrical portion, the two domes, the two Y-rings, and two skirts that attach to the fuselage structure, Figure 76. The cylindrical portion of the tank is probably best machined from plate. Various types of longitudinal, circumferential, and/or isogrid stiffening can be machined into one side of the plate

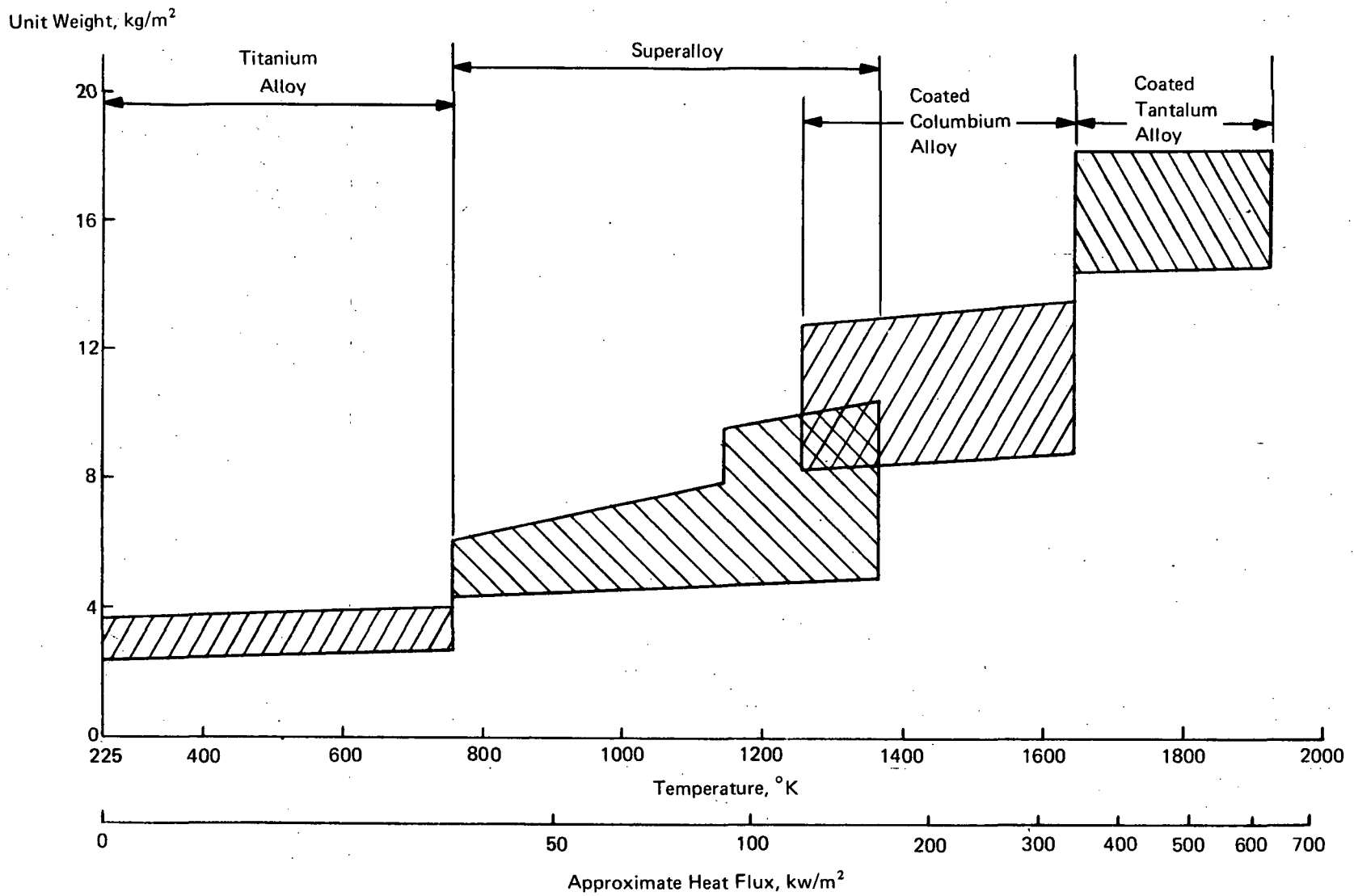


Figure 75a. Unit Weights for Heat Shield and Supports

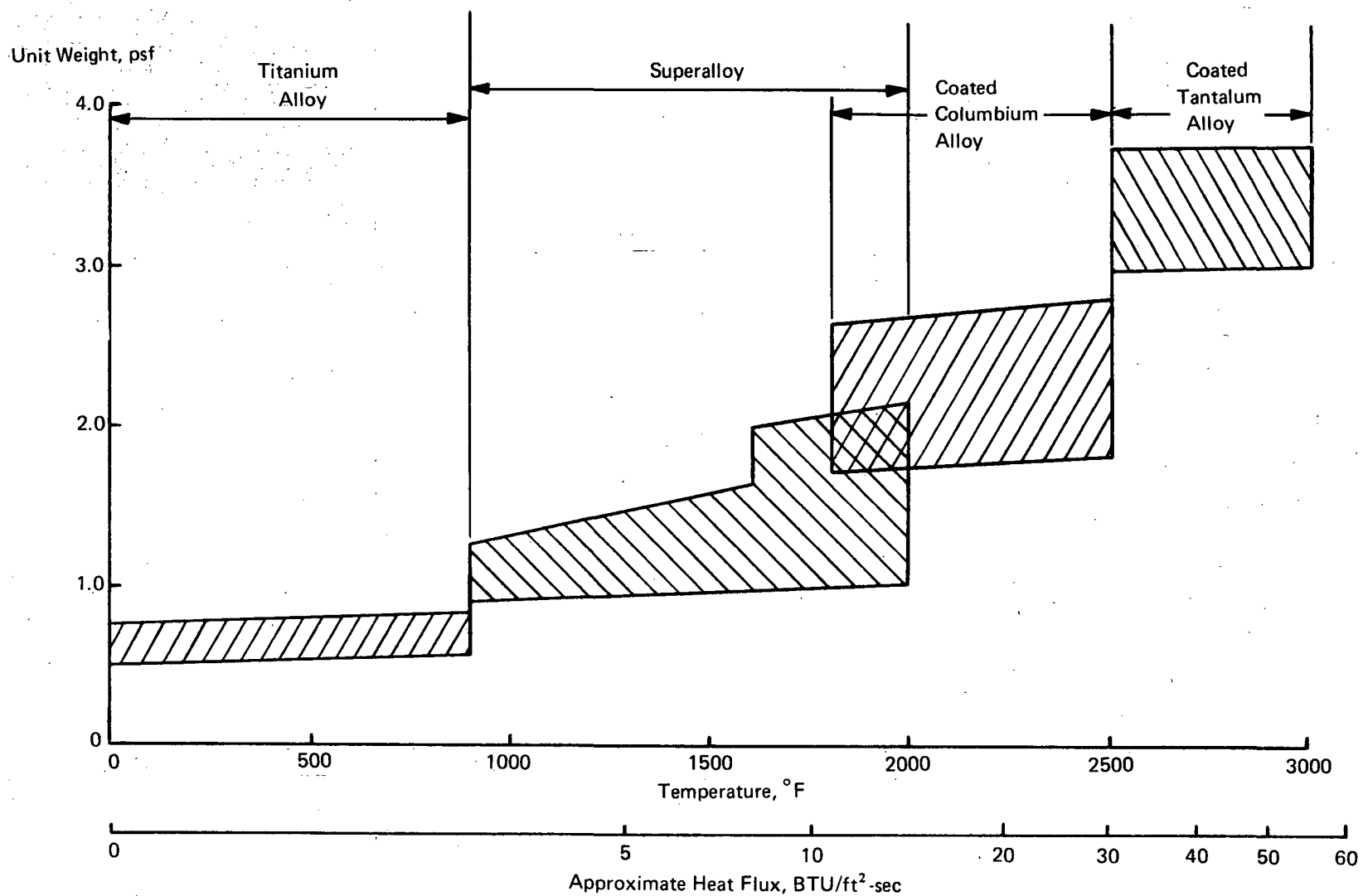


Figure 75b. Unit Weights for Heat Shield and Supports

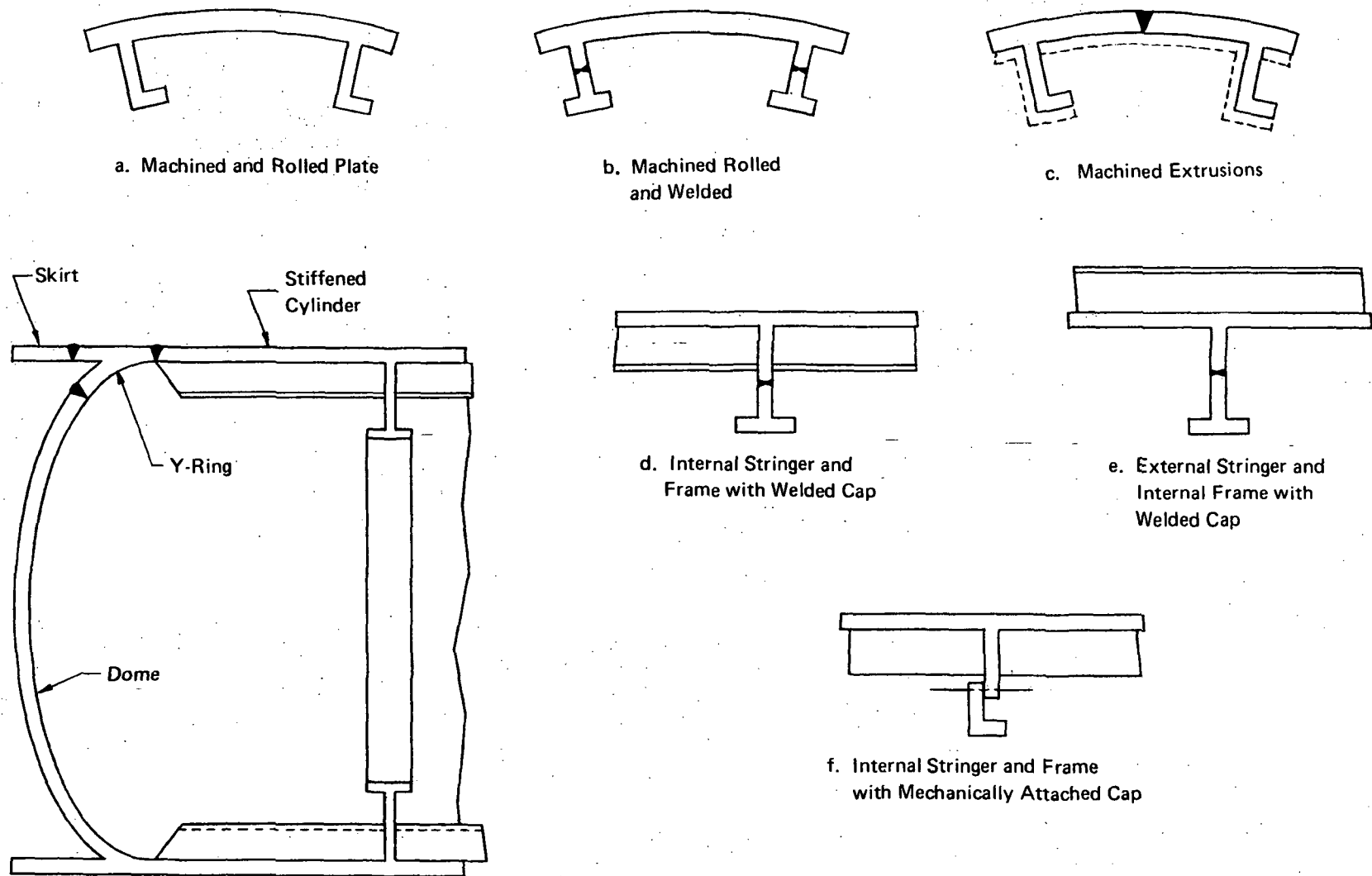


Figure 76. Typical Construction for Integral Tank

while the coolant passage network can be machined into the other side and subsequently covered by a smooth external sheet. The domes, Y-rings and cylindrical portion should be welded together before the cover skin is bonded, brazed, or soldered in place. Once the cover skin is installed welding would probably be detrimental. The fabrication of the cylindrical portion involves the greatest number of alternatives, see Figure 76.

A variety of types of shell stiffening can be considered such as stringers and frames and waffle grid plus frames. The stringers may be plain webs, tees, zeos, or jays. If the welding approach is used for incorporation of stiffeners, machining is reduced quite substantially since the stiffening network on the skins would have plain webs. Consideration might be given to the use of extrusions to minimize the amount of machining (detail C) but this would require a large number of longitudinal welds since the width of extruded plate would be relatively small compared to the circumference of the tanks. Manifold sections might be extruded separately and welded in place. Use of extruded planks would complicate the introduction of external coolant passages, particularly for noncircular cross sections, since the machining of the coolant passages would have to be done after the tank assembly was completed. However, this is possible; manual routing with surface templates offers one possible approach since the depth of the cuts for the coolant passages is small. Regardless of how the stringers are attached, the frames must be joined to the stiffened tank shell by means of welding or mechanical fastening, details D, E and F. The mechanical fastening approach might have advantages in that fit-up requirements may not be as stringent as if welding was used.

The tanks would be assembled by welding using the normal procedures for aerospace tankage. If the coolant passage networks had not been machined prior to welding they would be machined after this first stage of assembly. A final assembly operation would be that of covering the exterior surface of the tank with a skin that would close the coolant passages. For tanks of large size the attachment of this closure skin introduces practical problems. Autoclaves of adequate size may not be available and would be quite expensive to procure. Vacuum bags and heating blankets would eliminate expensive curing equipment but pressures across the joint between the skin and the tank wall would be relatively low thereby necessitating much greater care in providing a good fit between these items.

Stiffener geometries other than plain webs would complicate the installation of interior insulation. However, in some instances structural efficiency may be more important than the cost of installing the insulation. Even when internal insulation is used thermal stresses may be induced in the tanks due to the fact that a temperature gradient will exist from the external mold line surface (which will be slightly below ambient) and the interior flanges of the stiffeners and frames (which will be at a temperature somewhat above that of the cryogenic fuel). The wing support frames will be particularly difficult to integrate and to insulate because of the depth that will be required.

Coolant Passage Integration Into Tank Wall. - The manner in which the coolant passage can be integrated depends upon the details of the tank structure. For those schemes where the stiffening is located internally, coolant passages can be installed on the external surface of the tank with a minimum impact on structural interactions and with a smooth mold line being obtained through the use of cover sheets. Figure 77 illustrates typical coolant passage integration techniques with circumferential and axial orientation of coolant passages on the outside of an internally stiffened tank wall. If the cylindrical portion was machined from plate, the sections of distribution lines used to supply and return coolant from individual tankage panels could be machined into the tankage thereby eliminating a significant

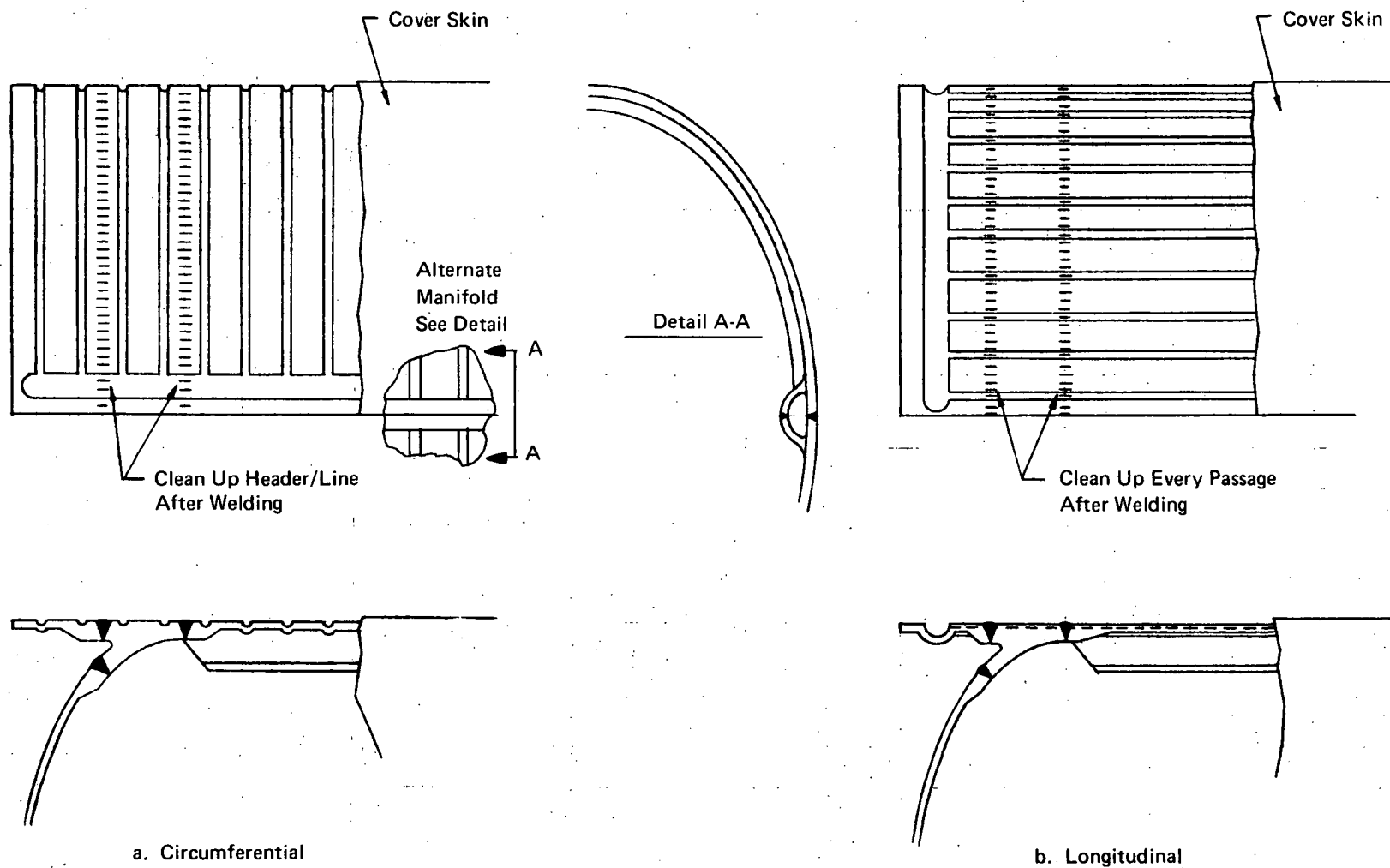


Figure 77. Coolant Passages Machined Into Exterior Tank Wall

number of connectors, see detail A-A. With such an approach, redundancy may be difficult to achieve. One alternative is to incorporate redundancy by providing externally mounted distribution lines. This requires the use of uncooled tunnel structure to cover the distribution lines that would be external to the tankage, Figure 78. By allowing the interior of the tunnel structure to radiate freely to the distribution lines and the cooled tank walls, it should be possible to use superalloy tunnel components for heat fluxes of up to about 39.0 w/cm^2 ($35 \text{ BTU/ft}^2 \text{ sec}$).

Coolant passage depth will depend upon particular design parameters such as flowrate requirements, length of coolant passages, and allowable pressure drops. Where passage depths are quite shallow, chemical milling might be an appropriate technique for material removal. For deeper passages a machining operation similar to milling or the template/router technique might be more appropriate. In either case, it is quite likely that the inside of the tank wall would have to be machined to accommodate the depth of the coolant passage. In order to minimize weight penalties, very close coordination of the interior and exterior contours around the coolant passage must be maintained or excess material must be provided to account for tolerances. One of the disadvantages of machining the coolant passage network after the tank fabrication has been completed is the significant financial loss that would result if the tank is damaged during the final machining operation. This may tend to favor chem milling if the coolant passages are to be cut after the tank has been welded.

Note that inspection may be difficult with the tank wall covered by insulation on the inside and on the outside by the coolant passage cover skin.

The alternative approach of installing coolant passages on the inside of the tank wall, as shown in Figure 79, offers some potential advantages. Machining of notches in the tank wall skin to provide coolant passages is eliminated since the internal cover skin can be formed with the coolant passage pattern. The coolant passage cover skin and the tank insulation are on the same side of the tank wall so that the primary tank wall can be inspected easily from the outside. And, the welded tank shell could act as a pressure containment wall during bonding of the internal cover skin. Unfortunately, there are also some disadvantages. Detection and repair of coolant passage leaks would be difficult when the passages are between the tank wall and the insulation; such leakage may degrade the insulation attachment. Hoop-wise orientation of the coolant passages would require a large number of holes through every stringer and does not appear to be practical. Therefore, longitudinal orientation of coolant passages seems necessary. With this orientation it would be possible to use either short passage lengths between frames or to provide holes through the frames. This latter approach may not be too difficult since the frames might be notched for the stringers anyway. Another possibility would be to use a frame spacing greater than optimum in order to simplify the coolant passage integration even though a structural weight penalty may be incurred. With the interior coolant cover skin approach integration of the manifolding is more complicated. If external tunnels are used the panel connections must penetrate the primary tank wall and will require careful local reinforcement. This may not be too serious; because of the limited number of connections the weight penalty should not be severe. Welding or bonding to the tank wall could be considered.

Externally Installed Cooled Panels. - A majority of the design interactions between the thermal and structural aspects of the propellant tankage can be eliminated by providing external panels that contain the coolant passages but that do not carry primary structural loads. Major advantages of using separate semi-structural cooled cover panels include:

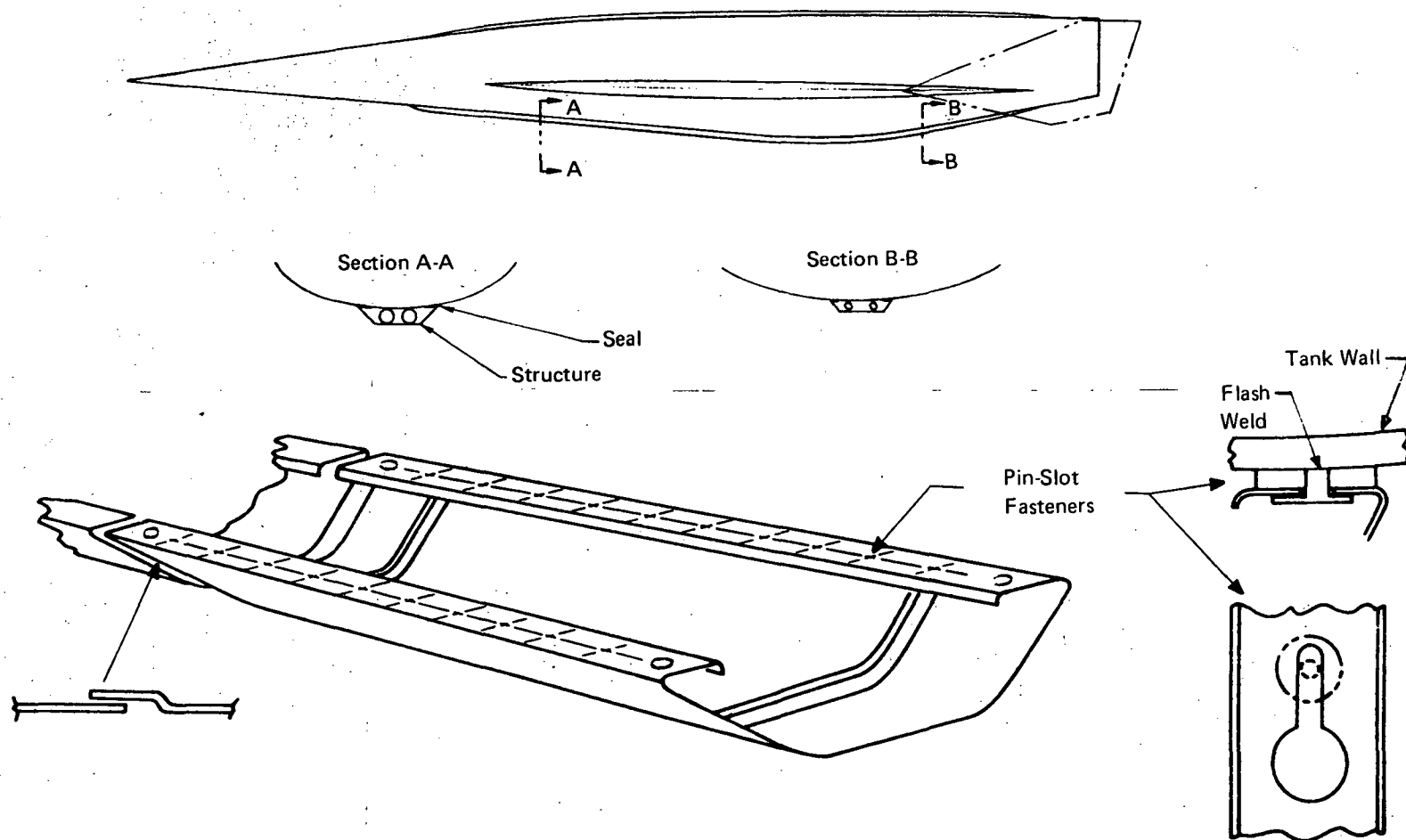
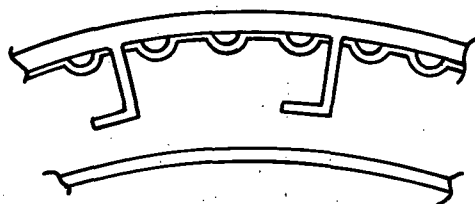
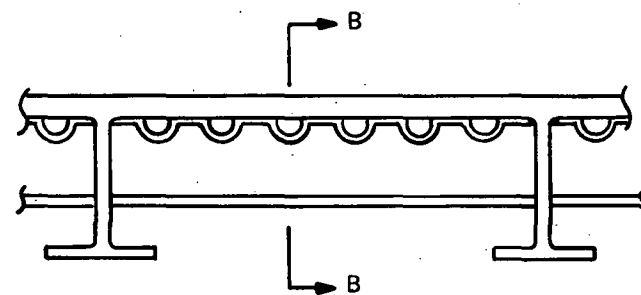
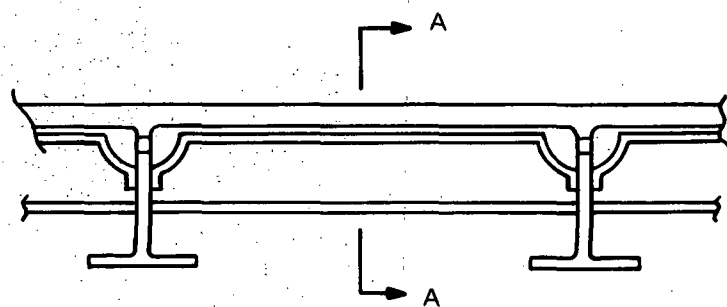
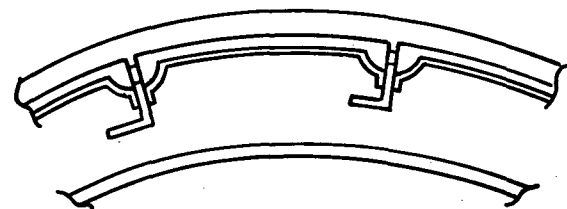


Figure 78. External Tunnel Structure



A-A



B-B

Figure 79. Coolant Passages Integrated on Inside of Tank Wall

- (1) Routing of coolant flow passages without regard to structural arrangement details such as stiffeners, frames, and joints.
- (2) Using different materials for the cooled panels and the load carrying structure.
- (3) Installing coolant distribution lines in the relatively accessible space between the cooled panels and the load carrying structure.
- (4) Reducing thermal stresses in primary load carrying tank wall.
- (5) Simplifying maintenance of cooled panels, such as replacement rather than repair.

Disadvantages include:

- (1) Increased weight associated with the semi-structural cooled panel, its attachments, in addition to the structural skin.
- (2) Need to remove the cooled panels to inspect the primary structure.
- (3) Higher cost because of additional parts.
- (4) Possible high local heating of primary structure due to flow of hot boundary gas around the edges of the cooled panels and into the space between the panels and the structure.

One approach for installing cooled structural panels on the integral tankage is to provide some type of wrap-around skin that fits tightly around the tank wall, Figure 80. Tunnels are required for the distribution lines and they could cover the latch-like attachments required to hold the individual cooled skins against the tank wall. A system design that permits the distribution lines to be nested in the wing root might be desirable.

Such a pretensioned skin with integral coolant passages could be pulled snugly against the tank wall in regions of relatively high curvature, but where large flat surfaces occur, local pressure distributions may result in the tendency to pull the cooled cover away from the tank walls in much the same manner as a very small transverse load will cause a tensioned string to sag. This type of deformation can be eliminated by providing small vent holes between coolant passages to prevent a pressure differential across the wrap-around cooled cover, but might cause gas flow between the cooled wrap-around skin and the tank wall which may cause an increase in local heating. The vents and gaps that occur between the wrap-around and the tank wall due to the finite height of the coolant passages may trap water, and, the vents might influence drag. Whether the drag change would be an increase or a decrease is difficult to ascertain since flow into one area would imply egress at another so as to constitute a boundary layer bleed in some regions and a transpiration effect in others.

A variation of the separate cooled skin approach is illustrated in Figure 81. Here, the integrally stiffened tank shell has external stringers and internal rings. This arrangement increases structural efficiency, simplifies the installation of the internal insulation, and permits a relatively simple installation of the cooled external skin. Machining of the plates is simplified since all machining cuts on one side

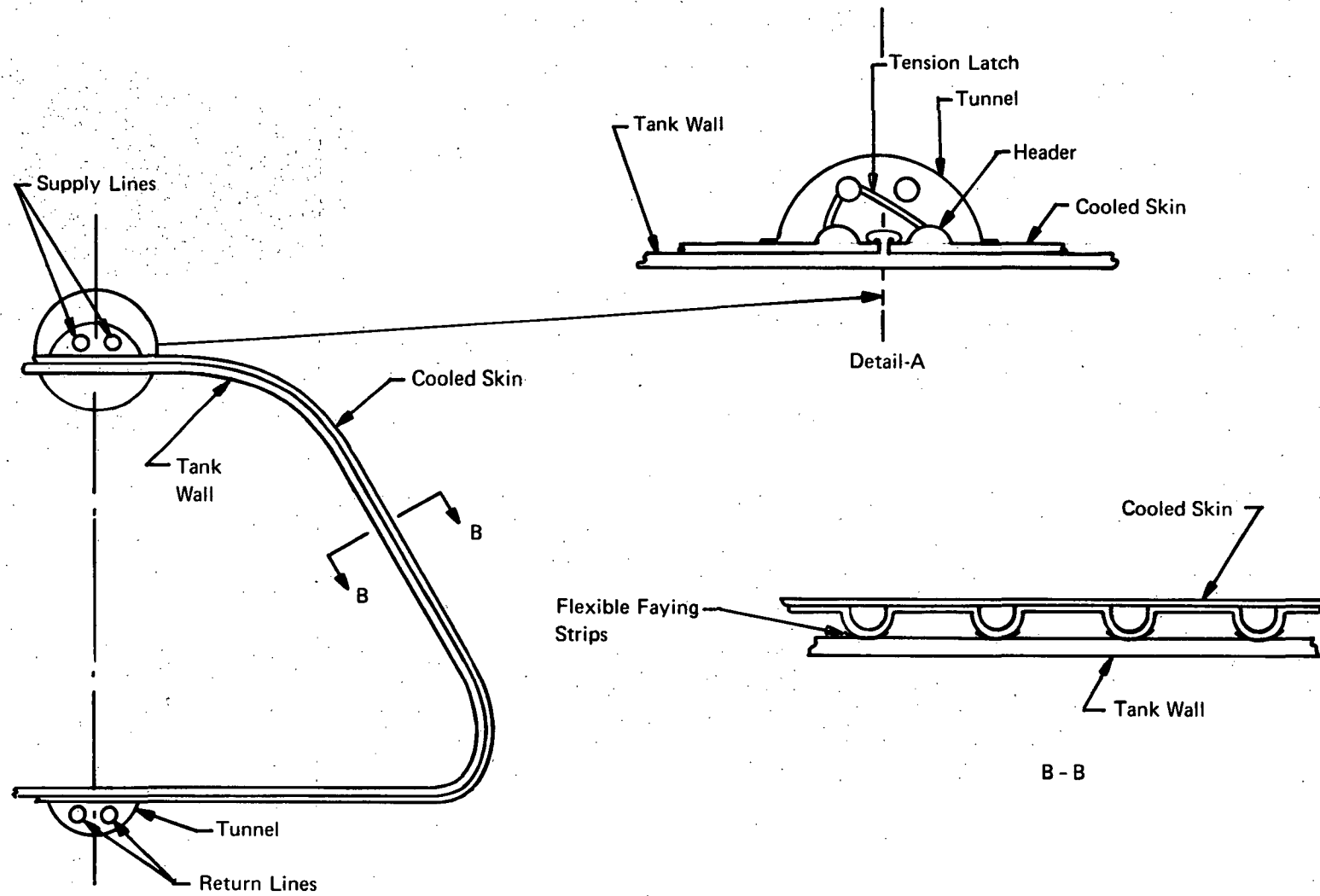


Figure 80. Wrap Around Cooled Skin

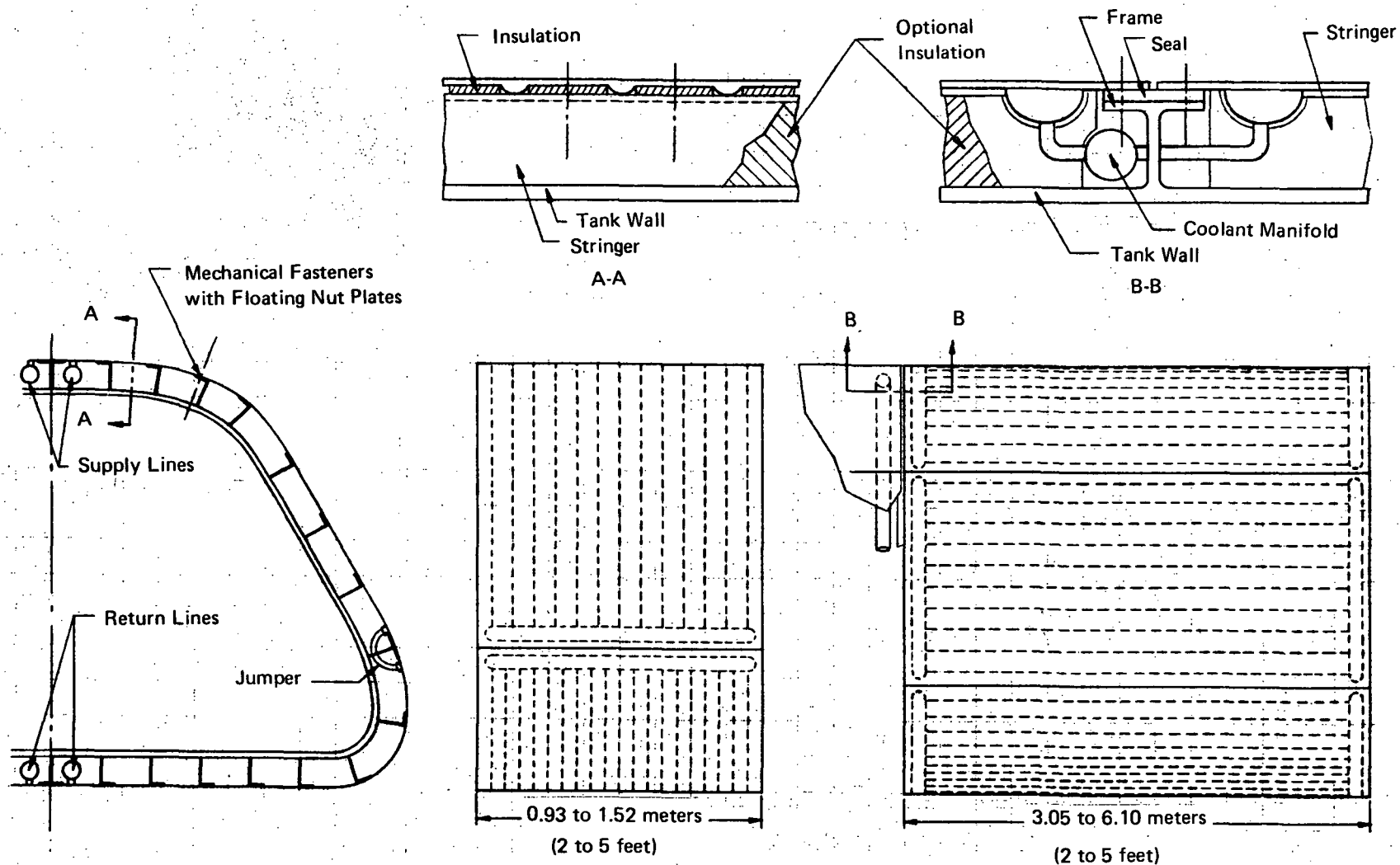


Figure 81. Actively Cooled Heat Shields

can be made in one direction and all those on the other are orthogonally oriented. The skins can be made to share load with the tank wall or can be essentially semi-structural depending upon the attachment technique used between the cooled skin and the tank stiffeners. Axial thermal stresses in the tank wall are reduced because the longitudinal stiffeners are not buried in the cryogenic installation. However, the thermal stresses in the frames may be relatively high.

This design approach reduces the usable volume within the tank. The loss could be reduced by installing the insulation, or at least some of it, between the tank wall and the cooled skin. However, this would increase thermal stresses. An advantage of installing the insulation between the tank wall and the cooled skin is the ability to inspect the inside surface of the tank which cannot be done with internal insulation and an external cooled skin. For LOX tankage, the thermal insulation would be placed in the cavity formed by the tank wall, the stringers, and the cooled panel. The cooled panels would be thermally isolated from the LOX tank by insulating strips along the flanges of the stringers. Sealed closed cell plastic foam could be installed on the exterior of the LOX tank to avoid frost buildup. If frost buildup is not considered to be a problem, a relatively thin layer of thermal insulation attached to the inside of the cooled external panel should prevent freezing of the coolant. Reference 50 examined this problem.

An alternative to the externally installed cooled skin panels is a sandwich tank wall construction with the inner face being the tank wall and the outer face being the cooled skin. Aluminum alloy or plastic core could be considered depending upon thermal and structural tradeoffs. This sandwich approach might eliminate longitudinal stiffeners with a substantial reduction in the cost of fabricating the tank. The bending rigidity of the sandwich concept would be particularly helpful in noncircular regions of the tank. In common with the other separate cooled skin approaches, the sandwich concept eliminates the need for cutting coolant passages into the tank walls. Figure 82 illustrates some details that might be used for the design of a double wall sandwich tank. The tank is assembled by welding in a normal fashion. The Y-ring elements contain an offset leg to permit installation of the sandwich core. It should be possible to adhesively bond the core to the tank wall by means of vacuum bags and heater blankets without the need for an autoclave cure since the surface to bond area ratio is about 50. The coolant passage patterns could be cut into the core either before or after the core is bonded to the tank wall. Prior machining of the grooves is a relatively simple operation which can be done on flat slabs, perhaps even before the core is expanded. However, with this approach allowances must be made for tolerances associated with core expansion and fit-up. A primary advantage of premachining the core is that the core can be bonded to both faces of the sandwich in one operation. The alternative approach of bonding the core to the tank wall and then to machining the coolant passage slots minimizes tolerance and fit problems but introduces a second bonding operation.

Connection Concepts

Design Considerations. - The airframe cooling system consists of a network of piping that connects the skin panels of the airframe with major system elements such as the pumps and heat exchangers so that the absorbed aerodynamic heat input can be rejected. Within this network, the lines must be joined to one another and attachments must be made between the lines and skin panel. Considerations for the design of such connections include pressure capability, induced bending, resonance, differential expansion, initial installation, maintenance and repair, and reliability. An extensive technology base is available from hydraulic and fuel system applications for adaptation to the cooled airframe application. Of particular importance are flexible connections designed to accommodate differential expansion, mechanical connectors that can be disconnected with relative ease, and methods of attaching coolant flow lines to the cooled panels.

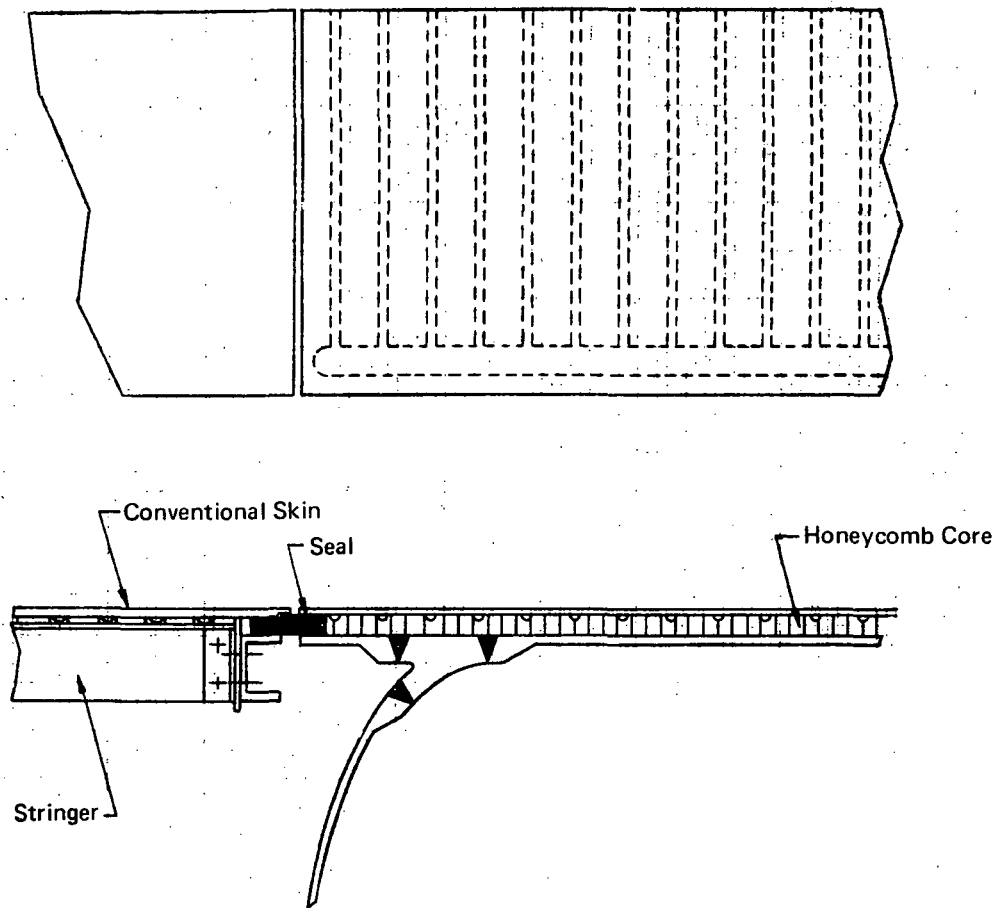


Figure 82. Actively Cooled Sandwich Tank

The cooled airframe is expected to operate properly through the environmental temperature range of 220°K (-65F) to 350°K (165F). Installation of the hardware will take place in a factory at 290°K (60F) to 300°K (85F). Under normal operating conditions, the coolant inlet temperature is likely to range from 256°K (0F) to 283°K (50F) while the coolant outlet temperature may range from 350°K (175F) to 380°K (225F) for aluminum alloy construction. Therefore, a temperature difference of as much as 834°K (150F) might be expected. For a line length of 25.4 m (1000 in.) this represent a length change of ± 5.0 cm (2 in.). Under operating conditions the temperature differences between the distribution lines and the structures from which they are supported are likely to be about 310°K (100F) so that relative length changes would be about 3.5 cm (1.4 in.) per 25.4m (1000 in.) of length. Even for very long line runs it should be possible to simply allow the relative motion between the lines and the structure and to accommodate the differential expansion in the connections between the distribution line and the skin panels. The alternative is to anchor the distribution line at intervals and to provide expansion joints between the anchors. While this will reduce the amount of differential expansion to be accommodated by the distribution line-to-panel connection details it does not eliminate the relative motion unless an expansion joint is provided between each set of panel connections.

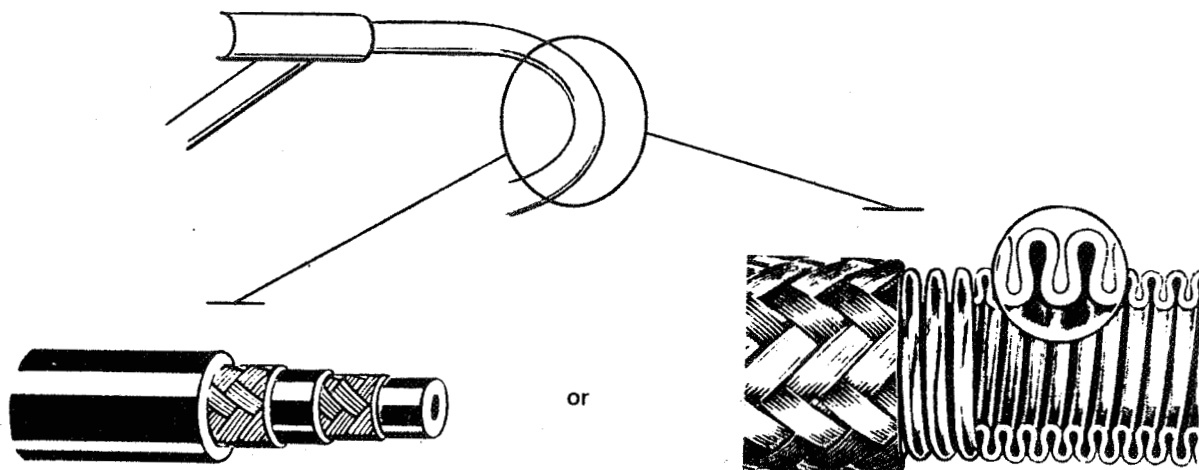
A review of expansion joint designs indicates three general possibilities, all of which have disadvantages: (1) loops, (2) bellows, (3) sliding sleeves. Swivel fittings are not permitted for aircraft hydraulic systems that must conform to MIL specs, without specific approval by the procuring agency. Where repeated, thermal expansions and contractions must be accommodated the length of the expansion loop must be at least 20 diameters to accommodate one diameter of deflection at a stress level that would be consistent with essentially infinite life. Based on representative temperature differences and distribution system proportions the differential expansion to be accommodated ranges between one diameter and 1/3 of a diameter. For a line diameter of 6.2 cm (2.5 in.) and a differential expansion of ± 3.0 cm (± 1.2 in.) a length to diameter ratio of about 15 would suffice, a loop length of about 90 cm (35 in.). Slip joints provide an alternative means of reducing relative deformation effects but such designs are used primarily for low pressure systems and where leakage would not constitute a significant problem. Metallic bellows provide the most practical means of accommodating differential expansion but the allowable relative motion compatible with long life is approximately 20% of the bellows free length. For ± 3.0 cm (1.2 in.) of differential expansion a free length of approximately 15.3 cm (6.0 in.) is needed so that the total bellows installation would be approximately 20.2 cm (8.0 in.) including end pieces. The outside diameter of a bellows tends to be about 1.5 times the line diameter and if high pressures are to be used guides are usually employed to control convolute deformation and to restrict total deformation. These guides and restraints can constitute a significant weight item.

Thus it appears that the various techniques for accommodating differential expansion are all quite unattractive when applied to lines of large diameters. If the differential expansion is accommodated at small lines such as those between the major distribution lines and the panel connectors, the size and weight of the piping installation will be minimized. Allowing the distribution line piping to expand freely is not difficult to accomplish. The network would be anchored at the point of the fore and aft split of the coolant flow and the other line supports would be of a roller type or equivalent. These supports could be located as required to minimize bending stresses in the distribution lines and to control the distribution line natural frequency. Even for very long runs of piping, as might be expected in a hypersonic transport, where relative expansion differences may be as much as 13.0 cm (5.0 in.) the axially unrestrained piping installation should be satisfactory.

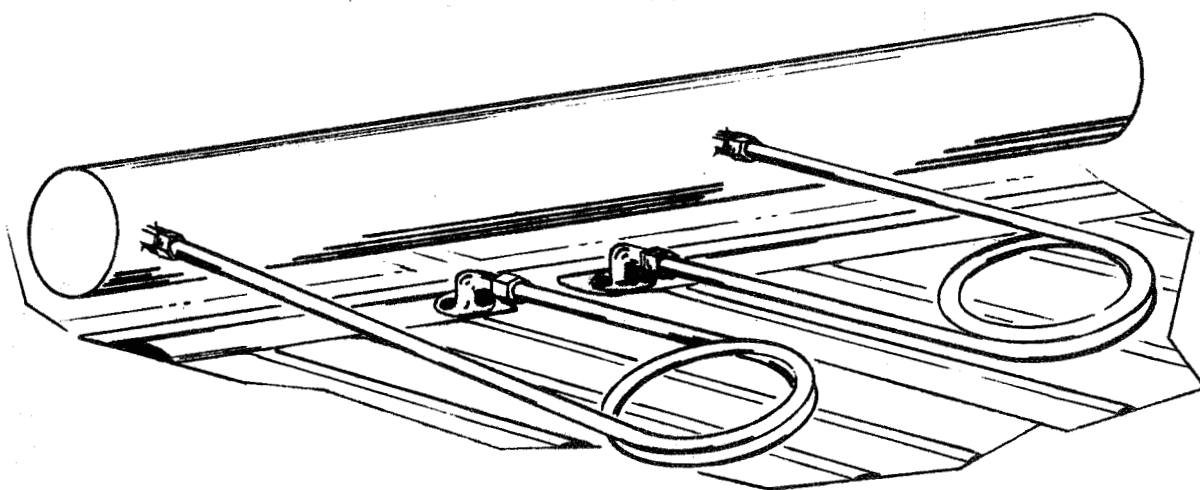
Primary Lines.- The connections within the primary line network could be made by welding, brazing, adhesive bonding, or by mechanical means. It is expected that the distribution lines would be assembled into an airframe structure during final assembly so that access would be attainable internally and externally with respect to the mold line. While this may preclude installation of completely preassembled lines large sections could be preassembled. It seems unlikely that torch welding would be done when the piping is within the airframe structure. However, if the piping material can be welded without the use of filler material, the Astroarc welding process can be applied. The successful use of 2021 or 2219 aluminum alloys, or stainless steel, are within the present state-of-the-art. The successful use of titanium alloys depends upon the ability to shield adequately. The practicality of brazing also depends upon the particular alloys used for the piping. The brazing approach is not particularly attractive for aluminum alloys because of the difficulty of removing flux. Soldering can be considered but the flux removal problem remains. Adhesive bonding and mechanical joining are least influenced by the choice of piping materials. For adhesive bonding careful consideration must be given to the details of the joints so that complete bonding is achieved. For mechanical joining bolted flange or Marman-type clamps can be considered. The latter approach is lighter and available designs are suitable for system burst pressures in excess of 6.9 MN/m^2 (1000 psi) for line diameters up to 30.5 cm (12 inches).

Primary Lines to Panels.- Connection of the skin panels to the main distribution lines can be accomplished by means of flexible hose, either metallic or non-metallic, by metal tubing whose geometry permits accommodation of differential expansion, or by incorporating a bellows section into the line, see Figure 83. Flexible metal hoses are available as commercial items up to 5 cm (2 in.) in diameter being suitable for pressure in excess of 6.9 MN/m^2 (1000 psi). For application involving intermittent flexing, the bend radius of the flexible hose should be about 10 times that of the hose diameter. Since the hose diameters for cooled structural skin panels are expected to be in the range from 0.6 cm to 2.5 cm (0.25 in. to 1.0 in.), depending upon vehicle flight conditions, the presence or absence of external thermal protection, etc. a modest amount of space is required for the installation. The non-metallic flexible hoses are available as commercial items also. Burst pressures exceed 6.89 MN/m^2 (1000 psi) for 5.0 cm (2.0 in.) diameter hose when only a single metallic reinforcement is used. The addition of more metallic braid reinforcements will increase burst pressure and the bend radius, (about 6 diameters for single braid reinforcement, about 10 for double braid reinforcement, and about 13 for triple braid reinforcement). Thus, as compared to the flexible metal hose, the nonmetallic hose offers no outstanding advantage other than reduced pressure drop. Its major disadvantage is that it tends to be susceptible to handling damage, particularly severe bending or collapse of the tube wall which may damage the braid in a manner that is not easily detected.

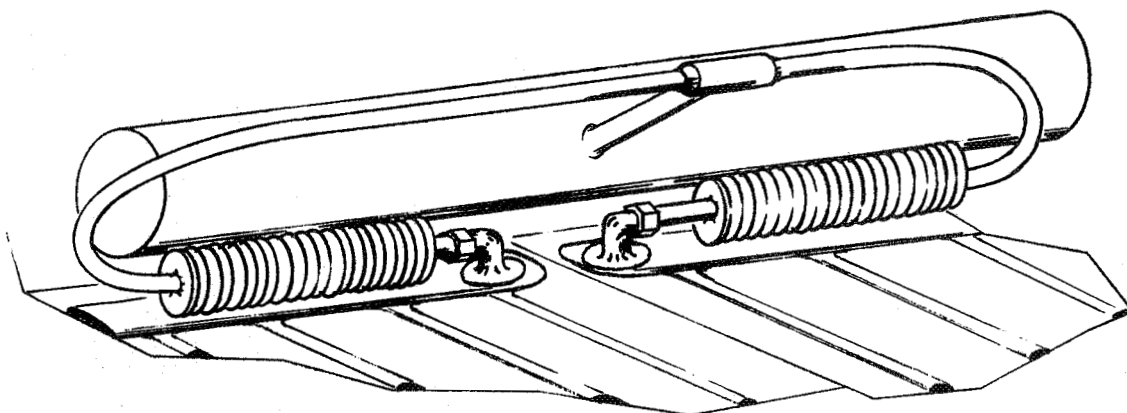
The general specification for hydraulic systems, MIL-H-5440 specifies the use of metallic tubing. Where differential expansion considerations are important, the type of configuration shown in Figure 83 b is recommended. The bend radius is approximately 4 times the tube diameter while the distance from the tubing connections to the center of the helix varies from 7 to 12 times the diameter with the largest factor associated with the smallest tubing. Thus, not only does this design approach offer a more reliable installation than flexible hoses, the installation is somewhat more compact. A further advantage is the higher stiffness of the tubing such that its natural frequency will be higher, and the adaptability of the helix to snubbing which would dampen adverse vibration tendencies. The bellows approach illustrated in Figure 83c is the most compact approach but is nonstandard and will undoubtedly be more expensive than the more conventional concepts. For the small sizes, associated with the lines from the distribution piping to the panels, pressure ratings should be no problem.



a. Flexible Hose



b. Coiled Tubing



c. Bellows

Figure 83. Concepts for Connecting Distribution Lines to Skin Panels

It is likely that mechanical fastening will be desirable in the piping, most probably near the cooled structural panels and near items of equipment that might need replacement. Figure 84 presents representative designs; types a and b are covered by military specifications for hydraulic and fuel systems. The other two designs are used in commercial applications. Leakage is a common problem with mechanical connectors but this problem is offset by the utilitarian advantages of mechanical joints.

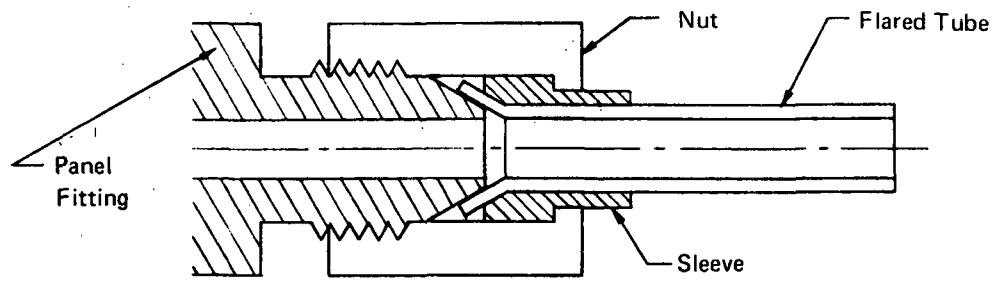
Panel Connectors.- The final type of connection to be considered is that made between the cooled skin panel and the fitting to which the flexible hose, tubing, or tubing/bellows piping is attached. The connector shown in Figure 85a is machined from a forging or from barstock. A prolongation of the fitting, with a rubber grommet located around the outside diameter is inserted into the hole of the header. A gasket is used as a secondary seal on the interface between the header passage and the outside face of the connector. A special tool is inserted through the connector and the protrusion is flared over and pulled tight on the inside surface of the header passage. A special tool is used for this operation in which the flare is formed by pulling down on an off-center L-shaped anvil. As this anvil is rotated, a nut on the expander is gradually tightened pulling the expander against the part thereby flaring it in place. This connector features two sealing surfaces in series to provide a double redundancy. However, it is impossible to remove the connector from the header without destroying the connector and getting chips into the coolant passages. Riveting and/or adhesive bonding eliminate loadings on the seals.

A more serviceable connector is shown in Figure 85b; Sealing is obtained by the pressure exerted between the faying surface of the connector and the header. The threaded ferrule is inserted into the hole of the header (the outside diameter of the flange on the ferrule is smaller than the inside diameter of the hole in the header). A split washer is threaded onto the ferrule and through the hole in the header passage. The primary portion of the connector is then threaded onto the ferrule which, in turn, is prevented from twisting by an Allen wrench inserted through the connector. The primary portion of the fitting contains two O-rings in series thereby achieving a redundant seal. A nylon insert is contained in the ferrule and provides a locking feature. To remove the connector from the header, the rivets are first drilled out and then the connector body is unscrewed. A pocket knife, or similar tool, is used to flick the washer end out and to start threading it back over the sheet. The ferrule then slides out easily. This particular connector design was patented by Bell Aerospace Company in the early 1960's.

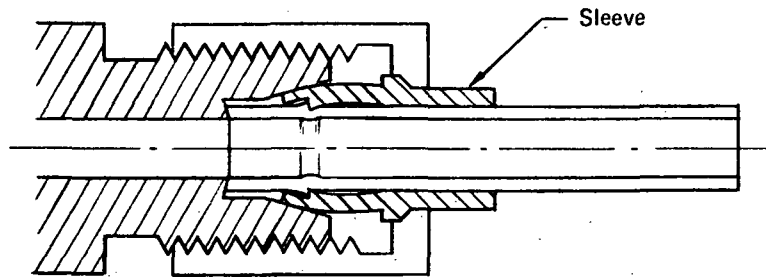
If the construction material of interest can be brazed or welded, a number of other possible connector design approaches can be considered, such as those shown in Figure 86. Figure 86a illustrates a concept assembled by brazing a machined internal member and a machined or drawn external sleeve. The two concentric elements of the fitting are of different major diameters to provide a gradual stiffness change from the header to the fitting. Two joints must fail before leakage occurs. A somewhat similar design that combines welding with brazing or adhesive bonding is illustrated in Figure 86b. The external sleeve provides redundancy and increases the area over which fitting loads are dissipated.

Control Surface Concepts

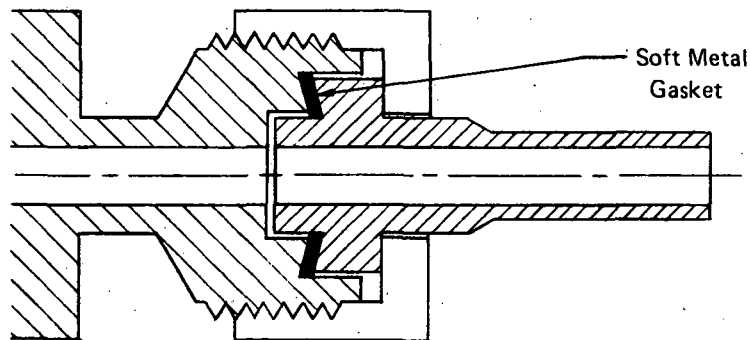
The complex flow fields in the vicinity of deflected aerodynamic control surfaces cause heating conditions that will require special attention to the design details for the applicable thermal protection system. Local incident heat fluxes are related to local pressure and velocity characteristics; these in turn are related to altitude, velocity, angle of attack, surface deflection angle, type of flow,



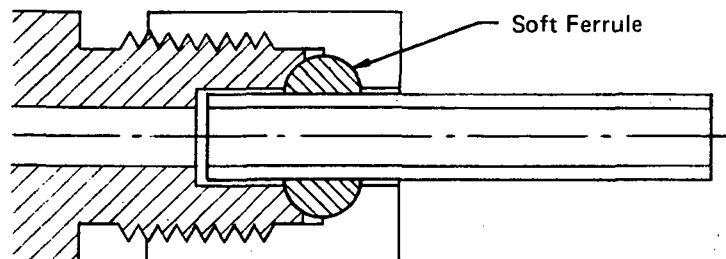
a. Flared



b. Flareless

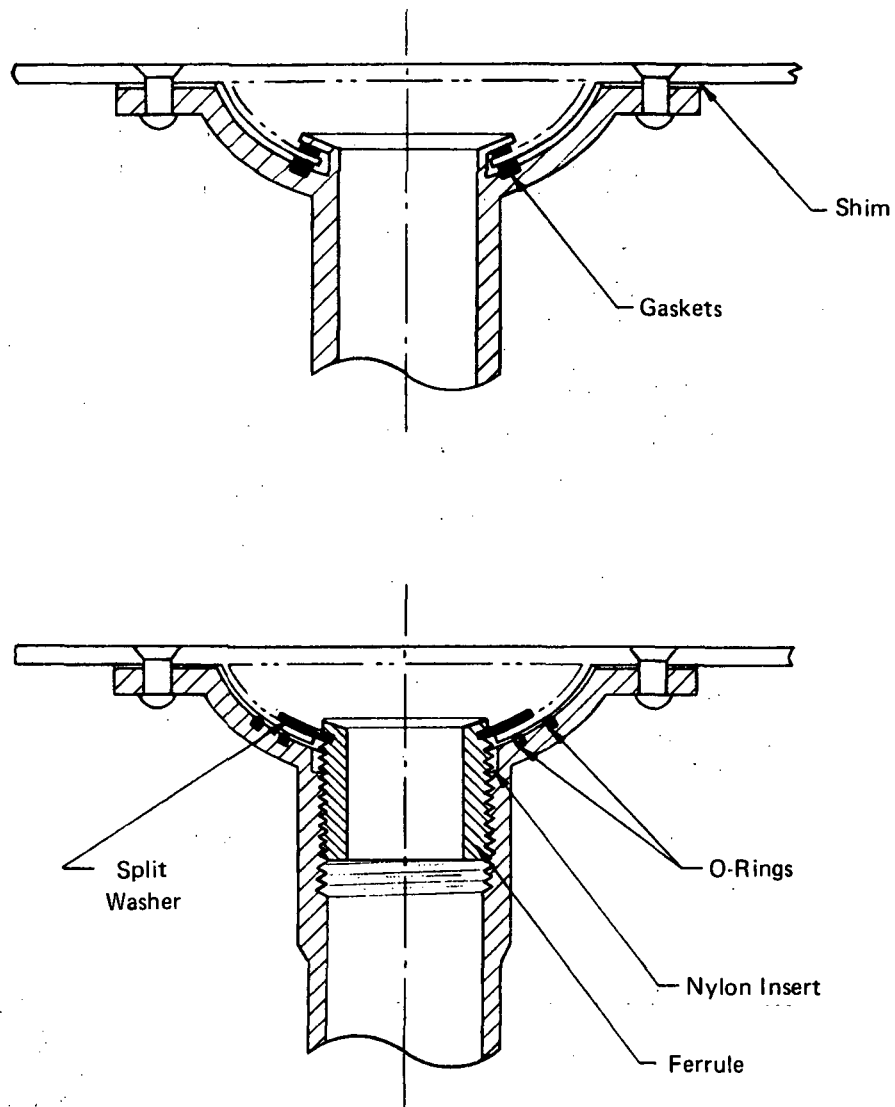


c. Marman Conoseal



d. Compression

Figure 84. Fitting Concepts



Patent Held by Bell Aerospace Company

Figure 85. Mechanically Attached Connectors

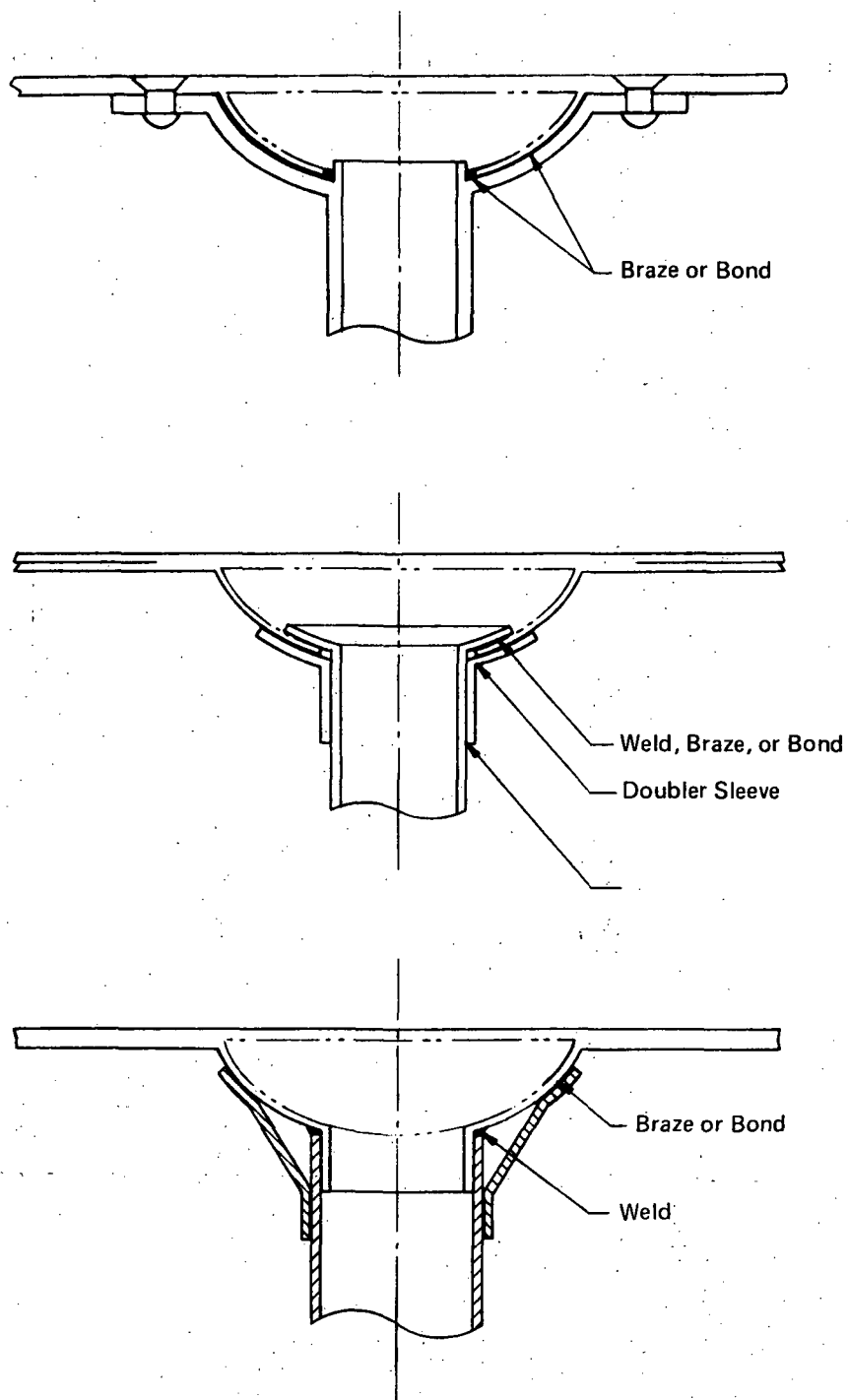


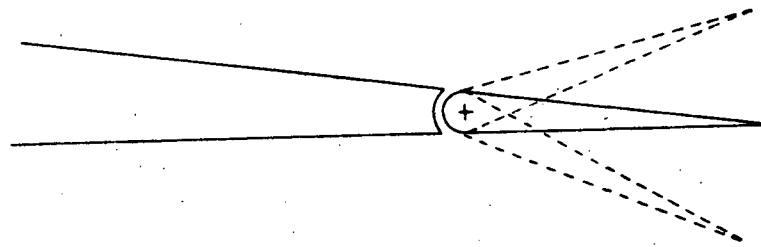
Figure 86. Metallurgically Attached Connectors

flow separation and reattachment, flow interference, flow reversal, and flow through the hinge line region, References 51 and 52. Under some circumstances the peak heat flux on the control surface might be greater than at the stagnation line. Recognition of high local heat fluxes is important in establishing candidate concepts for the control surfaces of hypersonic aircraft. The difficulty in identifying exact locations of maximum heating coupled with the high levels expected are likely to dictate design arrangements that feature closely spaced coolant passages (such as plate-fin or sphere-core sandwich construction) or techniques which attenuate the heat load to the cooled structure. Based on such design considerations, some cooled control surface concepts were identified and their relative merits and problem areas are discussed qualitatively.

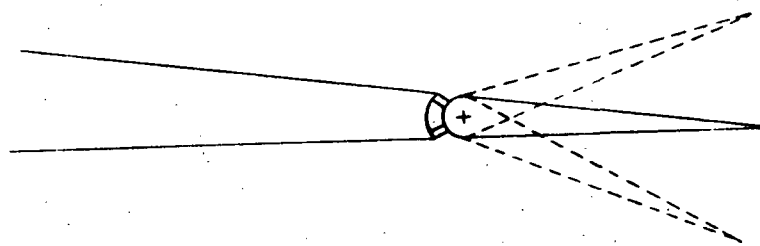
The two concepts shown in Figure 87 are similar to current control surface design practice. In addition to the flow separation and reattachment problems, the first design concept permits the flow of hot boundary layer gas between the fixed and movable aerodynamic surfaces. The second variation introduces seals across the gap so that flow cannot occur. The presence of the seal is likely to increase control forces since seal friction must be overcome. Assembly tolerances would have to be carefully controlled to insure an adequate seal. With a carefully designed actively cooled holder for the seals it should be possible to avoid excessive seal temperatures. A pressurized liquid cooled seal may reduce tolerance requirements as well as avoiding excessive temperature.

Figure 88 shows three arrangements that use metallic sheets to seal the cavity between the fixed and movable portion of the aerodynamic surface. The upper sketch employs extension of the skins from the movable surface as sliding seals. The high degree of flexibility required of these skins might be difficult to achieve when coolant passages must be incorporated. This complexity could be removed by introducing a spray cooling system for the sliding seals. The high heat of vaporization and high boiling heat transfer coefficient of water make it the ideal expendable coolant. The steam generated could be vented through slots to provide a degree of transpiration cooling for the movable surface thus reducing the heat load to the convective cooling system. The second sketch is a similar design but the metallic seals are extensions of the skins from the fixed surface. Note that with this approach the rear spar can be farther aft which is desirable. If spray cooling is employed, superalloy seals might be used. The third design utilizes an essentially continuous skin along the lower surface such that a portion between the fixed and the movable aerodynamic surface acts as a flexure plate. An uncooled high temperature metal seal might be used along the upper surface since the upper surface of the wing is an expansion area subjected to only modest heat fluxes even when the control surface is displaced. Should heating of this upper seal be a potential problem, the spray cooling technique could be employed. Obviously, control forces would be substantially greater than for conventional control surfaces which are mounted in bearings. Even a relatively thin cooled skin would introduce a significant resisting moment. In addition, wing deformation could have a serious effect on the stiffness of the flexural joint; imagine trying to bend the flexure plate when the wing shape was curved due to a high positive load factor.

Another concept is shown in Figure 89. Here, a hinge is incorporated along the upper surface but the actively cooled structure forms only the upper surface of the movable control. The lower surface is a superalloy or coated refractory metal, depending upon the heat flux. In basic concept this approach is similar to the radiation shield attenuator discussed previously. The lower surface material



a. Unsealed Gap



b. Sealed Gap

Figure 87. Control Surface Concepts, "Conventional"

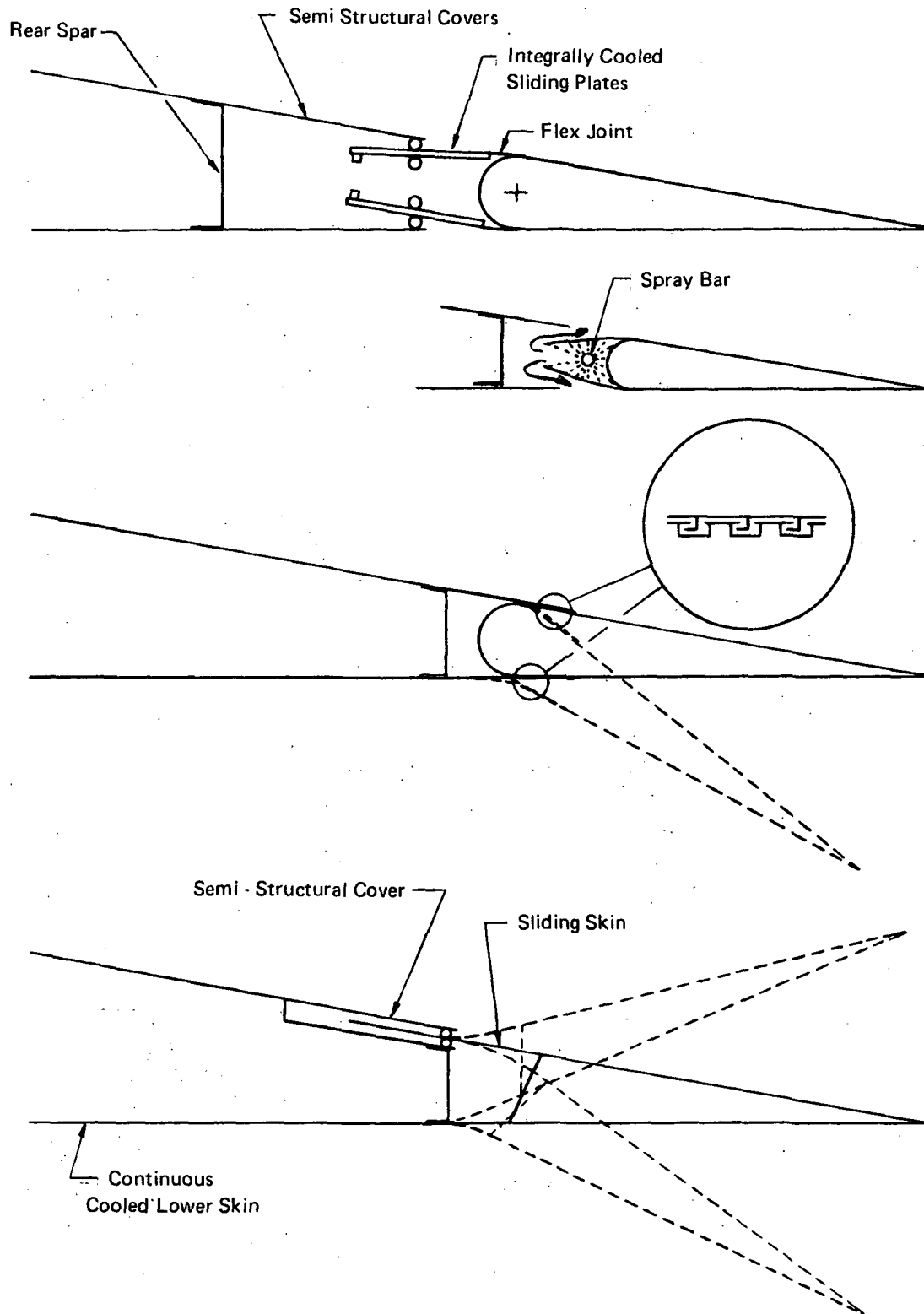


Figure 88. Control Surface Concepts, Metallic Seals

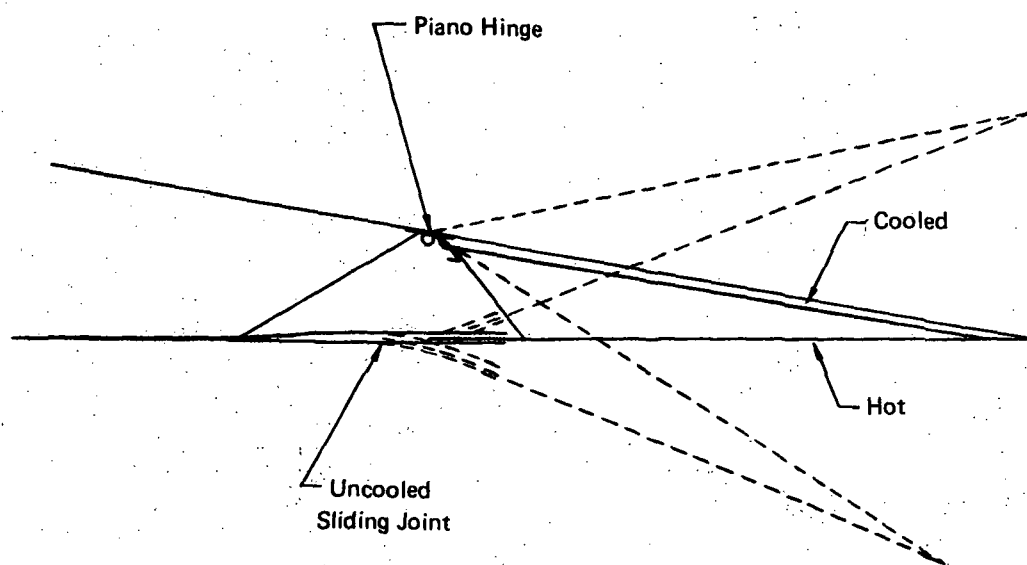


Figure 89. Heat Load Attenuated Control Surface Concept

radiates both to space and to the cooled upper skin. By painting the inner surface of the cooled skin black the effective thermal emittance of the hot skin is practically doubled. Thus, the radiation equilibrium temperature of the hot surface is substantially less than would be the case for an adiabatic surface or even for an uncooled movable control surface where the lower skin is free to radiate to an uncooled upper skin. In addition, the heat load to the cooled skin is lower than would be the case if a cooled lower skin was used.

In all the designs discussed, the movable control surface problem has been considered in a two dimensional sense. Reference to Figure 90 suggests that the flow field complexities at the sides of a movable control surface may induce severe local heating effects. It seems unlikely that such slits could be sealed; an alternative might be to round the edges of both stationary and movable surfaces in the vicinity of the slit. Still another technique might be to avoid end slits completely by allowing the movable control surface to blend out from the fixed surface in a gradual manner. Some control effectiveness will be lost but edge heating problems should be reduced.

The means of actuating control surface motion is of importance also. For tail surfaces it is possible to employ linear or rotary actuators located within the tail cone of the fuselage. The shallow depth near the trailing edge of wings may reduce the efficiency of such approaches; when coupled with higher torques due to sealing this will increase actuator forces and weights. Since the upper surface of the wing is an expansion region of relatively low heating, current actuation techniques can be adapted to the upper surface rather than to the lower. Somewhat larger fairings may be required but the increased size should be offset by reduced heating and smaller actuators.

Doors

One concern with the use of cooled airframe structure is that of incorporating the many doors required for various access purposes; they will complicate the design and impose a weight penalty. Therefore, a concerted effort should be made to minimize the number of doors required even to the extent of influencing the internal arrangement of equipment. For example, it would be highly desirable to locate as much equipment as possible adjacent to the wheel wells in order to avoid a larger number of small doors. It may even be desirable to provide short crawl spaces which can be entered from the wheel wells and which extend slightly into the airframe so as to increase the airframe volume accessible.

With respect to the doors themselves only a small effort was expended to be sure that design problems were not insurmountable. Figure 91 illustrates two concepts, one for a small access door and the other for a relatively large door, such as might be appropriate for a wheel well. If the door is small enough, a single serpentine coolant passage can be provided. Note that both the inlet and outlet are close to the hinge line to minimize the amount of flexible hose required to connect from the main skin to the door. A similar inlet and outlet manifold location is used for the large doors although this will require careful design of the coolant circuit within the door since the flow length through each passage is of different length. The presence of a door is likely to require some modification in that portion of the coolant passage network which is intercepted by the door. Similarly, the presence of the coolant passages is likely to introduce a design constraint on door configuration and location. Few, if any, round doors are likely to be employed in a cooled airframe structure because such a configuration tends to conflict with the straight line nature of the coolant passage run, regardless of whether a tubular, plate-fin or cooled stiffener approach is used.

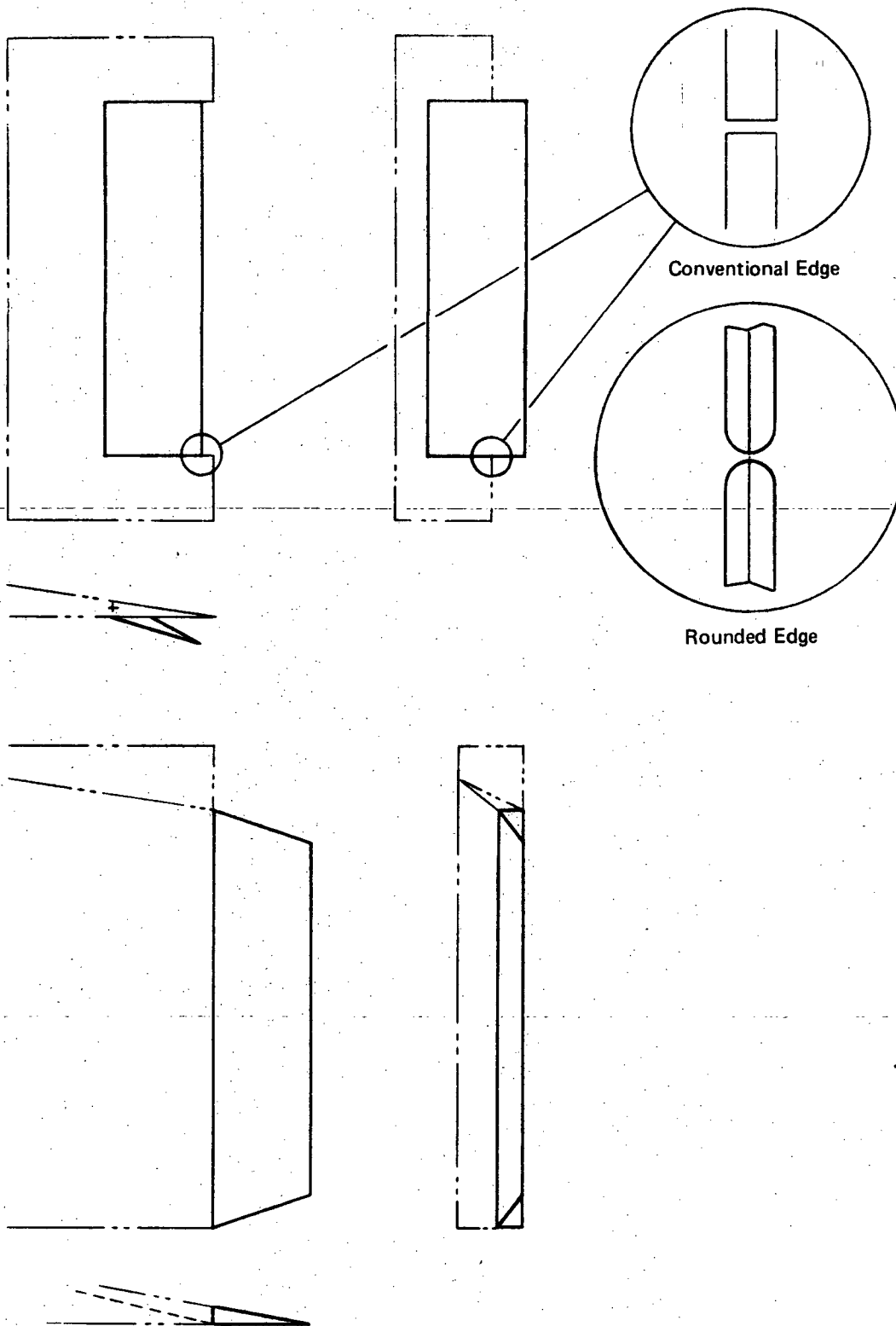


Figure 90. Extended Control Surface Concept

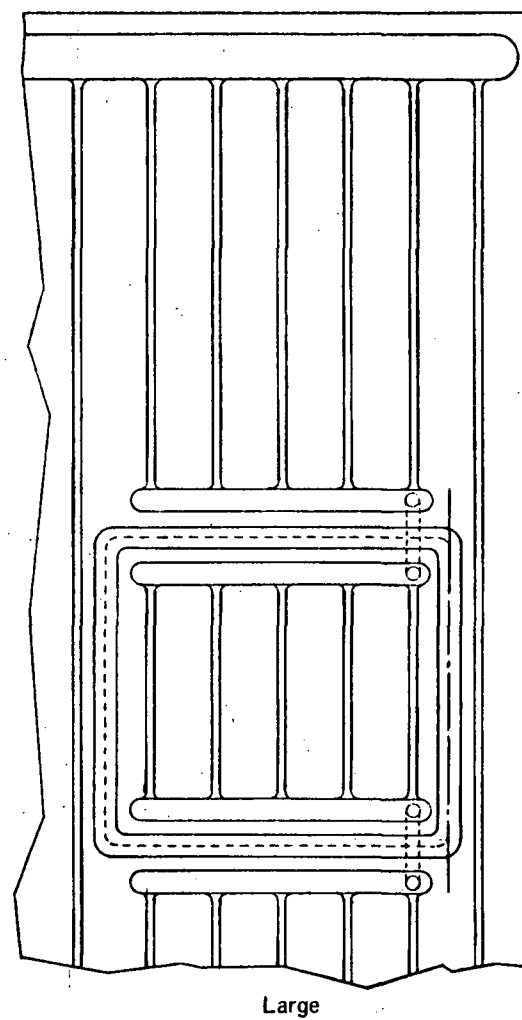
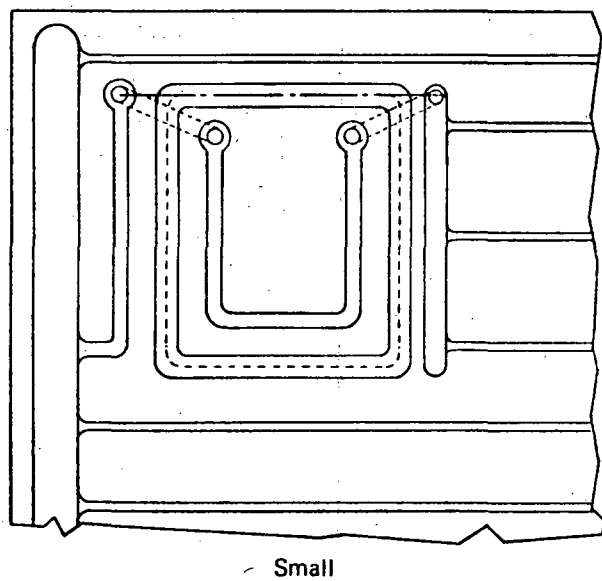


Figure 91. Typical Door Concepts

SYSTEM SUMMARIES

Preceding sections defined the characteristics of the two hypersonic aircraft of interest, (the transport and the research airplane), provided comparisons of materials and design concepts, and presented parametric data for use in evaluating various tradeoffs for cooled airframe structure. The results of these parametric comparisons are brought into focus here for the two aircraft of interest. Much work had been done previously (Ref 1, 2, and 3) on the cooling system for the hypersonic transport, with particular attention on thermal aspects. Therefore, this discussion emphasizes structural concepts and materials that would allow operating temperatures to 589°K (600F), refinement of weights for convective cooling systems that employ a variety of coolant types, and the integration of structural concept/material/panel design with the cooling systems for various types of coolants to obtain total airframe systems weights. Thermal aspects are treated in an abbreviated way, with attention given to matching of coolant requirements with fuel flow conditions. Reliability aspects are summarized, and fatigue and fracture characteristics are discussed for one construction material.

The discussions for the hypersonic research airplane parallel those for the transport in format but are generally more expensive in nature because this particular aircraft configuration had not been investigated previously. Due to the nearer-term nature of this aircraft only aluminum alloy construction was considered and emphasis was placed on conventional construction.

Since interest was focused on aluminum alloy construction, attention was devoted to coolants with maximum operating temperatures of about 394°K (250F). Consideration was given to various shielding arrangements as well as direct surface cooling. Thermal design aspects received relatively more attention than for the transport; panel temperatures were computed for dual and single mode operation of a redundant cooling system design. The relatively high heat flux associated with this aircraft lead to studies to define an approximate upper limit for the tubular type of panel. Fuel flow matching with coolant requirements is considered. Reliability studies compared various design alternatives to relate reliability and weight aspects. Fatigue and fracture considerations are also discussed.

Hypersonic Transport

Promising Structural Concepts. - The structural comparisons of panel concepts and materials indicated a number of possible candidates. These parametric studies were conducted on a theoretical basis with no considerations for practical constraints such as minimum gage thicknesses. As an aid in clarifying the relative merits of candidate approaches, minimum skin gages were defined for candidate materials when used in single sheet and in sandwich type construction (Table XXXI), and were applied to various forms of construction to obtain minimum equivalent thicknesses, as shown in Table XXXII. In turn, these were incorporated with the results of Tables XVI through XVIII so that integration provided the weight of the covers for fuselage and wing structure. The integrated fuselage shell weight for each material and structural approach was combined with a weight increment for frames and a weight estimate for the passenger compartment floor to obtain a subtotal for the fuselage weight as shown in Tables XXXIII and XXXIV for sandwich and Z-stiffened constructions, respectively. The incremental frame weight is dictated by internal pressurization requirements in excess of that needed to achieve structural stability for the fuselage shell. Nonoptimum weight allowances are included to account for nonoptimum structural proportions, as dictated by detailed design considerations, such as doors, inability to taper stringers, practical constraints on stiffener spacing, etc; the allowance was 15%

TABLE XXXIA
MINIMUM SKIN GAGES FOR CANDIDATE MATERIALS

Single Sheet Construction

| | |
|------------------|----------|
| Aluminum Alloys | 1.016 mm |
| Magnesium Alloys | 1.016 mm |
| Titanium Alloys | 0.762 mm |
| Steel Alloys | 0.635 mm |
| Beryllium | 1.016 mm |
| Boron/Aluminum | 1.016 mm |

Sandwich Construction, Sum of Both Faces

| | |
|------------------|----------|
| Aluminum Alloys | 1.270 mm |
| Magnesium Alloys | 1.270 mm |
| Titanium Alloys | 1.016 mm |
| Steel Alloys | 0.762 mm |
| Beryllium | 1.270 mm |
| Boron/Aluminum | 1.270 mm |

TABLE XXXIB
MINIMUM SKIN GAGES FOR CANDIDATE MATERIALS

Single Sheet Construction

| | |
|------------------|------------|
| Aluminum Alloys | 0.040 inch |
| Magnesium Alloys | 0.040 inch |
| Titanium Alloys | 0.030 inch |
| Steel Alloys | 0.025 inch |
| Beryllium | 0.040 inch |
| Boron/Aluminum | 0.040 inch |

Sandwich Construction, Sum of Both Faces

| | |
|------------------|------------|
| Aluminum Alloys | 0.050 inch |
| Magnesium Alloys | 0.050 inch |
| Titanium Alloys | 0.040 inch |
| Steel Alloys | 0.030 inch |
| Beryllium | 0.050 inch |
| Boron/Aluminum | 0.050 inch |

TABLE XXXIIA
MINIMUM EQUIVALENT THICKNESS

| Material | Minimum t, Millimeter | | | | |
|------------------|-----------------------|---------------|-------------|----------|-------------|
| | Ring +Z | Sand- wich | Double Bead | | Corrugation |
| | | | Symm | Non-Symm | |
| Aluminum | 1.778 | 1.778 | 2.159 | 2.540 | 1.829 |
| Magnesium Alloys | 1.778 | 1.778 | 2.159 | 2.540 | 1.829 |
| Titanium Alloys | 1.270 | 1.422 | 1.600 | 1.905 | 1.372 |
| Steel Alloys | 1.016 | 1.067 | 1.346 | 1.575 | 1.041 |
| Beryllium | 1.778 | 1.778 | 2.159 | 2.540 | 1.829 |
| Boron/Aluminum | 1.778 | 1.778 | 2.159 | 2.540 | 1.829 |

TABLE XXXIIB
MINIMUM EQUIVALENT THICKNESS

| Material | Minimum t, Inch | | | | |
|------------------|-----------------|---------------|-------------|----------|-------------|
| | Ring + Z | Sand- wich | Double Bead | | Corrugation |
| | | | Symm | Non-Symm | |
| Aluminum Alloys | 0.070 | 0.070 | 0.085 | 0.100 | 0.072 |
| Magnesium Alloys | 0.070 | 0.070 | 0.085 | 0.100 | 0.072 |
| Titanium Alloys | 0.050 | 0.056 | 0.063 | 0.075 | 0.054 |
| Steel Alloys | 0.040 | 0.042 | 0.053 | 0.062 | 0.041 |
| Beryllium | 0.070 | 0.070 | 0.085 | 0.100 | 0.072 |
| Boron/Aluminum | 0.070 | 0.070 | 0.085 | 0.100 | 0.072 |

TABLE XXXIIIA
WEIGHT OF SANDWICH CONSTRUCTION FUSELAGE, 311°K

| Material | Weight, kilograms | | | | | |
|----------------|-------------------|---------|-------|----------|-----------------------|--------|
| | Shell | Δ Frame | Floor | Subtotal | Non-Optimum Allowance | Total |
| Aluminum | 13,075 | 2,497 | 5,675 | 21,247 | 3,187 | 24,434 |
| Magnesium | 15,391 | 2,724 | 5,675 | 23,790 | 3,568 | 27,358 |
| Titanium | 14,483 | 2,361 | 5,675 | 22,519 | 3,378 | 25,897 |
| Beryllium | 10,215 | 2,225 | 5,085 | 17,525 | 2,629 | 20,154 |
| Boron/Aluminum | 10,823 | 2,225 | 5,085 | 18,133 | 2,683 | 20,816 |

TABLE XXXIIIB
WEIGHT OF SANDWICH CONSTRUCTION FUSELAGE, 100F

| Material | Weight, Pounds | | | | | |
|----------------|----------------|--------|--------|----------|-----------------------|--------|
| | Shell | ΔFrame | Floor | Subtotal | Non-Optimum Allowance | Total |
| Aluminum | 28,800 | 5,500 | 12,500 | 46,800 | 7,020 | 53,820 |
| Magnesium | 33,900 | 6,000 | 12,500 | 52,400 | 7,860 | 60,260 |
| Titanium | 31,900 | 5,200 | 12,500 | 49,600 | 7,440 | 57,040 |
| Beryllium | 22,500 | 4,900 | 11,200 | 38,600 | 5,790 | 44,390 |
| Boron/Aluminum | 23,840 | 4,900 | 11,200 | 39,400 | 5,910 | 45,310 |

TABLE XXXIVA
WEIGHT OF ZEE STIFFENED FUSELAGE, 311°K

| Material | Weight, kilograms | | | | | |
|----------------|-------------------|---------|-------|----------|-----------------------|--------|
| | Shell | Δ Frame | Floor | Subtotal | Non-Optimum Allowance | Total |
| Aluminum | 11,486 | 2,497 | 5,675 | 19,658 | 1,966 | 21,624 |
| Magnesium | 12,848 | 2,724 | 5,675 | 21,247 | 2,125 | 23,372 |
| Titanium | 13,529 | 2,361 | 5,675 | 21,565 | 2,157 | 23,722 |
| Beryllium | 7,264 | 2,225 | 5,085 | 14,574 | 1,457 | 16,031 |
| Boron/Aluminum | 8,876 | 2,225 | 5,085 | 16,186 | 1,616 | 17,802 |

TABLE XXXIVB
WEIGHT OF ZEE STIFFENED FUSELAGE, 100F

| Material | Weight, Pounds | | | | | |
|----------------|----------------|--------|--------|----------|-----------------------|--------|
| | Shell | ΔFrame | Floor | Subtotal | Non-Optimum Allowance | Total |
| Aluminum | 25,300 | 5,500 | 12,500 | 43,300 | 4,330 | 47,630 |
| Magnesium | 28,300 | 6,000 | 12,500 | 46,800 | 4,680 | 51,480 |
| Titanium | 29,800 | 5,200 | 12,500 | 47,500 | 4,750 | 52,250 |
| Beryllium | 16,000 | 4,900 | 11,200 | 32,100 | 3,210 | 35,310 |
| Boron/Aluminum | 19,550 | 4,900 | 11,200 | 35,650 | 3,560 | 39,210 |

for sandwich construction and 10% for the skin/stringer/frame construction. No weight allowance was included for major concentrated load points such as landing gear, wing, and tail attachments. It is expected that the weights of such items will be influenced more by the material of construction than by the type of construction. Such items might add about 5% to the fuselage weight, with a slightly lower percentage applicable to materials of highest strength and a slightly higher percentage applicable to materials of lesser strength because the problem of diffusing concentrated loads tends to be one of strength to weight ratio with little regard to stability considerations.

Examination of Tables XXXIII and XXXIV indicate the superiority of aluminum alloys over magnesium or titanium for near term applications, from 1360 to 2720 kg (3,000 to 6,000 lb) for sandwich construction and about 1820 kg (4,000 lb) for skin/stringer/frame construction. The use of beryllium or boron/aluminum would provide a very substantial reduction in fuselage weight, about 4540 kg (10,000 lb) which is about 20% of the aircraft payload. However, it should be noted that these trends are based on structural consideration and will be combined with thermal design considerations later. It is interesting to note that the weight of the fuselage structure as defined by Reference 2 was 23,200 kg (51,050 lb) while the weight predicted here is 21,400 kg (47,360 lb) for the skin/stringer/frame construction. This difference is reduced if an adjustment is made to account for the average structural temperature of about 366°K (200F); the fuselage weight becomes 23,300 kg (51,200 lb) and is almost identical to the prior estimate.

Weights of the wing covers based on Z-stiffened, symmetrical double beaded, and honeycomb sandwich skins were updated in a similar manner with results shown in Tables XXXV, XXXVI, and XXXVII. Cover weights include minimum gage constraints and reflected a weight increase of 100% over estimates based on axial loading alone in order to account for torsional and shear loading, based on the work of Reference 1. Rib and spar weights were estimated on the basis of past experience to be a percentage of the structural box weight with values of 27% and 30% for the Z-stiffened, and for the tubular and sandwich constructions respectively. Conservatively, the trailing edge flap and aileron structures were assumed to have the same unit weight as the structural box. The leading edge weight was computed in two steps; a total weight equivalent to a 0.63 cm (0.25 inch) thick plate of the construction material was assumed for the first 0.6 m (2 ft) and the rear 0.9 m (3 ft) was assumed to have the same unit weight as the wing box. Nonoptimum weight allowances were 10% for the Z-stiffened skins and 15% for the double beaded and sandwich constructions. With respect to construction types, the double beaded constructions do not appear to have any significant advantage. The lighter symmetrically beaded design has the definite disadvantage of surface roughness which would require external shielding to be aerodynamically acceptable. If such shielding is provided to attenuate the heat load, then the weight saving associated with this design concept might be worthwhile. Based on the studies of Reference 1 as adjusted for the load factor change to 2.5g a weight of about 16,800 kg (37,000 lb) would have been expected for the Z-stiffened aluminum alloy construction, the present weight projection is about 16,400 kg (36,000 lb) when the weights are corrected for the average wing temperature of 366°K (200F).

As in the case of the fuselage, aluminum alloy construction appears to be more desirable than other conventional materials. Significant weight benefits are possible through the use of beryllium or boron/aluminum, although the magnitude of the benefit depends on the type of construction employed. Between 912 and 5,000 kg (2,000 and 11,000 lb) could be saved through the use of these advanced materials. Other interesting observations were made during the comparisons of wing weights. Most of the wing was designed by the minimum gage constraint, outboard of buttline 30 for the more conventional materials and outboard of buttline 24 for the advanced materials. While the beryllium

TABLE XXXVA
WEIGHT OF ZEE STIFFENED WINGS*, 311°K

| Material | Weight, Kilograms | | | | | |
|----------------|-------------------|----------------|--------------|----------|-----------------------|--------|
| | Cover | Ribs and Spars | Leading Edge | Subtotal | Non-Optimum Allowance | Total |
| Aluminum | 8,263 | 3,087 | 2,116 | 13,466 | 1,348 | 14,814 |
| Magnesium | 9,915 | 3,705 | 2,097 | 15,717 | 1,571 | 17,288 |
| Titanium | 11,804 | 4,358 | 3,133 | 19,295 | 1,930 | 21,225 |
| Maraging Steel | 16,162 | 6,038 | 4,821 | 27,012 | 2,701 | 29,713 |
| Beryllium | 5,539 | 2,043 | 1,416 | 8,998 | 899 | 9,897 |
| Boron/Aluminum | 6,174 | 2,270 | 2,116 | 10,560 | 1,058 | 11,618 |

*For unsymmetrical double-beaded skin increase total weights by 10%.

TABLE XXXV B
WEIGHT OF ZEE STIFFENED WINGS*, 100 F

| Material | Weight, Pounds | | | | | |
|----------------|----------------|----------------|--------------|----------|-----------------------|--------|
| | Covers | Ribs and Spars | Leading Edge | Subtotal | Non-Optimum Allowance | Total |
| Aluminum | 18,200 | 6,800 | 4,660 | 29,660 | 2,970 | 32,630 |
| Magnesium | 21,840 | 8,160 | 4,620 | 34,620 | 3,460 | 38,080 |
| Titanium | 26,000 | 9,600 | 6,900 | 42,500 | 4,250 | 46,750 |
| Maraging Steel | 35,600 | 13,300 | 10,600 | 59,500 | 5,950 | 65,450 |
| Beryllium | 12,200 | 4,500 | 3,120 | 19,820 | 1,980 | 21,800 |
| Boron/Aluminum | 13,600 | 5,000 | 4,660 | 23,260 | 2,330 | 25,590 |

*For unsymmetrical double-beaded skin increase total weights by 10%.

TABLE XXXVIA
WEIGHT OF SYMMETRICAL DOUBLE BEADED WINGS, 311°K

| Material | Weight, Kilograms | | | | | |
|----------------|-------------------|----------------|--------------|----------|-----------------------|--------|
| | Cover | Ribs and Spars | Leading Edge | Subtotal | Non-Optimum Allowance | Total |
| Aluminum | 6,628 | 2,860 | 2,116 | 11,604 | 1,739 | 13,343 |
| Titanium | 7,555 | 3,223 | 3,133 | 13,911 | 2,088 | 15,999 |
| Beryllium | 5,675 | 2,452 | 1,416 | 9,543 | 1,430 | 10,973 |
| Boron/Aluminum | 6,265 | 2,679 | 2,116 | 11,060 | 1,657 | 12,717 |

TABLE XXXVIB
WEIGHT OF SYMMETRICAL DOUBLE BEADED WINGS, 100F

| Material | Weight, Pounds | | | | | |
|----------------|----------------|----------------|--------------|----------|--------------------|--------|
| | Covers | Ribs and Spars | Leading Edge | Subtotal | Non-Optimum Factor | Total |
| Aluminum | 14,600 | 6,300 | 4,660 | 25,560 | 3,830 | 29,390 |
| Titanium | 16,640 | 7,100 | 6,900 | 30,640 | 4,600 | 35,240 |
| Beryllium | 12,500 | 5,400 | 3,120 | 21,020 | 3,150 | 24,170 |
| Boron/Aluminum | 13,800 | 5,900 | 4,660 | 24,360 | 3,650 | 28,010 |

TABLE XXXVIIA
WEIGHT OF SANDWICH CONSTRUCTION WINGS, 311°K

| Material | Weight, Kilograms | | | | | |
|----------------|-------------------|----------------|--------------|----------|--------------------|--------|
| | Cover | Ribs and Spars | Leading Edge | Subtotal | Non-Optimum Factor | Total |
| Aluminum | 6,297 | 2,692 | 1,830 | 10,819 | 1,625 | 12,444 |
| Titanium | 6,347 | 2,733 | 2,265 | 11,345 | 1,703 | 13,048 |
| Beryllium | 5,380 | 2,315 | 1,426 | 9,121 | 1,362 | 10,483 |
| Boron/Aluminum | 5,734 | 2,474 | 1,730 | 9,938 | 1,489 | 11,427 |

TABLE XXXVII B
WEIGHT OF SANDWICH CONSTRUCTION WINGS, 100F

| Material | Weight, Pounds | | | | | |
|----------------|----------------|----------------|--------------|----------|--------------------|--------|
| | Covers | Ribs and Spars | Leading Edge | Subtotal | Non-Optimum Factor | Total |
| Aluminum | 13,870 | 5,930 | 4,030 | 23,830 | 3,580 | 27,410 |
| Titanium | 13,980 | 6,202 | 4,990 | 24,990 | 3,750 | 28,740 |
| Beryllium | 11,850 | 5,100 | 3,140 | 20,090 | 3,000 | 23,090 |
| Boron/Aluminum | 12,630 | 5,450 | 3,810 | 21,890 | 3,280 | 25,170 |

structure was lightest, the weight of the magnesium wing outboard of buttline 30 was equivalent. When considering magnesium as compared to beryllium for the outboard portion of the wing the cost savings associated with magnesium construction might possibly dictate its use even though the weights would be equivalent. When magnesium is compared to aluminum, costs favor aluminum and the weight savings of 73 kg (160 lb) is insufficient to warrant the use of two construction materials.

Total weights for the airframe structure are summarized in Table XXXVIII based on an assumed structural temperature of 315°K (100F), and the assumption that the unit tail weights are the same as for the wing. In all instances, the combination of a skin/stringer/frame fuselage, combined with a sandwich construction wing, yields lightest weight for any particular material, except for beryllium for which a Z-stiffened wing is slightly lighter. The second most promising combination depends upon the particular construction material. Based on these lightest weight combinations, and taking the aluminum alloy construction as a reference, the use of titanium would add about 8% or 2950 kg (6500 lb), while the use of boron/aluminum would reduce airframe weight by 14%, 5000 kg (11,000 lb), while beryllium would reduce weight by 23% or 8,600 kg (19,000 lb). The weight saving potential of the advanced materials is quite significant in view of the 21,800 kg (48,000 lb) payload of the baseline airplane.

Promising Thermal Concepts. - As a result of the studies of Reference 3, the most promising cooled airframe approach for the hypersonic transport, using essentially current technology for the structure, was aluminum alloy construction partially protected by superalloy heat shields to reduce the heat load to the glycol/water cooling system to acceptable levels, with respect to aircraft fuel flow. While the use of a single conventional construction material and a single cooling system simplifies fabrication and development efforts, it does not necessarily lead to an optimum aircraft. For example, when low cost aluminum alloy construction is used, heat shields are required, whereas if the maximum coolant temperature is increased, it should be possible to eliminate heat shielding. As an aid in establishing trends, heat load data were assembled in the form of the ratio of hydrogen required for airframe cooling, divided by the hydrogen required for thrust, and plotted as a function of load factor at the most critical times during cruise and descent for 30% shielded and unshielded transports with assumed wall temperatures of 366°K (200F), 478°K (400F), and 589°K (600F), see Figures 92 and 93. Conditions during cruise will be considered first. For the shielded vehicle the 366°K (200F) wall temperature is quite satisfactory for nominal flight, pull-up, and turn maneuvers and very mild push-overs. The largest discrepancy between hydrogen requirements and availability occurs near zero g, with conditions becoming more nearly satisfactory as the load factor is either increased or decreased. At the higher wall temperatures of 478 and 589°K (400 and 600F) the hydrogen flow availability is quite adequate for all maneuver conditions. For the unshielded vehicle, the 589°K (600F) wall temperature provides adequate hydrogen availability under all maneuver conditions. In fact, shielding can be eliminated at 544°K (525F) without necessitating any maneuver limitations. At a wall temperature of 478°K (400F) the hydrogen fuel flow rate is adequate to provide cooling for nominal flight, pullups, turns, and very mild or quite severe pushovers. In the range of zero-g where power requirements, and hence fuel flow requirements, are reduced there is not sufficient fuel flow to meet structural cooling needs. The situation becomes substantially worse as the airframe wall temperature is decreased for the unshielded vehicle as indicated in the plot for the 366°K (200F) structure. If a maneuver is assumed to last for 10 seconds, the use of excess hydrogen flow during cruise would amount to a maximum of 227 kg (500 lb) for a zero-g maneuver with an unshielded airframe operating at an average temperature of 366°K (200F) (hydrogen flow available and required are listed in Table III). Using the flight load spectrum defined previously for the HST and a more realistic average time of 3 seconds/maneuver a total of 545 kg (1200 lb) of excess hydrogen would be required.

TABLE XXXVIII A
TOTAL AIRFRAME STRUCTURAL WEIGHT

| Wing and Tail Fuselage | Total Airframe Structural Weight* kilograms | | |
|---------------------------|--|----------|---------------------|
| | Z Stiffened | Sandwich | Sym. Double Bead |
| Aluminum | | | |
| Z Stiffened | 40,601 | 37,441 | 38,486 |
| Sandwich | 43,411 | 40,252 | 41,296 |
| Titanium | | | |
| Z Stiffened | 50,875 | 40,406 | 43,924 |
| Sandwich | 53,050 | 42,581 | 46,099 |
| Beryllium | | | |
| Z Stiffened | 28,715 | 29,337 | 29,964 |
| Sandwich | 32,838 | 33,460 | 34,086 |
| Boron/Aluminum | | | |
| Z Stiffened | 33,047 | 32,347 | 33,868 |
| Sandwich | 35,816 | 35,117 | 36,638 |

*Fuselage, Wings, and Tail.

TABLE XXXVIII B
TOTAL AIRFRAME STRUCTURAL WEIGHT

| Wing and Tail Fuselage | Total Airframe Structural Weight* (lb) | | |
|---------------------------|---|----------|---------------------|
| | Z Stiffened | Sandwich | Sym. Double Bead |
| Aluminum | | | |
| Z Stiffened | 89,430 | 82,470 | 84,770 |
| Sandwich | 95,620 | 88,660 | 90,960 |
| Titanium | | | |
| Z Stiffened | 112,060 | 89,000 | 96,750 |
| Sandwich | 116,850 | 93,790 | 101,540 |
| Beryllium | | | |
| Z Stiffened | 63,250 | 64,620 | 66,000 |
| Sandwich | 72,330 | 73,700 | 75,080 |
| Boron/Aluminum | | | |
| Z Stiffened | 72,790 | 71,250 | 74,600 |
| Sandwich | 78,890 | 77,350 | 80,700 |

*Fuselage, wings and tail.

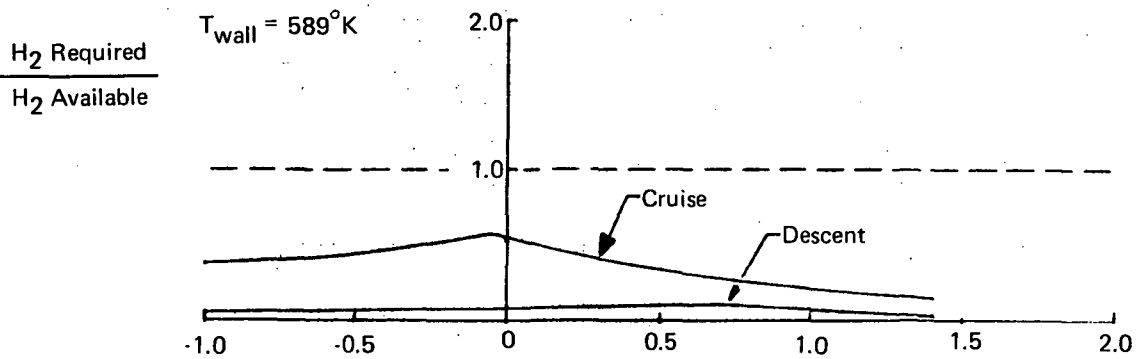
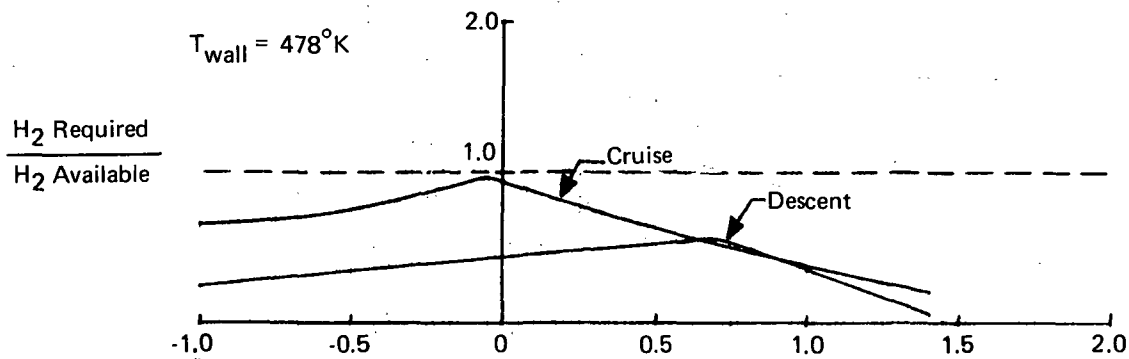
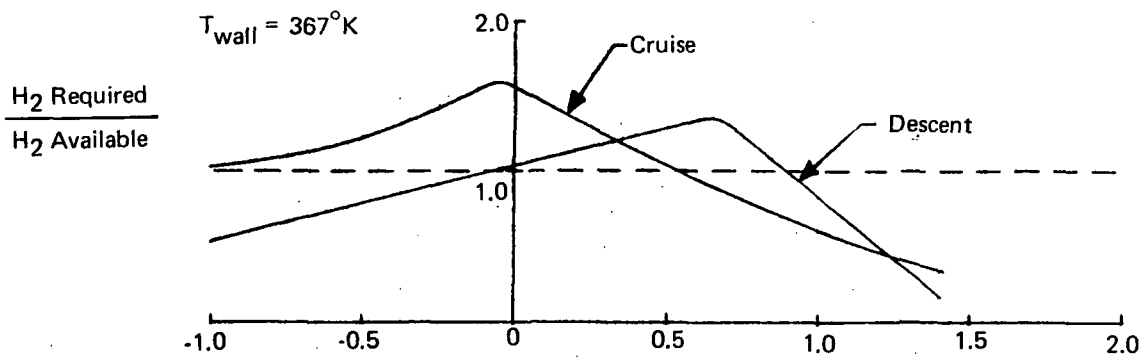


Figure 92a. Hydrogen Availability as a Function of Flight Load Factor for Structural Wall Temperatures at Critical Times During Cruise and Descent, Shielded Airframe, 920 m² (10,000 ft²) of Shielding

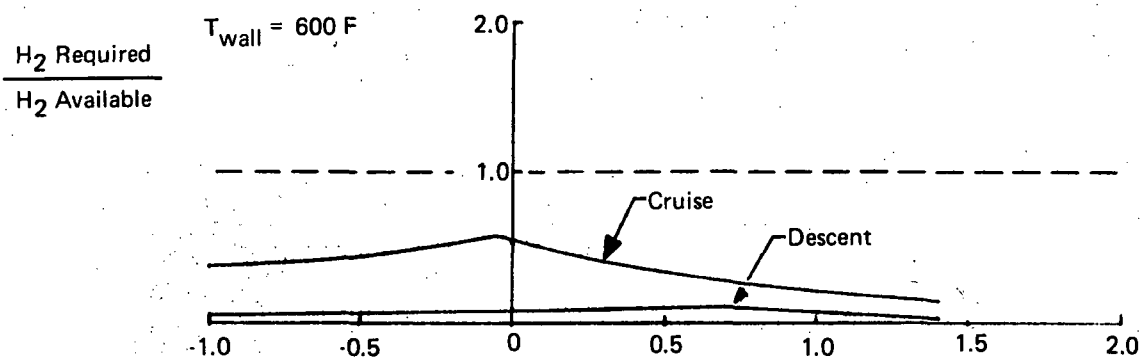
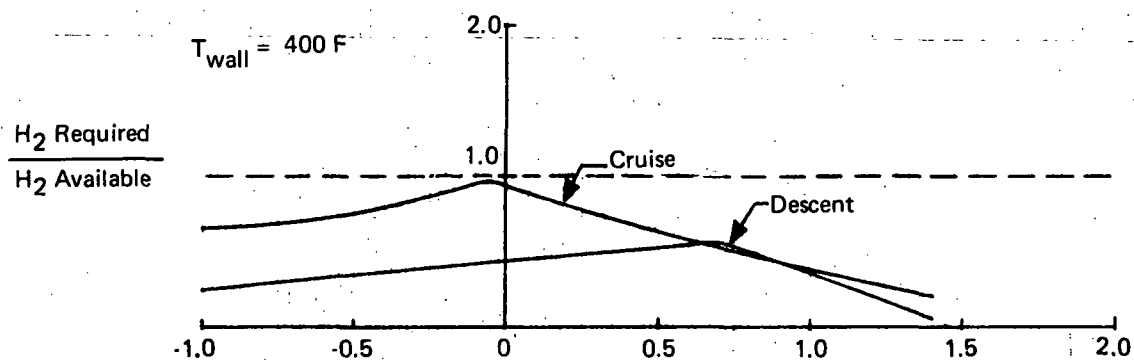
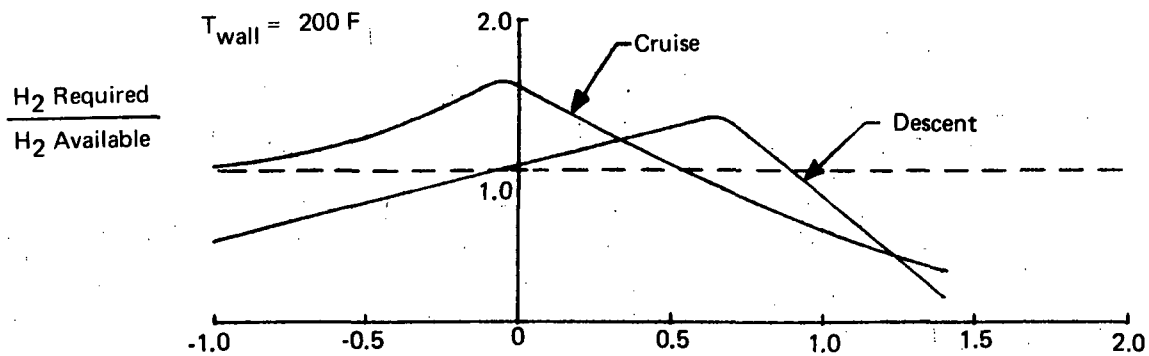


Figure 92b. Hydrogen Availability as a Function of Flight Load Factor for Structural Wall Temperatures at Critical Times During Cruise and Descent, Shielded Airframe

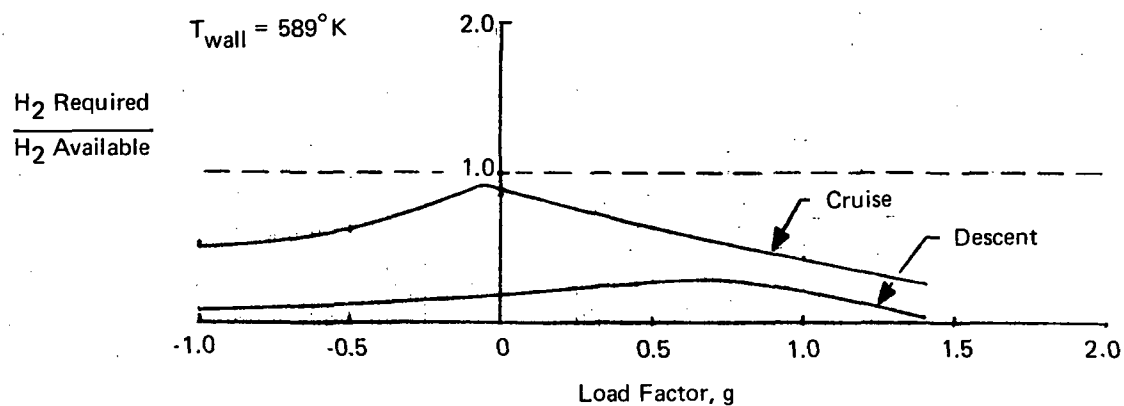
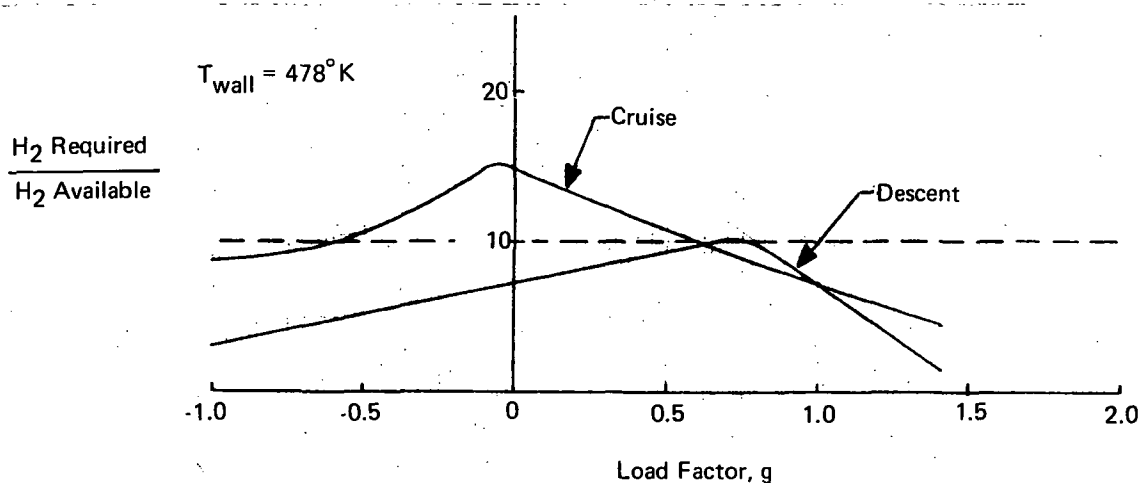
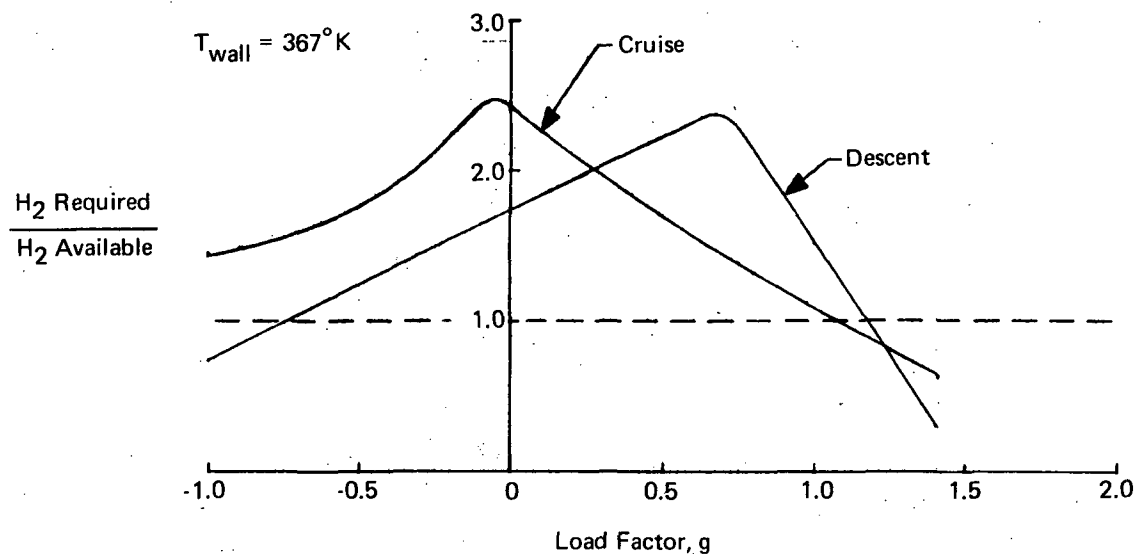


Figure 93a. Hydrogen Availability as a Function of Flight Load Factor for Structural Wall Temperatures at Critical Times During Cruise and Descent, Unshielded Airframe

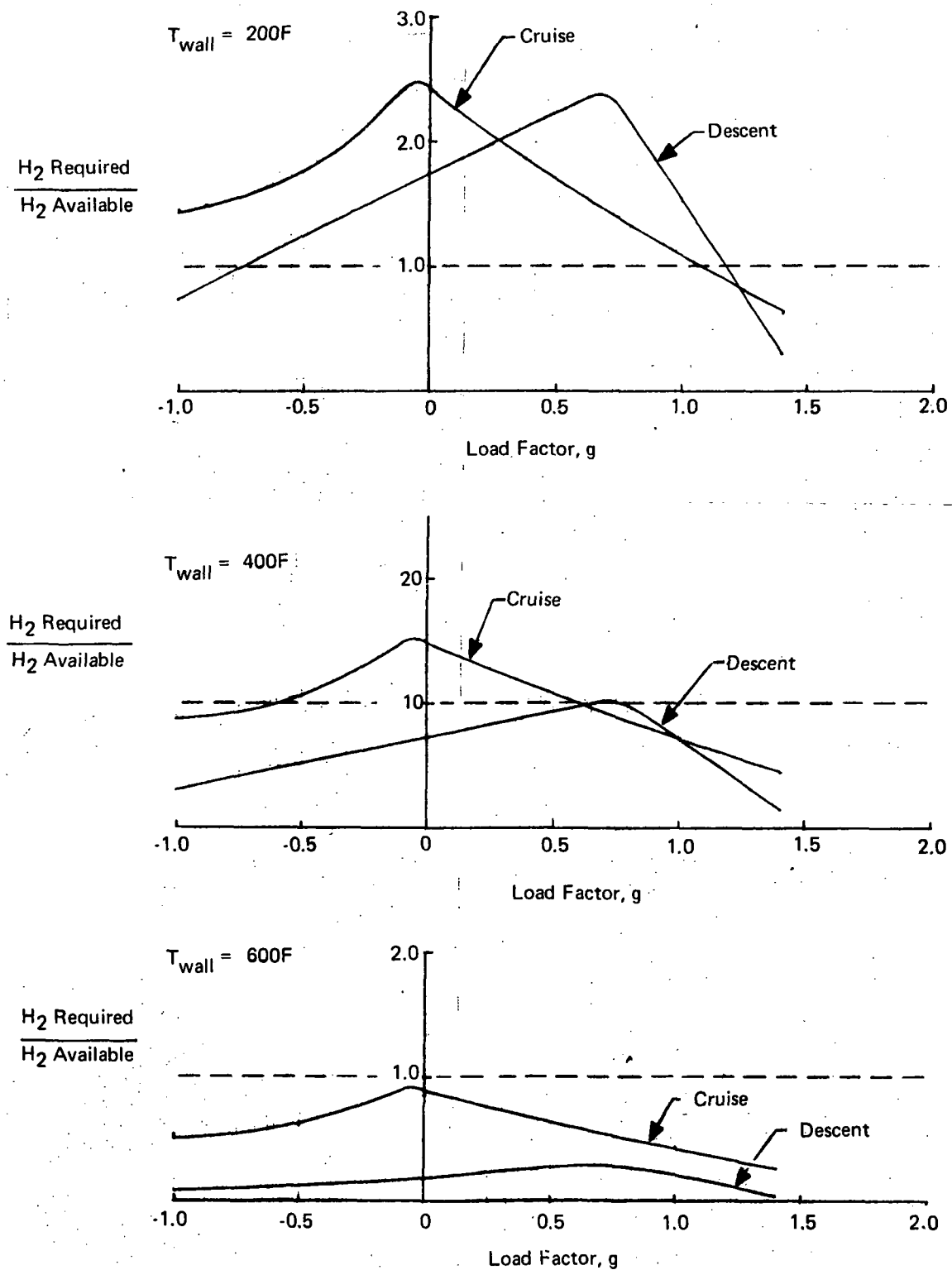


Figure 93b. Hydrogen Availability as a Function of Flight Load Factor for Structural Wall Temperatures at Critical Times During Cruise and Descent, Unshielded Airframe

A prohibitive increase in hydrogen quantity would be required for an unshielded 366°K (200F) structure during the cruise and descent portion of flight, about 10,500 kg (23,000 lb) compared to the approximately 5000 kg (11,000 lb) of excess hydrogen and heat shielding which is partially compensated for by a reduction in cooling system weight as indicated by References 2 and 3. When the average wall temperature is increased to about 478°K (400F), there is no need for shielding except for maneuvers that induce load factors between about $\pm 0.6g$; maneuvers within this range are infrequent and could be accommodated by carrying about 225 kg (500 lb) of hydrogen for cooling purposes; although controlling the flow of this excess fuel to match heat load requirements may be difficult.

In considering cooling system weights, both shielded and unshielded structures of different average operating temperatures should be compared. Heat load data and parametric results in prior sections of the report were used to assemble such comparative data as shown in Table XXXIX. Both nonredundant and completely redundant system concepts are indicated; such small differences as 865 to 1590 kg (1900 to 3500 lb) result from the assumption of 50% flow in each of the redundant loops under normal operating conditions. Also included in the comparison is a dual temperature cooling system concept that utilizes an unshielded aluminum alloy structure in all areas but those of leading edges, where a separate cooling system is used to permit a maximum transport coolant temperature of 533°K (500F) so that the maximum hydrogen temperature can be increased along with the quantity of heat that can be absorbed from the airframe.

Regardless of whether a nonredundant or redundant system is used, the ranking of the cooling systems concepts is not changed. The unshielded 589°K (600F) and the shielded 366°K (200F) systems are essentially comparable in weight followed by the shielded dual temperature system, the shielded 478°K (400F) system and the unshielded dual temperature system which are of comparable weight, and the unshielded systems for 478°K (400F) and 366°K (200F), which are essentially the same in weight. Note that the lowest ranking systems are about 50% heavier than the highest ranking systems. It is also interesting to note the significant reduction in cooling system weight between the nonredundant shielded 366°K (200F) system presented in Table XXXIX, 4750 kg (10,640 lb), and the weight projected for the same type of system in Reference 3, 5900 kg (13,000 lb). This weight reduction resulted from a more accurate optimization of cooling system distribution lines and a more detailed passage sizing in various panels over the airframe structure. In general, this suggests a degree of conservatism in prior analyses, inasmuch as refinements have led to lower weight estimates.

Cooled Airframe Weights. - Having considered the weight of various structural concepts/material combinations and of a variety of cooling system concepts that operate at different temperature levels, it is appropriate to consider integrated cooled airframe combinations in order to obtain estimates of weight and improvements in payload capability. In Table XL, the structural weights from Table XXXVIII, as corrected for operating temperature levels, are added to the cooling system weights from Table XXXIX and to other weight increments required to ensure operation functionality of the integrated cooled airframe structural concept. A review of the structural weights clearly indicates the advantage of using advanced types of construction material such as beryllium and metal matrix composites, of which boron/aluminum is typical. The slight differences in weight for these two advanced materials are not considered to be particularly significant, since the ply orientation used for the metal matrix composite was chosen somewhat arbitrarily such that weight reductions may be possible as a result of refined analyses. An examination of the total cooled airframe weight indicates a weight range from 40,000 kg (88,000 lb) to 62,500 kg (137,000 lb). The more sophisticated systems are lighter in general. The unshielded 366°K (200F) systems result in the highest weight because of the large quantity of hydrogen that must be carried specifically for structural cooling, because

TABLE XXXIXA
COOLING SYSTEM CONCEPT COMPARISON, HYPERSONIC TRANSPORT

| Item | Weights For Cooling System For Average Airframe Temperature Indicated, kilograms | | | | | | |
|--|---|---------------------|---------------------|--------------|---------------------|------------------------|------------------------|
| | Unshielded | | | Shielded | | Dual Temp | |
| | 366° K | 477° K | 588° K | 366° K | 477° K | 366/588 ⁽⁴⁾ | 366/588 ⁽⁵⁾ |
| Design Heat Load, 10⁶ Mw | 104.5 | 88.3 | 69 | 68 | 82 | 92.6 | 73.5 |
| REDUNDANT | | | | | | | |
| Distribution Lines ⁽¹⁾ | 4,122 | 3,995 | 2,851 | 2,847 | 3,146 | 3,746 | 3,246 |
| Heat Exchangers, Two | 1,889 | 1,271 | 953 | 1,226 | 1,153 | 1,589 | 1,362 |
| Pumps, Two | 240 | 227 | 159 | 145 | 163 | 240 | 222 |
| Panel Residual ⁽²⁾ | 1,503 | 1,934; 2,293 | 1,112; 1,317 | 1,117 | 1,430; 1,698 | 1,335 | 1,044 |
| Miscellaneous ⁽³⁾ | 772 | 774; 781 | 508; 530 | 422 | 586; 613 | 690 | 586 |
| Total | 8,526 | 8,172; 8,567 | 5,584; 5,811 | 5,684 | 6,433; 6,683 | 7,600 | 6,460 |
| NONREDUNDANT | | | | | | | |
| Distribution Lines ⁽¹⁾ | 3,746 | 3,632 | 2,592 | 2,588 | 2,860 | 3,405 | 2,951 |
| Heat Exchanger | 944 | 636 | 477 | 613 | 577 | 863 | 749 |
| Pump | 120 | 114 | 79 | 73 | 82 | 120 | 120 |
| Panel Residual ⁽²⁾ | 1,503 | 1,934; 2,293 | 1,112; 1,317 | 1,117 | 1,430; 1,698 | 1,335 | 1,044 |
| Miscellaneous ⁽³⁾ | 633 | 631; 667 | 945; 429 | 440 | 499; 522 | 574 | 488 |
| Total | 6,946 | 6,946; 7,341 | 4,676; 4,912 | 4,831 | 5,448; 5,739 | 6,297 | 5,353 |

- (1) Including piping, contained coolant, and APS fuel to drive pump (3 Step Flowrate Schedule as in Ref. 3)
- (2) Redundant and nonredundant entries are the same because half flow is in each of the redundant sets of passages
- (3) 10% to account for valves, controls, connectors, supports, etc.
- (4) Unshielded Aluminum/Beryllium Structure, Glycol/Water and Coolanol 45
- (5) Shielded Aluminum/Beryllium Structure, Glycol/Water and Coolanol 45
- (6) Glycol/Water Coolant Inlet/Outlet Temperatures of 50F/200F, Coolanol 45 Inlet/Outlet Temperatures of 50F/350F
- (7) Aluminum Structure, Glyco/Water
- (8) Left Column - Beryllium Structure, Coolanol 45
Right Column - Titanium Structure, Coolanol 45

TABLE XXXIXB
COOLING SYSTEM CONCEPT COMPARISON, HYPERSONIC TRANSPORT

| Item | Weights For Cooling System For Average Airframe Temperature Indicated, Pounds | | | | | | |
|--|--|-----------------------|-----------------------|---------------------|-----------------------|------------------------|------------------------|
| | Unshielded | | | Shielded | | Dual Temp | |
| | 200F ⁽⁶⁾ | 400F ⁽⁷⁾ | 600F ⁽⁷⁾ | 200F ⁽⁶⁾ | 400F ⁽⁷⁾ | 200/600 ⁽⁴⁾ | 200/600 ⁽⁵⁾ |
| Design Heat Load, 10⁶ BTU/hr | 357 | 301 | 235 | 232 | 280 | 316 | 252 |
| REDUNDANT | | | | | | | |
| Distribution Lines ⁽¹⁾ | 9,080 | 8,800 | 6,280 | 6,270 | 6,930 | 8,250 | 7,150 |
| Heat Exchangers, Two | 4,160 | 2,800 | 2,100 | 2,700 | 2,540 | 3,500 | 3,000 |
| Pumps, Two | 530 | 500 | 350 | 320 | 360 | 530 | 490 |
| Panel Residual ⁽²⁾ | 3,310 | 4,260; 5,050 | 2,450; 2,900 | 2,460 | 3,150; 3,740 | 2,940 | 2,300 |
| Miscellaneous ⁽³⁾ | 1,700 | 1,640; 1,720 | 1,120; 1,170 | 930 | 1,290; 1,350 | 1,520 | 1,290 |
| Total | 18,780 | 18,000; 18,870 | 12,300; 12,800 | 12,520 | 14,170; 14,720 | 16,740 | 14,230 |
| NONREDUNDANT | | | | | | | |
| Distribution Lines ⁽¹⁾ | 8,250 | 8,000 | 5,710 | 5,700 | 6,300 | 7,500 | 6,500 |
| Heat Exchanger | 2,080 | 1,400 | 1,050 | 1,350 | 1,270 | 1,900 | 1,650 |
| Pump | 265 | 250 | 175 | 160 | 180 | 265 | 265 |
| Panel Residual ⁽²⁾ | 3,310 | 4,260; 5,050 | 2,450; 2,900 | 2,460 | 3,150; 3,740 | 2,940 | 2,300 |
| Miscellaneous ⁽³⁾ | 1,395 | 1,390; 1,470 | 945; | 970 | 1,100; 1,150 | 1,265 | 1,075 |
| Total | 15,300 | 15,300; 16,170 | 10,300; 10,820 | 10,640 | 12,000; 12,640 | 13,870 | 11,790 |

- (1) Including Piping, Contained Coolant, and APS Fuel to Drive Pump (3 Step Flowrate Schedule as in Ref. 3)
- (2) Redundant and Nonredundant Entries are the same because Half Flow is in each of the Redundant Sets of Passages
- (3) 10% to Account for Valves, Controls, Connectors, Supports, Etc.
- (4) Unshielded Aluminum/Beryllium Structure, Glycol/Water and Coolanol 45
- (5) Shielded Aluminum/Beryllium Structure, Glycol/Water and Coolanol 45
- (6) Glycol/Water Coolant Inlet/Outlet Temperatures of 50F/200F, Coolanol 45 Inlet/Outlet Temperatures of 50F/350F
- (7) Aluminum Structure, Glycol/Water
- (8) Left Column - Beryllium Structure, Coolanol 45
Right Column - Titanium Structure, Coolanol 45

TABLE XLA
COOLED AIRFRAME WEIGHT SUMMARY, HYPERSONIC TRANSPORT

| System Combination of Average Structural Temperature | Cooled Airframe Structure Weight, Kilograms | | | |
|---|---|----------------|------------------|---------------|
| | Structure | Cooling System | Other | Total |
| 366° K Unshielded (1) (2) | | | | |
| Aluminum | 39,997 | 8,526 | 10,442 (6) | 58,965 |
| Beryllium | 30,781 | 8,526 | 10,442 (6) | 49,749 |
| Boron/Aluminum | 33,732 | 8,889 | 10,442 (6) | 53,063 |
| Titanium | 42,812 | 8,889 | 10,442 (6) | 62,143 |
| 477° K Unshielded (2) (3) | | | | |
| Beryllium | 32,597 | 8,172 | 226 (6) | 40,996 |
| Boron/Aluminum | 34,686 | 8,567 | 226 (6) | 43,479 |
| Titanium | 43,629 | 8,567 | 226 (6) | 52,423 |
| 588° K Unshielded (2) (4) | | | | |
| Beryllium | 37,727 | 5,584 | 0 | 43,311 |
| Boron/Aluminum | 38,499 | 5,811 | 0 | 44,310 |
| Titanium | 48,669 | 5,811 | 0 | 54,480 |
| 366° K Shielded (1) (2) | | | | |
| Aluminum | 39,997 | 5,684 | 50,394 (7) | 50,675 |
| Beryllium | 30,781 | 5,684 | 50,394 (7) | 41,460 |
| 477° K Shielded (2) (3) | | | | |
| Beryllium | 32,597 | 6,433 | 1271 (7) | 40,301 |
| Titanium | 43,629 | 6,683 | 1271 (7) | 51,583 |
| 366° K/588° K Unshielded (1) (2) (4) (5) | 38,454 | 7,600 | 3,178 (6) | 49,232 |
| 366° K/588° K Shielded (1) (2) (4) (5) | 38,454 | 6,460 | 1,271 (7) | 46,185 |

- (1) Glycol/Water Coolant
- (2) Structural weights of Table XXXVIII corrected for effect of average temperature
- (3) Coolanol 20 Coolant
- (4) Coolanol 45 Coolant
- (5) Aluminum and Beryllium Construction
- (6) Excess Hydrogen for Cooling, does not Include Containment
- (7) Heat Shielding and Excess Hydrogen, 10,000 lb and 1000 lb Respectively
- (8) Heat Shielding

TABLE XLB
COOLED AIRFRAME WEIGHT SUMMARY, HYPERSONIC TRANSPORT

| System Combination for Average Structural Temperature | Cooled Airframe Structure Weight, lb | | | |
|--|--------------------------------------|----------------|-------------|---------|
| | Structure | Cooling System | Other | Total |
| 200F Unshielded (1) (2) | | | | |
| Aluminum | 88,100 | 18,780 | 23,000 (6) | 129,880 |
| Beryllium | 67,800 | 18,780 | 23,000 (6) | 109,580 |
| Boron/Aluminum | 74,300 | 19,580 | 23,000 (6) | 116,880 |
| Titanium | 94,300 | 19,580 | 23,000 (6) | 136,880 |
| 400F Unshielded (2) (3) | | | | |
| Beryllium | 71,800 | 18,000 | 500 (6) | 90,300 |
| Boron/Aluminum | 76,400 | 18,870 | 500 (6) | 95,770 |
| Titanium | 96,100 | 18,870 | 500 (6) | 115,470 |
| 600F Unshielded (2) (4) | | | | |
| Beryllium | 83,100 | 12,300 | 0 | 95,400 |
| Boron/Aluminum | 84,800 | 12,800 | 0 | 96,600 |
| Titanium | 107,200 | 12,800 | 0 | 120,000 |
| 200F Shielded (1) (2) | | | | |
| Aluminum | 88,100 | 12,520 | 111,000 (7) | 111,620 |
| Beryllium | 67,800 | 12,520 | 111,000 (7) | 91,320 |
| 400F Shielded (2) (3) | | | | |
| Beryllium | 71,800 | 14,170 | 2,800 (8) | 88,770 |
| Titanium | 96,100 | 14,720 | 2,800 (8) | 113,620 |
| 200F/600F Unshielded (1) (2) (4) (5) | 84,700 | 16,740 | 7,000 (6) | 108,440 |
| 200F/600F Shielded (1) (2) (4) (5) | 84,700 | 14,230 | 2,800 (8) | 101,730 |

- (1) Glycol/Water Coolant
- (2) Structural weights of Table XXXVIII corrected for effect of average temperature
- (3) Coolanol 20 Coolant
- (4) Coolanol 45 Coolant
- (5) Aluminum and Beryllium Construction
- (6) Excess Hydrogen for Cooling, does not Include Containment
- (7) Heat Shielding and Excess Hydrogen, 10,000 lb and 1000 lb Respectively
- (8) Heat Shielding

the heat load and fuel flow histories do not match well. The actual aircraft weights would be even higher because no allowance has been made for containment of this additional hydrogen, nor for the increase in fuselage volume that would be necessary. Disregarding this particular category of aircraft type, reduces the range of weights to between 40,000 kg and 54,500 kg (88,000 and 120,000 lb), only 60% of the original spread.

For the unshielded vehicles it is interesting to note that minimum weight appears to be in the vicinity of the 478°K (400F) structural temperature and that the titanium systems are always relatively heavier than others in a particular class. The systems that use advanced structural materials (beryllium and boron/aluminum) result in lightest weights, but the various aluminum alloy structural approaches are attractive from a weight point of view. Of the aluminum alloy systems, the one employing beryllium stagnation regions and shielding over the portion of the fuselage forward of the wing results in lightest weight, followed by the unshielded dual temperature concept and the 366°K (200F) shielded approach.

The 366°K (200F) shielded airframe concept assumes that all regions of the aircraft that would have radiation equilibrium temperatures in excess of 810°K (1,000F) are protected by metallic heat shields with only a modest interchange of radiant energy between these shields and the cooled structure that they protect from the hot boundary layer. This represents about one-third of the total wetted area of the hypersonic transport, as shown in Figure 94, including the lower surface of the wing except for the first 1.5 m (5 ft), both sides of the horizontal and vertical tails except for the first 0.6 m (2 ft), and a portion of the fuselage beginning just behind the nose and extending rearward to Station 42 on the upper surface and blending into the wing region on the lower surface. The 478°K (400F) shielded concept is somewhat similar to the system just described, but shielding is eliminated from the lower surface of the wing and from the tails leaving shielded only that portion of the fuselage forward of Station 110 along the lower surface and forward of Station 42 along the upper surface. The shielding employed for the dual temperature 366°K/589°K (200F/600F) shielded concept is the same as the 478°K (400F) shielded concept, but in the dual temperature arrangement the first 1.5 m (5 ft) of the wing surface (top and bottom as measured perpendicular to the leading edge), the first 0.6 m (2 ft) of the horizontal and vertical tails, and a small portion of the fuselage nose utilize a separate high temperature cooling system with a beryllium or boron/aluminum structure. If a titanium structure is used for the high temperature portion the structural weight would be about 2470 kg (5400 lb) higher.

While the trends of cooled airframe weight are indicative of merit, a clearer picture of the ranking of the various cooled airframe structural concepts is provided by the data of Table XLI. Here, the various systems are compared for a takeoff gross weight of 232,000 kg (520,652 lb), the weight of an uncooled aircraft studied in Reference 4, of which the payload constitutes 21,800 kg (48,000 lb). Differences from this uncooled baseline aircraft are in the areas of the structure and thermal protection, the weight of tankage and insulation, and the payload. Other items were assumed to be of identical weight despite the fact that some subsystem benefits are likely with the cooled concepts. As the payloads in Table XLI are reviewed, it should be noted that the work in Reference 4 was performed in the mid 1960's and that a current assessment of the same aircraft might increase the 21,800 kg (48,000 lb) payload slightly. Also, some of the cooled airframe concepts require hydrogen fuel to be carried specifically for cooling purposes, and while the liquid hydrogen weight is included, the weights associated with its containment and with the additional fuselage volume required have not been subtracted from the payload gain. This weight increment is particularly detrimental to the 366°K (200F) unshielded aircraft category where it could amount to about 4540 kg (10,000 lb).

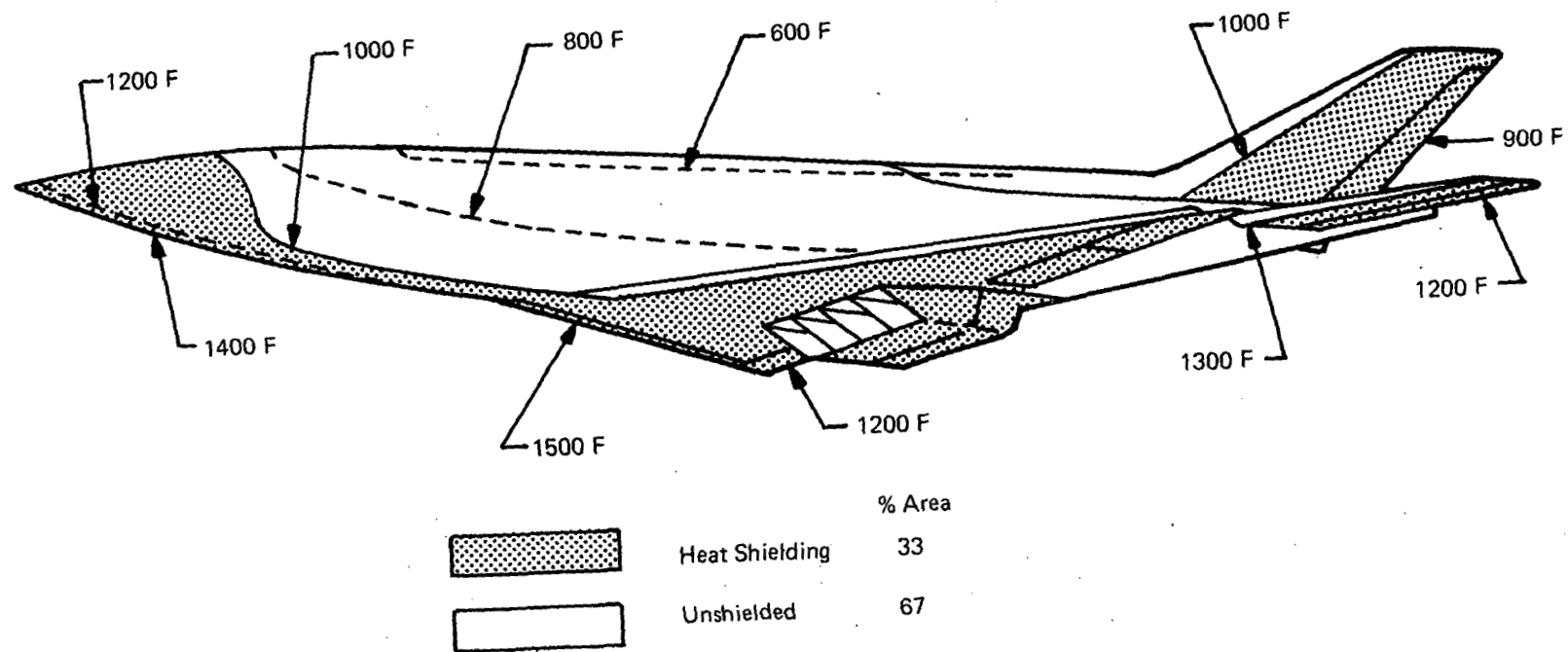


Figure 94. Shielding Hypersonic Transport Concept, 1000 F Shields

TABLE XLIA
IMPACT OF AIRFRAME COOLING ON PAYLOAD, HYPERSONIC TRANSPORT

| Airframe Concept | Weight, Kilograms | | Other | Payload | Payload Ratio |
|----------------------------|---------------------------|------------------------|---------|------------|---------------|
| | Weight, Structure and TPS | Tankage and Insulation | | | |
| Uncooled (1) | 63,139 | 16,192 | 135,244 | 21,792 | 1.00 |
| 366°K Unshielded (2) | | | | | |
| Aluminum | 58,966 | 11,078 (5) | 135,244 | 67,458 (2) | 1.40 |
| Beryllium | 49,749 | 11,078 (5) | ↑ | 39,842 (2) | 1.82 |
| Boron/Aluminum | 53,064 | 11,078 (5) | ↑ | 36,528 (2) | 1.67 |
| Titanium | 62,144 | 11,078 (5) | ↑ | 27,448 (2) | 1.26 |
| 477°K Unshielded (3) | | | | | |
| Beryllium | 41,450 | 16,344 (6) | ↑ | 43,832 (3) | 2.01 |
| Boron/Aluminum | 43,532 | 16,344 (6) | ↑ | 41,349 (3) | 1.92 |
| Titanium | 52,486 | 16,344 (6) | ↑ | 32,394 (3) | 1.48 |
| 588°K Unshielded | | | | | |
| Beryllium | 43,312 | 17,343 (7) | ↑ | 40,469 | 1.85 |
| Boron/Aluminum | 43,856 | 17,343 (7) | ↑ | 39,924 | 1.83 |
| Titanium | 54,480 | 17,343 (7) | ↑ | 29,300 | 1.34 |
| 366°K Shielded | | | | | |
| Aluminum | 50,721 | 11,078 (5) | ↑ | 38,870 (6) | 1.79 |
| Beryllium | 41,505 | 11,078 (5) | ↑ | 48,086 (6) | 2.21 |
| 477°K Shielded | | | | | |
| Beryllium | 40,318 | 16,344 (7) | ↑ | 44,563 | 2.04 |
| Titanium | 51,636 | 16,344 (7) | ↑ | 33,245 | 1.52 |
| 366°K/588°K Unshielded (4) | 49,232 | 11,078 (5) | 135,244 | 40,360 (4) | 1.85 |
| 366°K/588°K Shielded | 46,185 | 11,078 (5) | 297,894 | 43,406 | 1.99 |

- (1) From Reference 4
- (2) Weights do not include additional tankage, insulation, and fuselage (about 4,540 kilograms) to carry additional LH₂, thereby reducing payload.
- (3) Weights do not include additional tankage, insulation, and fuselage (about 90 kilograms) to carry additional LH₂, thereby reducing payload.
- (4) Weights do not include additional tankage, insulation, and fuselage (about 1,362 kilograms) to carry additional LH₂, thereby reducing payload.
- (5) From Reference 2, Inconel 718 tanks and sealed foam insulation.
- (6) Weights do not include additional tankage, insulation, and fuselage (about 180 kilograms) to carry additional LH₂, thereby reducing payload.
- (7) From Reference 2, Inconel 718 tanks and CO₂ frost insulation.
- (8) Based on data of Reference 2, Inconel 718 tanks.

TABLE XLIB
IMPACT OF AIRFRAME COOLING ON PAYLOAD, HYPERSONIC TRANSPORT

| Airframe Concept | Weight, lb | | Other | Payload | Payload Ratio |
|--------------------------|---------------------------|------------------------|---------|------------|---------------|
| | Weight, Structure and TPS | Tankage and Insulation | | | |
| Uncooled (1) | 139,073 | 35,665 | 297,894 | 48,000 | 1.00 |
| 200F Unshielded (2) | | | | | |
| Aluminum | 129,880 | 24,400 (5) | 297,894 | 67,458 (2) | 1.40 |
| Beryllium | 109,580 | 24,400 (5) | | 87,758 (2) | 1.82 |
| Boron/Aluminum | 116,880 | 24,400 (5) | | 80,458 (2) | 1.67 |
| Titanium | 136,880 | 24,400 (5) | | 60,458 (2) | 1.26 |
| 400F Unshielded (3) | | | | | |
| Beryllium | 90,300 | 36,000 (6) | | 96,430 (3) | 2.01 |
| Boron/Aluminum | 95,770 | 36,000 (6) | | 90,968 (3) | 1.92 |
| Titanium | 115,470 | 36,000 (6) | | 71,268 (3) | 1.48 |
| 600F Unshielded | | | | | |
| Beryllium | 95,400 | 38,200 (7) | | 89,138 | 1.85 |
| Boron/Aluminum | 96,600 | 38,200 (7) | | 87,938 | 1.83 |
| Titanium | 120,000 | 38,200 (7) | | 64,538 | 1.34 |
| 200F Shielded | | | | | |
| Aluminum | 111,620 | 24,400 (5) | | 85,718 | 1.79 |
| Beryllium | 91,320 | 24,400 (5) | | 106,018 | 2.21 |
| 400F Shielded | | | | | |
| Beryllium | 88,700 | 36,000 (6) | | 98,038 | 2.04 |
| Titanium | 113,620 | 36,000 (6) | | 73,138 | 1.52 |
| 200F/600F Unshielded (4) | 108,440 | 24,400 (5) | | 88,898 (4) | 1.85 |
| 200F/600F Shielded | 101,730 | 24,400 (5) | 297,894 | 95,608 | 1.99 |

- (1) From Reference 4
- (2) Weights do not include additional tankage, insulation, and fuselage (about 10,000 lb) to carry additional LH₂, thereby reducing payload.
- (3) Weights do not include additional tankage, insulation, and fuselage (about 200 lb) to carry additional LH₂, thereby reducing payload.
- (4) Weights do not include additional tankage, insulation and fuselage (about 3,000 lb) to carry additional LH₂, thereby reducing payload.
- (5) From Reference 2, Inconel 718 tanks and sealed foam insulation.
- (6) Weights do not include additional tankage, insulation, and fuselage (about 400 lb) to carry additional LH₂, thereby reducing payload.
- (7) From Reference 2, Inconel 718 tanks and CO₂ frost insulation.
- (8) Based on data of Reference 2, Inconel 718 tanks.

Examination of the last column in Table XLI suggests that payload improvements of from 50% to over 100% can be expected if cooled airframe technology is exploited in conjunction with advanced structural materials such as beryllium and metal matrix composite. The most attractive system is the 478°K (400F) shielded beryllium structure where the payload increase is about 140% of that for the uncooled baseline aircraft. However, it is rather surprising that a relatively state-of-the-art concept, the 366°K (200F) shielded aluminum alloy aircraft should permit a payload increase of about 80%.

Reliability. - The studies conducted to examine the overall question of reliability used the hypersonic transport cooling system shown in Figure 66 as a model. For a nonredundant system, 7 failures are expected per 1,000 flights; while for a completely redundant system, this decreases to only 4 failures per 100,000 flights. The comparison was made for a system that assumed glycol/water coolant and aluminum alloy construction. Reference to Table XXXIX indicates a weight difference of between 860 to 1600 kg (1,900 and 3,500 lb) between these two systems, a very small weight penalty indeed for such a substantial increase in reliability. With an equivalent weight increase, it would be possible to sustain a leakage rate of less than 0.2 kg/sec (0.5 lb/sec) during a total mission duration; this amounts to a leakage area of 1.30 mm² (0.002 in.²) for a system operating pressure of 2.07 MN/m² (300 psi). From a safety point of view, the completely redundant system approach seems more attractive.

In reviewing the reliability analysis of Table XXVII the skin panels and flexible hoses constituted the highest failure rates. Since the reliability analyses were based on panel having a width of 3 m (10 ft) and a length of up to 15 m (50 ft), the use of smaller panels would increase the failure rate because additional connections would be required between the coolant distribution lines and the cooled skin panels. To a first approximation, the failure rate of the total skin panel area would not increase; the increase in the number of panels would be offset by a decrease in failure rate because of reduced area of each panel. In actuality, a larger number of panels tends to mean an increased number of mechanical fasteners which tend to reduce reliability.

Fatigue and Fracture Considerations. - In the design of airframe structures, allowable stress levels must be established. As discussed in Reference 53, this involves consideration of static and fatigue strengths, as well as fracture toughness, and crack growth characteristics for various sizes of initial defects. As an aid to future design efforts, fatigue and fracture analyses were conducted. Both were based on the loading spectrum presented in Table VI. For the fatigue analysis, the stress/cycle data for the 2024-T3 alloy was obtained from Reference 21. For the fracture mechanics analyses, the correlations established for 2024-T3 alloy by Forman, Reference 54 were used. Fracture toughness values were obtained from References 21 and 56.

The fatigue life estimates were generated using an automated computational code based on the Miner cumulative damage theory. Theoretical stress concentration, factors of from 1.0 to 5.0 were used. The stress level corresponding to any particular load factor was computed by ratioing the applied load factor to the ultimate load factor and multiplying this ratio by an assumed design allowable ultimate stress level. This assumed stress level was varied from 27.5 to 45 kN/cm² (40,000 to 65,000 psi). The results are plotted in Figure 95, where the life scale is in increments of 10,000 hours. Based on fatigue considerations alone, and assuming a conservative stress concentration factor of 5.0 and a life scatter factor of 4.0, it is possible to estimate design allowable ultimate stress levels for various vehicle lives, as shown below:

0.276

Design Ultimate Tensile Stress, KN/cm²

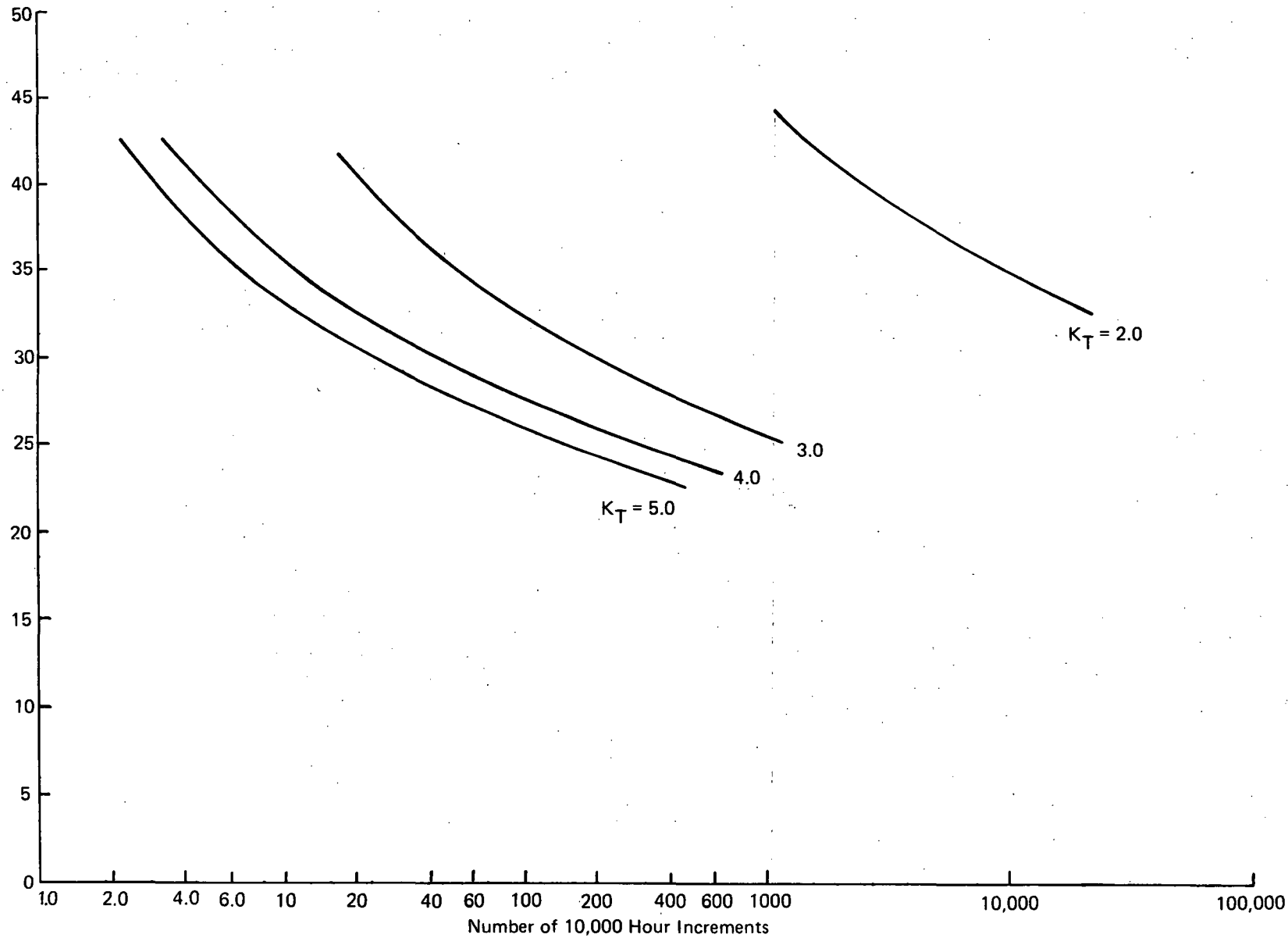


Figure 95a. Fatigue Characteristics of 2024-T3 Structure, HST Spectrum

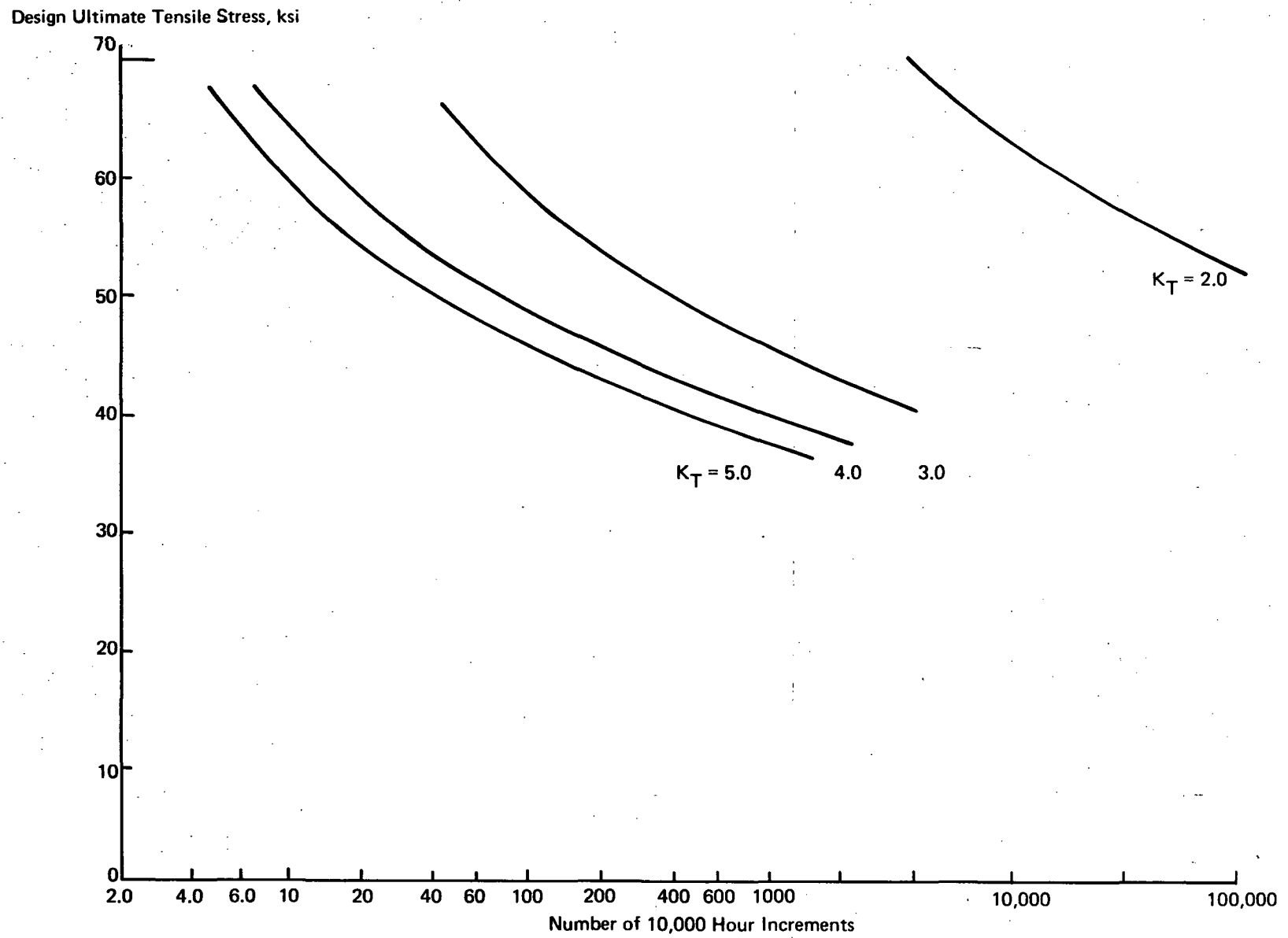


Figure 95b. Fatigue Characteristics of 2024-T3 Structure HST Spectrum

| Service Life, hours/flights | Design Life, hours | Design Allowable Ultimate Stress, kN/cm ² (psi) |
|--------------------------------|-----------------------|---|
| 10,000/5,000 | 40,000 | 45 (65,000) |
| 30,000/15,000 | 120,000 | 40 (58,000) |
| 50,000/25,000 | 200,000 | 37 (54,000) |

If the stress concentration factor is reduced by 5.0 to 4.0, the design allowable ultimate stress level increases by about 2.06 kN/cm² (3,000 psi). In reviewing the results, it appears that modest decreases in stress levels produce substantial increases in life and that realistic service lives can be expected at stress levels of the same magnitude as those that dictate the design of compressively loaded sheet metal structure. Significant benefits are obtained by minimizing stress concentrations.

Crack growth computations for the 2024-T3 alloys were made using the CRACKS computer code described in Reference 55. Conservatively, retardation effects were neglected. An infinite plate was assumed for the particular analysis conducted. Stress levels for the loading spectrum were obtained in the same manner as for the fatigue analyses. Defects of two types were considered: surface scratches and through cracks. Results predicted, using the Forman equations shown below, are presented in Figure 96:

$$da/dN = C_f (\Delta K)^{n_f} / (1-R) K_{cf} - K$$

where

$$C_f = 3 \times 10^{-13}, n_f = 3.0, \text{ and } K_{cf} = 83 \text{ ksi} \sqrt{\text{in.}}$$

Analyses conducted using the Paris correlation, Reference 57, provided more optimistic behavior predictions, while the use of the correlations of Hudson and Poe, References 58 and 59, would have lead to somewhat more conservative results. In Figure 96, the life shown for the surface scratch condition is the time required for the crack to propagate through the total thickness. At this point, the through crack results can be used to estimate the remaining life. For the surface scratch cases, the crack pops through the thickness after reaching a depth of 0.25 and 0.65 mm (10 and 25 mils), so that relatively little time is spent propagating the crack through the 2nd half of a laminated 1 mm (40 mil) sheet; assuming that the mid-thickness joint does not retard crack growth.

The results predicted for the surface scratches are considered to be conservative. The stress concentrating effects of a shallow surface scratch are relatively unknown; behavior may be more similar to fatigue than to fracture mechanics. For a laminated skin, the nature of the bond may modify the growth rate through the thickness, such that the progress of crack growth is retarded. This type of behavior has been observed for laminated aluminum alloy, Reference 60, and titanium alloy, Reference 61.

If it is assumed that surface scratches having a depth of more than 0.05 mm (2 mils) can be detected, and that through cracks of more than 0.25 mm (10 mils) are unlikely to be present in sheet material, the design allowable stress levels based on fracture mechanics considerations for representative service lives can be given as:

Ultimate Design Allowable Stress

———— Through Crack

----- Surface Flaw

A_o , Initial Crack Depth, cm -----

A_o , Initial Half Crack Size, cm ————

Number of 10,000 Hour Increments

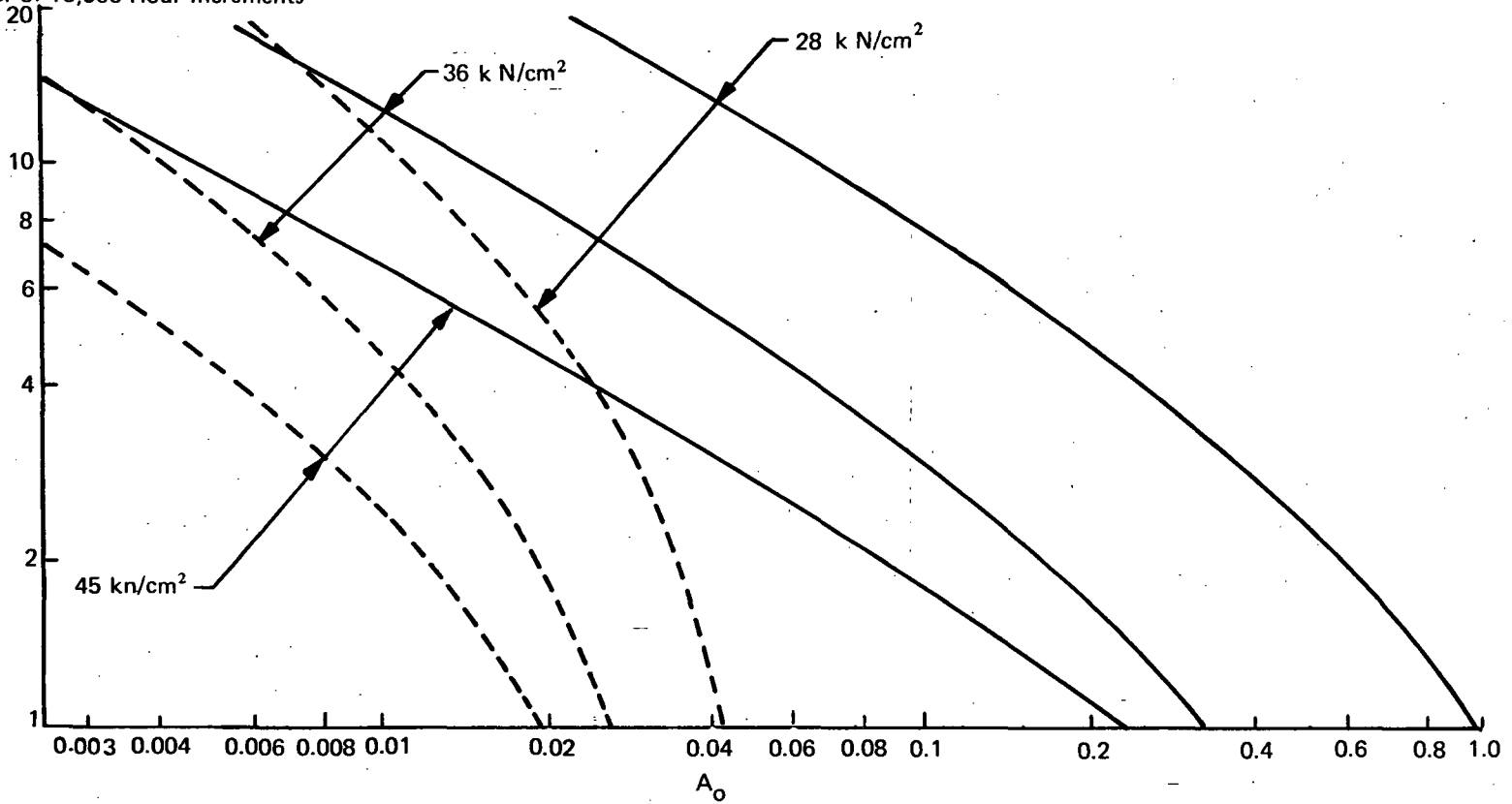


Figure 96a. Interaction of Life, Ultimate Design Allowable Stress and Initial Crack Size, Infinite.
2024-T3 Sheet, HST Spectrum

Ultimate Design Allowable Stress

———— Through Crack

----- Surface Flaw

A_o , Initial Crack Depth, Inch -----

A_o , Initial Half Crack Size, Inch ————

Number of 10,000 Hour Increments

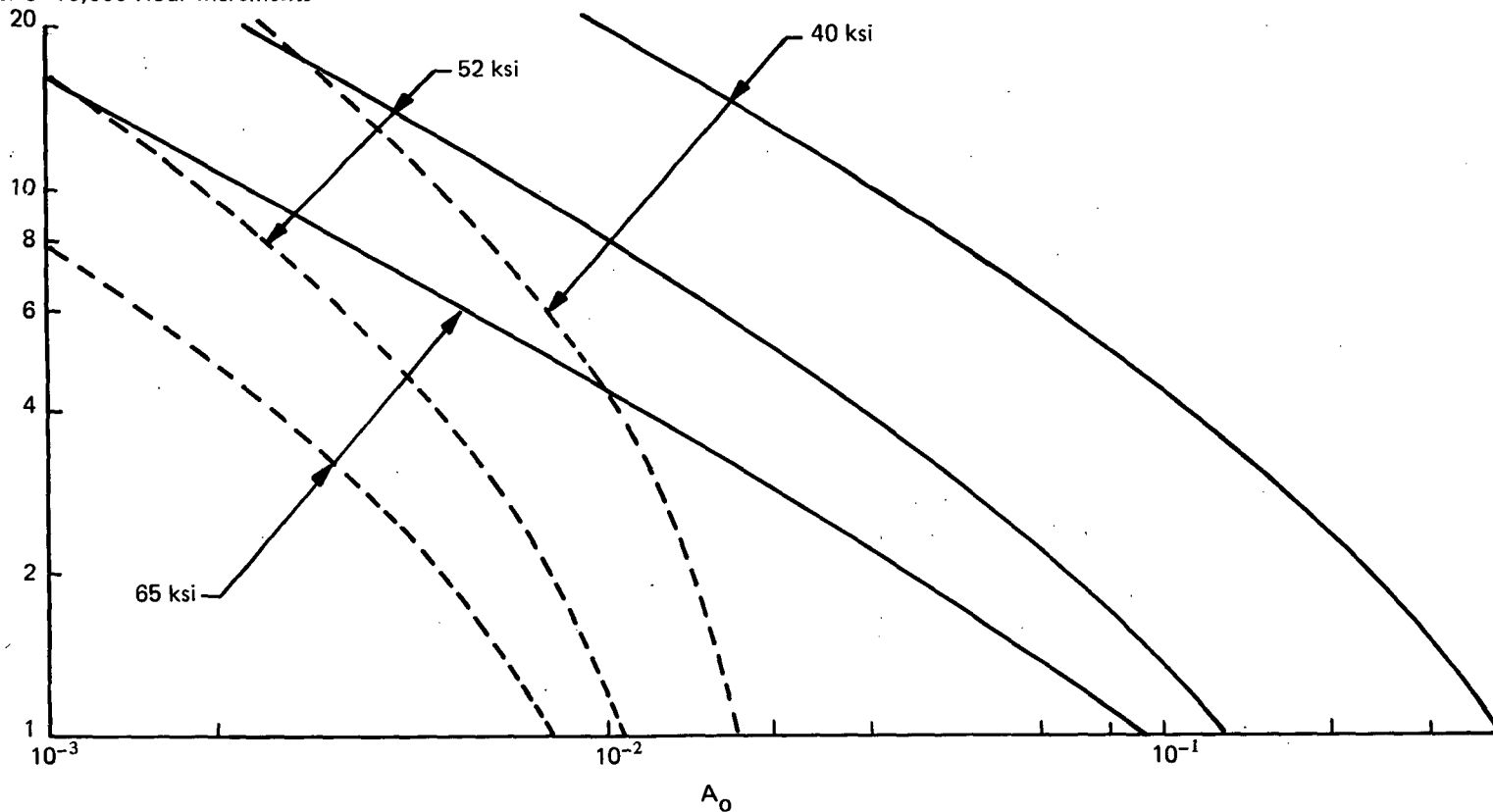


Figure 96b. Interaction of Life, Ultimate Design Allowable Stress and Initial Crack Size, Infinite 2024-T3 Sheet, HST Spectrum

| <u>Service Life, hours/flights</u> | <u>Design Life, hours</u> | <u>Design Allowable Ultimate Stress, Scratch/Through Crack, kN/cm² (psi)</u> | |
|--|-------------------------------|---|-----------------|
| 10,000/5,000 | 40,000 | 45/45 | (65,000/65,000) |
| 30,000/15,000 | 120,000 | 35/32 | (50,000/47,000) |
| 50,000/25,000 | 200,000 | 30/28 | (43,000/40,000) |

For a design life of 5,000 flights and the assumed initial defect sizes, fracture mechanics considerations do not influence the design. For the more realistic design lives of between 15,000 and 25,000 flights, fatigue and fracture considerations impose similar constraints of considerable magnitude upon the design.

Hypersonic Research Airplane

Structural Concepts. - Because of the nearer term potential of this aircraft as compared to the transport, structural considerations were limited to aluminum alloys. Based on the results obtained from comparing numerous structural concepts for the hypersonic transport over a range of loading intensities, the structural configuration for the HRA fuselage was assumed to be skin/stringer/frame construction with Z-stiffeners. For the wing structure, both the Z-stiffened skin and sandwich types of construction were considered. The structural weights were based on the loading intensities discussed previously. The maximum limit loading for the fuselage was only 1.0 kN/cm (560 lb/in.) while that for the wing was only 1.1 kN/cm (630 lb/in.) despite the very thin wing, only 32.8 cm (12.9 in.) thick at the root. With such low loading intensities, most of the airframe was designed by the minimum gage consideration. In the case of the wing structure, the minimum equivalent thicknesses for the stiffened and sandwich types of construction were the same, $\bar{t} = 1.8$ mm (0.070 in.) and $\bar{w} = 4.98$ kg/m² (1.02 psf). Because of the same equivalent thicknesses the stiffened approach was assumed because of its significantly lower cost. In addition, sizing studies were conducted for the propellant tankage which was assumed to be integral. Such analyses were not required for the transport because the baseline configuration employed nonintegral tanks, the weight of which was defined in Reference 2.

For both the fuselage and the wings, the weight estimation procedure involved sizing the covers for the loading intensity or the minimum equivalent thickness, whichever was greater, and using design experience factors to account for substructure, fittings, and nonoptimum considerations. Structural weight of the covers, skins plus stringers, were computed at various fuselage locations and were integrated circumferentially and axially to determine the cover weights. The minimum weight structure at the top centerline, bottom centerline, and vertical side was sized using a panel optimization program which accepted simultaneously applied axial, shear, and normal pressure loadings. A minimum gage thickness of 1 mm (0.04 in.) was introduced for the skin and for the stiffeners. The structure was sized conservatively to preclude buckling under ultimate load conditions so that there would be no distortions that might influence the cross sectional shape of any of the coolant passages. Checks with another optimization routine which permitted buckling under ultimate load conditions predicted a slight weight reduction potential. Even with the nonbuckling design constraint, the equivalent thickness of the non-tankage regions of the aircraft was 1.6 mm (0.063 in.), about 10% lighter than the 1.8 mm (0.070 in.) equivalent minimum gage defined previously for skin/stringer construction. The weight reduction results from increased stringer spacing in the forward fuselage structure.

Sizing of the structural elements at various locations in the forward fuselage are illustrated in Figure 97. The stringer design shown was specified as the minimum allowable so that the optimization tended to increase the spacing somewhat. Note that the stiffener spacings for the optimum designs are not compatible with an integer number of stiffeners. The digits in parentheses indicate the number of stiffeners at each station and the resultant spacing. The particular arrangements are not compatible with a logical decrease in the number of stiffeners from Station 360 forward. The numbers to the right of each sketch indicate a likely design arrangement and the corresponding spacing. While the various stations were not resized for the design that permitted a reasonable decrease in the number of stiffeners in the forward region of the fuselage the weight increase involved is expected to be less than 2%.

The relatively wide spacings of the stringers led to the consideration of the possibility of using a greater sheet thickness and still wider spacing. If the weight penalty is not too significant this would permit wider spacing for the coolant passages. However, it was found that relatively large weight penalties are associated with increasing the thickness of the structural skin. For example, if the skin thickness is doubled from 1 mm (0.040 in.) to 2 mm (0.08 in.) a weight increase of about 55% is incurred while the distance between coolant passages is increased by 40%. The increase in passage spacing will decrease the weight of residual coolant slightly but this benefit is small compared to the structural weight increase. However, if it is desirable to increase the passage spacing in the highly heated region of the forward fuselage a 60% structural weight increase in this region is not necessarily prohibitive, since the forward fuselage structure represents only about 180 kg (400 lb) (exclusive of fittings) out of a total fuselage weight of 2930 kg (6200 lb), amounting to approximately 115 kg (250 lb). Furthermore, if mechanical fastening is used between the skin and substructure there would be some cost saving since rivet spacing would be increased.

No detailed analyses were performed for the wing covers since the low loading intensities suggested the use of lighter structure than dictated on the basis of minimum equivalent thickness 1.78 mm (0.070 in.) for the stringer stiffened skin. Therefore, minimum weight construction of 4.98 kg/m² (1.02 psf) was used resulting in a cover weight of 365 kg (800 lb). Prior studies of low aspect ratio highly swept wings suggest that the wing covers constitute 60% to 65% of the wing weight. Thus, a weight of 227 kg (500 lb) was assumed for the substructure. A relatively high fitting weight, 137 kg (300 lb), was assumed since the main landing gear is mounted in the wing near the wing/fuselage intersection. A nonoptimal weight penalty of 910 kg (2000 lb) was also included to account for integration of the substructure with the cooled skin panels, access doors and the penalties involved with the large landing gear doors. The total wing weight was estimated to be 820 kg (1800 lb).

Since the loads on the vertical tails should be lighter than on the wings by virtue of the shorter tail spans, the tail weights were estimated on the basis of a minimum equivalent thickness of 1.8 mm (0.070 in.) for the covers, 330 kg (730 lb). Weight increments for the ribs and spars, the fittings, and the nonoptimum allowance were 160 kg (350 lb), 50 kg (110 lb), and 50 kg (110 lb) respectively. Thus the total tail weight was 590 kg (1300 lb).

In sizing the integral propellant tankage analytical emphasis was placed on the tank frames and heads since the skin is relatively easy to size. For purposes of these analyses the wing shears and bending moments were assumed to be transferred to the tank from the central third of the wing chord, 33% to 67%, through frames spaced approximately 0.51 m (20 in.) apart. The torsional load was taken by that portion of the wing from the 5% to the 67% chord. Loads from the rear captive flight hook and from the main landing gear were assumed to be reacted on a single frame at Station 721. The frames were sized initially for four conditions, namely ultimate tank pressure differential of 6.9 N/cm² (10 psi)

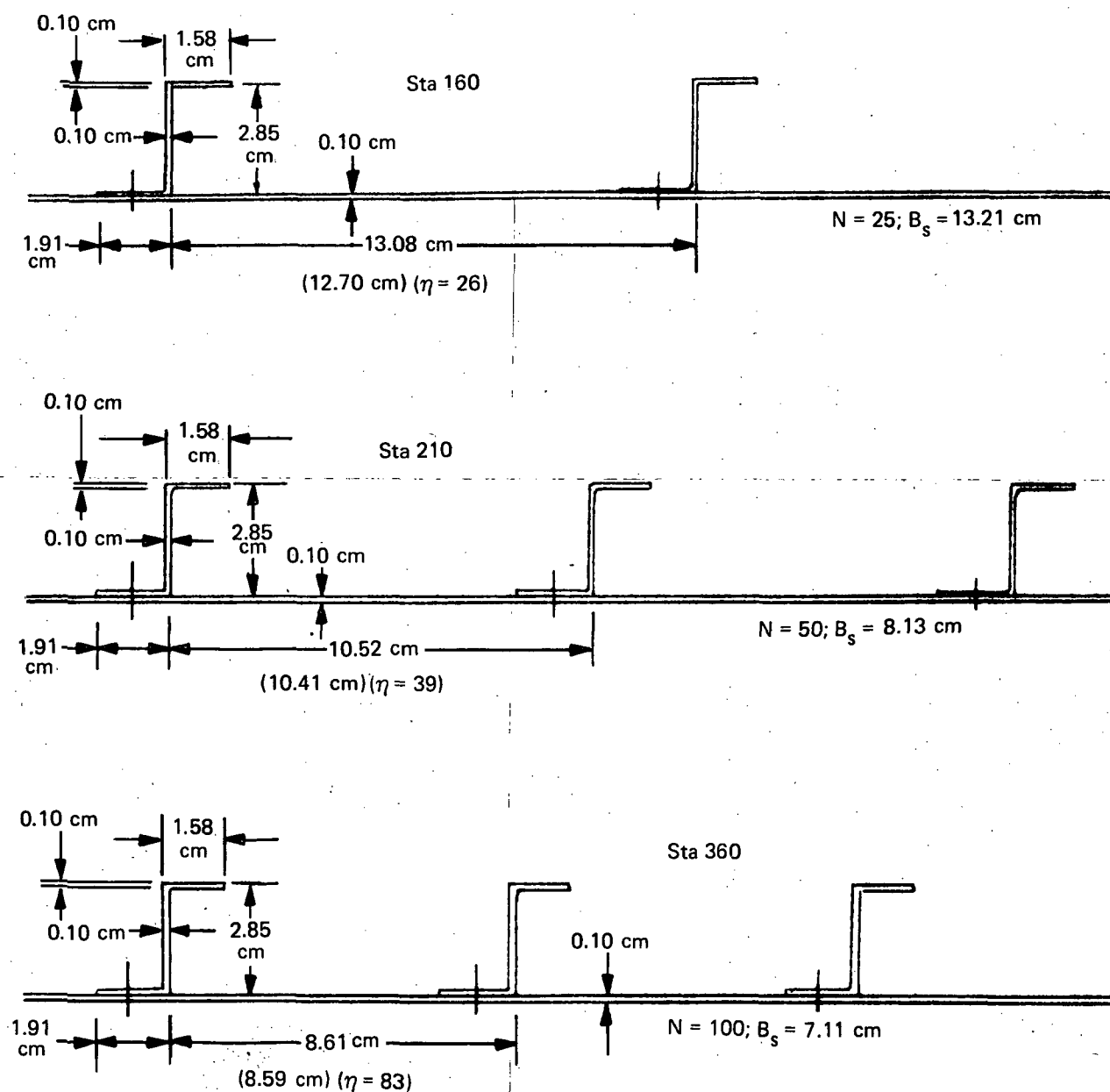


Figure 97a. Skin Stringer Dimensions for Hypersonic Research Aircraft

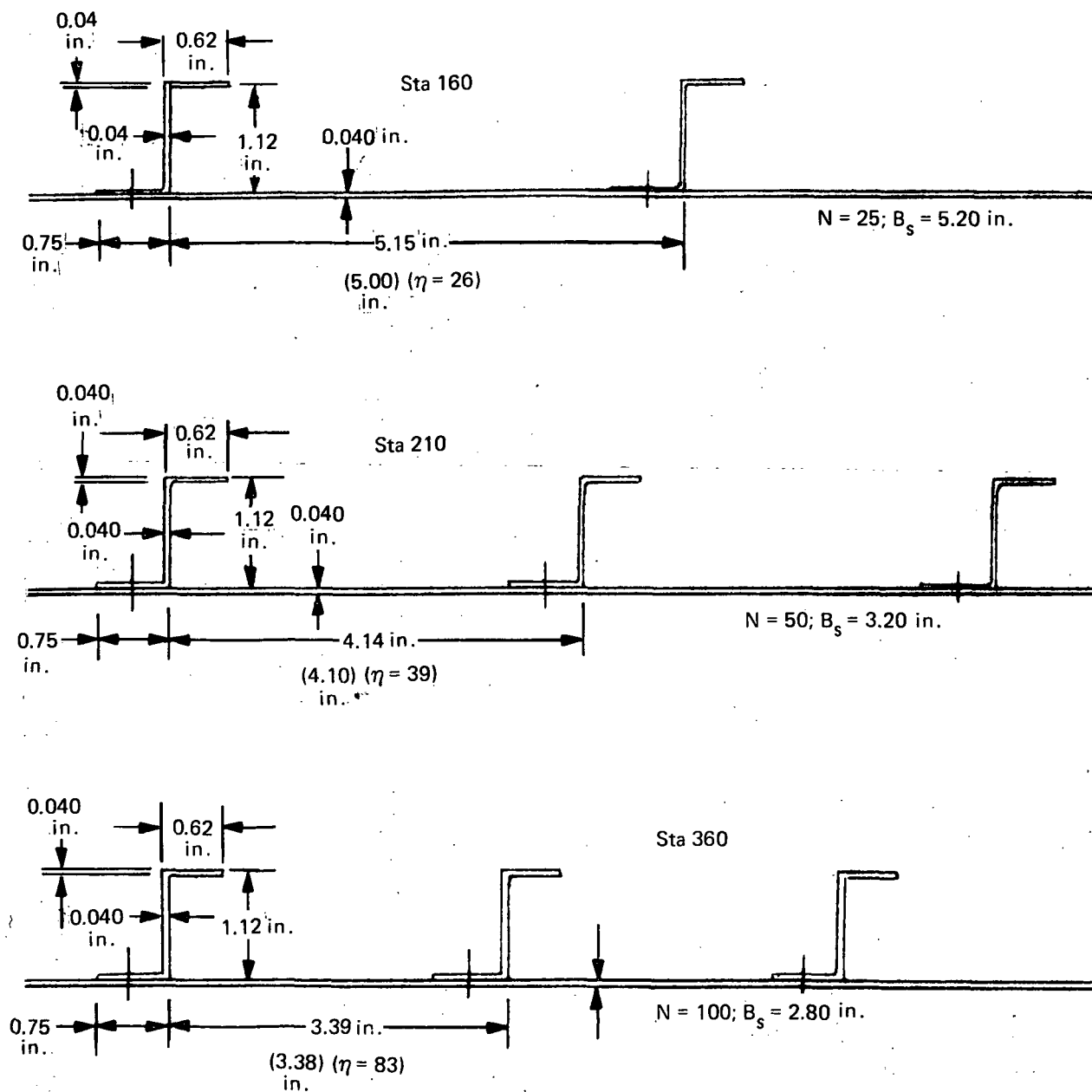


Figure 97b. Skin Stringer Dimensions for Hypersonic Research Aircraft

flight limit load factor of 3.0 g combined with a working tank pressure of 3.5 N/cm^2 (5 psi), captive limit load factor of 2.0 g combined with the working tank pressure of 3.5 N/cm^2 (5 psi), and landing loads combined with the working tank pressure of 3.5 N/cm^2 (5 psi). For purposes of analysis, the maximum depth of the frame at station 721 was 0.3 m (12 in.) while that for other frames was 0.25 m (10 in.). Initial analyses assumed constant frame depth and EI but after these initial solutions were obtained the frame characteristics were refined but were not fully optimized. Thus, the weight results should be slightly conservative. The tank heads were also sized in a somewhat conservative manner by assuming the heads to be flat plates, computing the unit weight of the head, and applying this unit weight to the actual head area.

The results of these initial analyses were used in estimating the airframe weight. However, to provide an indication weight trends with tank pressure level analyses were repeated with ultimate and limit tank pressures of 13.8 N/cm^2 (20 psi) and 6.9 N/cm^2 (10 psi), and of 27.6 N/cm^2 (40 psi) and 13.8 N/cm^2 (20 psi). The tankage weight increases were 318 kg (700 lb) and 1100 kg (2400 lb) respectively, due primarily to the noncircular cross section of the tankage. The introduction of a single vertical tension strap across each frame reduces the penalties to 38 kg (85 lb) and 235 kg (520 lb) respectively. Thus, if a vertical tie is used the $13.8/6.9 \text{ N/cm}^2$ (20 psi/10 psi) design condition can be met for essentially the same weight as that needed for the $6.9/3.5 \text{ N/cm}^2$ (10 psi/5 psi) condition without the tie.

The results of the fuselage sizing studies are shown as weight per unit length in Figure 98. This running weight includes the stiffened skins, frames, and tank ends: integration yields a fuselage weight of 2220 kg (4900 lb), 1740 kg (3825 lb) for covers and 480 kg (1055 lb) for frames. To this is added 600 kg (1320 lb) for fittings and the nonoptimum penalty bringing the total fuselage structural weight to 2850 kg (6220 lb). The wing and tail structure adds an additional 1410 kg (3100 lb) as shown in Table XLII bringing the airframe weight to 4250 kg (9320 lb).

Cooling System Concepts. - One potential objective of a hypersonic research airplane is to evaluate an actively cooled structure. The relatively near term of such a research airplane is likely to focus attention on conventional materials, with aluminum being the most promising. Because of this, the primary effort with respect to cooling system comparisons involved consideration of the most likely coolant choice. However, since it might be desirable to utilize the same construction material, coolant, and operating temperature level for the HRA as those expected to be used in a hypersonic transport, consideration was given also to other coolants which would permit structural temperatures of up to 589°K (600°F). In addition, consideration of heat load matching to fuel flow heat capacity suggested that some form of heat load attenuation or enhancement of available heat capacity of the fuel would be required after the initial acceleration phase as shown in Figure 99. An alternative is to carry hydrogen especially for cooling purposes. This would involve about 1530 kg (3400 lb) of hydrogen somewhat more than the scramjet fuel required to accelerate from 3.5 to Mach 8. In addition, it might be necessary to carry an additional 10% to 20% of hydrogen to deal with maneuver heat loads, thereby increasing the quantity of additional hydrogen to about 1820 kg (4000 lb). If direct surface cooling of the airframe is used for flight to Mach 10, the quantity of additional hydrogen required specifically for cooling purposes could approach 2720 kg (6000 lb).

The heat load attenuation techniques considered included the use of a higher average structural operating temperature to reduce the heat load and to simultaneously increase the available heat capacity of the hydrogen fuel since it would be possible to heat the hydrogen to about 450°K (350°F) rather than 340°K (150°F) as is the case for cooled aluminum structure. An increase in the average

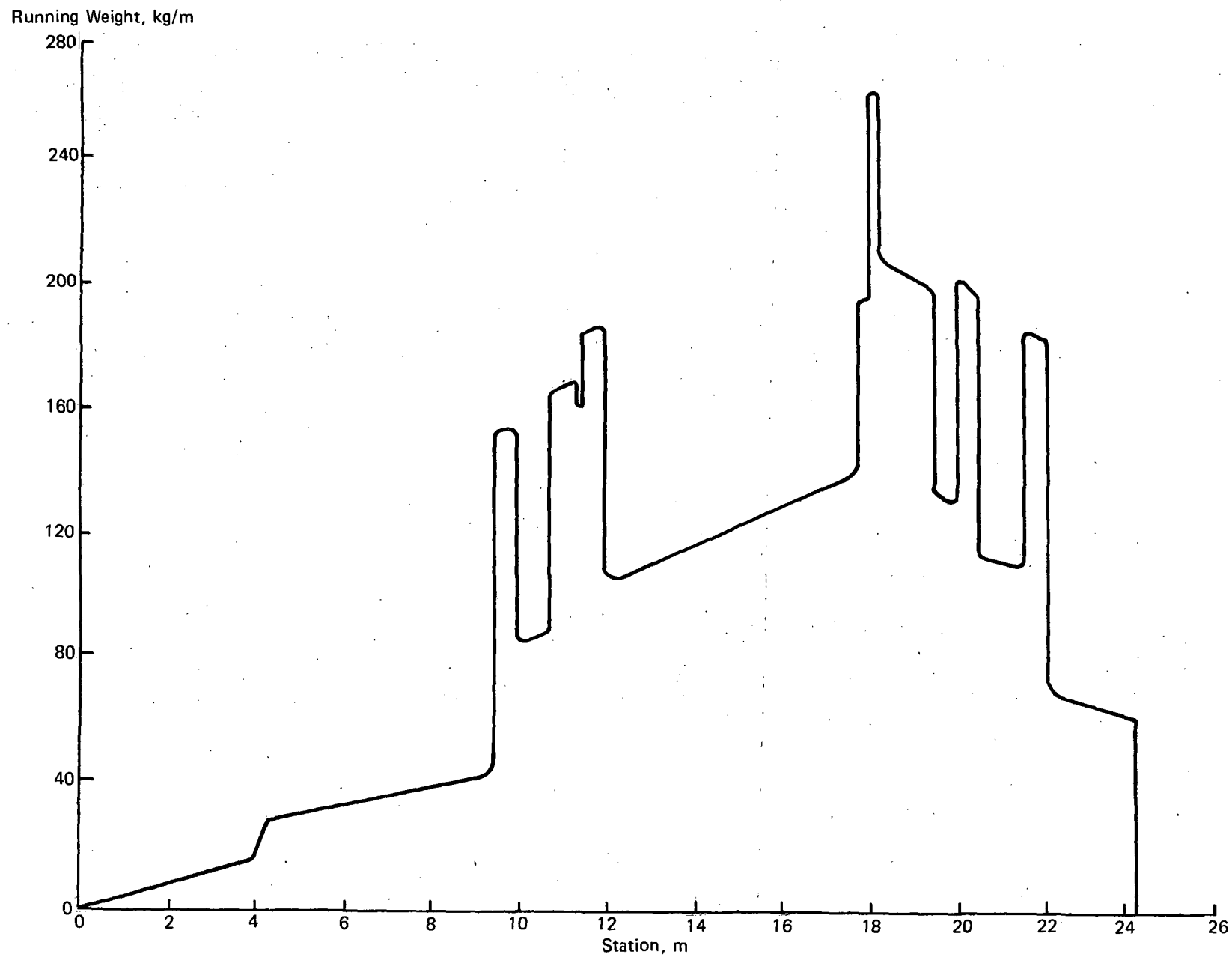


Figure 98a. Fuselage Running Weight, Shell and Frames

Running Weight, lb/in.

14

12

10

8

6

4

2

0

0

100

200

300

400

500

600

700

800

900

1000

Station, Inches

Figure 98b. Fuselage Running Weight, Shell and Frames

TABLE XLIIA
HRA AIRFRAME STRUCTURE WEIGHT SUMMARY

| | | |
|----------|---------------------|--------------------|
| Fuselage | Covers | Kilograms 1,746 |
| | Frames | 479 |
| | Fittings | 350 |
| | Non-Optimum Penalty | 250 |
| | | <u>2,825</u> |
| Wings | Covers | 363 |
| | Ribs and Spars | 227 |
| | Fittings | 136 |
| | Non-Optimum Penalty | 91 |
| | | <u>817</u> |
| Tails | Covers | 331 |
| | Ribs and Spars | 159 |
| | Fittings | 50 |
| | Non-Optimum Penalty | 50 |
| | | <u>590</u> |
| Total | | 4,232 |

TABLE XLIIB
HRA AIRFRAME STRUCTURE WEIGHT SUMMARY

| | | |
|----------|---------------------|-----------------|
| Fuselage | Covers | Pounds 3,845 |
| | Frames | 1,055 |
| | Fittings | 770 |
| | Non-Optimum Penalty | 550 |
| | | <u>6,220</u> |
| Wings | Covers | 800 |
| | Ribs and Spars | 500 |
| | Fittings | 300 |
| | Non-Optimum Penalty | 200 |
| | | <u>1,800</u> |
| Tails | Covers | 730 |
| | Ribs and Spars | 350 |
| | Fittings | 110 |
| | Non-Optimum Penalty | 110 |
| | | <u>1,300</u> |
| Total | | 9,320 |

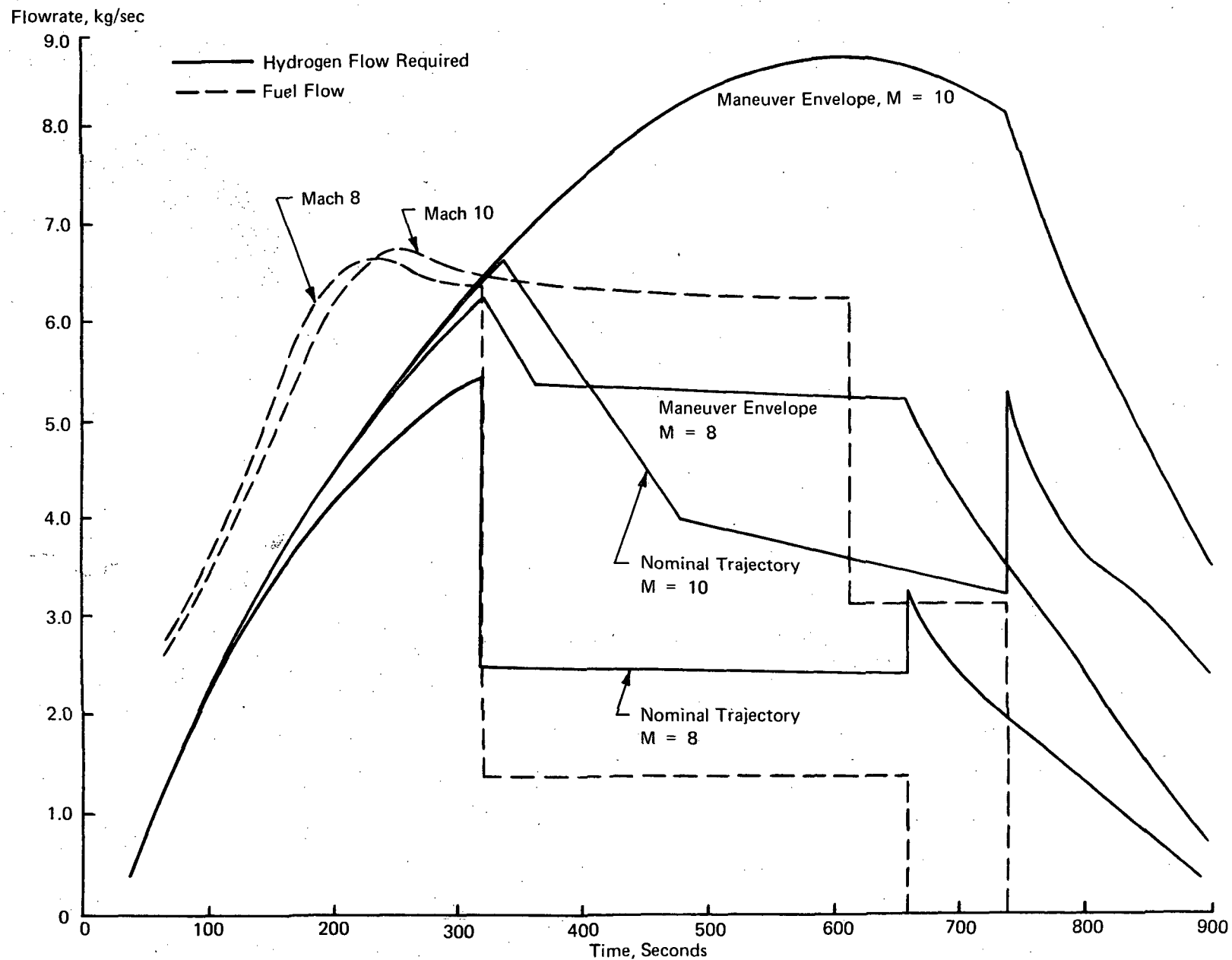


Figure 99a. Hydrogen Cooling Requirements and Fuel Flow Requirements for HRA,
Coolant Temperatures In/Out = 283/366°K
Maximum Structural Temperature = 394°K

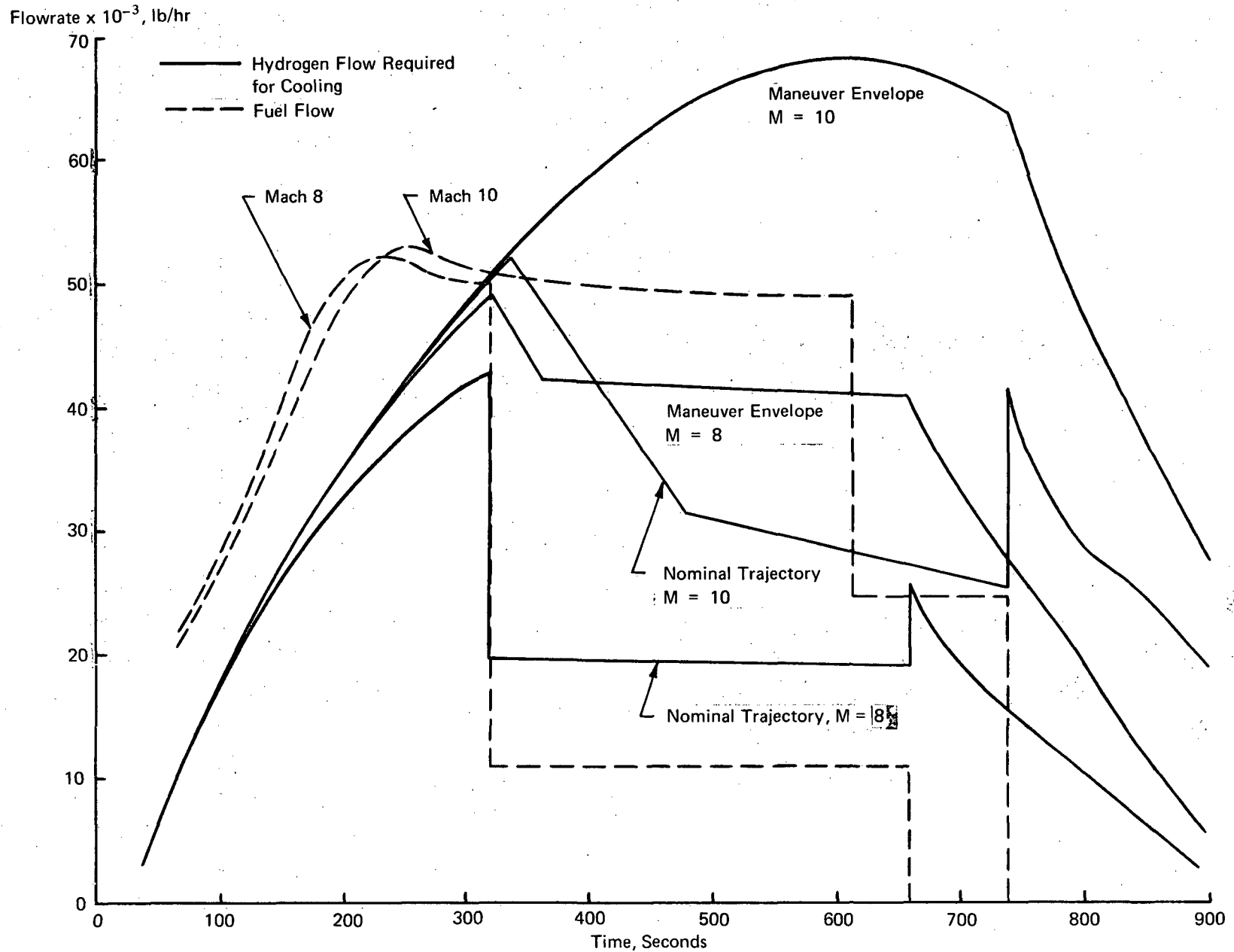


Figure 99b. Hydrogen Cooling Requirements and Fuel Flow Requirements for HRA, Coolant Temperatures In/Out = 50F/200F, Maximum Structural Temperature = 250F

structural temperature to 589°K (600F) reduces the heat load by about 16% while the higher temperature to which the hydrogen can be cooled increases the fuel heat capacity that is available for structural cooling by 35%. Both trends substantially reduce the amount of hydrogen that would have to be carried for cooling purposes. Thus, during cruise at Mach 8 the excess hydrogen required specifically for cooling would be only 183 kg (400 lb). The total quantity of additional hydrogen would be about 1360 kg (3000 lb). Another means of attenuating the heat load to the cooling system is to use external heat shielding or insulation. In fact, the plan for this particular HRA vehicle was to employ RSI to extend the flight speed capability from Mach 8 to 10. Several forms of insulation will be discussed later. The dual temperature cooling system also provides a means of enhancing the quantity of heat that can be rejected to the fuel flow.

Weights for convective cooling systems based on the configuration of Figure 100 are presented in Table XLIII for various coolants and airframe thermal protection concepts. Nonredundant systems tend to be about 20 to 25% lighter than redundant systems. The use of the methanol/water coolant results in a system that is about 8% lighter than for glycol/water. Although not shown in the table, other coolants were considered for the 366°K (200F) average temperature aluminum alloy structure; Coolanol 20, Coolanol 40 and FC-43 yielded systems that were significantly heavier than those based on aqueous solutions. The poor thermal performance of the non-aqueous solutions can be seen by comparing the unshielded 366°K (200F) systems to the unshielded 478°K (400F) system. Increasing the maximum structural temperature improves the thermal performance of the Coolanol system because the coolant temperature rise is increased and the heat load is reduced. The weight of the 589°K (600F) system is approximately equal to that of an unshielded 366°K (200F) ethylene-glycol/water system. A comparable weight can also be obtained with the dual temperature system concept. As shielding is added to the aircraft, the aerodynamic heat load to the cooling system is attenuated and cooling system weights decrease as shown.

The weights of Table XLIII represent only cooling system elements. Auxiliary items required for proper functioning of the thermal protection system in a total sense are not included in total. For any of the cooling systems, hydrogen must be carried specifically for cooling during descent since the vehicle as presently configured uses all of its fuel by the end of cruise, and unless hydrogen flow is continued for airframe cooling, the structure will overheat. Obviously the radiation shields and RSI incur weight increments. Total airframe weights will be discussed later.

Although weight considerations favor the use of methanol/water with aluminum alloy construction, practical considerations are involved in the selection between aqueous solutions of glycol and methanol as coolants. Both are electrically conductive and rely on inhibitors for corrosion resistance. Neither coolant type shows any decomposition below 394°K (250F). Primary disadvantages of methanol/water solutions are their high vapor pressure, flammability, and toxicity. The major advantage of methanol/water coolants is the ability to provide lower freezing points and the related characteristic of lower viscosity than water/glycol solutions at temperatures below about 255K (0F); at temperatures above about 255°K (0F) viscosity characteristics are about the same.

Although both the methanol and glycol solutions contain water, the vapor pressure characteristics are sufficiently different, such that a non-flammable water rich vapor is produced when a glycol solution evaporates while a flammable vapor is produced by the evaporation of a methanol/water solution. Thus, for manned systems the methanol containing coolants may be inferior to the glycols

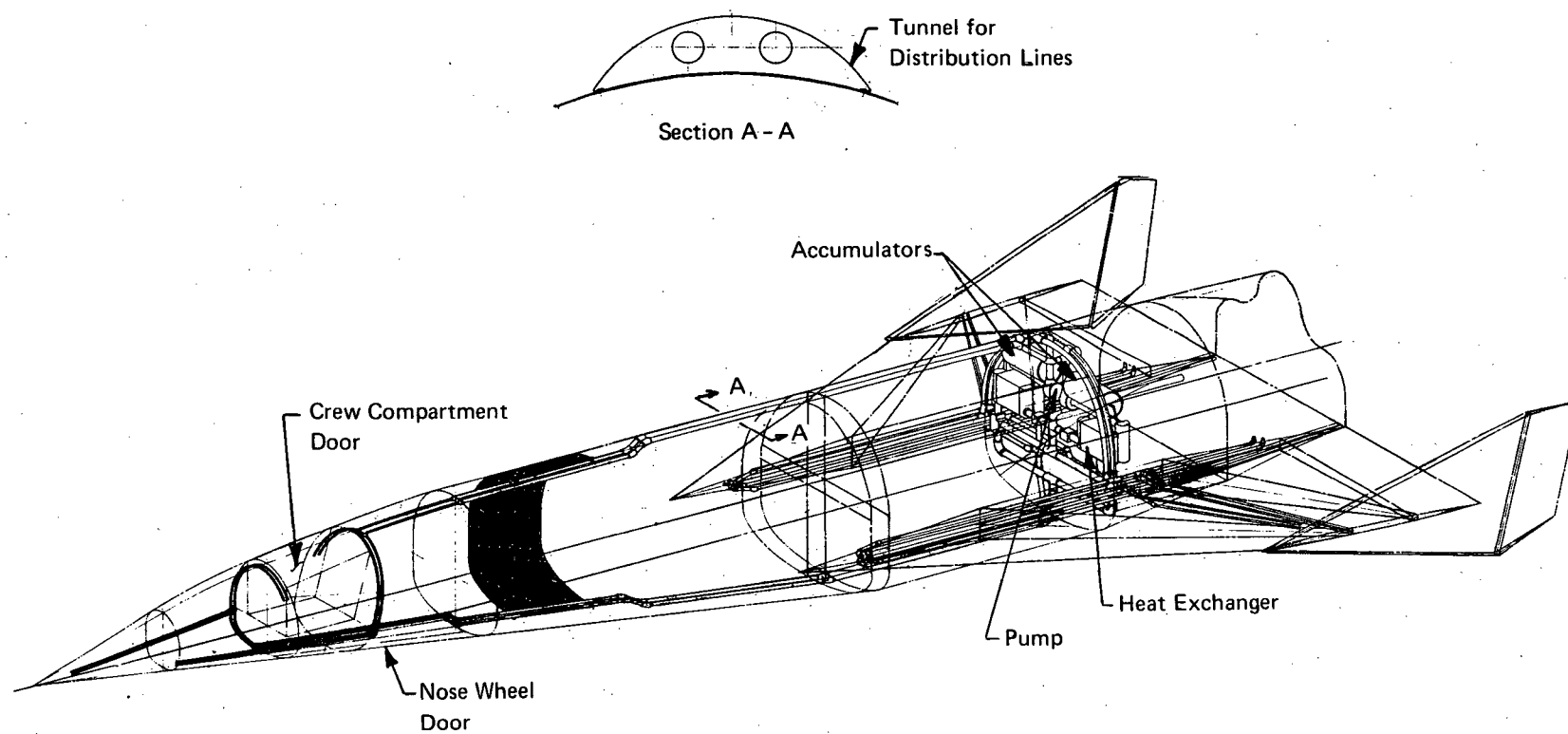


Figure 100. Distribution System Layout, Hypersonic Research Aircraft

TABLE XLIIIA
COOLING SYSTEM CONCEPT COMPARISON,
HYPERSONIC RESEARCH AIRPLANE BASELINE PANEL

| Item | Weights for Cooling System for Average Airframe Temperature Indicated, Kilograms ⁽³⁾ | | | | | | |
|-----------------------------------|--|-----------------------|-----------------------|----------------------------------|------------------|----------|---------------------------|
| | Unshielded | | | | 366° K, Shielded | | 366° K, RSI |
| | 366° K ⁽⁴⁾ | 477° K ⁽⁵⁾ | 588° K ⁽⁶⁾ | 366° K/ 588° K ⁽⁷⁾ | M = 8.0 | M = 10.0 | Optimized for M = 10.0 |
| Design Heat Load, Mw | 282 | 270 | 234 | 270 | 107 | 187 | 53 |
| REDUNDANT | | | | | | | |
| Distribution Lines ⁽¹⁾ | 717; 663 | 1,053 | 745 | 722 | 327 | 490 | 172 |
| Heat Exchangers, Two | 499; 468 | 654 | 354 | 463 | 177 | 327 | 81 |
| Pumps, Two | 36; 32 | 64 | 36 | 36 | 23 | 23 | 14 |
| Panel Residual ⁽²⁾ | 268; 241 | 345 | 400 | 295 | 204 | 295 | 109 |
| Miscellaneous ⁽³⁾ | 154; 140 | 213 | 154 | 159 | 73 | 114 | 39 |
| Total | 1,674; 1,544 | 2,329 | 1,689 | 1,675 | 804 | 1,249 | 415 |
| NONREDUNDANT | | | | | | | |
| Distribution Lines ⁽¹⁾ | 667; 622 | 972 | 690 | 667 | 281 | 436 | 168 |
| Heat Exchanger | 250; 234 | 327 | 177 | 232 | 91 | 163 | 41 |
| Pump | 18; 16 | 32 | 18 | 18 | 14 | 14 | 7 |
| Panel Residual ⁽²⁾ | 268; 241 | 345 | 400 | 295 | 204 | 295 | 109 |
| Miscellaneous ⁽³⁾ | 123; 114 | 168 | 127 | | 59 | 91 | 32 |
| Total | 1,326; 1,227 | 1,844 | 1,412 | 1,212 | 649 | 999 | 357 |

- (1) Lines, contained Coolant, and APS fuel to drive pump
- (2) Redundant and nonredundant entries are the same because half flow is in each of the two redundant sets of passages
- (3) 10% to account for valves, controls, supports, etc.
- (4) Glycol/Water; Methanol/Water Weights Account for Double Entries, Coolant Inlet/Outlet 283°K/360°K
- (5) Titanium Structure, Coolanol 20, Coolant Inlet/Outlet 283°K/394°K
- (6) Titanium Structure, Coolanol 40, Coolant Inlet/Outlet 283°K/450°K
- (7) Dual Temperature System, Glycol/Water and Coolanol 40

TABLE XLIIB
COOLING SYSTEM CONCEPT COMPARISON, HYPERSONIC RESEARCH AIRPLANE BASELINE PANEL

| Item | Weights For Cooling System For Average Airframe Temperature Indicated, Pounds ⁽³⁾ | | | | | | |
|---|---|---------------------|---------------------|------------------------------|----------------|----------|-------------------------|
| | Unshielded | | | | 200F, Shielded | | 200F, RSI |
| | 200F ⁽⁴⁾ | 400F ⁽⁵⁾ | 600F ⁽⁶⁾ | 200F/ 600F ⁽⁷⁾ | M = 8.0 | M = 10.0 | Optimized for M=10.0 |
| Design Heat Load, 10 ⁶ BTU/hr | 96 | 92 | 80 | 92 | 36 | 64 | 18 |
| REDUNDANT | | | | | | | |
| Distribution Lines ⁽¹⁾ | 1,580 ; 1,460 | 2,320 | 1,640 | 1,590 | 720 | 1,080 | 380 |
| Heat Exchangers, Two | 1,100 ; 1,030 | 1,440 | 780 | 1,020 | 390 | 720 | 180 |
| Pumps, Two | 480 ; 70 | 140 | 80 | 80 | 50 | 50 | 30 |
| Panel Residual ⁽²⁾ | 590 ; 530 | 760 | 880 | 650 | 450 | 650 | 240 |
| Miscellaneous ⁽³⁾ | 340 ; 310 | 470 | 340 | 350 | 160 | 250 | 85 |
| Total | 3,690 ; 3,400 | 5,130 | 3,720 | 3,790 | 1,780 | 2,750 | 915 |
| NONREDUNDANT | | | | | | | |
| Distribution Lines ⁽¹⁾ | 1,470 ; 1,370 | 2,140 | 1,520 | 1,470 | 620 | 960 | 370 |
| Heat Exchanger | 550 ; 515 | 720 | 390 | 510 | 200 | 360 | 90 |
| Pump | 40 ; 35 | 70 | 40 | 40 | 30 | 30 | 15 |
| Panel Residual ⁽²⁾ | 590 ; 530 | 760 | 880 | 650 | 450 | 650 | 240 |
| Miscellaneous ⁽³⁾ | 270 ; 250 | 370 | 280 | | 130 | 200 | 70 |
| Total | 2,920 ; 2,700 | 4,060 | 3,110 | 2,940 | 1,430 | 2,240 | 785 |

- (1) Lines, contained coolant, and APS fuel to drive pump
- (2) Redundant and nonredundant entries are the same because half flow is in each of the two redundant sets of passages
- (3) 10% to account for valves, controls, supports, etc.
- (4) Glycol/Water; Methanol/Water Weights Account for Double Entries, Coolant Inlet/Outlet 50F/200F
- (5) Titanium Structure, Coolanol 20, Coolant Inlet/Outlet 50F/250F
- (6) Titanium Structure, Coolanol 40 Coolant Inlet/Outlet 50F/350F
- (7) Dual Temperature System, Glycol/Water and Coolanol 40

because of the potential hazard caused by their higher vapor pressure and their lower flash points. While great care will be taken with the vehicle hydrogen fuel system, it is more difficult to determine the extent to which such care would be applied to the cooling system. If applied extensively, flammability of the coolant may be of little concern; if not, catastrophic consequences may result from coolant leakage. The possibility of leakage of a toxic fluid can have an adverse influence on the design of the life support system, perhaps including weight increases due to safety devices needed to minimize the influence of a toxic leak. Toxic fluids with high vapor pressures are particularly undesirable. While every effort would be taken to preclude leakage, it is impossible to ensure 100% prevention.

The lower freezing point and low temperature viscosity characteristics of methanol/water solutions make them particularly attractive for space radiator systems where internally generated heat loads are to be rejected. The complex control requirements and coolant flow stagnation, as experienced with the Apollo glycol/water radiator system, are essentially eliminated. If the vehicle of interest is unmanned the flammability and toxicity questions diminish in importance. With respect to an actively cooled airplane, where the skin panels absorb heat rather than reject it, the lower freezing point is of lesser significance and the low temperature viscosity characteristics have a reduced impact, influencing only the temperature gradient near the inlet of the skin panels and the allowable temperature rise in the coolant.

The cooling system weights presented in Table XLIII were based on the use of the baseline discrete tubular cooled skin concept. The choice of panel concept does influence the weight of the distribution lines and in particular the weight of the residual coolant within the cooled panels. To assess weight trends in this regard analyses were conducted for plate-fin panels and sphere-core panels.

Using the plate-fin weight optimization curves presented previously the weight of coolant within the plate-fin skin panels was computed and a cooling system weight based on the use of plate-fin skin panels was determined. Since the plate-fin concept is less sensitive to viscosity effects at low coolant temperatures it is possible to employ a lower inlet temperature than can be used for the discrete passage concept. Furthermore, the film temperature drop constitutes the only temperature gradient at the outlet end of the coolant flow path so that the coolant outlet temperature can be higher for the plate-fin concept than for the discrete passage concept. Thus, a total coolant temperature rise of 129°K (230°F) (255°K to 383°K (0°F to 230°F)) was used for the plate-fin concept as compared to 83°K (150°F) (283°K to 366°K (50°F to 200°F)) for the discrete passage approach. Although the same quantity of heat must be removed in either case, for the plate-fin approach the heat exchanger weight decreased due to the larger log mean temperature difference and the pump weight was reduced because of the lower flow rate due to a larger coolant temperature rise.

Weights of nonredundant and redundant cooling systems based on the use of plate-fin skin panels are presented in Table XLIV for three panel lengths. As panel length increases so does system weight. Note that although the flow area through the plate-fin panel is the same for both nonredundant and redundant design approaches the panel residual weight is much higher for the redundant system due to the fact that a 0.5 mm (20 mil) parting sheet was used between the stacked coolant passages. This additional material is not required for load carrying capability so that its weight was charged to the cooling system rather than to the structure. Some benefits might result from its presence since the stress level within the skin would be reduced. However, most of the airframe structure is designed by buckling considerations rather than by material strength limits so that stress levels are already quite low.

TABLE XLIVA
COOLING SYSTEM CONCEPT COMPARISON, HYPERSONIC RESEARCH AIRPLANE,
PLATE-FIN AND SPHERE-CORE PANELS, UNSHIELDED ALUMINUM STRUCTURE

| Item | Weights for Cooling System with Panel Types Indicated, kilograms | | | | | | | |
|------------------------|--|----------------|----------------|----------------|----------------|----------------|---------------------|-------------|
| | Plate-Fin | | | Sphere-Core | | | | |
| | | | | Close Pack | | | 6.10 m Open Pack | Baseline |
| | 1.52 m Long | 3.05 m Long | 6.10 m Long | 1.52 m Long | 3.05 m Long | 6.10 m Long | | |
| Nonredundant | | | | | | | | |
| Distribution Lines (1) | 536 | 558 | 590 | 683 | 745 | 858 | 854 | 667 |
| Heat Exchanger | 204 | 204 | 204 | 204 | 204 | 204 | 204 | 250 |
| Pump | 11 | 11 | 11 | 11 | 11 | 11 | 11 | 18 |
| Panel Residual (3) | 73 | 182 | 291 | 804 | 1026 | 1367 | 981 | 268 |
| Miscellaneous (2) | 82 | 95 | 109 | 173 | 200 | 245 | 204 | 123 |
| Total | 906 | 1050 | 1205 | 1875 | 2186 | 2685 | 2254 | 1326 |
| Redundant | | | | | | | | |
| Distribution Lines (1) | 595 | 608 | 649 | 772 | 844 | 935 | 922 | 717 |
| Heat Exchanger, Two | 409 | 409 | 409 | 409 | 409 | 409 | 409 | 499 |
| Pumps, Two | 23 | 23 | 23 | 23 | 23 | 23 | 23 | 36 |
| Panel Residual (3) | 277 | 386 | 495 | 1235 | 1457 | 1798 | 1412 | 268 |
| Miscellaneous (2) | 131 | 141 | 159 | 245 | 272 | 318 | 277 | 154 |
| Total | 1435 | 1567 | 1735 | 2684 | 3005 | 3483 | 3043 | 1674 |

- (1) Lines, Contained Coolant, and APS Fuel to drive the Pump, Coolant Inlet/Outlet 255°K/383°K.
(2) 10% to account for valves, controls, supports, etc.
(3) Includes 10 Mil splitter sheet between redundant passages since added strength is not needed for structural purposes.

TABLE XLIVB
COOLING SYSTEM CONCEPT COMPARISON, HYPERSONIC RESEARCH AIRPLANE,
PLATE-FIN AND SPHERE-CORE PANELS, UNSHIELDED ALUMINUM STRUCTURE

| Item | Weights for Cooling System with Panel Types Indicated, pounds | | | | | | | |
|------------------------|---|------------|------------|-------------|------------|------------|-----------------|----------|
| | Plate-Fin | | | Sphere-Core | | | | |
| | | | | Close Pack | | | 20 ft Open Pack | Baseline |
| | 5 ft Long | 10 ft Long | 20 ft Long | 5 ft Long | 10 ft Long | 20 ft Long | | |
| <u>Nonredundant</u> | | | | | | | | |
| Distribution Lines (1) | 1180 | 1230 | 1300 | 1505 | 1640 | 1890 | 1880 | 1470 |
| Heat Exchanger | 450 | 450 | 450 | 450 | 450 | 450 | 450 | 550 |
| Pump | 25 | 25 | 25 | 25 | 25 | 25 | 25 | 40 |
| Panel Residual (3) | 160 | 400 | 640 | 1770 | 2260 | 3010 | 2160 | 590 |
| Miscellaneous (2) | 180 | 210 | 240 | 380 | 440 | 540 | 450 | 270 |
| Total | 1995 | 2315 | 2655 | 4130 | 4815 | 5915 | 4965 | 2920 |
| <u>Redundant</u> | | | | | | | | |
| Distribution Lines (1) | 1310 | 1340 | 1430 | 1700 | 1860 | 2060 | 2030 | 1580 |
| Heat Exchanger, Two | 900 | 900 | 900 | 900 | 900 | 900 | 900 | 1100 |
| Pumps, Two | 50 | 50 | 50 | 50 | 50 | 50 | 50 | 80 |
| Panel Residual (3) | 610 | 850 | 1090 | 2720 | 3210 | 3960 | 3110 | 590 |
| Miscellaneous (2) | 290 | 310 | 350 | 540 | 600 | 700 | 610 | 340 |
| Total | 3160 | 3450 | 3820 | 5910 | 6620 | 7670 | 6700 | 3690 |

- (1) Lines, Contained Coolant, and APS Fuel to drive the Pump, Coolant Inlet/Outlet OF/230F.
- (2) 10% to account for valves, controls, supports, etc.
- (3) Includes 10 Mil splitter sheet between redundant passages since added strength is not need to structural purposes.

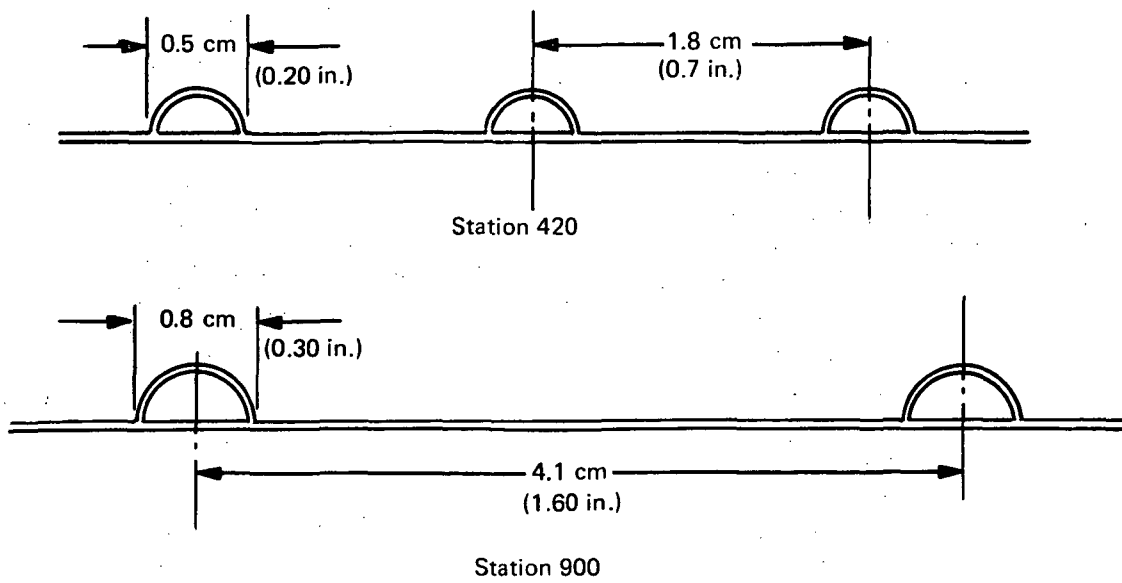
Weights for the sphere-core sandwich panel concept also are shown in Table XLIV for three lengths. As compared to the plate-fin design the relative weight of the sphere-core concept depends upon the manner of packing the spheres. When a tight packing is used relatively high pressure drops are encountered even though the sandwich thickness is increased relative to the plate-fin. The weight penalty associated with the pumping power and the thickness increase is not offset by the fact that about 50% of the sandwich volume is free of coolant because of the hollow spheres. With a square array of spheres weights are reduced because the decreased pressure drop permits a thinner sandwich with less residual coolant and less pumping power penalty, but the weight is still nearly twice that for the plate fin.

The cooling system weights for the plate-fin and sphere-core panels suggest that stagnation regions could incorporate either of these design approaches without significant weight penalties. Where design requirements include internal stiffening, benefits might be obtained by increasing stiffener spacing because of the inherent stiffness of the sandwich skins. In this regard the sphere-core design might be somewhat superior because of its greater depth for an equivalent weight. When extensive internal stiffening and equipment installations require more substructure the sandwich concepts are likely to prove less desirable than the discrete tubular passage approach because the latter is more easily integrated with present airframe fabrication technology. When tubular passages are used and spaced a finite distance apart it is possible to attach stiffening elements to the aircraft skins using conventional techniques such as riveting. When cooled sandwich panel construction is used all mechanical fastening locations must incorporate inserts to prevent leakage of the coolant.

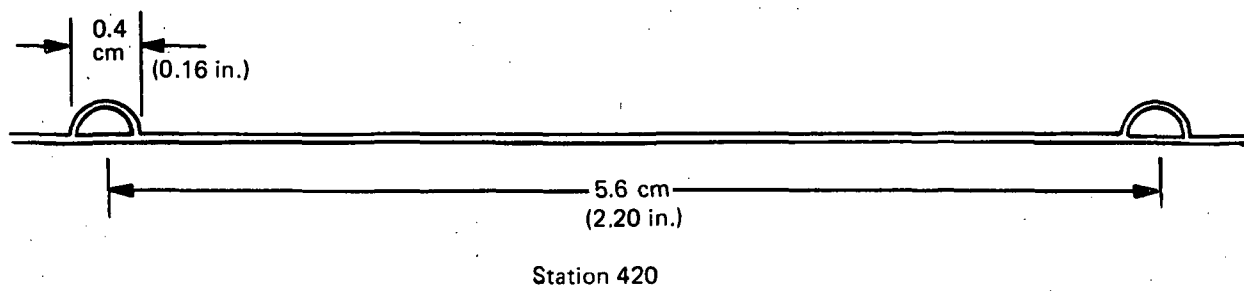
Panel Temperatures. - The operating temperature levels of the cooled sandwich panel concepts, plate-fin and sphere-core, are easily controlled because of the essentially continuous wetting of the wall by the coolant. However, temperature gradients exist when discrete passages are spaced at intervals on the aircraft skin. Passage sizing and spacing for two locations on the hypersonic research airplane are shown in Figure 101 to provide an indication of relative proportions for the unprotected cooled structure for Mach 8 and the insulated and cooled structure for Mach 10. Forward of Station 420 heating intensities increase and the space between coolant passages must decrease as will be discussed later. When an insulated and cooled structural approach is used coolant passage size decreases and spacing increases substantially so that integration with substructural elements is more easily accomplished.

Maximum temperatures between coolant passages were computed at Stations 420 and 900 for various load factor conditions assuming unprotected structure and Mach 8 flight at a dynamic pressure of 71.5 kN/m^2 (1500 psf.). For the nominal trajectory the heat load variation along the circumferential panel at Station 420 varies by a factor of almost 2; for the 3.0 g maneuver the factor is 5, and for the -1.0 g case the factor is about 2 but the panel inlet region (top of the fuselage) is heated higher than the outlet region (bottom of the fuselage). At Station 900 the heat fluxes from the upper center line to the beginning of the lower surface are quite low, a maximum of 5.65 W/cm^2 (5 BTU/ft² sec), but along the lower surface this section is heated by the scramjet exhaust for which a heat flux of 22.6 W/cm^2 (BTU/ft² sec) was assumed. Figures 102 and 103 show maximum temperatures between coolant passages along the length of the panels at Station 420 and 900 respectively. Under nominal flight conditions the maximum panel temperature reaches 400°K (260F) while under maneuver conditions 422°K (300F) is reached. These levels are essentially in agreement with the design criteria of 394°K (250F) for nominal flight conditions and 422°K (300F) for maneuver conditions.

Temperature histories for the two panel locations are presented in Figures 104 and 105, based on a constant coolant flow rate during the trajectory; flow rate modulation does not result in significant weight savings for the HRA as were found for the HST in Reference 3. The temperature



A. Bare Aluminum



B. Insulated and Cooled Aluminum

Figure 101. Coolant Passage Size and Spacing

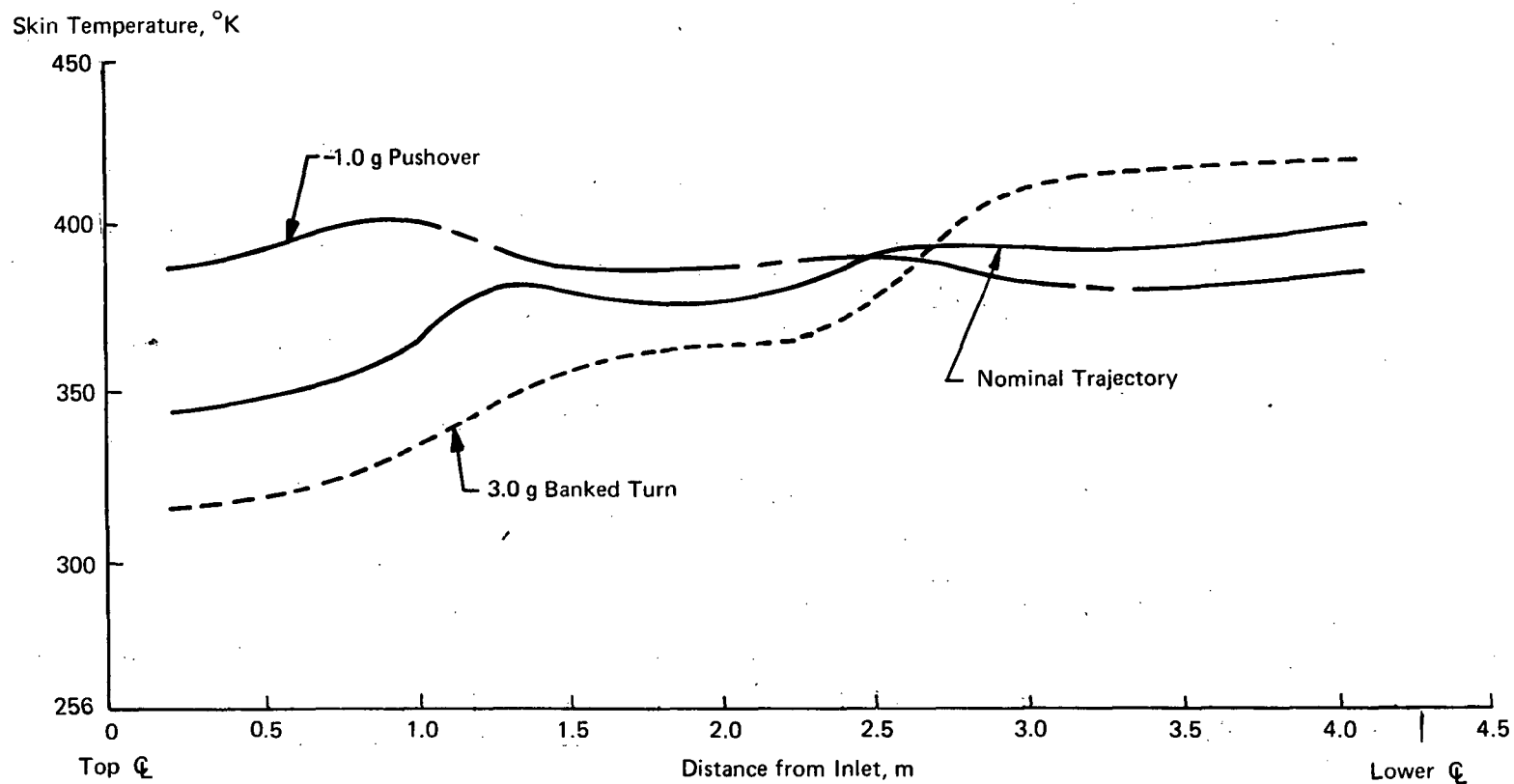


Figure 102a. Temperature Distribution Between Passages, Fuselage Station 420, Passage Spacing = 1.78 cm, Mach 8, 71.8 kN/m² Dynamic Pressure

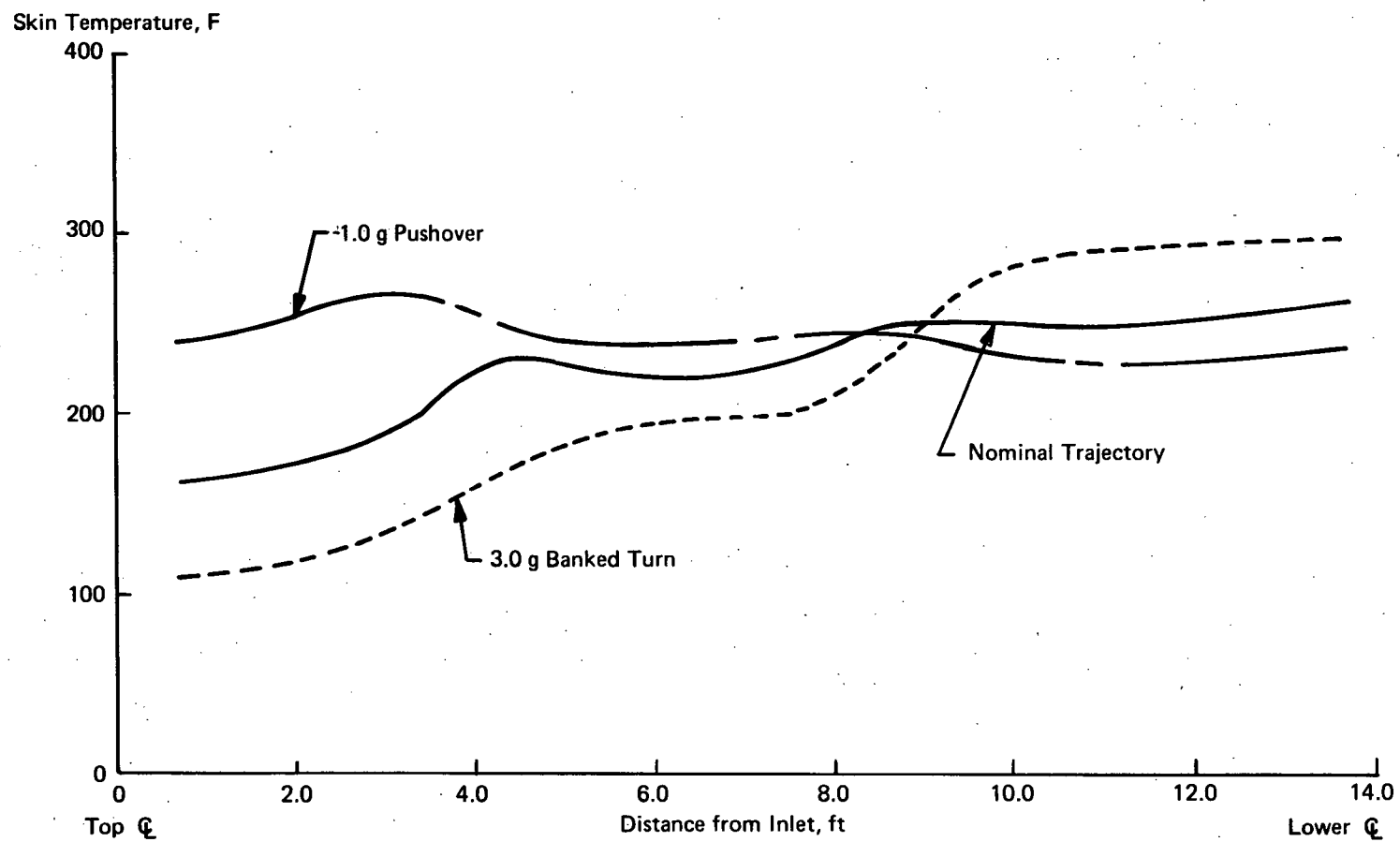


Figure 102b. Temperature Distribution Between Passages, Fuselage Station 420, Passage Spacing = 0.70, Mach 8, 1500 psf Dynamic Pressure

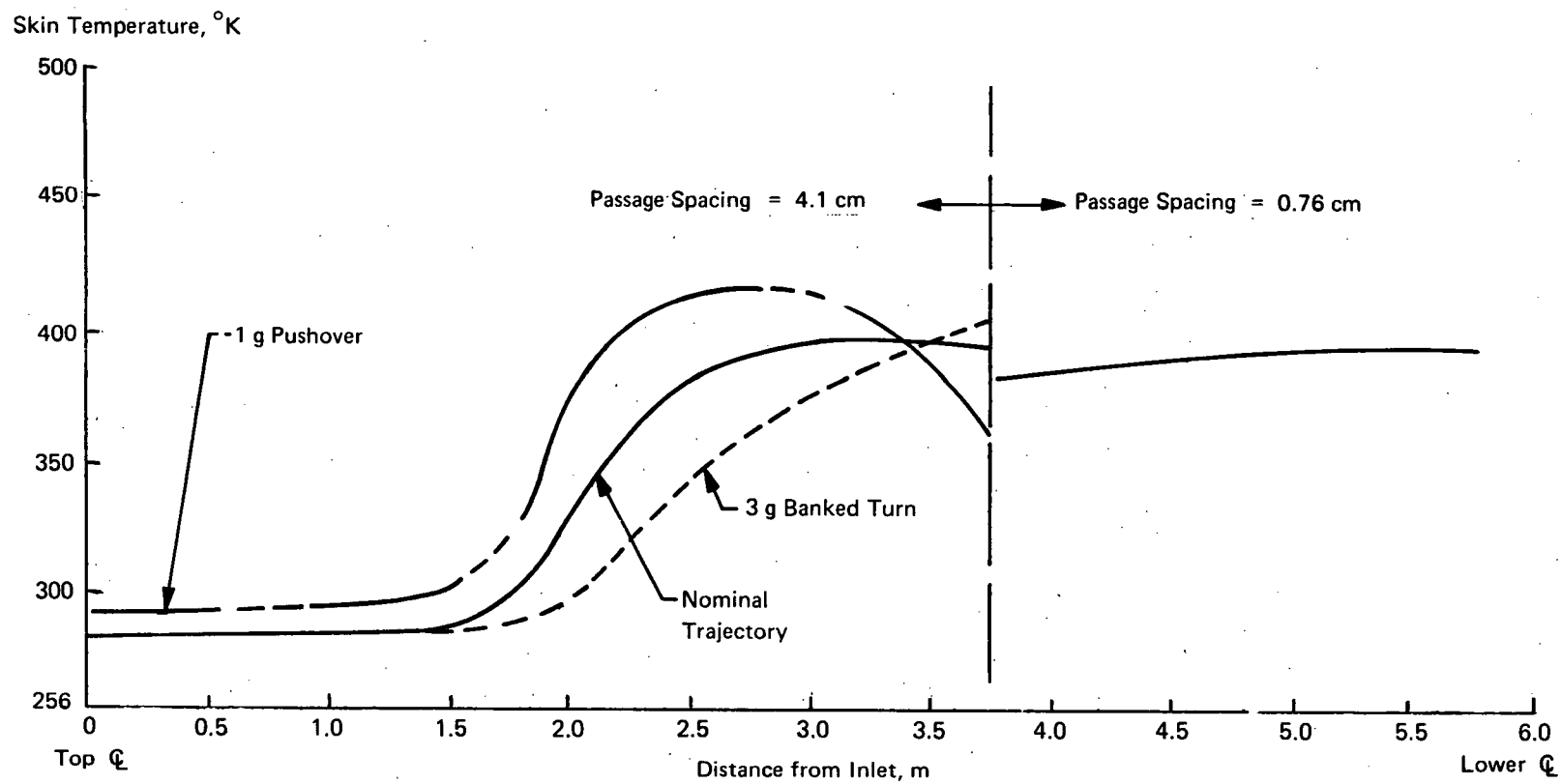


Figure 103a. Temperature Distribution between Passages, Fuselage Station 900,
Mach 8, 71.8 kNm² Dynamic Pressure including Effect of Engine Exhaust

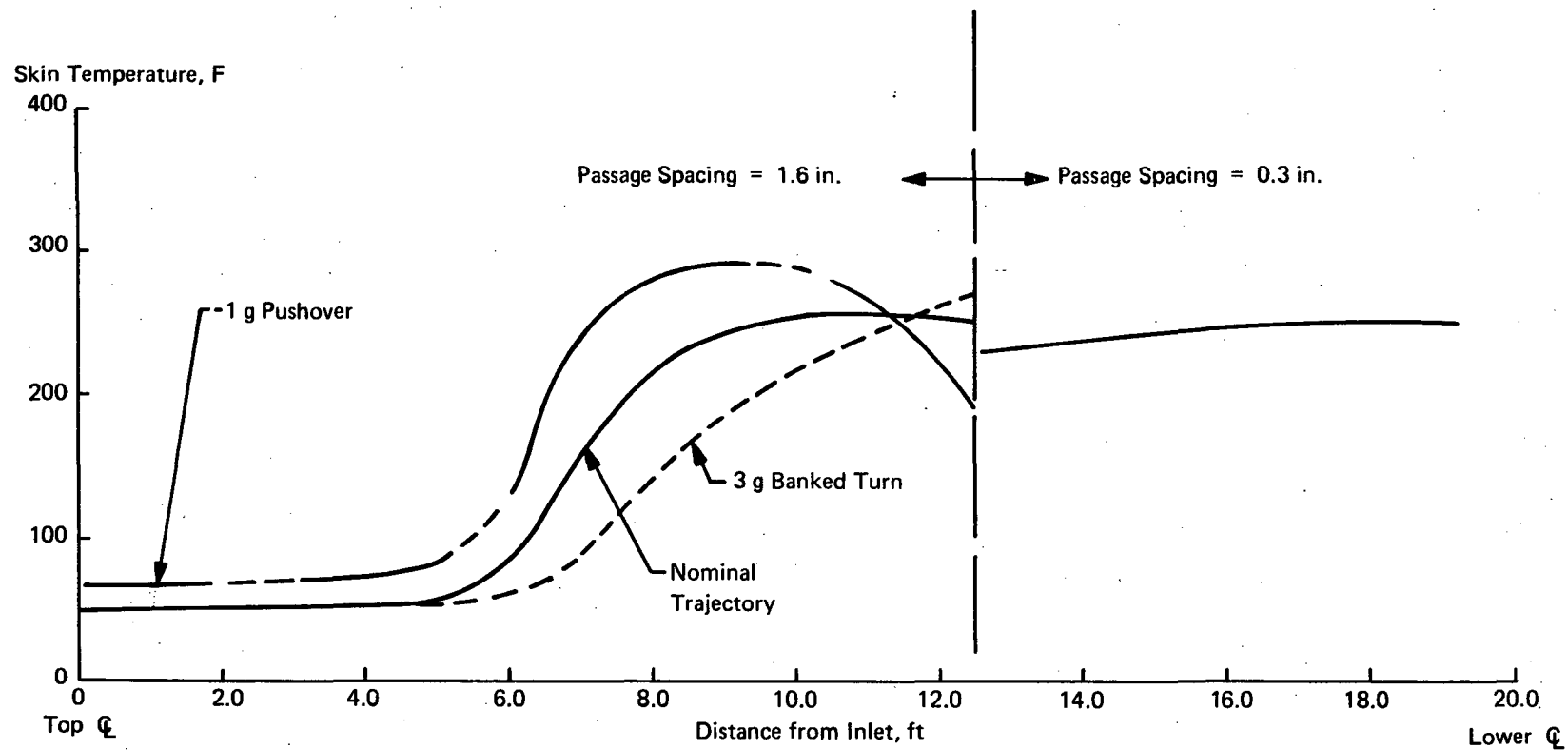


Figure 103b. Temperature Distribution Between Passages, Fuselage Station 900 Mach 8, 1500 psf Dynamic Pressure, Including Effect of Engine Exhaust

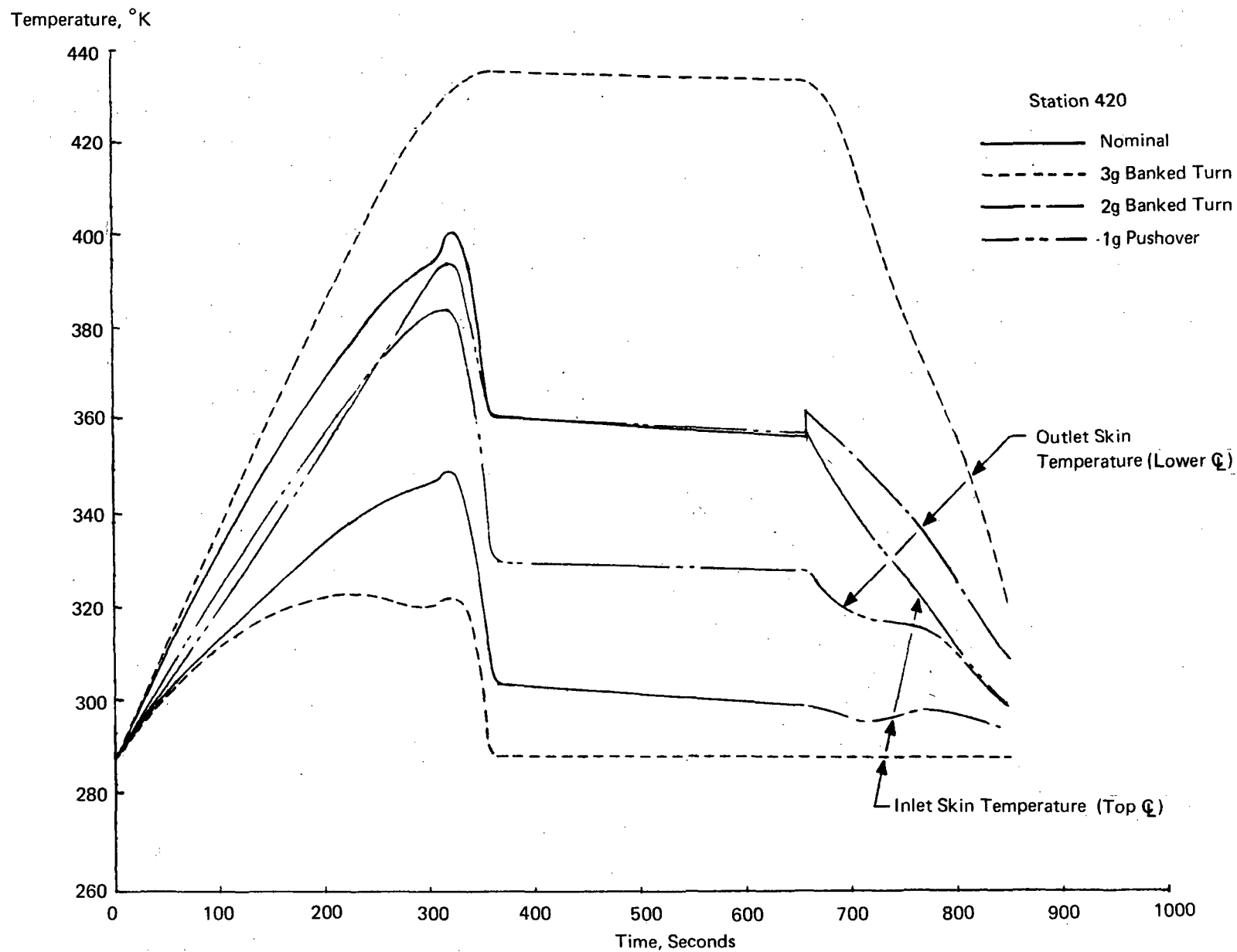


Figure 104a. Temperature History for Nominal Flight and Boundaries for Maneuvers, HRA Station 420

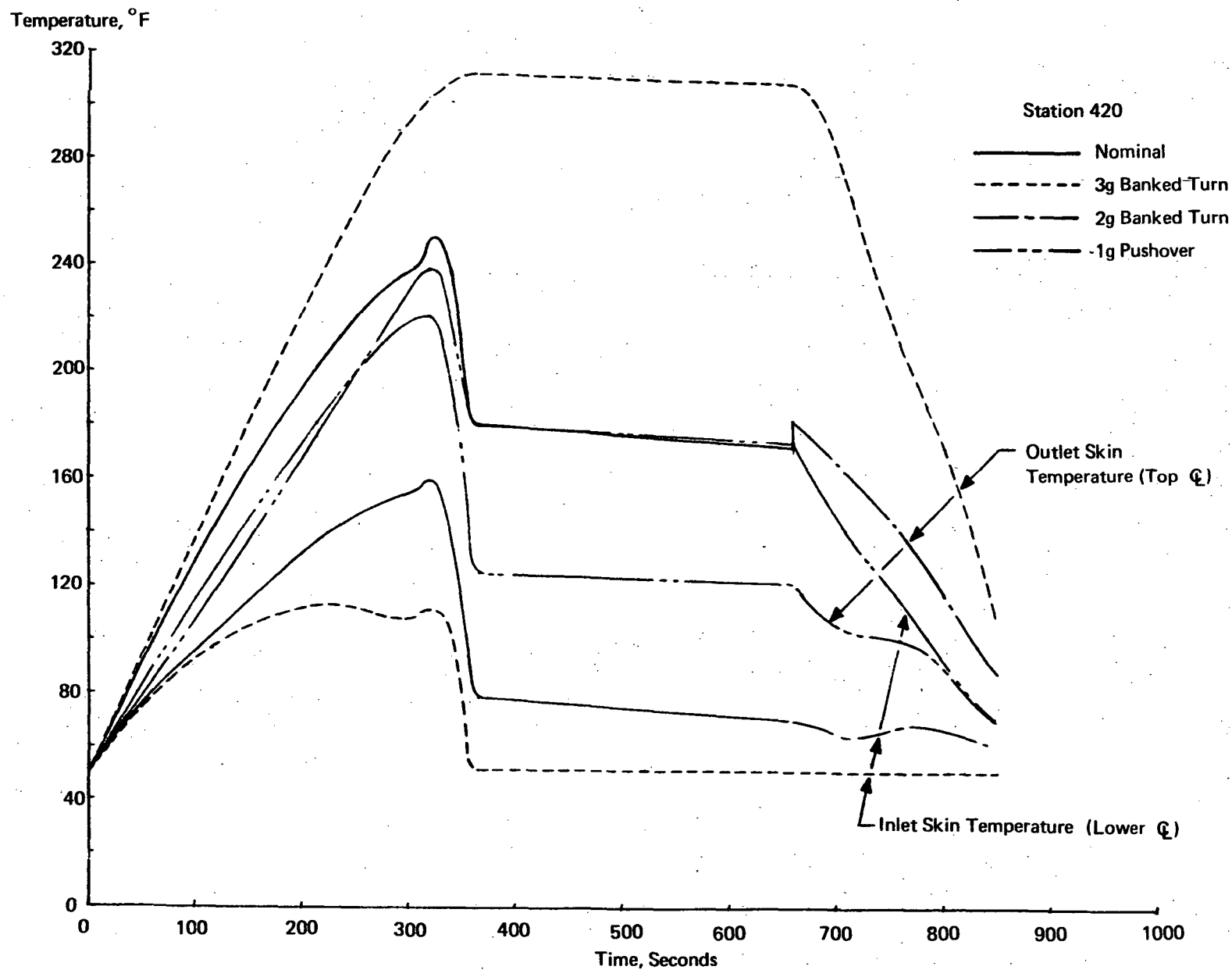


Figure 104b. Temperature History for Nominal Flight and Boundaries for Maneuvers, HRA Station 420

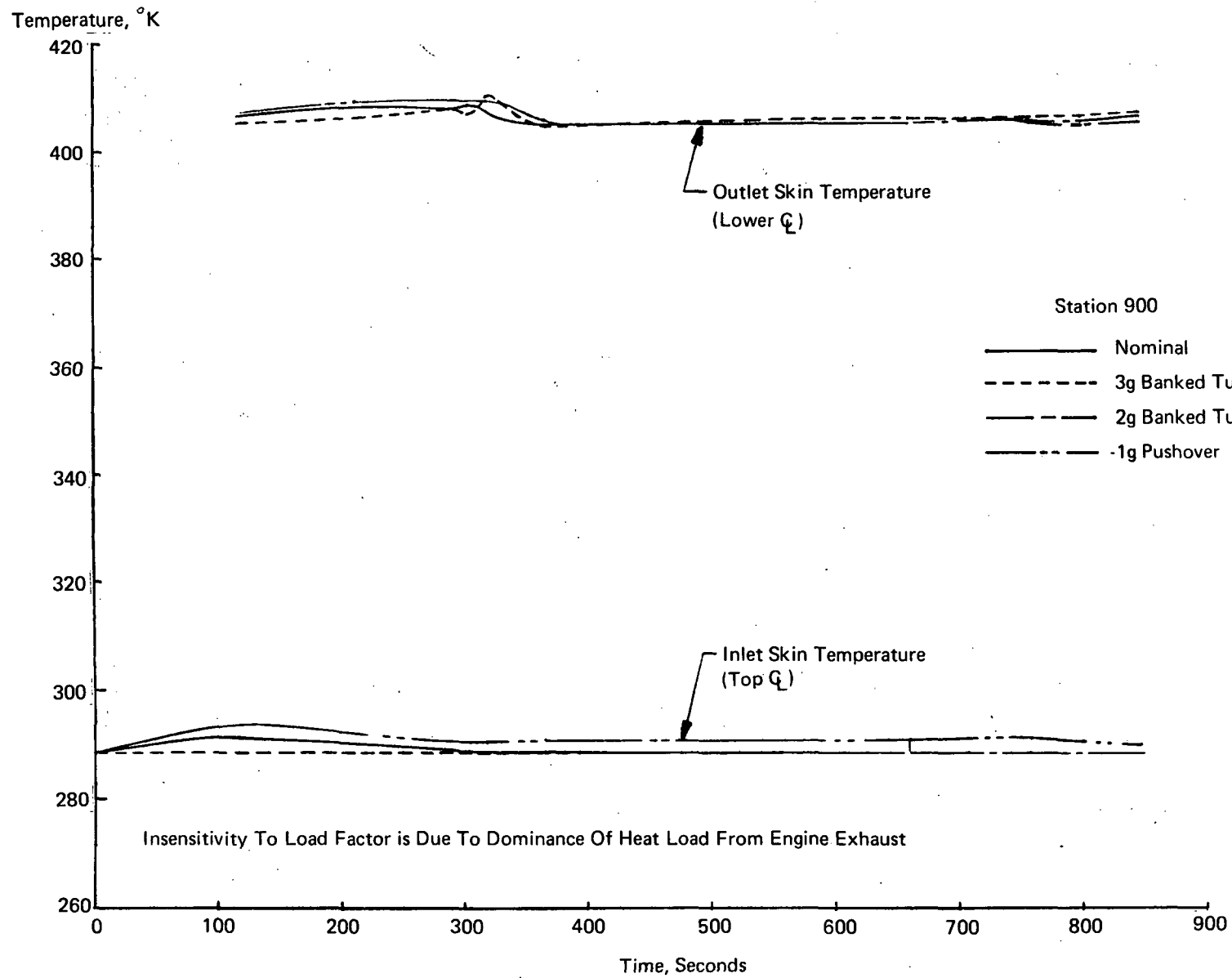


Figure 105a. Temperature History for Nominal Flight and Boundaries for Maneuvers, HRA Station 900

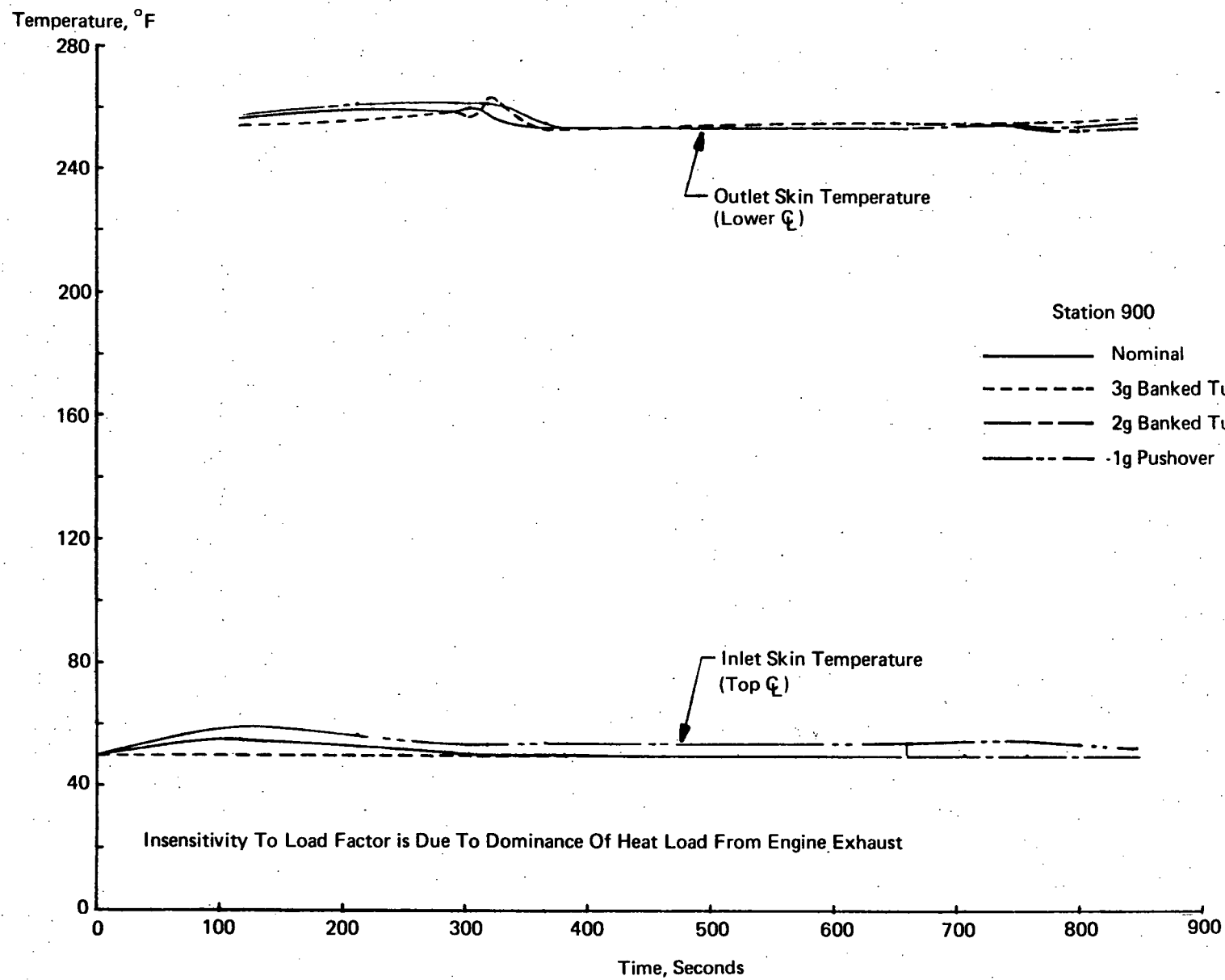


Figure 105b. Temperature History for Nominal Flight and Boundaries for Maneuvers, HRA Station 900

histories permit a clearer understanding of the suitability of designing the structure of this aircraft for a 422°K (300F) level under maneuver conditions. The temperature histories shown for the maneuver conditions represent envelopes and not continuous histories. In actual operation panel temperatures would follow the levels shown for nominal flight with only temporary excursion to the levels represented by the envelopes of the maneuver conditions. Therefore, higher temperature levels can be used for maneuver conditions without fear of adversely influencing the strength of the construction material.

In Figure 104 it can be noted that at Station 420 the maximum temperatures during nominal flight conditions are substantially lower (by nearly 45°K (80F) than the 394°K (250F) target except for about the last 200 seconds of the ascent. This suggests the possibility of increasing the allowable temperature rise of the coolant even when the baseline panel concept is used. Increasing the coolant temperature rise from 82°K (150F) to approximately 110°K (200F) would reduce system weight by about 282 kg (600 lb). An increase in the coolant temperature rise is implied also when the cooled sandwich panel concepts are considered but a somewhat smaller weight reduction would be expected.

It appears that rather detailed comparisons will be required to establish accurate weight comparisons for the plate-fin and baseline panel systems. Such a comparison must be based on complete thermal-structural designs because of the different aspects associated with airframe assembly for the two approaches and the likely need to use different alloys for each. Detailed design of representative sections of airframe structure corresponding to significantly different thermal and structural requirements may be desirable at some future date.

Temperature levels between coolant passages are of importance under emergency conditions despite the fact that the duration of such conditions is short. Two situations were examined for a side by side redundant cooling passage network, spaced as in Figure 101, prior to the worst heating conditions at Stations 420 and 900. First it was assumed that one loop of the redundant system failed but that the coolant flow in the operative loop was doubled immediately, Figures 106 and 107. Then, for Station 420 only, failure of one loop was assumed but the flow in the remaining loop was not increased, Figure 108. When the flow is doubled immediately the temperatures for one system out are not significantly different from the temperatures when both systems are operating despite the increase in passage spacing. This is due to the higher flow velocity that reduces the coolant film temperature drop thus increasing the allowable skin gradient. In either the fully laminar or the fully turbulent regions, the inlet and exit sections respectively, the temperatures are nearly the same since the product of heat transfer coefficient times the surface area is nearly constant. However, in the region of the panel where the flow is transitional, the increase in velocity for single mode operation results in a significantly higher heat transfer coefficient, hence the temperatures are actually lower for the single mode of operation.

Even though the panel temperatures are nearly the same, the pressure drop through the panel increases quite significantly. At Station 420 the pressure drop increases from 45 N/cm² (65 psi) to 208 N/cm² (300 psi) when one system is shut down. At Station 900 the pressure drop increases from 24 to 108 N/cm² (35 to 155 psi). In addition, the pressure drop in the distribution system will increase from 69 N/cm² (100 psi) to 280 N/cm² (410 psi) which results in a total system operating pressure of slightly more than 480 N/cm² (700 psi).

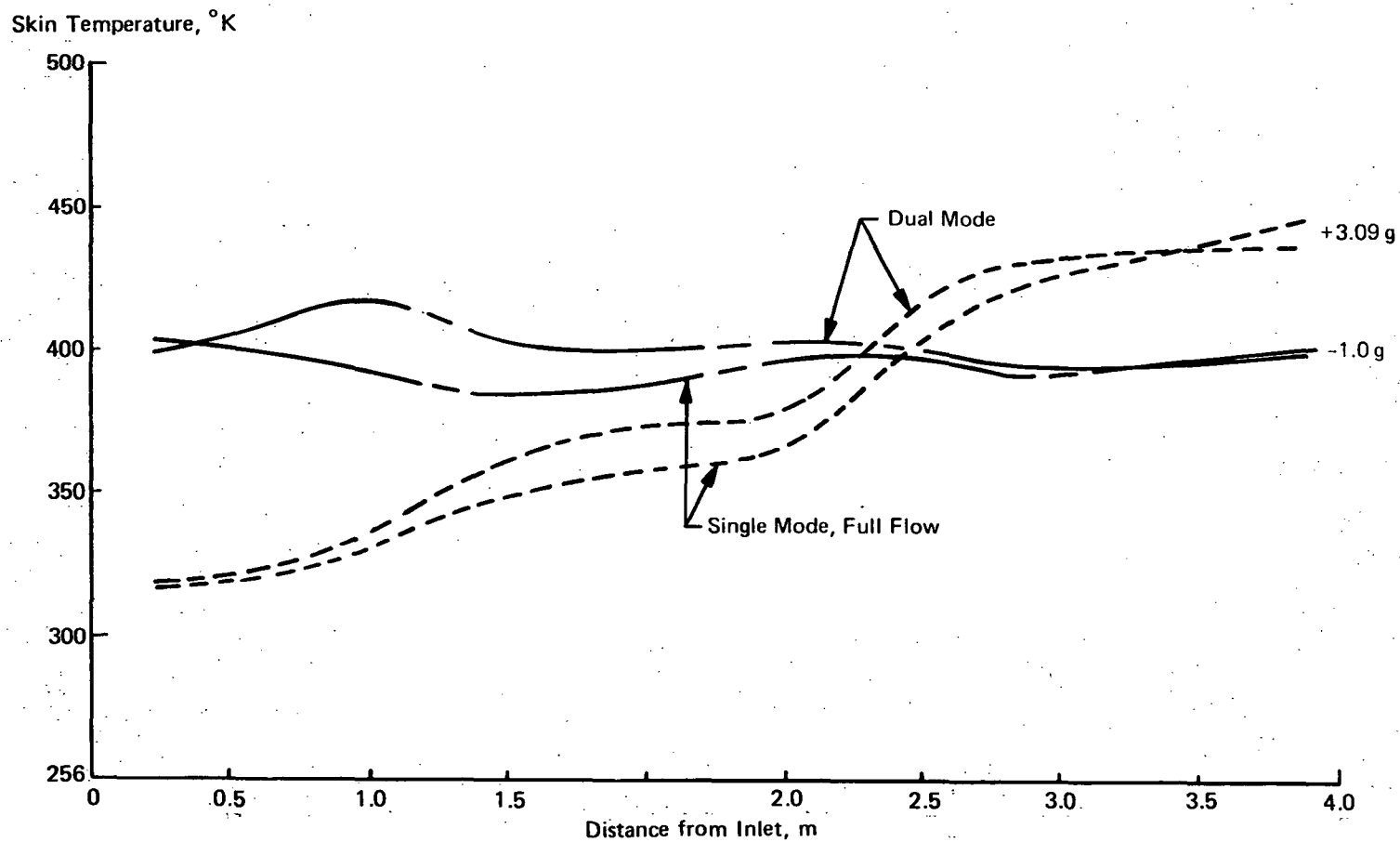


Figure 106a. Temperature Distribution Between Passages, Fuselage Station 420, Passage Spacing = 1.78 cm, Mach 8, 71.8 kN/m² Dynamic Pressure

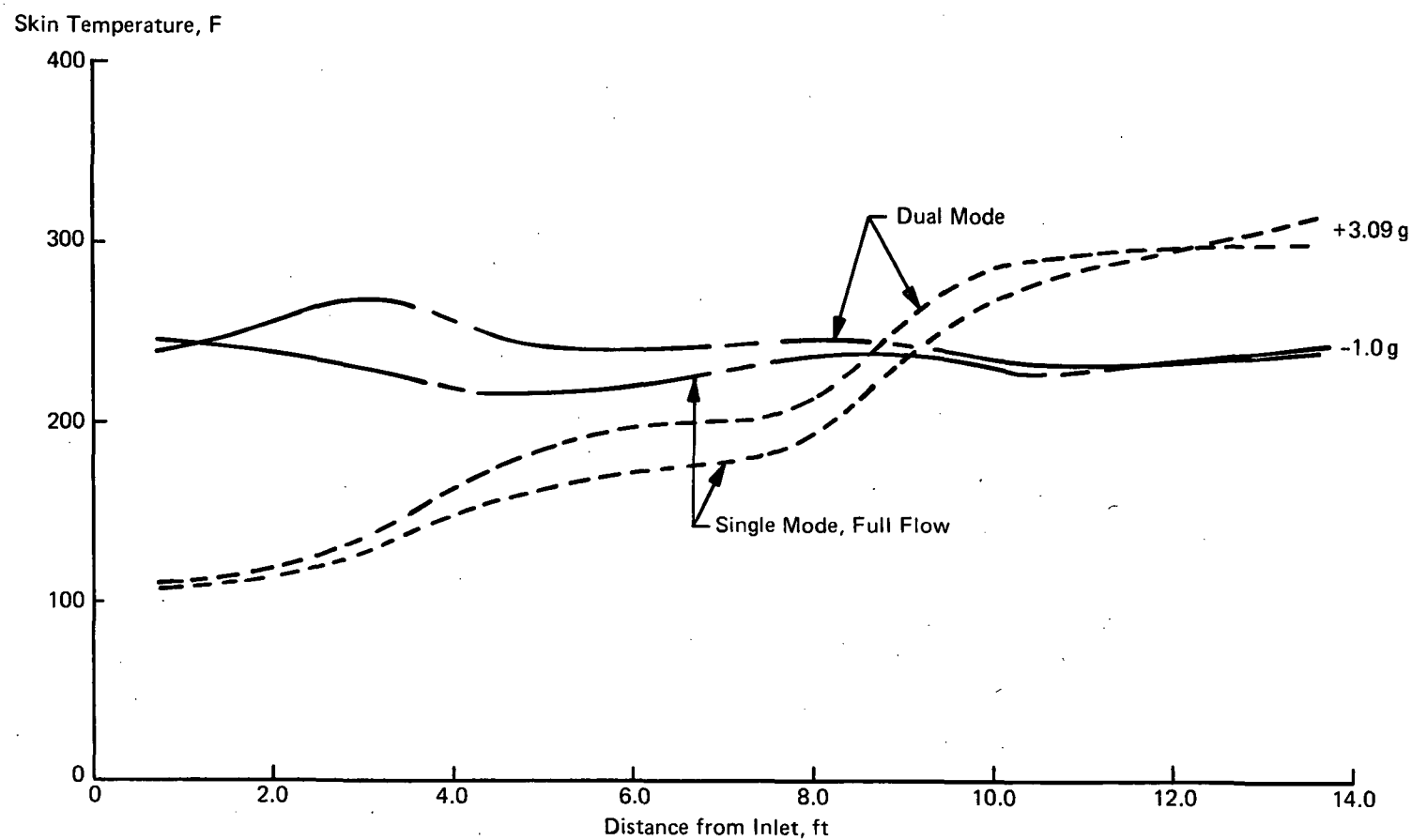


Figure 106b. Temperature Distribution Between Passages, Fuselage Station 420,
Passage Spacing = 0.70, Mach 8, 1500 psf Dynamic Pressure

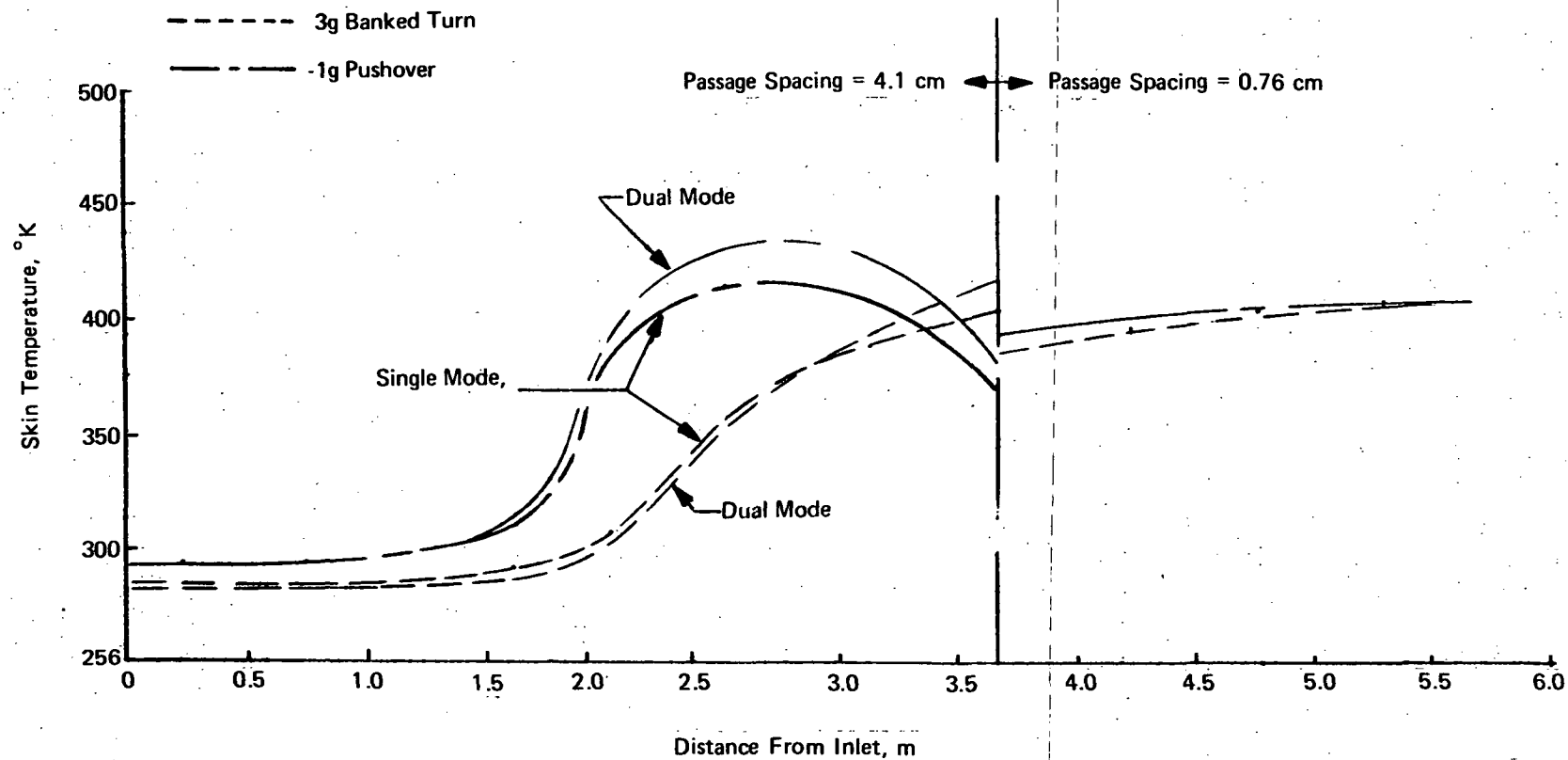


Figure 107a. Temperature Distribution Between Passages, Fuselage Station 900, Mach 8;
71.8 kN/m² Dynamic Pressure

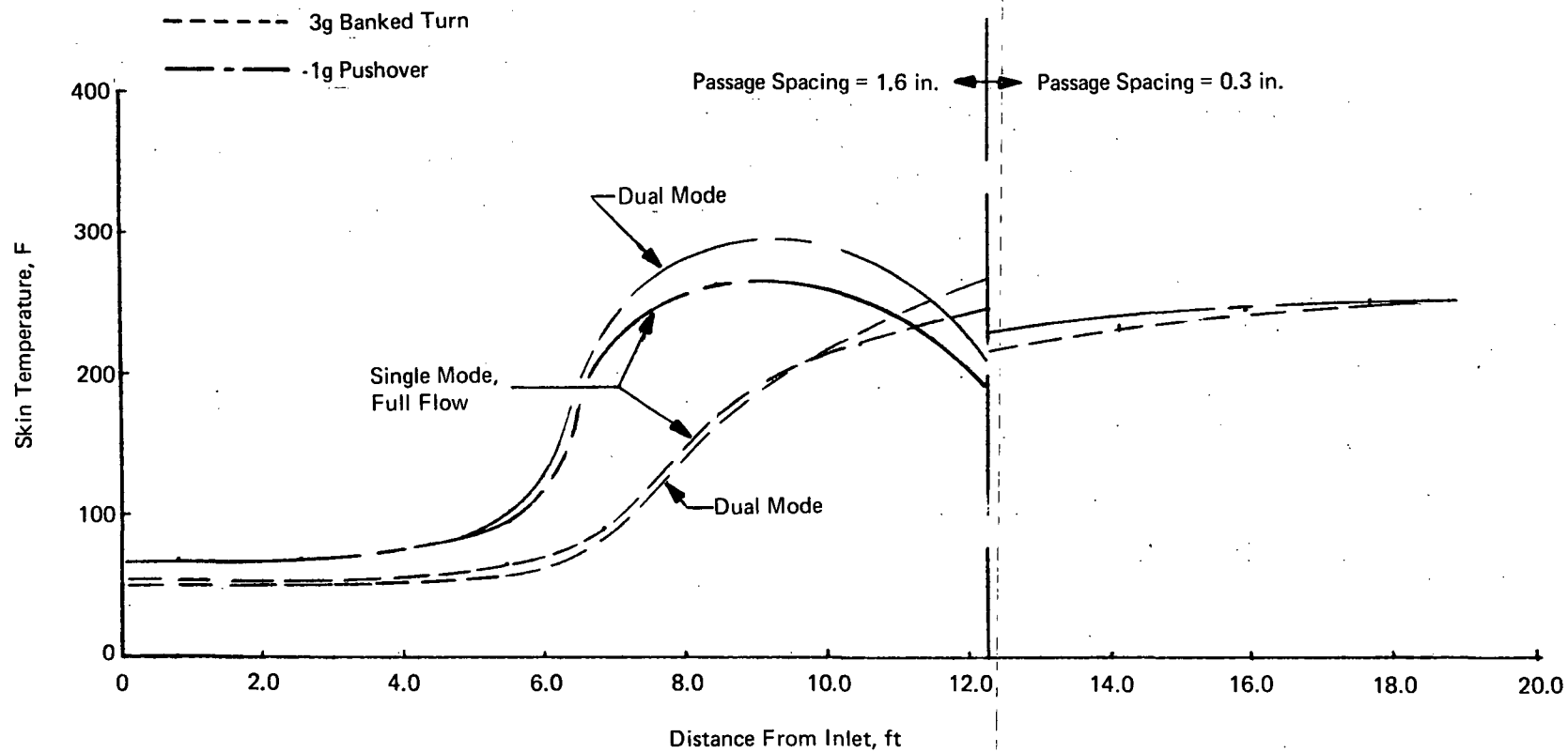


Figure 107b. Temperature Distribution Between Passages, Fuselage Station 900 Mach 8; 1500 psf Dynamic Pressure

Temperature, °K

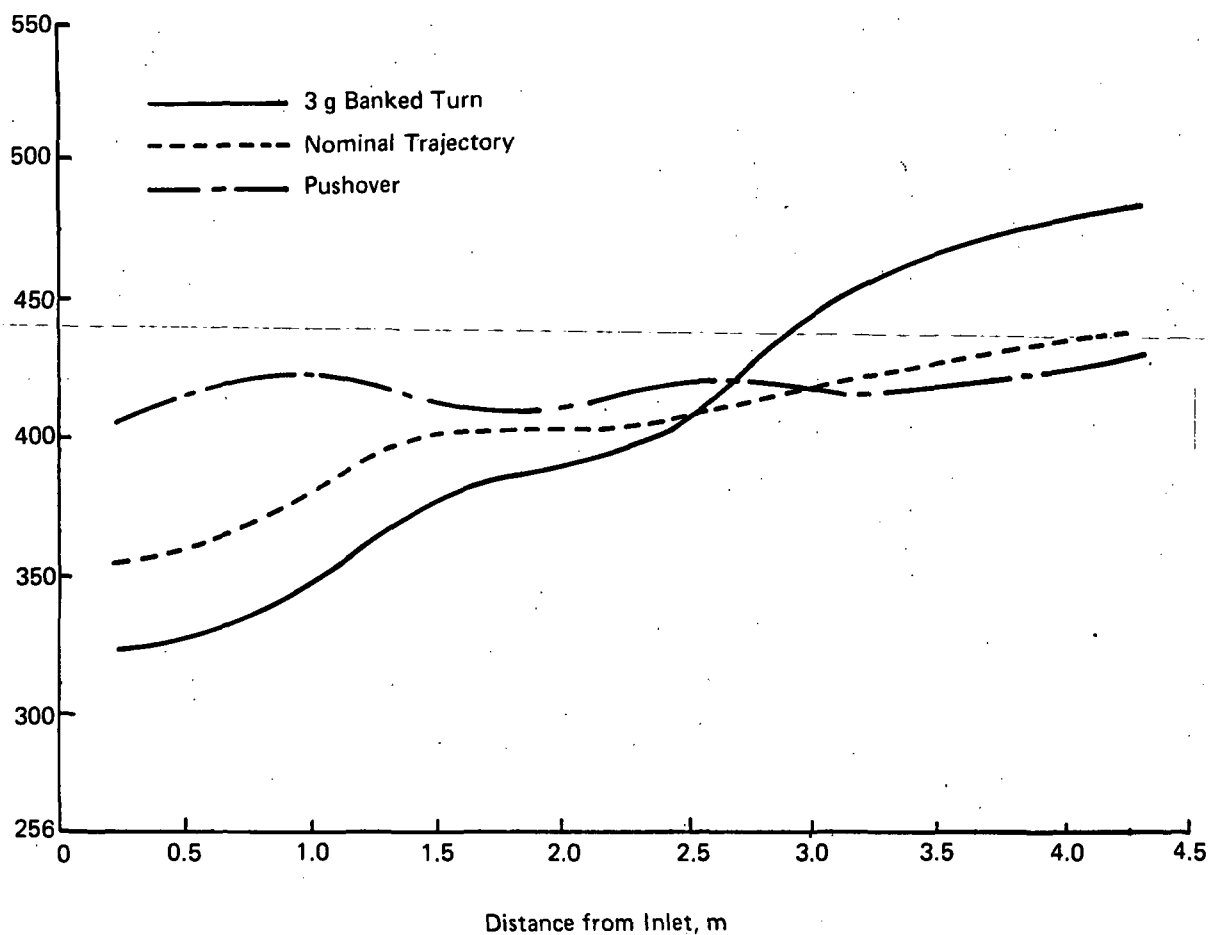


Figure 108a. Temperature Distribution along Panel inbetween Passages for Single-Mode Operation at 50% of Total Design Coolant Flow, Station 420

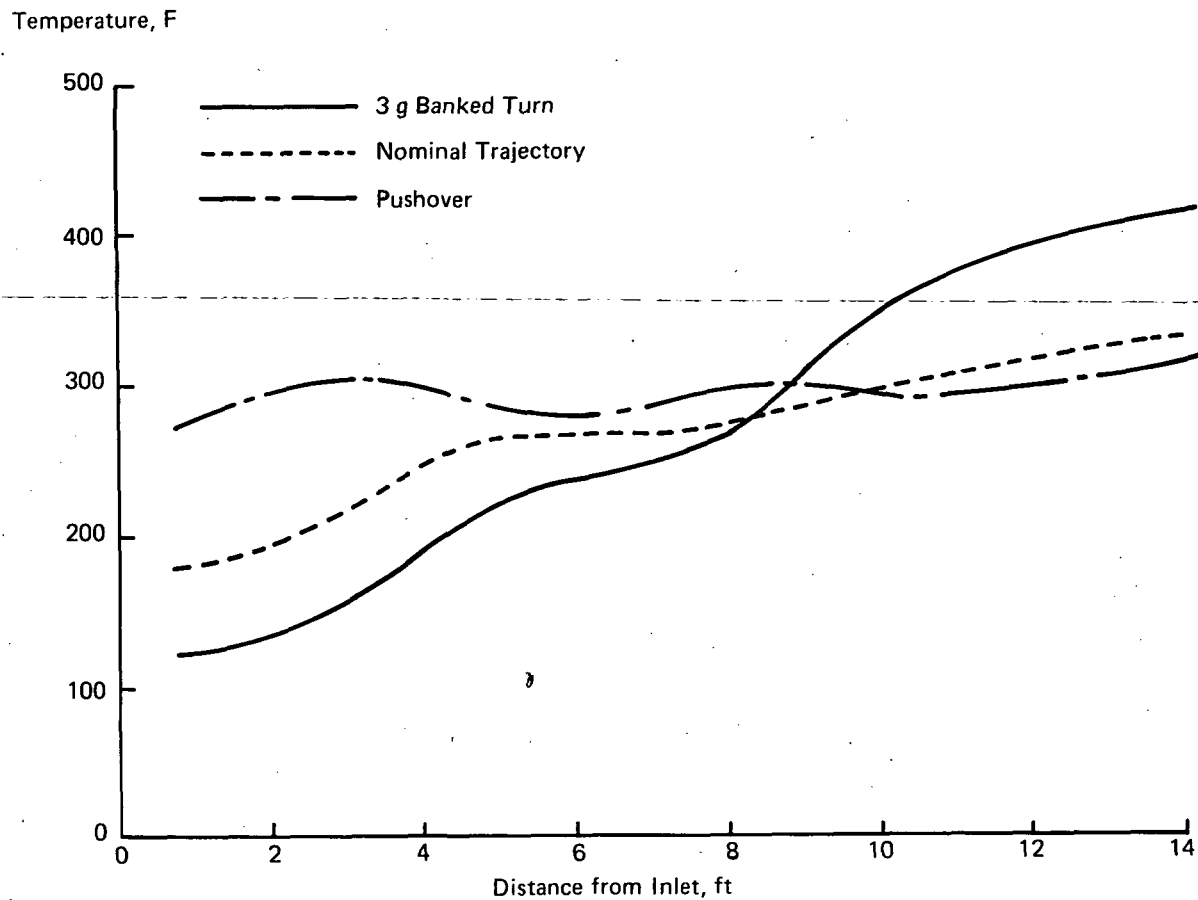


Figure 108b. Temperature Distribution along Panel inbetween Passages for Single-Mode Operation at 50% of Total Design Coolant Flow, Station 420

Analyses of the influence of flowrate on panel temperatures and pressure drops were conducted for Stations 420 and 900; results are summarized in Tables XLV and XLVI. As the coolant flowrate is decreased from 100% to 75% the panel pressure drop at Station 420 is decreased from 595% of the dual mode value to 328% while the 450°K (350F) temperature limit for emergency operation is exceeded slightly. The same decrease in flowrate decreases the panel pressure drop at Station 900 from 374% to 212% of the dual mode value but all temperatures are within desired limits. The relative insensitivity to flight conditions of the temperatures at Station 900 is due to the high constant exhaust heating on the panel. The pressure drop through the distribution lines would be about 172 N/cm² (250 psi) so that the total system pressure drop would be about 345 N/cm² (500 psi) during single mode of operation at 75% flow rate. When the flow rate is not increased at all for single mode operation the coolant temperature rise doubles and the pressure drop decreases slightly as compared to dual mode operation. Panel temperatures increase but not to catastrophic levels (Figure 108). In the very unlikely event of a cooling system malfunction occurring while a maximum load factor maneuver was being executed at the maximum speed and maximum dynamic pressure and the coolant flow was not increased by the flow control system, the aircraft would not be lost. Short time exposure to such emergency conditions under nominal flight conditions is unlikely to require any airframe rework although the source of cooling system malfunction would have to be repaired.

While the panels for Stations 420 and 900 are typical, the panels at the forward stations will be subjected to higher heat fluxes. In the nose region a structural approach such as plate-fin or sphere-core will be needed because of the high heat flux. This approach could be extended aft until the heat flux is reduced to a level where representative airframe structure could be used. Based on prior studies it appeared that the transition was likely to be made between 28 and 45 w/cm² (25 and 40 BTU/ft² sec). Since an exact location and/or heat flux is not critical at this time, analyses were conducted for a location 0.62 cm (0.25 in.) from the nose where the heat flux at the lower centerline was 36 w/cm² (32 BTU/ft² sec).

The panel was assumed to extend from Station 25 to Station 90 with passages oriented in the axial direction to be of rectangular planform and subjected to a constant heat flux. The coolant entered at 315°K (100°F) and was heated to 366°K (200 F) as it passed through the panel. Maximum skin temperature was varied from 394 to 450°K (250°F to 350 F) while pressure drop was varied to determine the (s-d) parameter and weight. Regardless of the maximum allowable structural temperature minimum weight is achieved at pressure drops between 34 to 48 N/cm² (50 and 70 psi) at unit weight values between 1.46 and 1.71 kg/m² (0.30 and 0.35 psf) (the sum of the residual coolant in the panel plus the pumping power penalty). For the rectangular panel shape, the corresponding (s-d) values for maximum structural temperatures of 394°K, 422°K and 450°K (250F; 300F and 350F) were approximately 0.68 cm, 1.21 cm and 1.58 cm (0.27 in., 0.48 in., and 0.63 in.) respectively. All of the spacings between coolant passages are acceptable from a fabrication point of view. Thus, at Station 25 for the maximum maneuver heat flux of 36 w/cm² (32 BTU/ft² sec), and the 422°K (300F) allowable temperature for maneuver conditions the distance between the edges of the coolant passages is 1.21 cm (0.48 in.). Demonstration assemblies fabricated as part of an in-house effort demonstrated the practicality of an assembly with an (s-d) of 0.62 cm (0.25 inch).

Examination of similar results for other heat fluxes in light of previously defined temperature limits of 394°K (250F) for nominal flight conditions, 422°K (300F) for maneuver conditions during dual mode operations of the cooling system, and 450°K (350F) for single mode operation indicated that the 394°K (250F) maximum temperature case is controlling for this particular structural location with an (s-d) value of 0.58 cm (0.23 inch). An increase in the heat flux from the nominal value of 19.2 w/cm² (17 BTU/ft² sec) to the 3 g maneuver value of 36 w/cm² (32 BTU/ft² sec) would raise a 394°K (250 F) temperature level to approximately 410°K (280 F). If the 422°K (300°F) limit was to be reached for maneuver conditions, the maximum structural temperature during nominal type

TABLE XLVA
SINGLE MODE OPERATION, STATION 420, 283°K COOLANT INLET TEMPERATURE

| Coolant Flowrate Ratio | Coolant Temperature Rise, °K | Panel Pressure Drop, Newtons/cm ² | Panel Pressure Drop Ratio | Maximum Skin Temperature °K | | |
|------------------------|------------------------------|--|---------------------------|-----------------------------|----------------|--------------|
| | | | | +3g Maneuver | Nominal Flight | -1g Maneuver |
| 1.00 | 338 | 266.8 | 5.95 | 428 | 389 | 377 |
| 0.86 | 352 | 193.1 | 4.31 | 443 | 401 | 388 |
| 0.75 | 366 | 146.9 | 3.28 | 458 | 413 | 400 |
| 0.50 | 422 | 44.8 | 1.00 | 520 | 481 | 468 |

TABLE XLVB
SINGLE MODE OPERATION, STATION 420, 50°F COOLANT INLET TEMPERATURE

| Coolant Flowrate Ratio | Coolant Temperature Rise, °F | Panel Pressure Drop, psi | Panel Pressure Drop Ratio | Maximum Skin Temperature °F | | |
|------------------------|------------------------------|--------------------------|---------------------------|-----------------------------|----------------|--------------|
| | | | | +3g Maneuver | Nominal Flight | -1g Maneuver |
| 1.00 | 150 | 387 | 5.95 | 311 | 241 | 219 |
| 0.86 | 175 | 280 | 4.31 | 339 | 263 | 240 |
| 0.75 | 200 | 213 | 3.28 | 365 | 284 | 261 |
| 0.50 | 300 | 65 | 1.00 | 476 | 406 | 384 |

TABLE XLVIA
SINGLE MODE OPERATION, STATION 900, 283°K COOLANT INLET TEMPERATURE

| Coolant Flowrate Ratio | Coolant Temperature Rise, °K | Panel Pressure Drop, Newton/cm ² | Panel Pressure Drop Ratio | Maximum Skin Temperature °K | | |
|------------------------|------------------------------|---|---------------------------|-----------------------------|----------------|--------------|
| | | | | +3g Maneuver | Nominal Flight | -1g Maneuver |
| 1.00 | 338 | 90.3 | 3.74 | 385 | 385 | 390 |
| 0.86 | 352 | 66.2 | 2.74 | 399 | 399 | 405 |
| 0.75 | 366 | 51.0 | 2.12 | 414 | 414 | 420 |
| 0.50 | 422 | 24.1 | 1.00 | 475 | 475 | 480 |

TABLE XLVIB
SINGLE MODE OPERATION, STATION 900, 50°F COOLANT INLET TEMPERATURE

| Coolant Flowrate Rate | Coolant Temperature Rise, °F | Panel Pressure Drop, psi | Panel Pressure Drop Ratio | Maximum Skin Temperature °F | | |
|-----------------------|------------------------------|--------------------------|---------------------------|-----------------------------|----------------|--------------|
| | | | | +3g Maneuver | Nominal Flight | -1g Maneuver |
| 1.00 | 150 | 131 | 3.74 | 233 | 234 | 242 |
| 0.86 | 175 | 96 | 2.74 | 259 | 259 | 270 |
| 0.75 | 200 | 74 | 2.12 | 286 | 285 | 297 |
| 0.50 | 300 | 35 | 1.00 | 395 | 396 | 404 |

conditions should be approximately 405°K (270 F). For single mode operation with 100% of total flow the 450°K (350 F) temperature level is not exceeded. However, inability to increase the flow in the remaining cooling system loop would permit maximum temperatures to reach the vicinity of 506°K (450 F). Even this is not a prohibitively high temperature since for a short time exposure the structural strength should be about 65% of its room temperature level. Thus, the baseline panel concept is suitable for use to heat fluxes of at least 36 w/cm² (32 BTU/ft² sec) within the established temperature and practical manufacturing constraints.

In addition to the high heat flux along the forward lower surface, the perimeters of the cross sections increase quite rapidly from front to midship and this can have a significant influence on panel design. If the coolant passages are oriented circumferentially the forward passage has a much shorter length than the aft passage. For a constant pressure drop through all passages, the passage diameter must be tailored to the flow length in conjunction with the variation of local heating intensity. For the modest axial variation of heating intensity on the forward portion of the HRA, little relief is obtained as a result of the decrease in heat flux in the aft direction. Figure 109 illustrates the problem. If the coolant passage diameter is constant, the pressure drop increases quite substantially as the ratio of coolant passage length is increased; the flow in the longer passage must increase because of the larger quantity of heat being removed along the longer length since the heat flux is practically constant. This is another way of saying that the longer passages will not receive the proper flow but will be starved. If the pressure drop through each coolant passage is to remain constant, so that flow will be uniform, the diameter must increase as the passage length is increased. Since the pressure drop and heat transfer characteristic are closely related, there is only a small change in heat transfer coefficient for the various passage lengths ratios when the pressure drop is held constant.

A second approach to minimizing the problem is to locate the inlet and outlet panel connections at that edge of the panel nearest to the longest coolant passage. Flow through the short passage must pass through the manifolds as well as the passage while flow through the long passage simply travels through the passage. However, since the pressure drop in the manifold tends to be relatively small compared to that through the coolant passages, a net pressure drop penalty may be incurred.

An alternate approach is to orient the coolant passages in the axial direction. This ensures essentially constant lengths as well as orienting the coolant passages perpendicular to lines of constant heat flux. If coolant passages are of the same diameter, the flow rate will be a function of slight differences in peripheral heating intensities. However, difficulties are encountered with the need to vary the coolant passage spacing to accommodate the difference in the perimeters of the vehicle cross sections. Analyses were conducted with the coolant inlet along the forward and rear edges of the panel, alternately at Stations 25 and 90. At first thought a forward inlet would seem preferable since the heating intensities are somewhat higher. However, the passage spacing at the aft edge is much greater if a constant number of passages are used. The perimeter ratio is 2.5. Because of this the aft location for the coolant inlet is more desirable. With this inlet location and a constant number of coolant passages from inlet to outlet, it would be necessary to increase the panel pressure drop substantially to retain the desired temperature levels and a practical passage spacing. However, there are more attractive alternatives. Using a coolant inlet temperature of 283°K (50F) and an outlet temperature of 340°K (150F) reduces the panel pressure drop from an intolerable 620 N/cm² (900 psi) to 276 N/cm² (400 psi). With this temperature range increasing the local maximum structural temperature between the most widely spaced passages to 422°K (300°F) under nominal flight conditions would reduce the pressure drop to about 98 N/cm² (140 psi) (double the optimum). Splitting the panel length is of most benefit because the taper ratio in each panel can be reduced from about 2.5 to 1.6 thereby minimizing the difference in spacing from one end to the other, and the flow length is reduced thereby allowing a higher pressure drop per unit length without exceeding the optimum allowable total pressure drop. Even with the taper effect considered splitting the panel into two unequal lengths would allow the (s-d) value to increase to about 0.68 cm (0.27 inch). Still another alternative is to vary the number of coolant passages along the flow length by using the technique illustrated in Reference 3.

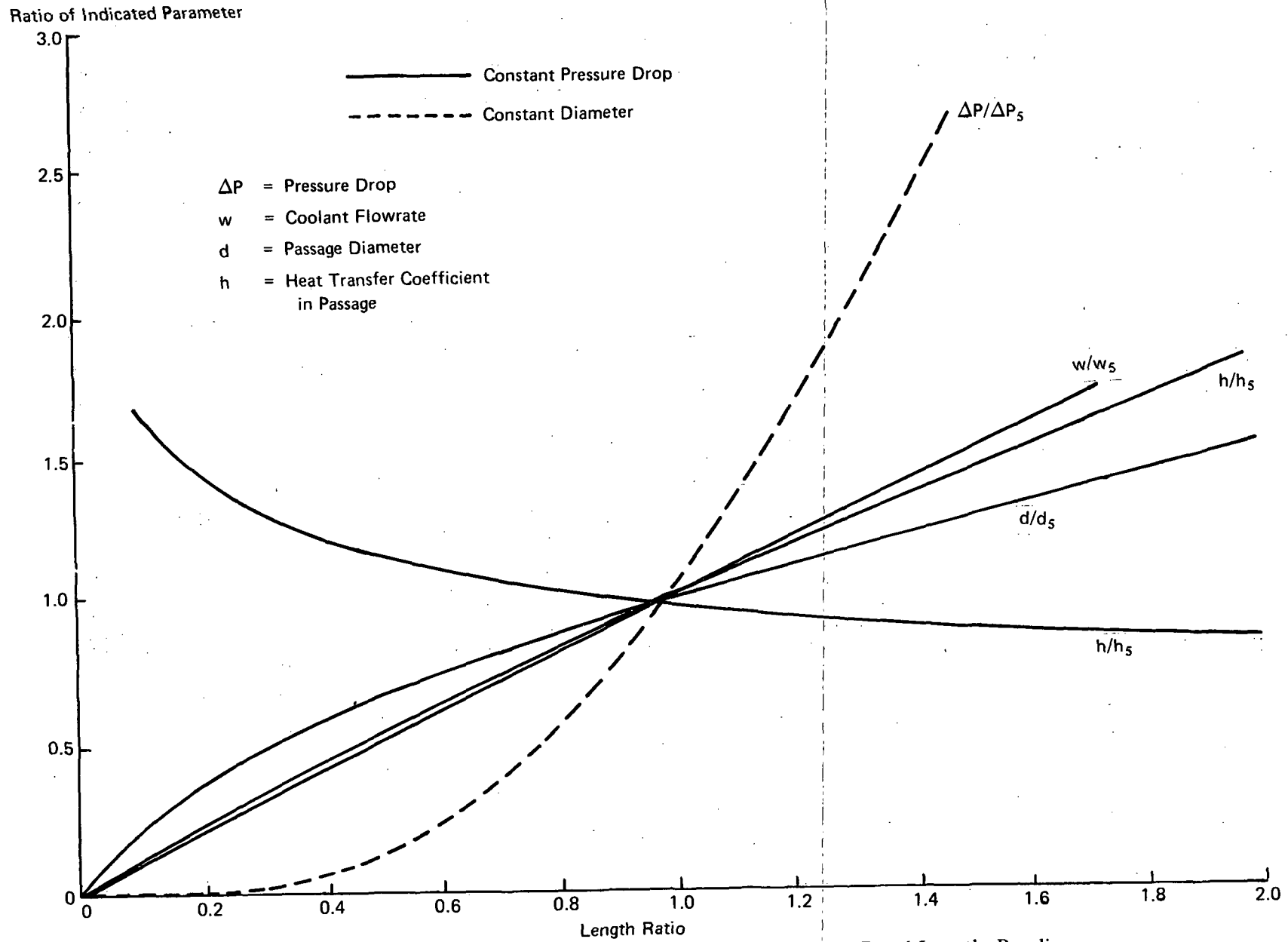


Figure 109. Dependence of Critical Passage Design Parameters on Panel Length, Baseline Length = 1.5 m (5.0 ft)

Cooled Airframe Weights.- The weight of the cooled airframe for various thermal protection systems concepts based on active cooling are presented in Table XLVII for the hypersonic research airplane. Aluminum alloy construction is assumed in all cases; maximum structural temperatures would be approximately 394° K (250F) under nominal flight conditions, 422° K (300° F) under maneuver conditions, and 450° K (300F) under emergency conditions when system redundancy is used, but would exceed this value for nonredundant systems. For comparison purposes, optimized uncooled RSI protected systems are included; weights were computed, using the data of Reference 42 and the techniques of Reference 41. These uncooled concepts are comparable to the heaviest of the cooled approaches.

While the optimized cooled RSI concept is the lightest (less than 5600 kg [13,000 lb]) thermal protection system for the hypersonic research airplane, it is not representative of concepts likely to be used for a hypersonic transport. In its present form, reusable surface insulation is too fragile for all weather operation and is probably too expensive in view of the high replacement and repair to be expected because of its frailty. Weight differences among the other four candidates employing the baseline tubular skin panel approach are comparable for similar operating conditions with weight differences of less than 10%. The similarity of cooled airframe weights suggests the possibility of designing the basic airframe for an unshielded Mach 8 capability to maximize the speed regime over which an unprotected airframe could be operated, and then evaluating both RSI and shielding concepts for the higher operating capabilities desired.

As compared to the baseline panel concept for the unshielded Mach 8 concept, the plate-fin design approach is expected to be slightly lighter, or slightly heavier, depending upon the size of the heat exchange skin panel that is used. The larger size leads to higher weight but less system complexity. The use of smaller panel sizes will reduce weight but will decrease reliability as indicated later.

It should be noted that in most cases, a significant increment of thermal protection weight is attributable to the hydrogen that must be carried specifically for cooling during the unpowered descent portion of flight. The magnitude of this additional weight of liquid hydrogen can be comparable to that of the redundant cooling system. Therefore, it would appear desirable to examine alternate flight paths and mission planning to see if a descent under power would be desirable, or at least, a descent with the 2.0 g turn imposed by the design trajectory specified for this study. A 1.0g descent could reduce 220 kg (500 lb) from the weight of hydrogen carried specifically for cooling.

Reliability. - The studies conducted to examine the question of reliability used the cooling system shown in Figure 100 as the model. For a nonredundant system, about 7 failures are expected per 10,000 flights, while for a completely redundant system the rate is approximately 1 failure per million flights. Because of this high reliability, studies were conducted to examine weight/reliability trades. Table XLVIII summarizes the influence of panel size on weight and reliability. While some weight can be saved by relaxing reliability requirements and using a larger number of panels the weight reductions seem to be quite small in comparison to the reliability that is lost, three times the failure rate to save 78 kg (170 lb) in the most favorable case.

An item identified as a potential problem area during the failure mode and effects analysis was the plate-fin heat exchanger. Therefore, consideration was given to the shell and tube design which is easier to manufacture and inspect, so that it should be more reliable. Such a heat exchanger was sized assuming coolant flow through the tubes with baffles on the hydrogen side. The minimum distance between tubes was 1.2 mm (0.05 in.) since fouling on the hydrogen side was considered to be remote. The thermal conductance on the hydrogen side was taken as 20% less than that on the

TABLE XLVIIA
COOLED AIRFRAME WEIGHT SUMMARY, HYPERSONIC RESEARCH
AIRPLANE, ALUMINUM ALLOY CONSTRUCTION

| Concept (1) | Cooled Airframe Structure Weight, kilograms | | | | | |
|------------------------|---|----------------|-----------|-----------|--------------|-----------|
| | Structure | Cooling System | | Other | Total | |
| | | Nonredundant | Redundant | | Nonredundant | Redundant |
| Unshielded, M = 8 | 4,231 | 1,326 | 1,675 | 1,680 (3) | 7,230 | 7,586 |
| No. 1 + RSI for M = 10 | 4,231 | 1,326 | 1,675 | 2,034 (4) | 7,591 | 7,940 |
| Optimized RSI, M = 10 | 4,231 | 356 | 415 | 1,140 (7) | 5,727 | 5,786 |
| Uncooled, RSI, M = 8 | 4,231 | - | - | 3,546 (8) | 7,777 | |
| Uncooled, RSI, M = 10 | 4,231 | - | - | 3,741 (8) | 7,972 | |
| Shielded, M = 8 | 4,231 | 649 | 808 | 1,870 (5) | 6,751 | 6,910 |
| Shielded, M = 10 | 4,231 | 1,017 | 1,249 | 2,279 (6) | 7,527 | 7,759 |
| Plate-Fin, 1.52 m (9) | 4,231 | 906 | 1,435 | 1,680 (3) | 6,817 | 7,346 |
| Plate-Fin, 3.05 m (9) | 4,231 | 1,051 | 1,566 | 1,680 (3) | 6,962 | 7,477 |
| Plate-Fin, 6.10 m (9) | 4,231 | 1,205 | 1,734 | 1,680 (3) | 7,116 | 7,645 |

- (1) Glycol/Water coolant, 283°K inlet/366°K outlet
(2) Unshielded, M = 8
(3) LHz needed for cooling during descent, including allowance for maneuvers
(4) 672 kg for RSI applied to 80% of surface area + 1362 kg of LH₂ for descent cooling
(5) 1189 kg for metallic heat shields applied to 80% of surface area + 861 kg of LH₂ for descent
(6) 1189 kg for metallic heat shields applied to 80% of surface area + 1090 kg of LH₂ for descent
(7) 745 kg for coating and strain isolator, 327 kg for insulation, 68 kg for descent cooling
(8) Computed using Reference 41
(9) Glycol/Water Coolant, 255°K/Inlet/383°K Outlet

TABLE XLVII B
COOLED AIRFRAME WEIGHT SUMMARY, HYPERSONIC RESEARCH
AIRPLANE, ALUMINUM ALLOY CONSTRUCTION

| Concept (1) | Cooled Airframe Structure Weight, pounds | | | | | |
|-------------------------|--|----------------|-----------|-----------|--------------|-----------|
| | Structure | Cooling System | | Other | Total | |
| | | Nonredundant | Redundant | | Nonredundant | Redundant |
| Unshielded, M = 8 | 9,320 | 2,920 | 3,690 | 3,700 (3) | 15,940 | 16,710 |
| No. 1 + RSI for M = 10 | 9,320 | 2,920 | 3,690 | 4,480 (4) | 16,720 | 17,490 |
| Optimized RSI, M = 10 | 9,320 | 785 | 915 | 2,510 (7) | 12,615 | 12,745 |
| Uncooled, RSI, M = 8 | 9,320 | - | - | 7,810 (8) | 17,130 | |
| Uncooled, RSI, M = 10 | 9,320 | - | - | 8,240 (8) | 17,560 | |
| Shielded, M = 8 | 9,320 | 1,430 | 1,780 | 4,120 (5) | 14,870 | 15,220 |
| Shielded, M = 10 | 9,320 | 2,240 | 2,750 | 5,020 (6) | 16,580 | 17,090 |
| Plate-Fin, 5 ft (2) (9) | 9,320 | 1,995 | 3,160 | 3,700 (3) | 15,015 | 16,180 |
| Plate-Fin, 10 ft (9) | 9,320 | 2,315 | 3,450 | 3,700 (3) | 15,335 | 16,470 |
| Plate-Fin, 20 ft (9) | 9,320 | 2,655 | 3,820 | 3,700 (3) | 15,675 | 16,840 |

- (1) Glycol/Water coolant, 50F inlet/200F outlet
(2) Unshielded, M = 8
(3) LHz needed for cooling during descent, including allowance for maneuvers
(4) 1480 lb for RSI applied to 80% of surface area + 3000 lb LH₂ for descent cooling
(5) 2620 lb for metallic heat shields applied to 80% of surface area + 1500 lb of LH₂ for descent
(6) 2620 lb for metallic heat shields applied to 80% of surface area + 2400 lb of LH₂ for descent
(7) 1640 lb for coating and strain isolator, 720 lb for insulation, 150 lb for descent cooling
(8) Computed using Reference 41
(9) Glycol/Water Coolant, 255°K Inlet/383°K Outlet

TABLE XLVIII
COOLING SYSTEM WEIGHT/RELIABILITY AS RELATED TO
PANEL SIZE, HYPERSONIC RESEARCH AIRPLANE

| Panel Description (1), m (ft) | | Number of Panels | Cooling System Characteristics | | | |
|----------------------------------|-----------------------|------------------------|--------------------------------|-------------|---|-----------|
| | | | Weight kg (lb) | | Reliability Failures/10 ⁶ Flights | |
| Width | Approximate Length | | | | Nonredundant | Redundant |
| 1.5 (5) | 6.1 (20) | 51 | 1330 (2920) | 1670 (3690) | 775 | 1 |
| | 3.0 (10) | 101 | 1310 (2890) | 1660 (3650) | 1280 | 2 |
| | 2.1 (7) | 151 | 1260 (2790) | 1600 (3520) | 1725 | 3 |
| 0.6 (2) | 6.1 (20) | 126 | 1300 (2860) | 1640 (3620) | 1400 | 2 |
| | 3.0 (10) | 251 | 1320 (2900) | 1660 (3660) | 2670 | 7 |
| | 2.1 (7) | 376 | 1270 (2800) | 1610 (3540) | 3785 | 14 |
| 0.3 (1) | 6.1 (20) | 251 | 1280 (2830) | 1630 (3580) | 2435 | 6 |
| | 3.0 (10) | 501 | 1330 (2920) | 1680 (3700) | 4990 | 25 |
| | 2.1 (7) | 751 | 1300 (2860) | 1640 (3610) | 7215 | 52 |

(1) Unshielded Glycol/Water System for Aluminum Alloy Structure

glycol/water side to account for leakage through the baffle. The lightest core weight consisted of 0.63 cm (0.25 in.) diameter tubes on 0.76 cm (0.30 in.) centers. The wet weight of this heat exchanger including the pumping power penalty was 368 kg (790 lb) for the Mach 8 unshielded aircraft, a weight increase of about 43%, as compared to the plate-fin type. If the spacing between tubes is increased to 0.63 cm (0.25 in.) to facilitate fabrication and inspection, the weight of the heat exchanger increases to 385 kg (850 lb), more than 55% heavier than the plate-fin design.

Various pump arrangements were also considered, as shown in Figure 110, with the nonredundant system shown for reference purposes. Since variations are with respect to only the pump and heat exchanger components all of the other items described in Table prior are shown schematically as the "Loop". These studies assume panels 1.5 m (5 feet) in width and extending from the upper fuselage centerline to the lower fuselage centerline and in the case of the wing, from root to tip. The predicted failure rate for the basic system (Figure 110b) is 7.7 failures per 10,000 flights. Removal of one pump, Figure 110a, increases the failure rate to 7.8 per 10,000 flights. Approximately 18 kg (40 lb) is saved by eliminating the pump.

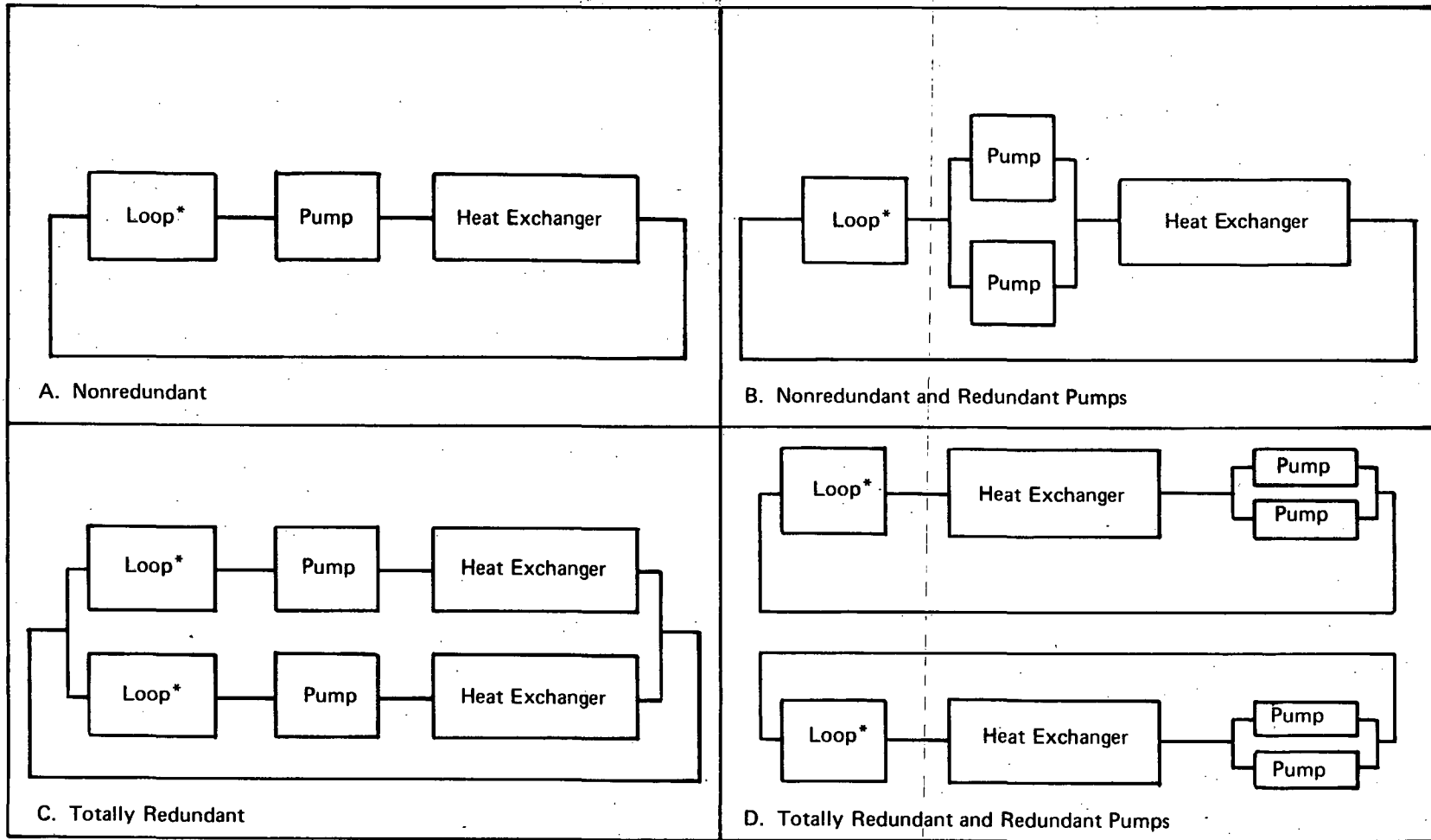
Dramatic increases in system reliability can be realized by total redundancy of the basic system. The reliability diagram for the totally redundant basic systems is depicted as Figure 110c and 110d for single and dual pump variations. For the single pump redundant system, only 6.1 failures per 10,000,000 missions are expected. For the dual pump redundant system, only 6.0 failures per ten million flights are expected. This indicates the insensitivity of the system reliability to the extra pump in each system.

It appears that relatively little weight can be saved by sacrificing reliability. Changing the cooling system weight by varying the number of panels rapidly becomes counter productive. For the first 45 kg (100 lb) weight reduction the failure rate triples, for the next 45 kg (100 lb) reduction the failure rate increases by a factor of about 25. There is no need for two pumps in a single coolant loop when system redundancy is employed. About 37 kg (80 pounds) would be added to a redundant system for a failure rate decrease of about 1 in 100 million missions. For a nonredundant system the weight increase would be only 18 kg (40 lb) and the failure rate would decrease by about 8 in 1 million missions.

Thus, with regard to weight/reliability trades the major decision is whether or not to employ a nonredundant or a redundant approach. The difference in weight is about 370 kg (800 lb,) which when saved increases the failure rate from 6 failures in 10 millions to about 8,000 failures in 10 million missions.

Fatigue and Fracture Considerations. - The fatigue and fracture analyses conducted for the hypersonic research airplane paralleled those for the hypersonic transport. The loading spectrum was presented previously in the baseline data section. Room temperature fatigue properties for the 2024-T3 alloy assumed for the airframe structure, exclusive of the propellant tankage, were obtained from Reference 21 while the crack growth correlation used for the fracture mechanics analysis was that of Forman as presented in the fatigue and fracture section for the hypersonic transport. Results are summarized on Figures 111 and 112 for the fatigue and fracture results respectively. The results are plotted in terms of design lifetimes which already include the scatter factor of 4.0. For this research airplane a service life of 250 hr was assumed (250 flights) so that the design life was 1000 hours.

The significance of fatigue and fracture considerations on the design of the airframe can be summarized in relation to the design allowable ultimate stress for two representative lifes.



* Includes all other Items

Figure 110. Pump Arrangements

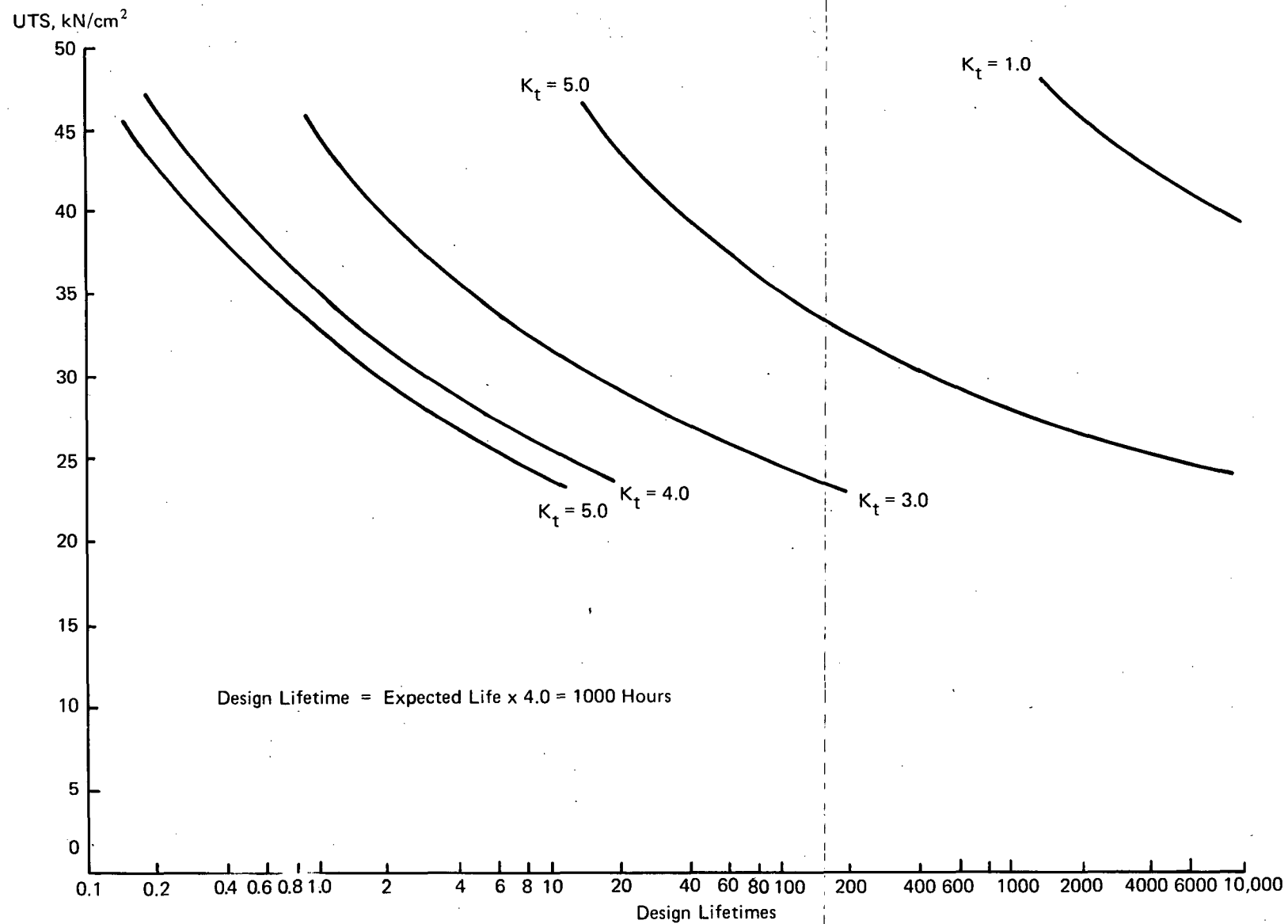


Figure 111a. Fatigue Characteristics of 2024-T3 Structure, Severe Research Airplane Spectrum

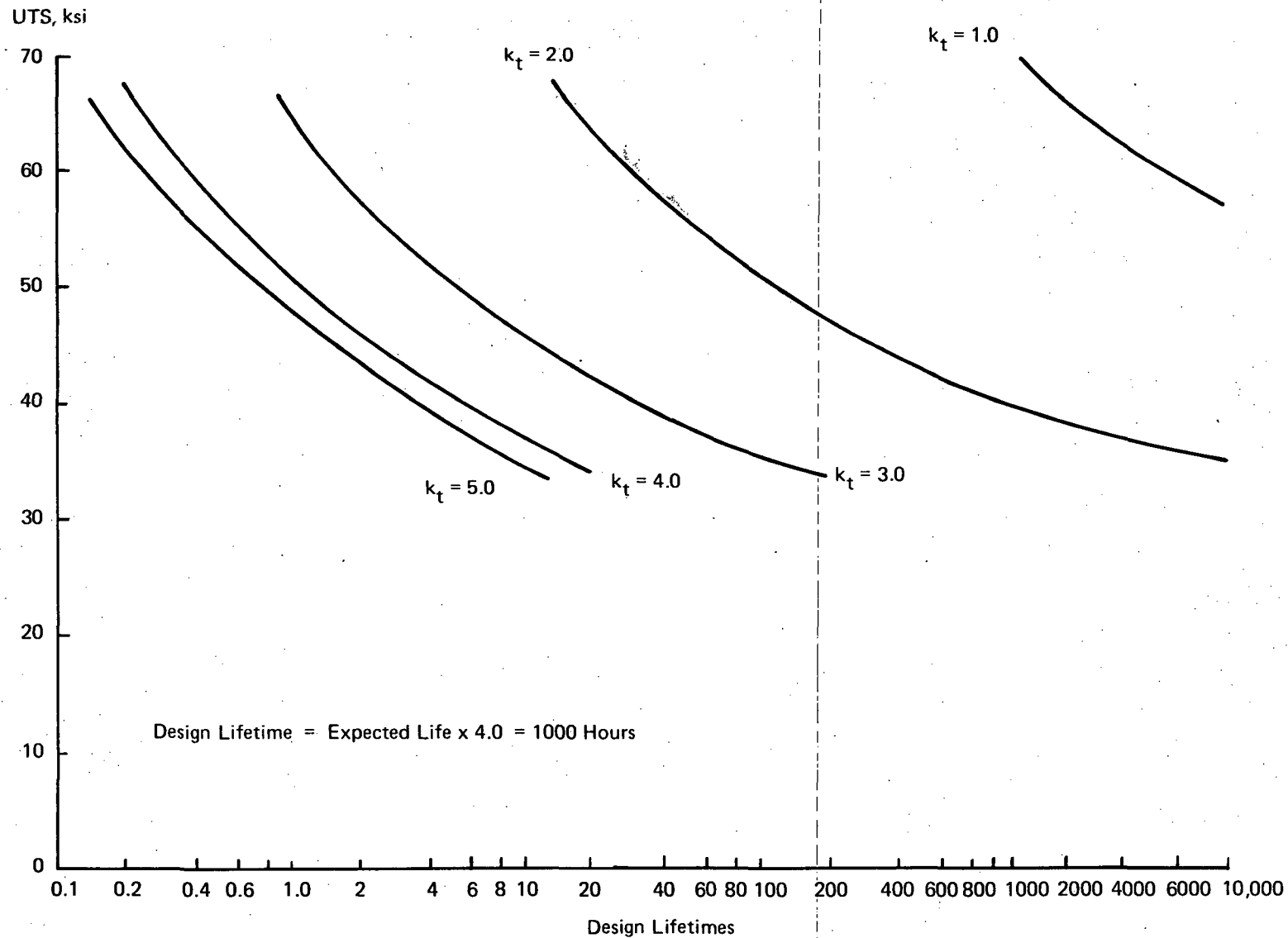


Figure 111b. Fatigue Characteristics of 2024-T3 Structure, Severe Research Airplane Spectrum

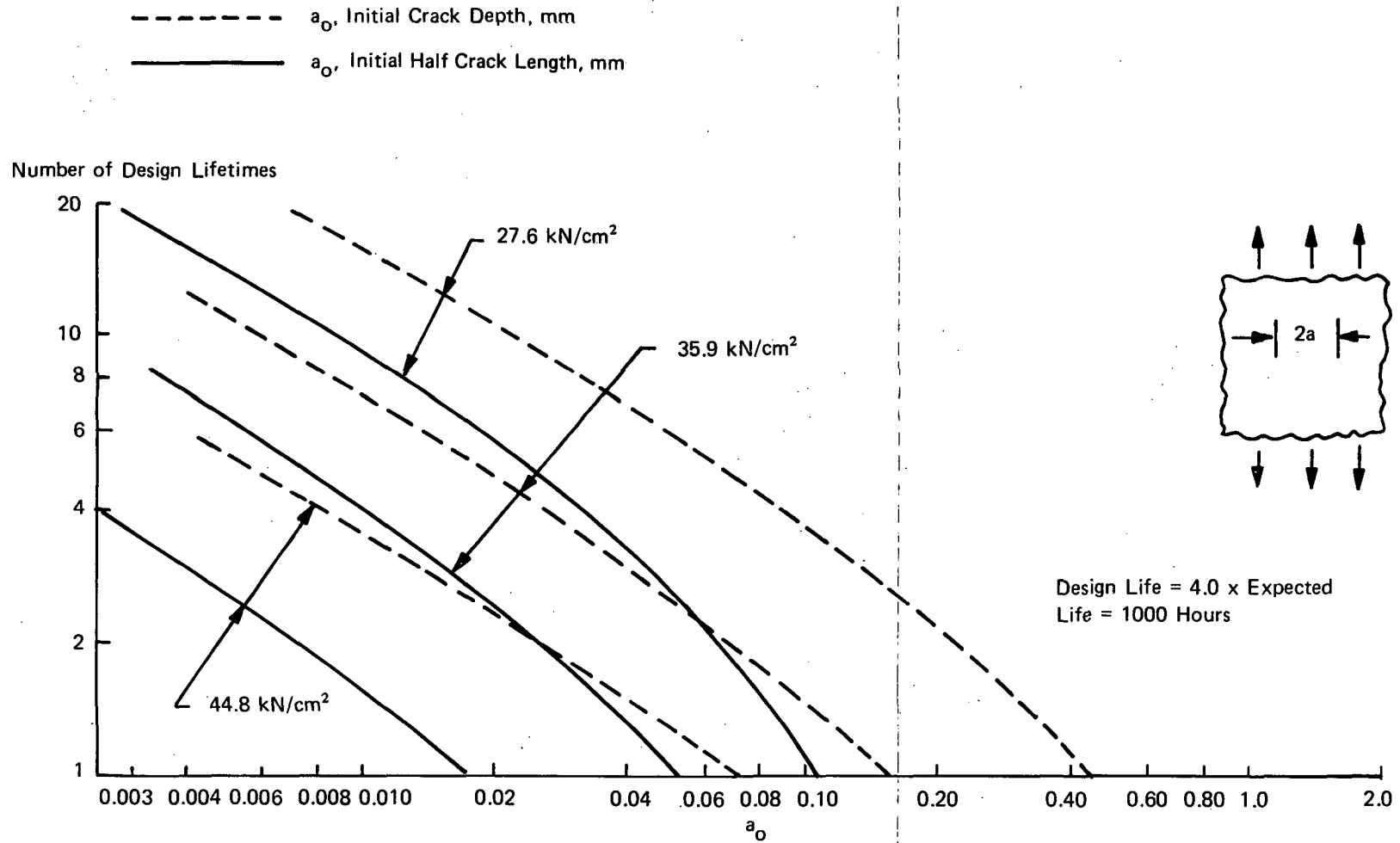


Figure 112a. Interaction of Life, Ultimate Design Allowable Stress, and Initial Crack Size for a Surface Crack and Through-Crack in an Infinite 2024-T3 Sheet, Hypersonic Research Airplane Spectrum

- - - a_o , Initial Crack Depth, in.
 — a_o , Initial Half Crack Length, in.

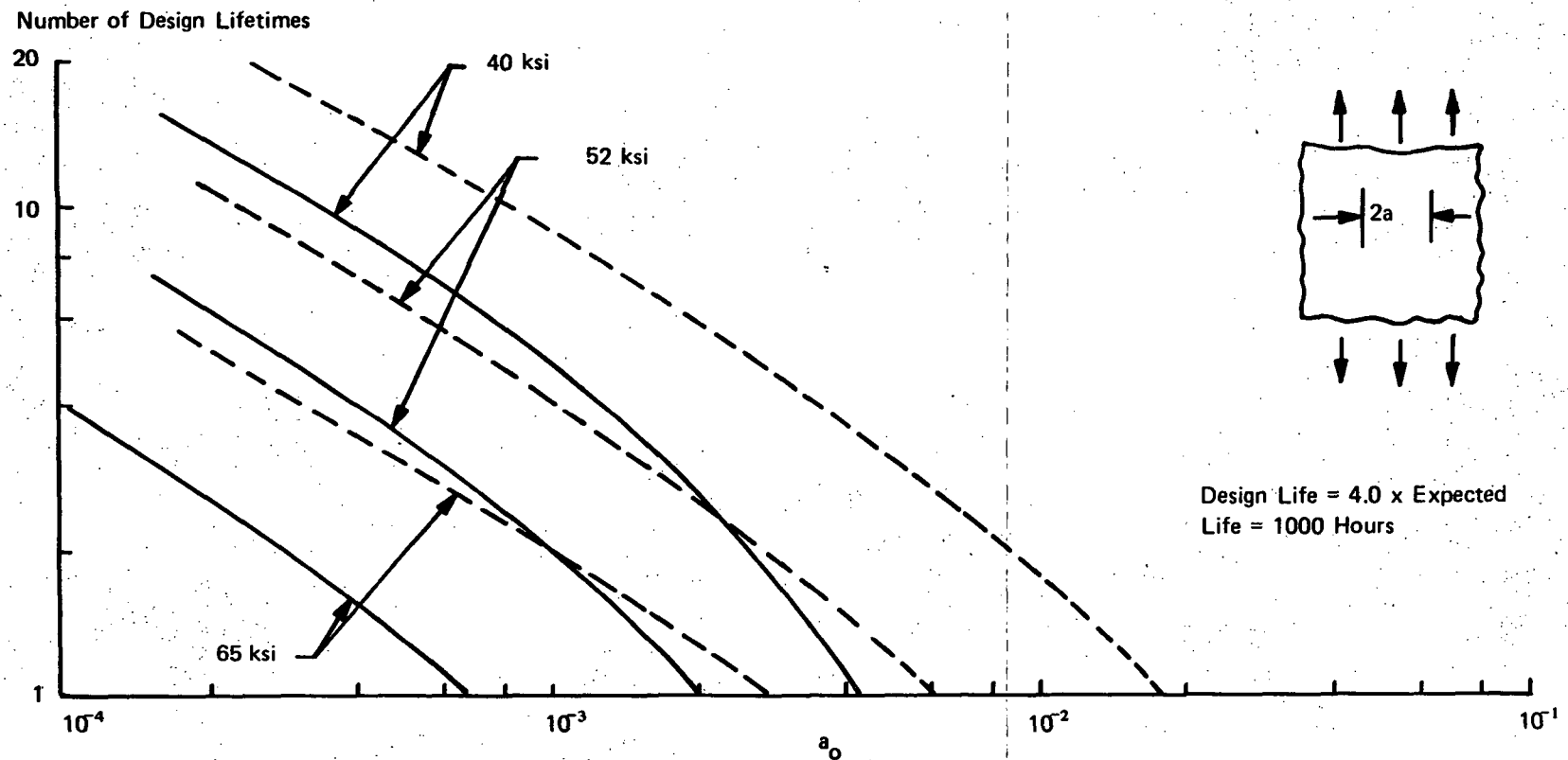


Figure 112b. Interaction of Life, Ultimate Design Allowable Stress, and Initial Crack Size
 for a Surface Crack and Through-Crack in an Infinite 2024-T3 Sheet,
 Hypersonic Research Airplane Spectrum

| <u>Design Consideration</u> | <u>1000 Hr. Design Life</u> | <u>2000 Hr. Design Life</u> |
|-----------------------------------|-----------------------------|-----------------------------|
| | kN/cm ² (psi) | kN/cm ² (psi) |
| Fatigue, $K_t = 5.0$ | 33.2 (48,000) | 29.8 (43,000) |
| Fatigue, $K_t = 4.0$ | 35.3 (51,000) | 31.8 (46,000) |
| Fatigue, $K_t = 3.0$ | 45.0 (65,000) | 39.4 (57,000) |
| Surface Scratch 0.06 mm, (2 mils) | 36.0 (52,000) | 30.5 (44,000) |
| Through Crack, 0.25 mm (10 mils) | 31.8 (46,000) | 27.0 (39,000) |

Based on these considerations, it appears that the fracture mechanics considerations are of primary importance particularly with respect to the presence of through cracks. The likelihood of such cracks being present is extremely remote and deserves further consideration before the design is penalized to the degree indicated. Surface scratches do not appear to be quite as significant as fatigue considerations. The above comments pertain to the airframe structure specifically and not to the propellant tankage. Because of the combined consideration of airframe loads and internal pressurization experienced by integral propellant tanks, the design allowable stress levels are likely to be somewhat lower for the tankage than for the airframe structure. In addition, the fatigue and fracture characteristics of the 2219 alloy are not quite as good as those for the 2024 alloy.

CONCLUSIONS AND RECOMMENDATIONS

Emphasis in this study was placed on convective cooling systems and primary load carrying structure with the objective of comparing materials and concepts. Because of this emphasis on concept examination and parametric comparisons, the efforts devoted to definition of the characteristics of the hypersonic transport and the hypersonic research airplane were limited to a level less than that associated with a preliminary design study. The net effect of the simplifying assumptions used is considered to be small with regard to comparisons, but may be somewhat larger when absolute magnitudes are considered.

The comparisons of the various cooled structural concepts for the hypersonic transport are made by comparing payloads for airplanes of the same gross weight, geometric configuration and dimensions. That is, the aircraft was not resized but rather it was assumed that the additional payload weight made possible by the lighter, cooled structure could be carried within the original volume. In some instances additional hydrogen was assumed to be carried specifically for cooling purposes, but the vehicle configuration was not altered to accommodate the increase in fuel volume associated with this additional hydrogen weight. These simplifications lead to optimistic estimates of payload increases.

The primary conclusion reached as a result of these extensive parametric and aircraft system analyses is that the potential benefit to be derived from actively cooled airframe structure may be greater than anticipated in earlier studies. When advanced structural materials are considered an actively cooled hypersonic transport could carry approximately 200% of the payload that could be carried by an uncooled vehicle of the same gross weight if the additional payload could be accommodated within the original vehicle configuration.

From a weight/payload point of view, the most attractive design utilized a beryllium airframe structure maintained at less than 394°K (250F) by a glycol/water cooling system. Approximately 30% of the external surface of the aircraft was shielded with superalloy panels to permit matching of the airframe heat load to the capacity available from the normal fuel flow schedule. The same basic concept, but with an aluminum alloy structure, served as the baseline system and indicated a payload of 180% of that for an uncooled structure. Both cooled designs employed completely redundant cooling systems.

In addition to the primary conclusion of the superior payload weight potential for the cooled airframe concept, a number of more detailed conclusions were reached with regard to various aspects of the total design picture; they are grouped into the following categories: (1) airframe concepts, (2) materials, (3) structural concepts for panels, (4) thermal concepts for panels, (5) reliability and safety, and (6) local areas requiring attention. Specific conclusions with respect to airframe concepts are as follows:

1. Matching the heat load absorbed by the cooling system to the heat capacity of the fuel flow schedule is a principle consideration in minimizing the weight of an actively cooled airframe structure. Several approaches including trajectory tailoring, external shielding and/or dual temperature airframe structures can be used to match cooling system heat load to fuel heat capacity.

2. To eliminate any form of external shielding or the carrying of excess hydrogen specifically for cooling purposes requires a structural operating temperature capability of about 575° K (575F) for the specific hypersonic transport studied.
3. For the hypersonic transport beryllium structure resulted in the lightest weight for all concept variations considered, with boron/aluminum almost as attractive. Payload increase varied for specific cooled airframe concept with the shielded 366° K (200F) system most beneficial, and the unshielded 366° K (200F) system least attractive.

With respect to construction materials and coolants, the following conclusions can be drawn from the results of the various studies:

1. As compared to aluminum alloy construction advanced materials might increase payload by more than 25%. Beryllium is most attractive with metal matrix composites only slightly less attractive.
2. There appears to be no major problem in finding compatible combinations of attractive construction materials and promising coolants based on the corrosion and stress corrosion tests conducted.
3. There are potential advantages for mixed material structures when this allows the hydrogen fuel to be heated to a higher temperature than possible when a single material is used.
4. Aqueous coolants are best for temperatures below about 394° K (250F), nonaqueous solutions are attractive when maximum coolant temperatures exceed about 394° K (250F).

While a large number of structural panel concepts were considered and compared, the relatively conventional skin/stringer/frame and the honeycomb sandwich approaches were most attractive for the fuselage and wings respectively. Lighter weights were indicated for symmetrically double beaded fuselage skin panels but this design poses major problems of integrating coolant passages with the structural arrangement.

With regard to the weight of panel designs as influenced by thermal factors, the following conclusions may be drawn:

1. The baseline tubular panel concept is most attractive from weight and assembly points of view for regions of modest heat flux and areas where minimum gage considerations set skin thickness requirements. The sandwiched tube concept appears particularly attractive.
2. The plate-fin panel concept is most attractive for high heat flux levels where the use of the tubular concept would impose weight penalties associated with high coolant flow rates, or preclude practical assembly because of very close passage spacing. The heat flux for changing of the panel concept will depend upon specific vehicle design requirements and requires further study.

3. While much heavier than the plate-fin concept the sphere-core panel concept may be useful in regions requiring double curvature.
4. The plain skin with cooled substructure appears to be attractive only for low heat flux levels unless metallurgical joining is used, in which case its primary advantage of damage tolerance is lost.
5. When aerodynamic heating is to be attenuated, metallic heat shields appear more attractive than high density ceramic external surface insulation.

Reliability considerations appear to dictate the use of the completely redundant cooling system designs for the hypersonic transport. While the weight penalty involved is about 1370 kg (3000 pounds) this is only about 0.6% of the takeoff gross weight, and the added safety appears to warrant such an approach. About half of the weight increment is due to a second heat exchanger. Therefore, the possibility of not doubling up on this item may warrant further investigation. The relatively small penalty associated with complete redundancy is due to an improved redundancy concept defined during the course of the project, flowing 50% of the required coolant in each of two adjacent coolant passage networks. Even if the flow rate in the single operating loop was not doubled under shutdown of one loop, structural temperatures would not rise catastrophically but the 1.5 design ultimate factor of safety will be reduced as a result of the temperature increase and strength reduction. The reduced size and shorter design life for the hypersonic research airplane made the need for complete redundancy uncertain. However, it may be desirable to include a redundant system as a means of testing the concept for later use on advanced transports. If redundancy is not used, a means of avoiding excessive temperatures of the load carrying structure will be needed to deal with possible emergencies associated with cooling system malfunction. Other conclusions reached with regard to reliability and safety include:

1. Redundant coolant passage networks can be provided in both the discrete tubular and plate-fin concepts with relatively small weight penalties by using concepts defined by this study.
2. The discrete tubular passage concept appears well suited to the incorporation of crack arrestors which should enhance the damage tolerance of actively cooled skin panels.
3. Failure mode and effects analyses indicate that the panel and connections should receive special attention during detail design.

Although the major portion of the cooled structure was studied in detail a few local areas still need attention, such as stagnation regions, areas subjected to interference heating effects, control surfaces, etc. Since the areas are rather localized even relatively inefficient solutions would not be expected to offset the advantages offered by the actively cooled airframe approach. Further comments regarding these areas are provided by the discussion of recommendations.

The studies conducted to date have demonstrated potential feasibility and potential performance advantages for actively cooled airframe structure. Future activities should be directed toward: (1) examination of areas that have not received much attention in the past, (2) demonstration of key design technology through experimental evaluations, (3) comparisons to identify the relative merits of seemingly comparable design approaches, and (4) an assessment of cost and operational considerations that may influence the design approaches that will lead to optimum hypersonic aircraft of the future. These future activities might be guided by recommendations derived from project studies and grouped into the following topic areas for convenience:

1. System trades
2. Material evaluations
3. Component demonstrations
4. System demonstrations

Based on the results of the present project, it appears that emphasis should be placed in the third area but concurrent activities in the first two areas are essential to insure and provide overall direction of component design and demonstration activities.

The system trade studies should have as their goal an initial assessment of design alternatives as they influence total aircraft characteristics and not only those directly related to the cooled structure. Items considered to be of importance include the following:

1. Investigation of alternatives to redundancy should be investigated since weight savings might be as much as 2% of the payload.
2. Methods of protecting against high local heating rates associated with flow interference will be needed, so that early consideration of design approaches is desirable.
3. The impact of cruise Mach number on the performance characteristics of cooled aircraft should be assessed. Reductions in heat flux will reduce cooling system weight and increase the spacing of coolant passages.
4. The areas of use for baseline and plate-fin panel concepts should be defined by analytical and design studies that combine thermal and structural considerations of airframe requirements such as doors, major fittings, etc.
5. Reliability, safety, and maintainability aspects of cooled airframe designs should be investigated in more depth with particular emphasis on such items as weight/reliability trends, component location/serviceability interactions, sensors for fault detection and isolation, and visual displays.

6. Since the presence of the airframe cooling system is likely to reduce the weight of other vehicle subsystems (such as environmental control, cooling of electronic equipment, and the auxiliary power supply) the impact of such benefits on payload should be defined along with any technology development implications.
7. Using data derived from component demonstrations, detailed system optimization and performance analyses should be conducted on various component malfunctions in order to identify the transient response of the system to operational conditions and malfunctions.

The recommendations made with respect to materials assume continuing activities for the identification and evaluation of promising new structural materials. Therefore, recommendations for future materials work relating to cooled structure are directed toward evaluations that are unlikely to be conducted in the course of normal material development activities. Future programs are considered necessary in the following areas:

1. Definition and evaluation of techniques for enhancing damage tolerance of actively cooled panels with particular attention to the influences of various candidate construction materials and damage tolerant features.
2. Comparison of candidate construction materials with respect to fracture and fatigue characteristics at operating temperature levels and with stresses induced by temperature gradients and internal pressurization as well as applied loadings.
3. Chemical compatibility testing of candidate coolants with construction materials and the non-metallics used for seals and similar purposes should be conducted at representative temperature levels using static and dynamic techniques. Studies of inhibitors may also be desirable.
4. The apparent advantages of some form of shielding over relatively small areas of the aircraft make it desirable to evaluate candidate metallic and ceramic materials for such shielding purposes.

No special programs are recommended with respect to the utilization of advanced composite materials. It is expected that a high level of activity will be maintained in this promising structural technology area. Hence, they should be considered as appropriate during the recommended material evaluation activities.

The major area for immediate attention with respect to cooled airframe structure involves the demonstration of the suitability of representative components. These are expected to involve external structural items (skin panels, stagnation components, movable surfaces, etc.) cooling system mechanical components, and structure/cooling interface items. Efforts should include design, fabrication and experimental evaluation. In many cases the concepts described in this report can form the basis for detailed design and development efforts, in others the results of the recommended system trade studies can be used. Damage tolerant designs should receive particular attention. Reliability and safety should be emphasized. Specific items should include:

1. Cooled skin panels of the type required for general usage on cooled airframes
2. Cooled skin panel concepts integrated with external shielding

3. Cooled skin panel concepts integrated with cryogenic propellant tankage
4. Cooling concepts for regions of interference heating
5. Cooled stagnation region structure, leading edges and nose caps
6. Cooled movable surfaces - Design studies should be preceded by wind tunnel tests to more accurately define aerodynamic heating, particularly around gaps and edges.
7. Mechanical components with particular emphasis on heat exchanger, fault detection devices, and connectors. Although the weight impact of connector designs is small the reliability and leakage aspects are very important.

While still quite far downstream, it is recommended that early consideration be given to planning for flight test and laboratory demonstrations of the cooled aircraft structure concept. An early flight demonstration on a subsonic aircraft is recommended as a means of evaluating reliability and maintainability aspects without jeopardizing safety. In addition, a demonstration of freedom from operational problems would do much to raise the level of confidence in the cooled airframe structural concept. The laboratory demonstration should employ a relatively large prototype structure on which mission profile heating and loading can be applied for thousands of simulated missions to evaluate thermal/structural interactions and to obtain long time data with respect to coolant/material compatibility, component reliability, and maintainability.

APPENDIX A EXPERIMENTAL EVALUATIONS

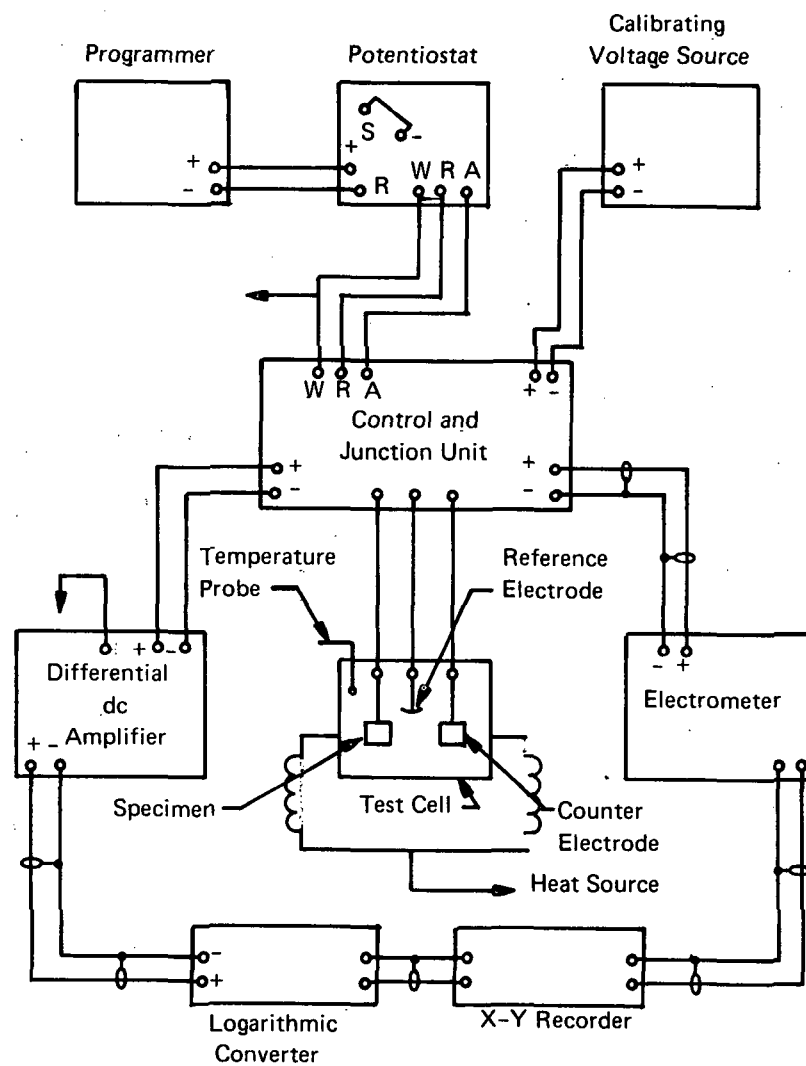
Since one of the potential applications for cooled structure is for hypersonic transports where long trouble free service life is essential, it is imperative that the construction material and the coolant be compatible. A review of available literature, References 8 through 20, provided limited information upon which only the most cursory screening of material combinations could be based. Because of the importance of the compatibility question experimental evaluations were undertaken. Three types of tests were conducted: (1) corrosion potential measurements, (2) weight change measurements, and (3) stress corrosion exposures. The purpose of the corrosion potential and weight change measurements was to obtain screening estimates of the compatibility of various construction material/coolant combinations at representative use temperatures. A relatively large number of combinations were investigated using the equipment illustrated schematically in Figure 113. The stress corrosion testing was more limited in nature and had as its purpose the identification of possible strength degradation when certain of the candidate construction materials were exposed to representative classes of coolants.

The materials and coolants were selected to provide data for various classes of materials and coolants rather than on the basis of picking combinations that are optimum. The objective of all testing was to screen candidates. Emphasis was placed on aluminum alloy construction materials because of the extensive experience level and low cost associated therewith, and on aqueous solutions of ethylene glycol and methanol because of their superior heat transfer characteristics over the range of temperatures of interest for aluminum alloy construction. The use of such material combinations would permit early attainment of an efficient and economical cooled structure. Consideration of other material classes and coolants, suitable for use to 589°K (600F) and at least 450°K (350F) respectively, provided a means of exploring the potential of more advanced systems which are expected to show improved aircraft performance in a later time frame than that associated with aluminum alloy construction.

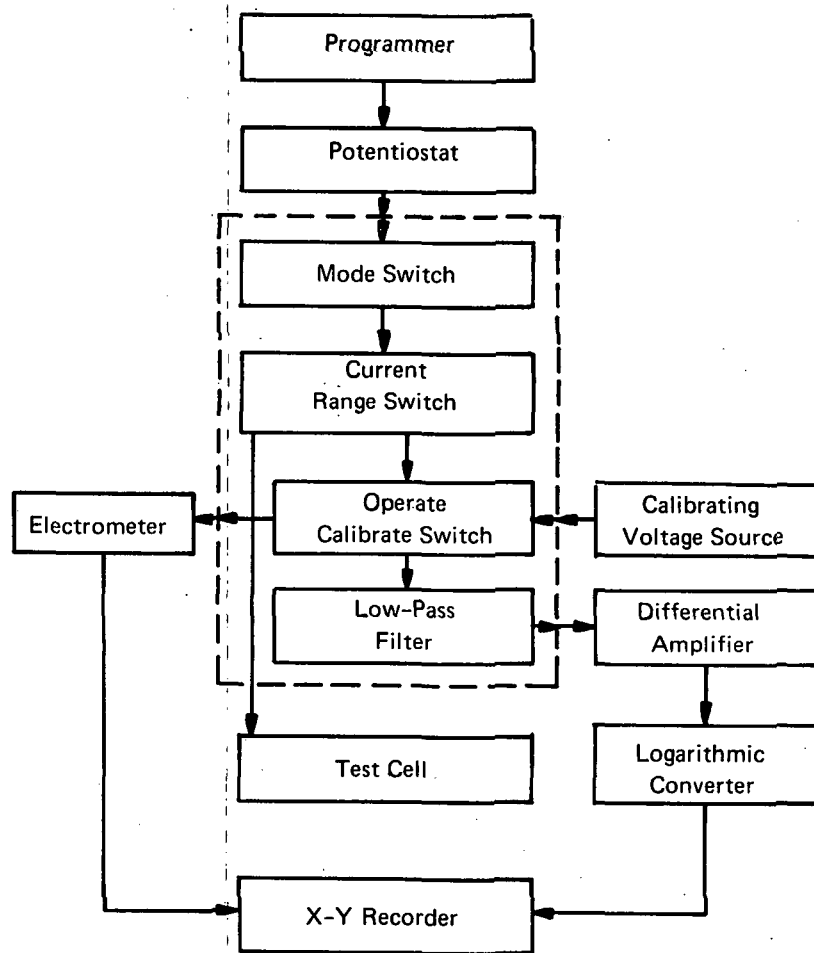
Corrosion Potential Measurements

A typical polarization diagram is shown in Figure 114. Voltage is referenced to platinum/silver chloride electrodes. The break in the anodic curve at 0.5 volts identifies the pitting potential while the point of rapid dropoff when polarizing in the negative direction identifies the crevice, or protection, potential. When the pitting potential is more positive than the protection potential pitting and crevice corrosion cannot occur. Furthermore, when these values are more positive than the redox potential of the coolant there will be no crevice or pitting corrosion in the combination as long as the coolant composition does not change. Redox potentials ranged from 0.10v to 0.30v indicating that only general corrosion would be of concern as long as coolant characteristics were controlled. The corrosion potential corresponds to the point where an extension of the cathodic polarization curve, the one sloping downward to the right, intersects the anodic polarization curve. The current density at this point of intersection is used to compute the corrosion rate.

Results of the corrosion potential measurement tests are summarized in Table XLIX. In addition to the materials of primary interest a few materials of relatively high corrosion resistance were included in the measurements to serve as relative references. No intentional attempt was made to



a. Schematic



b. Detail of Control and Junction Unit

Figure 113. Block Diagram of Automatic Polarization Apparatus

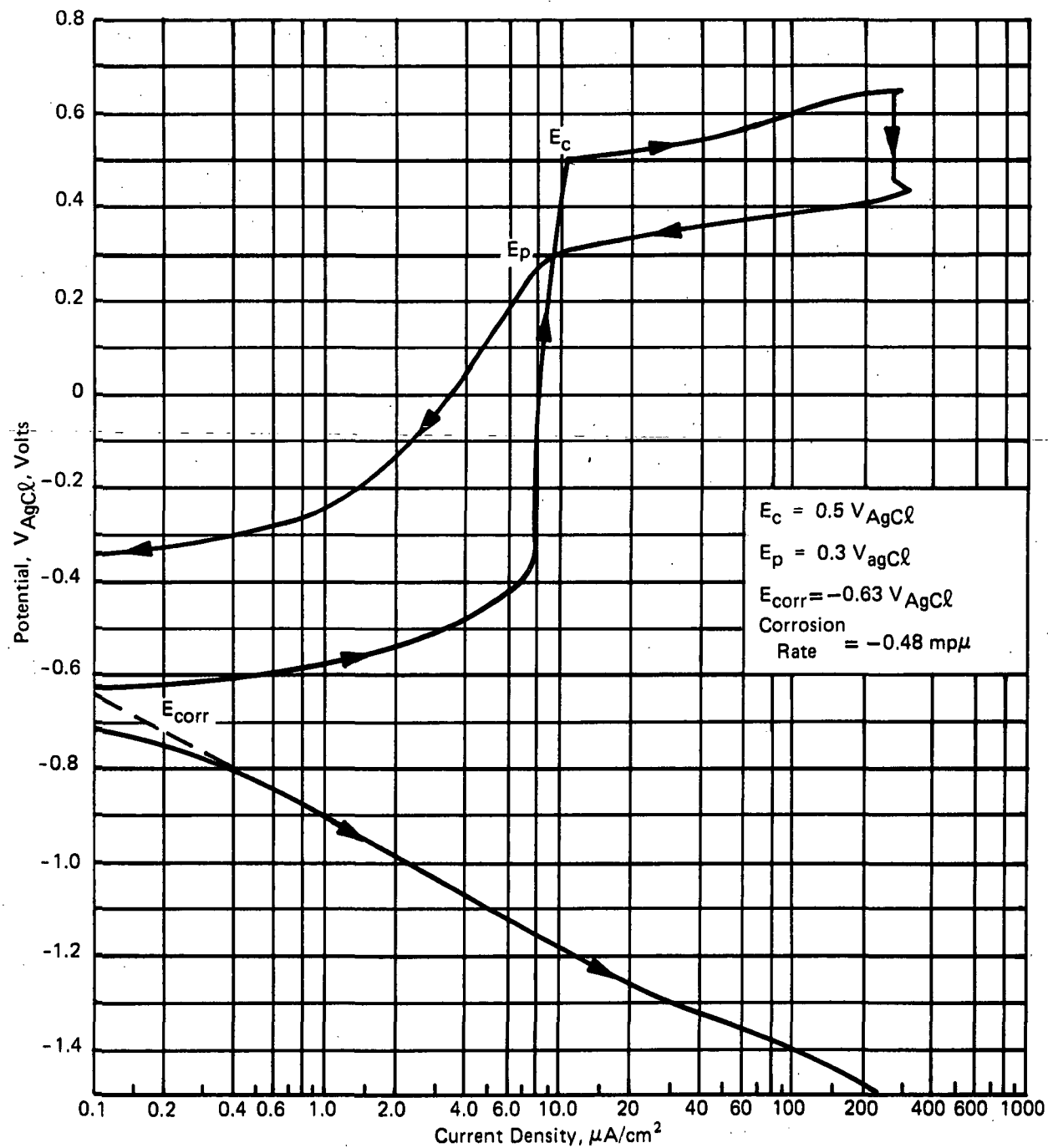


Figure 114. Polarization Diagram for 7075-T6 Aluminum Alloy Exposed To Apollo Grade 2 Ethylene Glycol at 200°F

TABLE XLIXA
CORROSION RATES IN AQUEOUS SOLUTIONS

| Construction Material | Corrosion Rate, $\mu\text{m/y}$ in Coolant Indicated | | | | |
|-----------------------|--|-------------|--------------|------------|----------------------|
| | 367° K | | | 344° K | |
| | Apollo 2* | Prestone* | Prestone II* | Methanol** | Inhibited Methanol** |
| Aluminum | | | | | |
| 1100-0 | 51.30 | 39.9 | 26.7 | 21.8 | 12.2 |
| 1145-H19 | 128.3 | - | - | - | - |
| 2021-T62 | 28.2 | 64.5 | 71.1 | 14.5 | 5.6 |
| 2024-T3 | 44.5 | 13.2 | 40.9 | 30.0 | 12.2 |
| 2024-T6 | 105.4 | - | - | - | - |
| X-2048-T851 | 21.1 | 27.7 | 13.5 | 15.5 | 22.4 |
| 2219-T87 | 78.7 | 90.9 | 31.0, 17.5 | 30.5 | 17.8 |
| 3003-0 | 34.3 | 28.7 | 24.4 | 11.2 | 13.5 |
| 5086-H117 | 41.1 | - | - | - | - |
| 5456-H117 | 23.1 | - | - | - | - |
| 6061-T6 | 18.8 | 3.3 | 5.6 | 8.4 | 11.4 |
| 7075-T6 | 12.2 | 114.3, 34.3 | 23.4, 19.6 | 53.3 | 38.9 |
| 7475-T61 | 55.4 | 55.4 | 26.7 | 25.7 | 11.2 |
| Others | | | | | |
| AZ31B-H24 | 45.7 | 3.18 | 125.7 | 16.5 | 26.7 |
| Beryllium | 38.1 | 83.8 | 9.7 | 40.6 | 16.5 |
| Lockalloy | 20.8 | 6.4 | 6.1 | 55.9 | 20.3 |
| Ti-6Al-4V-Ann | 7.62 | - | - | - | - |
| Ti-6Al-4V-STA | 6.86 | 261.6 | 67.1, 15.0 | 24.4 | 41.9 |
| Inconel 617 | 61.5 | - | 98.3 | 29.0 | 30.2 |
| Inconel 718 | 67.1 | 0.53, 45.7 | 40.1, 32.5 | 50.3 | 22.9 |
| Boron/Aluminum (1) | 95.5 | 43.4 | 44.5 | - | 58.9 |
| Boron/Aluminum (2) | 164.1 | 25.7 | 197.6 | 48.8 | 91.9 |
| Graphite/Aluminum (1) | 104.4 | 155.4 | 166.4 | 55.4 | 26.7 |
| Graphite/Aluminum (2) | 43.2 | - | 1290.3, 5.6 | 22.1 | 42.2 |

*66% Glycol/34% Water

**80% Methanol/20% Water (0.2 w/o Potassium Chromate in inhibited solution)

(1) Fibers parallel to surface

(2) Fibers perpendicular to surface

TABLE XLIXB
CORROSION RATES IN AQUEOUS SOLUTIONS

| Construction Material | Corrosion Rate, mpy in Coolant Indicated | | | | |
|-----------------------|--|-------------|--------------|------------|----------------------|
| | 200F | | | 160F | |
| | Apollo 2* | Prestone* | Prestone II* | Methanol** | Inhibited Methanol** |
| Aluminum | | | | | |
| 1100-O | 2.02 | 1.57 | 1.05 | 0.86 | 0.48 |
| 1145-H19 | 5.05 | | | | |
| 2021-T62 | 1.11 | 2.54 | 2.80 | 0.57 | 0.22 |
| 2024-T3 | 1.75 | 0.52 | 1.61 | 1.18 | 0.48 |
| 2024-T6 | 4.15 | | | | |
| X-2048-T851 | 0.83 | 1.09 | 0.53 | 0.61 | 0.88 |
| 2219-T87 | 3.10 | 3.58 | 1.22, 0.69 | 1.20 | 0.70 |
| 3003-O | 1.35 | 1.13 | 0.96 | 0.44 | 0.53 |
| 5086-H117 | 1.62 | | | | |
| 5456-H117 | 0.91 | | | | |
| 6061-T6 | 0.74 | 0.13 | 0.22 | 0.33 | 0.45 |
| 7075-T6 | 0.48 | 4.50, 1.35 | 0.92, 0.77 | 2.10 | 1.53 |
| 7475-T61 | 2.18 | 2.18 | 1.05 | 1.01 | 0.44 |
| Others | | | | | |
| AZ31B-H24 | 1.80 | 1.25 | 4.95 | 0.65 | 1.05 |
| Beryllium | 1.50 | 3.30 | 0.38 | 1.60 | 0.65 |
| Lockalloy | 0.82 | 0.25 | 0.24 | 2.20 | 0.80 |
| Ti-6Al-4V-Ann | 0.30 | | | | |
| Ti-6Al-4V- Sta | 0.27 | 10.3 | 2.64, 0.59 | 0.96 | 1.65 |
| Inconel 617 | 2.42 | | 3.87 | 1.14 | 1.19 |
| Inconel 718 | 2.64 | 0.021, 1.80 | 1.58, 1.28 | 1.98 | 0.90 |
| Boron/Aluminum (1) | 3.76 | 1.71 | 1.75 | | 2.32 |
| Boron/Aluminum (2) | 6.46 | 1.01 | 7.78 | 1.92 | 3.62 |
| Graphite/Aluminum (1) | 4.11 | 6.12 | 6.55 | 2.18 | 1.05 |
| Graphite/Aluminum (2) | 1.70 | 1.44 | 50.8, 0.22 | 0.87 | 1.66 |

* 66% Glycol/34% Water

** 80% Methanol/20% Water (0.2 w/o Potassium Chromate in Inhibited Solution)

(1) Fibers Parallel to Surface

(2) Fibers Perpendicular to Surface

form protective oxide surfaces on the samples. In general the samples were sanded lightly with 600 grit paper before testing. Since the tests involved a relatively short exposure, (about two hours in the coolant before measurements were started) some of the variation in corrosion rate data may be due to the detailed nature of the protective film formed on each alloy.

In the case of most conventional construction materials an aqueous coolant can be found that provides a corrosion rate of less than 25 micrometers per year (1 mil per year). This suggests that with some further optimization general corrosion should not restrict the choice of construction material/coolant combinations. It was surprising that in many cases uninhibited methanol had corrosion rates lower than the ethylene glycol/water solutions. This may be due to more rapid oxide formation in the absence of the particular inhibitors used in the glycols. Note that the 0.2 w/o of potassium chromate inhibitor in the methanol solution reduced corrosion rates still further in most instances. It should be noted that corrosion potential measurements provide useful trend data but are subject to significant scatter unless extreme care is taken in the preparation of specimens. An indication of the scatter is provided by spot rechecks shown as double entries in some of the columns.

In general, the composite materials tend to have higher corrosion rates regardless of the coolant used. This suggests that some further work will be required before the aluminum matrix composites can be used in contact with aqueous coolants for long time service. Since no studies of inhibitors for metal matrix composites have been conducted this is not surprising and should not be considered a deterrent to consideration of these metal matrix composites for future use. Rather, it points out a need for work in this area.

Weight Change Measurements

For the dielectric coolants it was not possible to obtain polarization curves since current flow could not be induced. Weight change measurements were used, therefore, to obtain an indication of the compatibility between candidate construction materials and representative dielectric coolants. Results are summarized in Tables L and LI. For the Coolanols (silicate esters), corrosion rates are generally less than 0.1 mil per year with many combinations showing no evidence of weight change after 1300 hours of exposure at 200F. Rather surprisingly the highest corrosion rate was indicated by 6061-T6 exposed in Coolanol 20. There was no weight loss for any of the candidate materials exposed in the Dow silicone fluid or in the prefluorinated hydrocarbons; therefore, there was no apparent corrosion during the 762 hours of exposure at 366° K (200F). The indications of weight gains suggest the formation of surface coatings. Since there was no flow during the tests the results should be considered as preliminary with regard to actual applications.

Stress Corrosion Exposures

The results of the stress corrosion tests are presented in Tables LII through LXI in the form of weight change data and visual observations. Both unnotched and notched specimens were stressed to 90% of the room temperature tensile strength. In the case of the notched specimens the induced stress was multiplied by the theoretical stress concentration factor of the notch. The specimen designs are shown in Figure 115. In reviewing the test results note that there were no failures despite the high stress induced in the bent strips. This indicates that all of the combinations examined can be used without a significant reduction in design allowable strength levels to allow for stress corrosion considerations. In general, corrosion rates are less than those determined by corrosion potential measurements. This is probably due to the longer exposures during the stress corrosion

TABLE L
CORROSION RATES FOR 1300 HOURS EXPOSURE
AT 366°K (200F) IN COOLANOLS

| Material | Weight Change,* mg | | | Corrosion Rate μm/gr (mpy) | | |
|-------------------|--------------------|-------------|-------------|-------------------------------|-------------|-------------|
| | Coolanol 20 | Coolanol 40 | Coolanol 45 | Coolanol 20 | Coolanol 40 | Coolanol 45 |
| 1100-0** | 0 | 0 | -0.3 | 0.00 (0.00) | 0.00 (0.00) | 2.75 (0.11) |
| 2021-T62 | -0.4 | -0.1 | -0.2 | 2.50 (0.10) | 0.50 (0.02) | 1.00 (0.04) |
| 2024-T3 | 0 | -0.1 | | 0.00 (0.00) | 0.50 (0.02) | 0.00 (0.00) |
| 2219-T87 | -0.4 | -0.4 | -0.1 | 1.50 (0.06) | 1.50 (0.06) | 0.50 (0.02) |
| 6061-T6 | -1.3 | +0.1 | -0.1 | 9.20 (0.37) | 0.00 (0.00) | 0.25 (0.01) |
| 7075-T6 | 0 | -0.1 | -0.3 | 0.00 (0.00) | 1.00 (0.04) | 1.25 (0.05) |
| 7475-T651* | -0.1 | -0.4 | -0.3 | 0.50 (0.02) | 2.25 (0.09) | 1.50 (0.06) |
| AZ31B-H24** | -0.1 | -0.1 | -0.3 | 0.75 (0.03) | 0.75 (0.03) | 3.00 (0.12) |
| Beryllium | 0 | -0.1 | +0.2 | 0.00 (0.00) | 2.50 (0.10) | 0.00 (0.00) |
| Lockalloy | 0 | | | 0.00 (0.00) | | |
| Ti-6Al-4V Sta | 0 | -0.3 | | 0.00 (0.00) | 4.50 (0.18) | 0.00 (0.00) |
| Inconel 617 | 0 | -0.1 | +0.2 | 0.00 (0.00) | 0.50 (0.02) | 0.00 (0.00) |
| Inconel 718 | +0.2 | | +0.1 | 0.50 (0.02) | 1.00 (0.04) | 0.00 (0.00) |
| Boron/Aluminum | -0.1 | +0.5 | -0.2 | 0.75 (0.03) | 0.00 (0.00) | 0.50 (0.02) |
| Graphite/Aluminum | +1.7 | +1.3 | +2.1 | 0.00 (0.00) | 0.00 (0.00) | 0.00 (0.00) |

* - is Weight Loss, + is Weight Gain

** 800 Hours Exposure

TABLE LI
WEIGHT CHANGE RESULTS IN DIELECTRIC
COOLANTS, 762 HOURS OF EXPOSURE AT 366°K (200F)

| Material | Weight Change, Milligrams | | |
|-----------------|---------------------------|-------|-----------|
| | Dow XF 1-3755 | FC-43 | Freon E-5 |
| 1100-0 | — | +1.0 | +0.3 |
| 2021-T62 | — | +0.7 | +1.2 |
| 2219-T87 | +0.8 | +0.9 | +1.6 |
| 2024-T3 | +0.3 | +0.7 | +1.3 |
| X-2048-T851 | +0.3 | — | +0.7 |
| 6061-T6 | +0.2 | +0.9 | +0.3 |
| 7075-T6 | +0.4 | +1.0 | +0.4 |
| 7475-T61 | +0.8 | +0.7 | +0.7 |
| AZ31B-H24 | +0.7 | +0.1 | +0.8 |
| Ti-6Al-4V | +0.7 | +0.7 | +0.7 |
| Inconel 617 | +0.6 | +0.7 | +0.6 |
| Inconel 718 | — | +0.5 | +0.3 |
| Lockalloy | +0.8 | +0.1 | +0.8 |
| Beryllium | +1.2 | +0.2 | +1.3 |
| Gr/Al Composite | +1.5 | +1.5 | +3.2 |
| B/Al Composite | +1.5 | +0.5 | +1.4 |

TABLE LII
RESULTS OF STRESS CORROSION TESTS IN APOLLO GRADE 2
ETHYLENE GLYCOL/WATER AT 366° K (200F), 90% OF YTS

| Material/Time | Sample | | Failure | Weight Change, Grams | Corrosion Rate, | | Comments |
|-----------------------------|----------|---------|---------|----------------------|-----------------|-------|---|
| | Type (1) | Number | | | μ m/y | mpy | |
| 2024-T3 4700 Hours | U | AI-7-S | No | -0.005 | 1.72 | 0.069 | Etched clean, scattered pitting |
| | U | AI-8-S | No | -0.006 | 2.07 | 0.083 | Same |
| | N | AI-7-N | No | -0.005 | 1.72 | 0.069 | Same |
| | N | AI-8-N | No | -0.005 | 1.72 | 0.069 | Same |
| 2048-T851 1750 Hours (2) | U | 48-1-S | No | 0 | 0 | 0 | Generally clean, etched surface, minor pitting |
| | U | 48-1-S | No | 0 | 0 | 0 | Same |
| | N | 48-1-N | No | +0.001 | 0 | 0 | Same |
| | N | 48-2-N | No | +0.001 | 0 | 0 | Same |
| 7475-T61 4700 Hours | U | 75-9-S | No | -0.013 | 4.50 | 0.180 | Little or no surface etching |
| | U | 75-10-S | No | -0.003 | 1.02 | 0.041 | Same |
| | N | 75-9-N | No | -0.002 | 0.70 | 0.028 | Same |
| | N | 75-10-N | No | -0.002 | 0.70 | 0.028 | Same |
| AZ31B-H24 4700 Hours | U | Z-7-S | No | -0.084 | 45.0 | 1.802 | Pitted and blackened |
| | U | Z-8-S | No | -0.073 | 38.8 | 1.566 | Same |
| | N | Z-6-N | No | -0.080 | 42.9 | 1.716 | Same |
| | N | Z-7-N | No | -0.075 | 40.1 | 1.609 | Same |
| Ti-6Al-4V Sta 4700 Hours | U | TS-7 | No | 0 | 0 | 0 | Light, tan surface stain, no pitting or corrosion |
| | U | TS-8 | No | 0 | 0 | 0 | Same |
| | N | TN-7 | No | +0.001 | 0 | 0 | Same |
| | N | TN-8 | No | +0.001 | 0 | 0 | Same |

TABLE LIII
RESULTS OF STRESS CORROSION TESTS IN PRESTONE*WATER
AT 366° (200F), 90% OF YTS

| Material/Time | Sample | | Failure | Weight Change, Grams | Corrosion Rate, | | Comments |
|-----------------------------|----------|---------|---------|----------------------|-----------------|-------|--|
| | Type (1) | Number | | | μ m/y | mpy | |
| 2024-T3 4700 Hours | U | AI-9-S | No | -0.007 | 2.41 | 0.097 | Little or no surface etching |
| | U | AI-10-S | No | -0.008 | 2.76 | 0.111 | Same |
| | N | AI-9-N | No | -0.005 | 1.72 | 0.069 | Same |
| | N | AI-10-N | No | -0.007 | 2.41 | 0.097 | Same |
| 2048-T851 (2) 1750 Hours | U | 48-3-S | No | +0.001 | 0 | 0 | Clean, etched surfaces, minor pitting |
| | U | 48-4-S | No | 0 | 0 | 0 | Same |
| | N | 48-3-N | No | +0.001 | 0 | 0 | Same |
| | N | 48-4-N | No | 0 | 0 | 0 | Same |
| 7475-T61 4700 Hours | U | 75-11-S | No | -0.008 | 2.76 | 0.111 | Etched, discolored, some pitting |
| | U | 75-12-S | No | -0.007 | 2.41 | 0.097 | Same |
| | N | 75-11-N | No | -0.006 | 2.07 | 0.083 | Same |
| | N | 75-12-N | No | -0.008 | 2.76 | 0.111 | Same |
| AZ31B-H24 4700 hours | U | Z-9-S | No | -0.056 | 30.1 | 1.201 | Very heavily pitted and blackened, Worst case. |
| | U | Z-10-S | No | -0.066 | 33.6 | 1.416 | Same |
| | N | Z-14-N | No | -0.013 | 6.90 | 0.279 | Same |
| | N | Z-15-N | No | +0.004 | 0 | — | Same |
| Ti-6Al-4V Sta 4700 Hours | U | T-S-9 | No | 0 | 0 | 0 | Dark blue discoloration, no pitting or corrosion |
| | U | T-S-10 | No | 0 | 0 | 0 | Same |
| | N | T-N-9 | No | +0.001 | 0 | 0 | Same |
| | N | T-N-10 | No | 0 | 0 | 0 | Same |

*Trademark, Union Carbide Corporation

(1) U - Unnotched, N - Notched

(2) Material received late in program.

(3) Apparently all residue was not removed

TABLE LIV

RESULTS OF STRESS CORROSION TESTS IN PRESTONE II*/WATER AT 366°K (200F), 90% YTS

| Material/Time | Sample | | Failure | Weight Change Grams | Corrosion Rate | | Comments |
|--|---------------------|---------|---------|---------------------|----------------|-------|---|
| | Type ⁽¹⁾ | Number | | | μm/y | mpy | |
| 2024-T3 4700 Hours | U | AI-11-S | No | -0.014 | 4.80 | 0.193 | gray-black discoloration, deepest pitting |
| | U | AI-12-S | No | -0.011 | 3.79 | 0.152 | Same |
| | N | AI-11-N | No | -0.004 | 1.38 | 0.055 | Same |
| | N | AI-12-N | No | -0.006 | 2.07 | 0.083 | Same |
| 2048-T851 1750 Hours ⁽²⁾ | U | 48-5-S | No | 0 | 0 | 0 | Gray-black discoloration, faint grain outline |
| | U | 48-6-S | No | -0.001 | 0.92 | 0.037 | Same |
| | N | 48-5-N | No | +0.001 | 0 | 0 | Same |
| | N | 48-6-N | No | +0.001 | 0 | 0 | Same |
| 7475-T61 4700 Hours | U | 75-13-S | No | -0.044 | 15.2 | 0.607 | Uniformly pitted |
| | U | 75-14-S | No | -0.041 | 14.1 | 0.566 | Same |
| | N | 75-13-N | No | -0.029 | 10.00 | 0.400 | Same |
| | N | 75-14-N | No | -0.027 | 9.30 | 0.373 | Same |
| AZ31B-H24 4700 Hours | U | Z-11-S | No | +0.005 | - | (3) | Pitted and blackened |
| | U | Z-12-S | No | +0.001 | - | (3) | Same |
| | N | Z-12-N | No | +0.006 | - | (3) | Same |
| | N | Z-13-N | No | -0.062 | 33.0 | 1.330 | Heavy localized pitting |
| Beryllium 3700 Hours ⁽⁴⁾ | U | B-1-S | No | +0.004 | 0 | 0 | Clean, slight surface etching |
| | U | B-2-S | No | +0.005 | 0 | 0 | Same |
| | N | B-15-N | No | +0.003 | 0 | 0 | Same |
| | N | B-16-N | No | +0.003 | 0 | 0 | Same |
| Ti-6 Al-4V-STA 4700 Hours | U | TS-11 | No | 0 | 0 | 0 | Clean surfaces, very little set |
| | U | TS-12 | No | 0 | 0 | 0 | Same |
| | N | TN-11 | No | 0 | 0 | 0 | White deposits on surface |
| | N | TN-12 | No | 0 | 0 | 0 | Same |

*Trademark, Union Carbide Corporation

⁽¹⁾ U - Unnotched, N - Notched⁽²⁾ Material received late in program⁽³⁾ Apparently some residue was adherent.⁽⁴⁾ Specimens received late.

TABLE LV

RESULTS OF STRESS CORROSION TESTS IN FC-43*, AT 366°K (200F), 90% YTS

| Material/Time | Sample | | Failure | Weight Change Grams | Corrosion Rate | | Comments |
|--|---------------------|---------|---------|---------------------|----------------|-------|--|
| | Type ⁽¹⁾ | Number | | | μm/y | mpy | |
| 2024-T3 4700 Hours | U | AI-13-S | No | 0 | 0 | 0 | Bluish tint, etched surface, scattered pitting |
| | U | AI-14-S | No | 0 | 0 | 0 | Same |
| | N | AI-13-N | No | 0 | 0 | 0 | Same |
| | N | AI-14-N | No | 0 | 0 | 0 | Same |
| 2048-T851 1750 Hours ⁽²⁾ | U | 48-7-S | No | 0 | 0 | 0 | Clean, shiny surfaces |
| | U | 48-8-S | No | 0 | 0 | 0 | Same |
| | N | 48-7-N | No | +0.001 | 0 | 0 | Same |
| | N | 48-8-N | No | +0.001 | 0 | 0 | Same |
| 7475-T61 4700 Hours | U | 75-15-S | No | -0.028 | 0.96 | 0.386 | Discolored, scattered pitting, faint grain outline |
| | U | 75-16-S | No | -0.002 | 0.70 | 0.028 | Same |
| | N | 75-15-N | No | -0.001 | 0.35 | 0.014 | Same |
| | N | 75-16-N | No | -0.001 | 0.35 | 0.014 | Same |
| AZ31B-H24 4700 Hours | U | Z-13-S | No | -0.001 | 0.51 | 0.021 | Scattered, shallow pitting, slight gray stain |
| | U | Z-14-S | No | 0 | 0 | 0 | Same |
| | N | Z-16-N | No | +0.001 | 0 | 0 | Etched surfaces |
| | N | Z-17-N | No | +0.001 | 0 | 0 | Same |
| Ti-6 Al-4V Sta 4700 Hours | U | TS-13 | No | +0.001 | 0 | 0 | Light tan to light blue discoloration-no corrosion |
| | U | TS-14 | No | +0.001 | 0 | 0 | Same |
| | N | TN-13 | No | 0 | 0 | 0 | Light brown discoloration - no corrosion |
| | N | TN-14 | No | 0 | 0 | 0 | Same |

*Trademark, 3M Company, Chemical Division

⁽¹⁾ U - Unnotched, N - Notched⁽²⁾ Material received late in program

TABLE LVI
RESULTS OF STRESS CORROSION TESTS IN
COOLANOL 45* AT 366°K (200F), 90% YTS

| Material/Time | Sample | | Failure | Weight Change Grams | Corrosion Rate, | | Comments |
|--|---------------------|---------|---------|---------------------|-----------------|-------|--|
| | Type ⁽¹⁾ | Number | | | μm/y | mpy | |
| 2024-T3 4700 Hours | U | AI-15-S | No | +0.001 | 0 | 0 | Stained surface |
| | U | AI-16-S | No | +0.002 | 0 | 0 | Same |
| | N | AI-15-N | No | -0.001 | 0.35 | 0.014 | Same |
| | N | AI-16-N | No | 0 | 0 | 0 | Same |
| 2048-T851 1750 Hours ⁽²⁾ | U | 48-9-S | No | +0.001 | 0 | 0 | Clean, shiny surfaces, no permanent set |
| | U | 48-10-S | No | +0.001 | 0 | 0 | Same |
| | N | 48-9-N | No | +0.001 | 0 | 0 | Same |
| | N | 48-10-N | No | +0.001 | 0 | 0 | Same |
| 7475-T61 4700 Hours | U | 75-17-S | No | -0.001 | 0.35 | 0.014 | Little or no surface etch. Faint grain outline. |
| | U | 75-18-S | No | -0.003 | 1.01 | 0.041 | Same |
| | N | 75-17-N | No | 0 | 0 | 0 | Little or no surface etching |
| | N | 75-18-N | No | -0.001 | 0.35 | 0.014 | Same |
| AZ31B-H24 4700 Hours | U | Z-15-S | No | -0.002 | 1.03 | 0.043 | Scattered, shallow pitting, slight gray stain |
| | U | Z-16-S | No | -0.001 | 0.50 | 0.021 | Same |
| | N | Z-18-N | No | -0.001 | 0.50 | 0.021 | Scattered, shallow pitting, lightly etched surface |
| | N | Z-19-N | No | -0.001 | 0.50 | 0.021 | Same |
| Beryllium 3700 Hours ⁽³⁾ | U | B-3-S | No | +0.001 | 0 | 0 | Clean, slight surface etching |
| | U | B-4-S | No | 0 | 0 | 0 | Same |
| | N | B-17-N | No | 0 | 0 | 0 | Same |
| | N | B-19-N | No | 0 | 0 | 0 | Same |
| Ti-6Al-4V Sta. 4700 Hours | U | TS-15 | No | +0.001 | 0 | 0 | Clean surface-no corrosion |
| | U | TS-16 | No | +0.001 | 0 | 0 | Same |
| | N | TN-15 | No | +0.001 | 0 | 0 | Same |
| | N | TN-16 | No | +0.001 | 0 | 0 | Same |

TABLE LVII
RESULTS OF STRESS CORROSION TESTS IN
COOLANOL 45* 450°K (350F), 90% YTS

| Material/Time | Sample | | Failure | Weight Change Grams | Corrosion Rate, | | Comments |
|--|---------------------|---------|---------|---------------------|-----------------|-------|---|
| | Type ⁽¹⁾ | Number | | | μm/y | mpy | |
| 2024-T3 4500 Hours | U | AI-1-S | No | 0 | 0 | 0 | Generally clean and shiny |
| | U | AI-2-S | No | 0 | 0 | 0 | Same |
| | N | AI-1-N | No | -0.001 | 0.35 | 0.014 | Same |
| | N | AI-2-N | No | -0.002 | 0.68 | 0.027 | Same |
| 2048-T851 1450 Hours ⁽²⁾ | U | 48-11-S | No | 0 | 0 | 0 | Clean, bright surface, faint grain outline |
| | U | 48-12-S | No | 0 | 0 | 0 | Same |
| | N | 48-11-N | No | -0.002 | 1.84 | 0.074 | Same |
| | N | 48-12-N | No | -0.002 | 1.84 | 0.074 | Same |
| 7475-T61 4500 Hours | U | 75-1-S | No | -0.003 | 1.01 | 0.041 | Faint grain outline. Little or no surface etch. |
| | U | 75-2-S | No | -0.001 | 0.35 | 0.014 | Same |
| | N | 75-1-N | No | -0.003 | 0.35 | 0.041 | Little or no surface etch. |
| | N | 75-2-N | No | +0.008 | 0 | 0 | |
| AZ31B-H24 4500 Hours | U | Z-1-S | No | -0.015 | 8.00 | 0.322 | Scattered, shallow pitting, slight gray stain |
| | U | Z-2-S | No | -0.013 | 6.98 | 0.279 | Same |
| | N | Z-1-N | No | -0.010 | 5.42 | 0.215 | Same |
| | N | Z-2-N | No | -0.012 | 6.32 | 0.251 | Same |
| Beryllium 3400 Hours ⁽³⁾ | U | B-9-S | No | +0.007 | 0 | 0 | Dark stain-scattered pits |
| | U | B-20-S | No | +0.056 | 0 | 0 | Clean, slight surface etching |
| Ti-6Al-4V Sta. 4500 Hours | U | TS-1 | No | +0.004 | 0 | 0 | Light brown surface stain-no corrosion |
| | U | TS-2 | No | +0.004 | 0 | 0 | Same |
| | N | TN-1 | No | +0.001 | 0 | 0 | Light blue surface stain-no corrosion |
| | N | TN-2 | No | +0.001 | 0 | 0 | |

*Trademark, Monsanto

(1) U - Unnotched, N - Notched

(2) Material received late in program

(3) Specimens received late

TABLE LVIII
RESULTS OF STRESS CORROSION TESTS IN
XF-1-3755* AT 450° K (350F), 90% YTS

| Material/Time | Sample | | Failure | Weight Change Grams | Corrosion Rate | | Comments |
|--|---------------------|---------|---------|---------------------|----------------|-------|---|
| | Type ⁽¹⁾ | Number | | | μ m/y | mpy | |
| 2024-T3 4500 Hours | U | AI-5-S | No | -0.015 | 5.21 | 0.210 | Clean, etched surface |
| | U | AI-6-S | No | -0.025 | 8.61 | 0.345 | Same |
| | N | AI-5-N | No | -0.010 | 3.45 | 0.138 | Same |
| | N | AI-6-N | No | -0.016 | 5.50 | 0.220 | Same |
| 2048-T851 1450 Hours | U | 48-15-S | No | -0.053 | 48.8 | 1.961 | Deeply etched and pitted-worst case |
| | U | 48-16-S | No | -0.050 | 46.0 | 1.850 | Same |
| | N | 48-15-N | No | -0.035 | 32.1 | 1.295 | Same |
| | N | 48-16-N | No | -0.043 | 39.6 | 1.591 | Same |
| 7475-T61 4500 Hours | U | 75-7-S | No | -0.012 | 4.11 | 0.166 | Little or no surface etching. Relatively clean |
| | U | 75-8-S | No | -0.002 | 0.68 | 0.027 | Same |
| | N | 75-6-N | No | -0.002 | 0.68 | 0.027 | Same |
| | N | 75-7-N | No | -0.001 | 0.35 | 0.014 | Same |
| AZ31B-H24 4500 Hours | U | Z-5-S | No | +0.010 | 0 | 0 | Etched bright and shiny |
| | U | Z-6-S | No | +0.010 | 0 | 0 | Same |
| | N | Z-8-N | No | +0.004 | 0 | 0 | Same |
| | N | Z-9-N | No | +0.005 | 0 | 0 | Same |
| Beryllium 3400 Hours ⁽³⁾ | U | B-13-S | No | +0.002 | 0 | 0 | Clean, slight surface etching, scattered pitting |
| | U | B-14-S | No | +0.003 | 0 | 0 | Same |
| Ti-6Al-4V Sta. 4500 Hours | U | TS-5 | No | +0.008 | 0 | 0 | Clean surface-translucent white deposit on surface |
| | U | TS-6 | No | +0.010 | 0 | 0 | Same |
| | N | TN-5 | No | 0 | 0 | 0 | Same |
| | N | TN-6 | No | +0.008 | 0 | 0 | Same |

*Trademark, Dow Corning Corporation

⁽¹⁾ U - Unnotched, N - Notched

⁽²⁾ Material received late in program

⁽³⁾ Specimens received late

TABLE LIX
RESULTS OF STRESS CORROSION TESTS IN E-5* AT 450° K (350F), 90% YTS

| Material/Time | Sample | | Failure | Weight Change Grams | Corrosion Rate, | | Comments |
|--|---------------------|---------|---------|---------------------|-----------------|-------|--|
| | Type ⁽¹⁾ | Number | | | μ m/y | mpy | |
| 2024-T3 4500 Hours | U | AI-3-S | No | +0.001 | 0 | 0 | Generally clean, some stain |
| | U | AI-4-S | No | +0.001 | 0 | 0 | Same |
| | N | AI-3-N | No | 0 | 0 | 0 | Same |
| | N | AI-4-N | No | +0.001 | 0 | 0 | Same |
| 2048-T851 1450 Hours ⁽²⁾ | U | 48-13-S | No | 0 | 0 | 0 | Gray-black discoloration, some minor, scattered pit |
| | U | 48-14-S | No | 0 | 0 | 0 | Same |
| | N | 48-13-N | No | +0.001 | 0 | 0 | Same |
| | N | 48-14-N | No | +0.001 | 0 | 0 | Same |
| 7475-T61 4500 Hours | U | 75-3-S | No | -0.002 | 0.68 | 0.027 | Little or no surface etching. Relatively clean |
| | U | 75-4-S | No | -0.005 | 1.72 | 0.069 | Same |
| | N | 75-4-N | No | -0.001 | 0.35 | 0.014 | Same |
| | N | 75-6-N | No | -0.001 | 0.35 | 0.014 | Same |
| AZ31B-H24 4500 Hours | U | Z-3-S | No | +0.001 | 0 | 0 | Scattered, shallow pitting, slight gray etch |
| | U | Z-4-S | No | +0.001 | 0 | 0 | Same |
| | N | Z-3-N | No | +0.001 | 0 | 0 | Same |
| | N | Z-4-N | No | +0.001 | 0 | 0 | Same |
| Beryllium 3400 Hours ⁽³⁾ | U | B-11-S | No | 0 | 0 | 0 | Blue to gray-black discoloration |
| | U | B-12-S | No | +0.001 | 0 | 0 | Same |
| Ti-6Al-4V Sta. 4500 Hours | U | TS-3 | No | 0 | 0 | 0 | Light blue surface stain-no corrosion |
| | U | TS-4 | No | +0.001 | 0 | 0 | Same |
| | N | TN-3 | No | 0 | 0 | 0 | Same |
| | N | TN-4 | No | +0.001 | 0 | 0 | Same |

*Trademark, E.I. DuPont De Nemours and Company, Inc.

⁽¹⁾ U - Unnotched, N - Notched

⁽²⁾ Material received late in program

⁽³⁾ Specimens received late

TABLE LX
RESULTS OF STRESS CORROSION TESTS IN COOLANOL 45* AT 535°K (500F), 90% YTS

| Material/Time | Sample | | Failure | Weight Change Grams | Corrosion Rate | | Comments |
|---------------------------|---------------------|---------|---------|---------------------|----------------|-------|---|
| | Type ⁽¹⁾ | Number | | | μm/y | mpy | |
| Ti-6Al-4V STA | U | T-S-17 | No | +0.001 | 0 | 0 | Light blue surface stain-no corrosion |
| 3700 Hours | U | T-S-18 | No | 0 | 0 | 0 | Same |
| | N | T-N-17 | No | +0.001 | 0 | 0 | Same |
| | N | T-N-18 | No | +0.002 | 0 | 0 | Same |
| Beryllium | U | B-5-S | No | 0 | 0 | 0 | Clean slight surface etch, shallow, scattered pit |
| 3700 Hours | U | B-6-S | No | +0.001 | 0 | 0 | Same |
| | N | B-21-N | No | 0 | 0 | 0 | Same |
| | N | B-22-N | No | 0 | 0 | 0 | Same |
| 2048-T851 | U | 48-17-S | No | 0 | 0 | 0 | Generally clean and bright, faint grain outline |
| 1750 Hours ⁽²⁾ | U | 48-18-S | No | +0.001 | 0 | 0 | Same |
| | N | 48-17-N | No | -0.001 | 0.92 | 0.037 | Same |
| | N | 48-18-N | No | -0.002 | 1.84 | 0.074 | Same |

*Trademark, Monsanto

(1) U - Unnotched, N - Notched

(2) Material received late in program

TABLE LXI
RESULTS OF STRESS CORROSION TESTS IN DOWTHERM G* AT 535°K (500F), 90% YTS

| Material/Time | Sample | | Failure | Weight Change Grams | Corrosion Rate | | Comments |
|---------------------------|---------------------|---------|---------|---------------------|----------------|-----|---|
| | Type ⁽¹⁾ | Number | | | μm/y | mpy | |
| Ti-6Al-4V STA | U | T-S-19 | No | +0.001 | 0 | 0 | Light brown surface stain-no corrosion |
| 3700 Hours | U | T-S-20 | No | 0 | 0 | 0 | Same |
| | N | T-N-19 | No | 0 | 0 | 0 | Same |
| | N | T-N-20 | No | +0.001 | 0 | 0 | Same |
| Beryllium | U | B-7-S | No | 0 | 0 | 0 | Clean, slight surface etching |
| 3700 Hours | U | B-8-S | No | 0 | 0 | 0 | Same |
| | N | B-23-N | No | 0 | 0 | 0 | Same |
| | N | B-24-N | No | 0 | 0 | 0 | Same |
| 2048-T851 | U | 48-19-S | No | 0 | 0 | 0 | Generally clean and bright, faint grain outline |
| 1750 Hours ⁽²⁾ | U | 48-20-S | No | 0 | 0 | 0 | Same |
| | N | 48-19-N | No | +0.001 | 0 | 0 | Same |
| | N | 48-20-N | No | 0 | 0 | 0 | Same |

*Trademark, Dow Chemical Company

(1) U - Unnotched, N - Notched

(2) Material received late in program

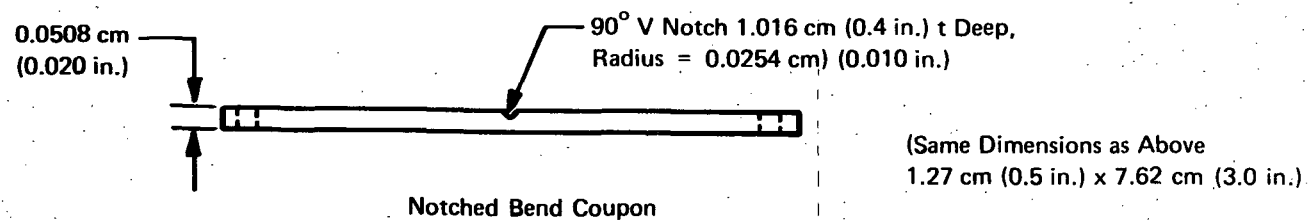
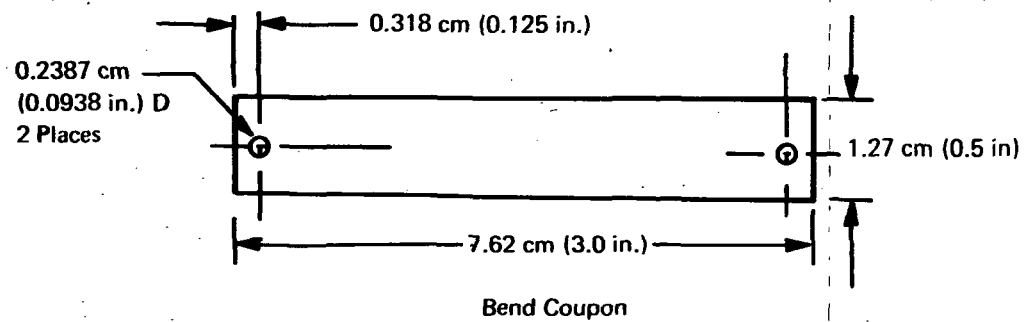


Figure 115. Beryllium Bend Coupon Specimen Configuration

tests that permitted formation of protective oxides that decreased corrosion rates during the stress corrosion exposures, in contrast to the short exposures of the corrosion potential testing.

With regard to the appearance of the specimens only two observations are particularly significant. Rather heavy black deposits were formed on the magnesium alloy specimens exposed in the glycol/water solutions. The deposits and precipitates were more pronounced for the Apollo Grade 2 and the Prestone coolants as compared to the Prestone II. The other significant observation was the presence of glassy like crystals on the surfaces of most of the specimens exposed to the Dow XF-1-3755 coolant. Before this silicone fluid is used in an aircraft cooling system more study of the nature of these crystals and their potential deleterious influences on cooling system components must be determined.

REFERENCES

1. McConarty, W.A. and Anthony, F.M.: Design and Evaluation of Active Cooling Systems for Mach 6 Cruise Vehicle Wings. NASA CR-1916, December 1971.
2. Helenbrook, R.G., McConarty, W.A., and Anthony, F.M.: Evaluation of Active Cooling Systems for a Mach 6 Hypersonic Transport Airframe. NASA CR-1917, December 1971.
3. Helenbrook, R.G., and Anthony, F.M.: Design of a Convective Cooling System for a Mach 6 Hypersonic Transport Airframe. NASA CR-1918, December 1971.
4. Jarlett, F.E.: Performance Potential of Hydrogen Fueled, Airbreathing Cruise Aircraft. Report Numbers GDC DCB 66-004/1/2/2A/3/4/, May 1966.
5. MIL-A-008861 (USAF): Airplane Strength and Rigidity, Flight-Loads. May 18, 1960.
6. MIL-A-008866 (USAF): Airplane Strength and Rigidity Reliability Requirements, Repeated Loads and Fatigue. May 1960.
7. Plank, P.P., et al.: Hypersonic Cruise Vehicle Wing Structure Evaluation. NASA CR-1568, Dec. 1969.
8. "Freon" Products Division, E.I. Du Pont De Nemours and Company Inc., Wilmington Delaware.
 - (a) Properties and Applications of the Freon Fluorocarbons. Technical Bulletin B-2, 1966.
 - (b) Transport Properties of Freon Fluorocarbons and other Fluorinated Compounds. Technical Bulletin C-30A, R.C. Downing, 1966.
 - (c) Freon E Series Fluorocarbons. Technical Bulletin EL-8B, 1967.
 - (d) Freon TF Dielectric. Technical Bulletin EL-14, 1969.
9. Electronic Products Division, Dow Corning Corp., Midland Michigan.
 - (a) Dielectric Coolants, Dow Corning 331 Fluid. Bull. No. 05-111, Dec. 1964.
 - (b) Aerospace Materials, Selection Guide to Fluids for Aerospace Applications. Bull. No. 05-136, Sept. 1965.
 - (c) Electronic Materials, Selection Guide to Fluids for Electronic Applications. Bull. No. 05-213, July 1968.
 - (d) Dow Corning XF-1-3755 Fluid.
10. Dowtherm Heat Transfer Fluids. . Efficient and Stable at Elevated Temperatures. The Dow Chemical Company, Functional Products and Systems Dept., Midland, Michigan, 1971.
11. Dowtherm G Heat Transfer Fluid for Low Pressure Systems. The Dow Chemical Company, Functional Products and Systems Dept., Midland Michigan, 1971.

12. 3M Brand Inert Fluorochemical Liquids. Minnesota Mining and Manufacturing Co., Chemical Division, St. Paul, Minnesota, 1965.
13. Coolanol 15, 25, 35, 45, Dielectric Heat Transfer Fluid for Electronic Equipment. Technical Bulletin O/AA-1, Monsanto, St. Louis, Missouri, 1967.
14. Coolanol 20, Coolanol 40, Dielectric Heat Transfer Fluids. Technical Bulletin O/FF-25, Monsanto, St. Louis, Missouri, 1970.
15. Stauffer 3664 Synthetic Lubricant. Specialty Chemical Division/Stauffer Chemical Company, New York, New York.
16. Glycols. Union Carbide Corporation, Chemicals Division, New York, 1964.
17. Jackson, J.D., Miller, P.D., Fink, F.W., and Boyd, W.K.: Corrosion of Materials by Ethylene Glycol-Water. Report DMIC 216, Office of the Director of Defense Research and Engineering, Defense Metals Information Center, May 10, 1965.
18. Godard, H.P., Jepson, W.B., Bothwell, M.R., and Kane, R.L.: The Corrosion of Light Metals. Sponsored by the Electrochemical Society, Inc., John Wiley & Sons, Inc. (from the Corrosion Monograph Series) 1967.
19. Fontana M.G. and Greene N.D.: Corrosion Engineering. McGraw-Hill Co., New York, 1967.
20. DMIC Report 242: Corrosion of Beryllium. Defense Metals Information Center, Battelle Memorial Institute, December, 1967.
21. Department of Defense: Metallic Materials and Elements for Aerospace Vehicle Structures. MIL-HDBK-5A, Revised 5 January 1970.
22. Weiss, V. and Sessler, ed.: Aerospace Structural Metals Handbook. Volumes I and II, Prepared by Syracuse University Research Institute for Air Force Materials Laboratory, March 1964.
23. Deel, O.L. and Mindlin, H.: Engineering Data on New and Emerging Structural Materials. Battelle Memorial Institute, TR-70-252, October 1970.
24. Stevens, E.C. and Hanink, D.K.: Titanium Composite Fan Blades. AFML-TR-70-180, July 1970.
25. Engler, E.E., and Cataldo, C.E.: Design and Test of Advanced Structural Components and Assemblies. NASA Space Shuttle Technology Conference, Paper No. 16, NASA TM X-2273, March 1971.
26. Figge, I.: Residual Static Strength of Several Titanium and Stainless Steel Alloys and One Superalloy at -109F, 70F and 550F. NASA TN D2331, 1964.
27. Hudson: Fatigue Properties of Several Titanium Alloys and Stainless Steel Alloys and One Superalloy at 80F, 550F, and 109F. NASA TN D2331, 1964.

28. Peterson, J.: Behavior of AM 350 Stainless Steel and Ti-8Al-1Mo-1V sheet at Room Temperature, 550F and 800F. NASA CR 23, May 1964.
29. Gideon, D., Marshall, C., Holden, F., and Hyler, W.: Exploratory Studies of Mechanical Cycling Fatigue Behavior of Materials for the Supersonic Transport. NASA CR 28, April 1964.
30. Cranford, R.F., and Burns, A.B.: Strength, Efficiency, and Design Data for Beryllium Structures. ASD TR61-692, February 1962.
31. Proceedings of the Beryllium Conference. National Materials Advisory Board, Volume I, July 1970.
32. Kaminski, B.E.: Development of Engineering Data for Advanced Composite Materials. AFML, TR70-108, August 1970.
33. Advanced Composite Design Guide. Third ed., January, 1973.
34. Boron and Graphite Reinforced Elevated Temperature Composites. Lockheed Georgia Company, ACDAP Report 2, July, 1971.
35. Levy, S.A. et al.: X2048, A High Strength, High Toughness Alloy for Aircraft Applications. AIAA Paper 73-385, March 1973.
36. Gallagher, R.H., Rattinger, I., and Krivetsky, A, "Minimum Weight Shells in Bending," Aerospace Engineering, February 1962.
37. Shideler, J.L., et al.: Optimum Mass-Strength Analysis for Orthotropic Ring-Stiffened Cylinders Under Axial Compression. NASA TN D-6772, July, 1972.
38. Giles, G.L.: Structural Efficiencies of Five Compression Panels with Curved Elements. TN-D-6479, December, 1971.
39. Madden, B. C., Jr., & Expanded - Sphere Sandwich Structure, ASME Preprint 70 - WA/Unt-7, November 1970.
40. Kays, W.M. and London, A.L.: Compact Heat Exchangers. National Press, 1955.
41. Anthony F.M., et al.: Reusable Space Shuttle Vehicle Thermal Protection. Bell Aerospace Co. Report No. 8629-950001, January 1972.
42. Space Shuttle Thermal Protection System Development. Lockheed Missiles and Space Co.; LMSC-D152738, January 1972.
43. Giles G.L., and Anderson, M.S.: Effects of Eccentricities and Lateral Pressure on the Design of Stiffened Compression Panels. TN-D-6784, June 1972.
44. Yurkowsky, W.: Nonelectronic Reliability Notebook. Hughes Aircraft Co., RADC-TR-69-458, March, 1970.

45. Farada: Failure Rate Data Handbook. Bureau of Naval Weapons; vol. 1B.
46. Autonetics Standards: Failure Rate Manual. July, 1965.
47. Failure Rate Pamphlet. Lockheed Missiles and Space Company.
48. Dukes, W.H., et al.: Manufacturing Methods for Insulated and Cooled Double Wall Structures. ASD-TR-61-7-799, volumes I and II, May, 1961.
49. NASA Space Shuttle Technology Conference: Dynamics and Aeroelasticity. Structures and Materials. NASA TM X-2570, July, 1972.
50. French, R.J.: Redesign of the Apollo Environmental Control System Radiator, Astronautics Division, LTV Aerospace Corp. Report No. 00.717, August, 1966.
51. Giles, H.L. and Thomas, J.W.: Analysis of Hypersonic Pressure and Heat Transfer Tests on a Flat Plate with a Flap and a Delta Wing with Body, Elevons, Fins and Rudders. NASA CR-536, 1966.
52. Nagel, A.L., et al.: Analysis of Hypersonic Pressure and Heat Transfer Tests on Delta Wings with Laminar and Turbulent Boundary Layers. NASA CR-535, 1966.
53. Elber, N. and Davidson, J.R.: A Material Selection Method Based on Material Properties and Operating Parameters. NASA TN-D-7221, April, 1973.
54. Forman, R.G. et al.: Numerical Analysis of Crack Propagation in Cyclic Load Structures. Journal of Basic Engineering, trans. ASME, Series D, vol. 89, No. 3, 1967, p. 459-464.
55. Engle, Robert, M., Sr.: Cracks, A FORTRAN IV Digital Computer Program for Crack Propagation Analysis. AFFDL-TR-70-107, October, 1970.
56. Damage Tolerant Design Handbook. Air Force Materials Laboratory, MCIC-HB-01, December, 1972.
57. Paris, P.C.: The Fracture Mechanics Approach to Fatigue. Fatigue - An Interdisciplinary Approach. Edited by Burke, N. Reed, N.L., and Weiss, V., Syracuse Univ. Press, 1964, pp 107-132
58. Hudson, C.M.: Effect of Stress Ratio on Fatigue - Crack Growth in 7075-T6 and 2024-T3 Aluminum-Alloy Specimens. NASA TN D-5390, 1969.
59. Poe, C.C.: Fatigue Crack Propagation in Stiffened Panels. ASTM STP 486, 1970.
60. Evaluation of Laminated Aluminum Plate for Shuttle Applications, Grumman Aerospace Corp. Final Report on Contract NAS 912387, 8 March 1973.
61. Hart, C.E.: Advanced Metallic Air Vehicle Structures Program. AFFDL-TR-73-77, July, 1973..